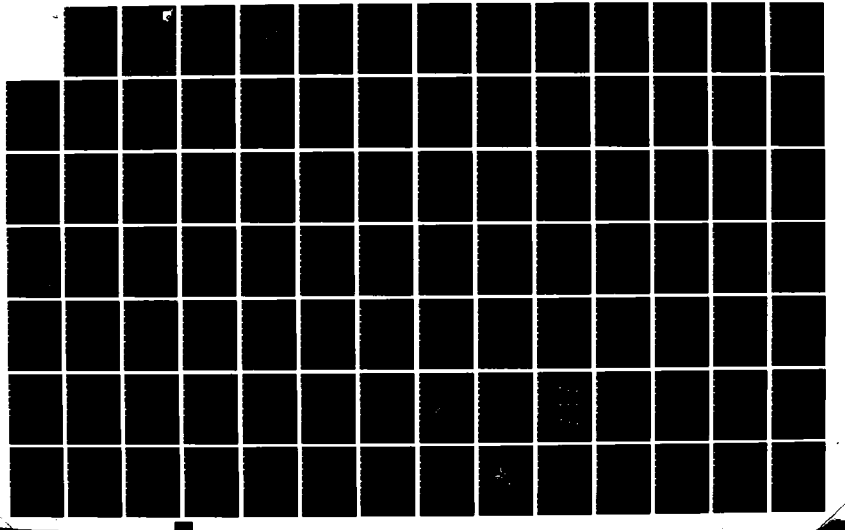
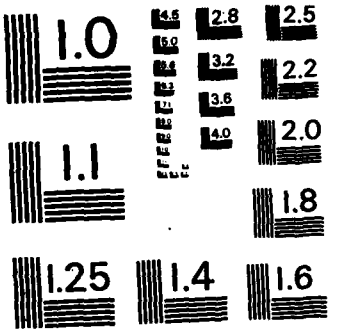
AD-A139 050 PROCEEDINGS OF THE WORKSHOP ON MULTIVARIABLE CONTROL SYSTEMS HELD AT WRIG.. (U) AIR FORCE WRIGHT AERONAUTICAL LABS WRIGHT-PATTERSON AFB OH M A MASI ET AL. SEP 83 1/7

UNCLASSIFIED AFWAL-TR-83-3093 FFG 1/3 NL






MICROCOPY RESOLUTION TEST CHART
NATIONAL BUREAU OF STANDARDS - 1963 - A

AFWAL-TR-83-3098

AD A139050

# PROCEEDINGS OF THE WORKSHOP ON MULTIVARIABLE CONTROL SYSTEMS

MICHAEL A. MASI
DANIEL E. RUSS

CONTROL SYSTEMS DEVELOPMENT BRANCH
FLIGHT DYNAMICS LABORATORY

SEPTEMBER 1983

FINAL REPORT - MARCH 1982 TO SEPTEMBER 1983

APPROVED FOR PUBLIC RELEASE; DISTRIBUTION UNLIMITED

FLIGHT DYNAMICS LABORATORY
AIR FORCE WRIGHT AERONAUTICAL LABORATORIES
AIR FORCE SYSTEMS COMMAND
WRIGHT-PATTERSON AIR FORCE BASE OH 45433

DTIC FILE COPY

DTIC
ELECTE
MAR 16 1984
E

84 03 13 151

*NOTICE*

*When Government drawings, specifications, or other data are used for any purpose other than in connection with a definitely related Government procurement operation, the United States Government thereby incurs no responsibility nor any obligation whatsoever; and the fact that the government may have formulated, furnished, or in any way supplied the said drawings, specifications, or other data, is not to be regarded by implication or otherwise as in any manner licensing the holder or any other person or corporation, or conveying any rights or permission to manufacture use, or sell any patented invention that may in any way be related thereto.*

*This report has been reviewed by the Office of Public Affairs (ASD/PA) and is releasable to the National Technical Information Service (NTIS). At NTIS, it will be available to the general public, including foreign nations.*

*This technical report has been reviewed and is approved for publication.*

DAVID W. POTTS, Capt, USAF
Program Manager
Control Techniques Group

EVARD H. FLINN, Chief
Control Systems Development Branch
Flight Control Division

*FOR THE COMMANDER*

JAMES D. LANG, Col, USAF
Chief, Flight Control Division
Flight Dynamics Laboratory

*"If your address has changed, if you wish to be removed from our mailing list, or if the addressee is no longer employed by your organization please notify* AFWAL/FIGL, *W-PAFB, OH 45433 to help us maintain a current mailing list".*

*Copies of this report should not be returned unless return is required by security considerations, contractual obligations, or notice on a specific document.*

# DISCLAIMER NOTICE

THIS DOCUMENT IS BEST QUALITY PRACTICABLE. THE COPY FURNISHED TO DTIC CONTAINED A SIGNIFICANT NUMBER OF PAGES WHICH DO NOT REPRODUCE LEGIBLY.

Unclassified

SECURITY CLASSIFICATION OF THIS PAGE (When Data Entered)

| REPORT DOCUMENTATION PAGE | | READ INSTRUCTIONS BEFORE COMPLETING FORM |
|---|---|---|
| 1. REPORT NUMBER<br>AFWAL-TR-83-3093 | 2. GOVT ACCESSION NO.<br>AD-A139 050 | 3. RECIPIENT'S CATALOG NUMBER |
| 4. TITLE (and Subtitle)<br>Proceedings of the Workshop on Multivariable Control Systems | | 5. TYPE OF REPORT & PERIOD COVERED<br>Final Report<br>March 1982-September 1983<br>6. PERFORMING ORG. REPORT NUMBER |
| 7. AUTHOR(s)<br>Michael A. Masi<br>Daniel E. Russ | | 8. CONTRACT OR GRANT NUMBER(s) |
| 9. PERFORMING ORGANIZATION NAME AND ADDRESS<br>AFWAL/FIGL<br>Wright-Patterson Air Force Base OH 45433 | | 10. PROGRAM ELEMENT, PROJECT, TASK AREA & WORK UNIT NUMBERS<br>62201F/24030277 |
| 11. CONTROLLING OFFICE NAME AND ADDRESS<br>AFWAL/FIGL<br>Wright-Patterson Air Force Base OH 45433 | | 12. REPORT DATE<br>September 1983<br>13. NUMBER OF PAGES<br>671 |
| 14. MONITORING AGENCY NAME & ADDRESS(if different from Controlling Office) | | 15. SECURITY CLASS. (of this report)<br>Unclassified<br>15a. DECLASSIFICATION/DOWNGRADING SCHEDULE |

16. DISTRIBUTION STATEMENT (of this Report)

Approved for Public Release; Distribution Unlimited.

17. DISTRIBUTION STATEMENT (of the abstract entered in Block 20, if different from Report)

18. SUPPLEMENTARY NOTES

19. KEY WORDS (Continue on reverse side if necessary and identify by block number)

Multivariable Control Laws
Multivariable Control Theory
Multivariable Control Systems
Flight Control Systems
Digital Control Systems

20. ABSTRACT (Continue on reverse side if necessary and identify by block number)

Proceedings are reported of a workshop held at Wright-Patterson Air Force Base on 3 December 1982. The workshop was organized and conducted by the Control Techniques Group, Flight Control Division, Flight Dynamics Laboratory, as part of an ongoing effort in flight control specification/criteria development.

The workshop focused on the results of applying multivariable control techniques to the development of flight control systems for present day aircraft.

DD FORM 1 JAN 73 1473 EDITION OF 1 NOV 65 IS OBSOLETE

Unclassified

SECURITY CLASSIFICATION OF THIS PAGE (When Data Entered)

This report contains condensed versions of the five papers presented at the workshop, as well as some general conclusions.

## FOREWORD

The Proceedings of the Workshop on Multivariable Control Systems represents a compilation of the results of the five papers presented. The presenters, M.S. students at the Air Force Institute of Technology, School of Engineering, were Mr A. Finley Farfield, Capt Jon Bauschlicher, Capt Mike Masi, Lt Tom Lewis, and Lt Dan Russ. The papers represent a condensation of their respective M.S. theses. The theses topics were sponsored by AFWAL/FIGL.

The workshop, also sponsored by AFWAL/FIGL, and coordinated by Mr Duane Rubertus and Capt Dave Potts, provided a useful interchange between the presenters and representatives of industry and the local engineering community.

Finally, a great deal of interest was expressed in the computer-aided-design package MULTI. The MULTI software, User's Manual, and Programmer's Manual are now available upon request.

Table of Contents


| | | Page |
|---|---|---|
| I | Introduction | 5 |
| II | Multivariable Digital Control Theory Using Singular Perturbation Methods | 7 |
| III | Conclusions | 30 |
| IV | Bibliography | 32 |
| V | VITA | 33 |
| | Appendix A(1) Multivariable Control Laws for the AFTI/F-16 | 39 |
| | Appendix B(2) Design of a Complete Multivariable Digital Flight Control System | 257 |
| | Appendix C(3) Digital Multivariable Tracker Control Laws for the C-141-A Starlifter Aircraft | 417 |
| | Appendix D(4) High-Gain Error Actuated Flight Control Systems for Continuous Linear Multivariable Plants | 515 |
| | Appendix E(5) Reconfigurable Digital Control Laws for the A-7D DIGITAC II Aircraft With Failed Primary Control Surfaces | 573 |



Accession For
NTIS GRA&I
DTIC TAB
Unannounced
Justification
By
Distribution/
Availability Codes
Dist | Avail and/or Special
A-1

DTIC COPY INSPECTED 2

# I. INTRODUCTION

The advent of highly augmented flight control systems, system integration at all levels, and the use of multiple function control surfaces, has led to the extensive requirement for multivariable multi-input/multi-output control systems.

The need for alternative multivariable design techniques has been documented. The present control law design methodologies of Linear Quadratic Regulator (LQR), eigenvalue/eigenvector assignment, and classical single input/output do not always meet the handling qualities performance and control system specifications, i.e., phase and gain margins and bandwidth, without modification to cope with the high dynamic uncertainties of an aircraft.

Professor Brian Porter's application of singular perturbation method of asymptotic eigenvalue assignment as applied to control systems has progressed from modal control theory through complete eigenstructure assignment to the use of high gain feedback to the use of output feedback for error-actuated tracker controllers using the method described her-in for the design of several multivariable control systems.

The purpose of the proceedings is to related the results of the five papers presented at the workshop. The papers investigate the applicability of Professor Porter's multivariable control technique to aircraft flight control system design. This multivariable technique can be used for the

design of both analog and digital controllers.

The workshop was very successful with the presenters providing those attending a better understanding of how the technique can be applied to real world plants, the simplicity of the design process, and the relative merits of the results achieved.

The exchange which took place during the workshop was excellent and brought to light some of the concerns of the engineering community about the possible limitations imposed by the technique, stability considerations (i.e., phase and gain margins), and the accuracy of simulating a digital implementation (i.e., failure to model time delays). These issues will be addressed in on-going application studies.

The proceedings provide a single chapter on the theory developed by Professor Porter. This chapter replaces the theory chapters which appear in each of the individual papers.

The conclusions drawn from the studies are then presented. The appendices of this proceedings are edited versions of the original papers and are condensed as much as possible, without deleting important information. Unedited papers may be obtained through NTIS.

## II Multivariable Digital Control Theory Using Singular Perturbation Methods

The control laws presented in each of the papers are based on the design techniques developed by Professor Brian Porter (Ref 1). These techniques utilize singular perturbation methods and are applicable to the design of both analog and digital controllers. These methods are applied to tracking systems incorporating high-gain error-actuated analog and fast-sampling error-actuated digital controllers.

The summary of the design technique is provided on the following pages; it is extracted from the thesis written by A. Finley Barfield. Mr Barfield's reference 6 is the same as the above Reference 1.

# Multivariable Control Law Theory

## Overview

The designs in this thesis are the result of the application of control law methods developed by Professor Brian Porter of the University of Salford, England. The techniques are presented in Reference 6. This chapter provides a summary of the techniques used in the design of high performance tracking systems for aircraft control. It also includes a discussion of important facets in their application. The theoretical discussions cover the discrete case and the corresponding continuous design equations. This approach is taken because, although the designs are for a digital implementation, the insight and experience with continuous design principles can be used effectively. The methods are essentially identical for continuous and discrete designs. It is often more meaningful to consider the s-plane root locations and migrations as opposed to z-plane analysis. For those cases where the continuous methods are employed, it should be kept in mind that sampling effects and discrete time delay must be examined prior to design acceptance.

The plant to be controlled is described by first-order linear differential equations written in state-space format:

$$\dot{\underline{x}} = \underline{A}\underline{x} + \underline{B}\underline{u} \tag{3.1}$$

$$\underline{y} = \underline{C}\underline{x} \tag{3.2}$$

where

A = the continuous-time plant matrix (n x n)

B = the continuous-time control matrix (n x m)

C = the continuous-time output matrix (p x n)

The dimensions are defined as n being the number of states, m the number of inputs, and p the number of outputs.

The $\underline{A}$, $\underline{B}$ and $\underline{C}$ matrices are partitioned to yield the following equations:

$$\begin{bmatrix} \dot{\underline{x}}_1 \\ \hline \dot{\underline{x}}_2 \end{bmatrix} = \left[\begin{array}{c|c} \underline{A}_{11} & \underline{A}_{12} \\ \hline \underline{A}_{21} & \underline{A}_{22} \end{array}\right] \begin{bmatrix} \underline{x}_1 \\ \hline \underline{x}_2 \end{bmatrix} + \begin{bmatrix} \underline{B}_1 \\ \hline \underline{B}_2 \end{bmatrix} \underline{u} \tag{3.3}$$

$$\underline{y} = \left[\begin{array}{c|c} \underline{C}_1 & \underline{C}_2 \end{array}\right] \begin{bmatrix} \underline{x}_1 \\ \\ \underline{x}_2 \end{bmatrix} \tag{3.4}$$

$\underline{B}_2$ is a square matrix with a row and column size equal to the number of inputs in the vector $\underline{u}$. $\underline{C}_2$ is also square with the number of rows and columns equal to the number of outputs. The designation of "inputs" for the aircraft model usually refers to the control surfaces, such as the elevator or rudder, available to command changes in the aircraft states. However, in designs where the $\underline{A}$ matrix is augmented with surface actuator states, "inputs" denote the

surface actuator input commands. Outputs are states or combinations of states of the aircraft such as angle of attack or pitch rate.

A requirement of the design method is that the number of inputs must equal the number of outputs, thus $\underline{B}_2$ and $\underline{C}_2$ have the same row and column dimensions. $\underline{A}_{22}$ also has the same dimensions. Knowing these dimensions allows the system matrices to be easily partitioned as shown above.

Two design methods are applicable to the aircraft under study using the regular and irregular designs. The design method used is determined by the type of plant being considered.

## Regular Versus Irregular Design

To be considered as a "regular" plant, the matrix representing the first Markov parameter, $[\underline{CB}]$, must have rank equal to the number of outputs. Since $\underline{C}$ is of order (p x n), and $\underline{B}$ is of order (n x m) with p=m, $[\underline{CB}]$ is a square matrix and must have full rank to fulfill the requirement of a regular plant. The gain matrix for feedback control is formed using the inverse of $[\underline{CB}]$. This cannot be accomplished without full rank.

Plants in which the first Markov parameter, $[\underline{CB}]$, is rank deficient are designated as "irregular." To allow the design to be accomplished, an $\underline{F}$ matrix is formed as shown and used in place of the $\underline{C}$ matrix:

$$\underline{F} = [\ \underline{F}_1 \mid \underline{F}_2\ ] \tag{3.5}$$

where

$$\underline{F}_1 = [\ \underline{C}_1 + \underline{MA}_{11}\ ] \tag{3.6}$$

$$\underline{F}_2 = [\ \underline{C}_2 + \underline{MA}_{12}\ ] \tag{3.7}$$

The elements of the measurements matrix $\underline{M}$ are selected to obtain a matrix $[\underline{FB}]$ having full rank and thus being invertable.

The control law is a proportional plus integral output feedback law expressed as:

$$\underline{u}(kT) = (1/T)[\underline{K}_0\underline{e}(kT) + \underline{K}_1\underline{z}(kT)] \tag{3.8}$$

where

$1/T$ is the sampling frequency

$\underline{K}_0$ is the proportional gain matrix for the error signal $\underline{e}(kT)$

$\underline{K}_1$ is the gain matrix for the backward difference of the error signal, which is designated as $\underline{z}(kT)$.

For the continuous case, the law is expressed as

$$\underline{u} = g(\underline{K}_0\underline{e} + \underline{K}_1\int\underline{e}\ dt) \tag{3.9}$$

where

g is the forward path gain

$\underline{K}_0$ is the proportional gain for the error signal

$\underline{K}_1$ is the gain for the integral of the error signal.

A block diagram of the system with this control law is presented in Figures 8 and 9 for both the continuous and discrete cases. The portion in broken lines is present only for irregular designs.

The gain factor in the figure is the sampling frequency (1/T) for the discrete system or a gain constant (g) for the continuous system. For the regular design the error vector $\underline{e}$ is expressed as $\underline{e} = \underline{v} - \underline{y}$. Each command in the $\underline{v}$ vector is summed with its corresponding output element in the $\underline{y}$ vector and is the input for the proportional plus integral gain paths. Thus, there exists a bank of integrators, one for each error signal developed. These integrators insure that the error signals are always driven to zero, resulting in the final value of the output equaling the input for step type commands.

In the irregular design the $\underline{e}$ vector is defined by

$$\underline{e} = \underline{v} - \underline{w} \tag{3.10}$$

where

$$\underline{w} = \underline{y} + \underline{M}\dot{\underline{x}} \tag{3.11}$$

These outputs $\underline{w}$ are developed with the measurement matrix $\underline{M}$ and the derivatives $\dot{\underline{x}}$ of the system states. Again for step inputs, the error signal is driven to zero. Rates of the system states also go to zero and, as before, the resulting output equals the commanded input.

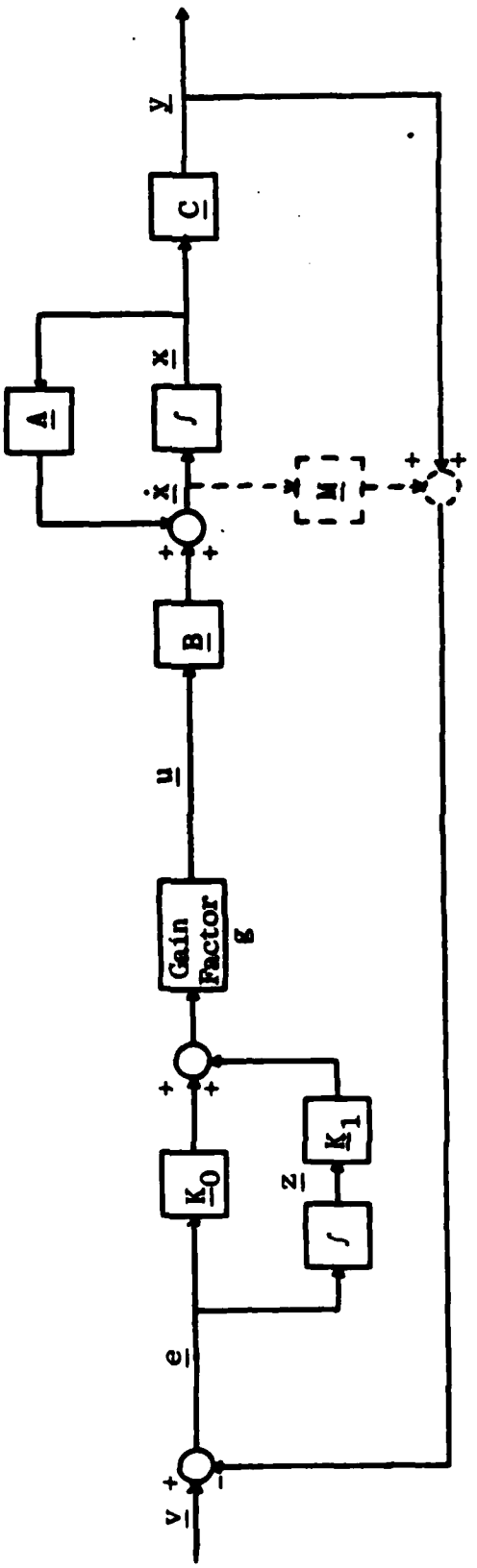



Figure 8. System Block Diagram - Continuous Design

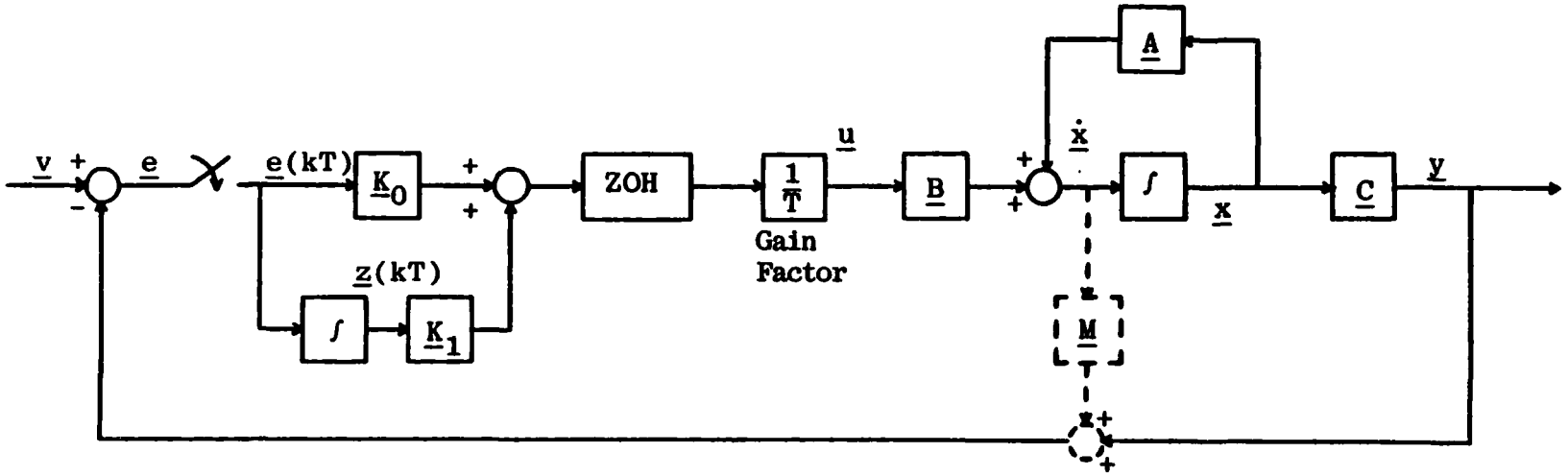



Figure 9. System Block Diagram - Discrete Design

At this point, the question of "do the state derivatives always go to zero as desired" must be asked. The answer is a qualified yes. For step commands to the system in which the outputs are states or linear combinations of states, the derivatives go to zero with one exception. This is precisely the reason for the large effort in this study developing state representation for quantities that are to be commanded. By establishing acceleration and pitch rate as system states, these quantities can be commanded, and for step inputs, the derivatives of the quantities go to zero in steady state. The exception concerns the situation in which one of the state derivatives is set equal to a state that is to be controlled. If the state is commanded to a constant value, the derivative reaches this constant value in the steady state. For example, consider a longitudinal design where, due to simplifying assumptions, the rate of change of pitch angle $\theta$ is set equal to body axis pitch rate q. It is assumed that q is a state of the system as well as an output. If it is desired to command a step in q, the state derivative $\dot{\theta}$ will eventually reach a constant value. This situation is one in which the system has a transmission zero at the origin. The significance of transmission zeros is discussed later in this chapter. For the time being, it is asserted that this situation provides an acceptable design if the measurement matrix elements are chosen so the system does not feedback the $\dot{\theta}$ state derivative.

## Output Feedback and the M Matrix

One of the major advantages of this design method is that it uses output feedback. Thus, all the states of the system are not required to be fed back for the design. The outputs are usually quantities of interest that are easily measured by existing sensors. Unfortunately, a measurement matrix is needed for all but the simplest design cases encountered. A number of points must be considered in selecting this measurement matrix as discussed later in this chapter. One such point relates to output feedback and is examined at this time.

It is important to select matrix elements that cause state derivatives to be fed back which can be either measured or derived from existing measurements. If this cannot be accomplished, the alternative is to form the derivative according to the state equation. In general, most of the derivative state equations involve combinations of essentially all the system states. Thus, to develop the proper state derivative, full-state or essentially full-state feedback is needed. This eliminates the tremendous advantage of output feedback and is avoided for design applications in this report. For the designs considered here, elements in the measurement matrix are selected to result in rotational accelerations being used as the rate derivative signals to be fed back. These signals are available from an inertial measurement system; however, such an approach for obtaining

rotational acceleration is not recommended due to reliability considerations. The technique selected for this study is as follows: considering the longitudinal case, $\dot{q}$ is selected as the derivative to be fed back as shown in Chapter IV. Equation (2.48) from Chapter II is repeated below:

$$A_{n_p} = A_{n_{cg}} + (\ell_x)\dot{q} \qquad (2.48)$$

The acceleration at the pilot station, $A_{n_p}$, is sensed by flight control accelerometers. Acceleration at the center of gravity, $A_{n_{cg}}$, can also be sensed by another set of flight control accelerometers. Using the above expression, a reasonably good approximation of $\dot{q}$ can be developed for use in the system. This same technique is used in the lateral-directional design.

Movement of the CG during flight introduces errors into the results. The CG variation in the x-body axis is approximately one percent of the MAC or 1.1 feet. Another source of error exists in the simplification used to develop Equation (2.48). Roll rate can be relatively large on the aircraft and may have to be considered in developing an expression for $\dot{q}$ using Equation (2.31). Time was not available in this study to evaluate the effects of such errors.

## Asymptotic Characteristics

For the design shown in Figure 8, as the gain factor increases, the system transfer function $\underline{G}(s) = \underline{C}(s\underline{I} - \underline{A})^{-1}\underline{B}$ assumes the asymptotic form

$$\underline{\Gamma}(\lambda) = \tilde{\underline{\Gamma}}(\lambda) + \hat{\underline{\Gamma}}(\lambda) \qquad (3.12)$$

where

$\tilde{\underline{\Gamma}}(\lambda)$ is the "slow" transfer function matrix and

$\hat{\underline{\Gamma}}(\lambda)$ is the "fast" transfer function matrix.

The poles of these transfer functions fall into three groups designated $Z_1$, $Z_2$, and $Z_3$. The slow modes correspond to poles contained in $Z_1$ and $Z_2$. As gain factor increases towards infinity, the poles of $Z_1$ become uncontrollable and the poles of $Z_2$ become unobservable. As this happens, the system response is increasingly dominated by the fast modes which correspond to the poles $Z_3$. Expressions for the asymptotic modes are given in Table 2.

As the gain factor is increased, tracking of the system's output to input commands becomes increasingly "tight." Reference 6 shows that with only moderate increases in gain factor, the output resembles an extremely fast first-order response. Although the dominant finite (fast) roots can be made complex, much of the experience to date has been with real roots.

The gain $\underline{K}_0$ is chosen such that

$$\underline{CBK}_0 = \text{diagonal } \{ \sigma_1, \sigma_2, \ldots \sigma_n \} \qquad (3.13)$$

Table 2

Asymptotic Equations for Zero-$B_2$ Form

System is represented by:

$$\begin{bmatrix} \dot{\underline{x}}_1 \\ \dot{\underline{x}}_2 \end{bmatrix} = \left[\begin{array}{c|c} \hat{\underline{A}}_{11} & \hat{\underline{A}}_{12} \\ \hline \hat{\underline{A}}_{21} & \hat{\underline{A}}_{22} \end{array}\right] \begin{bmatrix} \underline{x}_1 \\ \underline{x}_2 \end{bmatrix} + \begin{bmatrix} 0 \\ \hline \hat{\underline{B}}_2 \end{bmatrix} \underline{u} \qquad \text{and} \qquad \underline{y} = [\, \hat{\underline{C}}_1 \; \hat{\underline{C}}_2 \,] \begin{bmatrix} \underline{x}_1 \\ \underline{x}_2 \end{bmatrix}$$

| Continuous Case | Discrete Case |
|---|---|
| Gain Factor = g | Gain Factor = 1/T |
| (Poles are in the s-plane) | (Poles are in the z-plane) |
| $\tilde{\Gamma}(\lambda) = \underline{C}_o(\lambda \underline{I}_n - \underline{A}_o)^{-1}\underline{B}_o = 0$ | $\tilde{\Gamma}(\lambda) = \underline{C}_o(\lambda \underline{I}_n - \underline{A}_o)^{-1}\underline{B}_o$ |
| $\hat{\Gamma}(\lambda) = (\lambda \underline{I}_m + g\, \hat{\underline{C}}_2\hat{\underline{B}}_2\, \underline{K}_0)^{-1} g\, \hat{\underline{C}}_2\hat{\underline{B}}_2\, \underline{K}_0$ | $\hat{\Gamma}(\lambda) = (\lambda \underline{I}_m - \underline{I}_m + \hat{\underline{C}}_2\hat{\underline{B}}_2\, \underline{K}_0)^{-1}\hat{\underline{C}}_2\hat{\underline{B}}_2\, \underline{K}_0$ |
| (Finite roots) | |
| $\underline{Z}_1 = \lvert \lambda\, \underline{K}_0 + \underline{K}_1 \rvert = 0$ | $\underline{Z}_1 = \lvert \lambda \underline{I}_m - \underline{I}_m + T\, \underline{K}_0^{-1}\underline{K}_1 \rvert = 0$ |
| $\underline{Z}_2 = \lvert \lambda \underline{I}_{n-m} - \hat{\underline{A}}_{11} + \hat{\underline{A}}_{12}\, \hat{\underline{C}}_2^{-1}\hat{\underline{C}}_1 \rvert = 0$ | $\underline{Z}_2 = \lvert \lambda \underline{I}_{n-m} - T\, \hat{\underline{A}}_{11} + \hat{\underline{A}}_{12}\, \hat{\underline{C}}_2^{-1}\hat{\underline{C}}_1 \rvert = 0$ |
| (Infinite roots) | |
| $\underline{Z}_3 = \lvert \lambda \underline{I}_m + g\, \hat{\underline{C}}_2\hat{\underline{B}}_2\, \underline{K}_0 \rvert = 0$ | $\underline{Z}_3 = \lvert \lambda \underline{I}_m - \underline{I}_m + \hat{\underline{C}}_2\hat{\underline{B}}_2\, \underline{K}_0 \rvert = 0$ |

Table 2 (continued)

where:

$$\underline{A}_o = \left[\begin{array}{c|c} -\underline{K}_0^{-1}\underline{K}_1 & 0 \\ \hline \underline{A}_{12}\underline{C}_2^{-1}\underline{K}_0^{-1}\underline{K}_1 & \underline{A}_{11}-\underline{A}_{12}\underline{C}_2^{-1}\underline{C}_1 \end{array}\right]$$

$$\underline{B}_o = \left[\begin{array}{c} 0 \\ \hline \underline{A}_{12}\ \underline{C}_2^{-1} \end{array}\right]$$

$$\underline{C}_o = [\underline{K}_0^{-1}\underline{K}_1 \mid 0]$$

Equation (3.13) is used to calculate the proportional gain matrix $\underline{K}_0$. The elements of the $\underline{\Sigma}$ matrix, which is selected as a diagonal matrix, are chosen by the designer. These values determine the respective gains or the weighting of each error signal on the control surface or the system input being commanded by the control law.

$$\underline{K}_0 = [\underline{CB}]^{-1}\underline{\Sigma} \tag{3.14}$$

The integral gain matrix $\underline{K}_1$ is often determined by a scalar multiplication of the $\underline{K}_0$ matrix.

$$\underline{K}_1 = \bar{\alpha}\underline{K}_0 \tag{3.15}$$

The system transfer function G(s) approaches a diagonal asymptotic form of increasingly noninteracting control. Thus, the output responses become decoupled as gain increases. The asymptotic closed-loop transfer function of the digital system has the form:

$$\underline{\Gamma}(\lambda) = \text{diagonal } \{ \frac{\sigma_1}{\lambda-1+\sigma_1}, \frac{\sigma_2}{\lambda-1+\sigma_2}, \ \ldots \ \frac{\sigma_n}{\lambda-1+\sigma_n} \} \tag{3.16}$$

For the continuous system, the asymptotic transfer function has the form:

$$\underline{\Gamma}(\lambda) = \text{diagonal } \{ \frac{g\sigma_1}{\lambda+g\sigma_1}, \frac{g\sigma_2}{\lambda+g\sigma_2}, \ \ldots \ \frac{g\sigma_n}{\lambda+g\sigma_n} \} \tag{3.17}$$

For the irregular plant, the above equations are applied by replacing the $\underline{C}$ matrix with an $\underline{F}$ matrix. The

component $\underline{C}_1$ is replaced by $\underline{F}_1$ and $\underline{C}_2$ is replaced by $\underline{F}_2$ as calculated in Equations (3.6) and (3.7).

In the equations in Table 2 , the gain values $\underline{K}_0$ and $\underline{K}_1$ are the same as those developed from the equations that are not in zero-$B_2$ form. This is because

$$[\underline{CB}] = [\underline{C}_2\underline{B}_2] \quad \text{or} \quad [FB] = [\underline{F}_2\underline{B}_2] \tag{3.18}$$

The asymptotic closed-loop system roots can be calculated from the equations in Table 2 and are composed of the sets $Z_1$, $Z_2$ and $Z_3$. In the limit as gain approaches infinity, the following rules can be used to estimate root locations in the s-plane.

The $Z_1$ finite roots are m in number and equal to the ratio of integral to proportional gain values. The $Z_2$ finite roots are n-m in number and located at transmission zero locations.

The $Z_3$ infinite roots are m in number and for the continuous case they are located at a position on the real axis equal to $-g\sigma_i$ where g is the gain factor and $\sigma_i$ is the respective weighting element selected by the designer in the $\underline{\Sigma}$ matrix. For the discrete case the roots are located at $1-\sigma_i$ and are located near the origin.

Transmission Zeros

Transmission zeros are considered as regions in either the s-plane or the z-plane. These regions are asymptotic locations for certain finite or slow roots of the

system. Output feedback does not alter the location of transmission zeros (Ref 8). Such locations may coincide with conventional single input/single output transfer function zeros, or they may simply be regions in the plane that attract finite poles. Since the basic system transmission zeros cannot be altered by the controller design and since infinite gain cannot be used, the location of roots migrating towards these zeros does produce an effect on the system response.

Designing for a system with an unstable transmission zero is possible, but it means an upper stability limit must be established. Operation is possible only below that limit. Increasing gain eventually results in a pole migrating to the unstable location.

Using the zero-$B_2$ form, transmission zeros can be calculated from the equation in Table 2 where $Z_t = Z_2$. Although they cannot be altered by output feedback, transmission zeros can be changed in two ways. First, should the location of transmission zeros of the system be unacceptable, it is sometimes possible to select another $\underline{C}$ matrix that is acceptable for the design and yields different zero locations. Second, the measurement matrix modifies the transmission zeros, and it may be possible to alter the matrix elements to give both acceptable performance and acceptable transmission zero location.

## Measurement Matrix Elements

Some guidelines are available for the selection of the measurement matrix. Reference 9 presents a systematic approach to their selection for optimum decoupling. In addition, the following suggestions are offered:

1. make the measurement matrix as sparse as possible adding only enough non-zero elements to yield an $\underline{F}$ matrix and an $[\underline{FB}]$ matrix of full rank;

2. select values for the non-zero elements that give acceptable transmission zeros. In most cases, the values of the measurement elements result in transmission zero locations that are equal to the reciprocal of the element value. However, cases are encountered in this design effort in which this rule does not hold. This usually occurs when more than the minimum number of elements is specified. In these cases, the macro program in Appendix E proved to be a necessity in selecting proper elements; and

3. select the location of the non-zero elements to use a state derivative that can be easily obtained and is zero for steady-state step commands as discussed previously.

## Closed-Loop Roots

The design technique does not guarantee stability of the system unless it has stable transmission zeros and infinite gain. Even with stable transmission zeros, the root migrations can cross into the unstable region as the gain increases, and then return to the stable transmission

zero. With the desire to develop a system with only enough gain to do the job and being unfamiliar with the effects of design parameter variations on the system, it is desirable to be able to evaluate the closed-loop system roots for each design.

The equations for computing closed-loop roots are presented below. They are given for both the zero-$B_2$ and non-zero-$B_2$ formats. The zero-$B_2$ format solution is mechanized using macro programming of TOTAL. A listing of the program and instructions for its use are given in Appendix F.

Partitioning of the $\underline{A}$ and $\underline{B}$ system matrices is accomplished as before to yield $\underline{B}_2$ and $\underline{A}_{22}$ of order (m x m), where m is the number of inputs.

$$\dot{\underline{x}} = \left[\begin{array}{c|c} \underline{A}_{11} & \underline{A}_{12} \\ \hline \underline{A}_{21} & \underline{A}_{22} \end{array}\right] \underline{x} + \left[\begin{array}{c} \underline{B}_1 \\ \hline \underline{B}_2 \end{array}\right] \underline{u} \qquad (3.3)$$

$$\underline{y} = \left[\begin{array}{c|c} \underline{C}_1 & \underline{C}_2 \end{array}\right] \underline{x} \qquad (3.4)$$

or

$$\dot{\underline{x}}_1 = \underline{A}_{11}\underline{x}_1 + \underline{A}_{12}\underline{x}_2 + \underline{B}_1\underline{u} \qquad (3.19)$$

$$\dot{\underline{x}}_2 = \underline{A}_{21}\underline{x}_2 + \underline{A}_{22}\underline{x}_2 + \underline{B}_2\underline{u} \qquad (3.20)$$

$$\underline{y} = \underline{C}_1\underline{x}_1 + \underline{C}_2\underline{x}_2 \qquad (3.21)$$

$$\underline{e} = \underline{v} - \underline{y} \quad \text{and} \quad \underline{u} = g\underline{K}_0\underline{e} + g\underline{K}_1\int\underline{e}dt \qquad (3.22)$$

let $\dot{\underline{z}} = \underline{e}$ and $z = \int \underline{e} dt$ (3.23)

then $\dot{\underline{z}} = \underline{v} - \underline{y}$ (3.24)

$$\dot{\underline{z}} = -\underline{C}_1\underline{x}_1 - \underline{C}_2\underline{x}_2 + \underline{v} \quad (3.25)$$

$$\underline{u} = g\underline{K}_0\dot{\underline{z}} + g\underline{K}_1\underline{z} = g\underline{K}_0(-\underline{C}_1\underline{x}_1 - \underline{C}_2\underline{x}_2 + \underline{v}) + g\underline{K}_1\underline{z} \quad (3.26)$$

$$\underline{u} = -g\underline{K}_0\underline{C}_1\underline{x}_1 - g\underline{K}_0\underline{C}_2\underline{x}_2 + g\underline{K}_0\underline{v} + g\underline{K}_1\underline{z} \quad (3.27)$$

$$\dot{\underline{x}}_1 = \underline{A}_{11}\underline{x}_1 + \underline{A}_{12}\underline{x}_2 - \underline{B}_1 g\underline{K}_0\underline{C}_1\underline{x}_1 - \underline{B}_1 g\underline{K}_0\underline{C}_2\underline{x}_2 + \underline{B}_1 g\underline{K}_0\underline{v} + \underline{B}_1 g\underline{K}_1\underline{z} \quad (3.28)$$

$$\dot{\underline{x}}_1 = (\underline{A}_{11} - \underline{B}_1 g\underline{K}_0\underline{C}_1)\underline{x}_1 + (\underline{A}_{12} - \underline{B}_1 g\underline{K}_0\underline{C}_2)\underline{x}_2 + (\underline{B}_1 g\underline{K}_0)\underline{v} + (\underline{B}_1 g\underline{K}_1)\underline{z} \quad (3.29)$$

$$\dot{\underline{x}}_2 = \underline{A}_{21}\underline{x}_1 + \underline{A}_{22}\underline{x}_2 - \underline{B}_2 g\underline{K}_0\underline{C}_1\underline{x}_1 - \underline{B}_2 g\underline{K}_0\underline{C}_2\underline{x}_2 + \underline{B}_2 g\underline{K}_0\underline{v} + \underline{B}_2 g\underline{K}_1\underline{z} \quad (3.30)$$

$$\dot{\underline{x}}_2 = (\underline{A}_{21} - \underline{B}_2 g\underline{K}_0\underline{C}_1)\underline{x}_1 + (\underline{A}_{22} - \underline{B}_2 g\underline{K}_0\underline{C}_2)\underline{x}_2 + (\underline{B}_2 g\underline{K}_0)\underline{v} + (\underline{B}_2 g\underline{K}_1)\underline{z} \quad (3.31)$$

Writing Equations (3.25), (3.29) and (3.31) in matrix notation provides the description of the closed-loop system where $\underline{v}$ is the input command vector to the control system.

$$\begin{bmatrix} \dot{\underline{z}} \\ \dot{\underline{x}}_1 \\ \dot{\underline{x}}_2 \end{bmatrix} = \begin{bmatrix} 0 & -\underline{C}_1 & -\underline{C}_2 \\ \underline{B}_1 g\underline{K}_1 & \underline{A}_{11}-\underline{B}_1 g\underline{K}_0\underline{C}_1 & \underline{A}_{12}-\underline{B}_1 g\underline{K}_0\underline{C}_2 \\ \underline{B}_2 g\underline{K}_1 & \underline{A}_{21}-\underline{B}_2 g\underline{K}_0\underline{C}_1 & \underline{A}_{22}-\underline{B}_2 g\underline{K}_0\underline{C}_2 \end{bmatrix} \begin{bmatrix} \underline{z} \\ \underline{x}_1 \\ \underline{x}_2 \end{bmatrix} + \begin{bmatrix} \underline{I} \\ \underline{B}_1 g\underline{K}_0 \\ \underline{B}_2 g\underline{K}_0 \end{bmatrix} \underline{v} \tag{3.32}$$

Note that $\underline{z}$ is a vector of dimension (number of inputs) x 1. For irregular designs replace $\underline{C}_1$ and $\underline{C}_2$ with $\underline{F}_1$ and $\underline{F}_2$, respectively.

Some caution should be exercised in using these closed-loop equations. For the digital system, the control is piecewise continuous between samples and thus, by letting $1/T = g$ , these equations can be used to evaluate stability in a general sense. However, the effects of sampling such as quantization and zero order hold are not considered. Also, in any system using a real digital machine, such things as the computational time delay, harmonics generated by sampling, and the apparent rate limiting due to maximum sampling speed can cause instabilities. These effects are not considered in these equations. Nevertheless, the computation of the closed-loop roots provides an understanding of the effects of design changes on the system and can be the basis for realistic stability checks.

## MULTI Computer-Aided Design

The MULTI program was created by previous AFIT thesis research (Ref 10) and allows real-time computer-aided designs to be accomplished with the control law theories presented in this chapter. A users' guide is presented in

Reference 10. This design effort would have been impractical without such a package, along with the TOTAL program. Iterations and refinements are necessary as the design progresses. Time response data provide the basis for design decisions. The program allows on-line design changes and provides response plots to defined command inputs.

There are several differences between the MULTI program computations and the theoretical equations presented in this chapter which must be pointed out.

In the computation of the gain matrices, a number of flexibilities are provided. The actual MULTI computations are shown below.

For the regular design case:

$$\underline{K}_0 = \bar{\alpha}\ \varepsilon\ [\underline{CB}]^{-1}\underline{\Sigma} \tag{3.33}$$

$$\underline{K}_1 = \varepsilon\ [\underline{CB}]^{-1}\underline{\Sigma} \tag{3.34}$$

Both $\bar{\alpha}$ and $\varepsilon$ are scalars, and $\bar{\alpha}$ is used to set the ratio of proportional to integral gain. Unfortunately, it is the inverse of the usual method of varying this relationship. $\varepsilon$ is a scalar that can be used to change all the gain elements by any desired amount. For the digital design case, this proves useful for cases where the sampling frequency has been fixed by other design considerations. The system response can be altered by increasing $\varepsilon$, resulting in the same effect as increasing 1/T.

For the irregular design:

$$\underline{K}_0 = \bar{\alpha}\ \varepsilon\ [\underline{F}_2\underline{B}_2]^{-1}\underline{\Sigma} \tag{3.35}$$

$$\underline{K}_1 = \varepsilon\ [\underline{F}_2\underline{B}_2]^{-1}\underline{\Sigma} \tag{3.36}$$

It should be noted that the $[\underline{FB}]$ matrix must be used for the calculations if $\underline{B}$ is not in $\begin{bmatrix} 0 \\ \underline{B}_2 \end{bmatrix}$ form.

## III CONCLUSIONS

Based on the work done by five presenters, the following general conclusions are drawn:

1. The design of multivariable control laws is a relatively simple, straight-forward process; a basic understanding of the theory and some experience in applying the design procedures outlined in the papers is all that is required.

2. The results obtained in the five papers showed promise that the techniques can be used to obtain multivariable control laws for aircraft flight control systems.

3. The software package MULTI is an extremely useful design tool in obtaining control laws for a given plant. The capability of using MULTI interactively provides the engineer with the opportunity to design control laws quickly and to obtain a "feel" for how the adjustable parameters affect performance.

4. The method can be applied to both large (C-141A) and small (F-16, A-7) aircraft with positive results.

5. The design technique of Professor Porter yields controllers which are "robust" over a wide range of flight conditions and maneuvers. This is important since it may eliminate some gain scheduling and the associated memory that is required. In addition, the technique also yields control

laws which provide satisfactory performance in the event that a primary control surface becomes inoperative.

## IV BIBLIOGRAPHY


1. Porter, B. Design of High Performance Tracking Systems. USAME/DC/120/81. Air Force Flight Dynamics Laboratory, Wright-Patterson AFB, OH: October 1981.

2. Porter, B. and A. T. Shenton. "Singular Perturbation Methods of Asymptotic Eigenvalue Assignment in Multivariable Linear Systems", International Journal of Systems Science, 6 (1): 33-37 (January 1975).

3. Porter, B. "Singular Perturbation Methods in the Design of Observers and Stabilizing Feedback Controllers for Multivariable Linear Systems", Electronic Letters, 10 (23): 494-495 (November 14, 1974).

4. Porter, B. "Singular Perturbation Methods in the Design of Stabilizing Feedback Controllers for Multivariable Linear Systems", International Journal of Control, 20 §94): 689-692 (April 1974.

5. Porter, B. "Singular Perturbation Methods in the Synthesis of Feedback Control Laws for Eigenvalue Assignment in Multivariable Linear Systems", International Journal of Systems Science, 7 (5): 597-601 (May 1976).

6. Porter, B. and A. T. Shenton. "Singular Perturbation Analysis of the Transfer Function Matrices of a Class of Multivariable Linear Systems", International Journal of Control, 21 (4): 655-660 (April 1975).

# V VITA

Finley Barfield is a native of Norfolk, Virginia. He graduated from the Virginia Military Institute in Lexington, Virginia, in 1968 with a Bachelor of Science in Electrical Engineering. He was commissioned through the Air Force ROTC program and served on active duty for four years. During that time he was assigned to the Control System Development Branch, Flight Control Division of the Air Force Flight Dynamics Laboratory. His work involved the flight testing of an advanced terrain following system, development of multiplexing techniques for flight control application and research into self-adaptive control methods for tactical missiles

In 1972 he became a civilian employee of the Advanced Development Branch of the Air Force Flight Dynamics Laboratory's Flight Control Division. He has been assigned to both the Controlled Configured Vehicle (CCV) Bomber and Fighter Advanced Development Programs. Recently he served as the responsible Air Force engineer for flight control law development on the AFTI/F-16 Program. He is currently working towards an advanced degree at the Air Force Institute of Technology, Wright-Patterson AFB, Ohio.

# VITA

Jon M. Baushlicher was born in Milwaukee, Wisconsin on 13 April 1954 and was raised in Eustis, Florida. After completing his inital schooling in Eustis, he attended the United States Air Force Academy, Colorado Springs, Colorado, from July 1972 to June 1976. He was a distinguished graduate from the USAFA with a B.S. degree in History/Soviet Area Studies and was commissioned as an officer in June of 1976.

After completing Undergraduate Pilot Training at Reese AFB, Texas in June 1977 and Pilot Instructor Training at Randolf AFB, Texas, he served as a T-37 instructor pilot at Reese AFB until December 1980. He currently has approximately 1,500 hours of jet aircraft time.

He entered the School of Engineering, Air Force Institute of Technology in January 1981 and after completing six months of undergraduate work began working on his master's degree in Electrical Engineering/Guidance and Control. His next assignment is with the Weapons Laboratory at Kirtland AFB, New Mexico.

Permanent Home Address: Rt 2 Box 33
Umatilla FL

# VITA

Michael A. Masi was born in Sumter, South Carolina on 22 October 1951. Upon graduation from Sumter High School, he entered the University of South Carolina, Columbia, South Carolina. He received his Bachelor of Science Degree in Electrical Engineering in August 1974 and was commissioned through the four-year Air Force ROTC Program at USC.

After completion of Undergraduate Pilot Training at Laughlin AFB, Texas in February 1977, he was assigned to the 437th Military Airlift Wing at Charleston AFB, South Carolina. He has approximately 2500 total hours of jet aircraft time and left Charleston as a C-141 Aircraft Commander.

He entered the Graduate Electrical Engineering program at the School of Engineering, Air Force Institute of Technology in June 1981. His next assignment is with the Flight Dynamics Laboratory (AFWAL/FIGL), Wright-Patterson AFB, Ohio.

Permanent Home Address: 2 Henderson Street
Sumter, South Carolina
29150

# VITA

Thomas Lewis was born 27 January 1958 in Albert Lea, Minnesota. He graduated from Suffield Academy, Suffield Connecticut in 1976, and then attended Purdue University, West Lafayette Indiana, where he earned a Bachelor of Science degree in Aeronautical and Astronautical Engineering, graduating May 1981. He also received a reserve commission in the USAF through the ROTC program at Purdue. He immediately pursued a graduate degree by enrolling in the Air Force Institute of Technology, Department of Aeronautical Engineering, WPAFB Ohio, in June 1981.

# VITA

Daniel E. Russ was born in Bitburg, West Germany, on 31 July 1959. He attended Carnegie-Mellon University, Pittsburgh PA, from September 1977 to May 1981, with a four-year Air Force ROTC scholarship. He was graduated with the degree of Bachelor of Science in Electrical Engineering and Economics and received his reserve commission in the U.S. Air Force on 15 May 1981.

He enrolled in the School of Engineering, Air Force Institute of Technology in June 1981 as a direct accession selectee. His next assignment is with the Flight Dynamics Laboratory, Air Force Wright Aeronautical Laboratories, Wright-Patterson AFB, Ohio.

# Appendix A

PREVIOUS PAGE
IS BLANK

AFIT/GE/EE/83S-4

# MULTIVARIABLE CONTROL LAWS FOR THE AFTI/F-16

THESIS

Presented to the Faculty of the School of Engineering
of the Air Force Institute of Technology
Air University
in Partial Fulfillment of the
Requirements for the Degree of
Master of Science

by
A. Finley Barfield, B.S.E.E.
Graduate Electrical Engineer
July 1983

Approved for public release; distribution unlimited.

## Preface

Emphasis in this thesis is on the development of a preliminary design for a flight control system using recently evolved multivariable techniques and considering real world constraints. Such an approach is important because of concerns that exist in the engineering community about the application of modern control system designs with high gains and wide bandwidths.

The AFTI vehicle is chosen because of my experience with the control law development and knowledge of the implementation constraints. I would like to thank Mr. Jim Ramage, Chief Engineer for the AFTI/F-16 ADPO, for sponsoring this effort along with the ADPO Engineers for providing assistance and guidance during the study.

The theoretical background is based on techniques developed by Professor Brian Porter from the University of Salford, England. I would like to express my appreciation to Professors John J. D'Azzo and Constantine H. Houpis of the Department of Electrical Engineering at the Air Force Institute of Technology. The thesis would not have been possible without their guidance and suggestions.

This research was accomplished in parallel with four fellow students. I found the numerous and enlightening discussions with this group to be most helpful during the

thesis effort. My sincere thanks to Captain Jon Bauschlicker, Lieutenant Tom Lewis, Captain Mike Masi and Lieutenant Dan Russ who comprised this group.

Finally, I want to express my love and appreciation to my wife, Diane, for her patience and understanding during this research effort. I would also like to thank my parents and my brother, Travis, for all their love and support.

A. Finley Barfield

# Contents


Preface . . . . .

List of Figures . . . . .

List of Tables . . . . .

List of Symbols . . . . .

Abstract . . . . .

I. Introduction . . . . .

- Background . . . . .
- Assumptions . . . . .
- Pertinent Observations . . . . .
- Study Approach and Design Requirements . . .
- Presentation Sequence . . . . .

II. The AFTI/F-16 Aircraft . . . . .

- Aircraft Description . . . . .
- Aerodynamic Model . . . . .
- Validation Methods . . . . .

III. Multivariable Control Law Theory . . . . .

- Overview . . . . .
- Regular Versus Irregular Design . . . . .
- Output Feedback and the $\underline{M}$ Matrix . . . . .
- Asymptotic Characteristics . . . . .
- Transmission Zeros . . . . .
- Measurement Matrix Elements . . . . .
- Closed-Loop Roots . . . . .
- MULTI Computer-Aided Design . . . . .

IV. Philosophy and Details of the Design Method . . . . .

- Requirements . . . . .
- Inputs and Outputs . . . . .
- Controllability and Observability . . . . .
- Transmission Zeros . . . . .
- Integral Plus Proportional Compensation . .
- A Design Procedure . . . . .
- The Aircraft Model . . . . .
- Output Feedback Choices . . . . .

Checking the System Properties . . . . . .
Transmission Zeros and the M Matrix . . . .
Maximum Maneuver Estimates . . . . . .
Gain Scaling and the Weighting Matrix . . .
Integral Plus Proportional Adjustment . . .
Gain and Phase Margins . . . . . .
Evolution of a Final Design . . . . . .
Trial 1 . . . . . .
Trial 2 . . . . . .
Pilot Interface . . . . . .
Instabilities . . . . . .

V. Evaluation . . . . . .

Time Response Analysis . . . . . .
Neal-Smith Criterion . . . . . .
Bandwidth Comparison . . . . . .
Robustness versus Tailoring . . . . . .

VI. Conclusions and Recommendations . . . . . .

Design Results . . . . . .
Simplifying and Improving the Design Process . . . . . .
MULTI Improvements . . . . . .
Proposed Future Work . . . . . .

References . . . . . .

Appendix A: Aircraft Aerodynamic Data . . . . . .

Appendix B: Aircraft Equations of Motion . . . . . .

Appendix C: Maximum Command Responses . . . . . .

Appendix D: Conversion And Transformation (CAT) Program . . . . . .

Appendix E: TOTAL Macro Program to Calculate Transmission Zeros . . . . . .

Appendix F: A TOTAL Macro Program For Determining the Closed-Loop System Matrices . . . . .

Vita . . . . . .

## List of Figures


| Figure | | |
|---|---|---|
| 1 | Flight Envelope Design Points | |
| 2 | Direct Force Development Using Multiple Surfaces | |
| 3 | Longitudinal Direct Force Modes | |
| 4 | Lateral-Directional Direct Force Modes | |
| 5 | AFTI/F-16 Control Surface Location | |
| 6 | Longitudinal Static Stability Plot | |
| 7 | Axis Definition | |
| 8 | System Block Diagram - Continuous Design | |
| 9 | System Block Diagram - Discrete Design | |
| 10 | Longitudinal Two Input--Two Output Controller Block Diagram | |
| 11 | Response Plot for Initial Rate Controller Design with Short Period Approximation | |
| 12 | Surface Position Plot for Initial Rate Controller Design with Short Period Approximation | |
| 13 | Response Plot for Rate Controller with Short Period Approximation | |
| 14 | Surface Position Plot for Rate Controller with Short Period Approximation | |
| 15 | $\alpha$ Response of the Trial 2 Design to a 9g Step Command (0.9 Mach 20,000 feet) | |

Figure


16 Pitch Rate and Acceleration Response of the Trial 2 Design to a 9g Step Command (0.9 Mach 20,000 feet) . . . . .

17 Surface Response of the Trial 2 Design to a 9g Step Command (0.9 Mach 20,000 feet) . . . . . .

18 α Response of the Desired Preliminary Design to a 9g Step Command (0.9 Mach 20,000 feet) . . . . . .

19 Pitch Rate and Acceleration Response of the Desired Preliminary Design to a 9g Step Command (0.9 Mach 20,000 feet) . . . . . .

20 Surface Response of the Desired Preliminary Design to a 9g Step Command (0.9 Mach 20,000 feet) . . . . . .

21 α Response of the Desired Preliminary Design to a 1g Step Command (0.9 Mach 20,000 feet) . . . . . .

22 Pitch Rate and Acceleration Response of the Desired Preliminary Design to a 1g Step Command (0.9 Mach 20,000 feet). .

23 Pitch Angle Response of the Desired Preliminary Design to a 1g Step Command (0.9 Mach 20,000 feet) . . . . . .

24 Surface Position Response of the Desired Preliminary Design to a 1g Step Command (0.9 Mach 20,000 feet) . . . . . .

25 Forward Velocity Change of the Desired Preliminary Design to a 1g Step Command (0.9 Mach 20,000 feet) . . . . . .

26 α Response of the Initial Pitch Pointing System to a 2 deg/sec Pitch Rate Pulse of 0.9 sec Duration (0.9 Mach 20,000 feet) . . . . . .

Figure


27 Pitch Rate and Acceleration Response of the Initial Pitch Pointing System to a 2 deg/sec Pitch Rate Pulse of 0.9 sec Duration (0.9 Mach 20,000 feet) . . .

28 Surface Response of the Initial Pitch Pointing System to a 2 deg/sec Pitch Rate Pulse of 0.9 sec Duration (0.9 Mach 20,000 feet) . . . . . .

29 Pitch Angle and Velocity Change of the Initial Pitch Pointing System to a 2 deg/sec Pitch Rate Pulse of 0.9 sec Duration (0.9 Mach 20,000 feet) . . . . .

30 Roll Rate Response of the Initial Roll Rate Command System to 308 deg/sec Pulse Command (0.9 Mach 20,000 feet) . .

31 Aileron Response of the Initial Roll Rate Command System to a 308 deg/sec Pulse Command (0.9 Mach 20,000 feet) . . . . .

32 Sideforce and Output Feedback Response of the Initial Roll Rate Command System to a 10 deg/sec Pulse (0.9 Mach 20,000 feet) . . . . . .

33 Roll Rate and Sideslip Response of the Initial Roll Rate Command System to a 10 deg/sec Pulse (0.9 Mach 20,000 feet) . . . . . .

34 Yaw Rate and Sideforce Responses of the Sideforce System to a 0.8g Step Command (0.9 Mach 20,000 feet) . . . . .

35 Sideslip and Roll Rate Response of the Sideforce System to a 0.8g Step Command (0.9 Mach 20,000 feet) . . . . .

36 Roll Angle Response of the Sideforce System to a 0.8g Step Command (0.9 Mach 20,000 feet) . . . . . .

37 Surface Response of the Sideforce System to a 0.8g Step Command (0.9 Mach 20,000 feet) . . . . . .

Figure


| | |
|---|---|
| 40 | Pilot Interface for the Sideforce System . . . . . |
| 41 | Block Diagram of Longitudinal G-Command System With Pilot Interface Addition and Including the Pitch Pointing System . . . . . |
| 42 | Block Diagram of the Roll Rate Command System and Direct Sideforce System with Pilot Interface Addition (Yaw Pointing System is included) . . . . . |
| 43 | Response Plot for the Rate Controller to a 2 deg/sec Step Command (0.9 Mach 20,000 feet) . . . . . |
| 44 | Surface Position Plot for the Rate Controller to a 2 deg/sec Step Command (0.9 Mach 20,000 feet) . . . . . |
| 45a-d | G-Command System Response to a 1g Step Command (0.9 Mach 20,000 feet) . . . |
| 46a-b | Pitch Pointing System Response to a 1 deg/sec Step Command (0.9 Mach 20,000 feet) . . . . . |
| 47a-e | Roll Rate Command System Response to a 5 deg/sec Pulse Command (0.9 Mach 20,000 feet) . . . . . |
| 48a-d | Sideforce System Response to a 0.8g Step Command (0.9 Mach 20,000 feet) . . . . . |
| 49a-d | G-Command System Response to a 1g Step Command (1.6 Mach 30,000 feet) . . . |
| 50a-e | Roll Rate Command System Response to a 5 deg/sec Pulse Command (1.6 Mach 30,000 feet) . . . . . |
| 51a-d | Sideforce System Response to a 0.6g Step Command (1.6 Mach 30,000 feet) . . . . . |

Figure


| | |
|---|---|
| 52a-d | G-Command System Response to a 1g Step Command (0.6 Mach 30,000 feet) . . . . . |
| 53a-e | Roll Rate Command System Response to a 5 deg/sec Pulse Command (0.6 Mach 30,000 feet) . . . . . |
| 54a-d | Sideforce System Response to a 0.2g Step Command (0.6 Mach 30,000 feet) . . . . . |
| 55a-d | G-Command System Response to a 0.15g Step Command (0.2 Mach 30 feet) . . . |
| 56a-e | Roll Rate Command System Response to a 5 deg/sec Pulse Command (0.2 Mach 30 feet) . . . . . |
| 57a-d | Sideforce System Response to a 0.053g Step Command (0.2 Mach 30 feet) . . . |
| 58 | Neal-Smith Model for Pitch Attitude Control . . . . . |
| 59 | Neal-Smith Criterion for Fighter Maneuvering Dynamics . . . . . |
| 60 | Nichols Chart with Performance Standard Boundaries and Overlay of Amplitude-Phase Plot of $\theta/\theta_e$ with $\tau_{p_1}$ and $\tau_{p_2}$ Equal to Zero . . . . . |
| 61 | Criterion Graph with Design Evaluation Points . . . . . |
| 62 | Open-Loop Bandwidth Comparison for the Pitch Rate to Elevator Path . . . . . |
| 63 | Open-Loop Bandwidth Comparison for the Acceleration to Elevator Path . . . . . |
| 64a-d | G-Command System Response to a 9g Step Command--Nominal $C_{m_{\delta e}}$ (0.9 Mach 20,000 feet) . . . . . |
| 65a-d | G-Command System Response to a 9g Step Command--Reduced $C_{m_{\delta e}}$ (0.9 Mach 20,000 feet) . . . . . |

Figure


C-1a-d G-Command System Response to a 9g Step Command (0.9 Mach 20,000 feet) . . . . . .

C-2a-e Roll Rate Command System Response to a 308 deg/sec Pulse Command (0.9 Mach 20,000 feet) . . . . . .

C-3a-d G-Command System Response to a 8.5g Step Command (1.6 Mach 30,000 feet) . . . . . .

C-4a-e Roll Rate Command System Response to a 200 deg/sec Pulse Command (1.6 Mach 30,000 feet) . . . . . .

C-5a-d G-Command System Response to a 4.7g Step Command (0.6 Mach 30,000 feet) . . . . . .

C-6a-e Roll Rate Command System Response to a 300 deg/sec Pulse Command (0.6 Mach 30,000 feet) . . . . . .

C-7a-d G-Command System Response to a 0.3g Step Command (0.2 Mach 30 feet) . . .

C-8a-e Roll Rate Command System Response to a 35 deg/sec Pulse Command (0.2 Mach 30 feet) . . . . . .

## List of Tables


| Table | | |
|---|---|---|
| 1 | Aircraft Data for the 0.9 Mach and 20,000 Feet Flight Condition | . . . . . |
| 2 | Asymptotic Equations for Zero-$B_2$ Form | . . . . |
| 3 | Surface Position and Rate Limits | . . . . . |
| 4 | Maximum Command Estimates | . . . . . |
| 5 | CCV Maximum Capabilities | . . . . . |
| 6 | Gain and Phase Margin Requirements | . . . . . |
| 7 | Cooper-Harper Handling Qualities Rating Scale | . . . . . |
| A-1 | Aircraft Data for the 0.9 Mach and 20,000 Feet Flight Condition | . . . . . |
| A-2 | Aircraft Data for the 1.6 Mach and 30,000 Feet Flight Condition | . . . . . |
| A-3 | Aircraft Data for the 0.6 Mach and 30,000 Feet Flight Condition | . . . . . |
| A-4 | Aircraft Data for the 0.2 Mach and 30 Feet Flight Condition | . . . . . |

## List of Symbols

| | |
|---|---|
| $\underline{A}$ | Continuous-time plant matrix |
| AC | Aerodynamic center |
| $A_n$ | Longitudinal acceleration (positive upward along the negative z body axis) |
| $A_{n_{cg}}$ | Longitudinal acceleration at the center of gravity |
| $A_{n_p}$ | Longitudinal acceleration at the pilot's station |
| $A_y$ | Side acceleration (positive out the right wing along the y body axis) |
| $A_{y_{cg}}$ | Side acceleration at the center of gravity |
| $A_{y_p}$ | Side acceleration at the pilot's station |
| $\alpha$ | Angle of attack, perturbation angle of attack in perturbation equations |
| $\alpha_T$ | Trim angle of attack |
| $\alpha_1$ | Independent fuselage pitch pointing mode |
| $\bar{\alpha}$ | Ratio of proportional to integral feedback |
| $\underline{B}$ | Continuous-time plant matrix |
| b | Wing span |
| BW | Bandwidth |
| $\beta$ | Sideslip angle |
| $\beta_1$ | Independent fuselage yaw pointing mode |
| $\underline{C}$ | Continuous-time Output Matrix |
| c | Mean Aerodynamic Cord |
| CG, cg | Center of gravity |
| $C_D$ | Nondimensional coefficient of drag (along velocity vector) |

$C_{D_\alpha}$ Nondimensional variation of drag with angle of attack

$C_{D_\delta}$ Nondimensional variation of drag with elevator ($\delta e$) or flaperon ($\delta f$)

$C_{D_0}$ Nondimensional bias coefficient of drag at zero angle of attack

$C_{D_u}$ Nondimensional variation of drag with forward velocity perturbations from trim velocity

$C_L$ Nondimensional coefficient of lift (normal to velocity vector)

$C_{L_\alpha}$ Nondimensional variation of lift with angle of attack

$C_{L_{\dot{\alpha}}}$ Nondimensional variation of lift with the rate of change of angle of attack

$C_{L_\delta}$ Nondimensional variation of lift with elevator ($\delta e$) or flaperon ($\delta f$)

$C_{L_0}$ Nondimensional bias coefficient of lift at zero angle of attack

$C_{L_q}$ Nondimensional variation of lift with pitch rate

$C_{\ell_\beta}$ Nondimensional variation of rolling moment with sideslip angle

$C_{\ell_\delta}$ Nondimensional variation of rolling moment with aileron ($\delta a$), rudder ($\delta r$), canard ($\delta c$), or differential tail ($\delta_{DT}$)

$C_{\ell_p}$ Nondimensional variation of rolling moment with roll rate

$C_{\ell_r}$ Nondimensional variation of rolling moment with yaw rate

$C_m$ Nondimensional coefficient of pitching moment

$C_{m_\alpha}$ Nondimensional variation of pitching moment with angle of attack

$C_{m_\delta}$ Nondimensional variation of pitching moment with elevator ($\delta e$) or flaperon ($\delta f$)

$C_{m_0}$ Nondimensional bias coefficient of pitching moment at zero angle of attack

$C_{m_q}$ Nondimensional variation of pitching moment with pitch rate

$C_{m_u}$ Nondimensional variation of pitching moment with forward velocity perturbations

cmd Command

$C_{n_\beta}$ Nondimensional variation of yawing moment with sideslip angle

$C_{n_\delta}$ Nondimensional variation of yawing moment with aileron ($\delta a$), rudder ($\delta r$), canard ($\delta c$), or differential tail ($\delta_{DT}$)

$C_{n_p}$ Nondimensional variation of yawing moment with roll rate

$C_{n_r}$ Nondimensional variation of yawing moment with yaw rate

cos Cosine

$C_x$ Nondimensional x-force coefficient

$C_{x_\alpha}$ Nondimensional variation of x-force with angle of attack

$C_{x_\delta}$ Nondimensional variation of x-force with elevator ($\delta e$) or flaperon ($\delta f$)

$C_{x_0}$ Nondimensional bias x-force coefficient at zero angle of attack

$C_{x_q}$ Nondimensional variation of x-force with pitch rate

$C_{x_u}$ Nondimensional variation of x-force with forward velocity perturbation

$C_{y_\beta}$ Nondimensional variation of y-force with sideslip angle

$C_{y_\delta}$ Nondimensional variation of y-force with aileron ($\delta a$), rudder ($\delta r$), canard ($\delta c$), or differential tail ($\delta_{DT}$)

$C_{y_p}$ Nondimensional variation of y-force with roll rate

$C_{y_r}$ Nondimensional variation of y-force with yaw rate

| | |
|---|---|
| $C_z$ | Nondimensional z-force coefficient |
| $C_{z_\alpha}$ | Nondimensional variation of z-force with angle of attack |
| $C_{z_{\dot{\alpha}}}$ | Nondimensional variation of z-force with the rate of change of angle of attack |
| $C_{z_\delta}$ | Nondimensional variation of z-force with elevator ($\delta e$) or flaperon ($\delta f$) |
| $C_{z_0}$ | Nondimensional bias coefficient of z-force at zero angle of attack |
| $C_{z_q}$ | Nondimensional variation of z-force with pitch rate |
| $C_{z_u}$ | Nondimensional variation of z-force with forward velocity perturbation |
| deg | Degree |
| $\delta a$ | Aileron deflection |
| $\delta c$ | Canard deflection |
| $\delta_{DT}$ | Differential horizontal tail deflection (rolling tail) |
| $\delta e$ | Elevator or horizontal tail deflection |
| $\delta f$ | Flap deflection |
| e(t),$\underline{e}$ | Error vector |
| $\underline{e}$(kT) | Discrete error vector |
| $\varepsilon$ | Epsilon scalar multiplier |
| $F_s$ | Stick input |
| ft | Feet |
| $F_y$ | Sideforce in y-body axis |
| $F_z$ | Force in z-body axis |
| $F_{z_{cg}}$ | z-force at center of gravity |
| f | Sampling frequency |
| g | Gravity, type of pilot command, gain constant |

| | |
|---|---|
| $\underline{G}(s)$ | Transfer function matrix |
| $I_{xx}$ | Moment of inertia about x-axis |
| $I_{yy}$ | Moment of inertia about y-axis |
| $I_{zz}$ | Moment of inertia about z-axis |
| $I_{xz}$ | Product of inertia about xz-axes |
| $\underline{I}$ | Identity matrix |
| $K_i$ | Gain constant on surface position feedbacks |
| $\underline{K}_0$ | Proportional control law feedback matrix |
| $\underline{K}_1$ | Integral control law feedback matrix |
| $K_p$ | Gain constant in pilot model |
| Lat-Dir | Lateral-Directional |
| lbs | pounds |
| Long | Longitudinal |
| $\ell_x$ | Distance from CG to sensor location along x-axis |
| $\ell_y$ | Distance from CG to sensor location along y-axis |
| $\ell_z$ | Distance from CG to sensor location along z-axis |
| $L_\beta$ | Dimensional variation of rolling moment with sideslip angle |
| $L_\delta$ | Dimensional variation of rolling moment with aileron ($\delta a$), rudder ($\delta r$), canard ($\delta c$), or differential tail ($\delta_{DT}$) |
| $L_p$ | Dimensional variation of rolling moment with roll rate |
| $L_r$ | Dimensional variation of rolling moment with yaw rate |
| $\underline{M}$ | Measurement matrix |
| m | Aircraft mass, number of inputs |
| MAC | Mean Aerodynamic Cord |
| $M_\alpha$ | Dimensional variation of pitching moment with angle of attack |

| | |
|---|---|
| $M_{\dot{\alpha}}$ | Dimensional variation of pitching moment with the rate of change of angle of attack |
| $M_c$ | Controllability matrix |
| MD | MULTI Design |
| $M_o$ | Observability matrix |
| $M_q$ | Dimensional variation of pitching moment with pitch rate |
| $M_\theta$ | Dimensional variation of pitching moment with pitch angle |
| $M_x$ | Moment about the x-axis |
| $M_y$ | Moment about the y-axis |
| $M_z$ | Moment about the z-axis |
| n | Number of states |
| $N_\beta$ | Dimensional variation of yawing moment with sideslip angle |
| $N_\delta$ | Dimensional variation of yawing moment with aileron ($\delta a$), rudder ($\delta r$), canard ($\delta c$), or differential tail ($\delta_{DT}$) |
| $N_r$ | Dimensional variation of yawing moment with yaw rate |
| $N_p$ | Dimensional variation of yawing moment with roll rate |
| p | Number of outputs, roll rate |
| PR | Pilot Rating |
| q | Pitch rate |
| $\bar{q}$ | Dynamic pressure |
| r | Yaw rate |
| rad | Radians |
| S | urface area |
| s | Laplace operator |
| sec | Seconds |

| | |
|---|---|
| sin | Sine |
| $\sigma$ | Elements of the Sigma ($\Sigma$) matrix |
| $\Sigma$ | Sigma Gain Weighting matrix |
| $\underline{T}$ | Transformation matrix |
| T | Sampling period, Thrust |
| TWeaD, TWEAD | Tactical Weapon Delivery |
| U | Velocity along x-axis |
| $\Delta u, u$ | Perturbation velocity along x-axis |
| $\underline{u}$ | Input vector |
| V | Velocity along y-axis |
| v | Perturbation velocity along y-axis |
| $\underline{v}$ | Command input vector |
| $V_T$ | Forward Velocity |
| W | Velocity along z-axis, aircraft weight |
| w | Perturbation velocity along z-axis |
| $\underline{w}$ | Controller output vector |
| $\underline{x}$ | State vector |
| $X_\alpha$ | Dimensional variation of x-force with angle of attack |
| $X_{\dot{\alpha}}$ | Dimensional variation of x-force with the rate of change of angle of attack |
| $X_\delta$ | Dimensional variation of x-force with elevator ($\delta e$) or flaperon ($\delta f$) |
| $X_q$ | Dimensional variation of x-force with pitch rate |
| $X_u$ | Dimensional variation of x-force with forward velocity perturbation |
| $\underline{y}$ | Output vector |
| $Y_\beta$ | Dimensional variation of y-force with sideslip angle |

$Y_\delta$ Dimensional variation of y-force with aileron ($\delta a$), rudder ($\delta r$), canard ($\delta c$), and differential tail ($\delta_{DT}$)

$Y_p$ Dimensional variation of y-force with roll rate

$Y_r$ Dimensional variation of y-force with yaw rate

$\underline{z}(t), \underline{z}$ Integral of error vector

$\underline{z}(kT)$ Discrete Integral of error vector

$Z_\alpha$ Dimensional variation of z-force with angle of attack

$Z_{\dot{\alpha}}$ Dimensional variation of z-force with the rate of change of angle of attack

$Z_\delta$ Dimensional variation of z-force with elevator ($\delta e$) or flaperon ($\delta a$)

$Z_q$ Dimensional variation of z-force with pitch rate

$Z_u$ Dimensional variation of z-force with forward velocity perturbation

$Z_t$ Transmission zeros

$Z_{1,2}$ Finite system roots

$Z_3$ Infinite system roots

$\theta$ Pitch angle

$\theta_c$ Pitch angle command

$\theta_e$ Pitch angle error

$\phi$ Roll angle

$\Psi$ Yaw angle

$\Gamma(\lambda)$ Asymptotic transfer function matrix

## Abstract

Recently evolved multivariable design techniques are used to develop control laws for the AFTI/F-16. The techniques were developed by Professor Brian Porter of the University of Salford, England. In the study, designs are investigated to provide pilot control of vehicle rotational rates and accelerations. This line of inquiry is in contrast to the angle control concepts required in previous applications of these new techniques. A computer-aided design package called "MULTI" is used in refining the control laws to the preliminary design stage. It proves to be invaluable.

An aircraft model is developed in state space form for the AFTI vehicle from linearized aerodynamic data. This is accomplished at several points in the flight envelope. After validation, these models are used for the design and evaluation of the control laws.

AFTI is equipped with additional control surfaces to provide Direct Force (CCV) control. A requirement of the design is to demonstrate specific CCV capabilities. Major emphasis is placed on the ability to properly blend CCV and conventional control capabilities for combat maneuvering.

The methods employed to obtain a design are presented along with the evaluations of the final control laws.

Several instabilities encountered during the investigation are discussed. The multivariable techniques are shown to provide good designs with a very moderate expenditure of manpower. Additional areas of research are discussed along with proposed modifications to the "MULTI" package.

# MULTIVARIABLE CONTROL LAWS FOR THE AFTI/F-16

## I. Introduction

### Background

The advent of digital fly-by-wire control on advanced high performance aircraft has provided the pilot with control over pertinent motion variables. A stick input no longer simply commands a control surface deflection. The pilot's task is not restricted by the basic aerodynamic characteristics of the vehicle. The designer has the ability to develop a system which allows the pilot to command the type of aircraft response that has been found to be most useful. Such developments have opened the door to tailoring the control system for accomplishing specific mission phases with the promise of significant performance improvements. For a number of years, control theory has been applied to the design of limited authority augmentation systems to improve an aircraft's inherent short period and dutch roll damping throughout the flight envelope. Also, it has been employed in the design of autopilots to perform functions such as altitude hold, Mach hold, or heading hold and in the development of automatic landing systems. In the 1960 time period, flight

testing on the TWeaD F-4 program demonstrated active control could improve the ability of the pilot to use the aircraft as a weapons platform (Ref 1).

Recent emphasis has been on the incorporation of control concepts early in the aircraft design cycle to improve flight performance. The aerodynamic design is no longer restricted by requirements to provide natural damping and stability. In the case of statically unstable aircraft, the control system provides complete artificial stability and acceptable flying qualities.

The use of fly-by-wire requires the "electrical flight control system" to be as reliable and endurable as the mechanical system it replaces. This establishes rather severe requirements for the system, since flight safety is a paramount issue. The flight control system has to be designed to operate after several failures. In some cases this results in the use of four identical (redundant) channels within the flight control system so that monitoring and majority voting can identify and isolate failures. The required reliability is in the order of $1x10^{-7}$ failures per flight hour. Thus, only one failure is permitted for every 10 million flight hours (Ref 2).

Such stringent requirements result in the philosophy of having very few signal sources external to the system. Aircraft motion sensors used by the flight control system, although not possessing great accuracy, are extremely

reliable. Linear Variable Differential Transformers (LVDT) which are magnetically coupled are used as position sensors. Potentiometers are avoided because of their high failure rates and tendency to generate noisy signals.

This type of reliability is not necessary for other avionics systems or for limited authority outer-loop control functions such as autopilots. In these cases a failure is easily detected by the pilot and corrective action taken to counter the failure until the system can be removed from operation. This is not practical for full authority fly-by-wire systems. Because of their high authority and fast response, failures can result in aircraft loss.

Recent developments in Direct Force capabilities have provided the pilot with an additional dimension in maneuvering response resulting in a "new way to fly" (Ref 3). The proper application of these new Control Configured Vehicle (CCV) abilities to enhance combat effectiveness has been the subject of several research programs (Ref 4; 5).

Control design has been complicated by these new abilities. The designer is now faced with multiple input/output systems and an ever increasing number of feedback loops. Although classical methods can provide a means of design, application of these methods is becoming more and more time-consuming. Many iterations are required, as each new loop is closed, to satisfy the many varied and sometimes conflicting requirements.

The CCV YF-16 program carried such a classical design through flight testing with exceptionally good results. Attempts to design with modern control techniques have given less impressive results. This is unfortunate since these methods offer the potential of improved performance with a reduction in the design complexity. Requirements such as use of full state feedback, definition of a proper performance index, or selection of desired eigenvectors leave much to be desired in the currently available modern control techniques.

Recent theoretical work by Professor Brian Porter at the University of Salford, England, on high-gain error actuated methods has shown promise of enabling the design of exceptionally good performing systems without many of the drawbacks of current modern control methods. The theory of Professor Porter's work is presented in Chapter III and can also be found in Reference 6.

The problem undertaken in this thesis research is the development of an air-to-air combat control system for the AFTI/F-16 aircraft. Emphasis is placed on considerations for a practical implementation. The design is accomplished at several points in the flight envelope as shown in Figure 1. The point at 0.9 Mach and 20,000 feet is the primary design case. This is the condition where aerial combat generally begins. The other points are chosen to give a good variation in both the aerodynamic characteristics and static

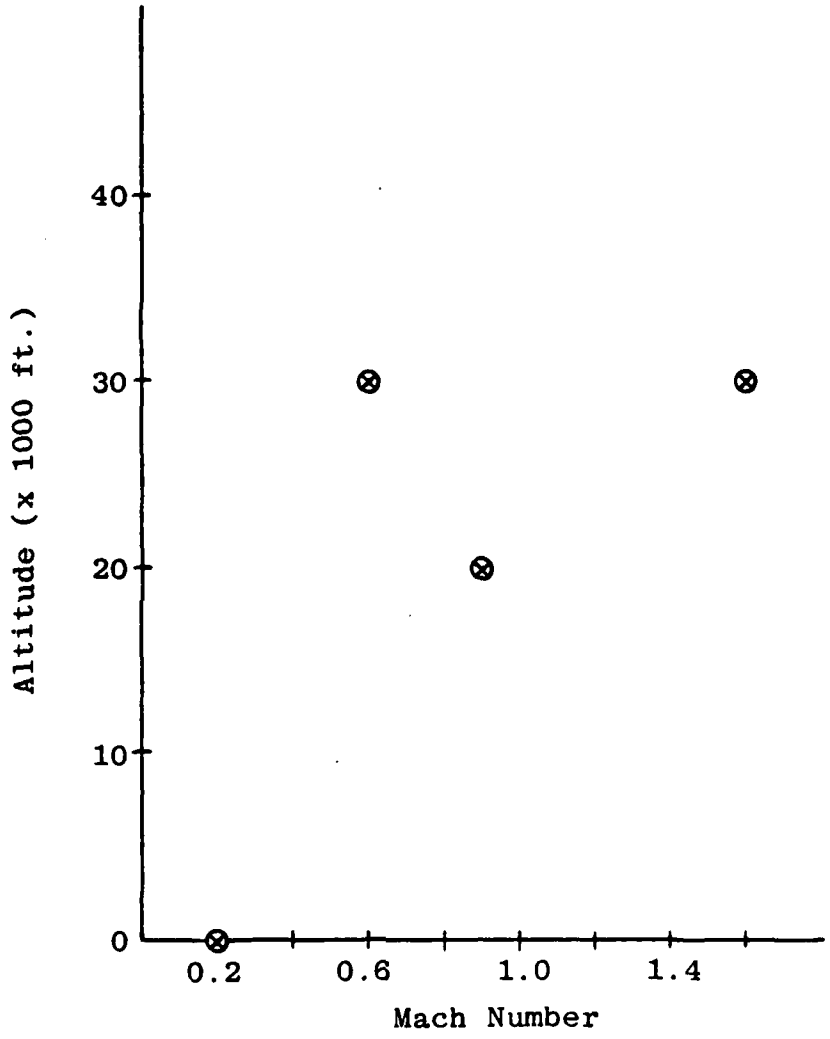



Figure 1. Flight Envelope Design Points

stability. Only cursory data is collected at the 0.2 Mach, sea level condition since combat capability is being stressed. This condition is included in the evaluation because it provides information on operation at elevated angle of attack. The 1.6 Mach, 30,000 feet point is selected due to the high "$\bar{q}$" condition and since some encounters actually begin supersonically. However, for such encounters, should a maneuvering engagement develop, airspeed drops quickly, and the subsonic region is entered.

Assumptions

Basic assumptions in the design effort are established to reduce the design complexity to a level equivalent to that of a "preliminary design" effort. These assumptions are listed below.

* The aircraft is a rigid body, and mass is constant.
* Thrust is not changing.
* The earth's surface is an inertial reference frame.
* The atmosphere is assumed fixed with respect to the earth.
* The equations of motion can be decoupled into a longitudinal and a lateral-directional set of equations.
* Linearization about an operating condition is acceptable for point designs.
* Aerodynamics are fixed for Mach and altitude.

A rigid aircraft model is employed in which any two points in the airframe remain fixed with respect to one

another. Flexibility due to structural modes of the aircraft are not considered in this study. However, requirements are developed with a consideration of such effects. As an example, flight control-structural interactions can cause several problems ranging from unwanted vibrations or control surface activity to structural failure and aircraft loss. With this in mind, the design goals are established to provide good performance at a minimum gain and bandwidth. In seeking to prevent structural interaction, the system is limited in bandwidth to only the range needed to do the job. High frequencies, where structural resonances are usually encountered, are attenuated. It is noted that flexibilized aerodynamic data is used in developing the linear aircraft model. In this way control surface deformation due to air loads is accounted for as dynamic pressure changes.

Mass variations for the aircraft are fairly large because of fuel usage during a mission. However, the control system responses being studied are in the range of one to ten seconds compared to a 1.5 hour mission. Fuel usage and the resulting mass change during a specific maneuver are very small and can be neglected.

Thrust is held constant throughout each maneuver to reduce the number of variables being altered in the design. It also provides a means of comparing design attempts. With constant thrust, the variation in velocity provides an indication of the drag penalty and energy loss for the same

maneuver for several candidate designs. In addition, an apriori scheme for varying thrust during a maneuver is not apparent. Although thrust adjustment can be added as an input to control velocity, it is felt that pilot control of thrust during combat maneuvering is very active and not easily predicted for use in design studies of this level. Such an extension can be examined for application to an automated or semi-automated attack system.

The inertial frame of reference is established as the earth's surface. This greatly simplifies the equation development and is valid for two reasons. First, the sensors used for flight control systems, although highly reliable, are not sensitive enough to detect the earth's rotational rate or the coriolis acceleration. Secondly, the maneuvers being considered have short durations compared to earth rate. Relative to the earth they are also "local" responses, and thus a flat earth with constant gravity gives fairly accurate results.

For this design effort, the atmosphere is assumed fixed to the surface of the earth. The limited scope of this preliminary design did not cover random gust, steady winds, or wind sheers during maneuvers. However, the effect of gust upset is considered in establishing design restraints that lead to a limited bandwidth control system with reduced gains. It also directs the selection of feedback signals to those which are not overly gust sensitive.

The full nonlinear equations of motion are developed in Appendix B and then simplified for the study. The first basic simplification is to assume that for this preliminary design work the equations can be broken into a set of longitudinal equations and a set of lateral-directional equations which do not interact. Since air combat maneuvering is a design goal, this assumption of being decoupled must be kept in mind. At times the assumption is altered to allow for consideration of special maneuvers such as the ability to roll about the velocity vector of the aircraft. That ability is very desirable for fighter aircraft and is addressed later.

Multiple design points are established in the flight envelope, and the simplified equations are linearized at these points. Perturbation equations about these points are then employed in the design phase. Such a strategy assumes that such point designs are fairly accurate representations at the selected points. To accomplish a full envelope design requires many such point designs with gain scheduling between points. This approach has been used for several existing aircraft control system designs and requires a great many points to be considered. The further the deviation from such "design" points, the less likely that the design is adequate since the model used for such designs becomes less and less realistic. In this study, only four design points are used as shown in Figure 1. These are

selected to provide a full range of aerodynamic variations for the controller design effort. For a practical design, a great many more points must be considered with a number of trimmed acceleration levels at each point being studied.

Although perturbations in velocity and altitude about trim are examined, the aerodynamic model is fixed at the trim point. Aerodynamic coefficients are constant throughout a maneuver. In general, the aerodynamic coefficients vary rather slowly (except in the transonic region), and the approximation is valid for reasonably small variations about the trim point.

The above assumptions with their resulting restrictions are typical of simplifications used in developing a preliminary design for an aircraft control system. They are considered to be appropriate for this study.

Pertinent Observations

Previous efforts applying Professor Porter's method have centered on the command of output functions such as pitch angle, flight path angle, or roll angle. That approach presents two problems for the application being considered in this thesis. First, these angular quantities are referenced to inertial space which in this case is the local earth coordinate system. Such measurements are usually obtained from an inertial navigation system or inertial measurements system which has a significantly lower reliability and failure detection capability than the flight

control system. Second, the pilot feels aircraft body angular rates and accelerations since he is physically attached to the aircraft. In actuality, he controls these quantities in flying the aircraft. For a right stick input, a fighter pilot expects to develop a proportional "right wing down" roll rate. Release of the stick input results in zero roll rate while the aircraft roll angle remains at a constant value. In pitch, the pilot expects constant stick force to result in a constant acceleration with an associated pitching rate. It is important to note that the pilot actually feels (and desires to command) accelerations at his position in the aircraft. This acceleration, $A_{n_p}$, is a combination of aircraft acceleration measured at the center of gravity, $A_{n_{cg}}$, and rotational acceleration, $\dot{q}$, as shown in the following simplified equation. The $\ell_x$ term is the distance from the center of gravity to the pilot's position.

$$A_{n_p} = A_{n_{cg}} + \ell_x(\dot{q}) \qquad (1.1)$$

For rudder commands, yaw rate is developed with a corresponding side acceleration ($A_y$) and sideslip ($\beta$). Based on such observations, the controller design strives to command these same inputs.

Recent flight testing on a highly modified F-16 has demonstrated some rather unique new capabilities. These capabilities are provided to the pilot through the use of

multiple control surfaces. The use of these control surfaces, coupled with the flight control system, allow "direct forces" to be developed by the aircraft (Figure 2). The direct force term is meant to imply the development of forces which are uncoupled from or not related to the aircraft's rotation. Using direct forces, six new control modes are available to the pilot as illustrated in Figures 3 and 4.

The "direct lift" mode provides a longitudinal acceleration while holding angle of attack constant. In this mode a pilot's command to the system causes the aircraft to change its flight trajectory by developing an additional lift force without an angle of attack change.

The "pitch pointing" mode allows the pilot to command an angle of attack change without developing an acceleration. With this mode, the pilot can actually point the nose of the aircraft up or down without changing the direction of flight.

"Longitudinal translation" results in the aircraft changing altitude or translating upward without rotating. A constant upward velocity is developed while maintaining a zero pitch rate.

These same capabilities also exist in the lateral-directional axis. The use of canards in conjunction with the rudder and various control system feedbacks allows direct force to be developed while moments are balanced on the aircraft. Ailerons are also used to counter unwanted rolling moments.

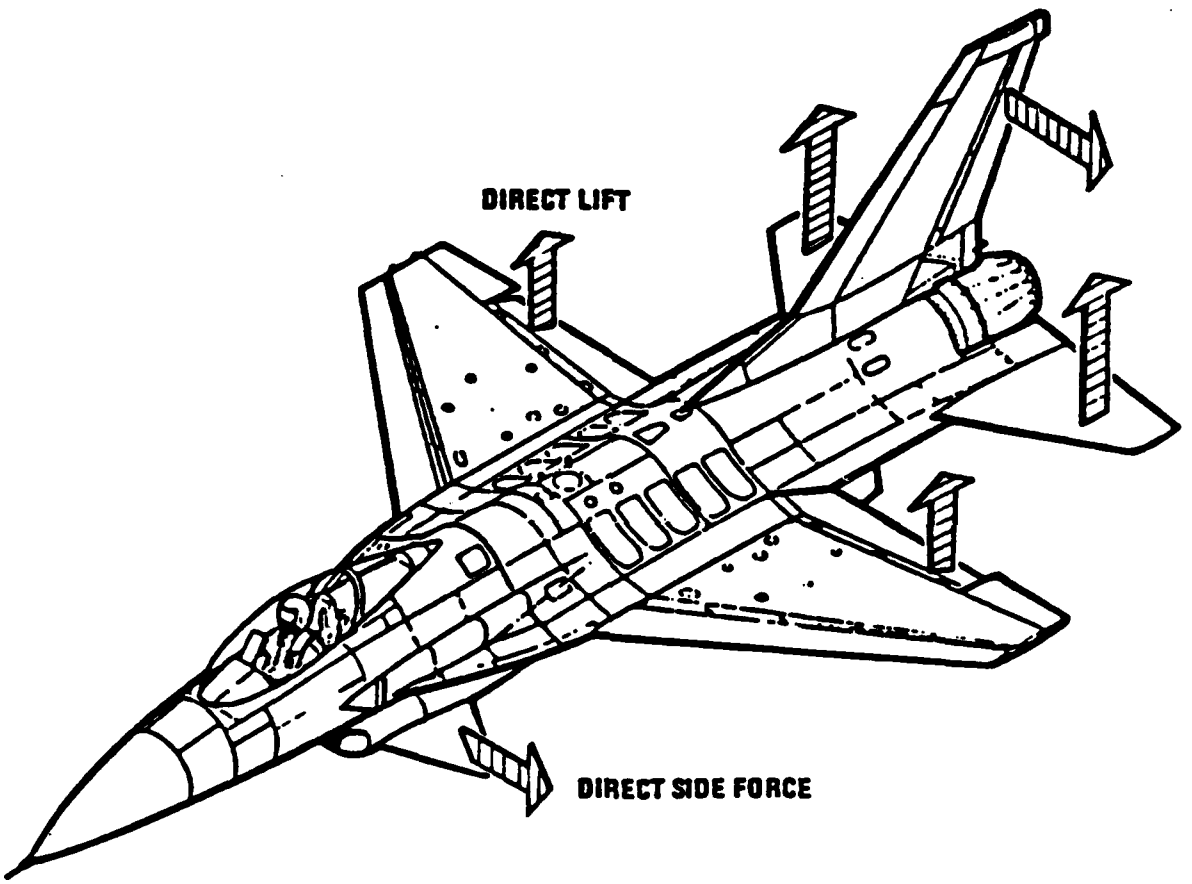
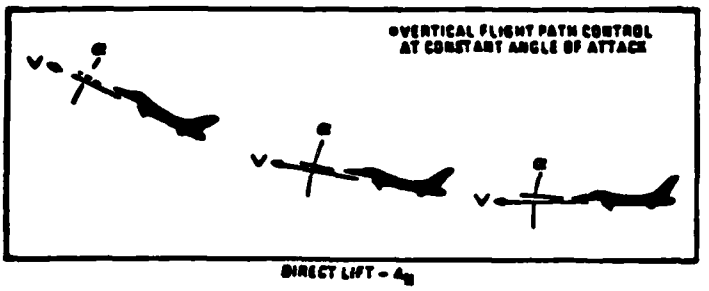
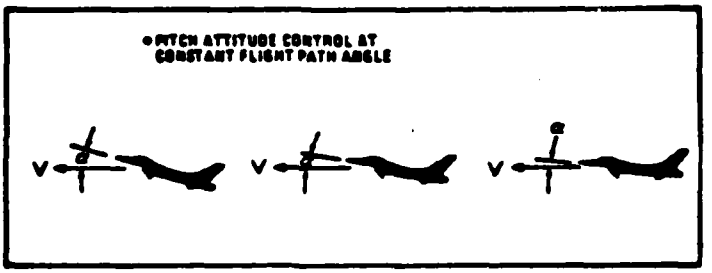


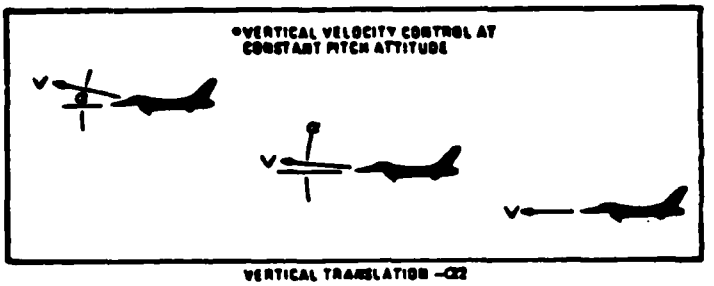

Figure 2. Direct Force Development Using Multiple Surfaces




DIRECT LIFT - $A_{z_\delta}$

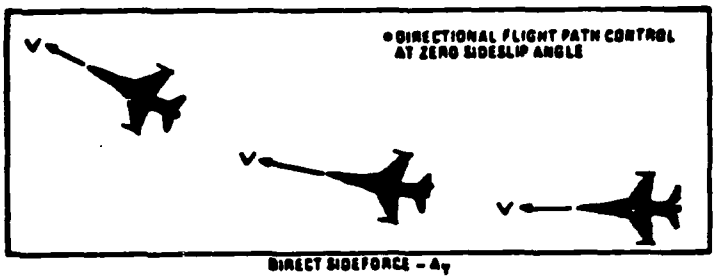


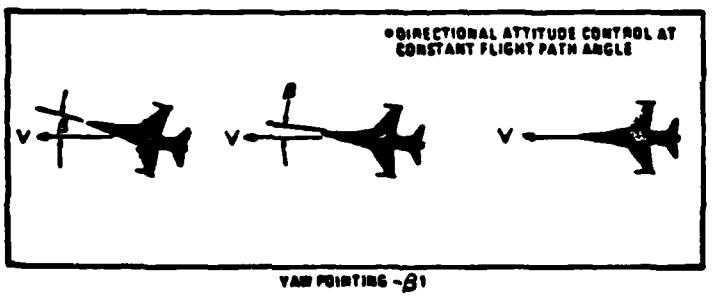

PITCH POINTING - $Z_1$




VERTICAL TRANSLATION - $Z_2$

Figure 3. Longitudinal Direct Force Modes



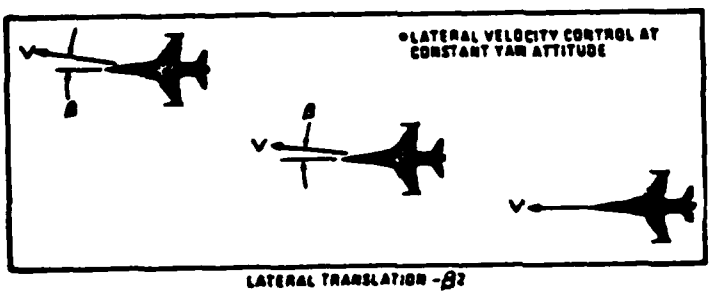




Figure 4. Lateral-Directional Direct Force Modes

A "direct sideforce" mode provides lateral acceleration to the pilot without inducing a sideslip angle. Using such a mode allows wings level turns to be performed in which a turn rate is developed without banking the aircraft or developing a sideslip. As in the longitudinal case, the aircraft is turning with the velocity vector as opposed to leading it in conventional maneuvers.

"Yaw pointing" provides the pilot with independent control over sideslip, beta. The aircraft's nose can be pointed right or left without developing a side acceleration or changing the direction of travel.

"Lateral translation" results in the aircraft being able to execute side-step maneuvers without having to bank. In this case, a constant side velocity is developed while maintaining a zero yaw rate.

These modes of operation are called Control Configured Vehicle (CCV) maneuvers in this report. It is acknowledged that the CCV concept encompasses much more than unconventional flight modes (Ref 7). The above descriptions of the unconventional modes differ from the definitions found in the open literature by the lack of the use of terms relative to an inertial reference such as flight path angle or pitch angle. This is deemed desirable since such definitions, while being correct for limited portions of flight, are not proper in maneuvering situations. As an example, consider the case of pitch pointing. This can be defined as changing

the aircraft's pitch attitude while maintaining flight path angle and heading angle. In wings level flight such a system provides the desired fuselage pointing. Should the aircraft be in a high "g" turn requiring a large bank angle, such a system cannot be employed. Heading angle is continually changing due to the turn. For a descending turn, flight path angle is also changing. Pitch attitude ($\theta$) is defined as the angle between the local horizon and the x-axis of the aircraft. Should the aircraft be banked at 88 or 89 degrees, changing theta results in a yawing motion. This is clearly not what is intended. It is advantageous to mechanize such CCV capabilities for "all aspect" operation. This was accomplished for the majority of modes on the CCV YF-16. Using the definitions specified in this report, a system is specified which is able to develop a change in angle of attack without an accompanying normal acceleration change. In this way fuselage pointing can be obtained without interfering with maneuvering turns. In fact, it can be commanded simultaneously with the turn.

Study Approach and Design Requirements

The general approach for this study is to design a multivariable control system for the AFTI/F-16 vehicle for combat maneuvering. Major emphasis is on the development of a controller with equivalent or improved performance as compared with the current AFTI Air-to-Air gunnery control mode but with reduced complexity. Each design attempt begins

with a very simple design and slowly increases in complexity until a realistic result is obtained. For example, at the 0.9 Mach, 20,000 feet case a short period approximation of the aircraft is initially employed in order to arrive at a basic design with the fewest variables to adjust. The design then proceeds to treating the full equations of motion and includes actuator and sensor models. Any time an unforeseen result or problem is encountered, the simplistic model is reinvestigated. This allows determination of the cause of such a result as either being inherent in the basic design or as having been created in the manipulation of variables or in the modeling of the more complex system. It also results in a tremendous time saver in finding problems and errors as shown later in the report.

Early in the study, a set of general design requirements is established to form a basis for the work. These requirements are listed below.

* The design will provide control and stability augmentation.
* Responses are to be fast and well-behaved.
* Surface position and rate limits must not be exceeded.
* Aircraft rates and accelerations will be directly controlled.
* Feedbacks can be reliably obtained with existing sensors.
* Conventional and specific CCV maneuver capabilities are available.

A brief discussion on the development of each of these requirements follows.

The controller is to augment the basic aircraft stability and in some cases, such as in the subsonic region, provide artificial stability for a statically unstable aircraft. In addition, it should provide the pilot with control over motion parameters that are important for the specific mission task of air-to-air gunnery.

In target acquisition and tracking, certain basic characteristics have been found to be advantageous. The main pilot task is precise pointing. The task can be broken into an acquisition phase and a fine tracking phase. Acquisition requires large roll and pitch changes. This translates into being able to pull onto the target rapidly, and thus, the acceleration response must be fast and well damped. Fine tracking requires precise attitude control which indicates that the pitch rate response must be fast and well damped.

In conventional aircraft, the pitch and acceleration responses are coupled, and this results in conflicting requirements. Generally, a fast "g" response produces a fast pitch rate response with large overshoots and low damping. If the design emphasizes a fast and well-damped pitch rate response, then it results in a relatively slow "g" response. The actual design which is implemented is usually a compromise of both responses, providing the best

overall results. Direct lift provides the designer with the capability of altering this basic relationship. Pitch rate and normal acceleration can be "decoupled." In this way, both responses can be tailored to provide fast well-damped behavior within the direct lift capability limits. Once these limits are exceeded, such decoupling is not possible.

The restrictions on surface position and rate limiting are imposed at the preliminary design stage as opposed to the conventional tendency for a new system to include them later in the design cycle. This restriction is established after a review of several applications of the design technique. In those cases it has been apparent that the exceptionally fast aircraft responses achieved were developed through large and extremely fast surface movements.

A design is sought that results in surface activity that does not encounter either of these limits. Running into a position limit results in loss of decoupling and prevents the required command from being reached. In cases where the control system is providing artificial stability, this results in loss of that stability. Rate limiting presents a problem that is a little more sinister but just as dangerous. Rate limiting is a nonlinear function that can result in a significant increase in phase lag in a feedback system. Such phase lag has been shown to cause loss of control and divergent oscillations that can result in aircraft loss for a full authority fly-by-wire system.

It is interesting to note that in early multivariable designs such as the CCV YF-16 (in which classical design techniques were used), aircraft stability and control, and basic flying qualities were provided by conventional control surfaces with appropriate feedbacks. Additional surfaces were used to provide the direct force capabilities. Rate or surface limiting of these additional surfaces resulted in loss of the direct force function with less than the desired responses, but augmentation was not impaired. Rate and position limiting is important for the conventional surfaces and such limiting is prevented in the design. In the current multivariable designs, surface rate and position limiting is an important consideration on all surfaces since the stability function, as well as the direct force function, is performed by the combination of all surfaces.

The desirability of controlling aircraft body rates and accelerations becomes more apparent when considering the complexity of interface to the pilot. The multivariable theory applied in this thesis allows as many independent aircraft states or linear combinations of states to be commanded as there are control surfaces (inputs). For the AFTI vehicle there are two longitudinal surfaces, and thus, it is possible to control two system outputs. It should be noted that both must be commanded to some value even if that value is zero. Suppose the command parameters are selected to be angle of attack and pitch angle. In maneuvering flight,

pitch angle is not completely a longitudinal parameter. In the case of a constant altitude turn, theta stays at zero. Additionally, how does the pilot know what value of these two parameters to command in order to perform the maneuver he desires? One answer is to develop a model of the aircraft. Conventional pilot commands can be input, and the resulting model parameters can provide the command inputs to the multivariable controller. This requires that a simple model must be developed which exhibits the response desired of the actual aircraft. With the wide variation of aerodynamic parameters, gain scheduling might be required in the model. If the control system is to be tailored to the specific task, the model must also be tailored.

If pitch rate and normal acceleration are employed for the command parameters, the problem can be eliminated. The pilot generally desires a specific "g" level and a corresponding pitch rate can be determined from the following relationship $q = (1845/U)(A_n)$. The choice of rate and acceleration makes sense as far as reliability, availability, pilot preference, interface complexity, and workload are concerned.

The required reliability of a flight control system which provides stability and control augmentation is discussed earlier in this chapter. Rate gyros and accelerometers that sense body motion can be incorporated in the flight control system design where redundant electrical

power and signal processing are available. They are low enough in cost and size that multiple sensors can be used for redundancy. Such redundancy considerations are not meant to infer that selection of feedback signals is limited to only rates and accelerations. It is to focus attention on the careful selection of signals. In the F-16, angle of attack is deemed necessary for use in the flight control system. A means of developing multiple independent and reliable sources has been found. In addition, the F-16 uses four longitudinal accelerometers, four lateral accelerometers, four pitch rate gyros, and four roll rate gyros. These are required to meet mission reliability and failure tolerance requirements.

Through several research and development programs, the CCV control modes have been examined for usefulness in combat scenarios. From this work, several of the modes are selected for design applications in this thesis.

The first of these is blending of the conventional maneuvering capability of the aircraft with the direct lift function in the longitudinal axis to provide improved performance. The decoupling of direct lift from aircraft rotation can be used to tailor the aircraft response in a conventional maneuver to provide optimum response for both acceleration and pitch rate. Thus, the longitudinal design is aimed at using direct lift and conventional aircraft blending. Fuselage pointing holds promise for automatically

nulling small aiming errors during target tracking or in obtaining a lock-on by the weapons system. The feasibility of providing longitudinal fuselage pointing by commanding rates and accelerations is examined. Direct sideforce has also been shown to be promising in air-to-air gunnery and may have possibilities for air-to-ground bombing applications. It may also be useful for evasive maneuvering or limited terrain avoidance maneuvers. Thus, it is selected for the directional design. Conventional roll rate control is selected for the lateral design. The controller design being sought is to provide the above combination of unconventional and conventional capabilities to the aircraft.

## Presentation Sequence

The material in this thesis consists of a description of the aircraft chosen for the study in Chapter II. The process of developing a model for the design, and the means of validating such a model is also presented. Chapter III contains a brief description of the multivariable design theory developed by Professor Brian Porter of the University of Salford, England. An important area of bounded stability is included. The design method and representative results at selected points in the flight envelope are presented in Chapter IV. A proposed design procedure is established. Inadequacies of the design method as well as advantages are discussed. The final design is evaluated in Chapter V against several criteria and compared with current state-of-the-art

designs. Conclusions are discussed in Chapter VI with recommendations for future efforts. A complete set of aerodynamic and transformed aircraft model data is included in Appendix A. Development of the equations of motion is covered in detail in Appendix B . Controller responses to the maximum estimated inputs to verify surface rate and position limits are presented in Appendix C. The last three Appendices document the three programs used in conjunction with MULTI in the designs. The programs provide methods to: (1) convert and transform aerodynamic data into the form necessary for developing a state space aircraft model; (2) calculate transmission zeros; and (3) determine the closed-loop system matrix. The last program is useful in obtaining both closed-loop roots and system transfer functions.

## II. The AFTI/F-16 Aircraft

### Aircraft Description

The AFTI vehicle is a highly modified F-16 aircraft. It has been changed to allow flight demonstration of the benefits possible from the integration of advanced technology features. Among the advanced features selected for demonstration are triple redundant digital flight control computers, and a flight control system tailored to the specific mission phase. Tailoring has resulted in eight separate control modes being implemented in the digital computers with extensive gain scheduling to provide unprecedented performance. Asynchronous computer operation is employed in which each of the three computers operates independently in calculating the flight control laws. A redundancy management system has been developed that uses comparison monitoring of the three computers along with internal self-test features to detect failed system elements, and provides a two-fail/operate capability. This means the system can withstand two similar failures and still continue to operate.

AFTI's major external modifications to date have been the addition of twin vertical canards mounted under the engine inlet and the installation of a dorsal fairing or "back pack" between the cockpit and vertical tail. The dorsal fairing houses avionics and instrumentation necessary

for the flight test effort. Although receiving an entirely new flight control system, the original F-16 sensors are retained. Body accelerations are measured at the pilot's station by longitudinal and lateral accelerometers. There are four identical sensors for each axis for redundancy. The F-16 flight control system employs all four since it is quadruply redundant. AFTI uses only three of these sensors to provide essentially the same fail/operate capability as the F-16. The fourth provides signals for flight test instrumentation. Body rotational rates are sensed by rate gyros located very close to the aircraft's center of gravity. There are four identical pitch rate gyros, four roll rate gyros, and four yaw rate gyros. In addition, angle of attack is sensed by two fuselage side-mounted cones, as well as, by a hemispherical differential pressure probe extending from one side of the aircraft. Although sideslip angle, beta, is not employed in the F-16, plans called for its use in the AFTI system. The same type of conical sensors used for angle of attack were to be installed to measure sideslip. Unfortunately, a suitable location, free of airflow irregularities around the fuselage, could not be found to provide good sideslip information.

The aircraft is shown in the drawing in Figure 5. The control surfaces used in this study are denoted by solid black. These consist of two fully movable horizontal tail surfaces which can be deflected symmetrically as an elevator

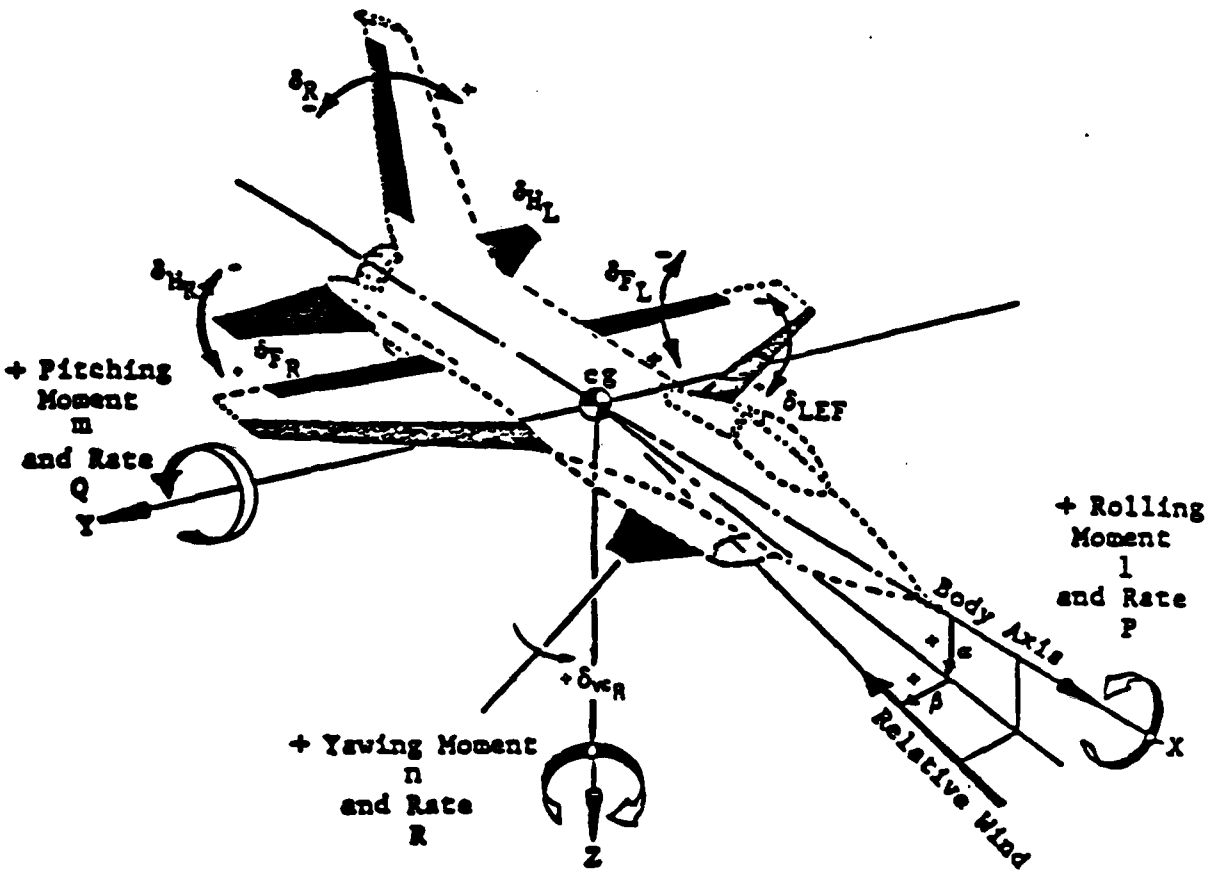



Figure 5. AFTI/F-16 Control Surface Location

or asymmetrically for augmenting roll control. Flaperons on the trailing edge of each wing can be moved symmetrically to act as flaps or asymmetrically as ailerons for primary roll control. The canards are used for sideforce control. Sign convention used in this study is also displayed in the figure.

Longitudinally the unaugmented aircraft (no control system) is statically unstable at subsonic flight conditions as illustrated in Figure 6. The center of gravity (CG) is located behind the aerodynamic center (AC) by design. The difference between the CG and AC is generally measured in percent of the mean aerodynamic cord (MAC). The figure shows the aircraft to be approximately three percent unstable subsonically. In the transonic region, the aircraft is neutrally stable. Although stable at supersonic speeds, there is also a reduction in stability when compared to conventional aircraft. The unstable condition eliminates the requirements for the elevator to continually develop a down load in trimmed flight. The tail is actually adding lift to the aircraft. Because of this design feature, the aircraft can obtain higher load factors and has reduced drag. This translates into faster turn rates and longer operational ranges. The unaugmented aircraft pitch angle-to-elevator deflection transfer function for the 0.9 Mach 20,000 feet condition is shown below. It should be noted that the short period roots of the aircraft are real, and

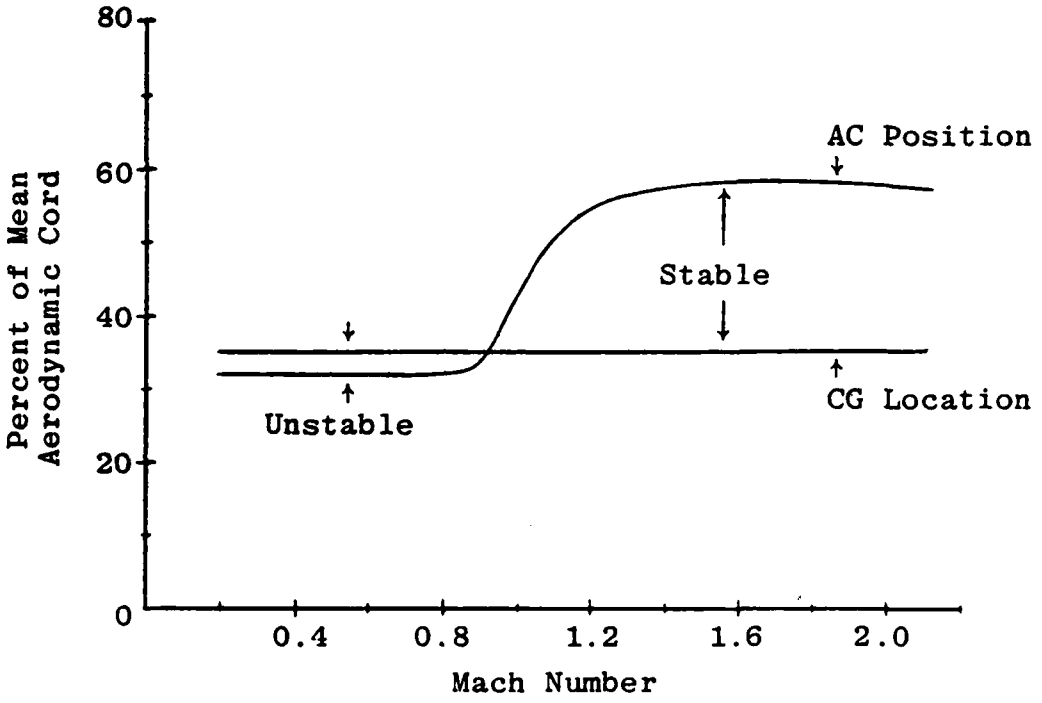



Figure 6. Longitudinal Static Stability Plot

one is unstable. This is the manner in which static instability is manifested.

$$\frac{q}{\delta_e} = \frac{-24.06(s)(s+0.0126)(s+1.51)}{(s+0.00757\pm j0.0543)(s-0.964)(s+3.222)} \qquad (2.1)$$

Phugoid Short Period

In the lateral-directional axis, the aircraft has very light dutch roll damping. This can be seen by examining the yaw rate-to-rudder deflection transfer function for the aircraft computed at the 0.9 Mach 20,000 feet point.

$$\frac{r}{\delta_r} = \frac{-5.81(s+0.323\pm j0.623)(s+2.482)}{(s+0.0272)(s+0.391\pm j2.961)(s+2.697)} \qquad (2.2)$$

Spiral Dutch Roll Roll

In its smallest sense, the control system design must provide longitudinal stability and improve dutch roll damping. In a larger sense, this is desired while providing an aircraft control system combination that is of most benefit to the pilot in performing specific tasks during a mission. The task considered in this study is air-to-air gunnery.

Aerodynamic Model

An extensive aerodynamic data package was developed by the General Dynamics Corporation of Fort Worth, Texas, for the AFTI/F-16 vehicle. The work was performed under contract to the AFTI/F-16 Advanced Development Program Office (ADPO) of the Flight Dynamics Laboratory. Wind

tunnel testing in both low and high speed tunnels provided data throughout the flight envelope for angle of attack ranges of 90 degrees to -40 degrees and large sideslip angles. F-16 wind tunnel data and flight test data were used as a baseline for the package.

A General Dynamics program was used to obtain linearized aerodynamic coefficients by trimming the aircraft at various flight conditions and load factors. Aircraft weight and inertias were also provided by the program. This data is listed in Table 1 for the major design point at 0.9 Mach and 20,000 feet. A complete set of data for all the points considered in the study is given in Appendix A. It should be noted that by convention, the static derivatives ($C_{m_\alpha}$ , $C_{L_\alpha}$ , etc.) are listed in units of per degree (1/deg). The dynamic derivatives, such as $C_{L_q}$ , $C_{L_{\dot{\alpha}}}$ , $C_{n_p}$ , are listed in units of per radian (1/rad). Also by convention, the aerodynamic derivatives are presented in the stability axis while mass properties, such as moments and products of inertias, and the position of the sensors, are referenced to the body axis of the aircraft. Figure 7 provides a definition of the axis systems. The data must be converted to a consistent reference frame to permit analyses to be conducted.

For conditions where angle of attack is small, such as in trimmed straight and level flight, the differences between body and stability axes can usually be ignored. In

Table 1

Aircraft Data for the 0.9 Mach and 20,000 Feet Flight Condition

## Aircraft Parameters

$\bar{q}$ (dynamic pressure - lbs/ft$^2$) = 552.113

S (wing reference area - ft$^2$) = 300.0

c (wing mean aerodynamic cord - ft) = 11.32

b (wing span - ft) = 30.0

$V_T$ (trim velocity - ft/sec) = 933.23

W (weight - lbs) = 21,018.0

Inertias: $I_{xx}$ (slug - ft$^2$) = 10,033.4

$I_{yy}$ (slug - ft$^2$) = 53,876.3

$I_{zz}$ (slug - ft$^2$) = 61,278.5

$I_{xz}$ (slug - ft$^2$) = 282.132

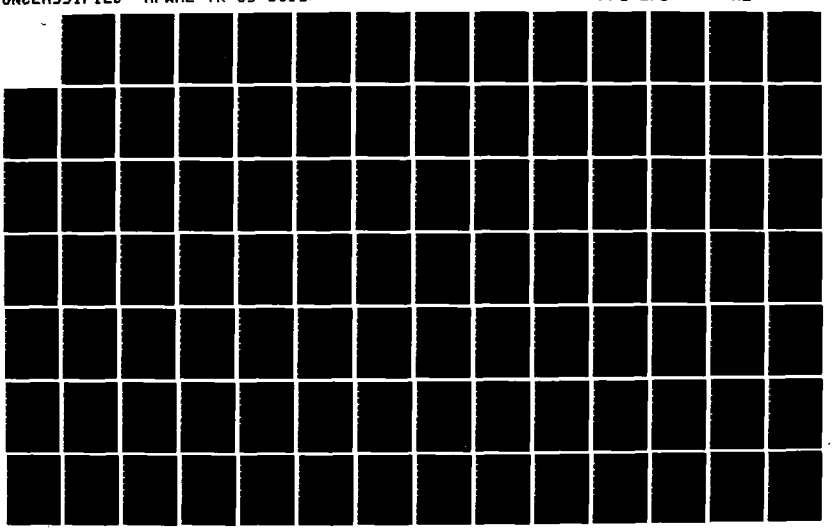
## Aircraft Aerodynamic Coefficients in the Stability Axis

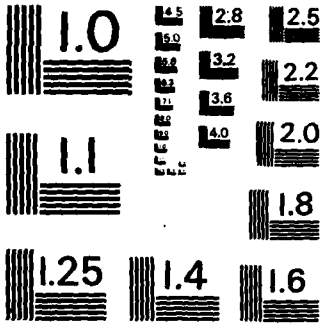
$\alpha$(deg) = 1.86

| | | |
|---|---|---|
| $C_L$ = 0.1262 | $C_m$ = 0.0 | $C_D$ = 0.02377 |
| $C_{L_\alpha}(\frac{1}{deg})$ = 0.09481 | $C_{m_\alpha}(\frac{1}{deg})$ = 0.001938 | $C_{D_\alpha}(\frac{1}{deg})$ = 0.002636 |
| $C_{L_{\delta_e}}(\frac{1}{deg})$ = 0.009578 | $C_{m_{\delta_e}}(\frac{1}{deg})$ = -0.01209 | $C_{D_{\delta_e}}(\frac{1}{deg})$ = 0.000173 |
| $C_{L_{\delta_f}}(\frac{1}{deg})$ = 0.01572 | $C_{m_{\delta_f}}(\frac{1}{deg})$ = -0.003280 | $C_{D_{\delta_f}}(\frac{1}{deg})$ = 0.000351 |

AD-A139 050 PROCEEDINGS OF THE WORKSHOP ON MULTIVARIABLE CONTROL SYSTEMS HELD AT WRIG..(U) AIR FORCE WRIGHT AERONAUTICAL LABS WRIGHT-PATTERSON AFB OH M A MASI ET AL. SEP 83 2/7

UNCLASSIFIED AFWAL-TR-83-3093 FFG 1/3 NL






MICROCOPY RESOLUTION TEST CHART
NATIONAL BUREAU OF STANDARDS - 1963 - A

Table 1 (continued)

| | | |
|---|---|---|
| $C_{L_q}(\frac{1}{rad}) = 3.1617$ | $C_{m_q}(\frac{1}{rad}) = -2.3822$ | |
| $C_{L_{\dot{\alpha}}}(\frac{1}{rad}) = -1.3578$ | $C_{m_{\dot{\alpha}}}(\frac{1}{rad}) = -1.3076$ | |
| $C_{L_u}(\frac{1}{ft/sec}) = -0.000442$ | $C_{m_u}(\frac{1}{ft/sec}) = -0.00006$ | $C_{D_u}(\frac{1}{ft/sec}) = 0.00016$ |
| $C_{y_\beta}(\frac{1}{deg}) = -0.02205$ | $C_{n_\beta}(\frac{1}{deg}) = 0.001675$ | $C_{\ell_\beta}(\frac{1}{deg}) = -0.001901$ |
| $C_{y_p}(\frac{1}{rad}) = 0.05756$ | $C_{n_p}(\frac{1}{rad}) = -0.005541$ | $C_{\ell_p}(\frac{1}{rad}) = -0.3512$ |
| $C_{y_r}(\frac{1}{rad}) = 0.5576$ | $C_{n_r}(\frac{1}{rad}) = -0.2791$ | $C_{\ell_r}(\frac{1}{rad}) = 0.02194$ |
| $C_{y_{\delta_r}}(\frac{1}{deg}) = 0.002377$ | $C_{n_{\delta_r}}(\frac{1}{deg}) = -0.001272$ | $C_{\ell_{\delta_r}}(\frac{1}{deg}) = 0.000331$ |
| $C_{y_{\delta_a}}(\frac{1}{deg}) = -0.000088$ | $C_{n_{\delta_a}}(\frac{1}{deg}) = -0.00016$ | $C_{\ell_{\delta_a}}(\frac{1}{deg}) = -0.001804$ |
| $C_{y_{\delta_{DT}}}(\frac{1}{deg}) = -0.001708$ | $C_{n_{\delta_{DT}}}(\frac{1}{deg}) = -0.000997$ | $C_{\ell_{\delta_{DT}}}(\frac{1}{deg}) = -0.001816$ |
| $C_{y_{\delta_c}}(\frac{1}{deg}) = 0.001716$ | $C_{n_{\delta_c}}(\frac{1}{deg}) = 0.001256$ | $C_{\ell_{\delta_c}}(\frac{1}{deg}) = 0.00023$ |

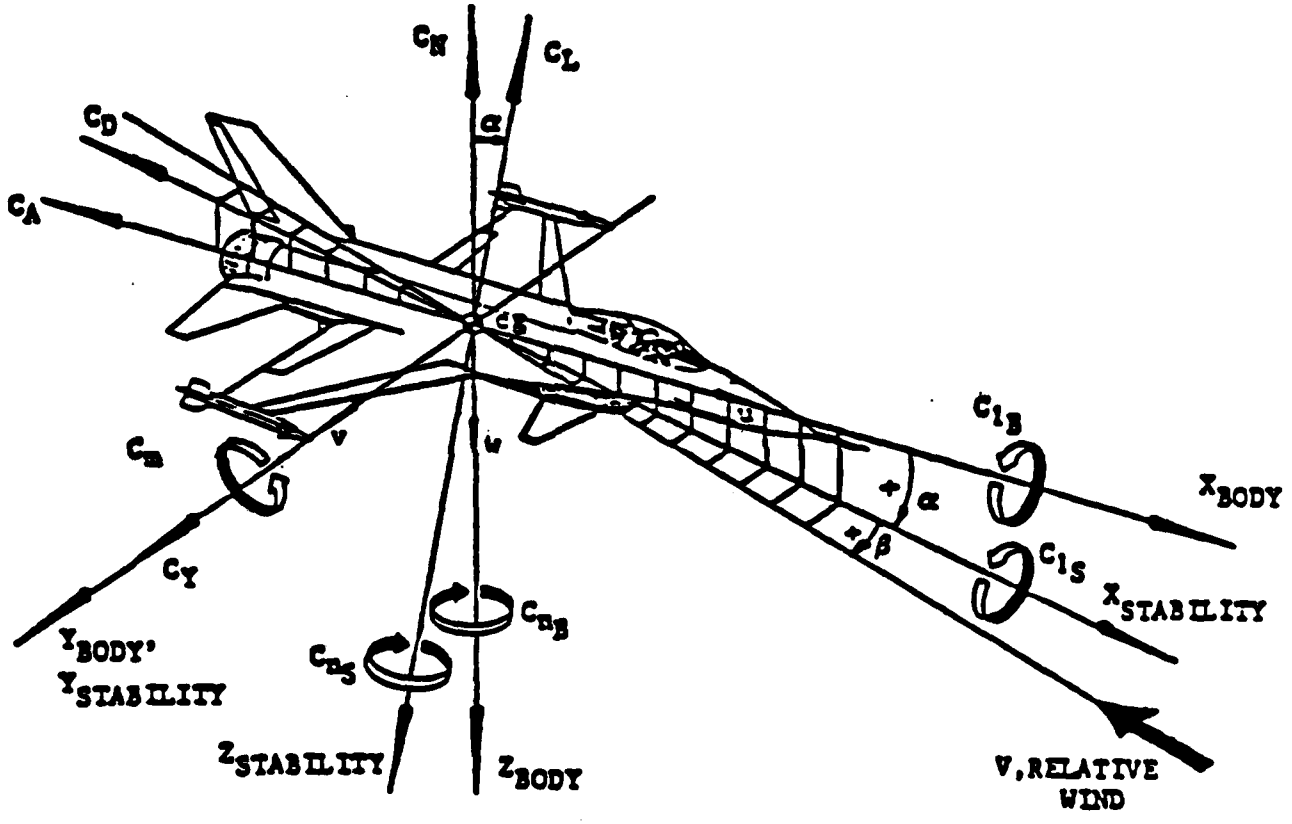



Figure 7. Axis Definition

stability analyses, it is often easier to convert a few inertia terms into stability axis data than to convert all of the aerodynamic derivatives into the body axis. Since the characteristic equation and corresponding aircraft roots are unaffected by this axis transformation, the determination of quantities such as short period damping can be made in either axis system.

However, as is shown later, there are major drawbacks to choosing the stability axis for design work. Conversion of inertia data to the stability axis yields numbers with no physical significance. In some cases, the converted products of inertia are negative. Thus, valuable insight into the mechanics of maneuvering flight needed by the design engineer is lost.

In fighter aircraft, fast rolls about the body axis at large angles of attack can result in unacceptably large sideslip angles. The design problem is to use body-sensed data in the flight control system to cause the aircraft to roll about the velocity vector. In this way, alpha remains essentially constant, and beta stays close to zero. If the design is accomplished in the stability axis, which is aligned with the velocity vector, rolling about the x axis produces the desired results. The signal being fed back to accomplish this is actually stability axis roll rate (a quantity which is not usually available within the flight control system). Thus, design in the stability axis can

lead to problems in implementation unless extreme care is taken. Designing in the body axis yields the same results but requires the engineer to explicitly attack the problem of obtaining an appropriate feedback signal. The signal must cause the proper rolling action with the available sensor information. As is shown later, this is usually accomplished by using body axis measurements of angle of attack, roll rate, yaw rate and side acceleration.

In this research, maneuvering flight characteristics are of primary interest. In elevated load factor or high "g" maneuvers, angle of attack can be a relatively large value, and the difference between body and stability axes becomes more significant. The body axis is chosen for this design for two main reasons in addition to those given in the previous discussions. First, the sensors providing feedback signals are actually measuring body accelerations and rates. Second, the pilot desires to control variables that he actually feels which are body accelerations and rates.

The transformation equations to convert to the body axis are based on data from Reference 20 and are given in Appendix B. The coefficients must also be dimensionalized for use in the equations of motion. These calculations are time-consuming and must be carried out for each flight condition being investigated. To aid in the conversion and transformation at a number of flight conditions, a computer

program called Conversion And Transformation (CAT) is developed to perform the necessary mathematical operations.

For the design effort, the equations of motion must be written as state equations in the form $\dot{\underline{x}} = \underline{A}\underline{x} + \underline{B}\underline{u}$. They represent a set of first-order differential equations. This operation is also carried out by the CAT program. The program's outputs are designated as primed derivatives. They are of the proper form to be directly inserted into the $\underline{A}$ matrix. The equations used in the conversion are presented in Appendix B. The computer listing is given in Appendix D.

The states in these equations do not include acceleration. Additional transformations are manually performed to obtain a state vector that includes accelerations at the pilot's station. The results of these transformations for the four flight conditions are listed in Appendix A. An example of the transformation method is shown below for the side velocity equation.

$$\dot{V} = \frac{\bar{q}S}{m}\left[C_{y_\beta}\beta + \{C_{y_{\dot{\beta}}}\dot{\beta} + C_{y_p}p + C_{y_r}r\}\frac{b}{2V_T} + C_{y_{\delta_a}}\delta_a + C_{y_{\delta_r}}\delta_r + C_{y_{\delta_c}}\delta_c\right] - rU + pW + g\cos\theta\sin\phi \quad (2.3)$$

or

$$\dot{V} = (Y_\beta)\beta + (Y_p)p + (Y_r)r + (Y_{\delta_a})\delta_a + (Y_{\delta_r})\delta_r + (Y_{\delta_c})\delta_c - rU + pW + g\cos\theta\sin\phi \quad (2.4)$$

Dividing by U and letting $\beta = V/U$, $\dot{\beta} = \dot{V}/U$, and $\alpha = W/U$ yields

$$\dot{\beta} = (\frac{Y_\beta}{U})\beta + (\frac{Y_p}{U})p + (\frac{Y_{\delta_a}}{U})\delta_a + (\frac{Y_{\delta_r}}{U})\delta_r + (\frac{Y_{\delta_c}}{U})\delta_c + (\frac{Y_r}{U})r - r + p\alpha + \frac{g}{U}\cos\theta\sin\phi \quad (2.5)$$

Also, let $\sin\phi = \phi$ in radians and $\alpha = 0.0$, which gives

$$\dot{\beta} = (\frac{Y_\beta}{U})\beta + (\frac{Y_p}{U})p + (\frac{Y_r}{U} - 1)r + (\frac{Y_{\delta_a}}{U})\delta_a + (\frac{Y_{\delta_r}}{U})\delta_r + (\frac{Y_{\delta_c}}{U})\delta_c + (g\frac{\cos\theta}{U})\phi \quad (2.6)$$

Redefining the coefficients yields

$$\dot{\beta} = (Y_\beta')\beta + (Y_p')p + (Y_r')r + (Y_{\delta_a}')\delta_a + (Y_{\delta_r}')\delta_r + (Y_{\delta_c}')\delta_c + (Y_\phi')\phi \quad (2.7)$$

These equations are simplified, and the restrictions discussed in Chapter I are applied. The resulting states represented by the simplified equations are pitch angle, forward velocity, angle of attack, and pitch rate in the longitudinal axis and roll angle, sideslip angle, roll rate, and yaw rate in the lateral-directional axes. In applying the restrictions, it is assumed that coupling between longitudinal, and lateral-directional axes can be neglected. Although this is not entirely correct for a high-performance fighter, the assumption is still generally applied in preliminary design efforts in order to simplify the problem. Exceptions are taken when necessary. Once a

preliminary design is complete, it is evaluated in a simulation with full nonlinear coupled equations of motion. Unfortunately, such an evaluation is beyond the scope of this research effort.

Acceleration at the pilot station is not one of the resulting states in the equations available for feedback design. Since this is a function which must be commanded, the solution to this dilemma is found by using the following relationships. The longitudinal force equation in the z body direction can be written as

$$F_{z_{cg}} = m(\dot{W} + pV - qU - g\cos\theta\cos\phi) \tag{2.8}$$

thus

$$A_{z_{cg}} = \frac{F_{z_{cg}}}{m} = \dot{W} + pV - qU - g\cos\theta\cos\phi \tag{2.9}$$

This is longitudinal acceleration in the z direction at the center of gravity. From Appendix B

$$\dot{W} = (Z_\alpha)\alpha + (Z_{\dot{\alpha}})\dot{\alpha} + (Z_q)q + (Z_u)\Delta U + (Z_{\delta_e})\delta_e + (Z_{\delta_f})\delta_f - pV + qU + g\sin\theta\cos\phi \tag{2.10}$$

Letting $\alpha = W/U$ and $\dot{\alpha} = \dot{W}/U$, this becomes

$$\dot{\alpha} = \left[\frac{1}{U}\right]\left[(Z_\alpha)\alpha + (Z_{\dot{\alpha}})\dot{\alpha} + (Z_q)q + (Z_u)\Delta U + (Z_{\delta_e})\delta_e + (Z_{\delta_f})\delta_f - pV + qU + g\sin\theta\cos\phi\right] \tag{2.11}$$

Gathering the terms with $\dot{\alpha}$ on the left-hand side of the equation yields

$$\dot{\alpha}(1 - \frac{Z_{\dot{\alpha}}}{U}) = \frac{1}{U}\,[(Z_{\alpha})\alpha + (Z_q)q + (Z_u)\Delta U + (Z_{\delta_e})\delta_e + (Z_{\delta_f})\delta_f - pV + qU + g\sin\theta\cos\phi] \quad (2.12)$$

Note: $\frac{Z_{\dot{\alpha}}}{U}$ is extremely small and is neglected.

From Equation (2.9)

$$A_{z_{cg}} = U(\dot{\alpha} + p\frac{V}{U} - q\frac{U}{U} - \frac{g}{U}\cos\theta\cos\phi) \quad (2.13)$$

and using Equation (2.12), gives

$$A_{z_{cg}} = U\{(\frac{1}{U})[(Z_{\alpha}\alpha + Z_q q + Z_u\Delta U + Z_{\delta e}\delta e + Z_{\delta f}\delta f - pV + qU + g\sin\theta\cos\phi)] + \frac{pV}{U} - \frac{qU}{U} - \frac{g}{U}\cos\theta\cos\phi\} \quad (2.14)$$

Simplification by cancelling terms yields

$$A_{z_{cg}} = (Z_{\alpha})\alpha + (Z_q)q + (Z_u)u + (Z_{\delta e})\delta e + (Z_{\delta f})\delta f \quad (2.15)$$

Acceleration at the center of gravity can be expressed as a combination of the available states previously defined plus contributions from the control surfaces. At this point, two methods of expressing acceleration in state space format are apparent.

The easiest and least complex method is to use the previously developed $\dot{\underline{x}} = \underline{A}\underline{x} + \underline{B}\underline{u}$ equations and form an output equation $\underline{y} = \underline{C}\underline{x} + \underline{D}\underline{u}$ where the output being sought is acceleration. The contributions from the control surfaces are included in the $\underline{D}$ matrix. The state space model has the form

$$\begin{bmatrix} \dot{\theta} \\ \dot{u} \\ \dot{\alpha} \\ \dot{q} \end{bmatrix} = \begin{bmatrix} 0 & 0 & 0 & 1 \\ X_\theta' & X_u' & X_\alpha' & X_q' \\ Z_\theta' & Z_u' & Z_\alpha' & Z_q' \\ M_\theta' & M_u' & M_\alpha' & M_q' \end{bmatrix} \begin{bmatrix} \theta \\ u \\ \alpha \\ q \end{bmatrix} + \begin{bmatrix} 0 & 0 \\ X_{\delta e}' & X_{\delta f}' \\ Z_{\delta e}' & Z_{\delta f}' \\ M_{\delta e}' & M_{\delta f}' \end{bmatrix} \begin{bmatrix} \delta e \\ \delta f \end{bmatrix} \tag{2.16}$$

$$\begin{bmatrix} A_{z_{cg}} \\ q \end{bmatrix} = \begin{bmatrix} 0 & Z_u & Z_\alpha & Z_q \\ 0 & 0 & 0 & 1 \end{bmatrix} \begin{bmatrix} \theta \\ u \\ \alpha \\ q \end{bmatrix} + \begin{bmatrix} Z_{\delta e} & Z_{\delta f} \\ 0 & 0 \end{bmatrix} \begin{bmatrix} \delta e \\ \delta f \end{bmatrix} \tag{2.17}$$

Unfortunately, the design method used in this report does not consider a $\underline{D}$ matrix. The problem is, therefore, to develop the equations of motion with a zero $\underline{D}$ matrix but with the contributions from the control surfaces included. The method used in this design effort is to augment the $\underline{A}$ matrix with the actuator states. In this manner an augmented state vector is produced which includes surface deflection as shown below. Using a first-order actuator transfer function model of $[20/(s+20)]$ for both the elevator and

flaperon surfaces results in the following equations.

$$\delta e = \left[\frac{20}{s + 20}\right] \delta e_{cmd} \tag{2.18}$$

$$\delta e(s + 20) = 20\ \delta e_{cmd} \tag{2.19}$$

$$\delta \dot{e} + 20\ \delta e = 20\ \delta e_{cmd} \tag{2.20}$$

$$\delta \dot{e} = -20\ \delta e + 20\ \delta e_{cmd} \tag{2.21}$$

In a similar computation, the flaperon actuator model results in a first-order equation of $\delta \dot{f} = -20\ \delta f + 20\ \delta f_{cmd}$. The input vector $\underline{u}$ is now the actuator command instead of surface position as shown previously. The state and output equations are

$$\begin{bmatrix} \dot{\theta} \\ \dot{u} \\ \dot{\alpha} \\ \dot{q} \\ \delta\dot{e} \\ \delta\dot{f} \end{bmatrix} = \begin{bmatrix} 0 & 0 & 0 & 1 & 0 & 0 \\ X_\theta' & X_u' & X_\alpha' & X_q' & X_{\delta e}' & X_{\delta f}' \\ Z_\theta' & Z_u' & Z_\alpha' & Z_q' & Z_{\delta e}' & Z_{\delta f}' \\ M_\theta' & M_u' & M_\alpha' & M_q' & M_{\delta e}' & M_{\delta f}' \\ 0 & 0 & 0 & 0 & -20 & 0 \\ 0 & 0 & 0 & 0 & 0 & -20 \end{bmatrix} \begin{bmatrix} \theta \\ u \\ \alpha \\ q \\ \delta e \\ \delta f \end{bmatrix} + \begin{bmatrix} 0 & 0 \\ 0 & 0 \\ 0 & 0 \\ 0 & 0 \\ 20 & 0 \\ 0 & 20 \end{bmatrix} \begin{bmatrix} \delta e_{cmd} \\ \delta f_{cmd} \end{bmatrix} \tag{2.22}$$

$$\begin{bmatrix} A_{z_{cg}} \\ q \end{bmatrix} = \begin{bmatrix} 0 & Z_u & Z_\alpha & Z_q & Z_{\delta e} & Z_{\delta f} \\ 0 & 0 & 0 & 1 & 0 & 0 \end{bmatrix} [\theta\ \ u\ \ \alpha\ \ q\ \ \delta e\ \ \delta f]^T \tag{2.23}$$

In this case, $A_{z_{cg}}$ can be controlled as an output of the system without having a $\underline{D}$ matrix. Unfortunately, to develop the output requires a combination of all but one longitudinal state. At this point a transformation is employed to provide $A_{z_{cg}}$ as a state in place of angle of attack. As shown earlier,

$$A_{z_{cg}} = Z_\alpha \alpha + Z_q q + Z_u u + Z_{\delta e} \delta e + Z_{\delta f} \tag{2.15}$$

thus

$$\begin{bmatrix} \theta \\ u \\ A_{z_{cg}} \\ q \\ \delta e \\ \delta f \end{bmatrix} = \begin{bmatrix} 1 & 0 & 0 & 0 & 0 & 0 \\ 0 & 1 & 0 & 0 & 0 & 0 \\ 0 & Z_u & Z_\alpha & Z_q & Z_{\delta e} & Z_{\delta f} \\ 0 & 0 & 0 & 1 & 0 & 0 \\ 0 & 0 & 0 & 0 & 1 & 0 \\ 0 & 0 & 0 & 0 & 0 & 1 \end{bmatrix} \begin{bmatrix} \theta \\ u \\ \alpha \\ q \\ \delta e \\ \delta f \end{bmatrix} \tag{2.24}$$

$\underline{z}$ $\underline{T}$ $\underline{x}$

$\underline{z} = \underline{T}\underline{x}$ where $\underline{T}$ is a transformation matrix to develop a $\underline{z}$ state vector containing $A_{z_{cg}}$ from the original state vector $\underline{x}$. The complete set of equations is transformed using $\underline{x} = \underline{T}^{-1}\underline{z}$. Thus

$$\dot{\underline{x}} = \underline{A}\underline{x} + \underline{B}\underline{u} \tag{2.25}$$

$$\underline{T}^{-1}\dot{\underline{z}} = \underline{A}\underline{T}^{-1}\underline{z} + \underline{B}\underline{u} \tag{2.26}$$

$$\dot{\underline{z}} = \underline{T}\underline{A}\underline{T}^{-1}\underline{z} + \underline{T}\underline{B}\underline{u} \tag{2.27}$$

and $$\underline{y} = \underline{C}\underline{x} \tag{2.28}$$

$$\underline{y} = \underline{C}\underline{T}^{-1}\underline{z} \tag{2.29}$$

The output equation is actually not needed. It gives the relationship for expressing the old states as a linearized combination of the new states. Since interest is in the acceleration as an output and a state, a new $\underline{C}$ matrix is formed to allow using $A_{z_{cg}}$ as a feedback.

Acceleration at another point on the aircraft other than the center of gravity can be computed as follows:

Note: $A_n = -A_z$ (2.30)

$$A_n = A_{n_{cg}} - (\ell_x)(pr - \dot{q}) - (\ell_y)(rq + \dot{p}) + (\ell_z)(p^2 + q^2) \tag{2.31}$$

where $\ell_x$, $\ell_y$, and $\ell_z$ are distances in the body axis from the point to the center of gravity.

Since $\ell_y$ and $\ell_z$ are much smaller than $\ell_x$ for the AFTI vehicle and since the assumption is made that the longitudinal and lateral-directional axes can be decoupled, the equation reduces to

$$A_n = A_{n_{cg}} + (\ell_x)\dot{q} \tag{2.32}$$

The units are ft/sec$^2$ for acceleration, feet for the $\ell_x$ distance, and rad/sec$^2$ for the rotational acceleration term ($\dot{q}$). In a similar manner, the lateral acceleration at a point

other than the center of gravity is computed as

$$A_y = A_{y_{cg}} - (\ell_x)(pq - \dot{r}) - (\ell_y)(p^2 + r^2) + (\ell_z)(qr - \dot{p}) \qquad (2.33)$$

which, using the same assumptions, becomes

$$A_y = A_{y_{cg}} + (\ell_x)\,\dot{r} \qquad (2.34)$$

Equations (2.32) and (2.34) are used to develop relationships for acceleration at the pilot's station in the aircraft. Since acceleration at the center of gravity is now a state and the equations developed from the last transformation give $\dot{q}$ as a summation of the new state vector $\underline{z}$, a final transformation can be made to obtain accelerations at the pilot's station for the z and y axes.

An example of the transformations at the design points of 0.9 Mach and 20,000 feet is presented below for the longitudinal axis. The complete transformations for this point are given in Appendix B. For the other flight conditions, only the final resulting state equations are listed in the appendix in the interest of brevity. The same transformation method is used in each case.

Using the primed aerodynamic coefficients from the CAT program, the following state equation is developed.

$$\begin{bmatrix} \dot{\theta} \\ \dot{u} \\ \dot{\alpha} \\ \dot{q} \\ \dot{\delta e} \\ \dot{\delta f} \end{bmatrix} = \begin{bmatrix} 0 & 0 & 0 & 1 & 0 & 0 \\ -32.1831 & -0.0120748 & 38.2418 & -30.135 & 2.001 & 2.3087 \\ -0.0011187 & -0.000022 & -1.4845 & 0.994789 & -0.149227 & -0.244924 \\ 0.0003086 & -0.00013 & 4.27172 & -0.777221 & -24.0581 & -6.47269 \\ 0 & 0 & 0 & 0 & -20 & 0 \\ 0 & 0 & 0 & 0 & 0 & -20 \end{bmatrix} \begin{bmatrix} \theta \\ U \\ \alpha \\ q \\ \delta e \\ \delta f \end{bmatrix} + \begin{bmatrix} 0 & 0 \\ 0 & 0 \\ 0 & 0 \\ 0 & 0 \\ 20 & 0 \\ 0 & 20 \end{bmatrix} \begin{bmatrix} \delta e_{cmd} \\ \delta f_{cmd} \end{bmatrix}$$

(2.35)

From the unprimed dimensional coefficients, the $\underline{T}_1$ matrix is formed.

$$\underline{T}_1 = \begin{bmatrix} 1 & 0 & 0 & 0 & 0 & 0 \\ 0 & 1 & 0 & 0 & 0 & 0 \\ 0 & -0.0207687 & -1385.34 & -4.86336 & -139.263 & -228.57 \\ 0 & 0 & 0 & 1 & 0 & 0 \\ 0 & 0 & 0 & 0 & 1 & 0 \\ 0 & 0 & 0 & 0 & 0 & 1 \end{bmatrix}$$

(2.36)

Performing the transformation yields the following state equations.

$$\begin{bmatrix} \dot{\theta} \\ \dot{u} \\ \dot{A}_{z_{cg}} \\ \dot{q} \\ \dot{\delta e} \\ \dot{\delta f} \end{bmatrix} = \left[\begin{array}{cccc:cc} 0 & 0 & 0 & 1 & 0 & 0 \\ -32.18 & -0.01265 & -0.02760 & -30.27 & -1.843 & -4.0 \\ 2.311 & 0.001208 & -1.469 & -1381 & 2904 & 4606 \\ 0.000309 & -0.000194 & -0.003084 & -0.7922 & -24.49 & -7.177 \\ \hdashline 0 & 0 & 0 & 0 & -20 & 0 \\ 0 & 0 & 0 & 0 & 0 & -20 \end{array}\right] \begin{bmatrix} \theta \\ U \\ A_{z_{cg}} \\ q \\ \delta e \\ \delta f \end{bmatrix} + \left[\begin{array}{cc} 0 & 0 \\ 0 & 0 \\ -2785 & -4571 \\ 0 & 0 \\ \hdashline 20 & 0 \\ 0 & 20 \end{array}\right] \begin{bmatrix} \delta e_{cmd} \\ \delta f_{cmd} \end{bmatrix}$$

(2.37)

Using the $\dot{q}$ expression from this state matrix in Eq. (2.32) results in the expression for acceleration at the pilot's station.

$$A_{n_p} = A_{n_{cg}} + [\ell_x] \begin{bmatrix} 0.000309 & -0.000194 & -0.003084 & -0.7922 & -24.49 & -7.177 \end{bmatrix} \begin{bmatrix} \theta \\ u \\ A_{n_{cg}} \\ q \\ \delta e \\ \delta f \end{bmatrix} \tag{2.38}$$

where $\ell_x = 13.95$ ft (2.39)

With Eq. (2.9), an expression can be developed for $\dot{\alpha}$ using the states available after the last transformation. Assuming $pV = 0$ and $\phi = 0$ results in

$$A_{z_{cg}} = \dot{W} - qU - g\cos\theta \tag{2.40}$$

Dividing by forward velocity, U, and letting $\alpha = \frac{W}{U}$ gives

$$\frac{A_{z_{cg}}}{U} = \dot{\alpha} - q - \frac{g}{U}\cos\theta \tag{2.41}$$

Solving for $\dot{\alpha}$ yields

$$\dot{\alpha} = \frac{A_{z_{cg}} + g\cos\theta}{U} + q \tag{2.42}$$

Expressed using incremental acceleration from 1g trimmed flight, the equation becomes

$$\dot{\alpha} = \frac{A_{z_{cg}}}{U} + q \tag{2.43}$$

The $\dot{\alpha}$ equation is added to the state equations, and a second transformation matrix $T_2$ is formed from Eq. (2.38).

Thus,

$$\begin{bmatrix} \dot{\alpha} \\ \dot{\theta} \\ \dot{u} \\ \dot{A}_{z_{cg}} \\ \dot{q} \\ \dot{\delta e} \\ \dot{\delta f} \end{bmatrix} = \begin{bmatrix} 0 & 0 & 0 & 0.001072 & 1 & 0 & 0 \\ 0 & 0 & 0 & 0 & 1 & 0 & 0 \\ 0 & -32.18 & -0.01265 & -0.0276 & -30.27 & -1.843 & -4.0 \\ 0 & 2.311 & 0.001208 & -1.469 & -1387 & 2904 & 4606 \\ 0 & 0.000309 & -0.000194 & -0.003084 & -0.7922 & -24.49 & -7.177 \\ 0 & 0 & 0 & 0 & 0 & -20 & 0 \\ 0 & 0 & 0 & 0 & 0 & 0 & -20 \end{bmatrix} \begin{bmatrix} \alpha \\ \theta \\ u \\ A_{z_{cg}} \\ q \\ \delta e \\ \delta f \end{bmatrix} + \begin{bmatrix} 0 & 0 \\ 0 & 0 \\ 0 & 0 \\ -2785 & -4571 \\ 0 & 0 \\ 20 & 0 \\ 0 & 20 \end{bmatrix} \begin{bmatrix} \delta e_{cmd} \\ \delta f_{cmd} \end{bmatrix}$$

(2.44)

and

$$\underline{I}_2 = \begin{bmatrix} 1 & 0 & 0 & 0 & 0 & 0 & 0 \\ 0 & 1 & 0 & 0 & 0 & 0 & 0 \\ 0 & 0 & 1 & 0 & 0 & 0 & 0 \\ 0 & -0.00431 & 0.00271 & 1.043 & 11.05 & 341.64 & 100.12 \\ 0 & 0 & 0 & 0 & 1 & 0 & 0 \\ 0 & 0 & 0 & 0 & 0 & 1 & 0 \\ 0 & 0 & 0 & 0 & 0 & 0 & 1 \end{bmatrix}$$

(2.45)

The transformation results in

$$\begin{bmatrix} \dot{\alpha} \\ \dot{\theta} \\ \dot{u} \\ \dot{A}_{z_p} \\ \dot{q} \\ \dot{\delta e} \\ \dot{\delta f} \end{bmatrix} = \begin{bmatrix} 0 & 0 & 0 & 0.001028 & 0.989 & -0.3511 & -0.1029 \\ 0 & 0 & 0 & 0 & 1 & 0 & 0 \\ 0 & -32.18 & -0.01258 & -0.02646 & -29.98 & 7.198 & -1.351 \\ 0 & 2.32 & 0.003152 & -1.502 & -1439 & -3562 & 2873 \\ 0 & 0.00030 & -0.000186 & -0.002957 & -0.7595 & -23.48 & -6.881 \\ 0 & 0 & 0 & 0 & 0 & -20 & 0 \\ 0 & 0 & 0 & 0 & 0 & 0 & -20 \end{bmatrix} \begin{bmatrix} \alpha \\ \theta \\ u \\ A_{z_p} \\ q \\ \delta e \\ \delta f \end{bmatrix} + \begin{bmatrix} 0 & 0 \\ 0 & 0 \\ 0 & 0 \\ 3928 & -2766 \\ 0 & 0 \\ 20 & 0 \\ 0 & 20 \end{bmatrix} \begin{bmatrix} \delta e_{cmd} \\ \delta f_{cmd} \end{bmatrix}$$

(2.46)

and the output equation is:

$$\begin{bmatrix} A_{z_p} \\ q \end{bmatrix} = \begin{bmatrix} 0 & 0 & 0 & 1 & 0 & 0 & 0 \\ 0 & 0 & 0 & 0 & 1 & 0 & 0 \end{bmatrix} = [\alpha \ \theta \ u \ A_{z_p} \ q \ \delta e \ \delta f]^T \tag{2.47}$$

The transformation to acceleration at the aircraft center of gravity is performed as an intermediate step at which point the $\dot{\alpha}$ equation is added. The same results are obtained by writing the $\dot{\alpha}$ equation twice in the original system equations and forming a combined transformation matrix to directly obtain acceleration at the pilot's station from Eqs. (2.15) and (2.32) as follows:

$$A_{n_p} = A_{n_{cg}} + \ell_x(\dot{q}) \tag{2.48}$$

and

$$A_{n_{cg}} = -A_{z_{cg}} = -Z_\alpha \alpha - Z_q q - Z_u u - Z_{\delta e}\delta e - Z_{\delta f}\delta f \tag{2.49}$$

Both $A_{n_{cg}}$ and $\dot{q}$ are expressed as combinations of the original state variables and can be combined to yield:

$$\begin{aligned} A_{n_p} = {} & (\ell_x M_\theta')\theta + (\ell_x M_u' - Z_u)\Delta U + (\ell_x M_\alpha' - Z_\alpha)\alpha \\ & + (\ell_x M_q' - Z_q)q + (\ell_x M_{\delta e}' - Z_{\delta e})\delta e \\ & + (\ell_x M_{\delta f}' - Z_{\delta f})\delta f \end{aligned} \tag{2.50}$$

Thus,

$$\begin{bmatrix} \alpha \\ \theta \\ u \\ A_{n_p} \\ q \\ \delta e \\ \delta f \end{bmatrix} = \begin{bmatrix} 1 & 0 & 0 & 0 & 0 & 0 & 0 \\ 0 & 1 & 0 & 0 & 0 & 0 & 0 \\ 0 & 0 & 1 & 0 & 0 & 0 & 0 \\ 0 & (\ell_x M_\theta{}') & (\ell_x M_u{}'-Z_u) & (\ell_x M_\alpha{}'-Z_\alpha) & (\ell_x M_q{}'-Z_q) & (\ell_x M_{\delta e}{}'-Z_{\delta e}) & (\ell_x M_{\delta f}{}'-Z_{\delta f}) \\ 0 & 0 & 0 & 0 & 1 & 0 & 0 \\ 0 & 0 & 0 & 0 & 0 & 1 & 0 \\ 0 & 0 & 0 & 0 & 0 & 0 & 1 \end{bmatrix} \begin{bmatrix} \alpha \\ \theta \\ u \\ \alpha \\ q \\ \delta e \\ \delta f \end{bmatrix} \tag{2.51}$$

This method is used on all subsequent transformations to develop pilot station acceleration as a state. In either method of arriving at this final state vector, the addition of the $\dot{\alpha}$ equation results in a transmission zero at the origin. The significance of transmission zeros is discussed in Chapter III. This does not affect the designs that are developed. They are evaluated with and without the $\dot{\alpha}$ equation. Transfer function checks show that with the inclusion of the $\dot{\alpha}$ equation both a pole and a zero are added to the system at the origin. This pole-zero combination cancels and contributes nothing to the output responses.

The equations are modified to have states, inputs and outputs in convenient units such as "g" for accelerations and degrees for surface deflections. In the resulting system equations, the B matrix is partitioned as shown below.

$$\underline{B} = \begin{bmatrix} 0 & 0 \\ 0 & 0 \\ 0 & 0 \\ 2.129 & -1.499 \\ 0 & 0 \\ \hline 20 & 0 \\ 0 & 20 \end{bmatrix} = \begin{bmatrix} \\ \underline{B}_1 \\ \\ \\ \hline \\ \underline{B}_2 \end{bmatrix} \qquad (2.52)$$

The row dimension of $\underline{B}_2$ is equal to the number of inputs or, in this case, surface commands. Thus, it is always a square matrix. For the design work, the system is transformed once more so that $\underline{B}_1$ is a zero matrix. Such an arrangement is hereafter referred to as the zero-$B_2$ form. Although not necessary for application of the design principles, this conversion is accomplished for the following reasons.

First, a knowledge of the location of transmission zeros of the system is desired. A relatively simple and reliable means of calculating transmission zeros is available for systems in the zero-$B_2$ form (Ref 6). The method of computation of transmission zeros is discussed in Chapter III. This method is computerized using macro programming of the TOTAL program. A listing of the macro program is included in Appendix E.

The second reason is based on a previous unfortunate implementation of the design equations in the MULTI program which has been corrected at the time of this report. The problem is discussed in Chapter IV after the design

equations are presented in Chapter III. With the original MULTI program, the design obtained without this last transformation results in a system that is not adequately decoupled to meet the design objectives.

A note of caution is necessary at this point. Transformation to the zero-$B_2$ form results in a new set of states. Unfortunately, pilot station acceleration is altered by the transformation. Since this is one of the states to be used for feedback, the design implementation is unduly complicated. With the modified MULTI program, the same design results can be obtained without transformation to this form. It is advantageous to design with $A_{n_p}$ and $A_{y_p}$ as states and to transform the final design only to check for transmission zeros which are not altered by such transformations.

## Validation Methods

One major concern in the development of the linear models for multivariable designs is the complexity of performing multiple conversions and transformations. Each operation can become a source of errors. Validation of the final model as a true representation of the aircraft becomes a paramount issue. Such validation is handled in the following manner.

The linearized aerodynamic data obtained from General Dynamics are checked for reasonableness of coefficient values. Any discrepancies are checked with the nonlinear

data plots available in the AFTI/F-16 ADPO. All discrepancies are resolved with the help of ADPO engineers.

The linearized data is used as input for the Transfer Function Program (TRANSF). This is an ADPO program that is available at AFIT. The program allows direct input of the data and provides stability axis transfer functions for each aircraft state to surface input. These are open-loop or unaugmented aircraft transfer functions. The results are compared with known aircraft data developed by General Dynamics such as longitudinal static stability and dutch roll damping at each flight condition.

Since linear transformations do not change a system's characteristic equation, this provides a general test of each transformation in the development of the desired state-space model. In addition, the transformations are hand calculated for one case and used to check each computer operation. The actual sequence consists of using the CAT program to go from nondimensional coefficients to dimensional body axis "primed" derivatives for the $\underline{A}$ matrix. The system states available at this point are shown below.

$$\underline{x}(\text{Long.}) = \begin{bmatrix} \theta \\ u \\ \alpha \\ q \end{bmatrix} \quad \text{and} \quad \underline{x}(\text{Lat.-Dir.}) = \begin{bmatrix} \phi \\ \beta \\ p \\ r \end{bmatrix} \tag{2.53}$$

The $\underline{A}$ matrix is then augmented to include the actuator states assuming a first-order actuator. The state vectors are now

$$\underline{x}(\text{Long.}) = \begin{bmatrix} \theta \\ u \\ \alpha \\ q \\ \delta e \\ \delta f \end{bmatrix} \qquad \underline{x}(\text{Lat.-Dir.}) = \begin{bmatrix} \phi \\ \beta \\ p \\ r \\ \delta a \\ \delta r \\ \delta c \end{bmatrix} \tag{2.54}$$

This system is then transformed to include accelerations at the center of gravity as previously discussed and finally transformed to acceleration at the pilot's station. The last transformations have replaced angle of attack and sideslip with longitudinal and side acceleration. Both angle of attack and sideslip are important parameters to monitor in maneuvering flight. To allow this, two new equations are added that express alpha and beta as a combination of the existing states. The final resulting state vectors are shown below.

$$\underline{x}(\text{Long.}) = \begin{bmatrix} \alpha \\ \theta \\ U \\ A_{n_p} \\ q \\ \delta e \\ \delta f \end{bmatrix} \qquad \underline{x}(\text{Lat.-Dir.}) = \begin{bmatrix} \beta \\ \phi \\ A_{y_p} \\ p \\ r \\ \delta a \\ \delta r \\ \delta c \end{bmatrix} \tag{2.55}$$

The TOTAL program is employed to perform the above transformations. System transfer functions are checked after every transformation. The transformations can be combined to simplify the effort. This is also done for each of the other flight conditions. Finally, prior to design, the state model is altered to provide the states, inputs, and outputs in convenient units. Accelerations are expressed in "g" units; rates are given in degrees per second; angles and surface deflections are in degrees; and velocities have units of feet per second. Transformation to zero-$B_2$ form is accomplished and results in the following set of states.

$$\underline{x}(\text{Long.}) = \begin{bmatrix} \alpha \\ \theta \\ U \\ A_{n_p} + K_1\delta e + K_2\delta f \\ q \\ \delta e \\ \delta f \end{bmatrix} \tag{2.56}$$

$$\underline{x}(\text{Lat.-Dir.}) = \begin{bmatrix} \beta \\ \phi \\ A_{y_p} + K_3\delta a + K_4\delta r + K_5\delta r \\ p \\ r \\ \delta a \\ \delta r \\ \delta c \end{bmatrix} \tag{2.57}$$

Chapter 3, Design Theory, Omitted

See Proceedings

# IV. Philosophy and Details of the Design Method

## Requirements

The following requirements must be satisfied in applying the design method:

1. The number of inputs must equal the number of outputs.

2. The system must be controllable and observable.

3. All transmission zeros must be stable.

4. Integral plus proportional control is applied to all forward loop signals.

Each of these requirements is considered in detail in the following paragraphs.

## Inputs and Outputs

The "inputs" refer to the number of controls that can be commanded to alter the aircraft's states. These are inputs to the aerodynamic (plant) model. For the AFTI/F-16 longitudinal case, the inputs consist of the flaperon and the horizontal tail (elevator) surface positions. For the lateral-directional case, they are the canard, aileron and rudder surface positions. These are designated by the $\underline{u}$ vector in the system equation. The "outputs" are the variables contained in the $\underline{y}$ vector and are the responses which are to be controlled. The outputs can be states of the

system or linear combinations of states. For this study, two sets of outputs for the longitudinal axis are considered. The first set is angle of attack and pitch rate. The second set consists of normal acceleration at the pilot's station and pitch rate. The lateral-directional outputs are chosen to be side acceleration at the pilot's station, roll rate, and yaw rate. An explanation of this selection is given in the design procedure section.

For each aircraft response that is to be independently controlled, a separate surface must be available. This is a requirement for a decoupled response and is independent of the design method. For a conventional pull up, only one surface is employed, the elevator, and the pilot has independent control of one aircraft state, normal acceleration. The angle of attack and pitch rate, which are developed, are directly related to the normal acceleration being commanded. In order to independently control both acceleration and angle of attack for a decoupled response such as Direct Lift, the use of an additional control surface, the flaperon, is required. A direct lift force can be developed with the flaps without rotating the aircraft, since the moments generated by the flaps are balanced by the elevator. Thus, to enable control of two outputs (responses), two inputs (surfaces) are required. This holds true for the multivariable techniques employed in this thesis. The procedure for selection of the proper commands for each control

parameter in order to perform specified maneuvers is discussed in detail later in the chapter.

Controllability and Observability

Controllability and observability are properties of the state-space representation of a system. Controllability implies that the inputs can affect each mode of the system. For a time invariant linear system, controllability can be checked by evaluating the rank of the controllability matrix $\underline{M}_c$ (Ref 11) where

$$\text{Rank } \underline{M}_c = \text{Rank } [\ \underline{B} \quad \underline{AB} \quad \ldots \quad \underline{A}^{n-1}\underline{B}\ ] = n$$

Observability implies that the outputs are affected by every mode. It also implies that the effects on the outputs of one state variable can be distinguished from the effects of other state variables. For a time invariant linear system, this property can be determined by evaluating the rank of the observability matrix $\underline{M}_o$, (Ref 11) where

$$\text{Rank } \underline{M}_o = \text{Rank } [\ \underline{C}^T \quad \underline{A}^T\underline{C}^T \quad \ldots \quad \underline{A}^{T(n-1)}\underline{C}^T\ ] = n$$

Controllability and observability are evaluated for each design. This is accomplished by employing the CESA (Ref 12) computer-aided design package available as an AFIT program on the CDC6600 system. In cases where the criteria are not met, the system model is redefined until controllability and observability are achieved. The majority of the

cases under investigation are found to be controllable and observable.

Transmission Zeros

As discussed in Chapter III, transmission zeros of the system are considered as regions toward which system roots migrate with increasing gain. As gain approaches infinity or sampling time approaches zero, the affected roots asymptotically approach the transmission zero locations. Output feedback does not alter transmission zeros. In the strictest sense, it is desired that all such zeros be stable in order to insure system stability with high gain. Such a selection does not guarantee stability for all system gain values since the locus of system roots may journey into the unstable region before arriving in the vicinity of the transmission zeros. Thus, for stable transmission zeros, stable operation is only assured for gain values approaching infinity. A controller design for a system with unstable transmission zeros can be developed with these techniques, but in such cases an upper gain boundary is established to prevent system roots from moving into the unstable region. Thus, the restriction is not absolute; however, failing to meet it does impose additional design considerations.

For irregular designs, when $\underline{CB}$ does not have full rank, additional transmission zeros are introduced by the measurement matrix $\underline{M}$. These can be altered by changing the matrix elements. If the measurement matrix is very sparse,

the location of the additional transmission zeros in the s-plane is the inverse of the values of the elements in the measurement matrix. Thus, a 0.25 element in the measurement matrix produces a transmission zero at -4.0 in the s-plane. This simple relationship breaks down as the number of measurement matrix elements increases. Reference 9 provides a guide to the selection of the measurement matrix. A computerized method to directly calculate the transmission zero locations is developed using equations from Reference 6 and macro programming of TOTAL. The program is discussed later in the report and is listed in Appendix E.

At this point the concept of global stability is considered, and its influence in the design method examined. Global stability or "bounded input-bounded output" stability implies that for any and all bounded inputs to a system, the outputs are also bounded. Because of the assumptions made in the equation development, controlling angular rate and acceleration results in the existence of a transmission zero at the origin. This is one of the major reasons previous efforts have not pursued rate or acceleration controllers. As discussed previously, controllers of this type are desired for fighter aircraft, and classical experience shows that such designs perform very well. The question that must be answered is, "Is global stability necessary?" By carefully considering the dynamics of a maneuver, the answer is a resounding no. For example, the transmission zero at the

origin results in an unbounded pitch attitude ($\theta$) response for a bounded pitch rate (q) input. This is exactly what is sought. For the simplified equations, the pitch angle is the integral of pitch rate, and thus a pitch rate step command should cause the pitch angle to ramp to infinity. For all other conceivable inputs, this is the only "unbounded output." The integration due to a pole located exactly at the transmission zero causes the unbounded output and is both predictable and desirable. In conventional fighter aircraft, a step change or bounded output of pitch attitude is manually obtained by the pilot developing a pitch rate and then reducing it to zero through the use of a pulse input.

In conclusion, for this application to the aircraft control problem, a transmission zero at the origin is not only acceptable but highly desirable. The system is considered conditionally stable, and such stability is appropriate for the designs under study. In all cases, any instability encountered during the design work is investigated to define its cause. Also, gain and phase margins are established for the system which must be met both analytically and by test of the actual implementation. This approach is used for classical designs, and the military specification governing control system design, MIL-F-9490D, establishes such margins for a system. Those margins are adopted for use in this investigation.

It is of interest to consider "guaranteed stability." Much has been said in the literature about control design methods that guarantee stability. If a set of conditions is met, then the system is always stable. Such a guarantee has been espoused as a major advantage for designs developed by linear quadratic methods (either the deterministic LQR or the nondeterministic LQG approach). In these approaches, the stability is "guaranteed" only for full state feedback. Such full state feedback is almost impossible to implement. States not contributing significantly to the response are generally eliminated to arrive at a practical design. In addition, a model of the process to be controlled is developed for design. As long as the model and process are exactly the same, and assuming full state feedback, stability is guaranteed. For aircraft applications, such models are only approximations to the real aircraft. Stability is not guaranteed for processes which do not exactly match the design model.

Early in a design cycle, such "guaranteed stability" is useful since the engineer does not have to continually check stability margins for each proposed concept. However, at this point the models are usually very simple, and an evaluation of stability is not a difficult task. Later in the cycle, when the full plant is considered with its inherent nonlinearities, stability checks must be made irrespective of any implied guarantee. The advantage of

guaranteed stability is more an academic nicety than a practical design benefit. For any realistic flight control application, gain and phase margins are specified, and testing is accomplished to prove compliance.

## Integral Plus Proportional Compensation

The requirement of integral plus proportional control on all forward loops is not considered a severe restraint. In fighter aircraft applications, integral plus porportional compensation is generally used in the pitch axis for the primary variable controlled by the pilot. For aircraft such as the F-16, this variable is normal acceleration. Pitch rate and angle of attack are fed back to tailor the response and to augment stability. Their values are not directly commanded by the pilot. The relationship between pitch rate, angle of attack, and acceleration varies with flight condition. This variation is natural for a pilot and provides a cue to his operating point in the flight envelope. Thus, use of integral plus proportional compensation is generally not necessary for these feedbacks. In the roll axis, a roll rate command system is used, but the response to a pilot input changes with flight conditions. Again, this variation is generally very natural for the pilot, and such compensation is not needed.

In redundant control systems, the integrators must be equalized. Consider the F-16 again as an example. The pitch axis has four separate but identical control channels

with exactly the same feedbacks. Four integral plus proportional networks exist in the path from pilot input to surface command; however, due to the signal selection method, multiple duplicates of only one channel are actually controlling the aircraft. The others are active and provide comparison signals with the ability to instantaneously take over control in the event of a failure. With such an arrangement, only one of the integrators can actually drive its input to zero by matching the aircraft's response to the pilot's command.

Although all the channels are trying to provide the same control, tolerance differences in the components in each channel cause the signals to be slightly different. The inputs to the three integrators that are not in direct control never go completely to zero.

With a constant input, these integrators ramp to infinity. In real applications, they simply saturate. The solution of the dilemma is to have the integrators equalize one another. Such equalization, although necessary, adds complexity. It also creates points in an otherwise separated system where failures can be propagated from one channel to another.

Thus, the addition of integral plus proportional compensation where it is not entirely necessary, increases complexity, and may endanger redundancy. Only through more complexity and a substantial amount of additional testing

can the integrity of the redundant system be preserved. As noted above, use of the compensation on all forward control paths can remove useful cues from the pilot relating to flight condition by forcing the steady-state response to equal the command.

When decoupled operation is desired, the addition of integrators to the forward paths is highly desirable. This is because, in such decoupling, several parameters must be exactly controlled. The use of integral plus proportional compensation on each forward signal path insures that the specified values commanded are reached in steady state.

Unfortunately, the decoupled capabilities are only auxiliary flight modes that aid in certain specific tasks. They are limited in authority and do not replace conventional controls, only augment them. For this reason, the requirement for integral plus proportional compensation on all feed forward paths may be a disadvantage.

## A Design Procedure

A procedure for developing a design is established, based on the efforts in this thesis. The basic steps in this procedure are outlined below and are then discussed in detail.

1. Formulate the aircraft design model into the proper format.

2. Validate the model.

3. Select the outputs to be controlled and the feedback signals that are required.

4. Check controllability and observability.

5. Calculate the transmission zeros and select the measurement matrix.

6. Estimate the maximum maneuvers.

7. Scale gains for stable response.

8. Vary weighting matrix elements for desired responses and to meet control input restraints.

9. Adjust proportional plus integral gain for timely steady-state behavior.

The Aircraft Model

Chapter II covers the formulation of an aircraft model in state space format necessary for this design application. It also covers the methods used to validate the model. These are two extremely important and usually error prone steps in the design process. Time spent in developing a controller design is wasted effort if the model for the plant is not an adequate representation. Each step in the model development must be checked and rechecked for accuracy. Automated methods are extremely useful in actual design efforts since multiple point designs at a number of flight conditions are accomplished. The model development for each of these points is usually very similar. However, such programs must themselves be adequately validated.

## Output Feedback Choices

Selection of the outputs to be commanded and the feedbacks to be used is dependent on three main items:

1. Pilot interface requirements.
2. Reliability and redundancy considerations.
3. Practicality of measuring the feedback signals required.

In the early design stage, selection of feedback signals is, at times, an arbitrary decision. Such decisions can have a dramatic impact on cost, complexity, and the reliable operation of the resulting system when it enters production. Use of easily obtained reliable signals is recommended.

## Checking the System Properties

Controllability and observability are checked for both the open-loop aircraft and the closed-loop design model prior to performing design variations. This is another area prone to error due to the tedium of performing operations on matrices with realistic elements. Automation can significantly reduce the computational burden. The CESA program available as an AFIT Library program is used throughout this investigation to check controllability and observability.

## Transmission Zeros and the M Matrix

The selection of measurement matrix elements and the calculation of transmission zeros are steps that are interrelated in the design. An initial selection is made for the

measurement matrix elements using data from Reference 6 and from previous study efforts. The transmission zeros are then calculated. Based on their locations, refinement of the measurement matrix elements is made. In some cases, unstable transmission zeros that are not created by the measurement matrix can be removed by redefining the $\underline{C}$ output matrix. The calculation is performed using the matrix methods of the TOTAL interactive program available at AFIT. A Macro program called AKEY is employed on TOTAL when the $\underline{B}$ matrix of the state equation is in the "zero-$B_2$" format shown at the top of Table 2 . After the system matrices are stored, AKEY requires only the entering of the measurement matrix elements for each trial calculation of transmission zeros. The equation implemented for irregular designs is shown below:

$$\underline{Z}_t = |\underline{\lambda}_{I_{n-\ell}} - \underline{A}_{11} + \underline{A}_{12}\underline{F}_2^{-1}\underline{F}_1| = 0 \qquad (4.1)$$

For regular designs, the same program is used except that $\underline{C}_1$ and $\underline{C}_2$ are entered in place of $\underline{F}_1$ and $\underline{F}_2$, respectively. A zero matrix of size $n-\ell$ by $\ell$ is entered for the measurement matrix. The program for TOTAL can be quickly created and kept on a permanent computer file for access throughout the design. A listing of the Macro steps is given in Appendix E. An alternate program called ZERO is also available for determining transmission zeros, but has not been completely debugged (Ref 13).

For the first design attempt, the $\bar{\alpha}$, $\Sigma$ and $\varepsilon$ parameters are set to one in MULTI. In almost all cases, this results in an unstable system. The gain is then reduced by decreasing $\varepsilon$ until stable operation is obtained. For those cases that are initially stable, gain is increased until the instability point is found. The gain is then reduced by the required margin.

Initial design attempts using the techniques of Professor Porter usually result in systems that respond rapidly to commands. The quickness of the response may require large control surface deflections and excessive surface rates. Therefore, the design must be modified. The control surface limits for the AFTI/F-16 are shown in Table 3.

Table 3

Surface Position and Rate Limits

| Surface | Position Limit (deg) | No Load Rate Limit (deg/sec) |
|---|---|---|
| Elevators | ±25 | 60 |
| Flaperons | ±20 | 52 |
| Rudder | ±30 | 120 |
| Canards | ±27 | 100 |

Maximum Maneuver Estimates

To stay within position limits, a method based on maximum commands is developed. At each condition, the maximum maneuvers that can be commanded are estimated. These estimated maximum maneuvers are used as inputs, and individual weighting matrix elements are varied until less than maximum surface positions are reached. The weighting matrix elements are also adjusted (ratioed with respect to one another) at the same time to provide the type of responses desired. Then, the proportional plus integral ratio ($1/\overline{\alpha}$) is adjusted so that steady-state behavior is reached within a desired time.

Maximum capability for conventional maneuvers may be limited by structural ability, pilot physiological constraints, control authority or departure limits. Table 4 lists the maximum longitudinal and roll commands used in the thesis.

Table 4

Maximum Command Estimates

| Flight Condition | | Axis (units) | |
|---|---|---|---|
| Mach | Altitude (ft) | Pitch (g) | Roll (deg/sec) |
| 0.2 | 30 | +3.1 | 150 |
| 0.6 | 30000 | +4.7 | 300 |
| 0.9 | 20000 | +9.0 | 300 |
| 1.2 | 30000 | +8.5 | 210 |

CCV maneuvers are limited by the direct force capability of the control surfaces. To develop the CCV maximum estimates, the equations of motion are solved for each maneuver of interest. Longitudinal authority is limited by the maximum deflection of the symmetric flaperons for both the direct lift and pitch pointing modes. In the lateral-directional modes, the canard deflection sets the maximum sideforce capability while the rudder deflection limit establishes the maximum yaw pointing capability. For the translational modes, a velocity is produced by developing a direct force and then, after an established time, reducing the force to zero. Thus, the maximum translational capabilities are determined by the integral of the direct forces. Since the time for direct force to be commanded is an arbitrary design selection, maximum estimates for translation are not shown. The solution of the system of equations for the CCV maximum estimates is found at each flight condition. Table 5 is a compilation of the results.

The input commands are very closely tracked by the controllers developed using this design method. For step inputs, the control surfaces are commanded instantaneously to maximum deflection. This would result in rate limiting in any actual implementation. Inclusion of an actuator model reduces the surface rates, but not to values within acceptable limits. Rates are kept below the limit by slowing down the input command. It is recommended that this be

Table 5

CCV Maximum Capabilities

| Flight Condition | | Mode | Capability |
|---|---|---|---|
| Mach | Altitude (ft) | | |
| 0.9 | 20000 | $A_n$ | 2.07 g |
| | | $\alpha_1$ | 2.72 deg |
| | | $A_y$ | 0.84 g |
| | | $\beta_1$ | 4.30 deg |
| 0.2 | 0 | $A_n$ | 0.16 g |
| | | $\alpha_1$ | 3.22 deg |
| | | $A_y$ | 0.05 g |
| | | $\beta_1$ | 2.77 deg |
| 0.6 | 30000 | $A_n$ | 0.70 g |
| | | $\alpha_1$ | 4.0 deg |
| | | $A_y$ | 0.20 g |
| | | $\beta_1$ | 4.68 deg |
| 1.6 | 30000 | $A_n$ | 0.94 g |
| | | $\alpha_1$ | 1.00 deg |
| | | $A_y$ | 0.60 g |
| | | $\beta_1$ | 1.48 deg |

accomplished by placing a first-order lag in each command input path. Output from the lag device is a continuous, well-behaved function that the controller tracks with good accuracy. This approach is used in classical designs presently being flown. The lag or "pilot command prefilter" does not interfere with the closed-loop stability but matches the aircraft's response to the pilot's response. Time delays from 1/4 second to 1/10 second are generally used. Higher-order filters can be used, but they tend to increase phase lag at higher frequencies. As discussed in Chapter V, it is beneficial to keep the phase lag as low as possible from such a filter in order to reduce pilot workload.

The MULTI computer-aided design program, at the time of this research, does not have the ability to handle filters on the command inputs to the controller. In work on a related thesis, a method has been developed to represent command inputs as ramp hold waveforms (Ref 14). The ramp hold input is used to approximate an input prefilter by slowing down the command and providing acceptable surface rates. This is not a one-to-one relationship since rates are also affected by feedback signals. However, the technique does result in acceptable surface rates and output responses. The time duration for the ramp is calculated from the maximum surface position divided by the maximum surface rate.

## Gain Scaling and the Weighting Matrix

Initially, responses are obtained for a given design to a maximum step input, and the surface rates are examined. The surface with the highest rate is used to establish the ramp time for the input. Then interactive fine tuning is performed to establish the fastest ramp that provides surface rates below the specified limits. The same ramp is used for all inputs.

Weighting matrix elements are varied to develop the desired time responses. After selection of the matrix elements, rate and position limits are again checked and iterated to result in a system that meets the requirements and provides the desired response.

At this point in a design attempt, it is very useful to understand the designation of the elements in the gain matrices. With such knowledge during the gain iteration step, it is possible to trace an undesirable response to its cause or to correct surface saturation problems with minimal impact on performance.

Figure 10 illustrates the element designation for the two input-two output longitudinal AFTI design, i.e.:

$$\underline{K}_0 = \begin{bmatrix} P_{11} & P_{12} \\ P_{21} & P_{22} \end{bmatrix} \quad \text{and} \quad \underline{K}_1 = \begin{bmatrix} I_{11} & I_{12} \\ I_{21} & I_{22} \end{bmatrix} \qquad (4.2)$$

The $\underline{C}$ matrix specifies the outputs to be used as feedbacks.

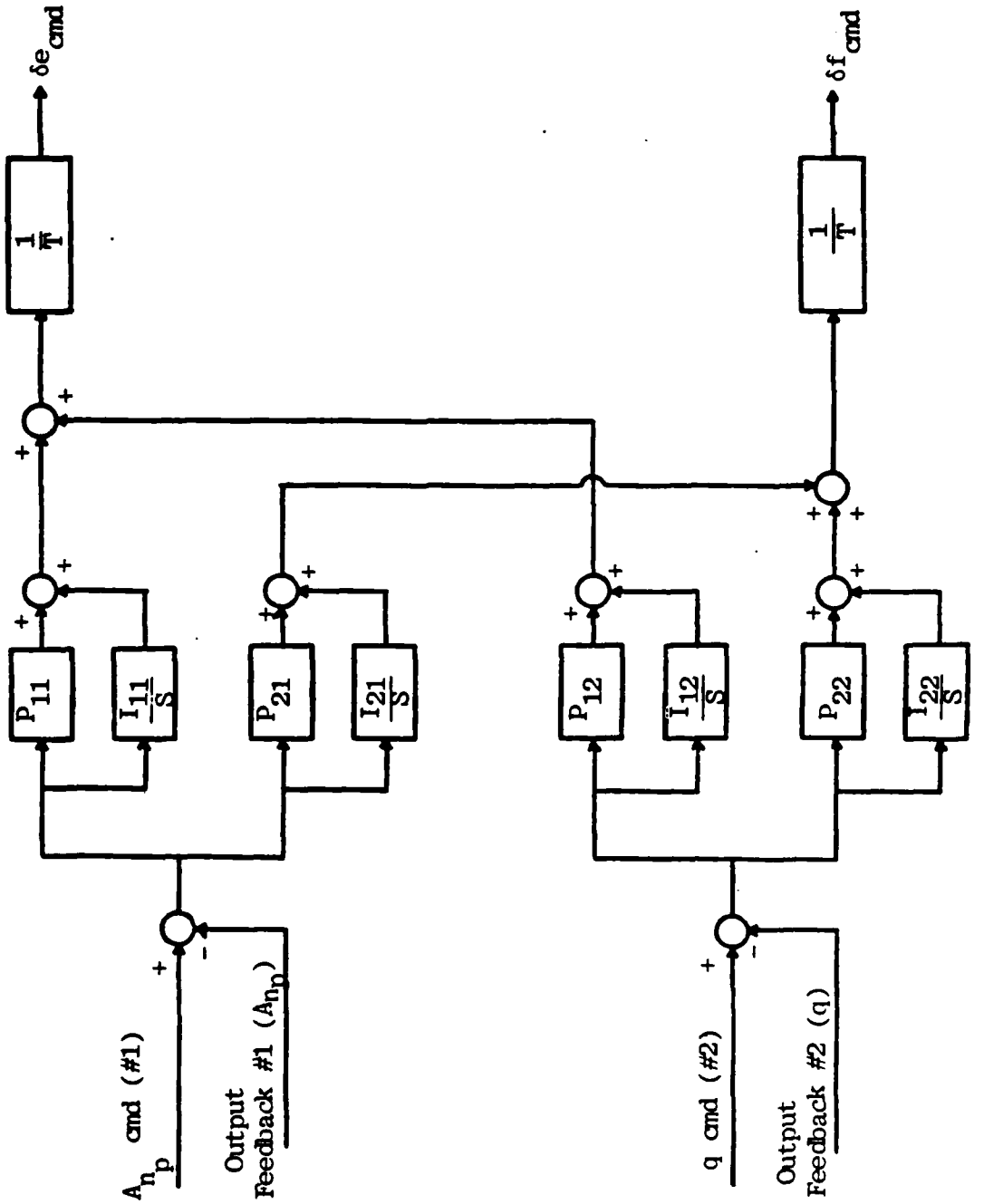



Figure 10. Longitudinal Two Input--Two Output Controller Block Diagram

$$y = \begin{bmatrix} 0 & 0 & 0 & 1 & 0 & 0 & 0 \\ 0 & 0 & 0 & 0 & 1 & 0 & 0 \end{bmatrix} \begin{bmatrix} \alpha \\ \theta \\ u \\ A_{n_p} \\ q \\ \delta_e \\ \delta_f \end{bmatrix} = \underline{cx} \qquad (4.3)$$

Feedback number one is the longitudinal acceleration at the pilot's station, $A_{n_p}$, and feedback number two is pitch rate. The elevator surface position is determined by the equation:

$$\delta_{e_{cmd}} = \{(A_{n_p} \text{ error})(P_{11})\} + \{\int(A_{n_p} \text{ error})(I_{11})\} + \{(q \text{ error})(P_{12})\} + \{\int(q \text{ error})(I_{12})\} \qquad (4.4)$$

Integral Plus Proportional Adjustment

The proportional plus integral ratio is adjusted until the system reaches the desired steady-state value in the time required. It is important to realize that the $\bar{\alpha}$ parameter in MULTI is the inverse of the ratio of integral to proportional gain. As shown in Chapter III:

$$\underline{K}_0 = \bar{\alpha}\ \varepsilon\ [\underline{F}_2\underline{B}_2]^{-1}\underline{\Sigma} \qquad (4.5)$$

and

$$\underline{K}_1 = \varepsilon\ [\underline{F}_2\underline{B}_2]^{-1}\underline{\Sigma} \qquad (4.6)$$

Varying $\alpha$ directly affects the proportional gains and system stability. What is actually desired is to hold the proportional gains constant while varying the integral gains to improve steady-state response. The method developed is to select the ratio of proportional to integral gain by varying the $\bar{\alpha}$ parameter and then modifying the gain matrix to return to the original proportional gain. This becomes a time-consuming process and can be eliminated by altering MULTI to move the parameter into the equation for the integral gains.

Gain and Phase Margins

Although not actually listed as part of the design method, gain and phase margins must be checked for any design. In real applications, there is no "guaranteed" stability. The model used in a design is, as the name states, just a model of the aircraft. All the inputs and states of the aircraft are never included in any design model. Aeroelastic interactions, gust disturbances, and nonlinear characteristics of the aircraft or control system can all result in unexpected instabilities.

The only guarantee is that produced by requiring a margin be established and to base the margin on the best estimate of the uncertainties in the model. The military flight control design specification establishes such margins for systems being developed. The table below is extracted from Reference 15. One of the easier methods to check gain

Table 6

Gain and Phase Margin Requirements

| Mode Frequency Hz \ Airspeed | Below $V_{O_{MIN}}$ | $V_{O_{MIN}}$ To $V_{O_{MAX}}$ | At Limit Airspeed ($V_L$) | At 1.15 $V_L$ |
|---|---|---|---|---|
| $f_M$ < 0.06 | GM = 6 db (No Phase Requirement Below $V_{O_{MIN}}$) | GM = ±4.5<br>PM = ±30 | GM = ±3.0<br>PM = ±20 | GM = 0<br>PM = 0<br>(Stable at Nominal Phase and Gain) |
| 0.06 ≤ $f_M$ < First Aero-Elastic Mode | | GM = ±6.0<br>PM = ±45 | GM = ±4.5<br>PM = ±30 | |
| $f_M$ > First Aero-Elastic Mode | | GM = ±8.0<br>PM = ±60 | GM = ±6.0<br>PM = ±45 | |

NOTE: Gain is in dB; Phase is in degrees.

where: $V_L$ = Limit Airspeed (MIL-A-8860).

$V_{O_{MIN}}$ = Minimum Operational Airspeed (MIL-F-8785).

$V_{O_{MAX}}$ = Maximum Operational Airspeed (MIL-F-8785).

Mode = A characteristic aeroelastic response of the aircraft as described by an aeroelastic characteristic root of the coupled aircraft/FCS dynamic equation-of-motion.

Table 6 (continued)

| | | |
|---|---|---|
| GM = Gain Margin | = | The minimum change in loop gain, at nominal phase, which results in an instability beyond that allowed as a residual oscillation. |
| PM = Phase Margin | = | The minimum change in phase at nominal loop gain which results in an instability. |
| $f_M$ | = | Mode frequency in Hz (FCS engaged). |
| Nominal Phase and Gain | = | The contractor's best estimate or measurement of FCS and aircraft phase and gain characteristics available at the time of requirement verification. |

and phase margins is to use frequency domain analysis methods (Bode plots or Nyquist plots). These are not presently available within MULTI but may be achieved with other programs such as TOTAL.

Note that the required margins in Table 6 are specified for all aerodynamically closed loops of the flight control system. In multiple loop systems, variations are made with all gain and phase values in the feedback paths held at nominal values except for the path under investigation.

In preliminary designs, since structural mode data may not be available, a general guideline is to use ±6db gain margin and ±45 degrees phase margin. The specified gain margin must be large enough to account for: (1) uncertainties in the aircraft model, and (2) system changes from age through the operating life. As more testing is accomplished with the aircraft and the uncertainties are removed, the margins may be reduced. In recent years, airframes have become more efficient, being manufactured with less strength and weight. At the same time, control system designs have increased in authority and gain. This trend has significantly increased the possibility of adverse interactions between the control system and the structure (servoelastic problems). At times such interactions include the aerodynamic feedback paths resulting in aeroservoelastic instabilities (Ref 21).

As a guard against such instabilities, it is prudent to limit the control system bandwidth. Most structural modes occur at higher frequencies than the functions of the control system. Thus, once a control bandwidth is found that provides acceptable performance, it is advisable to provide gain attenuation at all higher frequencies. Structural modes or interactions within the control system bandwidth must be handled with either notch filters or phase compensation techniques.

For this study, the ±6db gain margin and 45 degrees phase margin are specified. Bandwidth limiting is seen as a desirable characteristic for the system. This limiting is accomplished with the actuators. Compensation is not allowed to counter the gain roll off above the actuator break frequency in order to provide the desired bandwidth limiting. Even with this concept, it should be noted that both the F-16 and the AFTI/F-16 control system designs require the addition of notch filters to alleviate structural interactions.

As a final note on stability margins, the MULTI design package does not provide a means for altering individual system gains. The elements of the weighting matrix change all the gains associated with each output being fed back. Thus, to check stability, the elements of the gain matrix must be manually changed outside the MULTI program. Although not difficult, this is a time-consuming process. The

unavailability of frequency domain analysis methods in the MULTI package make phase measurements very difficult.

One method used in actual on-aircraft testing is to insert a compensation element of the form $[1-\tau s]/[1+\tau s]$ into each loop being tested. The time constant is increased until divergence occurs or until the 45 degree phase margin is demonstrated. It is desirable to include compensation filters within the MULTI design package. Presently, use of this approach requires regeneration of the aircraft model to include the compensation. The model has to be modified to allow evaluation with this element in each individual feedback loop. This addition to MULTI can provide a convenient means of measuring gain and phase margins. Only cursory phase margin checks are accomplished for the designs due to this limitation.

## Evolution of a Final Design

The design procedure is illustrated with a simple case in order to develop an understanding of the method being applied. Several interesting facts come to light from this approach. Many details of the design process are included in order to show the evolutionary process which leads to a successful design.

Trial 1. The longitudinal equations at 0.9 Mach and 20,000 feet are considered first. By arranging the equations with theta as the first state and by neglecting the drag

equation, a short period approximation is developed which is in the zero-$B_2$ form:

$$\begin{bmatrix} \dot{\theta} \\ \dot{\alpha} \\ \dot{q} \end{bmatrix} = \begin{bmatrix} 0 & 0 & 1 \\ -0.001187 & -1.4845 & 0.9948 \\ 0.000309 & 4.2717 & -0.7772 \end{bmatrix} \begin{bmatrix} \theta \\ \alpha \\ q \end{bmatrix} + \begin{bmatrix} 0 & 0 \\ -0.1492 & -0.2249 \\ -24.058 & -6.4727 \end{bmatrix} \begin{bmatrix} \delta_e \\ \delta_f \end{bmatrix} \quad (4.7)$$

$$\underline{y} = \begin{bmatrix} \alpha \\ q \end{bmatrix} = \begin{bmatrix} 0 & 1 & 0 \\ 0 & 0 & 1 \end{bmatrix} \begin{bmatrix} \theta \\ \alpha \\ q \end{bmatrix} \quad (4.8)$$

The system is controllable and observable with a transmission zero at the origin. The $\underline{C}$ matrix is created to provide control of angle of attack and pitch rate. The concept is to control pitch rate and longitudinal acceleration. Rewriting Equation (2.43)

$$A_{z_{cg}} = (\dot{\alpha} - q)U \quad (4.9)$$

Remembering that $A_n = -A_z$ and using Equation (2.32) yields

$$A_{n_p} = (q - \dot{\alpha})U + (\ell_x)\dot{q} \quad (4.10)$$

In a steady state pitch maneuver with constant acceleration, $\dot{\alpha}$ and $\dot{q}$ are zero. Converting the equation to the desired units of "g" and "degrees per second" yields

$$A_{n_p}(g) = \left[\frac{U(ft/sec)}{1845}\right] q(deg/sec) \quad (4.11)$$

This method can be applied to the lateral-directional axes giving a similar expression relating sideforce and yaw rate.

$$A_{y_p}(g) = \left[\frac{U(ft/sec)}{1845}\right] r(deg/sec) \qquad (4.12)$$

These two relationships are useful in meeting pilot interface requirements discussed later in this chapter. Since longitudinal acceleration is directly related to pitch rate, it is assumed that acceptable acceleration results by exercising proper control over pitch rate.

An initial value of one is selected for $\bar{\alpha}$, $\Sigma$ and the $\varepsilon$ elements. This results in an unstable design as shown in Figures 11 and 12. Adjustment of the weighting matrix elements produces the responses shown in Figures 13 and 14. In this case, the design parameters are:

$$\bar{\alpha} = 1.0 \qquad (4.13)$$

$$\varepsilon = 1.0 \qquad (4.14)$$

$$\Sigma = \begin{bmatrix} 0.1 & 0.0 \\ 0.0 & 2.35 \end{bmatrix} \qquad (4.15)$$

The inputs are step commands for angle of attack and pitch rate. The steps are not applied instantaneously. They are ramped in over a 0.4 second time interval. The interval is established by the flaperon rate limit and position limit.

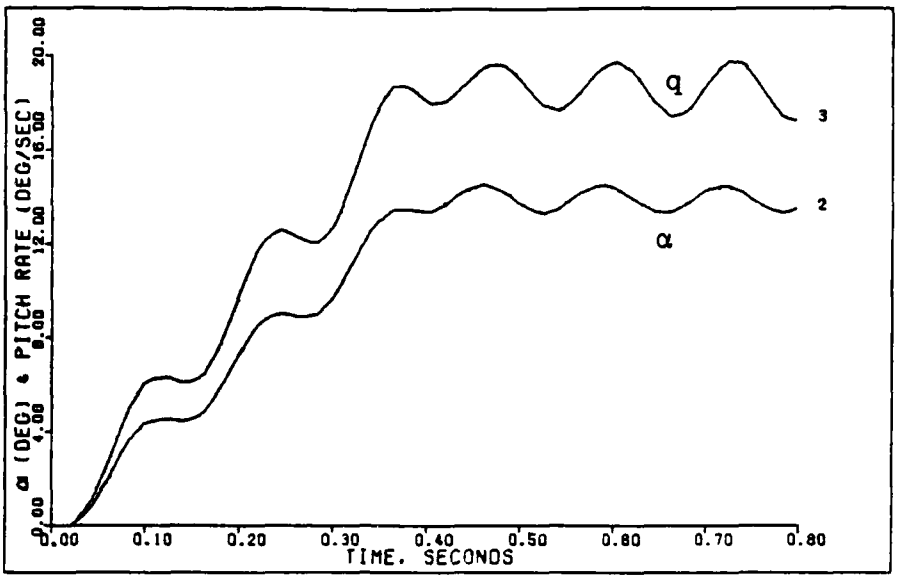



Figure 11. Response Plot for Initial Rate Controller Design with Short Period Approximation

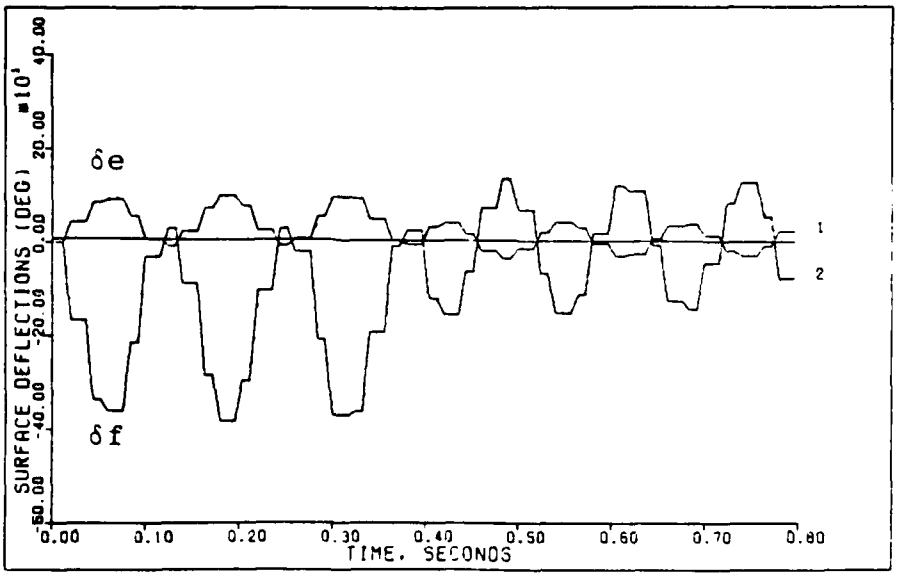



Figure 12. Surface Position Plot for Initial Rate Controller Design with Short Period Approximation

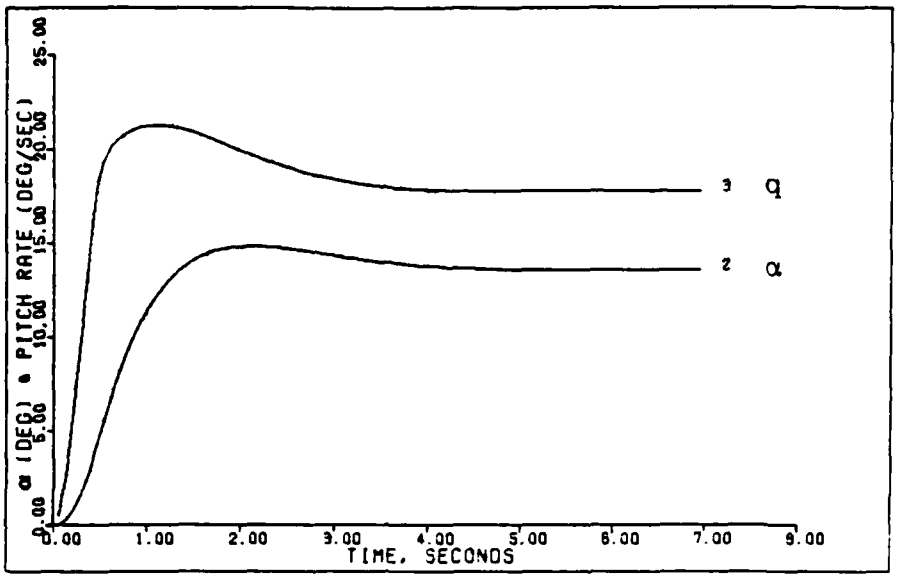



Figure 13. Response Plot for Rate Controller with Short Period Approximation

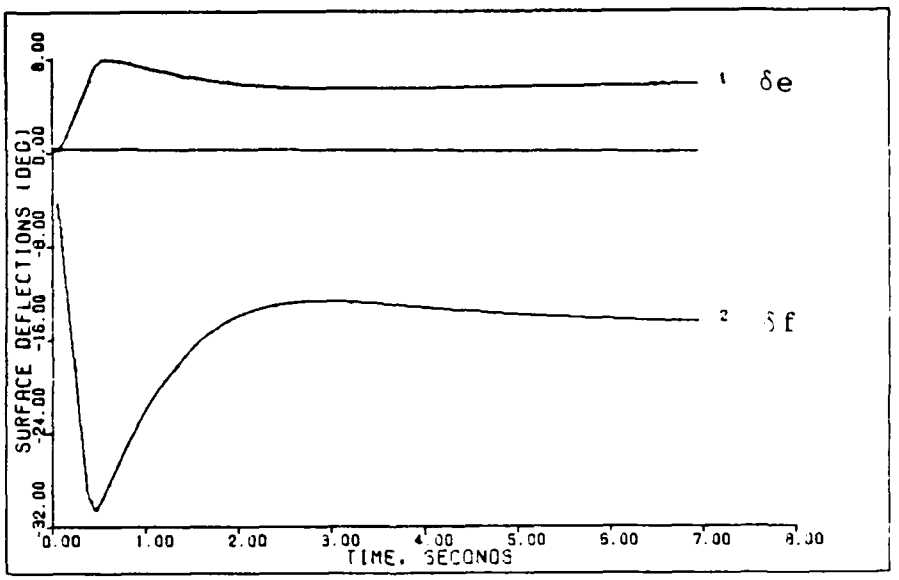



Figure 14. Surface Position Plot for Rate Controller with Short Period Approximation

$$\text{Ramp time} = \frac{\text{rate limit}}{\text{position limit}} \qquad (4.16)$$

The steady-state angle of attack command is determined by solving the aircraft equations for a trim solution at the desired acceleration level. This is a necessary calculation to obtain a coupled longitudinal maneuver with this type of design.

The responses appear acceptable, but two problems are evident. First, the required alpha command must be computed. Thus, pilot inputs must be converted into pitch rate and angle of attack commands through an aircraft model prior to input to the controller.

Second, the flaperons are deflecting in the wrong direction in Figure 14. The flaps are intended to aid in the maneuver by creating a positive instantaneous direct lift. For positive direct lift the flaps must be commanded to a positive position. By driving the flaperon in a negative direction, as shown, the controller is rotating the aircraft as rapidly as possible to develop the commanded pitch rate and angle of attack. The negative flaps are decreasing lift and adversely affecting acceleration. This appears to be contrary to the intended operation. Actually, the controller designed is responding exactly as specified. The step commands of angle of attack and pitch rate are in effect saying to rotate the aircraft rapidly. This is exactly what is being achieved.

Trial 2. The problem is in the concept of what should be happening. The concept assumes that by commanding alpha and q, acceleration is adequately controlled, based on Equation (4.11). However, the equation assumes a coupled aircraft, and this design method develops an essentially decoupled aircraft. Care must be exercised in selecting the states to be commanded, and in developing the proper relationship of these commands to recoupling the aircraft. The other problem is that the concept assumes for a specific load factor there is a unique value for both $\alpha$, q, and the elevator position in steady state. With two surfaces, there are multiple solutions to the steady-state trim problem. What is actually desired is a crisp, well-behaved step in pitch rate and acceleration with a corresponding step in angle of attack. What is commanded is a quick step in alpha and q irrespective of the acceleration. In other words, fast rotation is commanded and provided by the design, but it is really not desired.

The solution is to restructure the problem to actively command acceleration and pitch rate. Angle of attack is still important, and is monitored in the responses. The speed of response of acceleration and pitch rate determine the resulting angle of attack. Using Equation (2.43) and (2.32), the relationship can be defined by

$$\dot{\alpha} = \frac{A_{n_p}}{U} - \frac{(\ell_x)}{U}\dot{q} + q \qquad (4.17)$$

In the steady state $\dot{q}$ is zero, thus

$$\dot{\alpha} = \frac{A_{n_p}}{U} + q \qquad (4.18)$$

This solution requires a transformation of states to obtain acceleration. When performing the transformation as outlined in Chapter II, the angle of attack state is replaced by acceleration as a state. The importance of angle of attack must not be overlooked in the design. Too large a value can result in loss of directional stability and departure from controlled flight. Too small an angle of attack results in the use of a larger flaperon deflection than necessary to perform the desired maneuver. To allow angle of attack to be observed in the design attempts, it can be added as a redundant state equation as outlined in Chapter II, although this complicates the design. It increases the dimensions of the system matrices, adds a transmission zero at the origin, and results in the addition of a pole and a zero at the origin in the system transfer function. An alternative is to establish the proper $\underline{C}$ matrix which produces an acceleration output as well as an angle of attack output. This eliminates the need for augmenting the system matrix with redundant equations. MULTI cannot presently accept such a $\underline{C}$ matrix, since only those outputs that are commanded can be obtained. This is a proposed modification for MULTI.

A design with acceleration as a state is shown in Figures 15, 16 and 17. This illustrates that the same undesired response is obtained if care is not exercised in selecting elements of the measurement matrix. In the case shown, acceleration can now be observed and is initially negative. This is definitely not desirable. It is a result of the use of the flaps in the wrong direction causing an instantaneous loss of lift as the aircraft rotates. Rotation eventually results in an increase in alpha and an associated increase in lift. Figures 18 through 20 show response to a step for the same system with a measurement matrix selected to be as sparse as possible. The desired responses are obtained.

A cautionary note is provided. The maneuvers shown thus far are for step commands approximating the maximum aircraft capability. This is not to imply that the linearized perturbation equations used for the design are accurate for these maneuvers. It is only meant to give a general indication of the maximum surface rates and surface deflections commanded by the controller. Much smaller step responses are used to demonstrate the design. Responses with the full equations of motion and a 1g command are shown in Figures 21 through 25.

A pointing system is developed by using the same rate and acceleration commands. For fuselage pointing, a pulse command is input for pitch rate while a zero

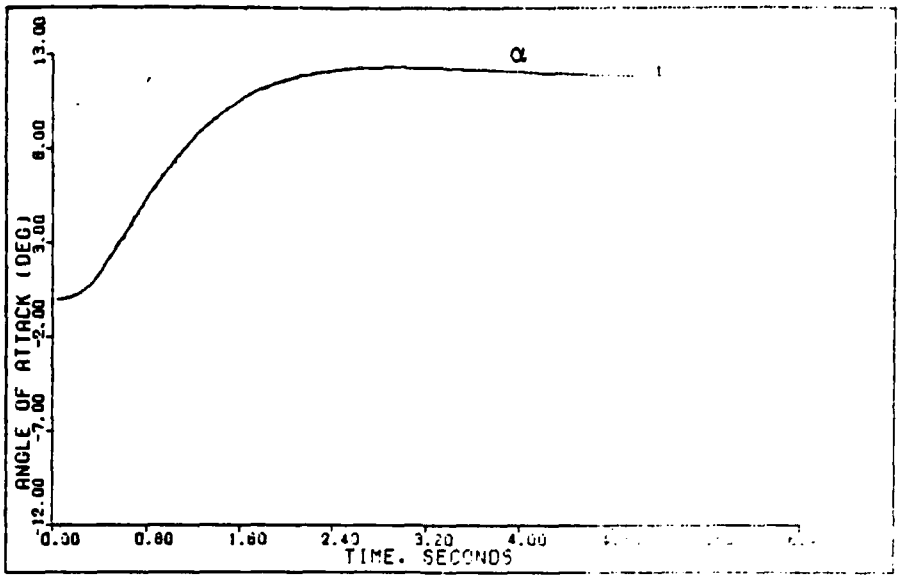



Figure 15. α Response of the Trial 2 Design to a 9g Step Command (0.9 Mach 20,000 feet)

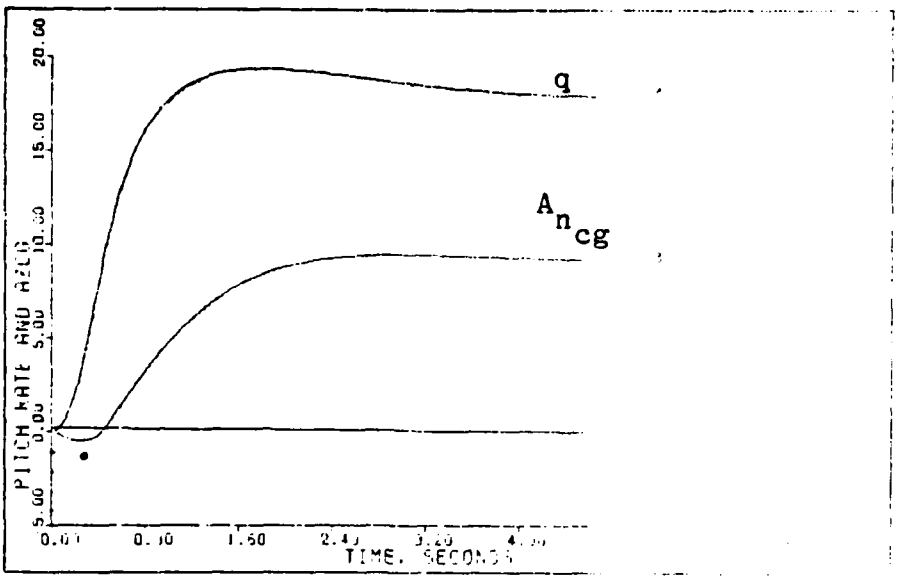



Figure 16. Pitch Rate and Acceleration Response of the Trial 2 Design to a 9g Step Command (0.9 Mach 20,000 feet)

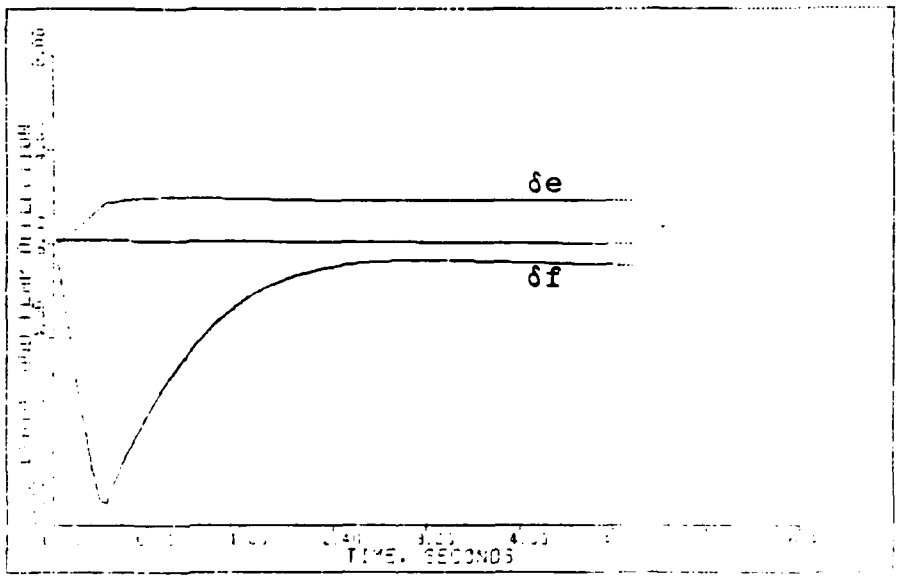



Figure 17. Surface Response of the Trial 2 Design to a 9g Step Command (0.9 Mach 20,000 feet)

Copy available to DTIC does not permit fully legible reproduction

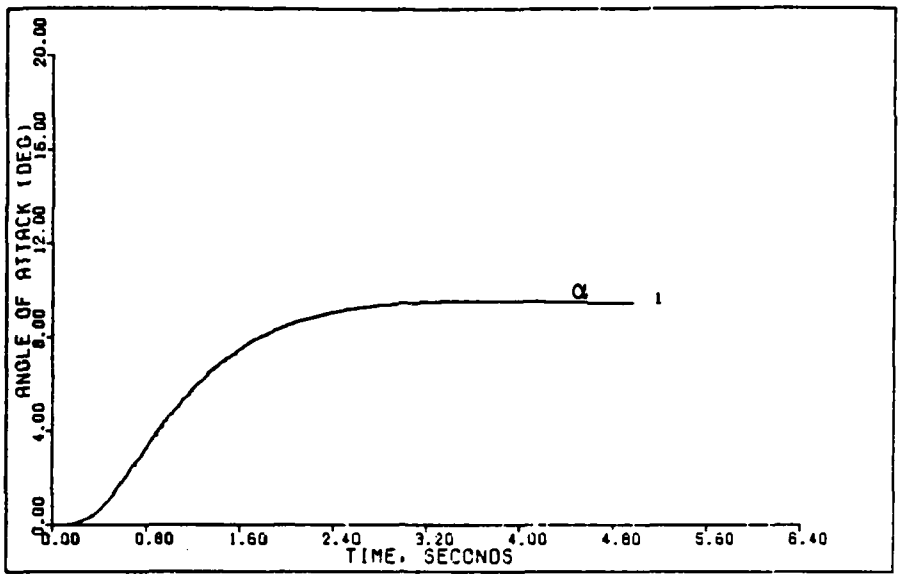



Figure 18. α Response of the Desired Preliminary Design to a 9g Step Command (0.9 Mach 20,000 feet)

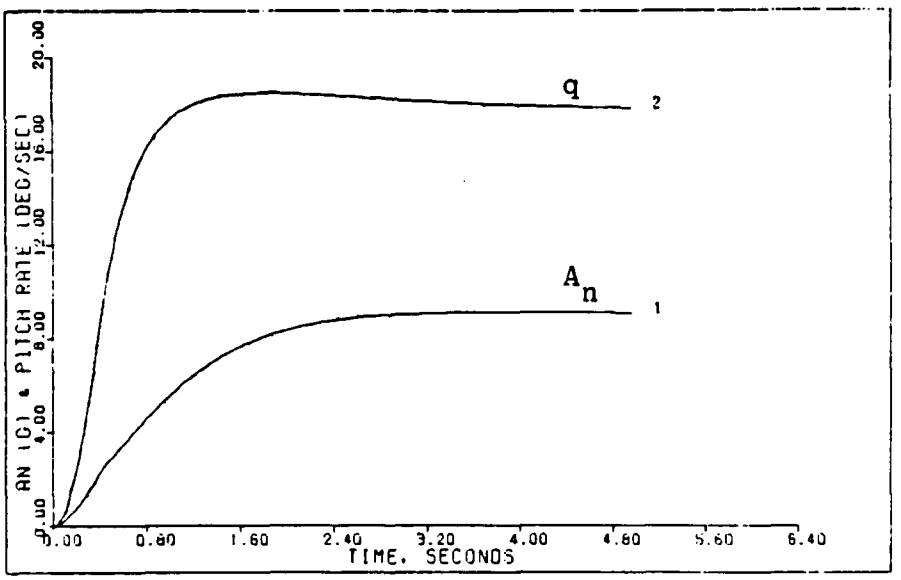



Figure 19. Pitch Rate and Acceleration Response of the Desired Preliminary Design to a 9g Step Command (0.9 Mach 20,000 feet)

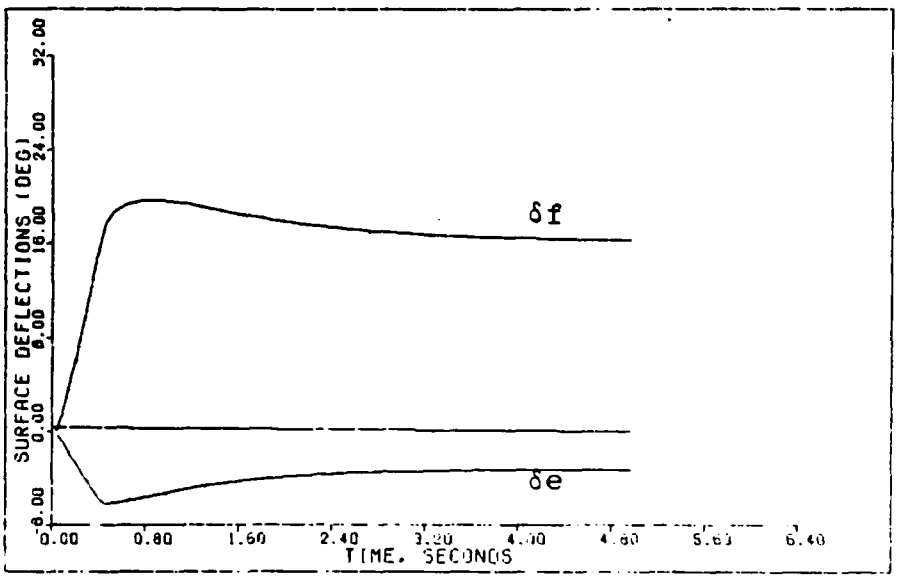



Figure 20. Surface Response of the Desired Preliminary Design to a 9g Step Command (0.9 Mach 20,000 feet)

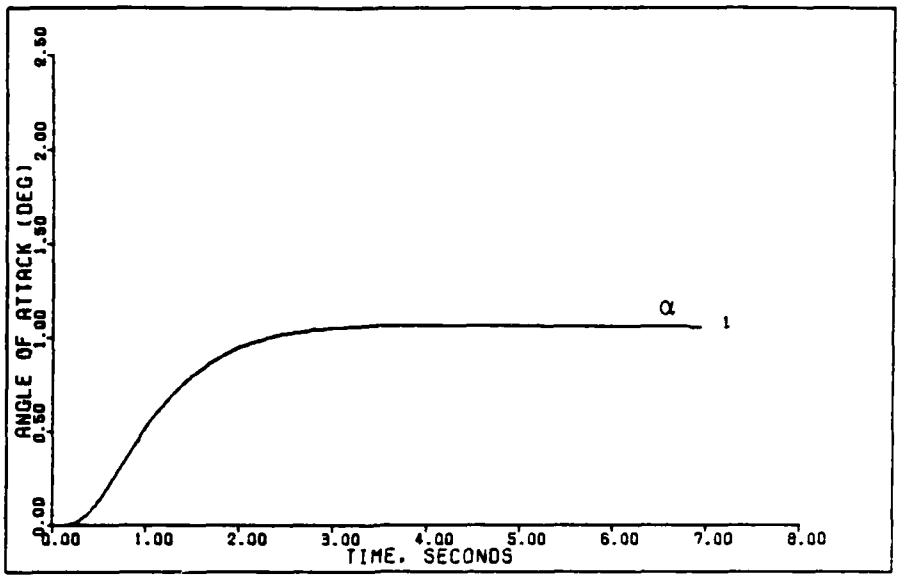



Figure 21. α Response of the Desired Preliminary Design to a 1g Step Command (0.9 Mach 20,000 feet)

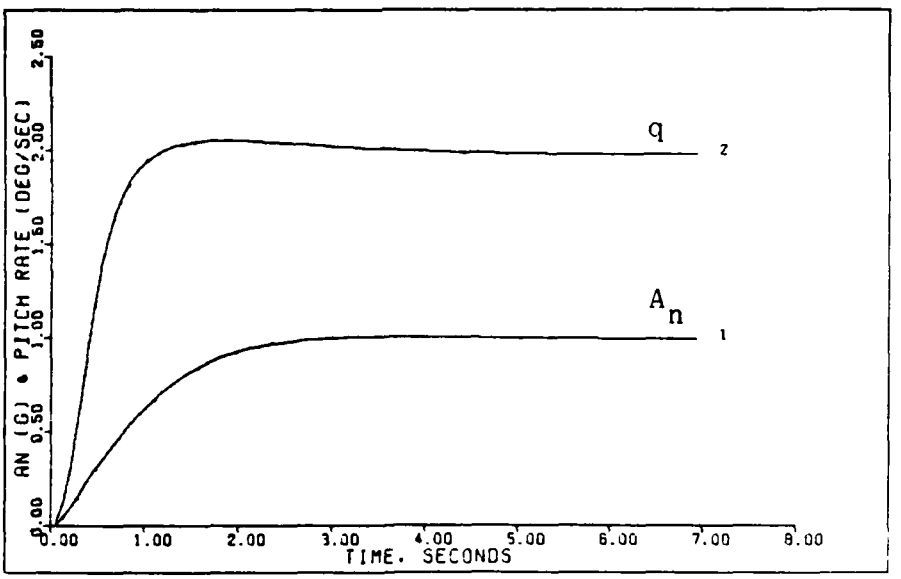



Figure 22. Pitch Rate and Acceleration Response of the Desired Preliminary Design to a 1g Step Command (0.9 Mach 20,000 feet)

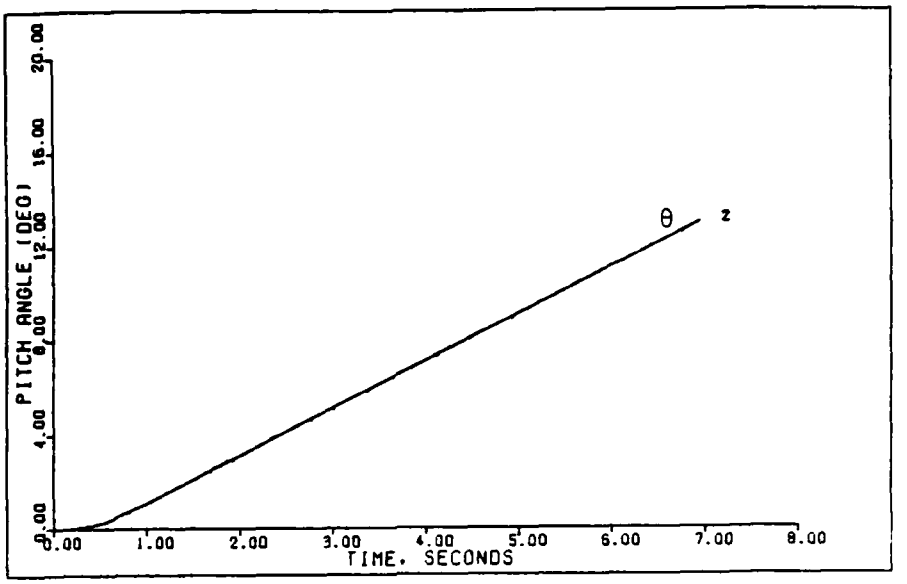



Figure 23. Pitch Angle Response of the Desired Preliminary Design to a 1g Step Command (0.9 Mach 20,000 feet)

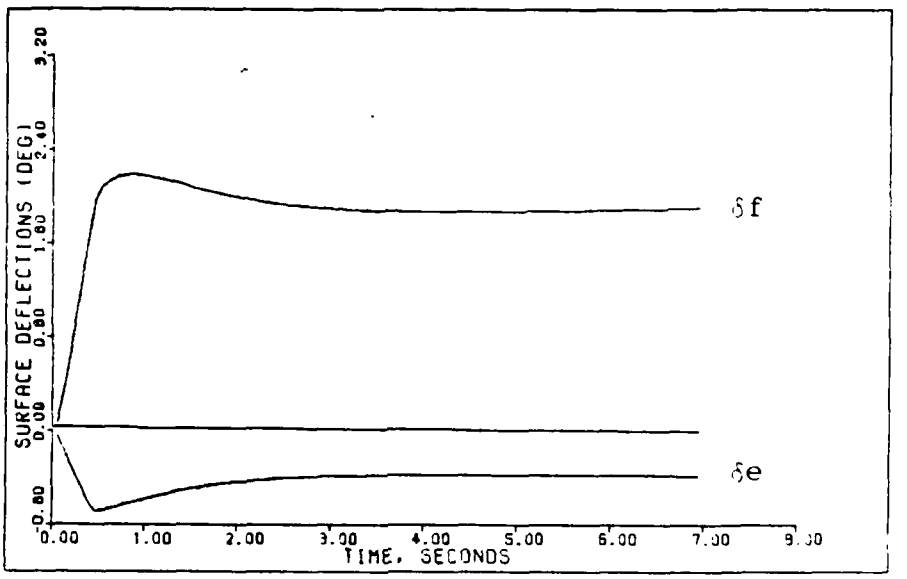



Figure 24. Surface Position Response of the Desired Preliminary Design to a 1g Step Command (0.9 Mach 20,000 feet)

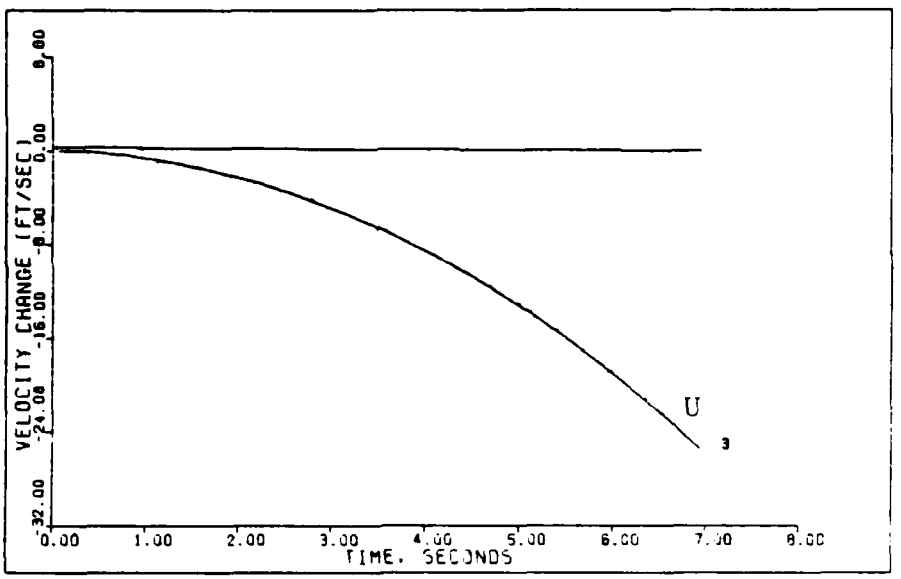



Figure 25. Forward Velocity Change of the Desired Preliminary Design to a 1g Step Command (0.9 Mach 20,000 feet)

acceleration command is simultaneously sent to the controller. Pitch rate develops and then reduces to zero, in the steady state, while acceleration is held at zero. The aircraft rotates, developing an angle of attack, without experiencing longitudinal acceleration. The aircraft nose is pointed upward without altering the flight trajectory (Figures 26 through 29).

With the design, pointing can be accomplished while in an accelerated turn. For example, a 4 "g" turn can be commanded with the appropriate acceleration and pitch rate steps. Pointing during the turn can be accomplished by adding a pitch rate pulse on top of the steady-state command while keeping the acceleration command at its steady-state value. This same technique is successfully applied in the lateral-directional axis to develop yaw pointing. A pulse yaw rate command is applied while side acceleration is held constant.

A trade-off exists between speed of response and pureness of the maneuver. As illustrated by Figure 27, the pointing maneuver is not completely decoupled, and a small amount of acceleration is generated. Pointing can be quickened by making the command pulse larger in amplitude while reducing its duration. However, as larger pulses are commanded, more acceleration results. If duration is not reduced, a larger pointing angle is commanded than can be generated. The surfaces then saturate while attempting to

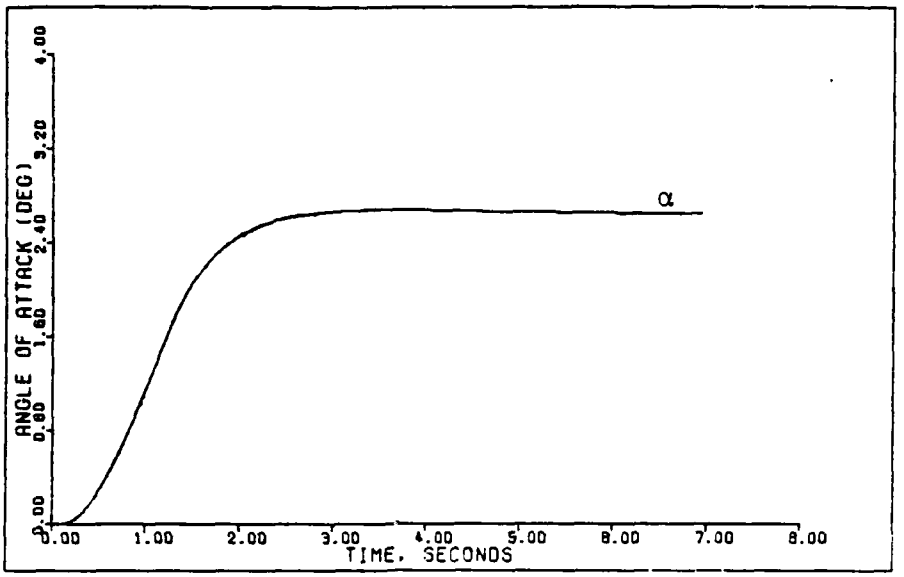



Figure 26. α Response of the Initial Pitch Pointing System to a 2 deg/sec Pitch Rate Pulse of 0.9 sec Duration (0.9 Mach 20,000 feet)

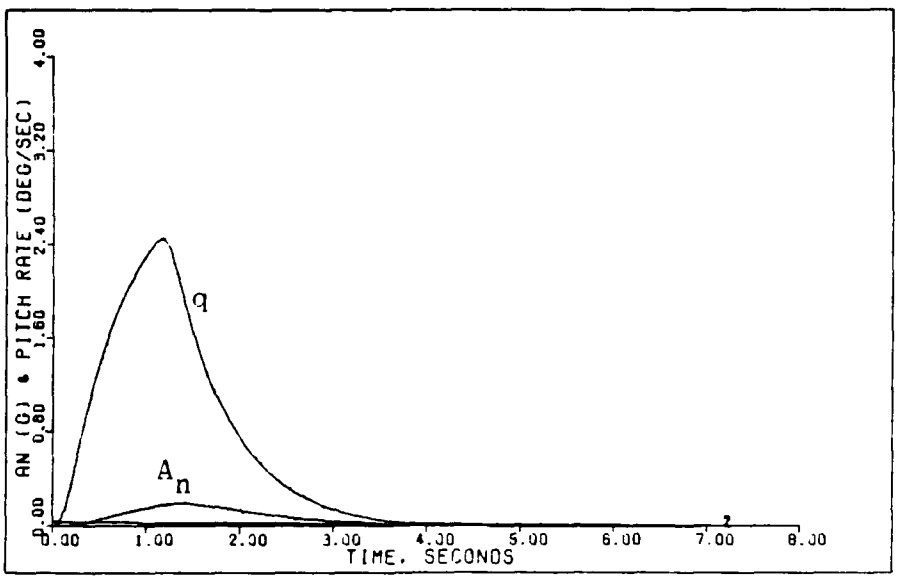



Figure 27. Pitch Rate and Acceleration Response of the Initial Pitch Pointing System to a 2 deg/sec Pitch Rate Pulse of 0.9 sec Duration (0.9 Mach 20,000 feet)

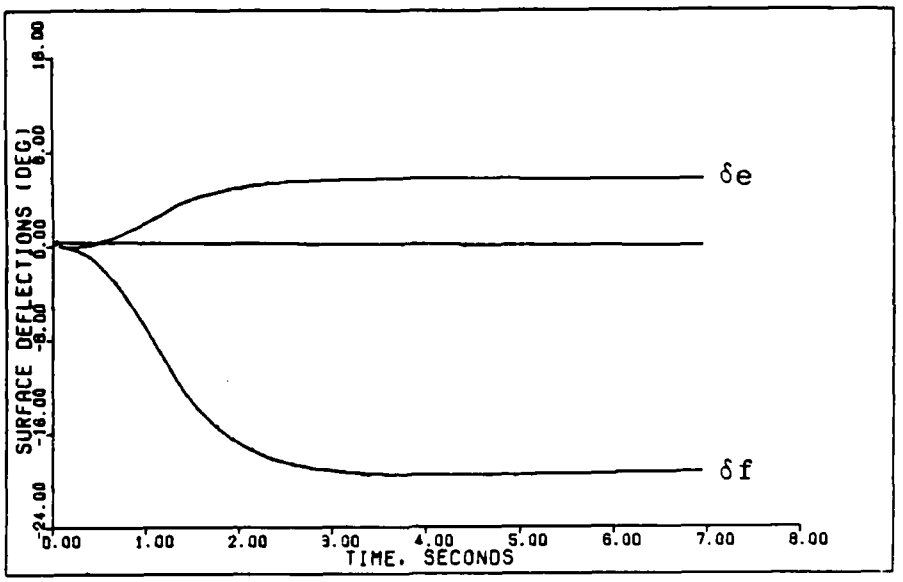



Figure 28. Surface Response of the Initial Pitch Pointing System to a 2 deg/sec Pitch Rate Pulse of 0.9 sec Duration (0.9 Mach 20,000 feet)

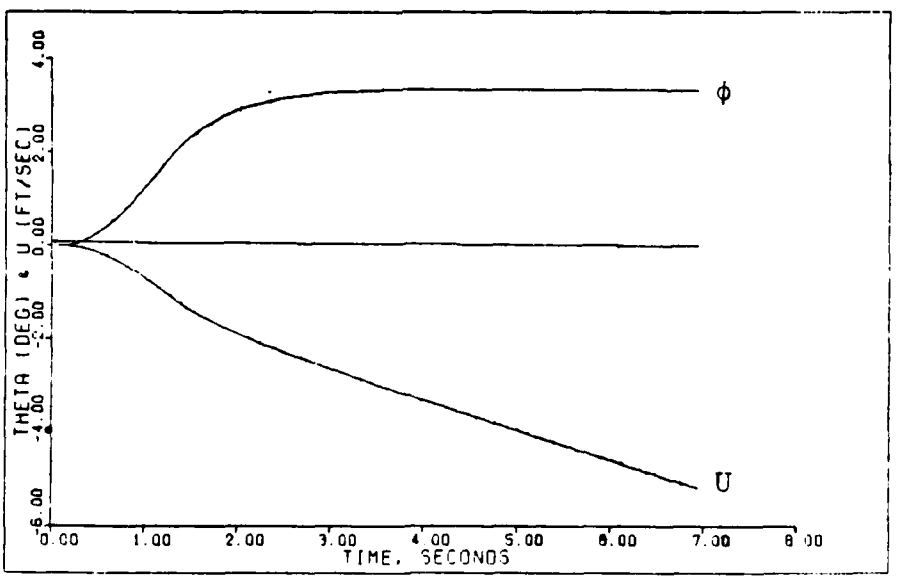



Figure 29. Pitch Angle and Velocity Change of the Initial Pitch Pointing System to a 2 deg/sec Pitch Rate Pulse of 0.9 sec Duration (0.9 Mach 20,000 feet)

satisfy the command, and thus decoupling is lost. If these surfaces are providing stability augmentation, that is also lost. As can be seen in Figure 28, surface rate limiting is not a problem for this design. Maximum Pointing of 2.7 degrees is achieved with a full upward flap deflection of -20 degrees.

The final design sets the pulse peak at a point determined by a compromise between quickness and purity. Pulse duration is selected so that the product of the pulse peak and pulse duration does not exceed the maximum pointing capability. Proportional control of pointing is obtained by varying the pulse value from zero to this peak value while holding the pulse width constant.

The final lateral-directional design results in a system in which roll rate, yaw rate, and side acceleration are commanded. The system provides conventional roll rate response and direct sideforce control. Lateral pointing can be accomplished in the same manner as employed for longitudinal pointing. The roll rate system requires further discussion. The equation for side force, including the gravitational force, can be written as:

$$F_{y_{cg}} = m(\dot{V} + Ur - pW) - gm\cos\theta\sin\phi \qquad (4.19)$$

Dividing by m, multiplying the right hand side by $\frac{U}{U}$, and letting $A_{y_{cg}} = \frac{F_{y_{cg}}}{m}$ yields:

$$A_{y_{cg}} = U(\dot{\beta} + r - p\alpha - \frac{g}{U}(\sin\phi\cos\theta)) \qquad (4.20)$$

The desire is to roll about the velocity vector without developing a sideslip angle or side acceleration on the aircraft. Conventionally, the method employed is to feed back an estimate of $\dot{\beta}$ to the rudder so that as the aircraft rolls, $\beta$ is driven to zero. Equation (4.20) is solved for $\dot{\beta}$:

$$\dot{\beta} = \frac{A_{y_{cg}}}{U} - r + p\alpha + \frac{g}{U}\sin\phi\cos\theta \qquad (4.21)$$

Using Equation (2.34):

$$\dot{\beta} = \frac{A_{y_p}}{U} - \frac{(\ell_x)\dot{r}}{U} - r + p\alpha + \frac{g}{U}\sin\phi\cos\theta \qquad (4.22)$$

For steady state rolls, r is a constant and $\dot{r}$ is zero; therefore

$$\dot{\beta} = \frac{A_{y_p}}{U} - r + p\alpha + \frac{g}{U}\sin\phi\cos\theta \qquad (4.23)$$

$$\dot{\beta} \approx \frac{A_{y_p}}{U} - r + p\alpha \qquad (4.24)$$

The approximation comes about in the following way. If the aircraft is simply rolling, the $\frac{g}{U}\sin\phi\cos\theta$ term should be included. Usually, rolling is a means of developing a desired bank angle to develop a turn. In such cases the longitudinal lift force is increased by the pilot to hold altitude constant (assuming a level turn). Thus, the

$\frac{g}{U}\sin\phi\cos\theta$ term is exactly cancelled by a portion of the lift force. In the analyses in this thesis, the longitudinal and lateral-directional axes are decoupled. Thus, there is no way of including that portion of the lift force into the lateral-directional equations.

If the aircraft is rolled into a bank without inclusion of the lift force, the rudder is deflected to counter the side acceleration component developed by the gravitational force. This is not desired for a turn. For the investigation at hand, this poses a problem. How to simulate a 360 degree roll and a banked turn with the equations that have been developed? For pure rolling maneuvers, such as 360 degree rolls, the full equations should be used since generally no additional lift force is developed to counter the gravity term. However, the assumption that $\sin\phi = \phi$(radians) is used in the equations developed for the aircraft model. This assumption is used to simplify the equations, but above a roll angle of ten degrees, it is invalid. Thus, for both 360 degree rolls and turns, the gravity term is dropped from both the $\beta$ and sideforce equations.

The controller developed for rolling response commands the acceleration $A_{y_p}$ to zero, roll rate to the desired level, and yaw rate to a value developed by solving Equation (4.23) for r assuming $\dot{\beta}$ is zero.

$$r = -\dot{\beta} + p\alpha + \frac{A_{y_p}}{U} + \frac{g}{U}\sin\phi\cos\theta \qquad (4.25)$$

$$r = p\alpha + \frac{A_{y_p}}{U} + \frac{g}{U}\sin\phi\cos\theta \qquad (4.26)$$

For turning flight, this becomes:

$$r = p\alpha + \frac{A_{y_p}}{U} \qquad (4.27)$$

Assuming sideforce is kept close to zero, the $A_{y_p}$ term can be neglected. Figures 30 and 31 are the results of the roll rate design for maximum inputs at 0.9 Mach and 20,000 feet. Responses for a 10 degree per second command at the same flight condition are shown in Figures 32 and 33.

Sideforce is developed by commanding $A_{y_p}$ to a constant value and roll rate to zero. Yaw rate is commanded to the value developed using Equation (4.12)

$$r = \left[\frac{1845}{U}\right] A_{y_p} \qquad (4.28)$$

A maximum sideforce maneuver is commanded at 0.9 Mach 20,000 feet for this design in Figures 34 through 37.

As in the longitudinal axis, sideforce can be developed while the aircraft is in turning flight or during a combat maneuver with the design by superimposing those commands over the normal roll commands.

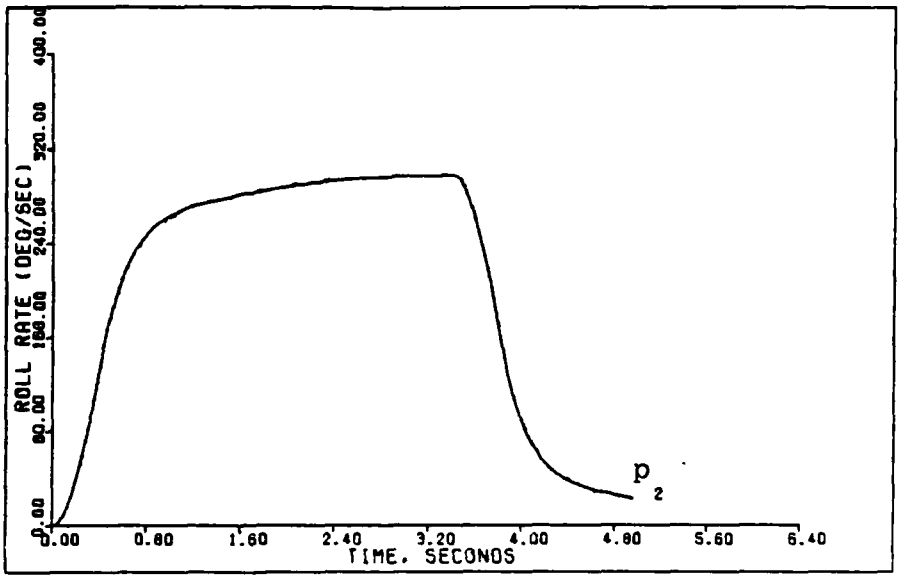



Figure 30. Roll Rate Response of the Initial Roll Rate Command System to 308 deg/sec Pulse Command (0.9 Mach 20,000 feet)

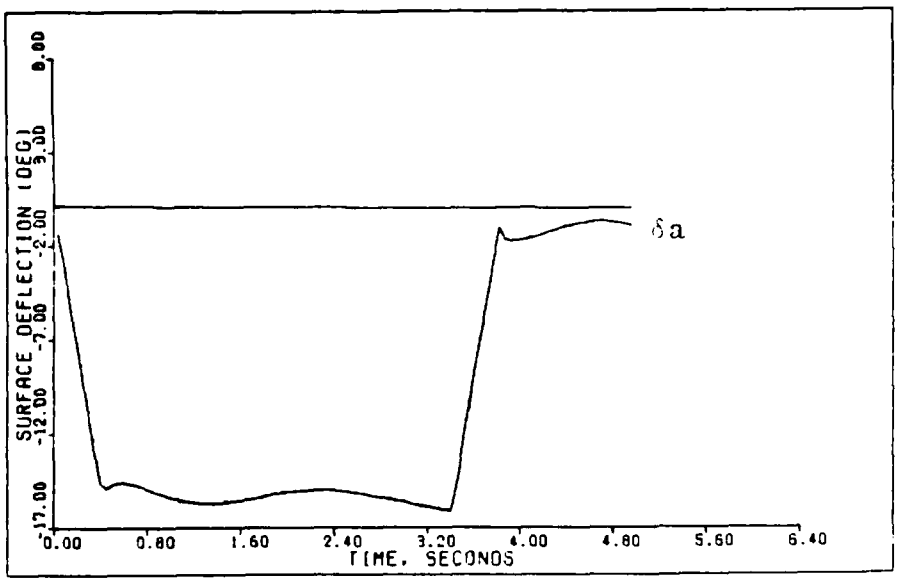



Figure 31. Aileron Response of the Initial Roll Rate Command System to a 308 deg/sec Pulse Command (0.9 Mach 20,000 feet)

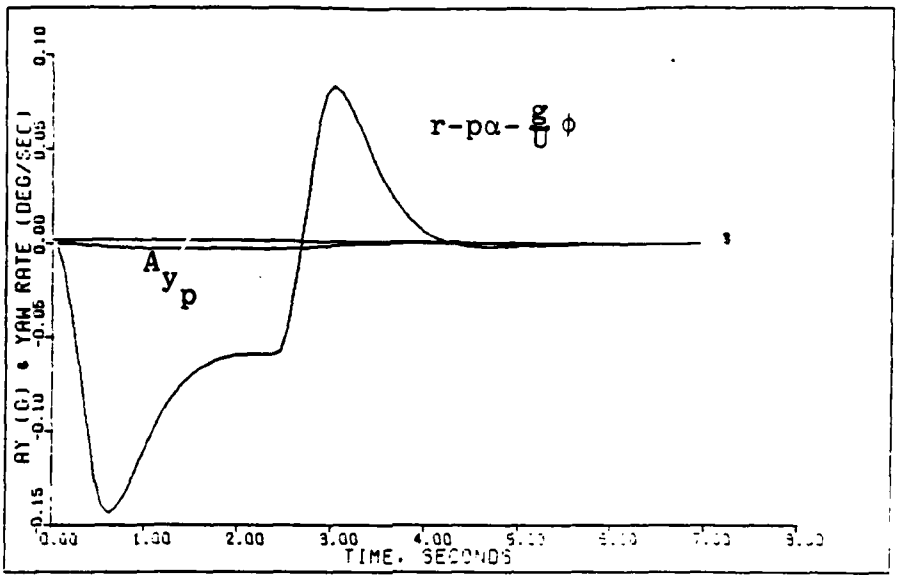



Figure 32. Sideforce and Output Feedback Response of the Initial Roll Rate Command System to a 10 deg/sec Pulse (0.9 Mach 20,000 feet)

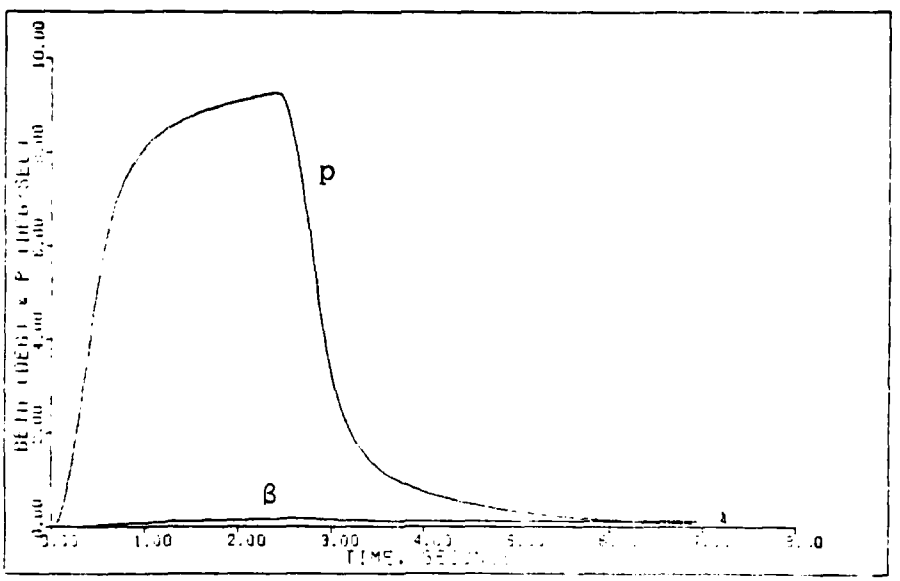



Figure 33. Roll Rate and Sideslip Response of the Initial Roll Rate Command System to a 10 deg/sec Pulse (0.9 Mach 20,000 feet)



Reproduced from best available copy.

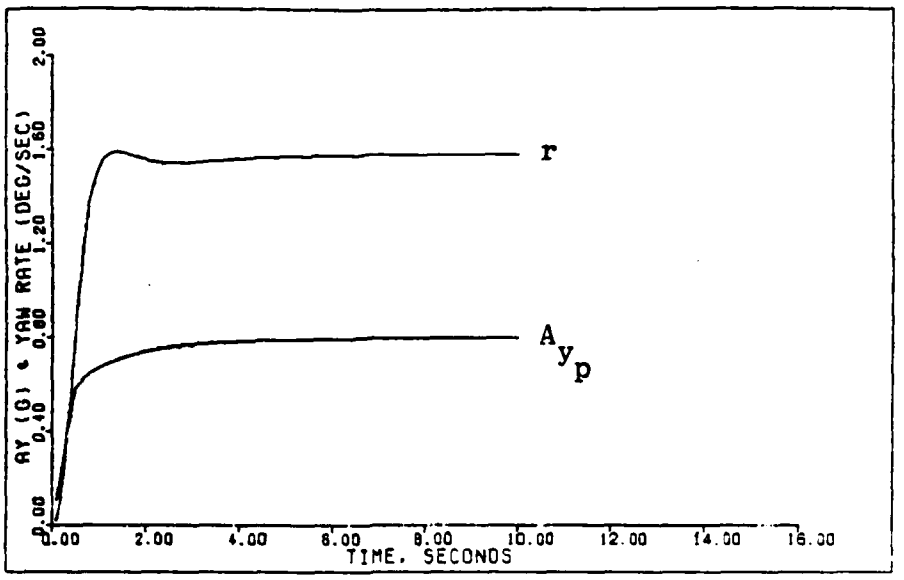



Figure 34. Yaw Rate and Sideforce Responses of the Sideforce System to a 0.8g Step Command (0.9 Mach 20,000 feet)

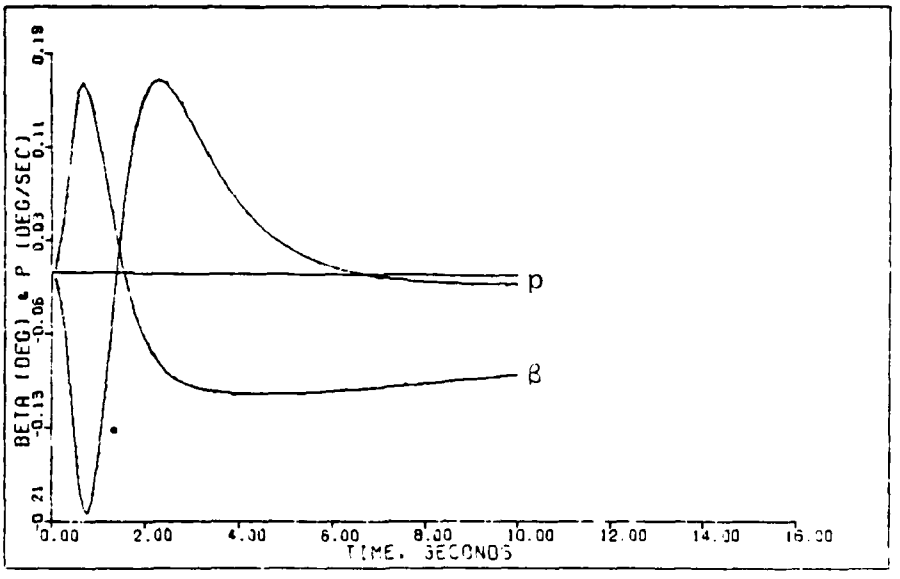



Figure 35. Sideslip and Roll Rate Response of the Sideforce System to a 0.8g Step Command (0.9 Mach 20,000 feet)

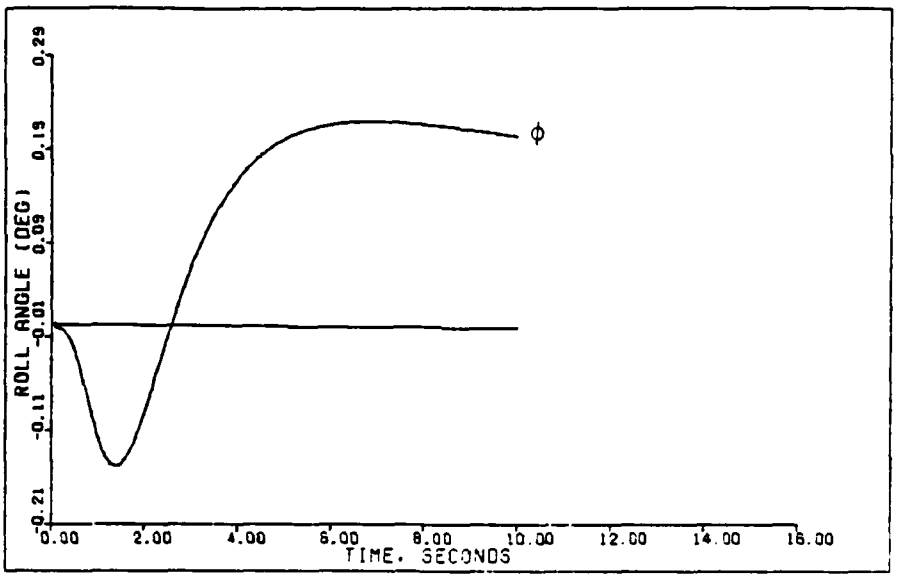



Figure 36. Roll Angle Response of the Sideforce System to a 0.8g Step Command (0.9 Mach 20,000 feet)

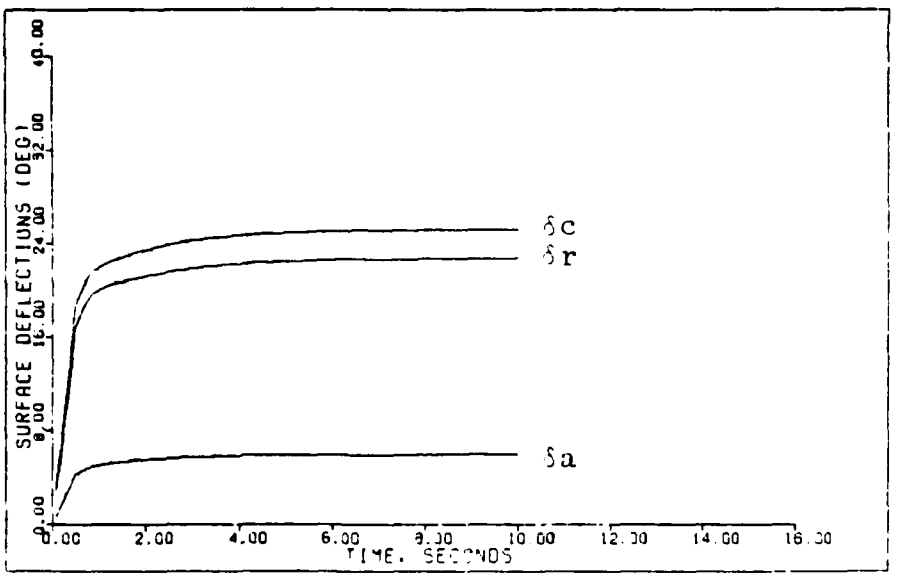



Figure 37. Surface Response of the Sideforce System to a 0.8g Step Command (0.9 Mach 20,000 feet)

## Pilot Interface

A major design consideration for any control system is the means by which the pilot injects his commands. In current fighter aircraft, the pilot is usually flying with one hand on the stick and the other on the throttle. Because of the highly maneuverable nature of combat with the associated high workload and the criticality of fast response, it is important to provide complete control without requiring the pilot to release either stick or throttle. At last count, the pilot had six functions to perform with switches on the throttle (not including thrust control itself) and up to seven functions on the stick in addition to conventional pitch and roll control. It is not practical to add extra input devices and expect anything but reduced performance.

The approach taken in this study is to preserve the conventional pilot control input methods. This is accomplished by an interface computation that provides the digital controller with the proper inputs for normal operation. In all cases, these interface computations are kept extremely simple. Note that in each case, all inputs to the controller must be specified. Two are required for pitch, while three are needed for the lateral-directional controller. In pitch control, the conventional stick input is accepted as a "g" command, and the two inputs needed by the controller are developed from Equation (4.11) as shown in Figure 38. In

roll, the commands to the controller are developed as illustrated in Figure 39. For sideforce control, the rudder pedal input is used as illustrated in Figure 40. The development of a yaw rate input is from Equation (4.12).

Roll and sideforce command methods can be combined for the lateral-directional system. The zero input to the $A_{y_p}$ command path, needed for a roll rate response system, can be supplied by the rudder pedal transducer when no force is applied by the pilot. The same can be said for the zero roll rate command for the sideforce system. The zero input can be provided by the roll stick transducer.

Pointing is assumed to be commanded from an automated fire control system. However, manual control can be provided using a twist throttle for pitch pointing command and switching the rudder pedal signal so that it provides an input to the lateral pointing system.

The complete control system block diagrams are shown in Figures 41 and 42 with the pilot interface and controller separated by the dot-dash line. The portion in dashed lines indicates the pointing system.

## Instabilities

As discussed in Chapter I, because of the need for a controller that commands rates and accelerations, conditional stability is accepted for the designs. However, care is exercised to identify all instabilities encountered in the design process. Two general types of instabilities are

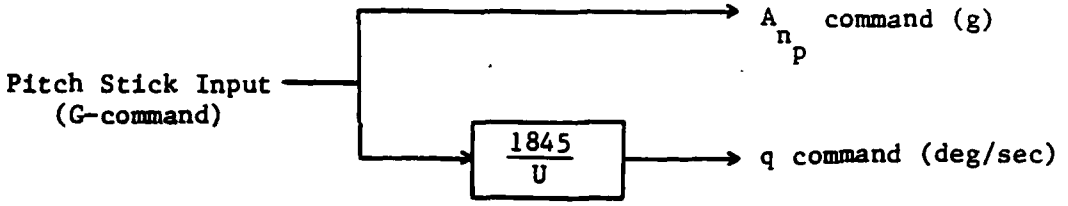



Figure 38. Pilot Interface for the G-Command System

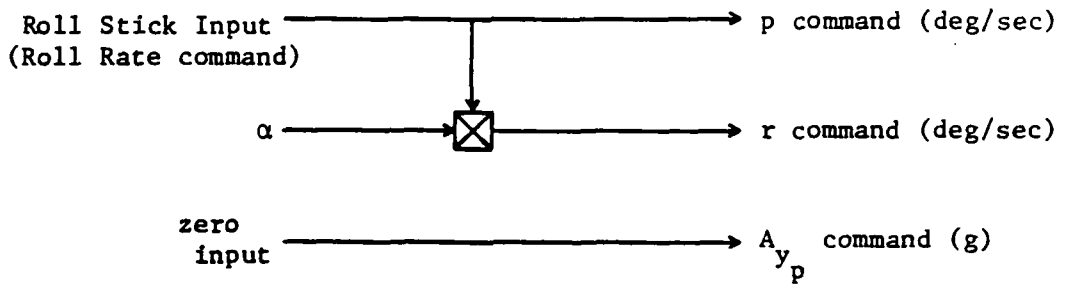



Figure 39. Pilot Interface for the Roll Rate Command System

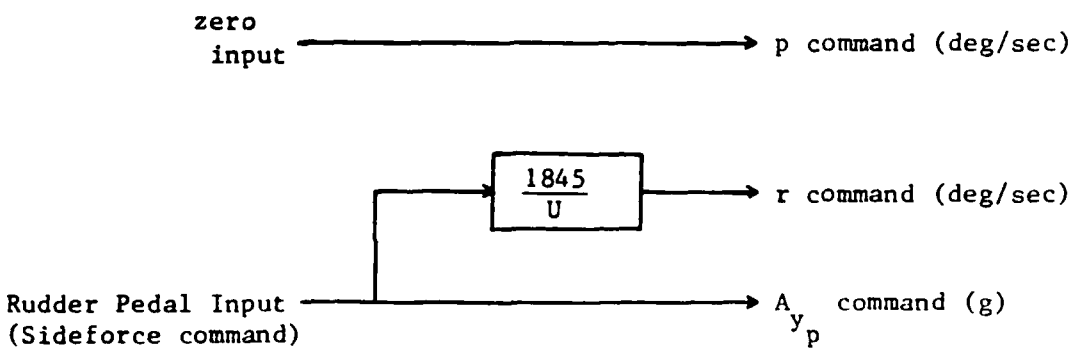



Figure 40. Pilot Interface for the Sideforce System

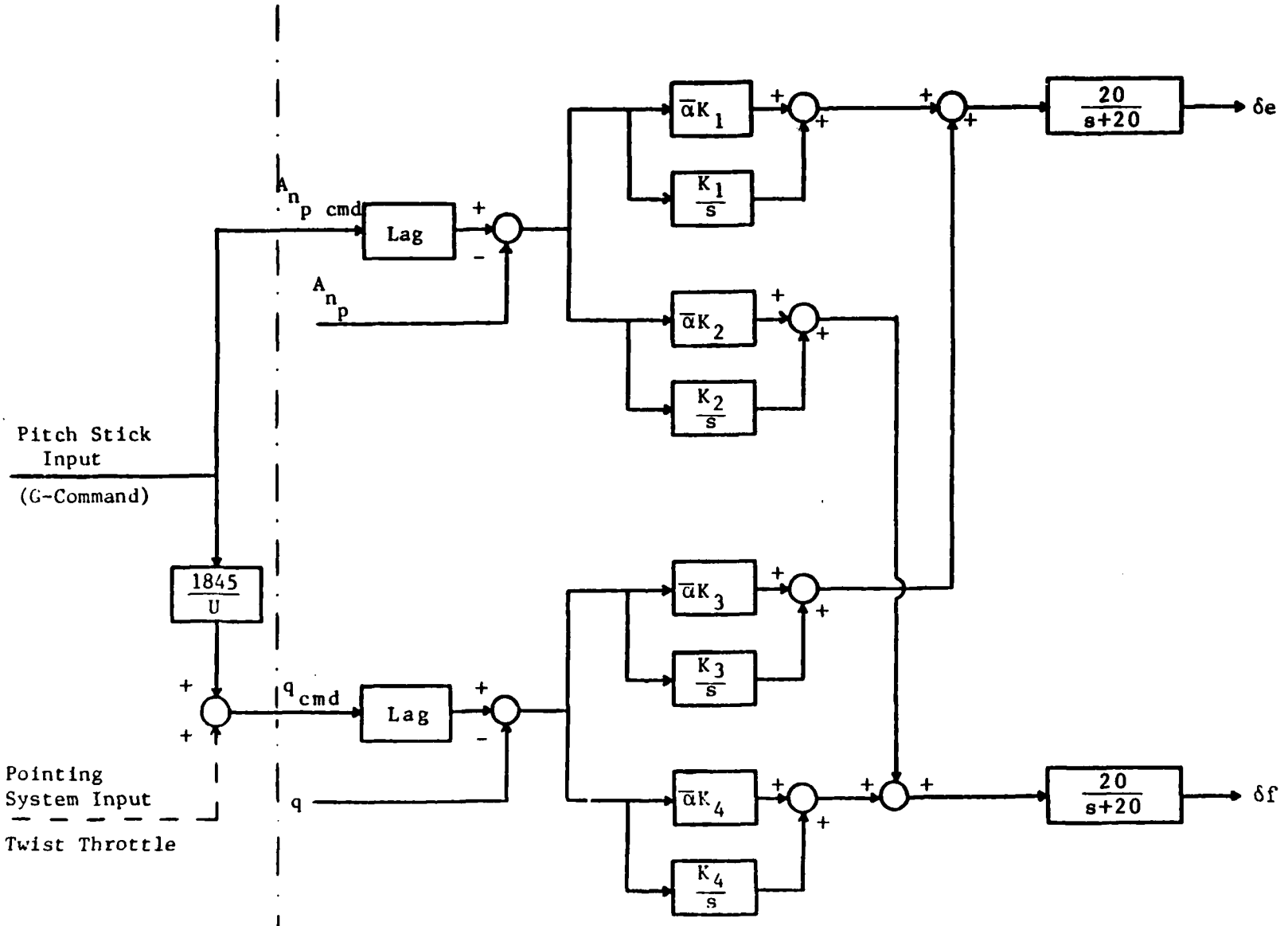



Figure 41. Block Diagram of Longitudinal G-Command System With Pilot Interface Addition and Including the Pitch Pointing System

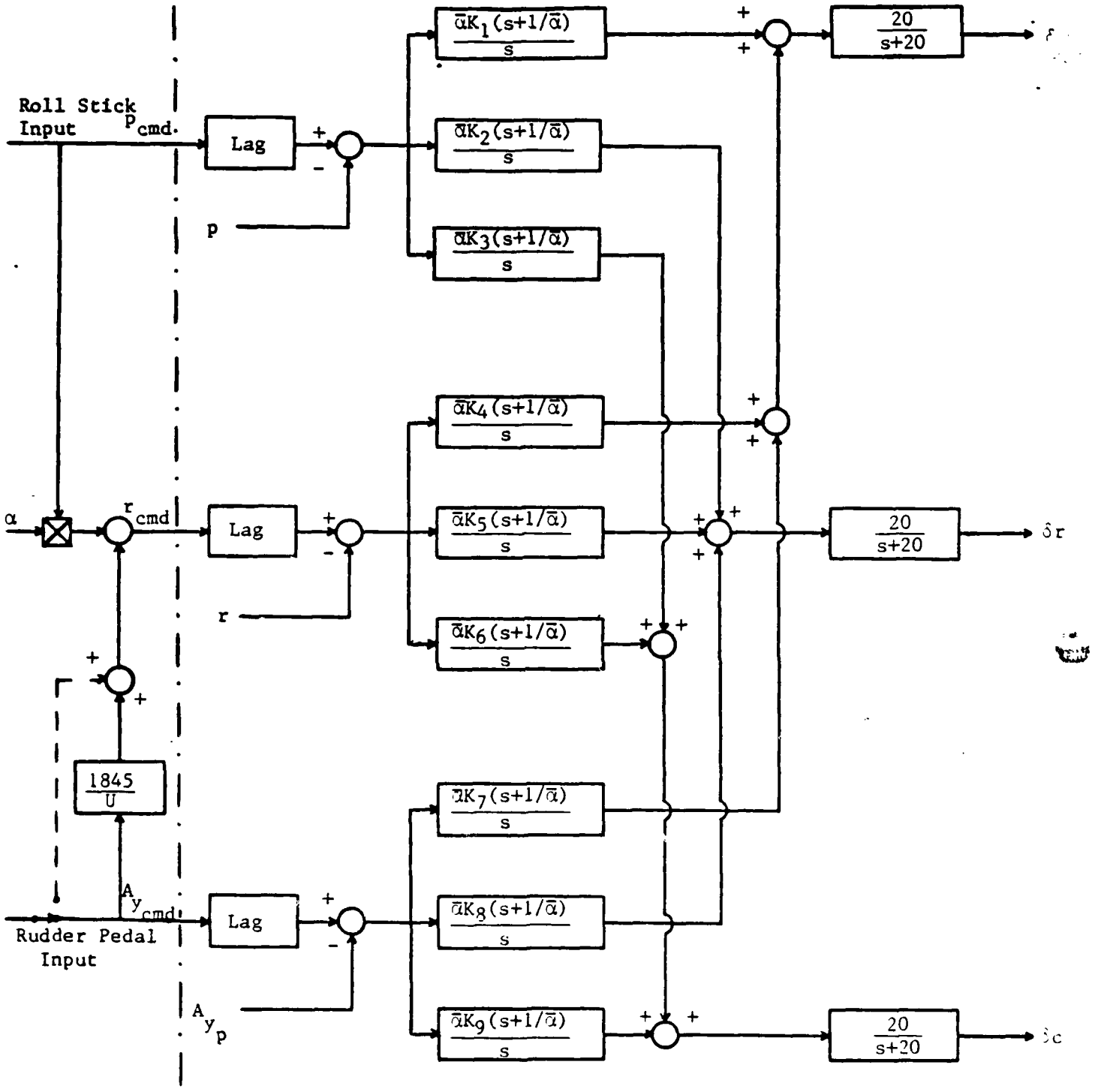



Figure 42. Block Diagram of the Roll Rate Command System and Direct Sideforce System with Pilot Interface Addition (Yaw Pointing System is included)

found. These consist of a low gain instability and a high gain instability. The low gain stability is seen in the longitudinal designs and is the result of having a statically unstable aircraft. As control system gain is reduced, a point is reached where the unstable aircraft reappears; adequate augmentation is not being provided. This establishes a lower gain boundary for all subsonic longitudinal designs.

In both longitudinal and lateral-directional designs, an oscillation is consistently encountered for high gains. An example is shown in Figures 43 and 44. This is the longitudinal design at 0.9 Mach and 20,000 feet with parameters of $\bar{\alpha} = 1.0$ , $\varepsilon = 1.0$ , and $\Sigma$ elements equal to one. Figures 11 and 12 illustrate the same high gain instability in the very simple regular design discussed earlier in this chapter. It is apparent that the instability occurs regardless of the inclusion of sensor or actuator dynamics or a measurement matrix. The observed frequency of the oscillation is always a subharmonic of the sampling frequency. Further investigation is warranted to enable the setting of boundaries for such an instability. The system roots are checked and are stable for the system responses shown. The initial attempt of each design generally results in this instability. As gain is reduced, the oscillation dies out. It is fortunate that this high gain limit usually does not compromise performance of the designs. The gain

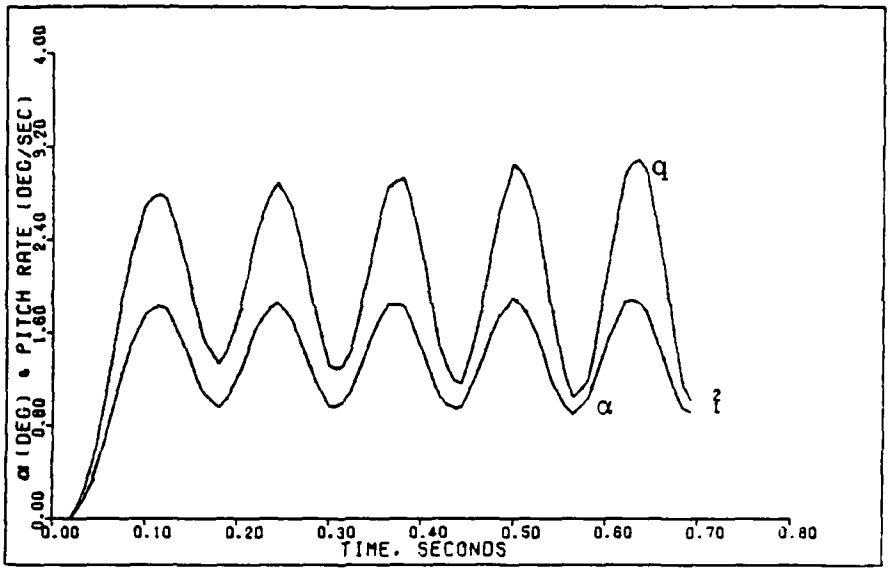



Figure 43. Response Plot for the Rate Controller to a 2 deg/sec Step Command (0.9 Mach 20,000 feet)

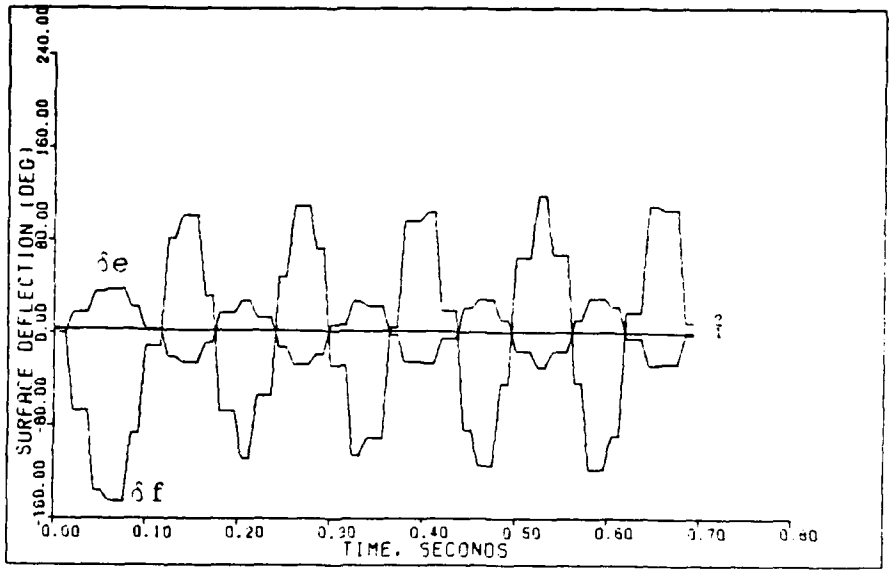



Figure 44. Surface Position Plot for the Rate Controller to a 2 deg/sec Step Command (0.9 Mach 20,000 feet)

reductions required to meet surface rate limit requirements prevent the instability. However, as faster actuators become available, this should be considered as a limiting condition in design performance.

# V. Evaluation

## Time Response Analysis

For the longitudinal designs, time responses for 1 g step commands are presented for each flight condition under study. Five degree per second roll rate pulses are used to evaluate the roll rate design. Maximum step commands are used for the sideforce design demonstrations. In addition, fuselage pitch pointing is shown at the 0.9 Mach 20,000 feet condition for a pitch rate step command.

The time responses presented exhibit the properties desired of the design. Stability is adequate, and the system provides proper, fast, well-behaved responses. The outputs are free of ringing or oscillations. Control surface deflections are within both rate and position limits for all maneuvers. Control of body rates and accelerations is provided using reliable feedbacks.

The designs are established using maximum estimated commands for each flight condition to provide system gains which do not exceed surface rate or position limits. Responses for maximum commands are presented in Appendix C. Such maximum maneuvers are not meant to imply that the aircraft model is an adequate representation for such large commands; they are used only to give an indication of the maximum acceptable system gains to prevent exceeding hardware limits.

Prior to each set of resp ses, the design values, controller gains, and measurement atrix elements are specified.

- - - - - - - - - - - - - - - - - - - - - - - - - - - - - - - - - - - - - -

**Design Data for the G- mmand System**

**Flight Condition: .9 Mach 20,000 feet**

$T = 0.02$

$\bar{\alpha} = 1.0$

$$\underline{\Sigma} = \begin{bmatrix} 0.1 & 0.0 \\ 0.0 & 2.35 \end{bmatrix}$$

$\varepsilon = 1.0$

$$\underline{M} = \begin{bmatrix} 0 & 0 & 0 & 0 & 0 \\ 0 & 0 & 0 & 0 & 0.1 \end{bmatrix}$$

$$\underline{K}_0 = \underline{K}_1 = \begin{bmatrix} -0.01299 & -0.0 & 34 \\ 0.04827 & -0.0 & 16 \end{bmatrix}$$

Input ramp time: 0.4 sec ds

Input commands: $A_{n_p}$ = 1g tep

$$q = \left[\frac{184}{U}\right] A_{n_p} = 1.977 \text{ deg/sec}$$

NOTE: Step inputs are ramped to eady state over a specified time. This time is design ed as the "input ramp time" given above.

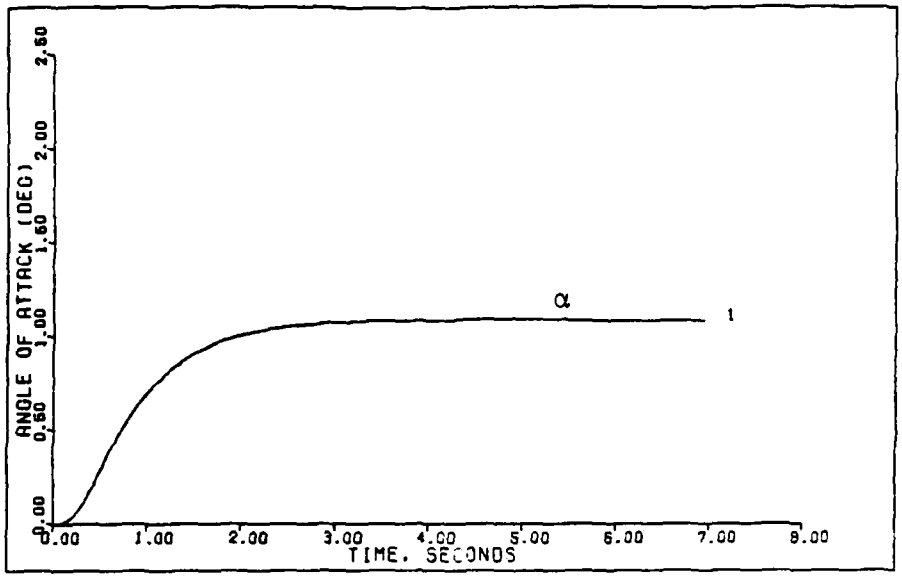



Figure 45a. G-Command System Response to a 1g Step Command (0.9 Mach 20,000 feet)

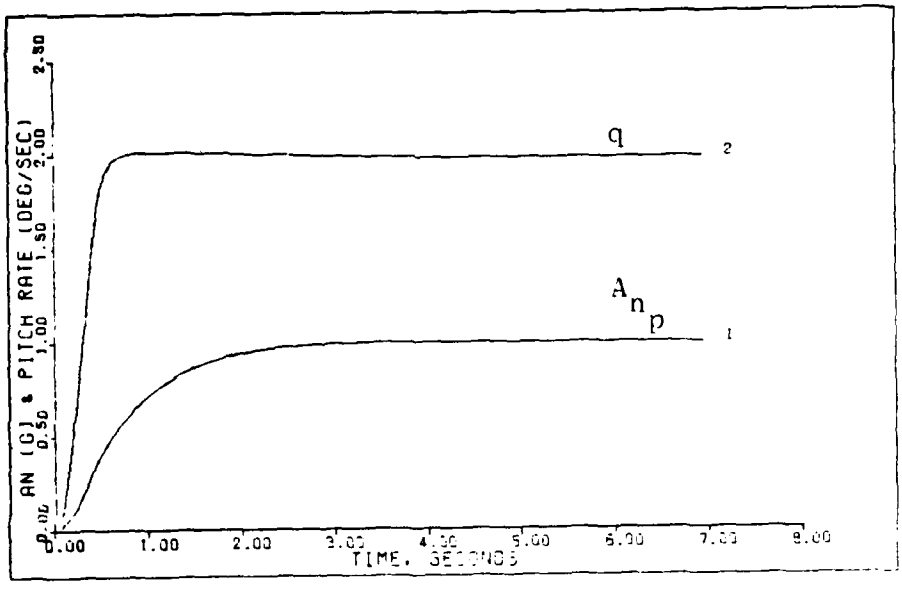



Figure 45b. G-Command System Response to a 1g Step Command (0.9 Mach 20,000 feet)

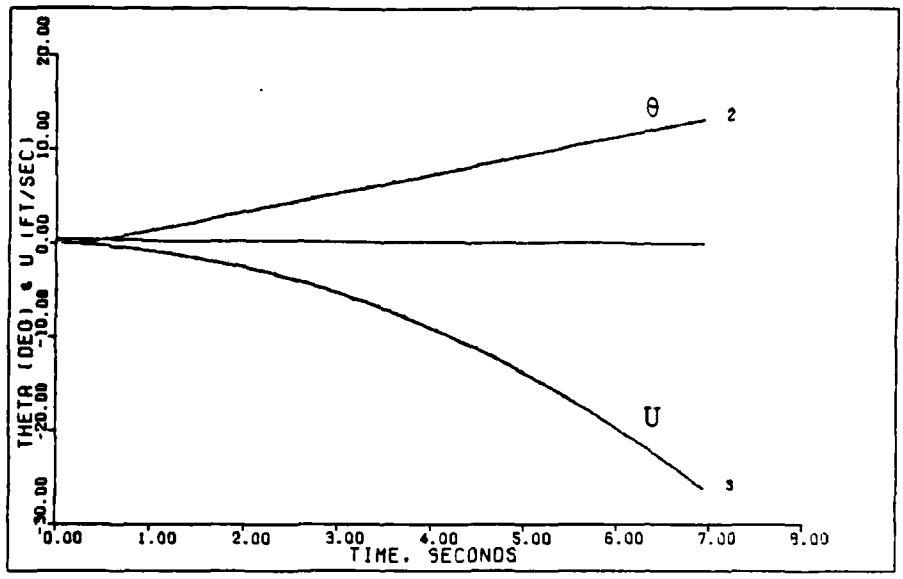



Figure 45c. G-Command System Response to a 1g Step Command (0.9 Mach 20,000 feet)

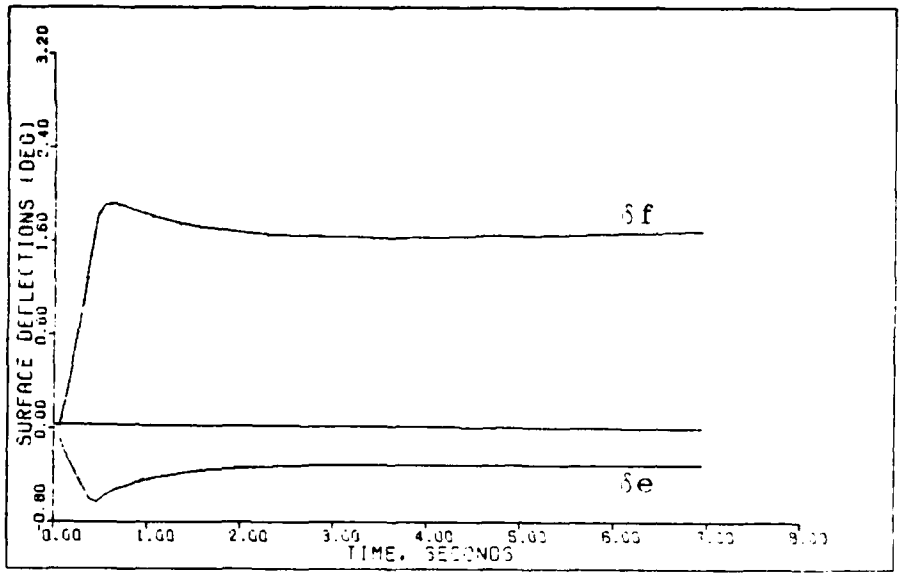



Figure 45d. G-Command System Response to a 1g Step Command (0.9 Mach 20,000 feet)

Design Data for the Pitch Pointing System

Flight Condition: 0.9 Mach 20,000 feet

$T = 0.02$

$\bar{\alpha} = 0.5$

$$\underline{\Sigma} = \begin{bmatrix} 2.5 & 0 \\ 0 & 1.0 \end{bmatrix}$$

$\varepsilon = 1.0$

$$\underline{M} = \begin{bmatrix} 0 & 0 & 0 & 0 & 0 \\ 0 & 0 & 0 & 0 & 0.1 \end{bmatrix}$$

$$\underline{K}_0 = \begin{bmatrix} -0.1623 & -0.007519 \\ 0.6034 & -0.01067 \end{bmatrix}$$

$$\underline{K}_1 = \begin{bmatrix} -0.3247 & -0.01504 \\ 1.207 & -0.02135 \end{bmatrix}$$

Input ramp time: 0.0 seconds

Input command: $A_{n_p} = 0.0$

$q = 1.0$ deg/sec step

NOTE: Step commands are ramped to steady state over a specified time. This time is designated as the "input ramp time" given above.

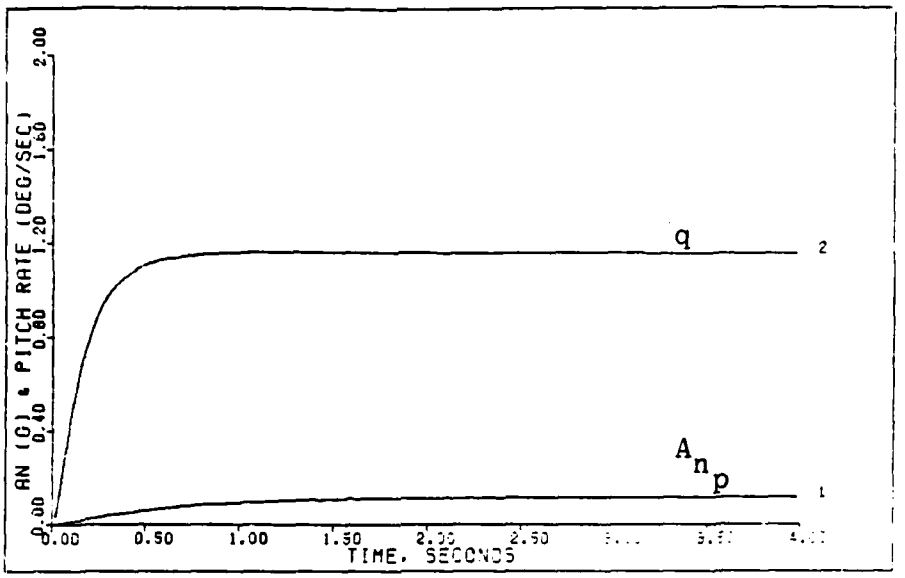



Figure 46a. Pitch Pointing System Response to a 1 deg/sec Step Command (0.9 Mach 20,000 feet)

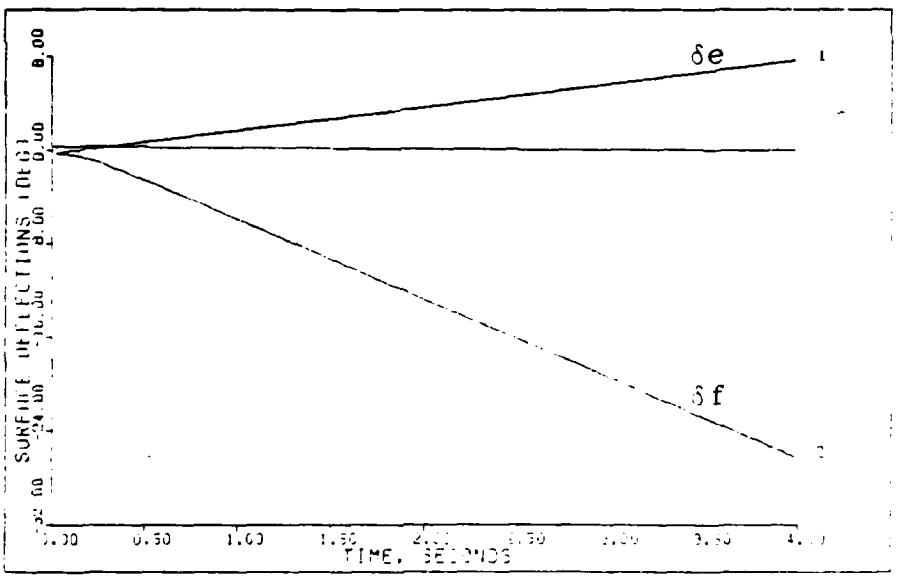



Figure 46b. Pitch Pointing System Response to a 1 deg/sec Step Command (0.9 Mach 20,000 feet)

## Design Data for the Roll Rate Command System

Flight Condition: 0.9 Mach 20,000 feet

$T = 0.02$

$\bar{\alpha} = 1.0$

$$\underline{\Sigma} = \begin{bmatrix} 1 & 0 & 0 \\ 0 & 1 & 0 \\ 0 & 0 & 1 \end{bmatrix}$$

$\varepsilon = 1.0$

$$\underline{M} = \begin{bmatrix} 0 & 0 & 0 & 0 & 0 \\ 0 & 0 & 0 & 0.25 & 0 \\ 0 & 0 & 0 & 0 & 0.25 \end{bmatrix}$$

$$\underline{K}_0 = \underline{K}_1 = \begin{bmatrix} 0.377 & -0.0030510 & -0.0120 \\ 1.460 & 0.0008075 & -0.0583 \\ 1.601 & -0.0005162 & -0.0287 \end{bmatrix}$$

Input ramp time: 0.4 seconds

Input command: $A_{y_p} = 0.0$

$p = 5$ deg/sec pulse for 3 sec duration

$r = p\alpha$ where $\alpha = 0.0325$ radians

NOTE:
1. Pulse inputs are ramped to a maximum value over a specified time. This time is designated as the input ramp time given above. The input is held at a maximum value for a duration time and then ramped back to zero. Both ramp times have the same value.
2. Rolls are performed about the velocity vector.

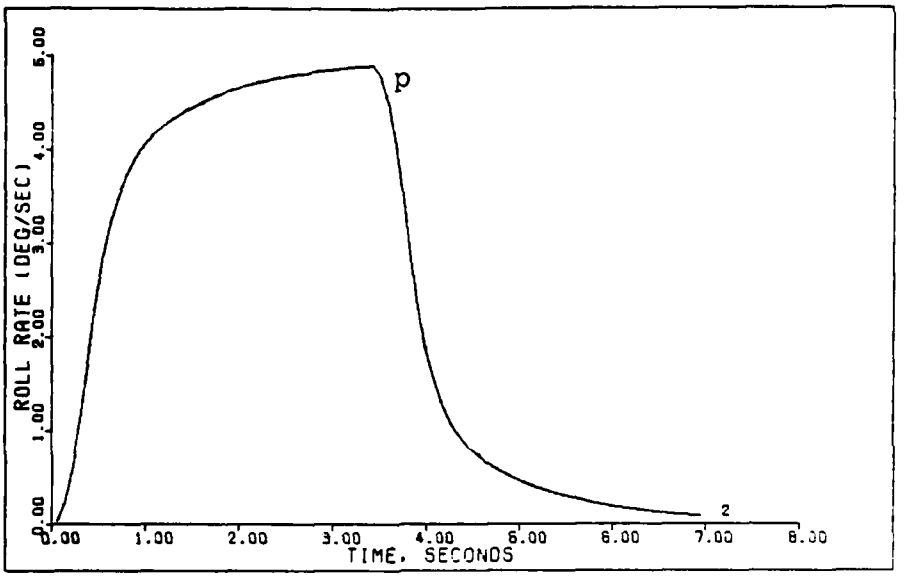



Figure 47a. Roll Rate Command System Response to a 5 deg/sec Pulse Command (0.9 Mach 20,000 feet)

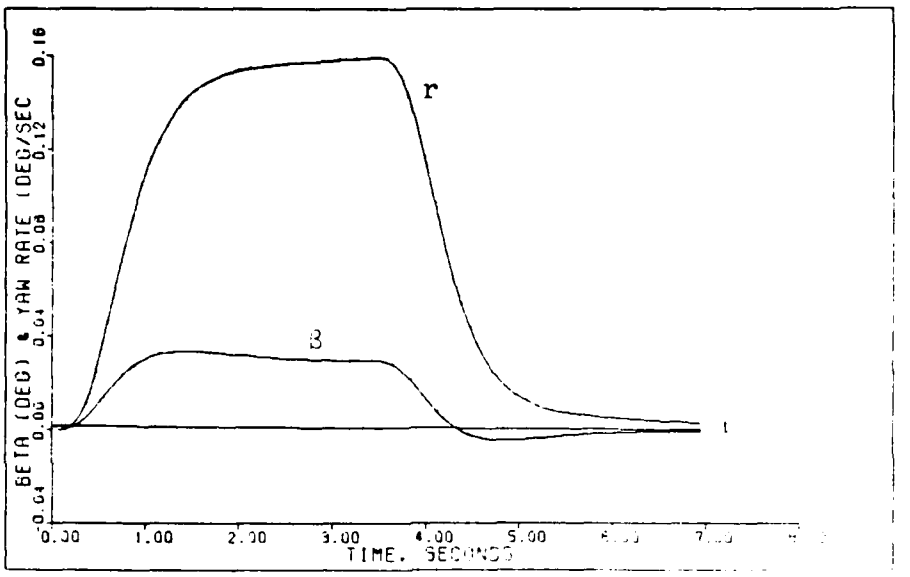



Figure 47b. Roll Rate Command System Response to a 5 deg/sec Pulse Command (0.9 Mach 20,000 feet)

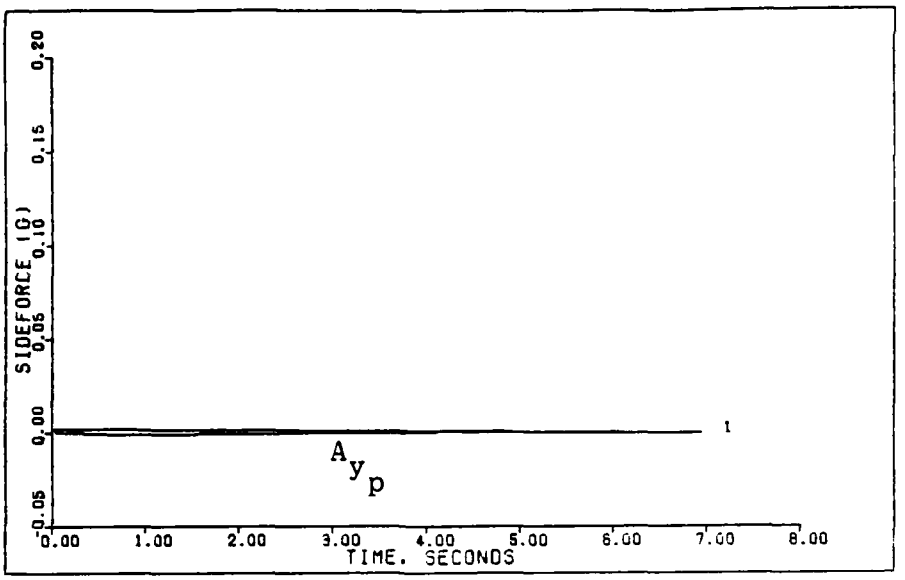



Figure 47c. Roll Rate Command System Response to a 5 deg/sec Pulse Command (0.9 Mach 20,000 feet)

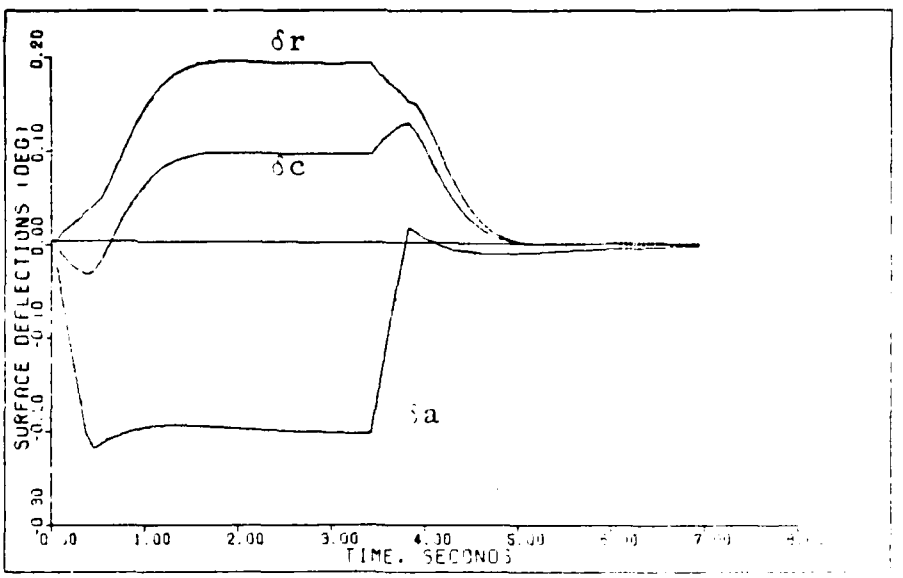



Figure 47d. Roll Rate Command System Response to a 5 deg/sec Pulse Command (0.9 Mach 20,000 feet)

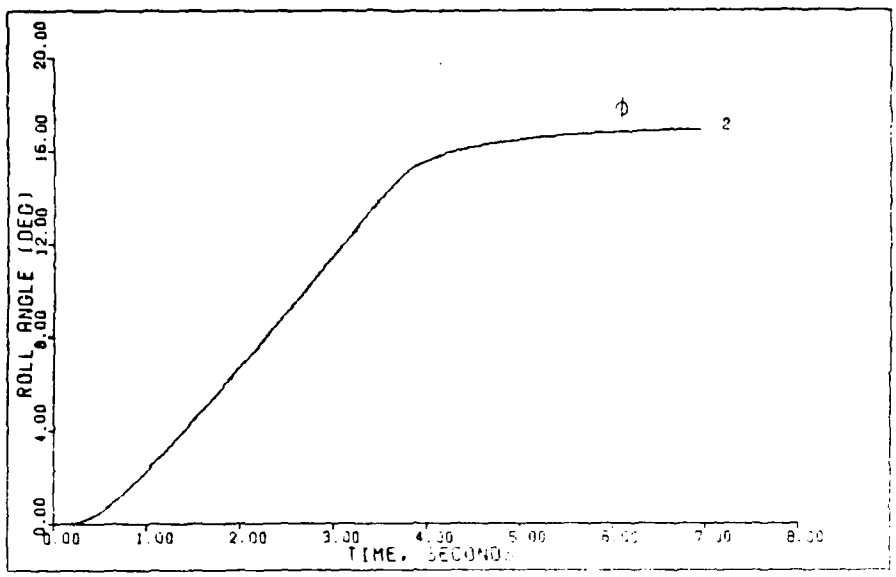
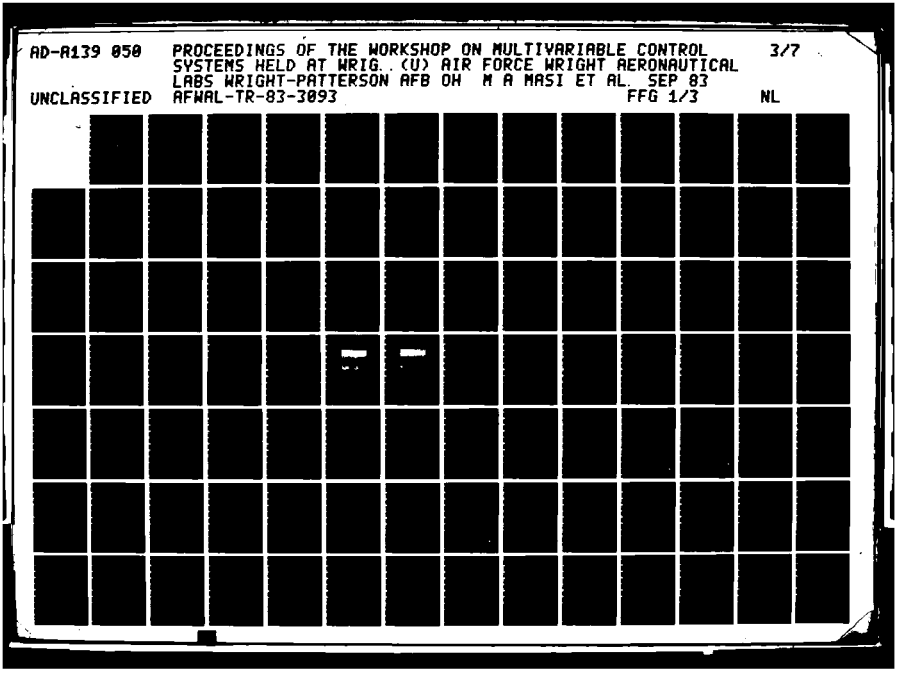
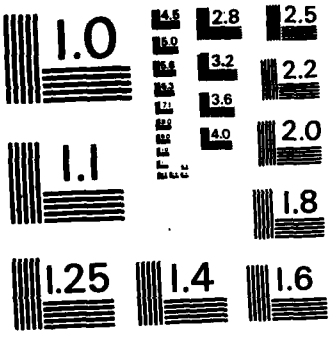



Figure 47e. Roll Rate Command System Response to a 5 deg/sec Pulse Command (0.9 Mach 20,000 feet)

AD-A139 050 PROCEEDINGS OF THE WORKSHOP ON MULTIVARIABLE CONTROL SYSTEMS HELD AT WRIG.. (U) AIR FORCE WRIGHT AERONAUTICAL LABS WRIGHT-PATTERSON AFB OH M A MASI ET AL. SEP 83 3/7

UNCLASSIFIED AFWAL-TR-83-3093 FFG 1/3 NL






MICROCOPY RESOLUTION TEST CHART
NATIONAL BUREAU OF STANDARDS-1963-A

## Design Data for the Sideforce System

### Flight Condition: 0.9 Mach 20,000 feet

$T = 0.02$

$\bar{\alpha} = 1.0$

$$\underline{\Sigma} = \begin{bmatrix} 1.0 & 0 & 0 \\ 0 & 2.3 & 0 \\ 0 & 0 & 1.0 \end{bmatrix}$$

$\varepsilon = 1.0$

$$\underline{M} = \begin{bmatrix} 0 & 0 & 0 & 0 & 0 \\ 0 & 0 & 0 & 0.25 & 0 \\ 0 & 0 & 0 & 0 & 0.25 \end{bmatrix}$$

$$\underline{K}_0 = \underline{K}_1 = \begin{bmatrix} 0.377 & -0.007018 & -0.0120 \\ 1.460 & 0.001857 & -0.0583 \\ 1.601 & -0.001187 & -0.0287 \end{bmatrix}$$

Input ramp time: 0.5 seconds

Input commands: $A_{y_p} = 0.8g$ step

$p = 0.0$

$r = \left[\frac{1845}{U}\right] A_{n_p} = 1.5816$ deg/sec

NOTE: Step inputs are ramped to steady state over a specified time. This time is designated as the input ramp time given above.

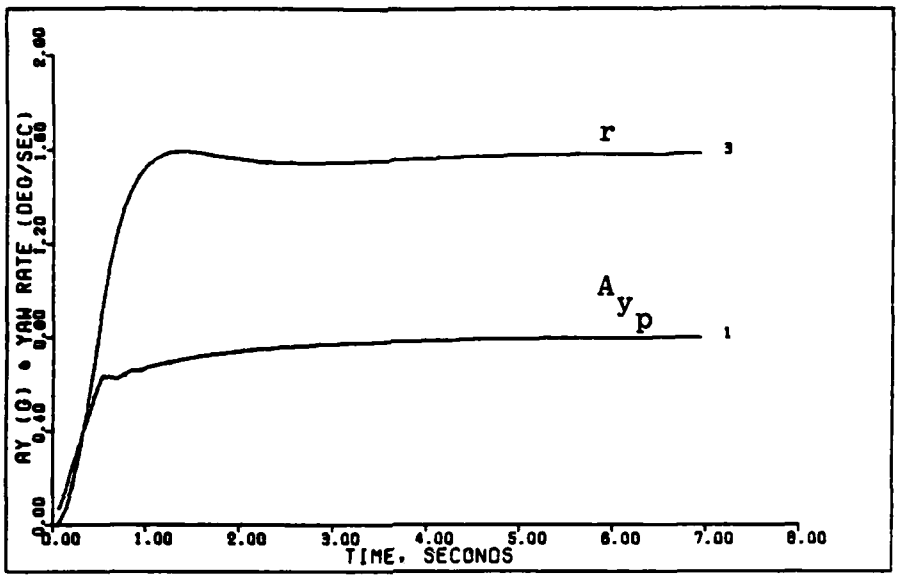



Figure 48a. Sideforce System Response to a 0.8g Step Command (0.9 Mach 20,000 feet)

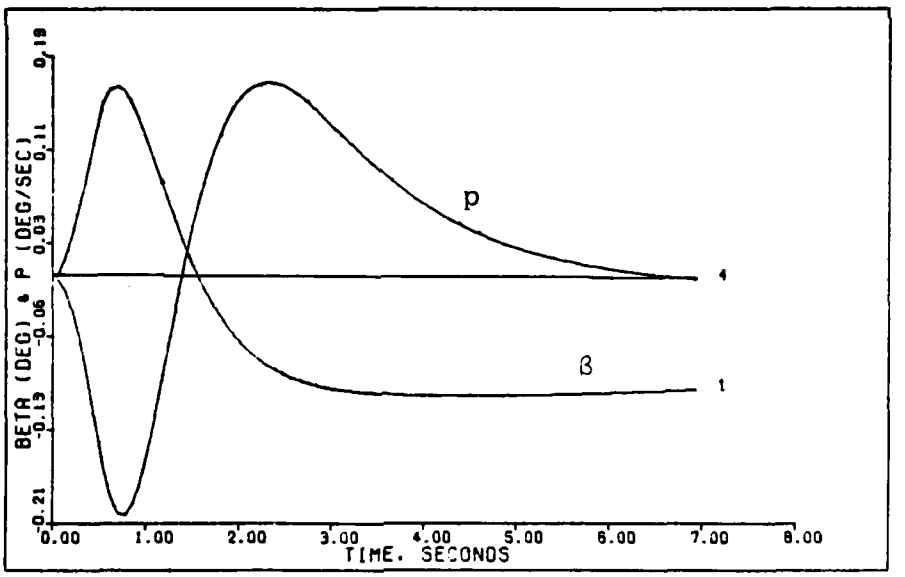



Figure 48b. Sideforce System Response to a 0.8g Step Command (0.9 Mach 20,000 feet)

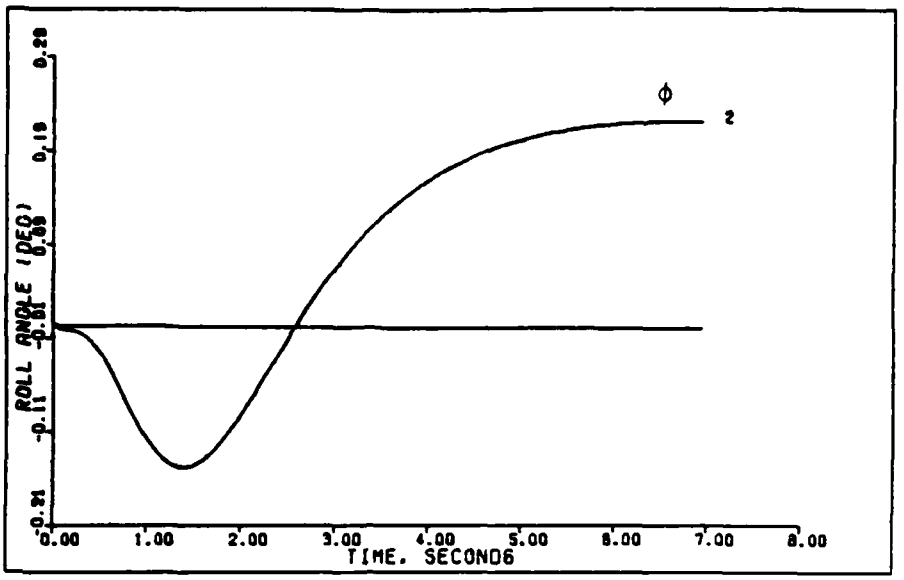



Figure 48c. Sideforce System Response to a 0.8g Step Command (0.9 Mach 20,000 feet)

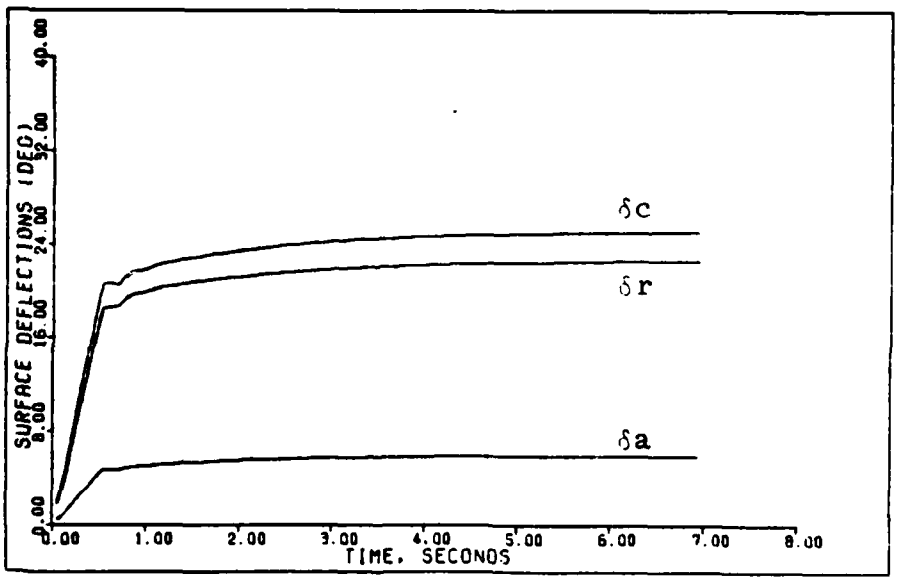



Figure 48d. Sideforce System Response to a 0.8g Step Command (0.9 Mach 20,000 feet)

## Design Data for the G-Command System

### Flight Condition: 1.6 Mach 30,000 feet

$T = 0.02$

$\bar{\alpha} = 0.2$

$$\underline{\Sigma} = \begin{bmatrix} 0.045 & 0 \\ 0 & 4.5 \end{bmatrix}$$

$\epsilon = 2.5$

$$\underline{M} = \begin{bmatrix} 0 & 0 & 0 & 0 & 0 \\ 0 & 0 & 0 & 0 & 0.1 \end{bmatrix}$$

$$\underline{K}_0 = \begin{bmatrix} -0.00425 & -0.01493 \\ 0.02389 & -0.1084 \end{bmatrix}$$

$$\underline{K}_1 = \begin{bmatrix} -0.02125 & -0.07464 \\ 0.1195 & -0.5419 \end{bmatrix}$$

Input ramp time: 0.4 seconds

Input commands: $A_{n_p}$ = 1g step

$$q = \left[\frac{1845}{U}\right] A_{n_p} = 1.159 \text{ deg/sec}$$

NOTE: Step inputs are ramped to steady state over a specified time. This time is designated as the input ramp time given above.

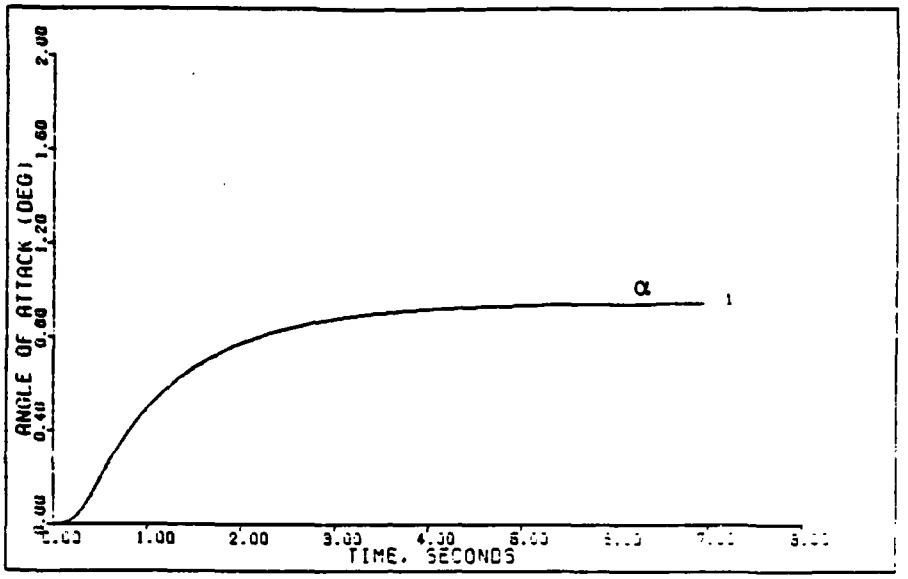



Figure 49a. G-Command System Response to a 1g Step Command (1.6 Mach 30,000 feet)

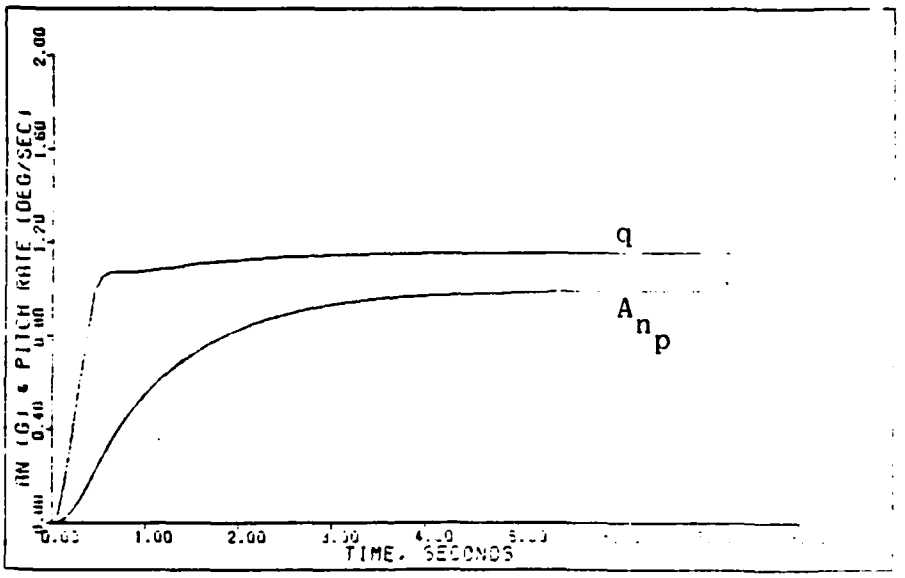



Figure 49b. G-Command System Response to a 1g Step Command (1.6 Mach 30,000 feet)

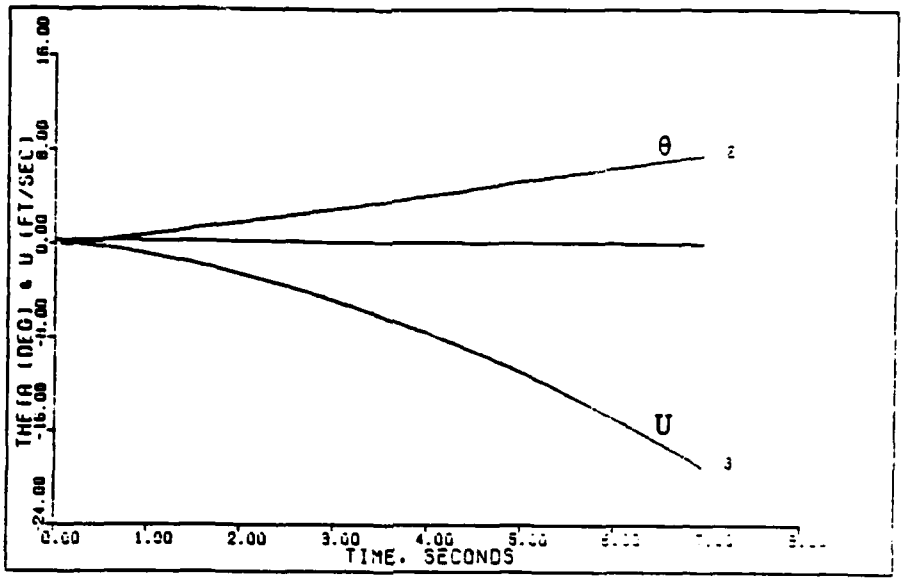



Figure 49c. G-Command System Response to a 1g Step Command (1.6 Mach 30,000 feet)

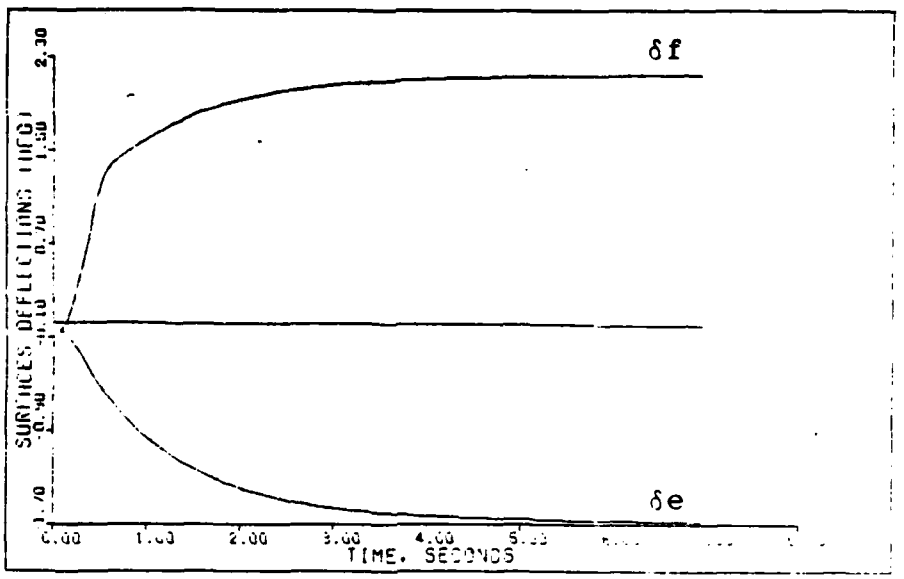



Figure 49d. G-Command System Response to a 1g Step Command (1.6 Mach 30,000 feet)



Copy available to DTIC does not permit fully legible reproduction

## Design Data for the Roll Rate Command System

**Flight Condition: 1.6 Mach 30,000 feet**

$T = 0.02$

$\bar{\alpha} = 1.0$

$$\underline{\Sigma} = \begin{bmatrix} 1.0 & 0 & 0 \\ 0 & 1.0 & 0 \\ 0 & 0 & 1.0 \end{bmatrix}$$

$\varepsilon = 1.0$

$$\underline{M} = \begin{bmatrix} 0 & 0 & 0 & 0 & 0 \\ 0 & 0 & 0 & 0.25 & 0 \\ 0 & 0 & 0 & 0 & 0.25 \end{bmatrix}$$

$$\underline{K}_0 = \underline{K}_1 = \begin{bmatrix} 0.8775 & -0.006716 & -0.02719 \\ 2.0680 & 0.005948 & -0.09214 \\ 1.0260 & -0.0002461 & -0.02024 \end{bmatrix}$$

Input ramp time: 0.3 seconds

Input commands: $A_{y_p} = 0.0$

$p$ = 5 deg/sec pulse for 3 sec duration

$r = p\alpha$ where $\alpha = 0.02932$ radians

NOTE:
1. Pulse inputs are ramped to a maximum value over a specific time. This time is designated as the input ramp time above. The input is held at a maximum value for a duration time and then ramped back to zero. Both ramp times have the same value.
2. Rolls are performed about the velocity vector.

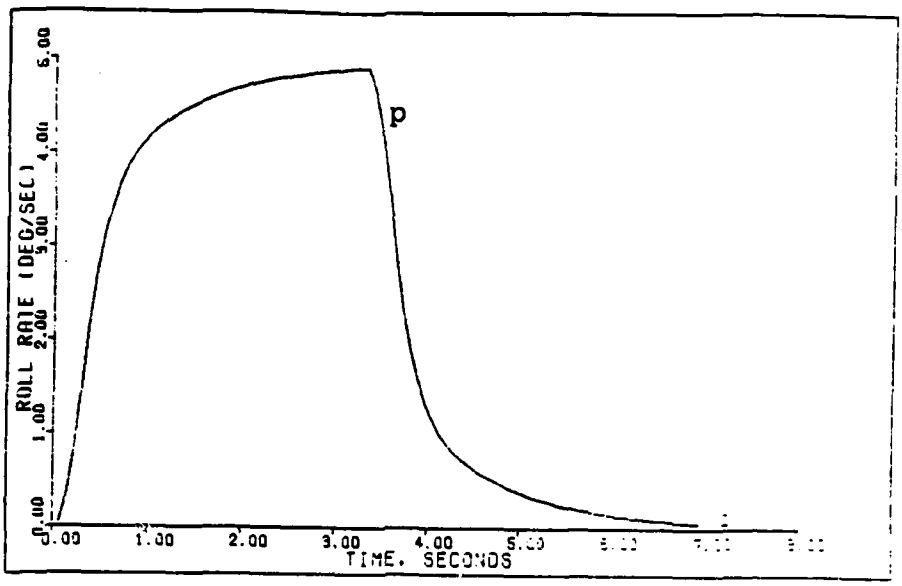



Figure 50a. Roll Rate Command System Response to a 5 deg/sec Pulse Command (1.6 Mach 30,000 feet)

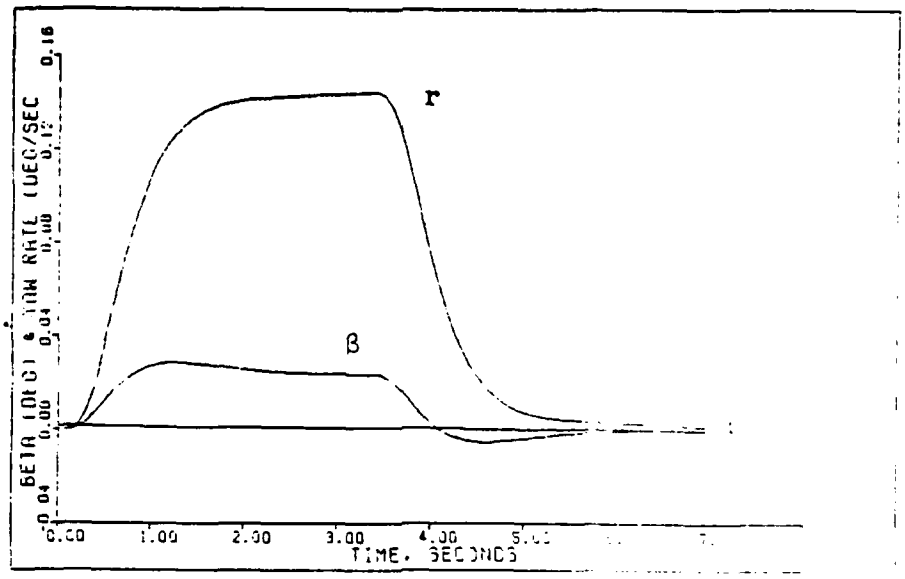



Figure 50b. Roll Rate Command System Response to a 5 deg/sec Pulse Command (1.6 Mach 30,000 feet)



Copy available to DTIC does not permit fully legible reproduction

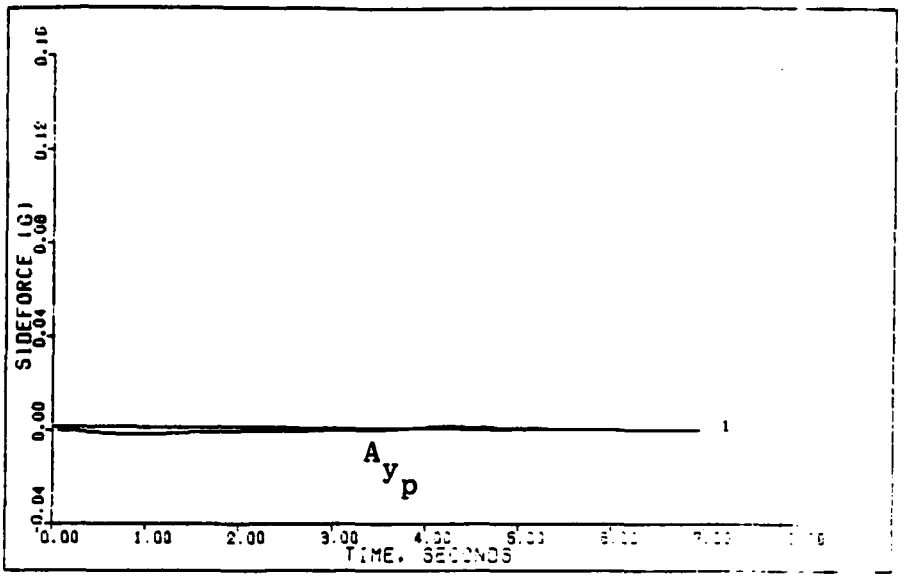



Figure 50c. Roll Rate Command System Response to a 5 deg/sec Pulse Command (1.6 Mach 30,000 feet)

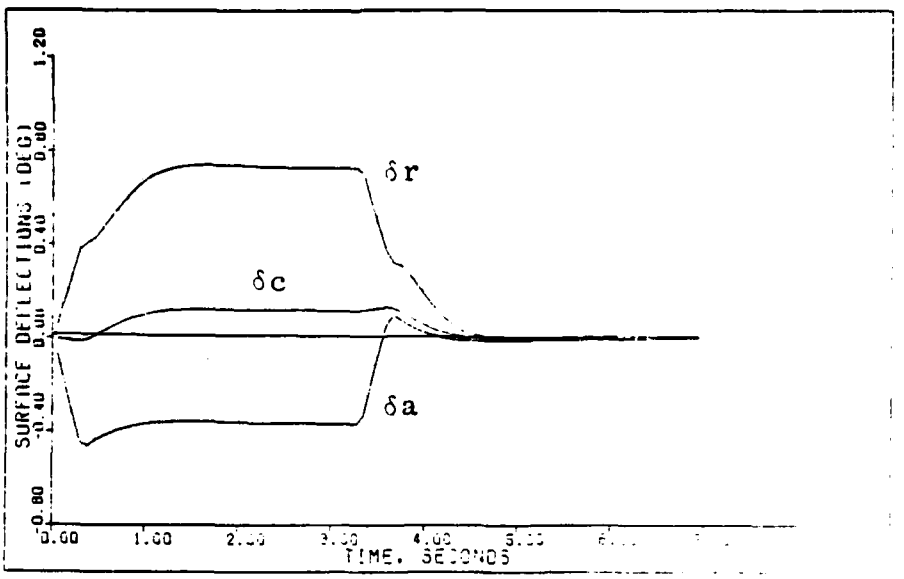



Figure 50d. Roll Rate Command System Response to a 5 deg/sec Pulse Command (1.6 Mach 30,000 feet)

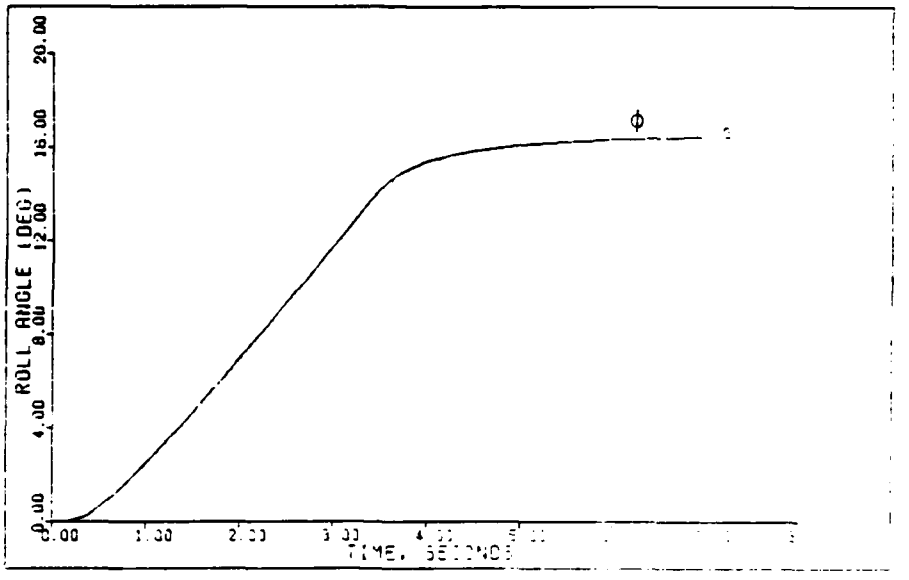



Figure 50e. Roll Rate Command System Response to a 5 deg/sec Pulse Command (1.6 Mach 30,000 feet)



Copy available to DTIC does not permit fully legible reproduction

## Design Data for the Sideforce System

**Flight Condition: 1.6 Mach 30,000 feet**

$T = 0.02$

$\bar{\alpha} = 1.0$

$$\underline{\Sigma} = \begin{bmatrix} 1.0 & 0 & 0 \\ 0 & 1.0 & 0 \\ 0 & 0 & 1.0 \end{bmatrix}$$

$\varepsilon = 1.0$

$$\underline{M} = \begin{bmatrix} 0 & 0 & 0 & 0 & 0 \\ 0 & 0 & 0 & 0.1 & 0 \\ 0 & 0 & 0 & 0 & 0.1 \end{bmatrix}$$

$$\underline{K}_0 = \underline{K}_1 = \begin{bmatrix} 0.8775 & -0.016790 & -0.06799 \\ 2.0680 & 0.014870 & -0.23040 \\ 1.0260 & -0.0006154 & -0.05060 \end{bmatrix}$$

Input ramp time: 0.5 seconds

Input commands: $A_{y_p} = 0.6g$ step

$p = 0.0$

$r = \left[\frac{1845}{U}\right] A_{y_p} = 0.7$ deg/sec

NOTE: Step inputs are ramped to steady state over a specific time. This time is designated as the input ramp time given above.

Design Data for the G-Command System

Flight Condition: 0.6 Mach 30,000 feet

$T = 0.02$

$\bar{\alpha} = 1.0$

$$\underline{\Sigma} = \begin{bmatrix} 0.02 & 0 \\ 0 & 1.0 \end{bmatrix}$$

$\varepsilon = 1.0$

$$\underline{M} = \begin{bmatrix} 0 & 0 & 0 & 0 & 0 \\ 0 & 0 & 0 & 0 & 0.167 \end{bmatrix}$$

$$\underline{K}_0 = \underline{K}_1 = \begin{bmatrix} -0.00102 & -0.04998 \\ 0.02827 & -0.03316 \end{bmatrix}$$

Input ramp time: 0.4 seconds

Input commands: $A_{n_p}$ = 1g step

$$q = \left[\frac{1845}{U}\right] A_{n_p} = 3.091 \text{ deg/sec}$$

NOTE: Step inputs are ramped to steady state over a specified time. This time is designated as the input ramp time given above.

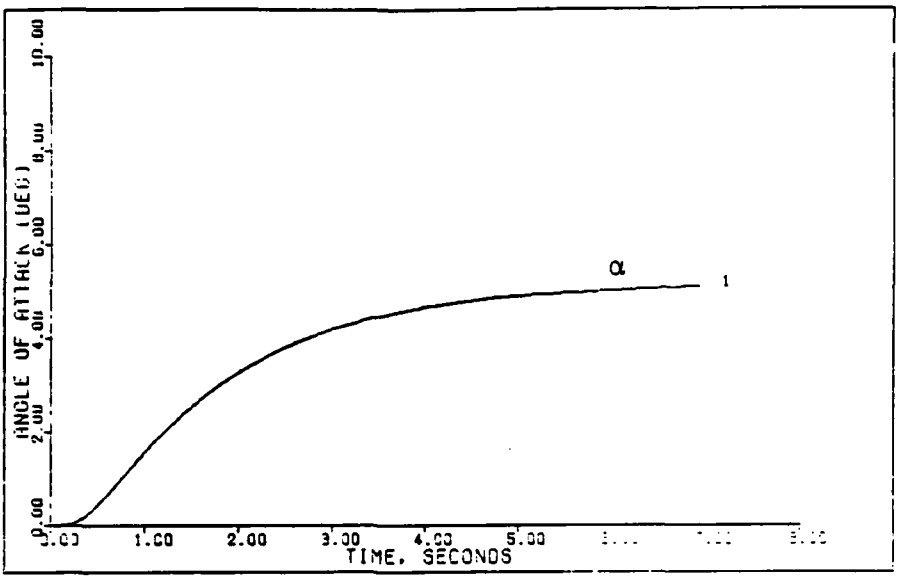



Figure 52a. G-Command System Response to a 1g Step Command (0.6 Mach 30,000 feet)

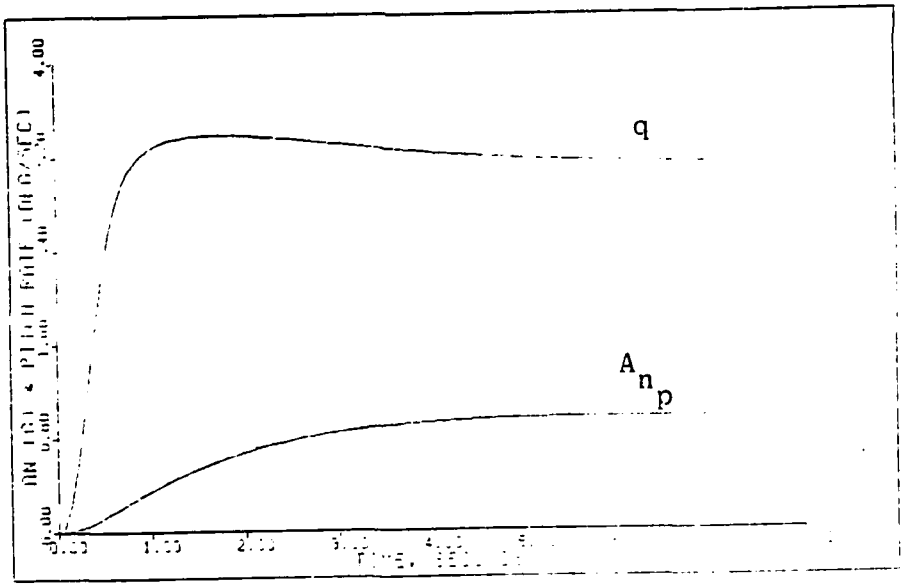



Figure 52b. G-Command System Response to a 1g Step Command (0.6 Mach 30,000 feet)

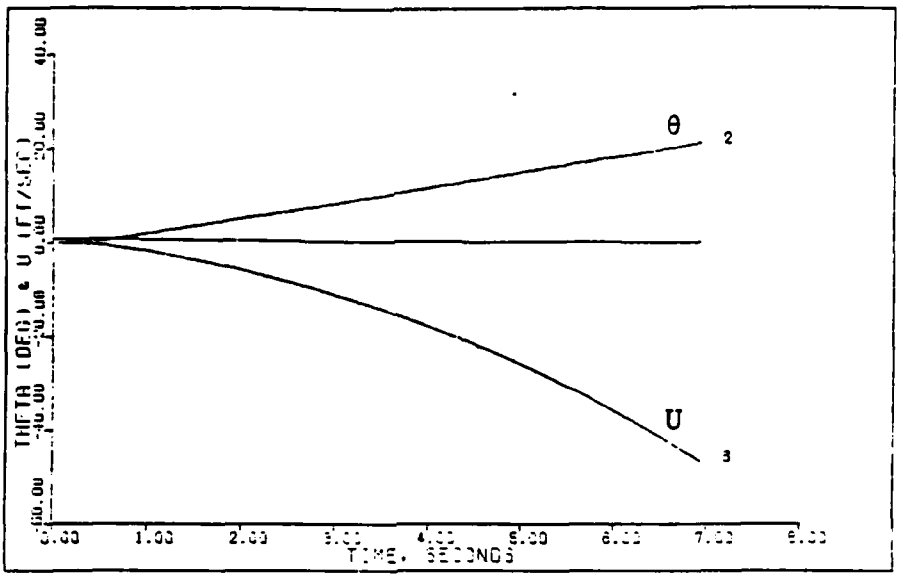



Figure 52c. G-Command System Response to a 1g Step Command (0.6 Mach 30,000 feet)

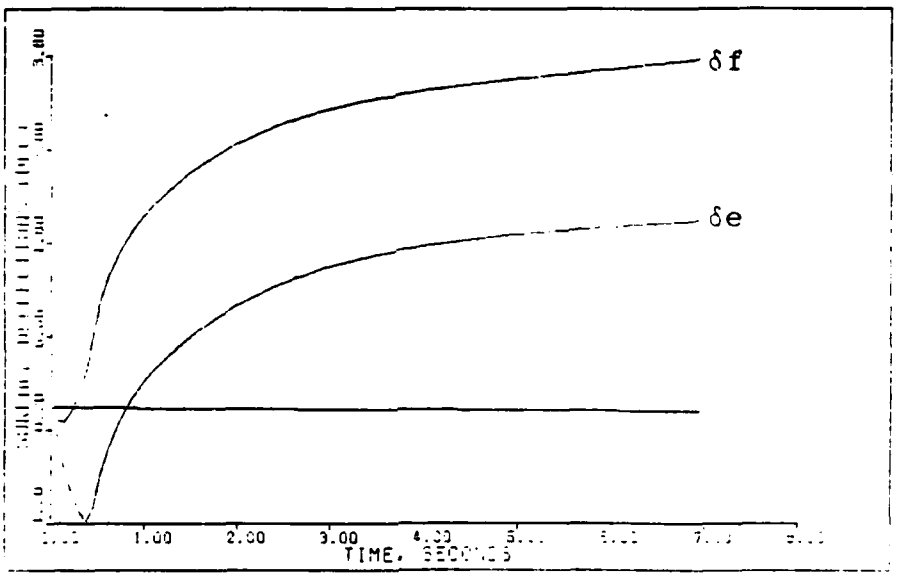



Figure 52d. G-Command System Response to a 1g Step Command (0.6 Mach 30,000 feet)

## Design Data for the Roll Rate Command System

**Flight Condition: 0.6 Mach 30,000 feet**

$T = 0.02$

$\bar{\alpha} = 1.0$

$$\underline{\Sigma} = \begin{bmatrix} 1.0 & 0 & 0 \\ 0 & 0.24 & 0 \\ 0 & 0 & 0.5 \end{bmatrix}$$

$\varepsilon = 0.25$

$$\underline{M} = \begin{bmatrix} 0 & 0 & 0 & 0 & 0 & 0 \\ 0 & 0 & 0 & 0 & 0.1 & 0 \\ 0 & 0 & 0 & 0 & 0 & 0.1 \end{bmatrix}$$

$$\underline{K}_0 = \underline{K}_1 = \begin{bmatrix} 0.2589 & -0.001383 & -0.01103 \\ 1.1990 & 0.000319 & -0.05492 \\ 1.6710 & -0.000175 & -0.03482 \end{bmatrix}$$

Input ramp time: 0.3 seconds

Input commands: $A_{y_p} = 0.0$

$p = 5$ deg/sec pulse for 3 sec duration

$r = p\alpha$ where $\alpha = 0.082115$ radians

NOTE:
1. Pulse inputs are ramped to a maximum value over a specific time. This time is designated as the input ramp time above. The input is held at a maximum value for a duration time and then ramped back to zero. Both ramp times are the same value.
2. Rolls are performed about the velocity vector.

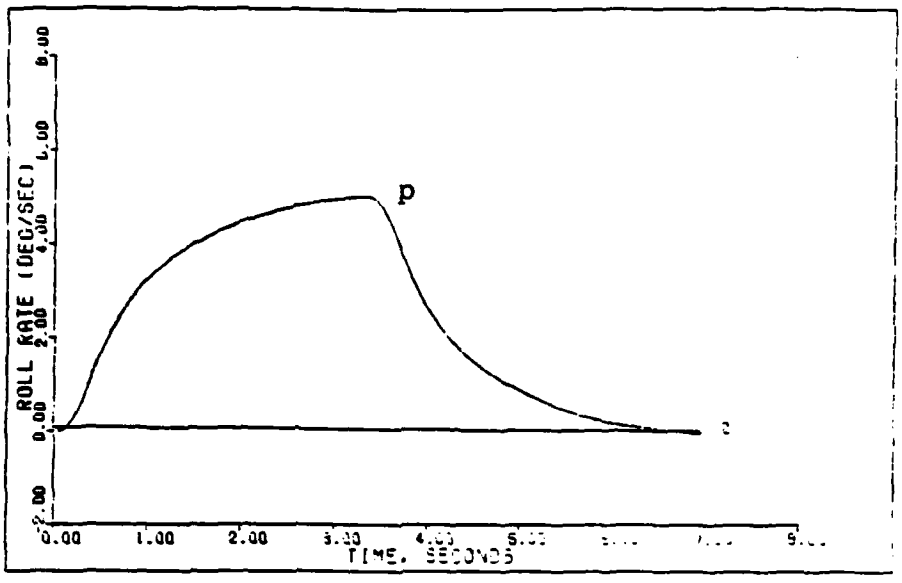



Figure 53a. Roll Rate Command System Response to a 5 deg/sec Pulse Command (0.6 Mach 30,000 feet)

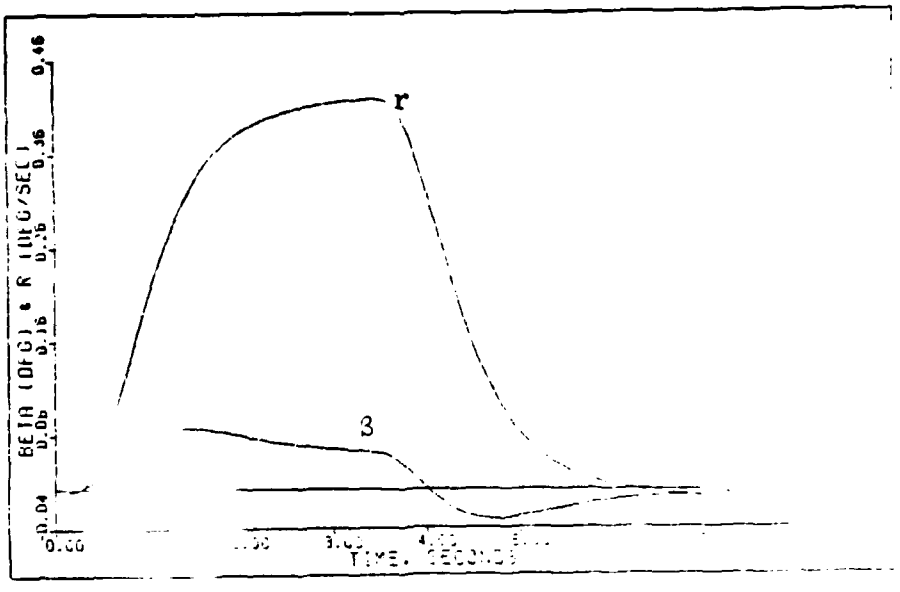



Figure 53b. Roll Rate Command System Response to a 5 deg/sec Pulse Command (0.6 Mach 30,000 feet)

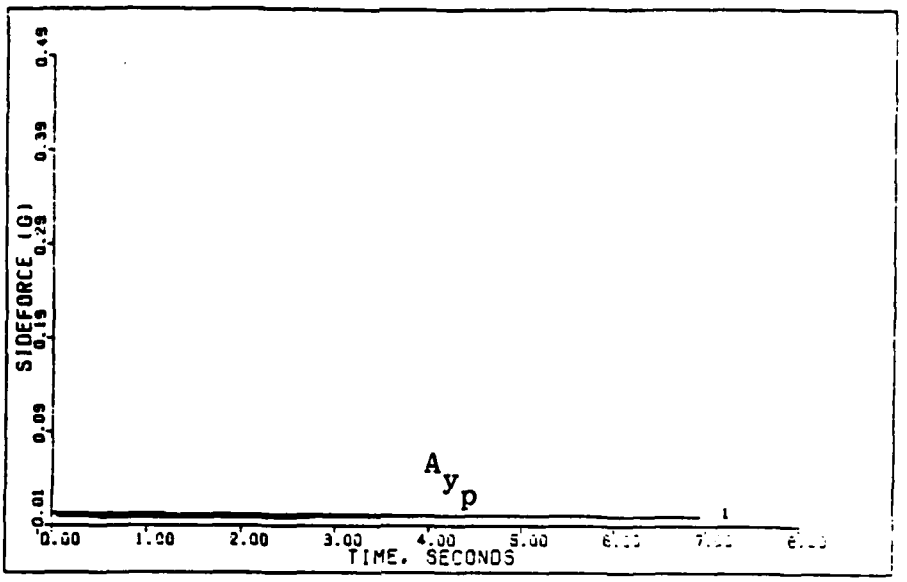



Figure 53c. Roll Rate Command System Responses to a 5 deg/sec Pulse Command (0.6 Mach 30,000 feet)

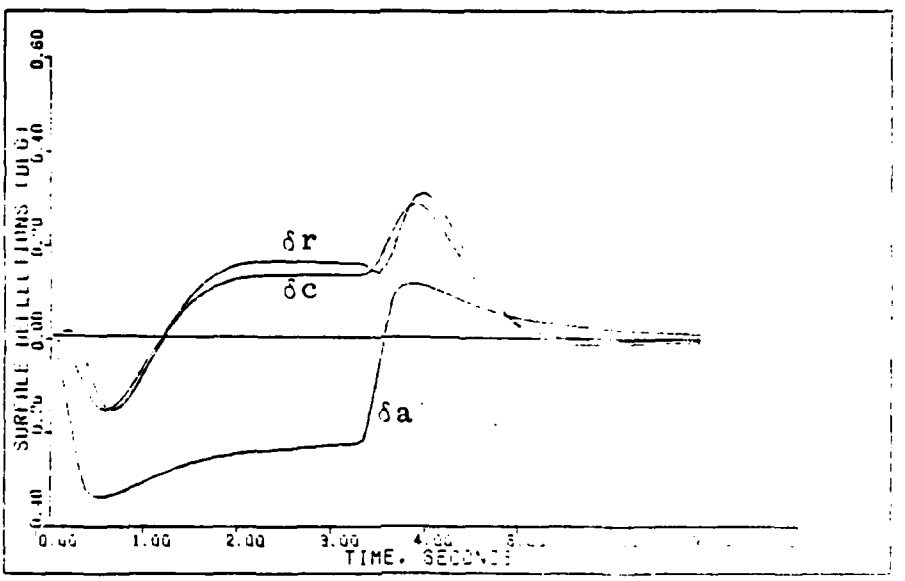



Figure 53d. Roll Rate Command System Response to a 5 deg/sec Pulse Command (0.6 Mach 30,000 feet)

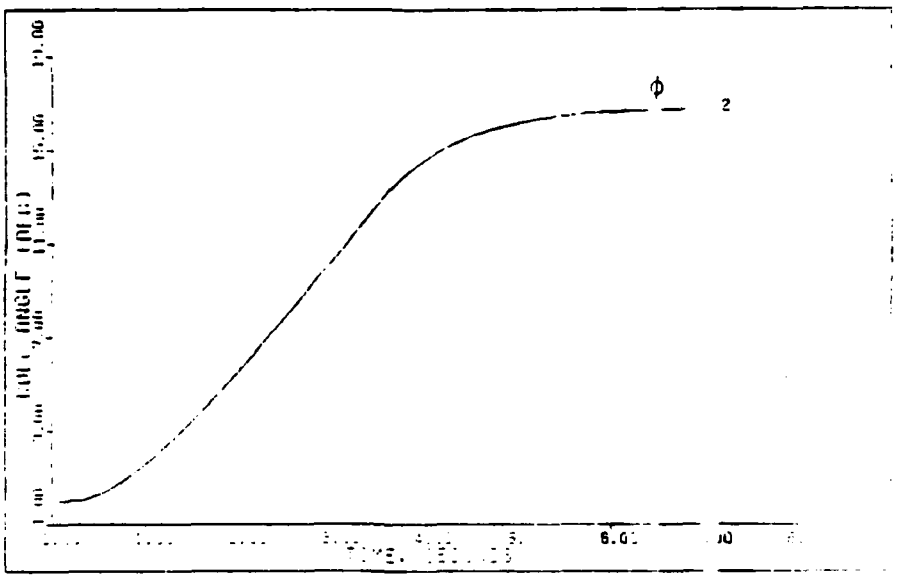



Figure 53e. Roll Rate Command System Response to a 5 deg/sec Pulse Command (0.6 Mach 30,000 feet)

## Design Data for the Sideforce System

**Flight Condition: 0.6 Mach 30,000 feet**

$T = 0.02$

$\bar{\alpha} = 1.0$

$$\underline{\Sigma} = \begin{bmatrix} 1.0 & 0 & 0 \\ 0 & 1.0 & 0 \\ 0 & 0 & 1.0 \end{bmatrix}$$

$\varepsilon = 1.0$

$$\underline{M} = \begin{bmatrix} 0 & 0 & 0 & 0 & 0 \\ 0 & 0 & 0 & 0.1 & 0 \\ 0 & 0 & 0 & 0 & 0.1 \end{bmatrix}$$

$$\underline{K}_0 = \underline{K}_1 = \begin{bmatrix} 1.036 & -0.02305 & -0.08824 \\ 4.794 & 0.05318 & -0.43930 \\ 6.684 & -0.02917 & -0.27850 \end{bmatrix}$$

Input ramp time: 0.5 seconds

Input commands: $A_{y_p} = 0.2g$ step

$p = 0.0$

$$r = \left[\frac{1845}{U}\right] A_{y_p} = 0.618 \text{ deg/sec}$$

NOTE: Step inputs are ramped to steady state over a specific time. This time is designated as the input ramp time given above.

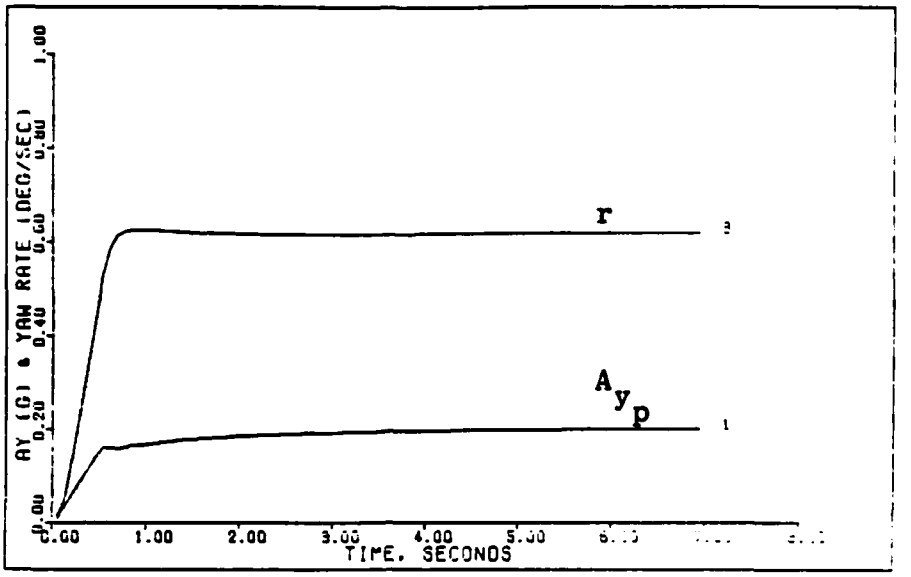



Figure 54a. Sideforce System Response to a 0.2g Step Command (0.6 Mach 30,000 feet)

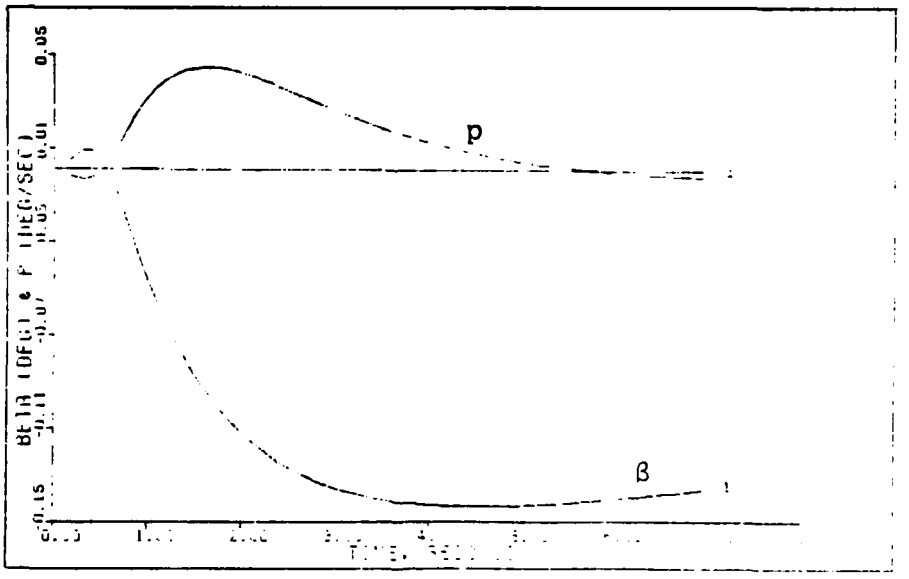



Figure 54b. Sideforce System Response to a 0.2g Step Command (0.6 Mach 30,000 feet)



Copy available to DTIC does not permit fully legible reproduction

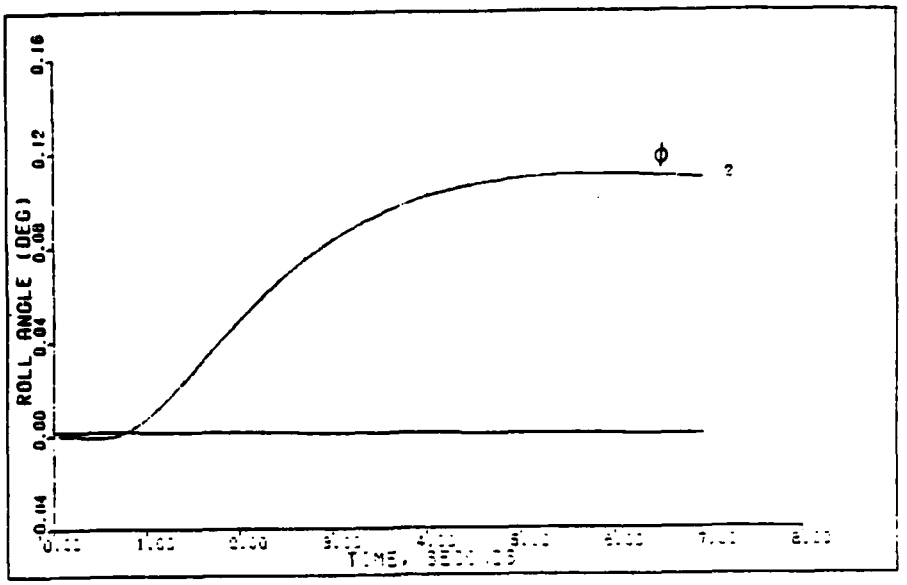



Figure 54c. Sideforce System Response to a 0.2g Step Command (0.6 Mach 30,000 feet)

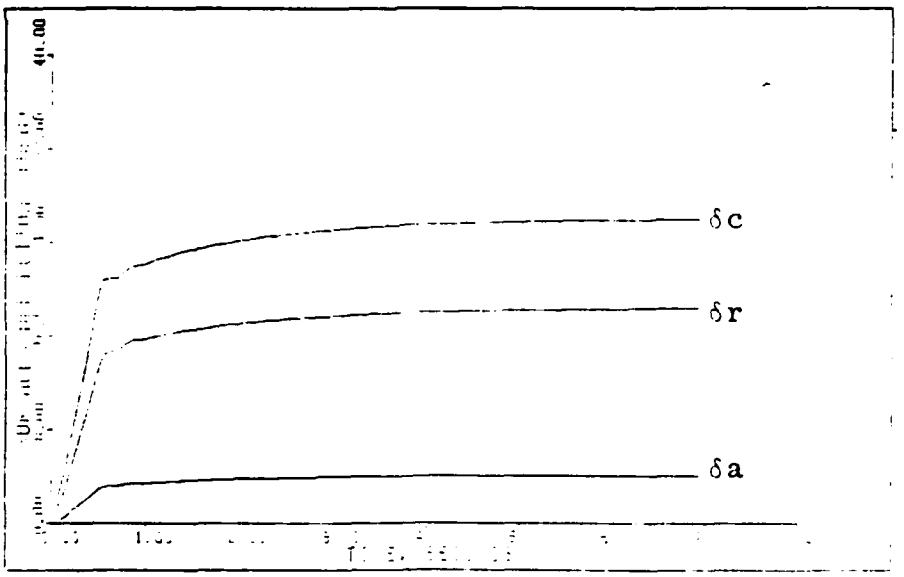



Figure 54d. Sideforce System Response to a 0.2g Step Command (0.6 Mach 30,000 feet)

Design Data for the G-Command System

Flight Condition: 0.2 Mach 30 feet

$T = 0.02$

$\bar{\alpha} = 1.0$

$$\underline{\Sigma} = \begin{bmatrix} 0.1 & 0 \\ 0 & 0.1 \end{bmatrix}$$

$\varepsilon = 1.0$

$$\underline{M} = \begin{bmatrix} 0 & 0 & 0 & 0 & 0 \\ 0 & 0 & 0 & 0 & 0.25 \end{bmatrix}$$

$$\underline{K}_0 = \underline{K}_1 = \begin{bmatrix} 0.06429 & -0.09859 \\ 0.59430 & -0.08450 \end{bmatrix}$$

Input ramp time: 0.4 seconds

Input commands: $A_{n_p}$ = 0.15g step

$q$ = 1.0 deg/sec

NOTE: Step inputs are ramped to steady state over a specific time. This time is designated as the input ramp time given above.

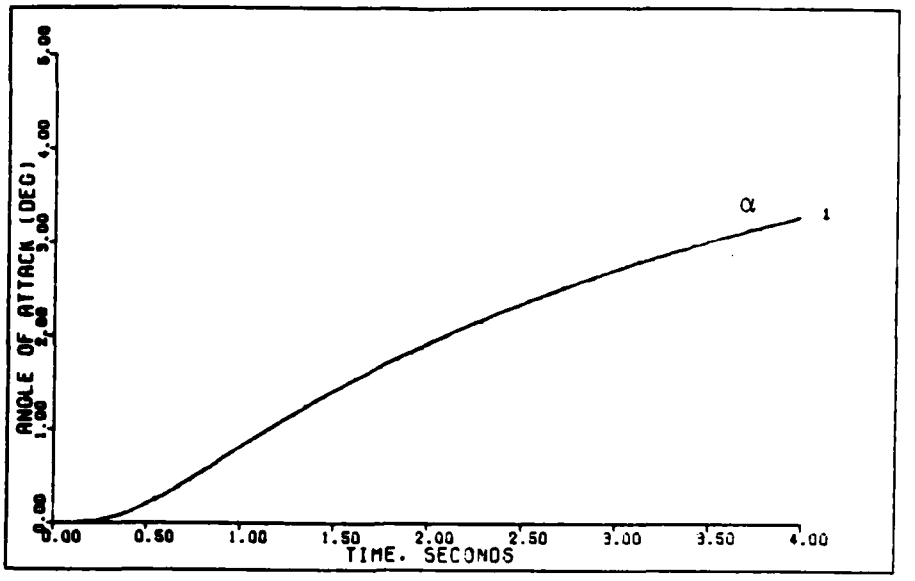



Figure 55a. G-Command System Response to a 0.15g Step Command (0.2 Mach 30 feet)

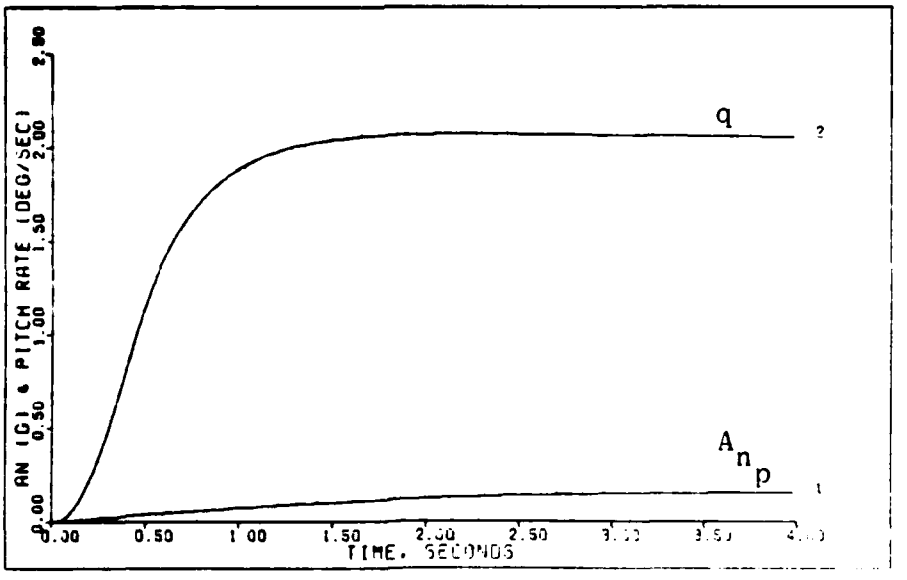



Figure 55b. G-Command System Response to a 0.15g Step Command (0.2 Mach 30 feet)

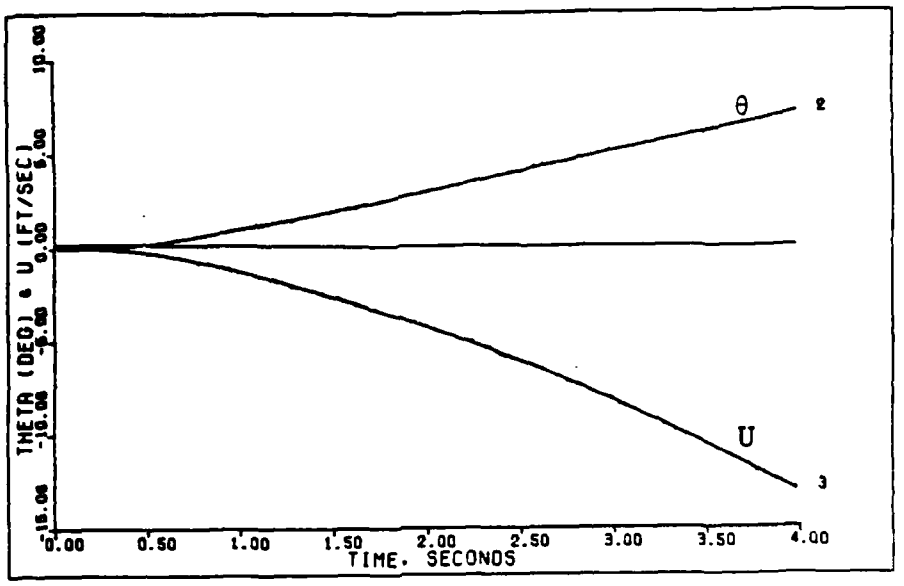



Figure 55c. G-Command System Response to a 0.15g Step Command (0.2 Mach 30 feet)

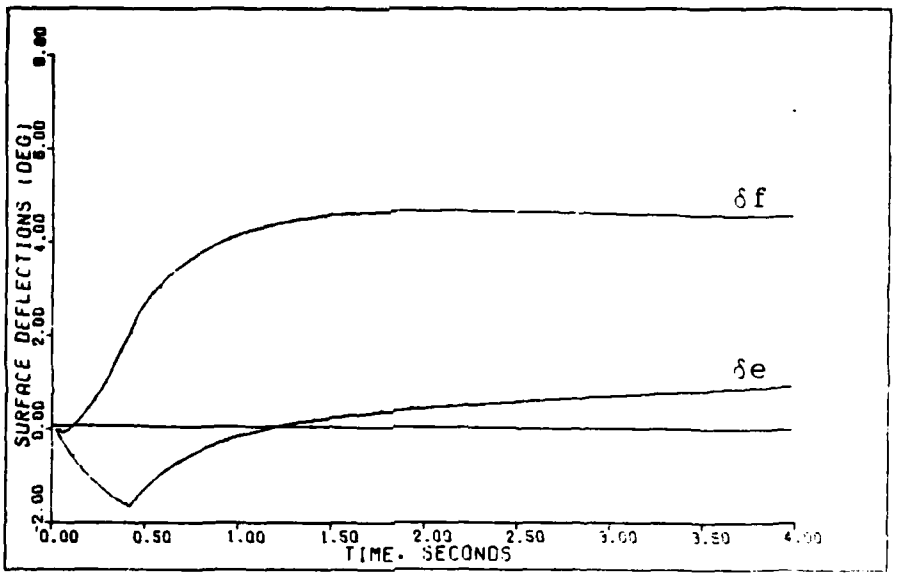



Figure 55d. G-Command System Response to a 0.15g Step Command (0.2 Mach 30 feet)

## Design Data for the Roll Rate Command System

Flight Condition: 0.2 Mach 30 feet

$T = 0.02$

$\bar{\alpha} = 1.0$

$$\underline{\Sigma} = \begin{bmatrix} 1.0 & 0 & 0 \\ 0 & 1.0 & 0 \\ 0 & 0 & 0.6 \end{bmatrix}$$

$\varepsilon = 1.0$

$$\underline{M} = \begin{bmatrix} 0 & 0 & 0 & 0 & 0 \\ 0 & 0 & 0 & 0.25 & 0 \\ 0 & 0 & 0 & 0 & 0.25 \end{bmatrix}$$

$$\underline{K}_0 = \underline{K}_1 = \begin{bmatrix} 1.291 & -0.03368 & -0.04875 \\ 10.520 & 0.01574 & -0.24040 \\ 26.420 & 0.03132 & -0.24260 \end{bmatrix}$$

Input ramp time: 0.3 seconds

Input commands: $A_{y_p} = 0.0$

$p$ = 5 deg/sec pulse for 3 sec duration.

$r = p\alpha$ where $\alpha = 0.26143$ radians

NOTE:
1. Pulse inputs are ramped to a maximum value over a specific time. This time is designated as the input ramp time above. The input is held at a maximum value for a duration time and then ramped back to zero. Both ramp times are the same value.
2. Rolls are performed about the velocity vector.

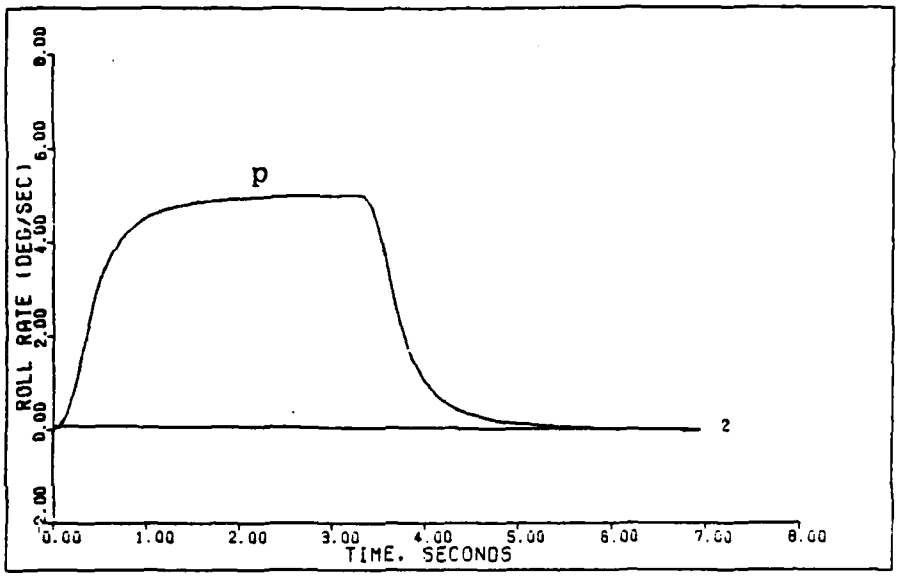



Figure 56a. Roll Rate Command System Response to a 5 deg/sec Pulse Command (0.2 Mach 30 feet)

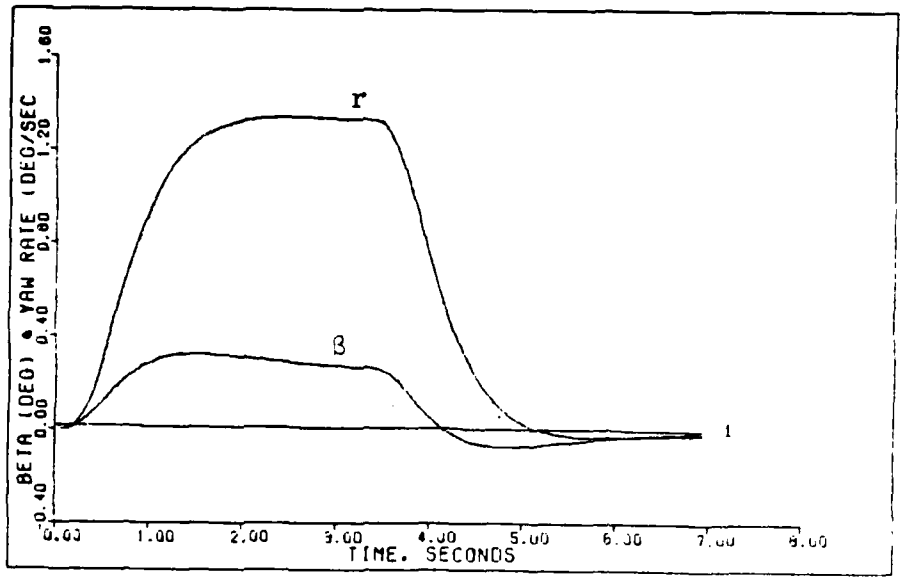



Figure 56b. Roll Rate Command System Response to a 5 deg/sec Pulse Command (0.2 Mach 30 feet)

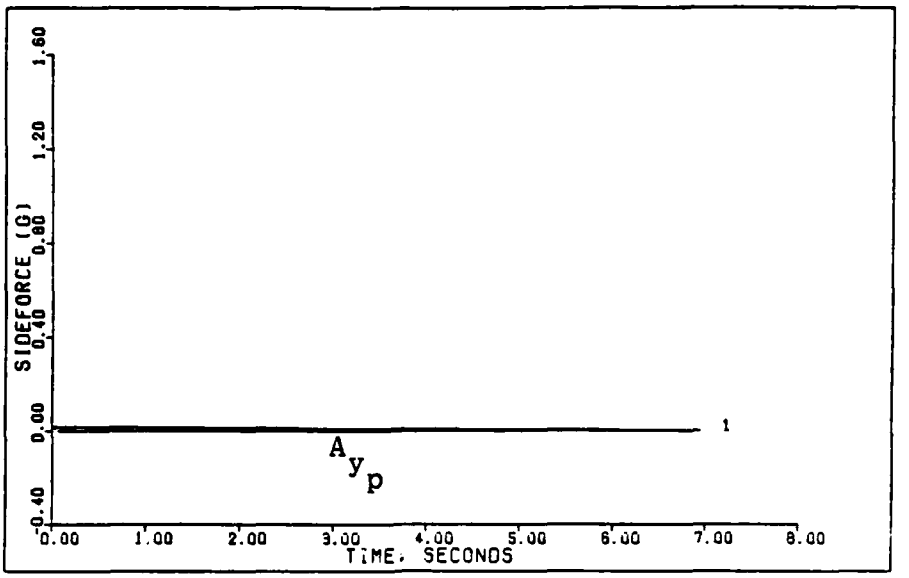



Figure 56c. Roll Rate Command System Response to a 5 deg/sec Pulse Command (0.2 Mach 30 feet)

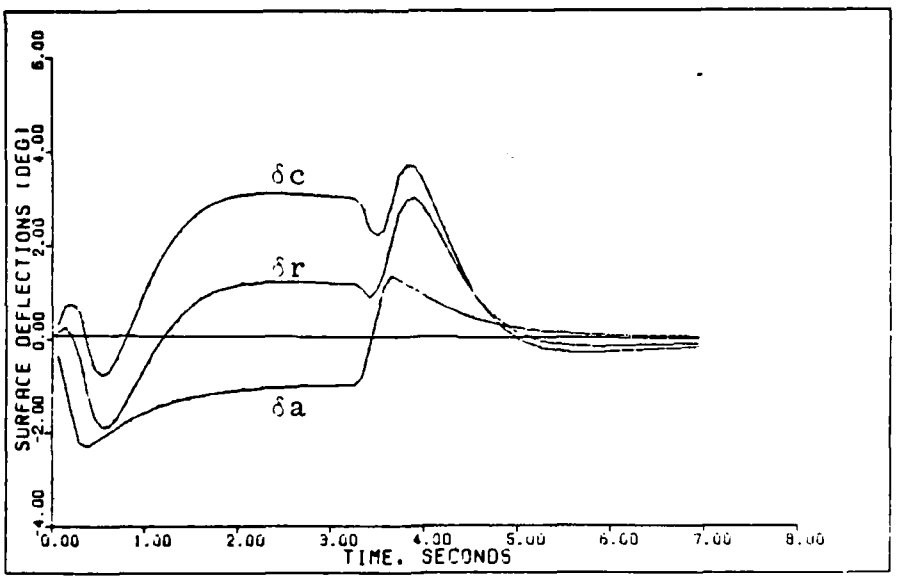



Figure 56d. Roll Rate Command System Response to a 5 deg/sec Pulse Command (0.2 Mach 30 feet)

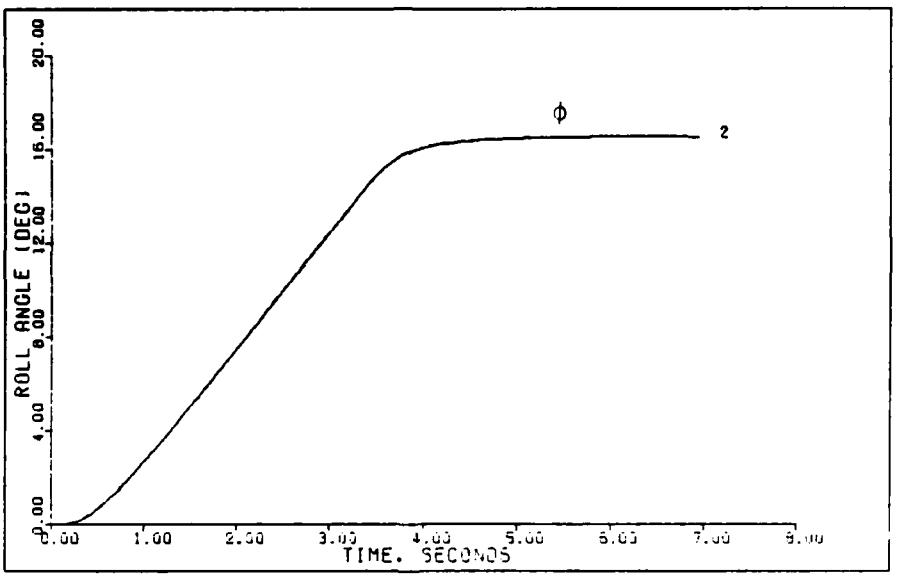



Figure 56e. Roll Rate Command System Response to a 5 deg/sec Pulse Command (0.2 Mach 30 feet)

**Design Data for the Sideforce System**

**Flight Condition: 0.2 Mach 30 feet**

$T = 0.02$

$\bar{\alpha} = 1.0$

$$\underline{\Sigma} = \begin{bmatrix} 1.0 & 0 & 0 \\ 0 & 1.0 & 0 \\ 0 & 0 & 1.0 \end{bmatrix}$$

$\varepsilon = 1.0$

$$\underline{M} = \begin{bmatrix} 0 & 0 & 0 & 0 & 0 \\ 0 & 0 & 0 & 0.1 & 0 \\ 0 & 0 & 0 & 0 & 0.1 \end{bmatrix}$$

$$\underline{K}_0 = \underline{K}_1 = \begin{bmatrix} 1.291 & -0.08420 & -0.2031 \\ 10.520 & 0.03936 & -1.0020 \\ 26.420 & 0.07829 & -1.0110 \end{bmatrix}$$

Input ramp time: 0.3 seconds

Input commands: $A_{y_p} = 0.053g$ step

$p = 0.0$

$r = \left[\frac{1845}{U}\right] A_{y_p} = 0.438$ deg/sec

NOTE: Step inputs are ramped to steady state over a specific time. This time is designated as the input ramp time given above.

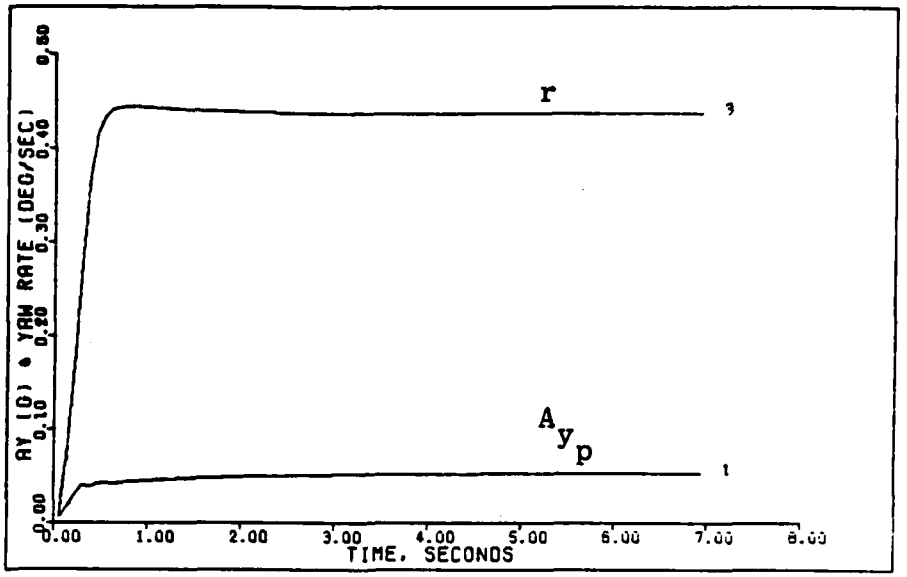



Figure 57a. Sideforce System Response to a 0.053g Step Command (0.2 Mach 30 feet)

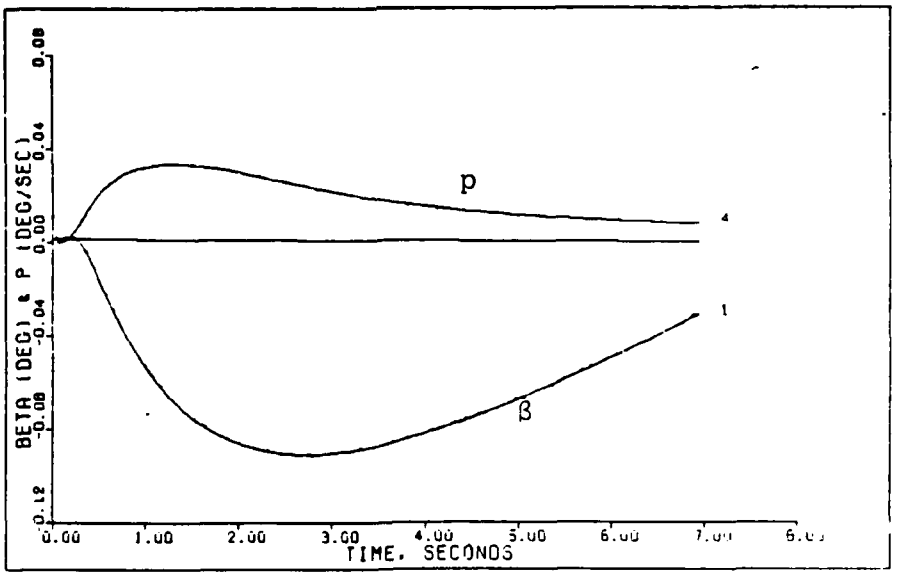



Figure 57b. Sideforce System Response to a 0.053g Step Command (0.2 Mach 30 feet)

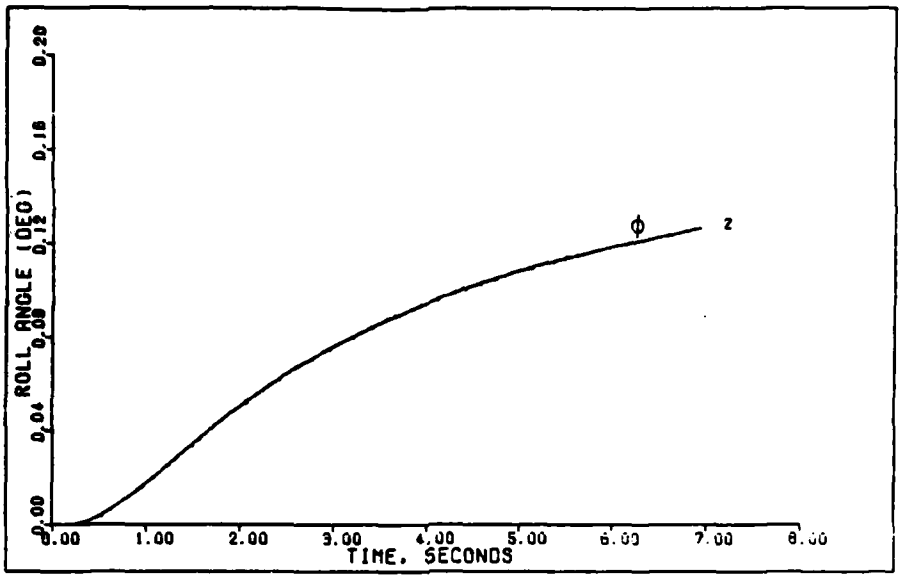



Figure 57c. Sideforce System Response to a 0.053g Step Command (0.2 Mach 30 feet)

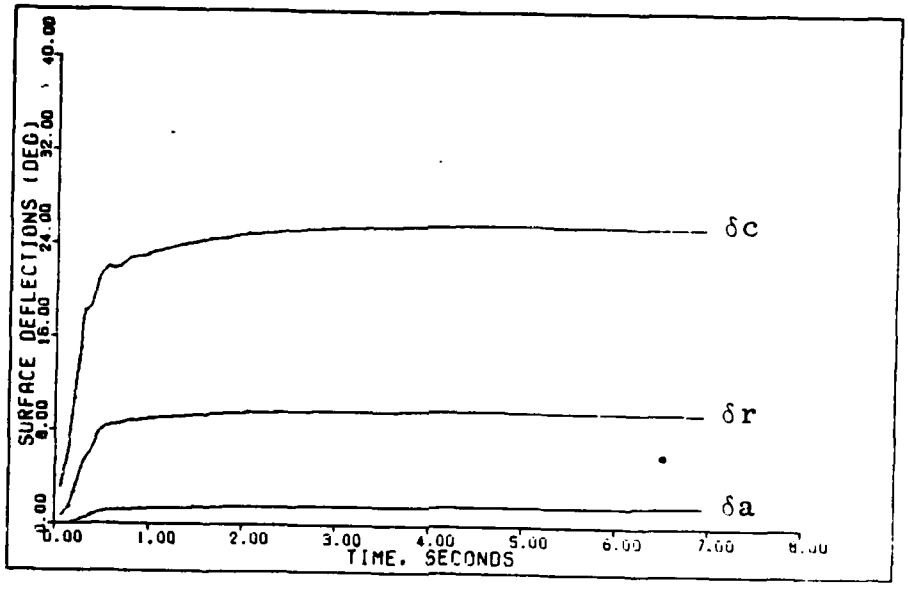



Figure 57d. Sideforce System Response to a 0.053g Step Command (0.2 Mach 30 feet)

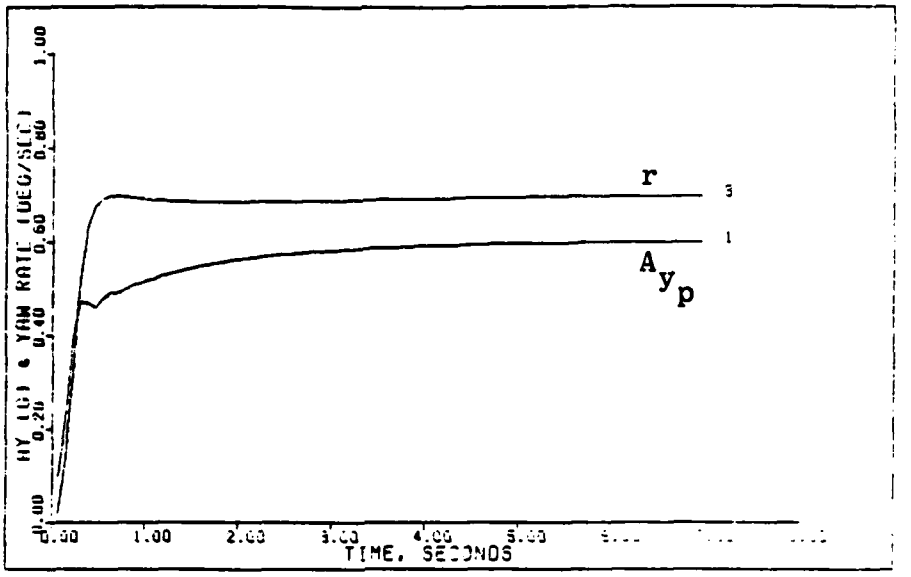



Figure 51a. Sideforce System Response to a 0.6g Step Command (1.6 Mach 30,000 feet)

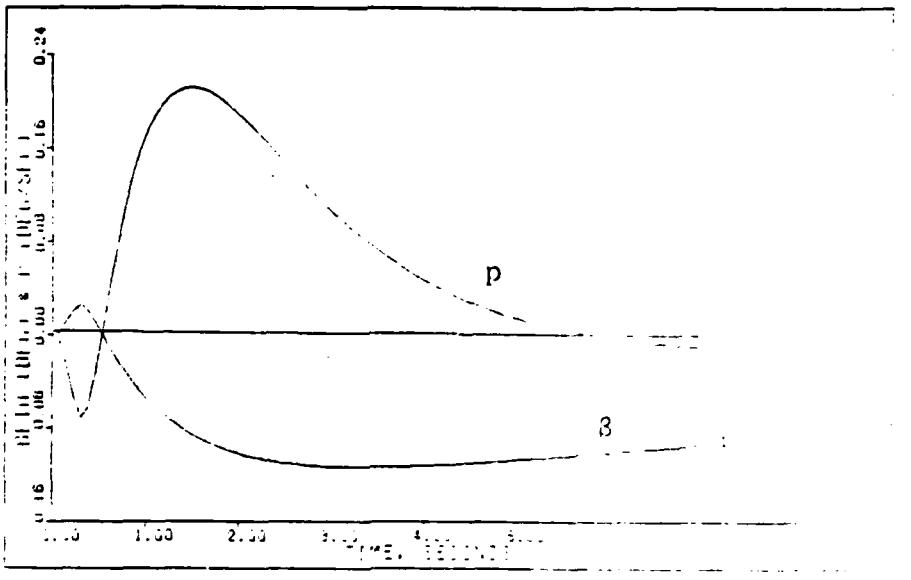



Figure 51b. Sideforce System Response to a 0.6g Step Command (1.6 Mach 30,000 feet)



Copy available to DTIC does not permit fully legible reproduction

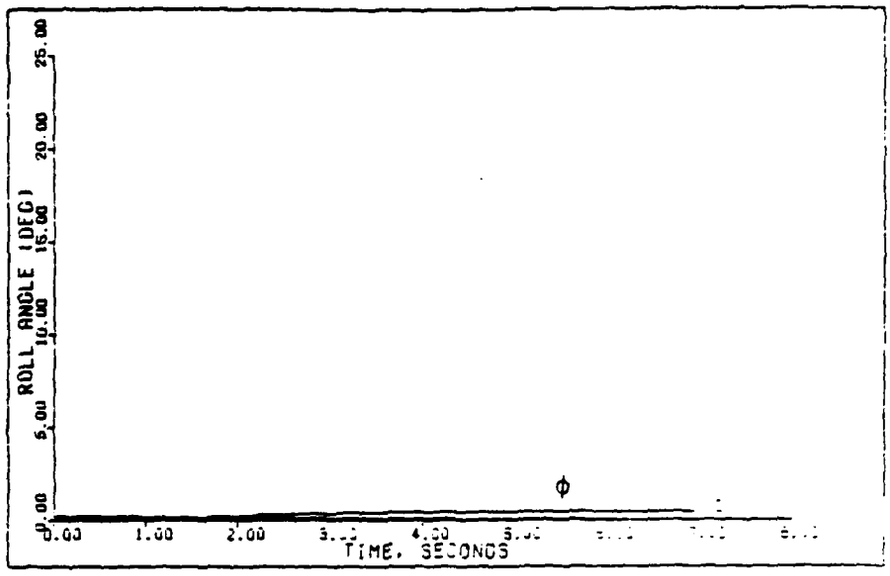



Figure 51c. Sideforce System Response to a 0.6g Step Command (1.6 Mach 30,000 feet)

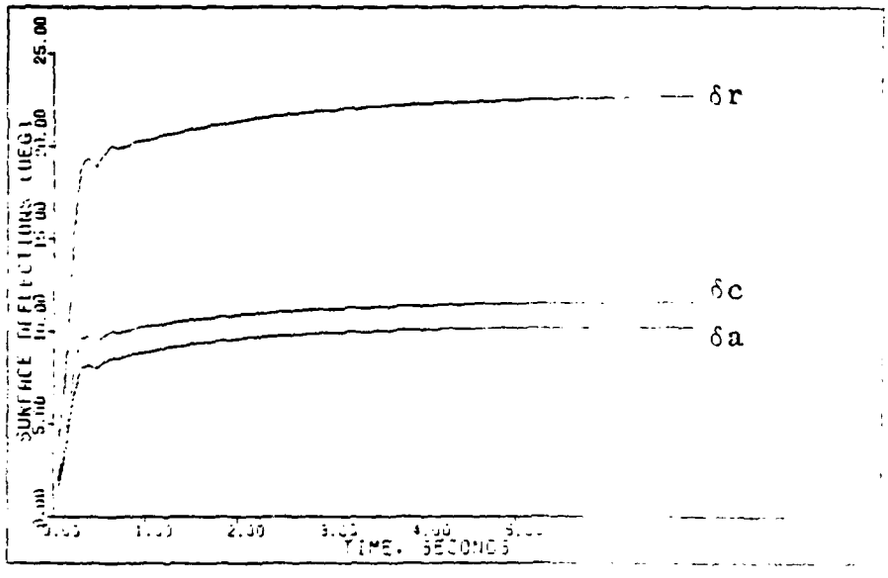
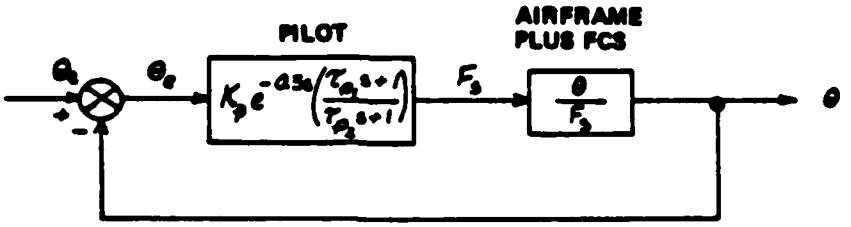



Figure 51d. Sideforce System Response to a 0.6g Step Command (1.6 Mach 30,000 feet)

## Neal-Smith Criterion

The acceptance of a design by the pilot is always an issue of utmost importance that must be addressed in any flight control work. Professor Porter's method, as applied in this effort, results in a closed-loop system with either all real roots or complex conjugate pairs with very high damping ratios. In light of this fact, a means of assessing pilot acceptance is needed.

One method of predicting pilot ratings for a longitudinal compensatory tracking task was suggested by Peter Neal and Roger Smith in Reference 16. The complete theoretical basis and the data used for the criterion development are provided in the reference. A summary of the technique is presented here. The assumption is made that the acceptability of an aircraft's maneuvering response in performing a specific task can be expressed in terms of the pilot compensation needed to achieve some "minimum standard of performance" with the least tendency to develop a pilot induced oscillation (PIO). The standard of performance is established by the task which is required of the pilot. For the final phase of a fighter's combat maneuvering, precise control of pitch attitude is assumed to be the critical task in the reference. The control of pitch attitude is modelled as shown in Figure 58. This model and the definitions presented are direct extracts from Reference 16.




Using this model, the following terms are defined:

Bandwidth (BW): Bandwidth is defined as the frequency for which the closed-loop Bode phase, $\angle(\theta/\theta_c)$, is equal to -90 degrees. It is a measure of how quickly the pilot can move the airplane's nose toward the target.

Droop: Droop is defined as the maximum excursion of closed-loop Bode amplitude, $|\theta/\theta_c|$, below the 0 dB line for frequencies less than BW. In the absence of large oscillations, droop is a measure of how slowly the nose settles down on target.

Standard of Performance: A minimum bandwidth, $(BW)_{min}$, of 3.5 rad/sec, and a maximum droop of 3 dB:

$\angle(\theta/\theta_c)$ greater than (-90) degree
and $|\theta/\theta_c|$ greater than (-3) dB
} for $\omega$ less than 3.5

PIO Tendency: The tendency to oscillate or PIO is defined in terms of the Bode magnitude of any closed-loop resonant peak, $|\theta/\theta_c|_{max}$, that results from the pilot's efforts to achieve the performance standards.

Pilot Compensation: The pilot's physical and mental workload required to achieve the standard of performance is defined in terms of the phase of his compensation at $\omega = (BW)_{min}$:

$$\angle_{pc} = \angle\left(\frac{j\omega\tau_{p_1}+1}{j\omega\tau_{p_2}+1}\right)_{\omega=(BW)_{min}}$$

Figure 58. Neal-Smith Model for Pitch Attitude Control

To evaluate a design, the engineer selects values of $K_p$, $\tau_{p1}$, and $\tau_{p2}$ in the pilot model that yield the smallest maximum value for $|\theta/\theta_c|$ for the closed-loop system while maintaining a minimum bandwidth of 3.5 radians per second and a maximum droop of -3 dB. The method of this selection is covered later.

For each specific selection of pilot model parameters, the maximum value of $|\theta/\theta_c|$ and the phase angle at the 3.5 rad/sec frequency are determined for the closed-loop system using a Nichols chart. These values are plotted in Figure 59 and evaluated against the boundaries in the figure to determine a prediction of a pilot rating (PR) and the acceptability of the design. The PR boundaries in the figure correspond to the Cooper-Harper Pilot Ratings given in Table 7.

To employ this method, the airframe plus flight control system transfer function, $\theta/F_s$ , must first be determined for the longitudinal system. With two inputs and two outputs, $\underline{G}(s)$ is a two-by-two transfer function matrix as expressed below.

$$\underline{G}(s) = \begin{bmatrix} \frac{A_{n_p}}{v_1} & \frac{A_{n_p}}{v_2} \\ \\ \frac{q}{v_1} & \frac{q}{v_2} \end{bmatrix} \qquad (5.1)$$

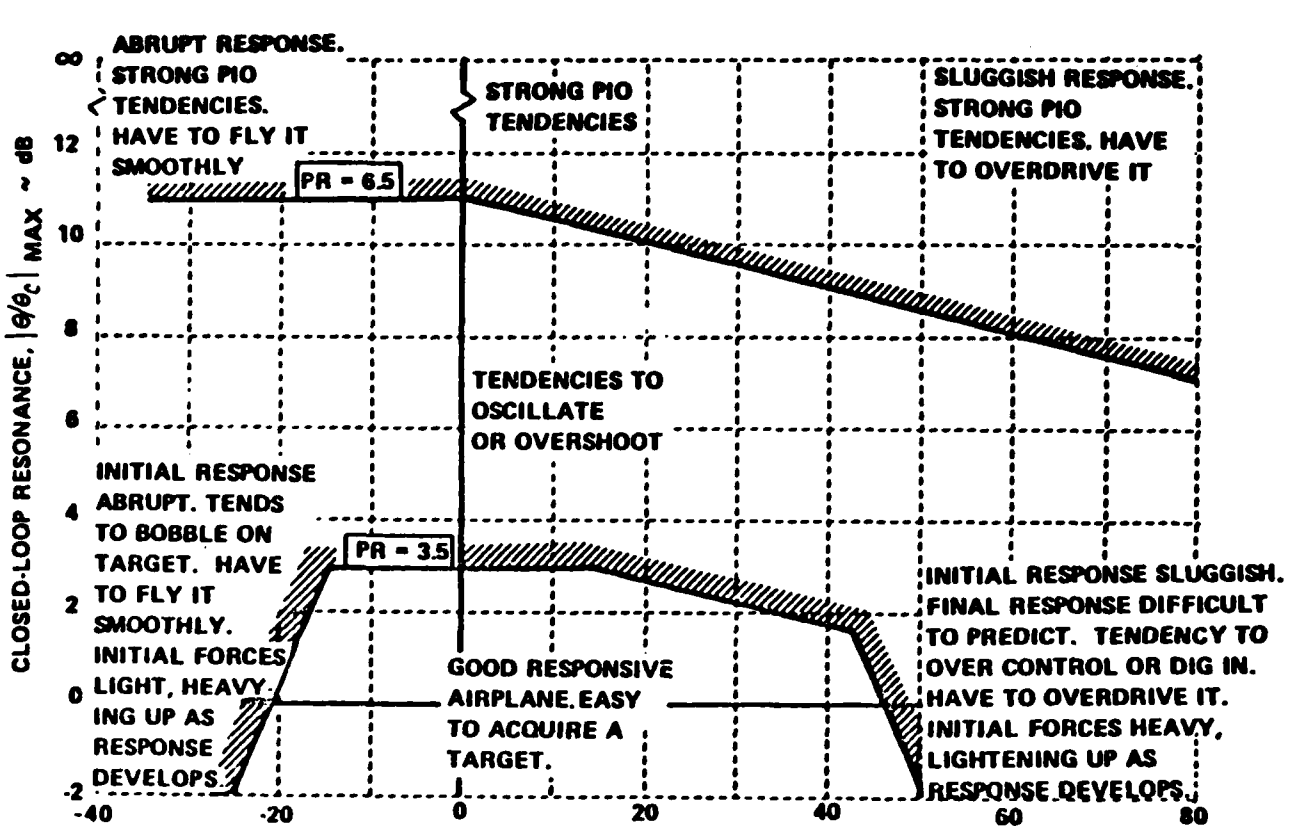
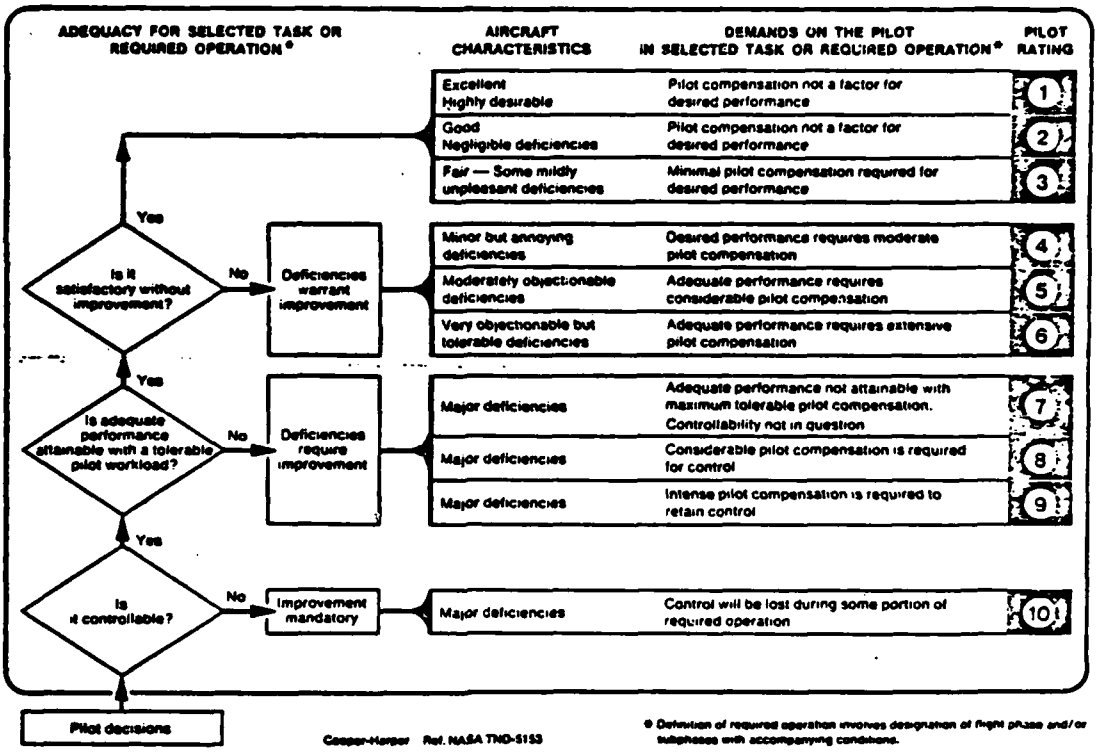



Figure 59. Neal-Smith Criterion for Fighter Maneuvering Dynamics

Table 7

Cooper-Harper Handling Qualities Rating Scale




The contribution from both inputs must be considered in the pitch attitude output since the aircraft is not completely decoupled. The system mechanization chosen for the longitudinal design shown in Figure 41 of Chapter IV relates stick force input ($F_s$) to the control commands $v_1$ and $v_2$ by

$$v_1 = F_s \quad \text{and} \quad v_2 = \left[\frac{1845}{U}\right] F_s \tag{5.2}$$

thus

$$q = \frac{q}{v_1} v_1 + \frac{q}{v_2} v_2 = \frac{q}{v_1} (F_s) + \frac{q}{v_2} \left[\frac{1845}{U}\right] (F_s) \tag{5.3}$$

and

$$\frac{q}{F_s} = \frac{q}{v_1} + \frac{q}{v_2}\left[\frac{1845}{U}\right] \tag{5.4}$$

$$\frac{\theta}{F_s} = \frac{1}{s}\left\{\frac{q}{v_1} + \frac{q}{v_2}\left(\frac{1845}{U}\right)\right\} \tag{5.5}$$

At the 0.9 Mach 20,000 feet flight condition, this transfer function is

$$\frac{\theta}{F_s} = \frac{929.5(s + 1)(s + 1.4)}{s(s + 1.065 \pm j\ 0.4189)(s + 3.75)(s + 133.8)} \tag{5.6}$$

Magnitude and phase values are calculated for frequencies between 0.1 and 10 radians per second from this transfer function. The next step is to establish values for the pilot model that allow the standard of performance to be met.

Initially, a check is made to find if varying only $K_p$, the pilot's gain, can provide a solution. This is accomplished by letting $\tau_{p1}$ and $\tau_{p2}$ equal zero and setting $K_p$ to one. The phase angle from the exponential term in the pilot model is $(57.3)(0.3)(\omega)$ and is added to the phase values of $\theta/F_s$. This establishes the open-loop $\theta/\theta_e$ magnitude and phase information.

The standard of performance (closed-loop) boundaries are established on a Nichols chart (Figure 60). The open-loop amplitude-phase plot of $\theta/\theta_e$ is then overlaid and moved vertically to determine if any value of $K_p$ allows the closed-loop tracking system $\theta/\theta_c$ to meet the standards.

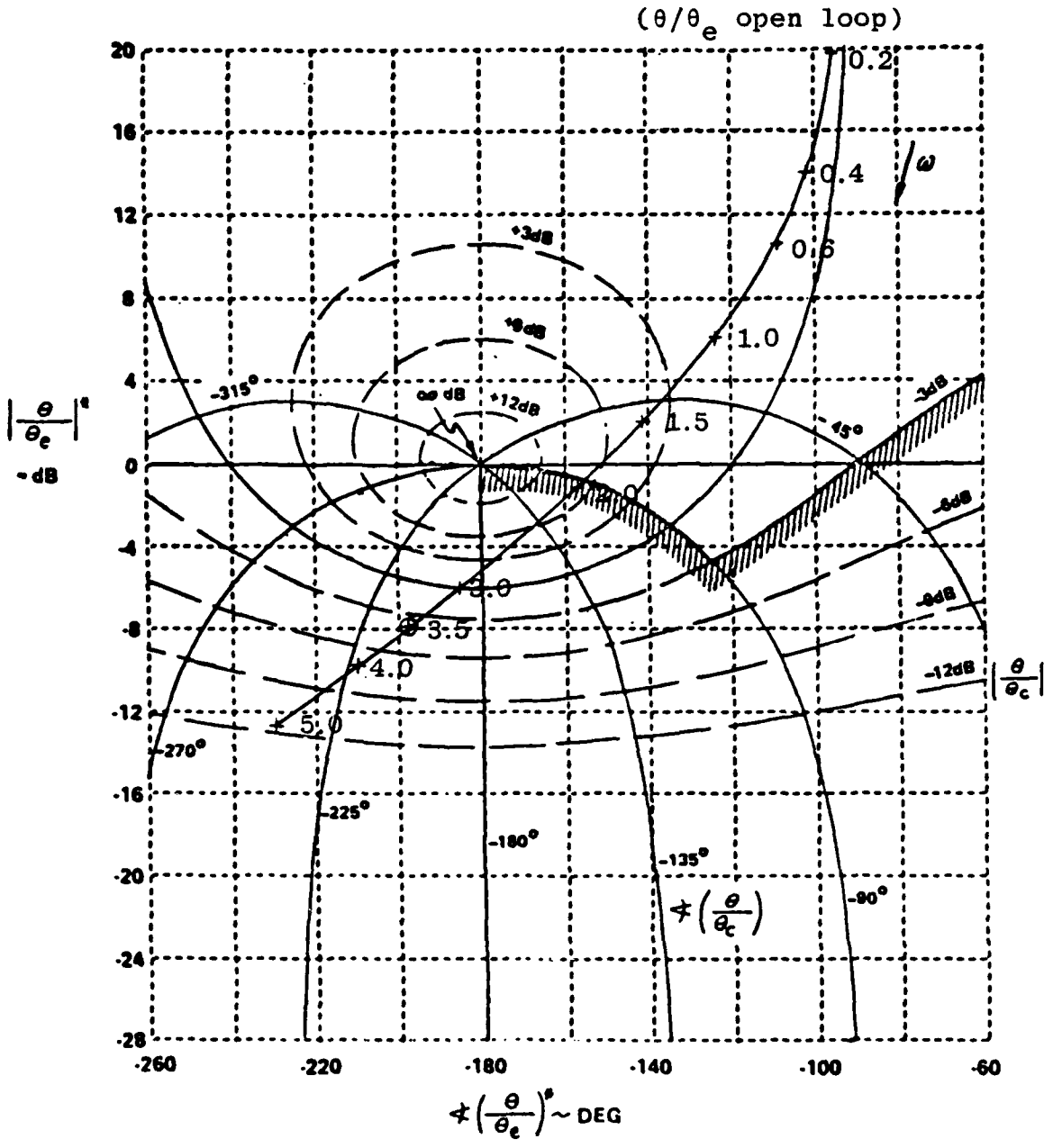



Figure 60. Nichols Chart with Performance Standard Boundaries and Overlay of Amplitude-Phase Plot of $\theta/\theta_e$ with $\tau_{p_1}$ and $\tau_{p_2}$ Equal to Zero

This plot indicates that $K_p$ alone can not satisfy the standard. The 3.5 radian per second point on the amplitude-phase plot needs a reduction in phase angle indicating lead compensation by the pilot.

Reference 16 provides a plot of amplitude-phase curves for optimum pilot compensation which simplifies the selection of $\tau_{p1}$ and $\tau_{p2}$. Two pilot models are selected for the design being analyzed. The first with $\tau_{p1} = 0.94$ and $\tau_{p2} = 0.0$ meets both the bandwidth and droop requirements. This means that the pilot must generate over 73 degrees of lead at the 3.5 rad/sec frequency. The resulting $|\theta/\theta_c|$ max is plotted (as a dot) versus pilot compensation angle on the criterion graph in Figure 61. The point falls outside the desired PR = 3.5 boundary. A second pilot compensation is found with $\tau_{p1} = 0.57$ and $\tau_{p2} = 0.0$ that requires the pilot to generate 62 degrees of lead at 3.5 rad/sec and meets the bandwidth requirement while exceeding the droop requirement. This point is also plotted (as a dot) in Figure 61. Although moving closer to the desired region, both are outside the "good response area." The lead angle required by the pilot must be reduced if the design is to receive good pilot ratings from this evaluation technique.

An examination of the transfer function reveals that the root at -3.75 contributes slightly over 45 degrees of phase lag at the 3.5 rad/sec bandwidth frequency used to select the pilot compensation. This root is of interest

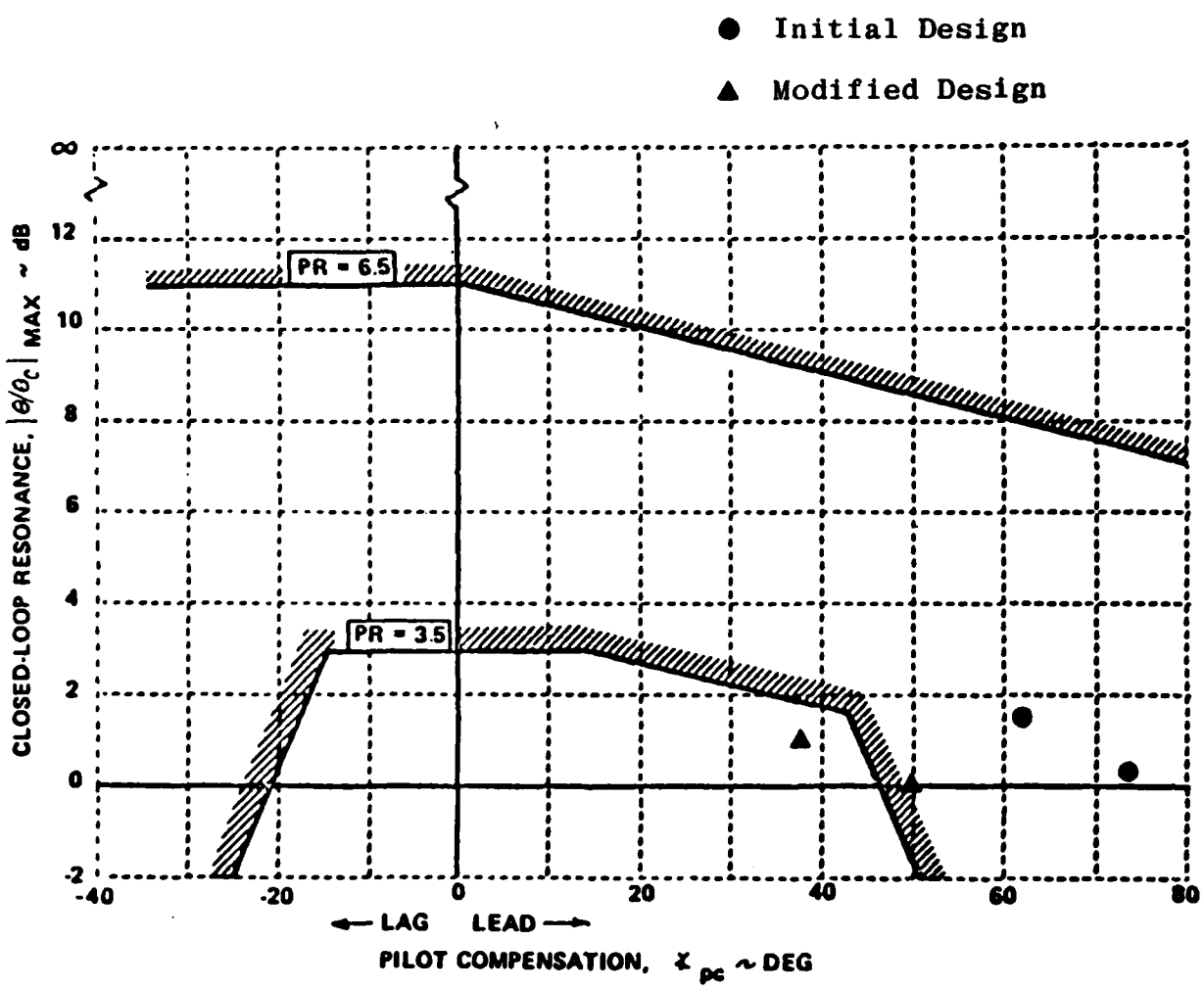



Figure 61. Criterion Graph with Design Evaluation Points

because its location is determined by the elements of the measurement matrix. The elements of $\underline{M}$ are changed to 0.1, and the system responses that result are shown in Figure 45. In this case, the first-order root is very close to -10 in the s-plane. Again, two pilot models are chosen and plotted as triangles in Figure 61. The first with $\tau_{p1} = 0.34$ and $\tau_{p2} = 0.0$ meets both constraints. It requires 50 degrees of pilot lead. The second meets the bandwidth condition and exceeds the droop requirement. For this case with $\tau_{p1} = 0.23$ and $\tau_{p2} = 0.0$, a pilot lead of 37 degrees is required.

The last choice yields a design which gives a pilot rating of 3.5 or less. Thus, after several well-placed changes, it appears that this design may be very useful for tracking cases. However, several cautionary notes are provided. The phase lag due to digital computer implementation and the lag from a pilot prefilter have not been included in this evaluation. An estimate for the digital design can be established by using a first-order Padé approximation for a zero-order hold and a factor of (1/T) for the sampling action (Ref 22). This indicates a phase lag of approximately 2 degrees at the 3.5 rad/sec bandwidth. The prefilter is of the order of 7.5/(s + 7.5) and adds as much as 25 degrees to the system. These additions again place the design outside the desired boundary. The prefilter may be increased to 10/(s + 10) or slightly higher depending on the actual surface rates encountered. The current design is conservative

since this is an indirect way to limit such rates, and the ramp times are calculated based on estimated maximum rates. Fine tuning of the prefilter has not been accomplished and can reduce the phase lag considerably.

These additional factors (which are present for any digital controller implementation) tend to cause the design points to fall to the lower right of the 3.5 PR boundary. This may not be a serious deficiency. Review of similar evaluations of both the F-16 and the AFTI/F-16 designs shows they fall in the same general region outside the 3.5 PR boundary.

The Neal-Smith Criterion is only one of several currently being proposed for flight control design evaluations (Refs 17, 18 and 19). Its use has highlighted areas of improvement for the current design; however, its validity in predicting pilot ratings is by no means unquestioned. Thus, further analyses with other criteria are needed to properly evaluate the designs. Ideally, conclusions on the acceptability of the design from these criteria should eventually be validated in a realistic piloted simulation evaluation.

Bandwidth Comparison

Chapter IV includes a discussion of the desirability of limiting the control system bandwidth. The major reason for this is to reduce undesirable effects from structural interaction. Designs with Professor Porter's techniques

can result in extremely fast responses. It is, therefore, important to assess the bandwidth of the designs under consideration. Time permitted only one such assessment in this study. The longitudinal design is compared with the F-16 and AFTI/F-16 control systems. Figures 62 and 63 are plots for the open-loop control system from sensor input to elevator position output. The MULTI Designs (MD) exhibit slightly less bandwidth at high frequencies than either the F-16 or the AFTI/F-16 systems for this path. In the acceleration path the MULTI Design falls between the other two systems and matches AFTI for very high frequencies. The plot for the AFTI design is for the air-to-air mode.

The plots were completed after the design gains had been established. Thus, they illustrate that the Porter design method employing maximum estimated maneuvers and considering limits on surface position and rates results in designs with acceptable bandwidths. The initial designs obtained before such considerations were taken into account had much higher gain values and would indeed have resulted in large bandwidths.

The high gain at low frequencies is due to integral compensation on all MULTI Design feedforward paths. Note that AFTI uses this compensation only in the pitch rate path, and the F-16 uses it only in the normal acceleration path.

A final word of caution must be given. Although the bandwidth of the longitudinal design compares favorably with

Note: $\frac{\delta e}{q}$ Transfer Function Comparisons

Gain set for 0.9 Mach 20,000 feet

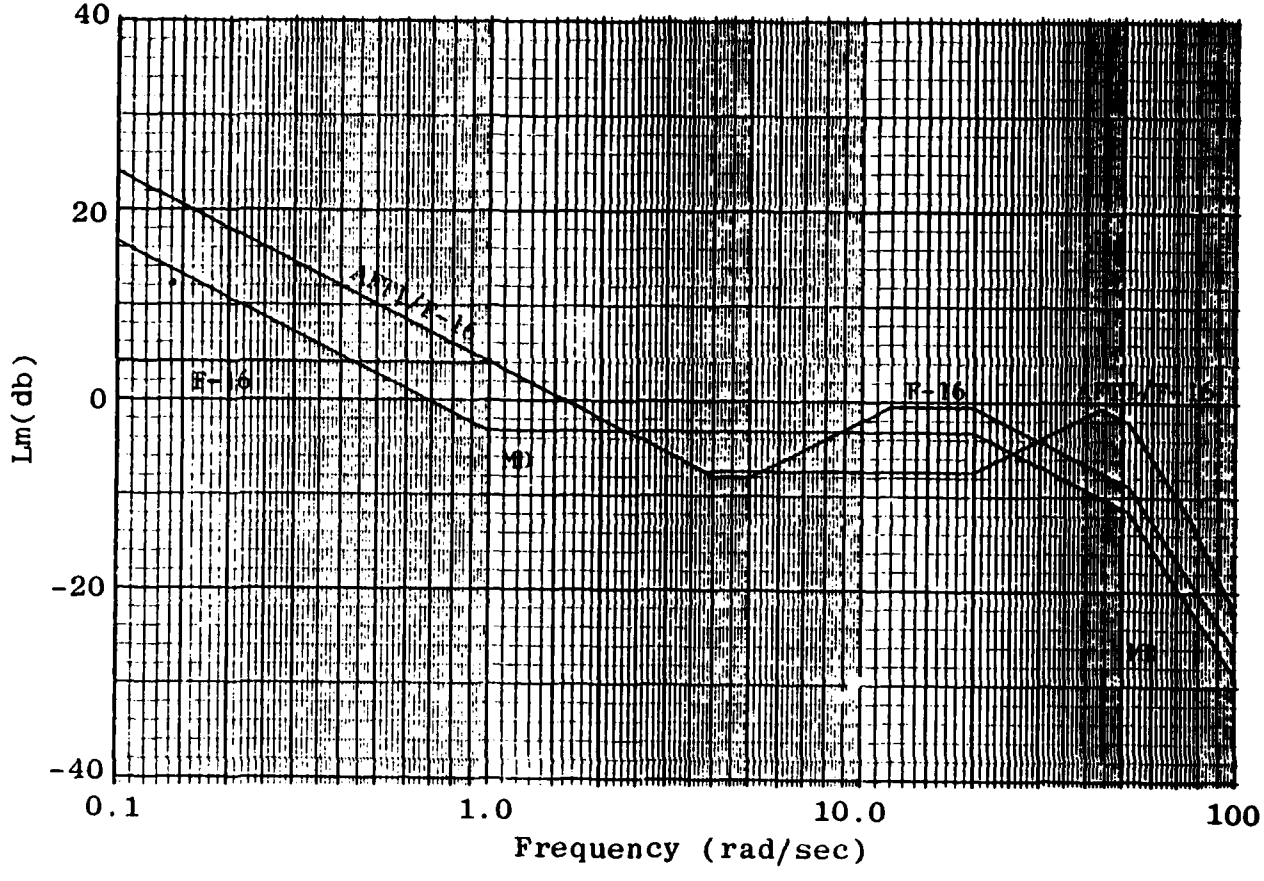



Figure 62. Open-Loop Bandwidth Comparison for the Pitch Rate to Elevator Path

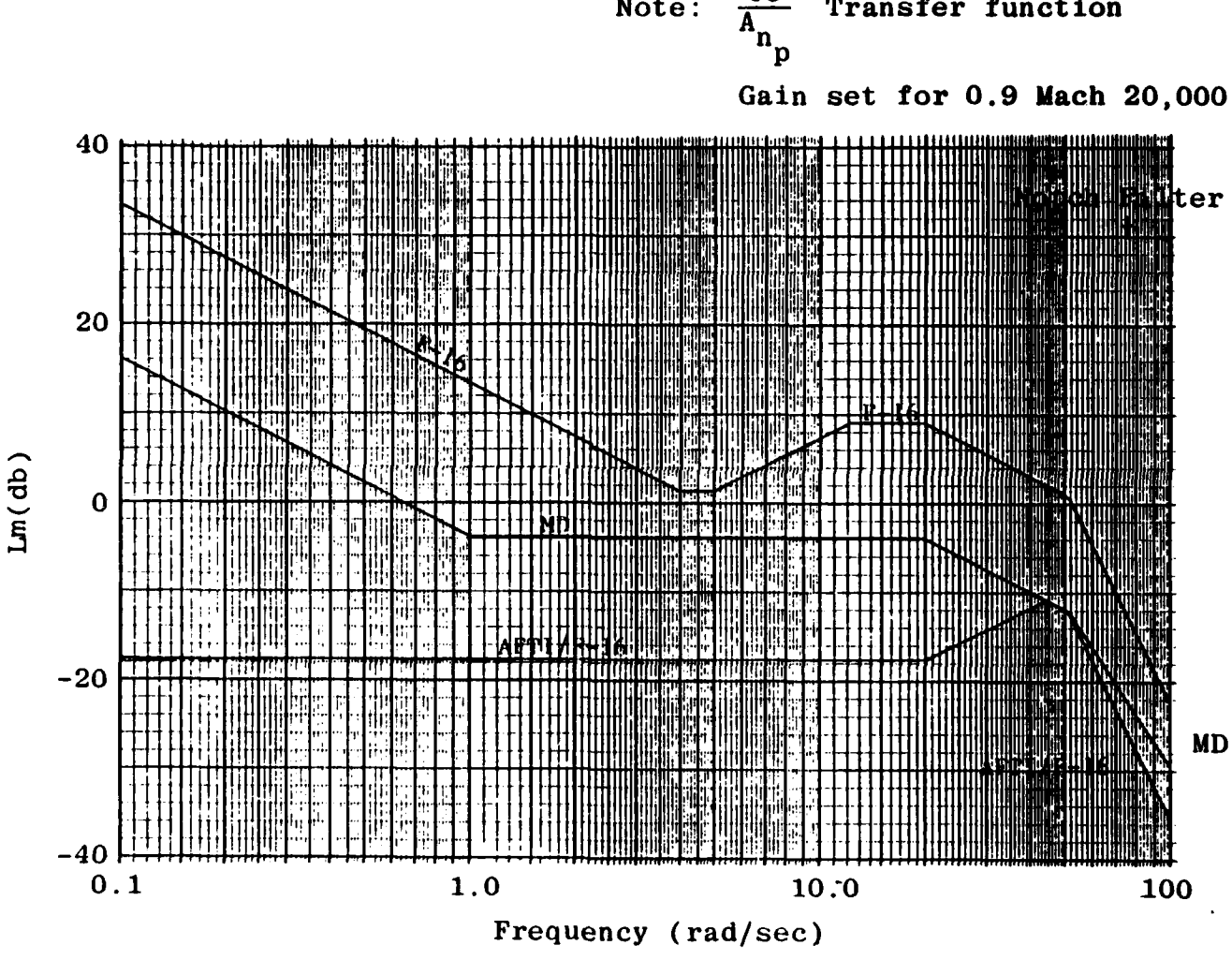



Figure 63. Open-Loop Bandwidth Comparison for the Acceleration to Elevator Path

the F-16 and the AFTI/F-16 systems, both of these systems have been modified with notch filters to eliminate structural interaction problems. The center frequency of the AFTI double notch filter is marked on Figure 63. Thus, even with the present system design, notch filters may be required once installation and testing begin. The design must be able to accept such filters without undue degradation. The ability to evaluate such filter additions is needed in the computer-aided design package and is recommended in Chapter VI.

The comparisons are accomplished for only one surface at one flight condition. A complete survey is needed for all sensor-to-surface paths at all flight conditions so that a realistic overall bandwidth assessment can be made. Such an extensive evaluation is recommended for any future efforts with these designs.

Robustness versus Tailoring

One measure of robustness is the ability of a control system design, with fixed gains, to provide acceptable performance over a wide range of flight conditions. However, in this study, emphasis is placed on tailoring the control system design at each flight condition to provide responses that improve the accomplishment of a specific task. The specific task of concern is air-to-air gunnery. To establish one set of gains for all flight conditions results in

a compromise in performance for the sake of reduced complexity. Two points need to be considered. First, gain scheduling is easily accomplished with current digital flight hardware. Second, since flight conditions change rather slowly, the update rate for gain scheduling is relatively low. In the AFTI system, the control commands are solved 64 times per second, but the gains are calculated only once a second. Considering both of these points and the desire for improved performance, a compromise in performance is not acceptable.

In this report, a design is considered robust if it can tolerate uncertainties in the aircraft model. A design to give specific performance is based on an aircraft model developed from wind tunnel data with an accuracy of 3 to 5 percent. A test of robustness is the ability of a design to yield acceptable performance for an inaccurate parameter in the aircraft model. Such an ability significantly reduces the fine tuning and redesign at late stages in the development of a new system.

To illustrate the robustness, the design developed for the 0.9 Mach 20,000 feet condition is evaluated with an aircraft model in which the pitching moment coefficient of the elevator ($Cm_{\delta e}$) is decreased by 15 percent. The results are shown in the comparison responses in Figures 64 and 65. The aircraft responses are essentially the same although

some difference in the surface positions are apparent. Using this measure, these designs are considered robust.

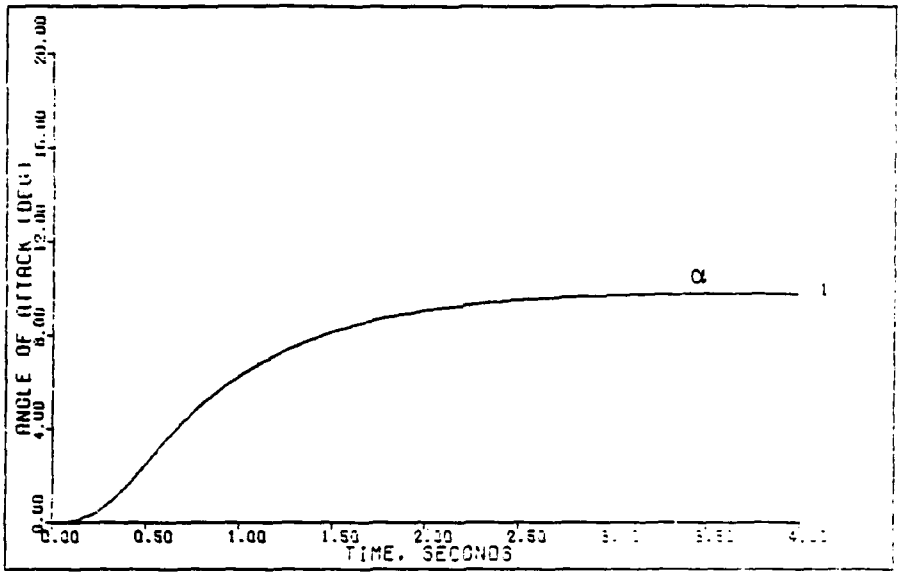



Figure 64a. G-Command System Response to a 9g Step Command--Nominal $C_{m_{\delta e}}$ (0.9 Mach 20,000 feet)

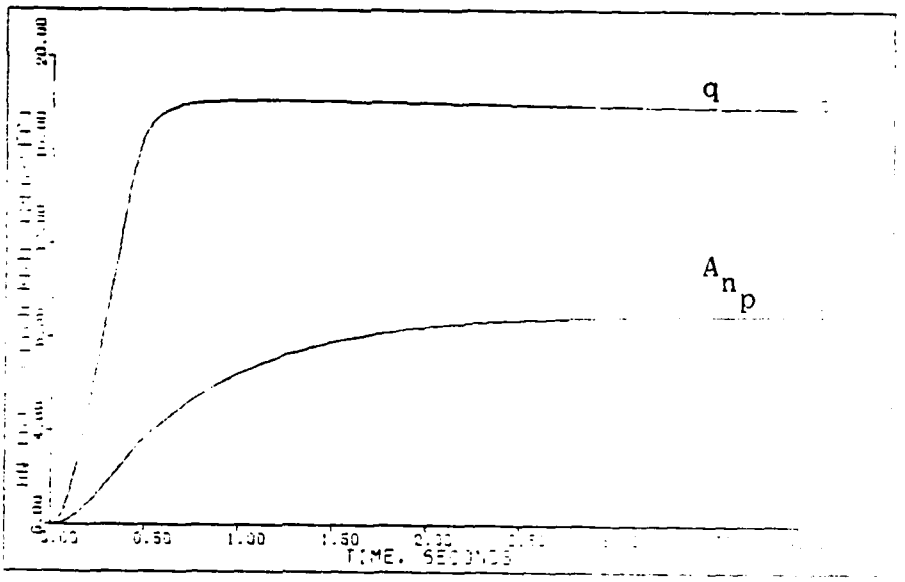



Figure 64b. G-Command System Response to a 9g Step Command--Nominal $C_{m_{\delta e}}$ (0.9 Mach 20,000 feet)

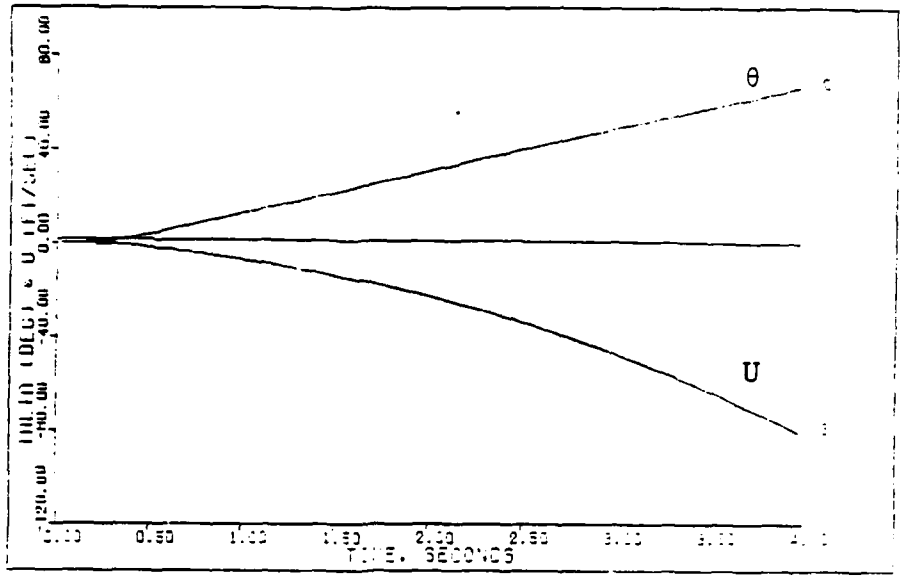



Figure 64c. G-Command System Response to a 9g Step Command--Nominal $C_{m_{\delta e}}$ (0.9 Mach 20,000 feet)

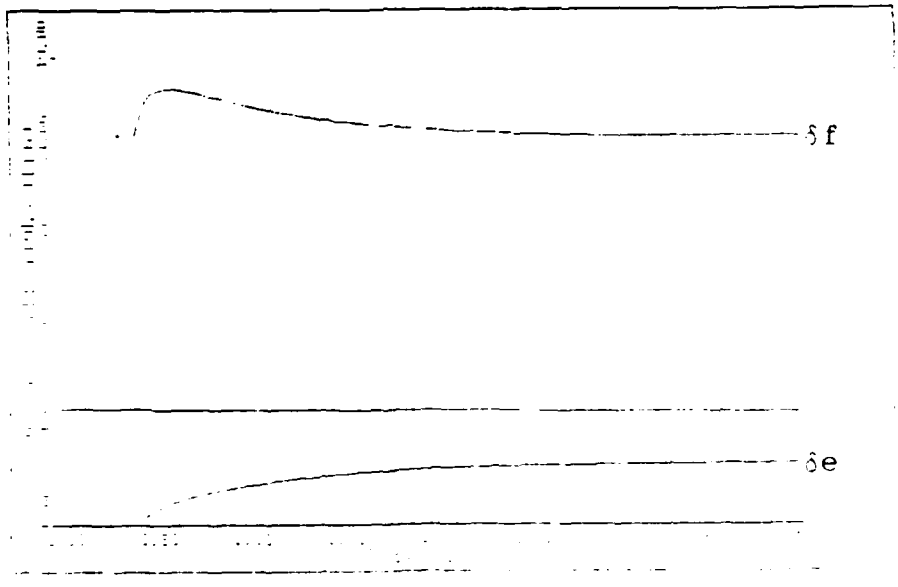



Figure 64d. G-Command System Response to a 9g Step Command--Nominal $C_{m_{\delta e}}$ (0.9 Mach 20,000 feet)



Copy available to DTIC does not permit fully legible reproduction

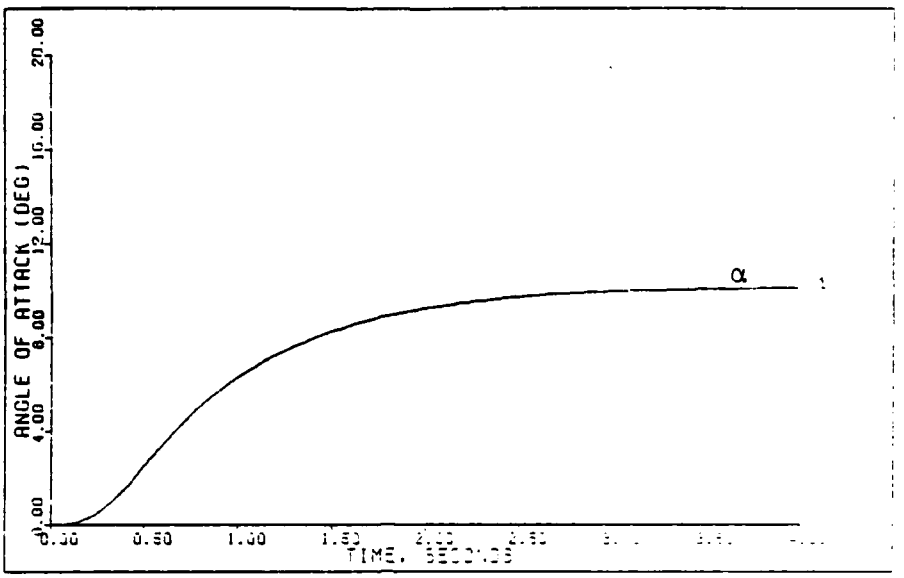



Figure 65a. G-Command System Response to a 9g Step Command--Reduced $C_{m_{\delta e}}$ (0.9 Mach 20,000 feet)

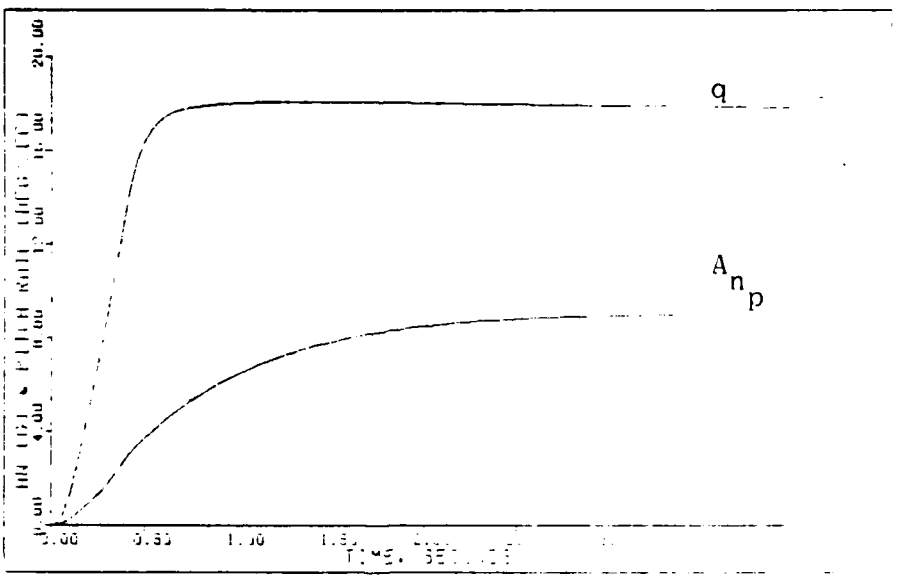



Figure 65b. G-Command System Response to a 9g Step Command--Reduced $C_{m_{\delta e}}$ (0.9 Mach 20,000 feet)

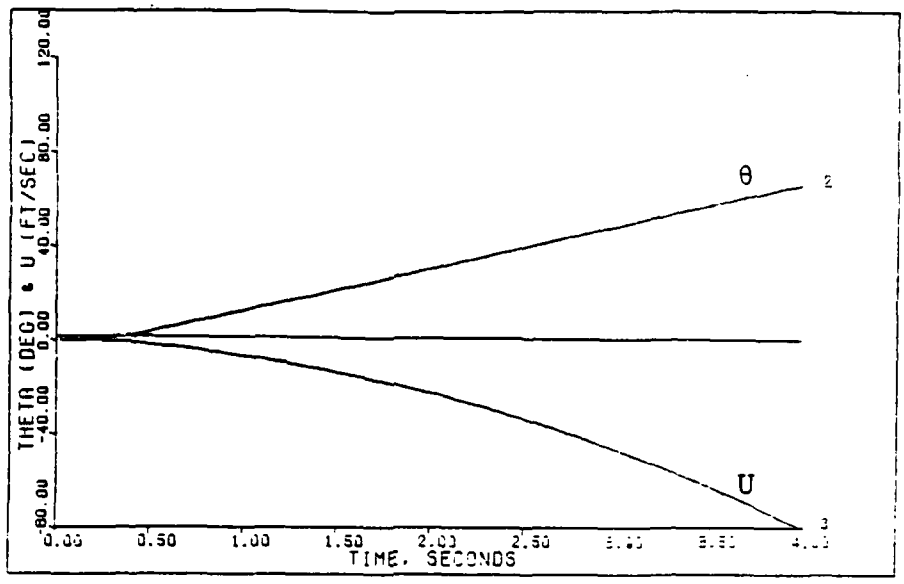



Figure 65c. G-Command System Response to a 9g Step Command--Reduced $C_{m_{\delta e}}$ (0.9 Mach 20,000 feet)

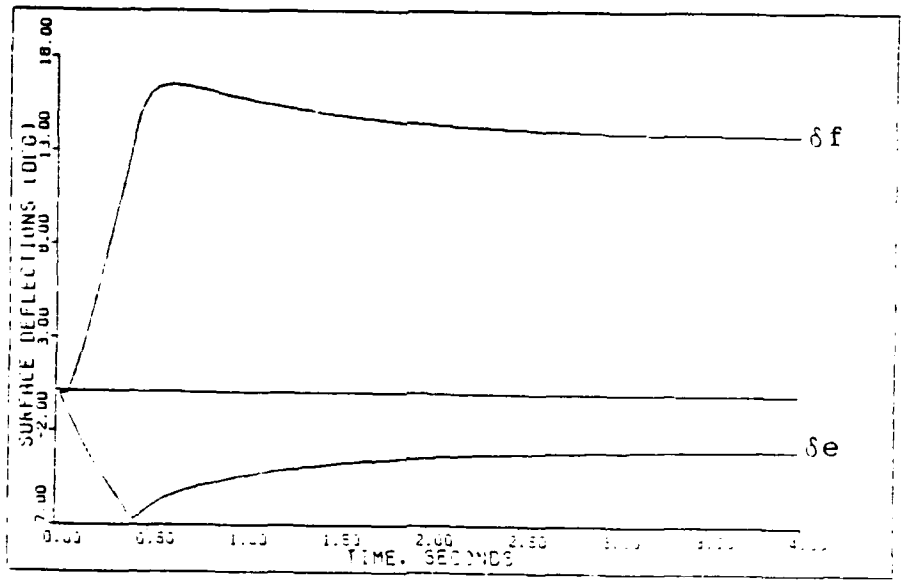



Figure 65d. G-Command System Response to a 9g Step Command--Reduced $C_{m_{\delta e}}$ (0.9 Mach 20,000 feet)

# VI. Conclusions and Recommendations

## Design Results

Very good performance is obtained from the controller designs developed with Professor Porter's techniques in tbis study. The time responses exhibit the desired characteristics and meet the established requirements. The techniques are found to be extremely flexible. A design method is formulated that can be used in the synthesis of conventional multivariable control laws and decoupled (CCV) control laws. Controllers are developed that provide the pilot with precise control over aircraft body rates and accelerations without increasing workload. The interactive capability of the MULTI program results in an efficient and cost effective design method.

The flight control design structure consists of a g-command system in the longitudinal axis. It accepts inputs in the form of acceleration commands from the pilot's sidestick and provides a blend of direct lift and conventional aircraft control. In the lateral axis, a roll rate system accepts pilot commands from lateral forces on the sidestick and develops the desired roll rate about the aircraft's velocity vector. For directional control, direct sideforce is available through the rudder pedals. In addition, independent fuselage pointing in both the pitch and yaw axes can be commanded through this same structure.

It is acknowledged that the designs are not optimum in every sense; however, the design method is a viable alternative and has many advantages compared with the currently available multivariable techniques. These advantages become more attractive when recognizing that the iterative process of fine tuning is an inherent requirement of any design method. The major advantages are:

1. The ease of design and the ability to fine tune to specific requirements.

2. The use of output feedback without the need of full state information.

3. The high degree of decoupling available.

4. The similarity in developing continuous and discrete designs.

It must be noted that these conclusions are based on a "preliminary design" effort. Because the techniques may result in high gain controllers, caution must be exercised in selecting final design values. It is recommended that surface rate and position limits be considered in the early design work. Use of estimated maximum maneuvers at each design point provides a means of scaling gains to prevent exceeding surface position limits.

Considerable effort is expended in the development of a proper aircraft model for the design. However, this problem is encountered with any design method. Once the modelling is achieved, the designs in this report are

accomplished in a simple, straightforward manner. An understanding of the fundamental physics of the aircraft's response cannot be overemphasized. It is through such an understanding that a realistic and desirable system design is established.

## Simplifying and Improving the Design Process

From the experience gained in this research, several changes are suggested to simplify the design process. First, the use of s-plane closed-loop root migrations and open-loop frequency response data can reduce trial and error design time and allow conventional gain and phase margin testing.

Second, the ability to directly observe the influences of surface rate limits provides valuable insight into the implementation restrictions imposed on a design. With such an ability, gain values can be quickly determined which yield acceptable and practical designs.

Third, a means of including compensation filters in the design process allows a more realistic assessment to be made. The ability of a chosen design to accept such filter additions can then be determined early in the synthesis process.

Fourth, a way to directly vary the integral gains without altering proportional gains can simplify the design process.

Finally, considerable effort and implementation complexity can be saved by designing in a non zero-$B_2$ format with nonredundant equations.

MULTI Improvements

All of the simplifications and improvements for the design process relate directly to changes in the MULTI package. To be able to use frequency domain techniques in the design, MULTI has been altered to provide both open-loop and closed-loop transfer functions. However, it is necessary at present to go to another program (TOTAL) to obtain frequency response plots. In addition, it will be beneficial to calculate the closed-loop roots for each design iteration. A plot from these iterations will provide a pseudo closed-loop root locus for the system. In this way, the powerful frequency domain techniques can be utilized.

To provide the ability to observe the effects of surface rate limits, the actuator model option must be altered to include these nonlinearities in the same way that position limits are currently provided. In this way, instabilities that might be encountered due to rate limits can be seen immediately. Designs with reduced but practical gains will result.

An option is needed to allow compensation filters to be added at the system inputs and to allow notch filters to be inserted between the controller outputs and the

actuator models. The influence of such filters (that will almost certainly be added during flight test) can be evaluated at this early design stage.

As MULTI is presently configured, changing the $\bar{\alpha}$ parameter varies the proportional gains, directly affecting stability, while holding the integral gains constant. When the integral-to-proportional gain ratio is varied to alter the time to reach steady state, $\bar{\alpha}$ is changed and $\varepsilon$ must be adjusted to return the proportional gain to its original value. This unnecessarily complicates the design effort. Only a minor modification to MULTI is needed to eliminate this problem.

The method of calculating gains with $[\underline{F}_2\underline{B}_2]$ requires an additional transformation to zero-$B_2$ form if a design is to be developed with a minimum number of measurement matrix elements. This transformation results in feedback states that include components of surface deflections for the designs in this study. Although an adequate design can be obtained, this adds complexity to the system. Equivalent performance and decoupling can be achieved without this complication if $[\underline{FB}]$ is used for gain calculations. (Note: This change is currently being made to the MULTI program.)

The use of redundant equations results in unnecessary complexity in the design activity and can cause numerical computation problems. The equations are included so that pertinent aircraft parameters such as angle of attack

and sideslip angle can be evaluated while controlling rates and accelerations. This requires that MULTI be modified to plot any combination of states instead of only those output which are being controlled. In this same light, it will be advantageous to provide a means to plot state derivatives or combinations of state derivatives and states. With such an expanded capability, almost any aircraft parameter of interest can be monitored during the design. Currently, this requires significant modifications to the matrix of system equations.

## Proposed Future Work

The major uncertainty with the designs presented in this report concerns their performance in a real world environment. The effects of gust inputs, sensor measurement noise, and structural mode interference need to be evaluated. The system's behavior with digital time delays, quantization effects and nonlinear aerodynamics must be ascertained. It is proposed that the current designs be carried into a nonlinear simulation evaluation where a realistic operational environment can be provided.

The Neal-Smith Criterion is applied to obtain an indication of pilot rating in a compensatory tracking task for one longitudinal design. This is only a cursory check with one of several methods. Recent work has been accomplished on a modified flying qualities evaluation method (Ref 19). Several other evaluation methods such as the step

target tracking technique and the bandwidth criteria are also available (Ref 17 and 18). The current designs should be evaluated using these methods.

The high gain instabilities illustrated in Figures 43 and 44 of Chapter IV should be examined in detail and a method developed to accurately predict the stability boundaries. This work can be a part of the simulation evaluation discussed previously.

## References


1. Rubertus, Duane P. "TWEAD Control Augmentation System." Paper presented at the National Aerospace Electronics Conference, Dayton, Ohio, 15-17 May 1972.

2. Sutherland, J.P. "Fly-by-Wire Flight Control System." Paper given at the Joint Meeting of Flight Mechanics and Guidance Control Panels of AGARD, Oslo, Norway, September 1968.

3. Whitmoyer, Robert A., and James K. Ramage. "The Fighter Control Configured Vehicle (CCV) Program Development and Flight Test Summary." Paper presented at the Eighth Annual Symposium of the Society of Flight Test Engineers, Washington, D.C., 10-12 August 1977.

4. McAllister, J.D. Task Oriented CCV Control Modes. (Phase VIII Report), FZM-620-058, General Dynamics, Fort Worth, Texas, 28 September 1979.

5. Barfield, A. Finley. "Flight Experience with Manually Controlled Unconventional Aircraft Motions." Paper presented at the 14th Annual Conference on Manual Control, Los Angeles, California, April 1978.

6. Porter, B. Design of High Performance Tracking Systems. USAME/DC/120/81. Air Force Flight Dynamics Laboratory, Wright-Patterson AFB, Ohio.

7. Johannes, Robert P., and Robert A. Whitmoyer. "AFFDL Experience in Active Control Technology." AGARD Conference Proceedings No. CP262 on Aerodynamic Characteristics of Control, Pozzuoli, Italy, 14-17 May 1979.

8. Rosenbrock, H.H. "The Zeros of a System," International Journal of Control, 18 (2): 297-299 (1973).

9. Ridgely, D. Brett, Siva S. Banda, and John J. D'Azzo. "Decoupling of High Gain Multivariable Tracking Systems." Paper No. 83-0280 presented at the AIAA 21st Aerospace Sciences Conference, Reno, Nevada, 10-13 January 1983.

10. Porter, Douglas S. Design and Analysis of a Multivariable Digital Controller for the A-7D DIGITAC II Aircraft and the Development of an Interactive Computer Design Program. MS Thesis. Air Force Institute of Technology, Wright-Patterson AFB OH, December 1981.

11. D'Azzo, John J., and Constantine H. Houpis. Linear Control Systems Analysis and Design (Second Edition). New York: McGraw-Hill Book Company, 1981.

12. Kennedy, Thomas A. The Design of Digital Controllers for the C-141 Aircraft Using Entire Eigenstructure Assignment and the Development of an Inter-Active Computer Design Program. MS Thesis. Air Force Institute of Technology, Wright-Patterson AFB OH, March 1979.

13. Lewis, Tom. High-Gain Error Actuated Flight Control Systems for Continuous Multivariable Plants. MS Thesis. Air Force Institute of Technology, Wright-Patterson AFB OH, December 1982.

14. Bauschlicher, Jon M. Design of a Complete Multivariable Digital Flight Control System. MS Thesis. Air Force Institute of Technology, Wright-Patterson AFB OH, December 1982.

15. Townsend, James L., and Eugene T. Raymond. Background Information and User Guide for Mil-F-9490D Flight Control Systems - Design, Installation and Test of Piloted Aircraft, General Specification for. AFFDL-TR-74-116, Air Force Flight Dynamics Laboratory, Wright-Patterson AFB, Ohio, January 1975.

16. Neal, Peter T., and Rogers E. Smith. An In-Flight Investigation to Develop Control System Design Criteria for Fighter Aircraft. AFFDL-TR-70-74, Volume 1. Air Force Flight Dynamics Laboratory, Wright-Patterson AFB, Ohio, December 1970.

17. Hoh, Roger H., Thomas T. Myers, Irving L. Ashkenas, Robert F. Ringland, and Samual J. Craig. Development of Handling Quality Criteria for Aircraft With Independent Control of Six Degrees of Freedom. AFWAL-TR-81-3027. Flight Dynamics Laboratory, Wright-Patterson AFB, Ohio, April 1981.

18. Onstott, E.D., and W.H. Faulkner. Prediction, Evaluation, and Specification of Closed Loop and Multiaxis Flying Qualities. AFFDL-TR-78-3. Air Force Flight Dynamics Laboratory, Wright-Patterson AFB, Ohio, February 1978.

19. Smith, Ralph H., and Norman D. Geddes. Handling Quality Requirements for Advanced Aircraft Design: Longitudinal Mode. AFFDL-TR-78-154. Air Force Flight Dynamics Laboratory, Wright-Patterson AFB, Ohio, August 1979.

20. Roskam, J. Airplane Flight Dynamics and Automatic Flight Controls. Lawerence, Kansas: Roskam Aviation and Engineering Corporation, 1976.

21. Barfield, A. Finley, and Larry R. Felt. "Aeroservoelasticity - A Merging of Technologies." Paper presented at the 7th Annual Symposium of the Society of Flight Test Engineers, Eastsound, Washington, 4-6 August 1976.

22. Lamont, Gary B., and Constantine H. Houpis. Digital Control System: Theory, Hardware, Software. McGraw-Hill Book Company, to be published.

Appendix B

PREVIOUS PAGE
IS BLANK

AFIT/GE/EE/82D-18

# DESIGN OF A COMPLETE MULTIVARIABLE DIGITAL FLIGHT CONTROL SYSTEM

THESIS

Presented to the Faculty of the School of Engineering
of the Air Force Institute of Technology
Air University
in Partial Fulfillment of the
Requirements for the Degree of
Master of Science

by

Jon M. Bauschlicher
Captain USAF
Graduate Engineering
December 1982

Reproduced from best available copy.

Approved for public release, distribution unlimited.

# PREFACE

This thesis follows up work done by Douglas Porter and Joseph Smyth in their thesis efforts at the Air Force Institute of Technology. It was supported by the Air Force Dynamics Lab/Control Division at Wright-Patterson Air Force Base and Duane P. Robertus and Elisha Rochovitsky in particular.

Before thanking all those who worked with me in the thesis effort itself, let me first thank those who worked the hardest and "suffered" the most--my family. Without their complete support and understanding, none of this would have been possible. Thank you Valerie, April, Kurt, and Shalyn.

My thanks goes out to Elisha Rochovitsky and Duane Robertus for their support and that of the Flight Dynamics Lab throughout this effort. Special thanks goes to Dr. John J. D'Azzo who gave me a valuable amount of his time examing my results, answering my questions, and suggesting alternatives in the developement and writing of this thesis. Many thanks also to Dr. Constantine H. Houpis who is always there when you need his support to get things done. Thanks also to Captain Aaron Q. Dewispelare who took the time to read and analyse initial drafts of this thesis and offer valuable suggestions.

Without the suggestions and ideas of my colleagues Mr. Finley Barfield, Captain Michael Massi, Lt Daniel Russ and Lt Thomas Lewis (all of them have produced theses examining various aspects of this design technique) much of this thesis would not have been possible. My thanks goes to them for taking

time out from their thesis work to examine and comment on my thesis work.

Captain Jon M. Bauschlicher

CONTENTS


Title

Preface .....

List of Figures .....

List of Tables .....

List of Symbols .....

Abstract .....

I Introduction .....

Background .....
Problem .....
Current Knowledge .....
Support .....
Overview .....

II Design Methodology Using Singular Perturbation Methods .....

Introduction .....
Unknown Plant .....
Known Plant .....
Known/Regular Plants .....
Known/Irregular Plant .....

III VFW Aircraft and Model Description .....

Introduction .....
Aircraft Description .....
Observations .....

IV Complete Controller Design .....

Introduction .....
Lateral Controller .....
Maneuver Description .....
Lateral Model .....
Measurement Matrix Development .....
Controller Design .....
Longitudinal Controller .....
Maneuver Description .....
Longitudinal Model .....
Measurement Matrix Development .....
Controller Design .....
Combining Lateral and Longitudinal Controllers ..
Conclusion .....

Title


V Robustness Testing on Complete Controller .....

Introduction .....
Universal Controller .....
0.6 Mach, Sea Level Flight Condition .....
0.9 Mach, 30,000 ft. Flight Condition .....
2.3 Mach, 40,000 ft. Flight Condition .....
Conclusions .....

VI Results, Conclusions and Recommendations .....

Introduction .....
Results .....
Advantages .....
Disadvantages .....
Recommendations .....
Design Method .....
MULTI .....

Bibliography .....

Appendix A: Modifications to Interactive Design Tool MULTI .....

Appendix B: Data for 0.9 Mach, 30,000 Ft. and 2.3 Mach, 40,000 Ft. Flight Conditions .....

Appendix C: Examination of Steady-State Control Inputs .....

Vita .....

# LIST OF FIGURES


| Figure | Title |
|---|---|
| 1 | Block Diagram of Basic Plant/Controller Structure ..... |
| 2 | Block Diagram of Known/Irregular Plant/ Controller Structure ..... |
| 3 | FPCC Aircraft and Jet Flap ..... |
| 4 | 1.5-g Horizontal Translation (.6M, SL) ..... |
| 5 | 60 Degree Rollover (.6M, SL) ..... |
| 6 | 1-g Flat Turn (.6M, SL) ..... |
| 7 | 4 Degree Yaw Pointing (.6M, SL) ..... |
| 8 | 4 Degree Yaw Pointing (.6M, SL) ..... |
| 9 | 1-g Horizontal Translation (.9M, 30K) ..... |
| 10 | 60 Degree Rollover (.9M, 30K) ..... |
| 11 | 0.5-g Flat Turn (.9M, 30K) ..... |
| 12 | 4 Degree Yaw Pointing (.9M, 30K) ..... |
| 13 | 4 Degree Yaw Pointing (.9M, 30K) ..... |
| 14 | 0.5-g Horizontal Translation (2.3M, 40K) .... |
| 15 | 60 Degree Rollover (2.3M, 40K) ..... |
| 16 | 0.5-g Flat Turn (2.3M, 40K) ..... |
| 17 | 4 Degree Yaw Pointing (2.3M, 40K) ..... |
| 18 | 4 Degree Yaw Pointing (2.3M, 40K) ..... |
| 19 | 1.75 Degree Pitch Pointing (.6M, SL) ..... |
| 20 | 1.5-g Direct Lift (.6M, SL) ..... |
| 21 | 1.5-g Vertical Translation (.6M, SL) ..... |
| 22 | 1.75 Degree Pitch Pointing (.9M, 30K) ..... |
| 23 | 2.0-g Direct Lift ..... |
| 24 | 1-g Vertical Translation (.9M, 30K) ..... |
| 25 | 0.5 Degree Pitch Pointing (2.3M, 40K) ..... |
| 26 | 0.5-g Direct Lift (2.3M, 40K) ..... |
| 27 | 0.5-g Vertical Translation (2.3M, 40K) ..... |
| 28 | 60 Degree Rollover (.9M, 30K) ..... |
| 29 | 60 Degree Rollover (.9M, 30K) ..... |
| 30 | 60 Degree Banked Level Coordinated Turn (.6M, SL) ..... |
| 31 | 60 Degree Banked Level Coordinated Turn (.9M, 30K) ..... |
| 32 | 60 Degree Banked Level Coordinated Turn (.9M, 30K) ..... |
| 33 | 1.5-g Horizontal Translation (.6M, SL) ..... |
| 34 | 1.5-g Horizontal Translation (.6M, SL) ..... |
| 35 | 60 Degree Rollover (.6M, SL) ..... |
| 36 | 60 Degree Rollover (.6M, SL) ..... |
| 37 | 1-g Flat Turn (.6M, SL) ..... |
| 38 | 1-g Flat Turn (.6M, SL) ..... |
| 39 | 4 Degree Yaw Pointing (.6M, SL) ..... |
| 40 | 4 Degree Yaw Pointing (.6M, SL) ..... |
| 41 | 1.75 Degree Pitch Pointing (.6M, SL) ..... |
| 42 | 1.75 Degree Pitch Pointing (.6M, SL) ..... |




Copy available to DTIC does not permit fully legible reproduction

| Figure | Title |
|---|---|
| 43 | 1.8-g Direct Lift (.6M, SL) ..... |
| 44 | 1.8-g Direct Lift (.6M, SL) ..... |
| 45 | 0.8-g Vertical Translation (.6M, SL) ..... |
| 46 | 0.8-g Vertical Translation (.6M, SL) ..... |
| 47 | 1-g Horizontal Translation (.9M, 30K) ..... |
| 48 | 1-g Horizontal Translation (.9M, 30K) ..... |
| 49 | 0.8-g Horizontal Translation (.9M, 30K) ..... |
| 50 | 0.8-g Horizontal Translation (.9M, 30K) ..... |
| 51 | 60 Degree Rollover (.9M, 30K) ..... |
| 52 | 60 Degree Rollover (.9M, 30K) ..... |
| 53 | 0.6-g Flat Turn (.9M, 30K) ..... |
| 54 | 0.6-g Flat Turn (.9M, 30K) ..... |
| 55 | 0.6-g Flat Turn, Modified R Input (.9M, 30K). |
| 56 | 0.6-g Flat Turn, Modified R Input (.9M, 30K). |
| 57 | 3 Degree Yaw Pointing (.9M, 30K) ..... |
| 58 | 3 Degree Yaw Pointing (.9M, 30K) ..... |
| 59 | 3 Degree Pitch Pointing (.9M, 30K) ..... |
| 60 | 3 Degree Pitch Pointing (.9M, 30K) ..... |
| 61 | 2.4-g Direct Lift (.9M, 30K) ..... |
| 62 | 2.4-g Direct Lift (.9M, 30K) ..... |
| 63 | 1-g Vertical Translation (.9M, 30K) ..... |
| 64 | 1-g Vertical Translation (.9M, 30K) ..... |
| 65 | 0.7-g Horizontal Translation (2.3M, 40K) .... |
| 66 | 0.7-g Horizontal Translation (2.3M, 40K) .... |
| 67 | 30 Degree Rollover (2.3M, 40K) ..... |
| 68 | 30 Degree Rollover (2.3M, 40K) ..... |
| 69 | 0.6-g Flat Turn (2.3M, 40K) ..... |
| 70 | 0.6-g Flat Turn (2.3M, 40K) ..... |
| 71 | 1 Degree Yaw Pointing (2.3M, 40K) ..... |
| 72 | 1 Degree Yaw Pointing (2.3M, 40K) ..... |
| 73 | 0.5 Degree Pitch Pointing (2.3M, 40K) ..... |
| 74 | 0.5 Degree Pitch Pointing (2.3M, 40K) ..... |
| 75 | 2-g Direct Lift (2.3M, 40K) ..... |
| 76 | 2-g Direct Lift (2.3M, 40K) ..... |
| 77 | 1-g Vertical Translation (2.3M, 40K) ..... |
| 78 | 1-g Vertical Translation (2.3M, 40K) ..... |
| A-1 | Sample Input ..... |
| A-2 | Pulse Input ..... |
| A-3 | Ramped-Up Input ..... |
| A-4 | Step Input Value ..... |

# LIST OF TABLES


| Table | Title |
|---|---|
| I | Summary Listing of Initial CPCC Reference Aircraft Point Design Guidelines and Constraints ..... |
| II | Control Surface Limits and Dynamics ..... |
| III | Input Vector, $\underline{u}$ ..... |
| IV | State Vector, $\underline{x}$ ..... |
| V | Output Vector, $\underline{y}$ ..... |
| VI | Summary of Time Responses for Lateral Controller ..... |
| VII | Summary of Time Responses for Longitudinal Controller ..... |
| VIII | Summary of Time Responses for Integrated Controller ..... |

# LIST OF SYMBOLS

Symbols

Definition of State Matrix Parameters .....

Definition of Method Parameters .....

Definition of Partitioned Matrix Parameters .. ....

Definition of Aircraft State Equation Parameters ....

## ABSTRACT

This thesis investigates the application of a singular perturbation method in the design of a complete (lateral and longitudinal) multivariable, error-actuated, tracking, digital flight controller. The aircraft model used to test the method is a hypothisized design proposed by Lockheed with augmented flight control surfaces including horizontal and vertical canards, and jet-flaps.

Separate lateral and longitudinal controllers are designed for each of three flight conditions - 0.6 Mach, sea level; 0.9 Mach, 30,000 ft. altitude; and 2.3 Mach, 40,000 ft. altitude. The lateral and longitudinal controllers for each flight condition are then combined, yielding a controller for each of the three flight conditions capable of accomplishing lateral and longitudinal maneuvers. The controllers are tested by commanding seven decoupled six degree-of-freedom maneuvers and one coupled three degree-of-freedom maneuver. Figures of Merit (rise time, percent overshoot, and settling time) are presented for the decoupled maneuvers. Tests are conducted to find a single controller capable of commanding all of the decoupled maneuvers over the entire range of the three flight conditions examined. The controller is found and it's performance documented by recording the figures of merit (same figures as previously mentioned) for the seven decoupled maneuvers at the three flight conditions specified above. The design process and necessary considerations are outlined as th

controllers are synthesized. Finally, the computer aided design tool MULTI is modified and it's capabilities are enhanced.

The results of this thesis show that multivariable tracker control laws can be designed for the aircraft model examined here equiped with augmented control surfaces - ailerons, rudder, maneuver flaps, canards, and jet flaps. The controllers all perform very satisfactorily at the flight condition for which they are designed. In addition the thesis shows that a "universal" controller can be found that is capable of producing satisfactory responses for the three flight conditions previously mentioned, eliminating much of the gain scheduling required with present digital flight controllers.

FOLLOWING
Reproduced from best available copy.
PAGES

# CHAPTER I

# INTRODUCTION

## Background

Digital computers are rapidly becoming an integral part of aircraft flight control systems. This computer-operated digital flight control system must include the capability of the flight control system to handle multiple inputs by the pilot and to command multiple outputs simultaniously, thus maximizing aircraft performance over a very wide range of flight conditions.

There are many advantages to using a digital flight control system. A computer-operated digital flight control system has the ability to handle many more control surfaces than can currently be handled by the pilot. With digital control, surfaces such as jet flaps and canards may be controlled simultaniously along with ailerons, rudder, and elevator. This permits the maximizing of maneuver performance over a wide range of flight conditions. Now, instead of commanding a surface deflection directly to perform a maneuver, the pilot commands a maneuver at some desired rate and the computer controlled control surfaces operate to maximize performance and efficiency at a given flight condition.

Presently, controllers for such multiple input/multiple output (MIMO) systems are designed using classic single input/single output (SISO) and LQG methods each having some drawbacks. The well known classical SISO methods require much

trial and error and may yield a satisfactory design, however, they allow only a single input/output combination to be examined at a time. LQG methods can handle MIMO systems, but all states are required to be accessable or a state estimator is needed. This method also requires complex mathmatics and usually much trial and error to derive the appropriate cost function.

Professor Brian Porter and his associates of the University of Salford, U.K., have proposed a simple design technique capable of synthesizing a controller which can handle and decouple the outputs of multiple input/multiple output systems (Ref 14). Initial attempts to synthesize an aircraft flight control system using Porter's techniques have proven successful (Ref 25 and 28). Still, much remains to be studied concerning the design technique and it's refinement for use by the practical engineer before a design can be implemented on future aircraft.

Lockheed, Honeywell, and Pratt-Whitney have hypothesized an advanced aircraft under contract to the Air Force Flight Dynamics Lab. The hypothesized aircraft is statically unstable and incorporates several advanced concepts in aircraft flight control such as employing canards and jet flaps, all designed to enhance aircraft maneuverability (Ref 6). Due to these enhanced flight control surfaces, the aircraft is also capable of accomplishing decoupled six degree-of-freedom maneuvers. The contractors involved in this hypothesized design have provided the Flight Dynamics Lab with a computer simulation pro-

gram, FPCC Sim (Ref 8), which simulates the aircraft performance at various flight conditions.

AFIT students have composed a computer aided design tool (CAD) which aids in synthesizing a controller using Porter's design technique. The program, called MULTI (Ref 25), is very sound and improvements are being added to increase its capabilities.

Problem

This thesis first applies Professor Porter's design technique to develop three multi-variable tracker control laws for the hypothesized jet-flap aircraft, one controller for each of three flight conditions. Each controller is capable of performing both lateral or longitudinal, coupled or decoupled, maneuvers. A "universal" controller is then synthesized, capable of producing stable responses at all of the three flight conditions examined - 0.6 Mach, sea level; 0.9 Mach, 30,000 ft altitude; and 2.3 Mach, 40,000 ft altitude. The outputs of this "universal" controller are compared with those of the controllers designed to operate at a particular flight condition.

Finally, the thesis incorporates improvements to MULTI. Capabilities are increased by allowing pulse inputs (ramped-up and ramped-down), terminal or calcomp plots of pilot command input to the system $y$, and a printout of CPU time used at any point while running the program.

## Current Knowledge

Professor Porter and his associates have published numerous papers on the design technique employed in this thesis (Ref 2, 3, 12-21, 23, 24). Several related theses have been written at AFIT concerning the design technique, but none have attacked the problem of synthesizing a complete controller capable of commanding both lateral and longitudinal maneuvers, or a combination of these. This thesis builds on the work of Joseph Smyth completed in December of 1981 (Ref 28) in proposing a longitudinal MIMO control law for the jet flap aircraft. The thesis also builds on the work of Douglas Porter completed in December of 1981 (Ref 25) in composing the CAD tool, MULTI. The reports submitted by Lockheed on the jet flap aircraft and its simulation program FPCC Sim (Ref 6,8) are used in both the controller design and aircraft simulation.

## Support

The CDC computer system at Wright-Patterson Air Force Base, and those computer facilities at both AFIT and the Air Force Flight Dynamics Laboratory are used extensively. Also, the experience of the AFWAL/FIG division, and Mr. Elisha Rochovitsky of the Flight Dynamics Lab in particular, are used throughout this study.

## Overview

Chapter II describes briefly the theory under[illegible] the design method used in this study. Chapter III describes the jet flap aircraft and the simulation program FPCC [illegible] plus

IV begins by describing the modifications made to the data from FPCC Sim to accomplish the controller design. Next, Chapter IV follows the development of first the lateral and then the longitudinal controller for each of the three flight conditions examined. This is followed by an explaination of how these separate controllers are combined at each flight condition, yielding a complete controller capable of performing lateral, longitudinal, or combined lateral and longitudinal maneuvers. These controllers are tested by commanding seven decoupled and two coupled maneuvers and plotting the outputs of the system. Chapter V describes how the "universal" controller is synthesized and compares its performance at different flight conditions against controllers designed to operate at a specific flight condition. Chapter VI summarizes the results of this thesis and enumerates some conclusions made from the study including advantages and disadvantages found in employing Porter's design technique. Finally, recommendations are made for possible further study.

Chapter 2. Design Theory, Omitted

See Proceedings

# CHAPTER III

## *FPCC AIRCRAFT AND MODEL DESCRIPTION*

### Introduction

The aircraft model used in this thesis is a hypothesized advanced design - the result of a joint design effort by Lockheed, Pratt and Whitney, and Honeywell. The model incorporates many advanced flight control concepts. The name given to the aircraft, "Flight-Propulsion-Control-Coupling" (FPCC), designates what is probably the most significant of these control concepts - that of incorporating thrust vectoring into the control inputs available to the pilot to accomplish a given in-flight maneuver. Other advanced flight control technologies are used on the model and are described below.

The model was developed during the period of June 1976 through June 1977 - before the Air Force became interested in developing an aircraft capable of accomplishing decoupled, six-degree-of-freedom maneuvers such as pitch-pointing and flat turns. However, the aircraft does have the capability of developing direct side force because of the flight control surfaces incorporated in the design. Because of this capability, and the current Air Force interest in developing an aircraft with increased agility, this model was selected to test Professor Porter's multivariable design technique. The controller designed is thus capable of accomplishing decoupled six-degree-of-freedom maneuvers, equivalent to those currently being flight tested on the AFTI-16 aircraft.

## Aircraft Description

The aircraft configuration is shown in Figure 3. It is a single seat, supersonic fighter designed for air combat with a secondary role as a surface weapons delivery system. Flight control surfaces and other flight control inputs used by this aircraft consist of conventional surfaces such as rudder and ailerons coupled with surfaces not used on most present day Air Force Aircraft - horizontal and vertical canards, jet flaps (see Figure 3), and maneuver flaps (presently used only on the F-16). The vertical canards, rudder, and ailerons generate the side forces required to perform the laterally decoupled maneuvers. A combination of the jet flaps, maneuver flaps, and horizontal canards enable the aircraft to accomplish decoupled, longitudinal maneuvers. A summary of FPCC aircraft design guidelines and constraints is presented in Table I. Table II presents the control surface limits, servo dynamics, and sensor dynamics used in the simulation. For the purposes of this thesis, the horizontal canards, vertical canards, jet flaps, and maneuver flaps are deflected symmetrically. The rudder and ailerons work as they do on present day aircraft. On the original design, the jet flap was restricted to operate from 0° to 90° and the maneuver flaps were restricted to $\pm$ 15° because the aircraft was not designed to accomplish the six-degree-of-freedom maneuvers. For the purpose of this thesis, these limits are adjusted to those displayed in Table II. These are the only modifications made to the original paper design submitted by Lockheed. It should be noted that the

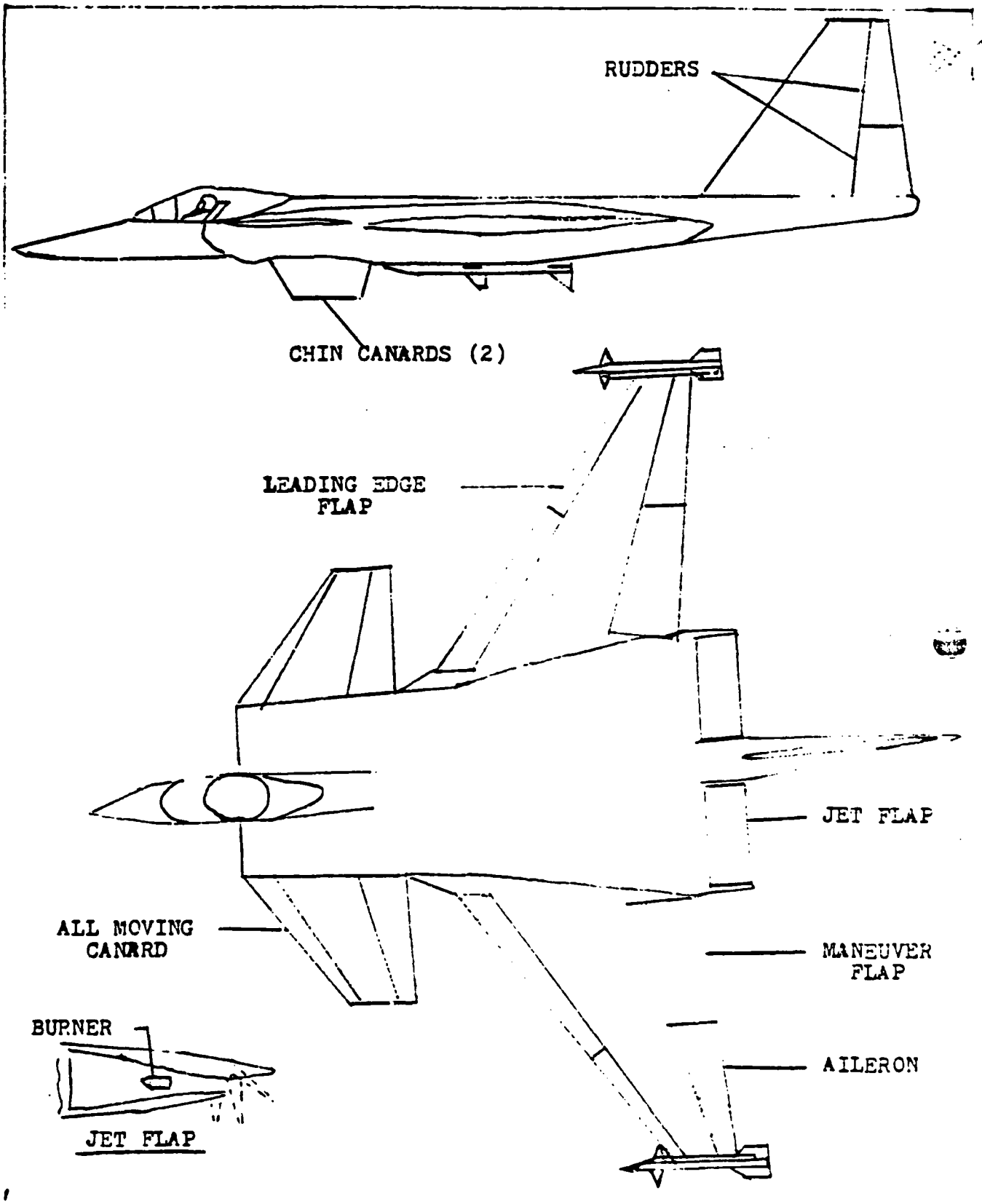



Fig 3. FPCC Aircraft And Jet Flap

TABLE I

SUMMARY LISTING OF INITIAL FPCC REFERENCE AIRCRAFT POINT DESIGN GUIDELINES AND CONSTRAINTS (REF 6)

1. Primary aircraft design mission -- supersonic/transonic air superiority

   Secondary aircraft design mission -- transonic close air support

   Aircraft dash speed capability -- within the range of Mach 2.2 through 3.0

2. Advanced CTOL or STOL design emphasizing air combat maneuvering and air combat tracking requirements for high subsonic/transonic air-to-air and air-to-ground tasks

3. Mission range, payload, takeoff and landing distance requirements are to be considered of secondary importance

4. Aircraft and propulsion design not constrained to any specification except for those noted in the RFP Statement of Work

5. Flight control designs may include any advanced feature such as Relaxed Static Stability (RSS) and Direct Side Force Control (DSFC)

6. Aircraft design may include modulatory type Aerodynamic/Propulsive Interactive Force (APIF) systems

7. Digital control and fly-by-wire assumed

8. The supersonic engine air inlet shall be of the external or mixed compression type consistent with the selected aircraft dash speed Mach number. Inlet bypass air may be used for aircraft maneuvering augmentation

9. Aircraft design thrust to weight (T/W) ratio shall be higher than 1.0 with dry engine operation. However, engines shall incorporate afterburning. Engine control may include

   - variable fan guide vane angle
   - variable compressor stator angle
   - variable turbine area
   - variable exhaust nozzle area

   Engine bleed capabilities may be considered consistent with APIF system

10. The Lockheed reference aircraft point design will incorporate the current state of the art Pratt and Whitney aircraft F-100-PW-100 afterburning turbofan engine and controls

TABLE II

CONTROL SURFACE LIMITS AND DYNAMICS

| Control Surface | Deflection Limits M<1.0 | M>1.0 | Servo Dynamics | Sensor Dynamics |
|---|---|---|---|---|
| Maneuver Flap ($\delta_{MF}$) | $\pm 30°$ | $\pm 15°$ | $\frac{25}{s+25}$ | $\frac{100}{s+100}$ |
| Jet Flap ($\delta_j$) | $\pm 90°$ | $\pm 90°$ | $\frac{25}{s+25}$ | $\frac{100}{s+100}$ |
| Horizontal Canard ($\delta_{HC}$) | $\pm 20°$ | $\pm 10°$ | $\frac{25}{s+25}$ | $\frac{100}{s+100}$ |
| Thrust ($F_{TOT}$) | - | - | $\frac{0.574}{s+0.574}$ | $\frac{100}{s+100}$ |
| Aileron ($\delta_a$) | $\pm 20°$ (per side) | $\pm 20°$ (per side) | $\frac{25}{s+25}$ | $\frac{100}{s+100}$ |
| Rudder ($\delta_r$) | $\pm 30°$ | $\pm 15°$ | $\frac{25}{s+25}$ | $\frac{100}{s+100}$ |
| Vertical Canard ($\delta_{VC}$) | $\pm 35°$ | $\pm 15°$ | $\frac{25}{s+25}$ | $\frac{100}{s+100}$ |

aircraft is statically unstable at 0.9 Mach (Ref 6).

FPCC Sim Program

The data used to represent the aircraft model chosen for this thesis is generated by a non-linear six degree-of-

freedom computer simulation program called "FPCC Sim". The program was developed by Lockheed under contract to the Air Force as part of the FPCC program and is available through the Air Force Flight Dynamics Lab. The computer program includes a simulation of the F-100 engine, along with many other variables not needed for this study. This model is appropriate, since the objective of this thesis is simply to design a digital flight controller. Due to the enormity of the FPCC Program (16,000 lines of FORTRAN code) and the large amount of computer time required to run the program, FPCC Sim was modified by Mr. John Houtz of the Flight Dynamics Lab to provide only the data needed for this thesis. This data consists of the state equations, in matrix form, for the flight conditions:

1) .6 Mach, Sea level
2) .9 Mach, 30,000 ft altitude
3) 2.3 Mach, 40,000 ft altitude

These three flight conditions provide a large range to test the robustness of the flight controller. A drawback to testing such a large range is that there are many areas in the flight envelope which are not explored. Given the constraints of this thesis (limited amount of time, the thesis objectives of designing both a lateral and longitudinal controller, and finally, testing the controller's robustness), these flight conditions are determined to be the best of those available to test the controller quickly over a very wide range of flight conditions.

As stated earlier, the data for each flight condition is provided as state equations in the matrix form:

$$\dot{\underline{x}} = \underline{A}\,\underline{x} + \underline{B}\,\underline{u} \tag{46}$$

$$\dot{\underline{y}} = \underline{C}\,\underline{x} + \underline{F}\,\underline{u} \tag{47}$$

An example of this data is listed in equations (48) and (49) exactly as it is given to the user from Mr. Houtz's modification to the FPCC Sim program. The example is for the flight condition 0.6 Mach at sea level (rounded off data):

$$\begin{bmatrix} \dot{p} \\ \dot{r} \\ \dot{v} \\ \dot{\phi} \\ \dot{\psi} \\ \dot{y} \\ \dot{q} \\ \dot{w} \\ \dot{u} \\ \dot{\theta} \\ \dot{h} \\ \dot{x} \end{bmatrix} = \begin{bmatrix} -2.35 & 1.47 & -.010 & 0. & 0. & 0. & 0. & 0. & 0. & 0. & 0. & 0. \\ .256 & -.989 & .019 & 0. & 0. & 0. & 0. & 0. & 0. & 0. & 0. & 0. \\ 13.2 & -666. & -.687 & 32.1 & 0. & 0. & 0. & 0. & 0. & 0. & 0. & 0. \\ 1.0 & .018 & 0. & 0. & 0. & 0. & 0. & 0. & 0. & 0. & 0. & 0. \\ 0. & 1. & 0. & 0. & 0. & 0. & 0. & 0. & 0. & 0. & 0. & 0. \\ 0. & 0. & 1. & -12.0 & 669 & 0. & 0. & 0. & 0. & 0. & 0. & 0. \\ 0. & 0. & 0. & 0. & 0. & 0. & -.463 & .064 & -.001 & 0. & 0. & .000 \\ 0. & 0. & 0. & 0. & 0. & 0. & 674 & -2.82 & -.057 & -.577 & -.0005 & -.0005 \\ 0. & 0. & 0. & 0. & 0. & 0. & -12.1 & .105 & -.030 & -32.1 & 0. & .000 \\ 0. & 0. & 0. & 0. & 0. & 0. & 1. & 0. & 0. & 0. & 0. & 0. \\ 0. & 0. & 0. & 0. & 0. & 0. & 0. & 1. & .018 & 669. & 0. & 0. \\ 0. & 0. & 0. & 0. & 0. & 0. & 0. & .018 & 1. & 0. & 0. & 0. \end{bmatrix} \begin{bmatrix} p \\ r \\ v \\ \phi \\ \psi \\ y \\ q \\ w \\ u \\ \theta \\ h \\ x \end{bmatrix}$$

$$+ \begin{bmatrix} .198 & 0. & 0. & .166 & -.0275 & .0487 & .000005 & -.000005 & -.968 & .968 \\ .007 & 0. & 0. & -.188 & .0368 & .0015 & .00003 & -.00003 & -10.3 & 10.3 \\ 0. & 0. & 0. & 1.78 & .581 & 0. & 0. & 0. & 0. & 0. \\ 0. & 0. & 0. & 0. & 0. & 0. & 0. & 0. & 0. & 0. \\ 0. & 0. & 0. & 0. & 0. & 0. & 0. & 0. & 0. & 0. \\ 0. & 0. & 0. & 0. & 0. & 0. & 0. & 0. & 0. & 0. \\ 0. & .640 & -.0966 & 0. & 0. & -.043 & -.000002 & -.000002 & 0. & 0. \\ 0. & -1.43 & -4.73 & 0. & 0. & -.616 & -.00003 & -.00003 & 0. & 0. \\ 0. & .518 & .0198 & 0. & 0. & .0009 & .0011 & .0011 & -387 & -.387 \\ 0. & 0. & 0. & 0. & 0. & 0. & 0. & 0. & 0. & 0. \\ 0. & 0. & 0. & 0. & 0. & 0. & 0. & 0. & 0. & 0. \\ 0. & 0. & 0. & 0. & 0. & 0. & 0. & 0. & 0. & 0. \end{bmatrix} \cdot \begin{bmatrix} \delta a \\ \delta c \\ \delta mf \\ \delta r \\ \delta vc \\ \delta j \\ F_1 \\ F_2 \\ CDI_1 \\ CDI_2 \end{bmatrix} \tag{48}$$

$$
\begin{bmatrix} \alpha' \\ \beta \\ VEL \\ ACGX \\ ACGY \\ ACGZ \end{bmatrix} =
\begin{bmatrix}
0. & 0. & 0. & 0. & 0. & 0. & 0. & .0015 & -.0000 & 0. & 0. & 0. \\
0. & 0. & .0015 & 0. & 0. & 0. & 0. & 0. & 0. & 0. & 0. & 0. \\
0. & 0. & 0. & 0. & 0. & 0. & 0. & .0179 & 1 & 0. & 0. & 0. \\
0. & 0. & 0. & 0. & 0. & 0. & -.0713 & .105 & -.030 & 0. & .000 & -.000 \\
1.18 & 3.94 & -.687 & 0. & 0. & 0. & 0. & 0. & 0. & 0. & 0. & 0. \\
0. & 0. & 0. & 0. & 0. & 0. & 4.08 & -2.82 & -.0568 & 0. & -.000 & -.000
\end{bmatrix}
\begin{bmatrix} p \\ r \\ v \\ \phi \\ \psi \\ y \\ q \\ w \\ u \\ \theta \\ h \\ x \end{bmatrix}
$$

$$
+
\begin{bmatrix}
0. & 0. & 0. & 0. & 0. & 0. & 0. & 0. & 0. & 0. \\
0. & 0. & 0. & 0. & 0. & 0. & 0. & 0. & 0. & 0. \\
0. & 0. & 0. & 0. & 0. & 0. & 0. & 0. & 0. & 0. \\
0. & .518 & .0198 & 0. & 0. & .001 & .011 & .011 & -387. & -387. \\
0. & 0. & 0. & 1.78 & .581 & 0. & 0. & 0. & 0. & 0. \\
0. & -1.43 & -4.73 & 0. & 0. & -.616 & -.0000 & -.0000 & 0. & 0.
\end{bmatrix}
\begin{bmatrix} \delta a \\ \delta c \\ \delta mf \\ \delta r \\ \delta vc \\ \delta j \\ F_1 \\ F_2 \\ CDI_1 \\ CDI_2 \end{bmatrix} \quad (49)
$$

Tables III, IV, and V define the vectors $\underline{u}$, $\underline{x}$, and $\underline{y}$.

TABLE III

INPUT VECTOR, $\underline{u}$*

| Variable | Units | Description |
|---|---|---|
| $\delta a$ | deg | sum of both aileron deflections |
| $\delta c$ | deg | horizontal canard deflection |
| $\delta mf$ | deg | maneuver flap deflection |
| $\delta r$ | deg | rudder deflection |
| $\delta vc$ | deg | vertical canard deflection |
| $\delta j$ | deg | Jet flap deflection WRT fuselage ref line |
| $F_1$ | lbs | Net thrust engine 1 |
| $F_2$ | lbs | Net thrust engine 2 |
| $CDI_1$ | - | Inlet drag coefficient engine 1 |
| $CDI_2$ | - | Inlet drag coefficient engine 2 |

TABLE IV

STATE VECTOR, $\underline{x}$*

| Variable | Units | Description |
|---|---|---|
| p | rad/sec | Body axis roll rate |
| r | rad/sec | Body axis yaw rate |
| v | ft/sec | Body axis side velocity |
| $\phi$ | rad | Roll angle |
| $\psi$ | rad | Yaw angle |
| y | ft | Cross-range position reference to initial body axis |
| q | rad/sec | Body axis pitch rate |
| w | ft/sec | Body axis vertical velocity |
| u | ft/sec | Body axis forward velocity |
| $\theta$ | rad | Pitch angle |
| h | ft | Altitude |
| x | ft | Down-range position referenced to initial body axis |

TABLE V

OUTPUT VECTOR, $\underline{y}$*

| Variable | Units | Description |
|---|---|---|
| $\alpha$ | rad | Angle-of-attack |
| $\beta$ | rad | Sideslip angle |
| VEL | ft/sec | Total airspeed |
| ACGX | $ft/sec^2$ | Accel. of c.g. along x-body axis |
| ACGY | $ft/sec^2$ | Accel. of c.g. along y-body axis |
| ACGZ | $ft/sec^2$ | Accel. of c.g. along z-body axis |

* All variables are perturbations from nominal. The FPCC program also gives the trim angle-of-attack as 1.03 degrees and dynamic pressure as 533.04, and forward velocity as 670.5 ft/sec for the 0.6 Mach sea level flight condition.

## Observations

While reading through this study, it is important to keep in mind that this aircraft was not originally designed to accomplish decoupled six degree-of-freedom maneuvers. As a result, some modifications are required on the control limits. Other modifications to the original design such as adding a horizontal tail and allowing the thrust to be vectored to either side or up and down, could further enhance aircraft performance and agility. However, the original design with the minor modifications made in this thesis is very capable of performing those maneuvers currently considered important.

# CHAPTER IV

# COMPLETE CONTROLLER DESIGN

## Introduction

This chapter describes the design of a complete aircraft controller for combined lateral and longitudinal maneuvers. As mentioned earlier, only separate longitudinal or lateral controllers have previously been designed and examined for this aircraft using Professor Porter's multivariable design method. (Ref 11, 14, 25, 26 and 28). For the jet flap aircraft examined here, a separate longitudinal controller has been designed and examined (Ref 28). While that design demonstrated the feasability of the method, transient control surface deflections often exceeded the limits described in Table II. This is due in part to the fact that the aircraft model combined the maneuver flaps and jet flaps into one equivalent control surface. Retaining the actual control surfaces in the aircraft model is more realistic and leads to increased maneuverability. Also, the previous design had an oscillation of very small amplitude but long duration in the velocity, due to slow engine thrust response. While that oscillation was eliminated by compensating (Ref 31) for slow engine dynamics it is possible to achieve a design that does not require compensation. The controller designed in this thesis is complete - it can command a lateral maneuver, a longitudinal maneuver, or some combination of both lateral and longitudinal motion. This is

typically required for advanced aircraft control systems. The problems mentioned with the previous longitudinal controller (Ref 28) have been overcome, resulting in a very "believable" controller that uses only the amount of control surface available to it and does not exceed those limits while still accomplishing the prescribed maneuvers with very satisfactory time responses.

In examining equations (48) and (49) it can be seen that designing a 12 state combined lateral and longitudinal controller would be a very formitable task. In order to simplify this task, the complete, combined lateral and longitudinal controller is designed in parts. First a suitable lateral controller is designed and tested, and then the longitudinal controller. These two controllers are then combined, resulting in a new controller capable of commanding lateral, longitudinal, or combined maneuvers. This method of controller design is well adapted to industry - two control engineer groups could come up with separate lateral and longitudinal designs and then combine their results. Minimum redesign is then required on the final controller, depending on the degree of coupling between the lateral and longitudinal modes of the particular aircraft. Another important point to be noted from this study is that the optimal values for the controller parameters $\underline{\Sigma}$, $\underline{\alpha}$, $\varepsilon$ and the measurement matrix $\underline{M}$ seem to remain optimum or very close to optimum at all flight conditions, resulting in a minimum requirement to redesign at different flight conditions. The control system is therefore very robust over a

wide range of flight conditions.

The controllers constructed in this thesis and the simulations made to test the different controller designs are accomplished using an interactive, multivariable design program called "MULTI" (Ref 25). MULTI was initially designed in the fall of 1981 by AFIT students to assist them in accomplishing a controller design using Porter's techniques. The program is very sound and provides the user with a tool which is critical to accomplishing the controller design. Some modifications and additions have been made by both the author of this thesis and other AFIT students involved in using Porter's techniques to design aircraft flight controllers. The result is an even better version of MULTI that is more flexible then before. A complete listing of MULTI and its options can be found in the MULTI Users Manual available from the AFIT Department of Electrical Engineering. The modifications to MULTI made during this study are included in Appendix A of this thesis. By use of the program MULTI the designer can rapidly investigate a number of design parameters and achieve an excellent control system.

This chapter contains a discussion of the lateral maneuvers to be tested, the design of the lateral controller, and simulation of the lateral maneuvers at the three flight conditions mentioned in Chapter III - 0.6 Mach, sea level, 0.9 Mach, 30,000 ft., and 2.3 Mach, 40,000 ft., using three different controllers, each designed for that particular flight condition. The longitudinal controller is then developed in an

identical manner. Finally, all controllers are combined and tested yielding three complete controllers, one for each flight condition (In the following chapter, the suitability of using one controller for all three flight conditions is examined).

## Lateral Controller

Maneuver Description. Laterally, four maneuvers are examined to test the controller. Three of these maneuvers, the flat turn, yaw pointing, and horizontal translation, are the lateral maneuvers being currently evaluated on test aircraft. These maneuvers are selected because they are considered by pilots and engineers to be those most beneficial for an air-combat/ground-weapon delivery fighter. An additional maneuver, called the rollover, is also examined to test the decoupled roll response of the controller.

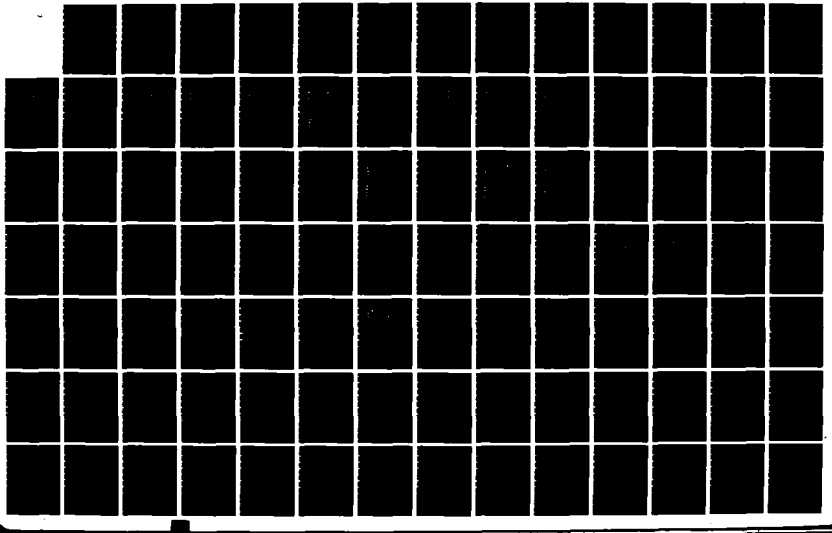
The flat turn maneuver is accomplished by commanding a body axis yaw rate r while commanding body axis side velocity v and roll angle $\phi$ to zero. The side acceleration Ay (in g's) produced by this command can be determined from the formula:

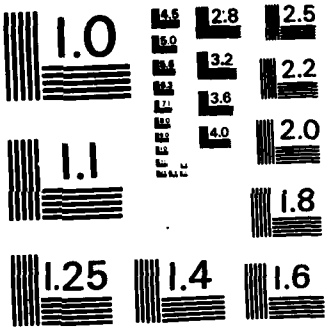
$$Ay = \frac{(r)(u)}{(57.3)(32.2)} \qquad (50)$$

Yaw pointing is accomplished by commanding a body axis yaw rate r equal and opposite in sign to the rate of change of either body axis side velocity v or sideslip angle $\beta$. Since body axis side velocity is used as an output in this thesis rather than $\beta$, sideslip angle can be approximated as:

AD-A139 050 PROCEEDINGS OF THE WORKSHOP ON MULTIVARIABLE CONTROL SYSTEMS HELD AT WRIG. (U) AIR FORCE WRIGHT AERONAUTICAL LABS WRIGHT-PATTERSON AFB OH M A MASI ET AL. SEP 83 4/7

UNCLASSIFIED AFWAL-TR-83-3093 FFG 1/3 NL






MICROCOPY RESOLUTION TEST CHART
NATIONAL BUREAU OF STANDARDS-1963-A

$$\beta \approx \frac{v}{u} \tag{51}$$

Horizontal translation is accomplished by commanding a body axis side velocity v while commanding both roll angle $\phi$ and body axis yaw rate r to zero.

The rollover maneuver is accomplished by commanding roll angle $\phi$ to some value while commanding v and r to zero.

Lateral Model. In order to meet the conditions associated with Porter's design method discussed in Chapter II, some modifications are made to the data available for each flight condition as shown in equations (48) and (49). These modifications are made to the data in equations (48) and (49) (flight condition 0.6M, S.L.), and for the other two flight conditions tested (0.9M, 30,000 ft. and 2.3M, 40,000 ft.). The data for these two other flight conditions from FPCC Sim and the modified versions are contained in Appendix B.

The first task is to take equations (48) and (49) and to separate the lateral state equations and outputs from the $\underline{A}$, $\underline{x}$, $\underline{B}$, and $\underline{u}$. The lateral states in equation (48) are p, r, v, $\phi$, y, and $\psi$. The lateral inputs are $\delta a$, $\delta r$, $\delta vc$, $F_1$, $F_2$, $CDI_1$, and $CDI_2$. The lateral outputs available from FPCC Sim are $\beta$ and ACGY. In order to accomplish the lateral maneuvers discussed earlier in this chapter the required outputs are v, r, and $\phi$. The states y and $\psi$ can be eliminated to simplify the plant and controller design, with no degradation of the model. Since this controller design is for an aircraft, if no approximations are used, the matrix product $\underline{C}_2\underline{B}_2$ does not have full

rank. The design requires that the number of inputs m equals the number of outputs ℓ. By using only the minimum number of outputs required, the resulting controller design is the simplest possible (Consideration is given to using side acceleration ACGY instead of v as an output. However, this results in a transmission zero at the origin which, when coupled with a small sampling time, yields a closed-loop root near the origin in the continuous domain or on the unit circle in the discrete domain and could result in slow settling times). In this case, there are a minimum of three outputs-therefore, there must be only three inputs in the $\underline{u}$ matrix. Of the inputs available, those having the most significant contribution to lateral control are δa, δr, and δvc. Other combinations of inputs and outputs are tried in an attempt to keep $F_1$, $F_2$ or $CDI_1$, $CDI_2$ in the input matrix $\underline{u}$, but this results in either $\underline{B}_2$ not having full rank, or a resulting $\underline{C}_2$ matrix for which no measurement matrix, $\underline{M}$, could be found that would produce full rank for $\underline{F}_2$ (See equations (31) and (32)). These are both requirements of the control technique. Since accelerations are the only elements in the $\underline{y}$ vector that have elements in the feed forward matrix, and accelerations are not used as outputs in this design, the $\underline{F}$ matrix can be dropped from equation (47) (If accelerations are used, the $\underline{F}$ matrix is still eliminated by incorporating the servo inputs as states, resulting in an augmented $\underline{A}$ matrix with $\underline{F}$ incorporated into $\underline{A}$).

The resulting modified version of the state and output equations (48) and (49) used for the design of the lateral

controller at flight condition 0.6 Mach and sea level is:

$$\begin{bmatrix} \dot{\phi} \\ \dot{v} \\ \dot{r} \\ \dot{p} \end{bmatrix} = \begin{bmatrix} 0 & 0 & .018 & 1.0 \\ 32.1 & -.687 & -666. & 13.2 \\ 0 & .019 & -.989 & .256 \\ 0 & -.0103 & 1.47 & -2.35 \end{bmatrix} \begin{bmatrix} \phi \\ v \\ r \\ p \end{bmatrix} +$$

$$\begin{bmatrix} 0 & 0 & 0 \\ 0 & 1.78 & .581 \\ .00727 & -.188 & .0368 \\ .198 & .166 & -.0275 \end{bmatrix} \begin{bmatrix} \delta a \\ \delta r \\ \delta vc \end{bmatrix} \qquad (52)$$

$$\begin{bmatrix} v \\ \phi \\ r \end{bmatrix} = \begin{bmatrix} 0 & 1 & 0 & 0 \\ 1 & 0 & 0 & 0 \\ 0 & 0 & 1 & 0 \end{bmatrix} \begin{bmatrix} \phi \\ v \\ r \\ p \end{bmatrix} = \underline{y} = \underline{v} \qquad (53)$$

This system is checked on a program available at AFIT called "CESA" (Ref 10) and is found to be both controllable and observable (ie - no decoupling zeroes) - two more requirements of Porter's technique. The system matrix:

$$\underline{P}(s) = \begin{bmatrix} \lambda \underline{I} - \underline{A} & \underline{B} \\ -\underline{C} & \underline{0} \end{bmatrix} \qquad (54)$$

is checked for transmission zeroes and none are found (if there are any, they must be stable - in the left half s-plane). Having met all these criteria, the design can continue.

The matrix product $\underline{C}\ \underline{B} = \underline{C}_2\underline{B}_2$ does not have full rank as expected, so the next task is to design the measurement matrix $\underline{M}$ to feedback certain rate information so that the resulting

$\underline{F}_2$ matrix has full rank (see equations (30), (31) and Figure 2). The design of the $\underline{M}$ matrix for this system is accomplished as prescribed in Ref 27 and is described below.

Measurement Matrix Development. The $\underline{C}$ matrix in equation (53) is separated into two parts, $\underline{C}_1$ and $\underline{C}_2$.

$$\underline{C}_1 = \begin{bmatrix} 0 \\ 1 \\ 0 \end{bmatrix} \qquad \underline{C}_2 = \begin{bmatrix} 1 & 0 & 0 \\ 0 & 0 & 0 \\ 0 & 1 & 0 \end{bmatrix} \tag{55}$$

The measurement matrix must have dimensions $\ell x(n-\ell) = 3x1$. Therefore,

$$\underline{M} = \begin{bmatrix} m_1 \\ m_2 \\ m_3 \end{bmatrix} \tag{56}$$

Using the methods of Ref 27,

$$\{d_1, d_2, d_3\} = \{0, 0, 0\} \tag{57}$$

and

$$\underline{B}^* = \begin{bmatrix} 0 & 0 & 0 \\ 0 & .018 & 1 \\ 0 & 0 & 0 \end{bmatrix} \tag{58}$$

$\underline{f}_2$ is obtained by using equations (30) and (31):

$$\underline{f}_2 = \begin{bmatrix} 1 & .018m_1 & 0 \\ 0 & .018m_2 & m_2 \\ 0 & 1+.018m_3 & 0 \end{bmatrix} \tag{59}$$

The elements of $\underline{M}$ appearing in $\underline{f}_2$ may be selected to have nonzero values only when the corresponding elements of B* are nonzero. Satisfying this requirement while making sure that $\underline{f}_2$ has full rank, results in the measurement matrix:

$$\underline{M} = \begin{bmatrix} 0 \\ m_2 \\ 0 \end{bmatrix} \tag{60}$$

Examination of this $\underline{M}$ matrix and Figure 2 shows that in addition to $\phi$, r, and v being fed back, now $\dot{\phi}$ is also in the feedback loop. This $\underline{M}$ matrix results in:

$$\underline{f}_2^{-1} = \begin{bmatrix} 1 & 0 & 0 \\ 0 & 0 & 1 \\ 0 & 1/m_2 & -.018 \end{bmatrix} \tag{61}$$

By using equation (61) along with equation (44), the discrete asymtotic transfer function is determined to be:

$$\underline{\Gamma}(\lambda) = \hat{\underline{\Gamma}} + \tilde{\underline{\Gamma}} = \begin{bmatrix} \frac{\sigma_1}{\lambda_1 - 1 + \sigma_1} & 0 & 0 \\ 0 & \frac{T/m_2}{\lambda_2 - 1 + T/m_2} & 0 \\ 0 & 0 & \frac{\sigma_3}{\lambda_3 - 1 + \sigma_3} \end{bmatrix} \tag{62}$$

The discrete asymtotic transfer function of equation (62) reveals several facts concerning the lateral system. First, the transfer function is diagonal and thus the outputs are decoupled as gain goes to infinity or sampling time

T becomes very small. The desired closed loop eiganvalues, $\lambda_1 = 1 - \sigma_1$, $\lambda_2 = 1 - T/m_2$ and $\lambda_3 = 1 - \sigma_3$ are selected by choosing the values $\sigma_1$, $m_2$, and $\sigma_3$ (Ref 27). Therefore, the values chosen for $\sigma_1$, $m_2$, and $\sigma_3$ in the controller design have a very significant impact on the time response of the system.

The new system matrix $\underline{P}(s)$ with $\underline{f}$ in place of $\underline{C}$ is now checked in equation (54) for unstable transmission zeroes. The result of this check reveals that there is one transmission zero at $-(1-T/m_2)$.

Controller Design. Armed with the information acquired up to this point, the lateral controller can be designed and the time responses can be checked. During this actual design phase, an interactive computer design tool such as MULTI is a necessity. The final design is the culmination of many iterations on MULTI and is achieved by varying the parameters in $\underline{M}$, $\underline{\Sigma}$, $\underline{\alpha}$, and $\varepsilon$. A good starting point is to set all the parameters to unity, compute $\underline{K}_0$ and $\underline{K}_1$, run a simulation and check the time response. The time response may be unstable.

The next step is to decrease $\varepsilon$, recompute $K_0$ and $K_1$, and check the time response to a command until the system becomes stable. Next the designer must vary the values in the $\underline{\Sigma}$ matrix to achieve the desired responses to command inputs. The elements of the $\underline{\Sigma}$ matrix are related directly to the elements of the output matrix $\underline{y}$. In this design, increasing $\sigma_1$ causes a decrease in the rise time and settling time of the first element of $\underline{y}$, side velocity v. The amount of each con-

trol surface deflection also increases, as does the transient part of the surface deflection. Increasing or decreasing a value of $\underline{\Sigma}$ also has an indirect effect on other outputs in $\underline{y}$ besides the direct effect described above. Thus, the final design of $\underline{\Sigma}$ is a compromise between the effects of each $\sigma_i$ on all elements of $\underline{y}$. It is found in this study that one set of values for $\underline{\Sigma}$ may be the optimum to accomplish one of the four prescribed lateral maneuvers, but not for the others. Thus, the final choise of $\underline{\Sigma}$ is another compromise. However, if computer space is available to store a different $\underline{K}_0$, $\underline{K}_1$ pair for each maneuver, the aircraft performance for the maneuvers described here can be better than that shown. The degree of improvement varied from one maneuver to the next.

Varying the value of $m_2$ in $\underline{M}$ has some effect on the overall settling time and the transients of the time response. Varying $\alpha$ seems to most significantly affect the control inputs to the system $\underline{u}$ (control surface deflections). Decreasing $\alpha$ decreases the peak transient value of control surface deflections and increases the steady state value, thus smoothing the control input. This often results in a slight increase in the settling time and rise time of the output response. The opposite effect happens when $\alpha$ is increased.

It must be remembered that these responses to a parameter variation may not occur the same way in all systems. This difference in response to a particular parameter variation from one system to the next can be compared to the difference in response to parameter variation which occurs in SISO systems when

trying to compare a second order system to a higher order system. In MIMO systems as well as in higher order SISO systems, poles and zeroes interact, often resulting in an unexpected time response.

The final values selected for the lateral controller are listed below. These values are found to be "optimal", or "nearly optimal", for all flight conditions. Therefore the same values of $\underline{\Sigma}$, $\underline{M}$, $\alpha$, and $\varepsilon$ are used for all three flight conditions tested.

$$\underline{\Sigma} = \begin{bmatrix} 0.2 & 0 & 0 \\ 0 & 0.5 & 0 \\ 0 & 0 & 3.0 \end{bmatrix} \tag{63}$$

$$\alpha = 1.5 \tag{64}$$

$$\varepsilon = 0.1, \; T = 0.01 \tag{65}$$

$$\underline{M} = \begin{bmatrix} 0 \\ 1 \\ 0 \end{bmatrix} \tag{66}$$

For the 0.6 Mach, sea level flight condition:

$$\underline{K}_0 = \begin{bmatrix} -.000790 & .3676 & 1.795 \\ .006299 & .008885 & -1.453 \\ .03234 & -.02722 & 4.451 \end{bmatrix} \tag{67}$$

$$\underline{K}_1 = \begin{bmatrix} -.000527 & .2450 & 1.197 \\ .004199 & .005923 & -.9686 \\ .02156 & -.01815 & 2.967 \end{bmatrix} \tag{68}$$

The $\underline{K}_0$, $\underline{K}_1$ pairs for the 0.9 Mach, 30,000 ft. and 2.3 Mach, 40,000 ft. flight conditions can found in Appendix B.

The time responses for the four lateral maneuvers for the 0.6 Mach, sea level flight condition appear in Figures 4 through 8. Time responses for the 0.9 Mach, 30,000 ft. flight condition are shown in Figures 9 through 13. Finally, time responses for the 2.3 Mach, 40,000 ft. flight condition are shown in Figures 14 through 18. The approximate figures of merit and commanded inputs for each maneuver and flight condition are summarized in Table VI.

Longitudinal Controller

Maneuver Description. Longitudinally, three maneuvers are examined to test the controller. The maneuvers are pitch pointing, vertical translation, and direct lift and are chosen because they are considered to be most useful to a pilot during an air-to-air or air-to-ground engagement.

Pitch pointing is accomplished by varying $\alpha$ and $\theta$ by equal amounts. Since flight path angle $\gamma$ equals $\theta$ minus $\alpha$, flight path angle remains constant while the aircraft pitches up or down around its lateral axis.

Vertical translation is accomplished by commanding $\alpha$ to some value while commanding $\theta$ to zero. Thus, for a negative $\alpha$ command, $\gamma$ increases and the aircraft translates vertically without pitching up.

The final maneuver, direct lift, is accomplished by commanding $\theta$ to some value while commanding $\alpha$ and u to zero. The resulting maneuver is a pitch up with increasing $\theta$ and g-loading

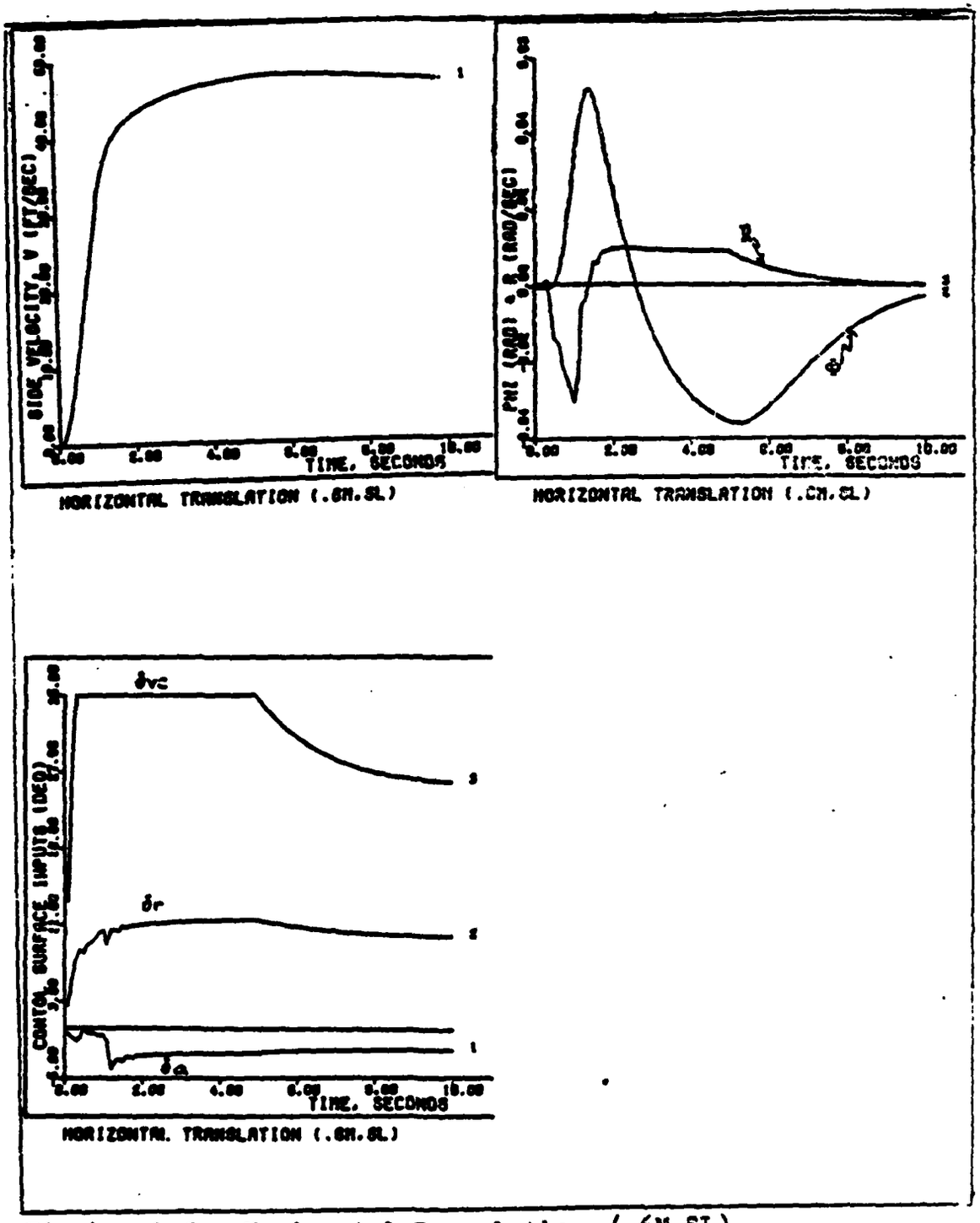



Fig 4. 1.5-g Horizontal Translation (.6M,SL)

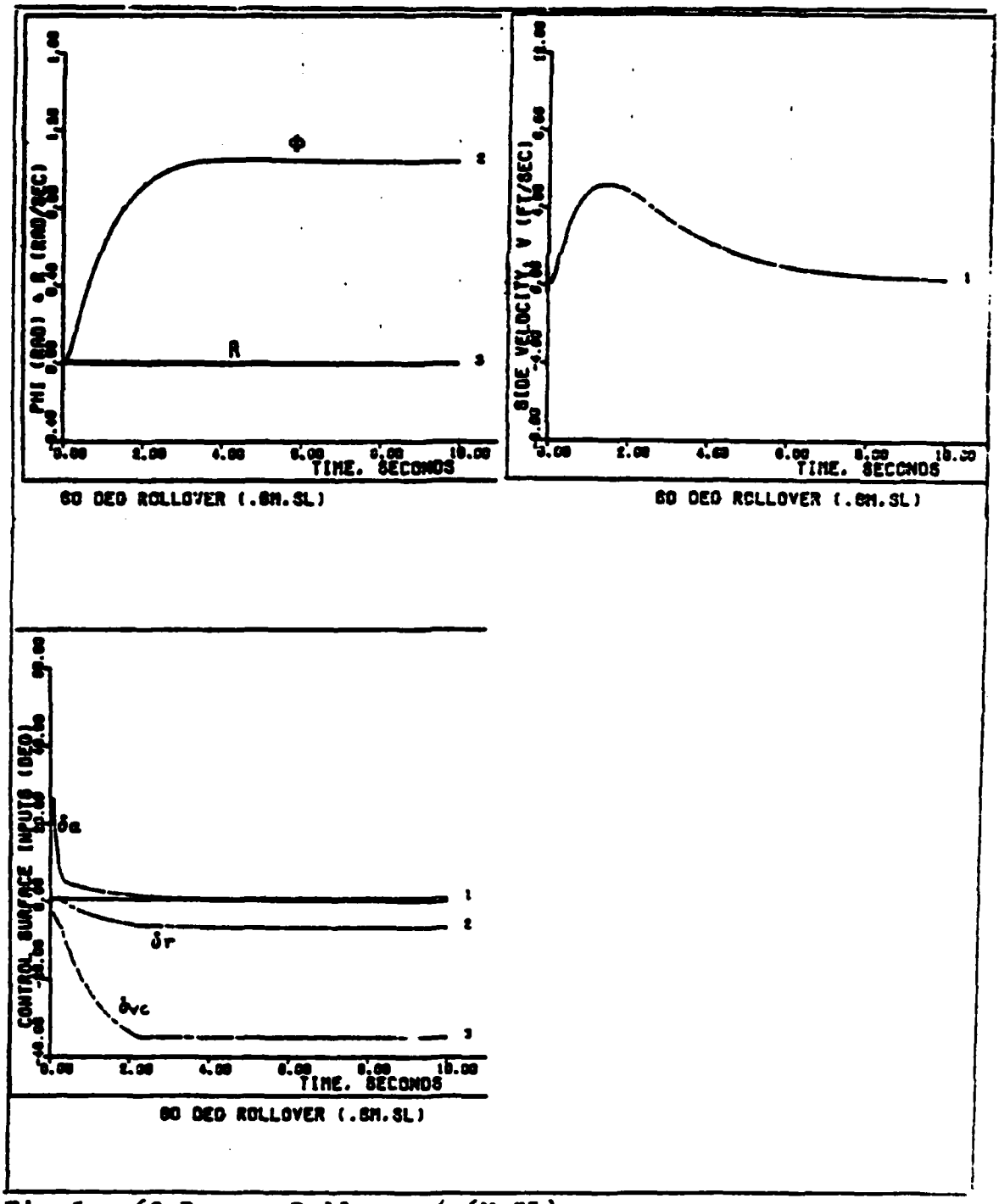



Fig 5. 60 Degree Rollover (.6M,SL)

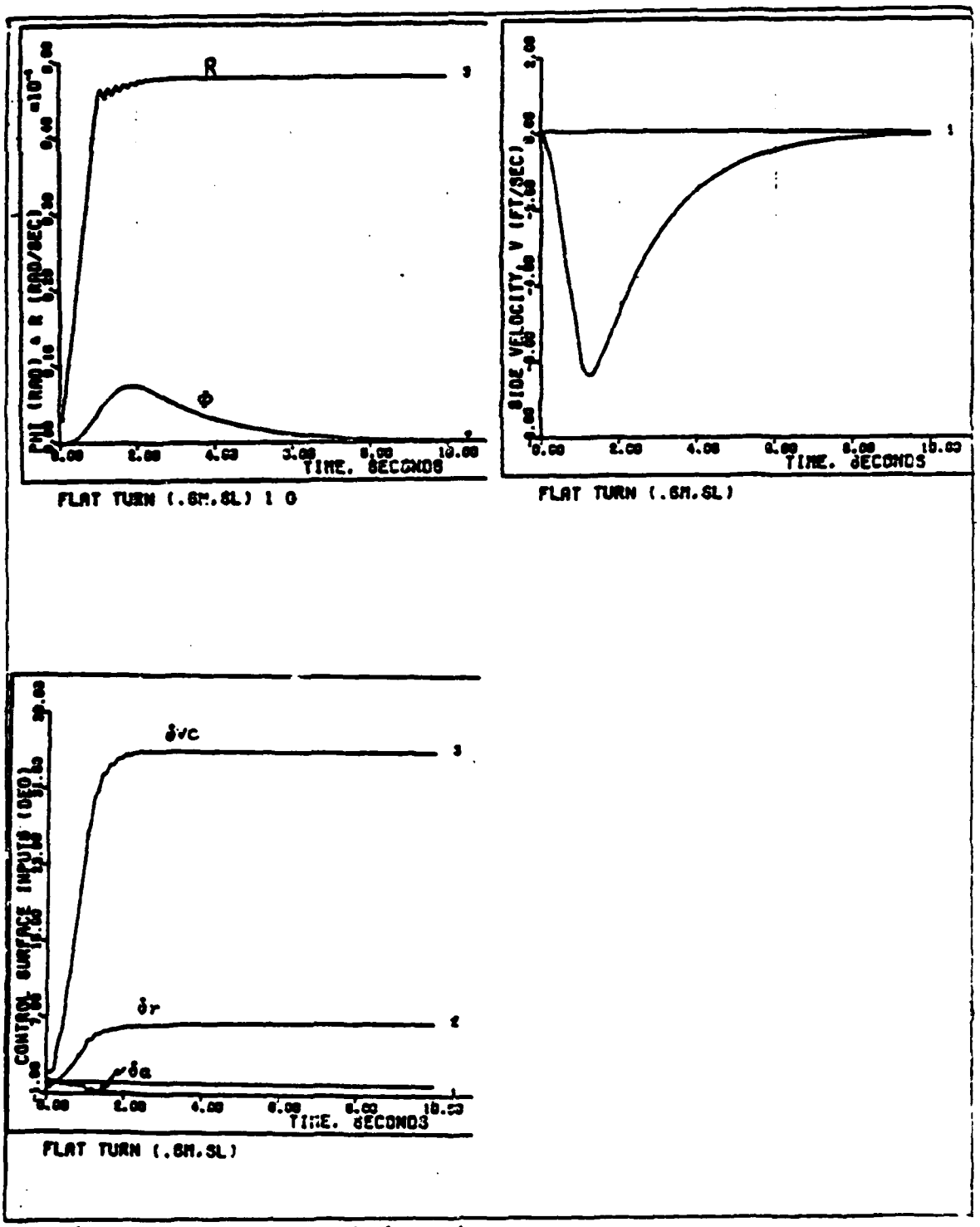



Fig 6. 1-g Flat Turn (.6M,SL)

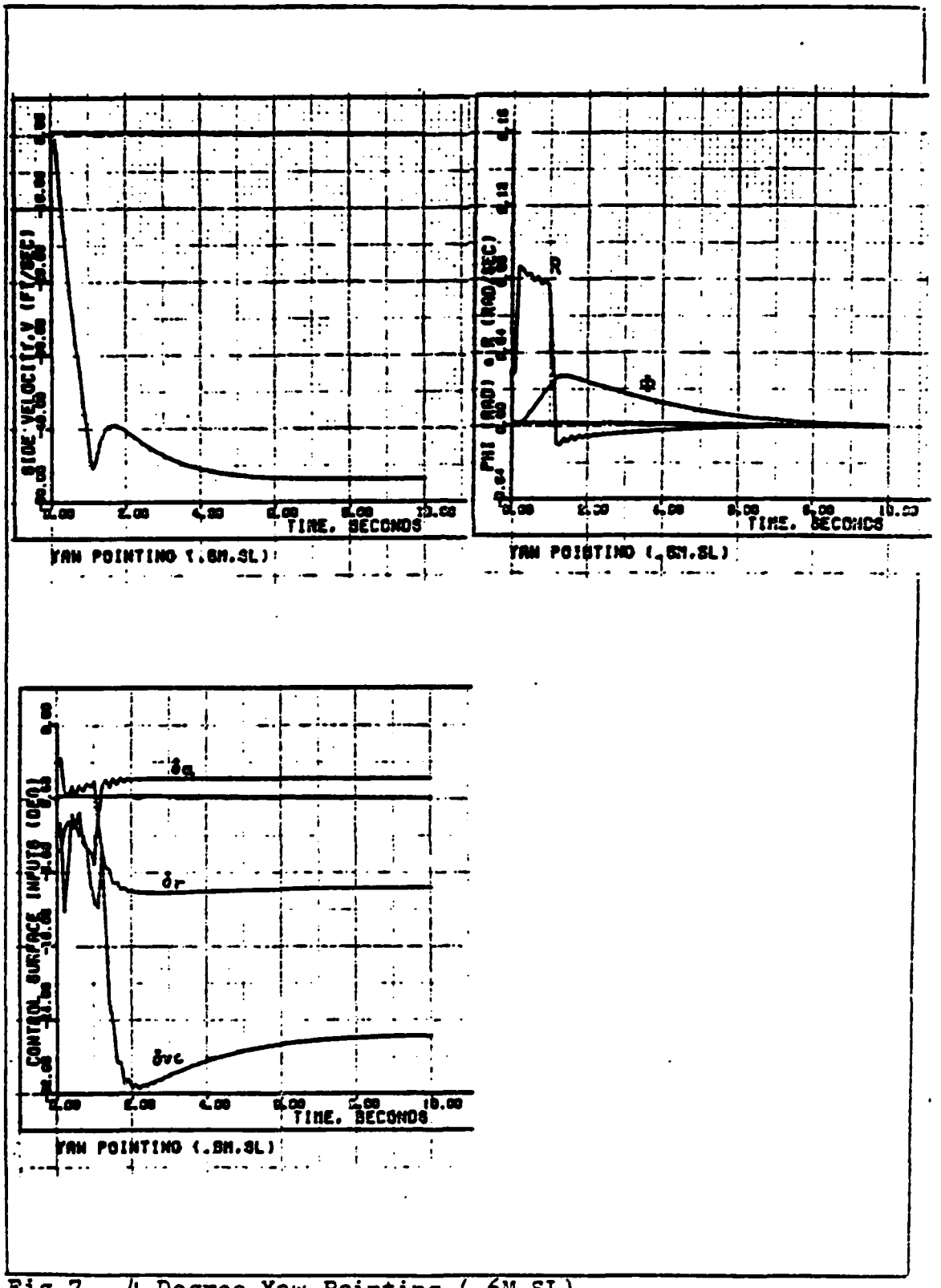



Fig 7. 4 Degree Yaw Pointing (.6M,SL)

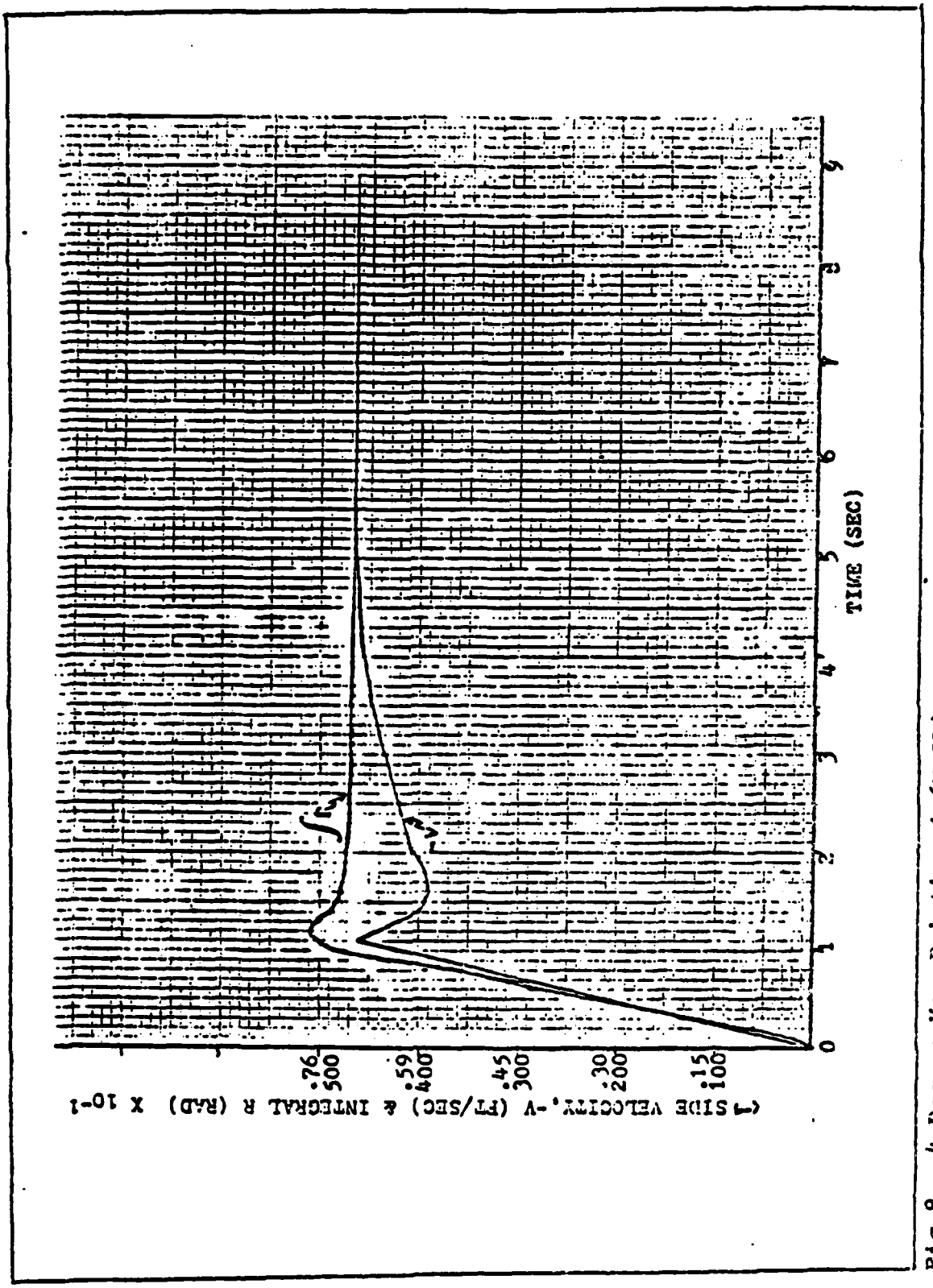



Fig 8. 4 Degree Yaw Pointing (.6M,SL)

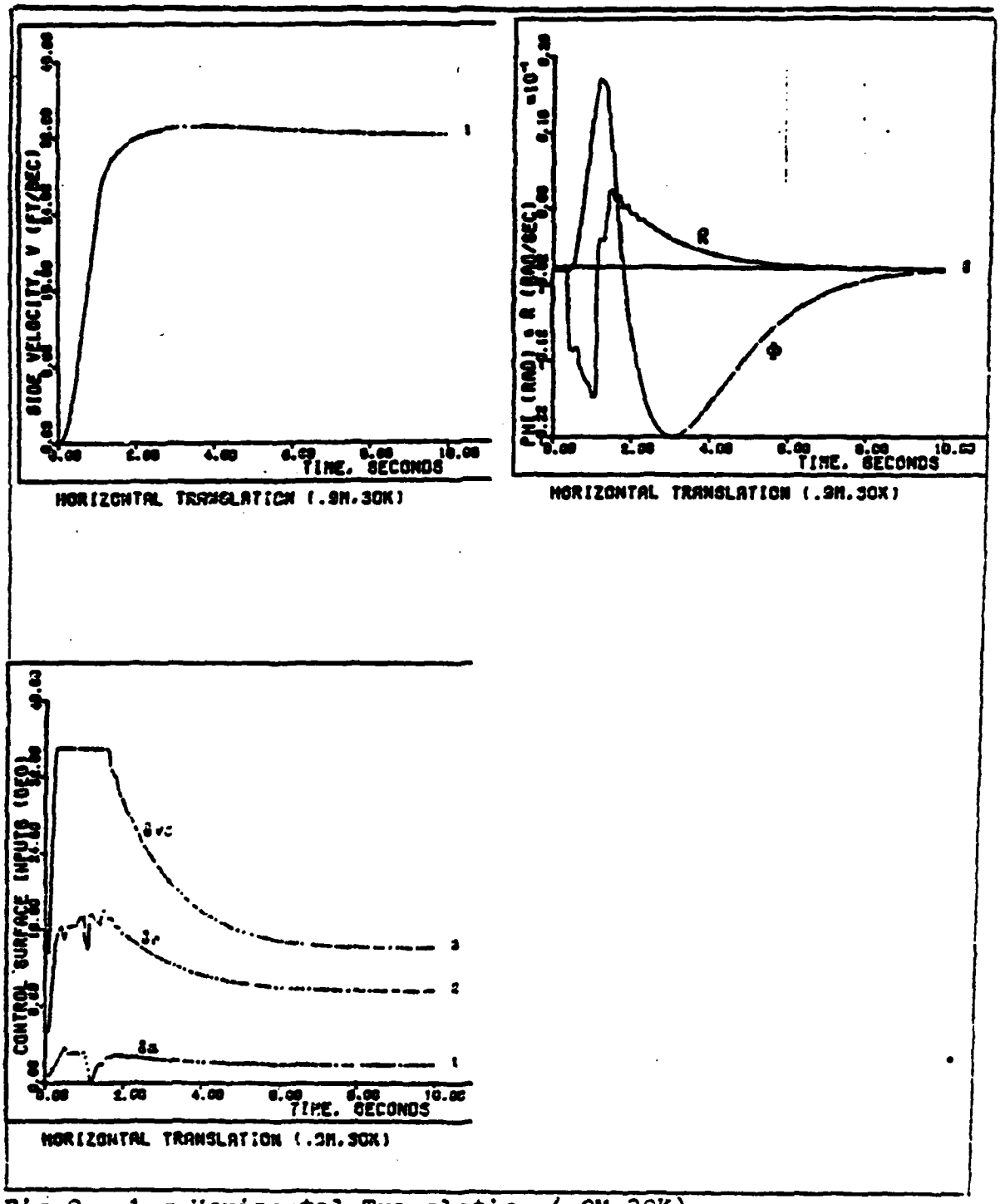



Fig 9. 1-g Horizontal Translation (.9M,30K)

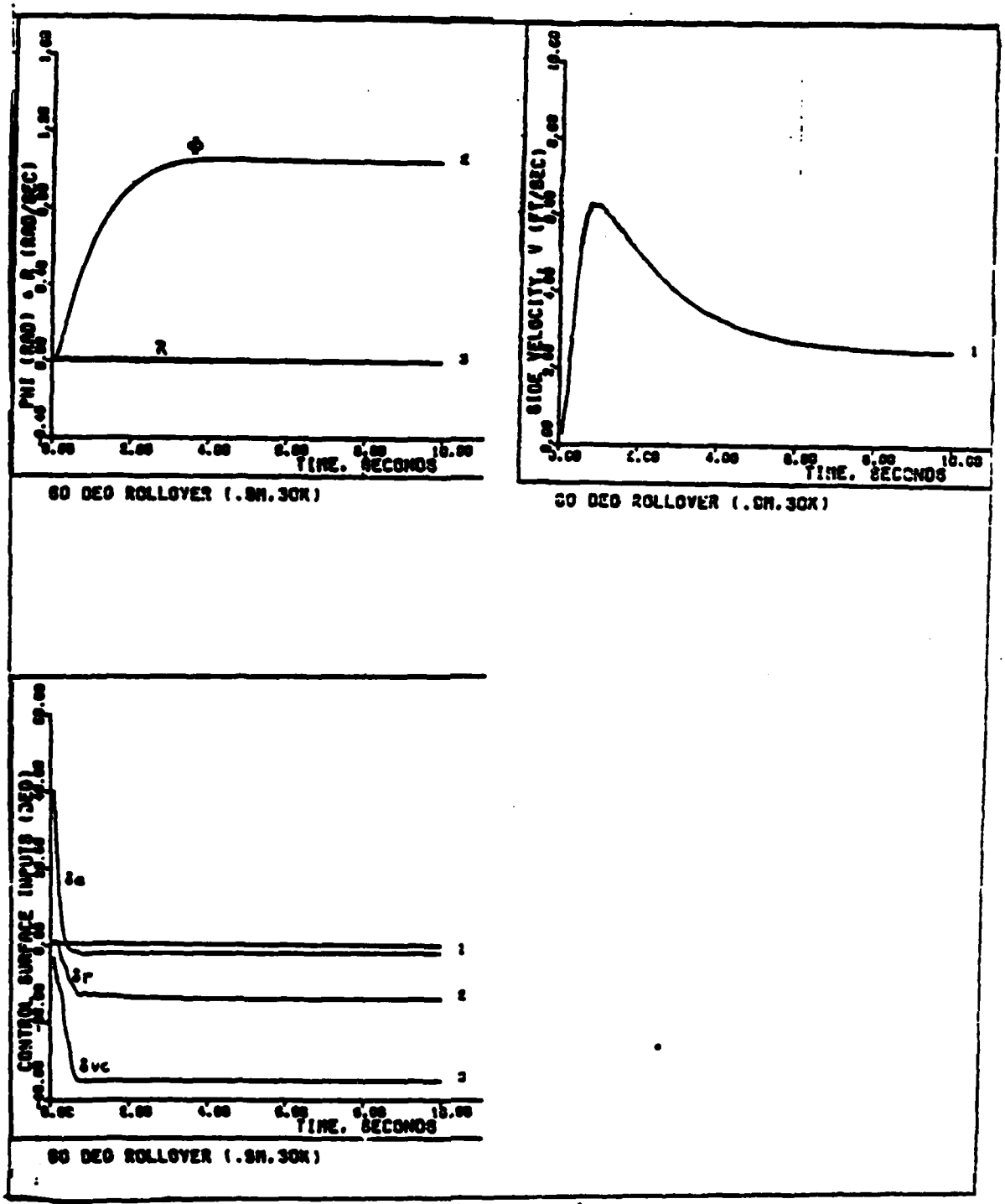



Fig 10. 60 Degree Rollover (.9M,30K)

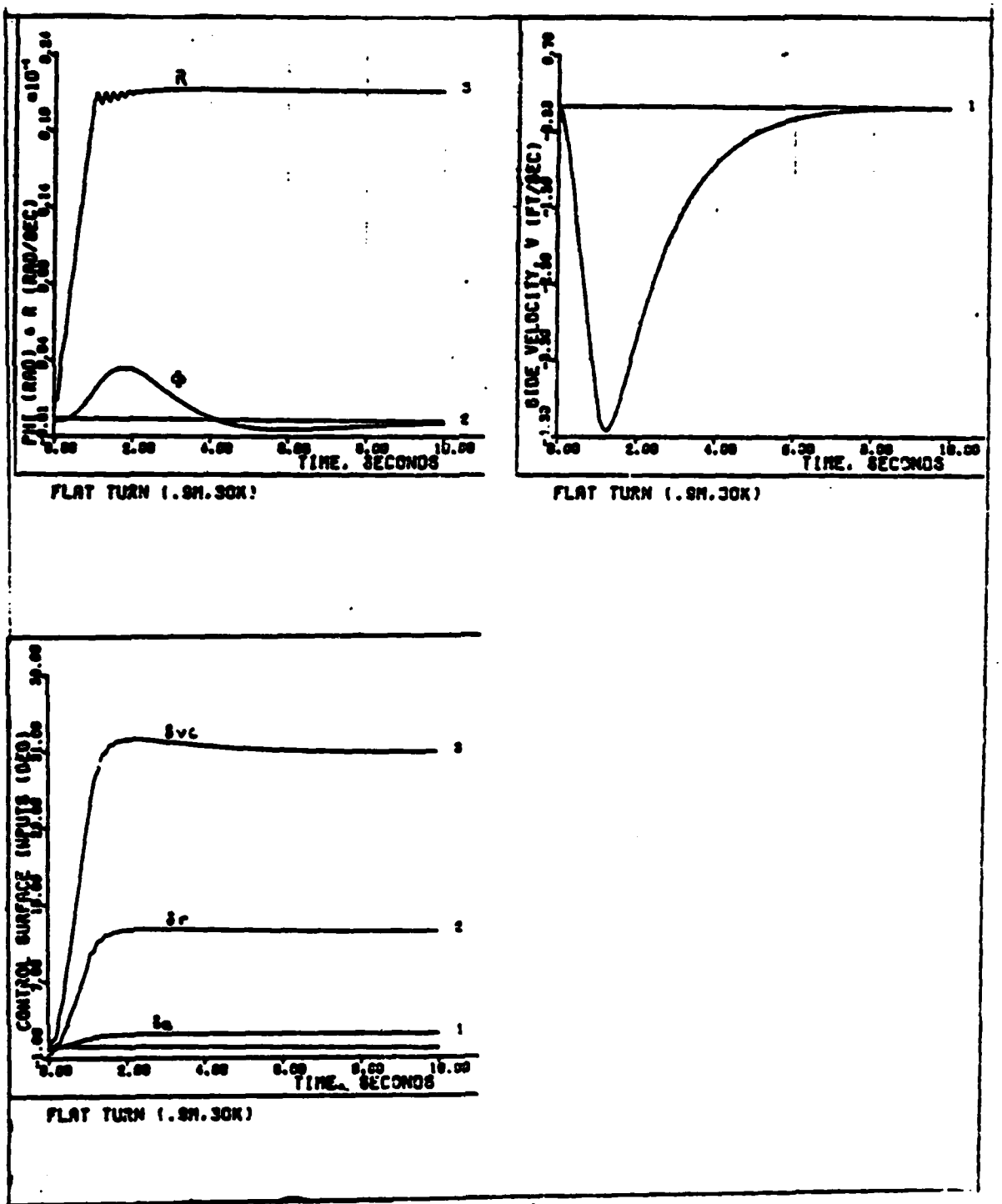



Fig 11. 0.6-g Flat Turn (.9M,30K)

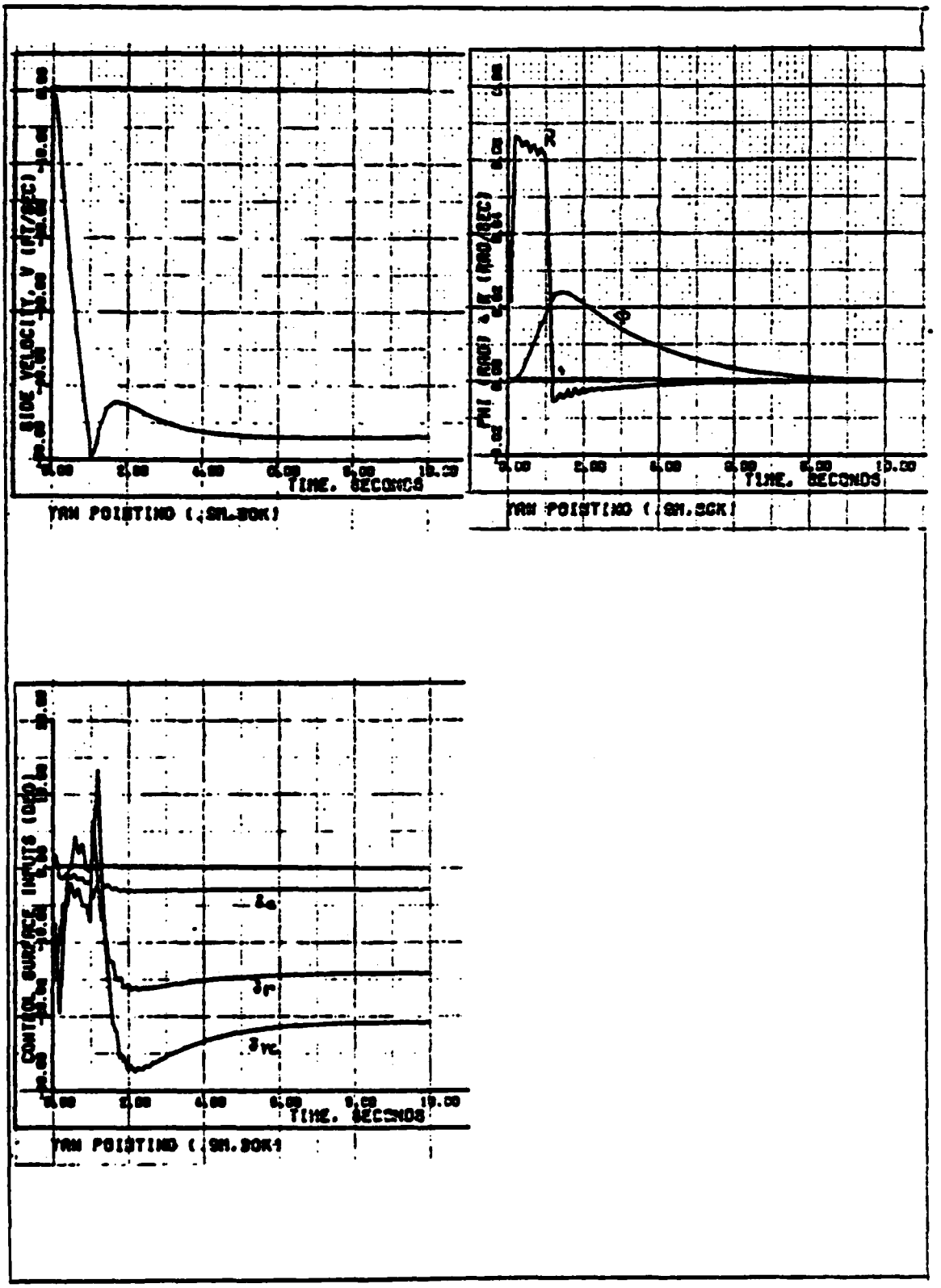



Fig 12. 3 Degree Yaw Pointing (.9M,30K)

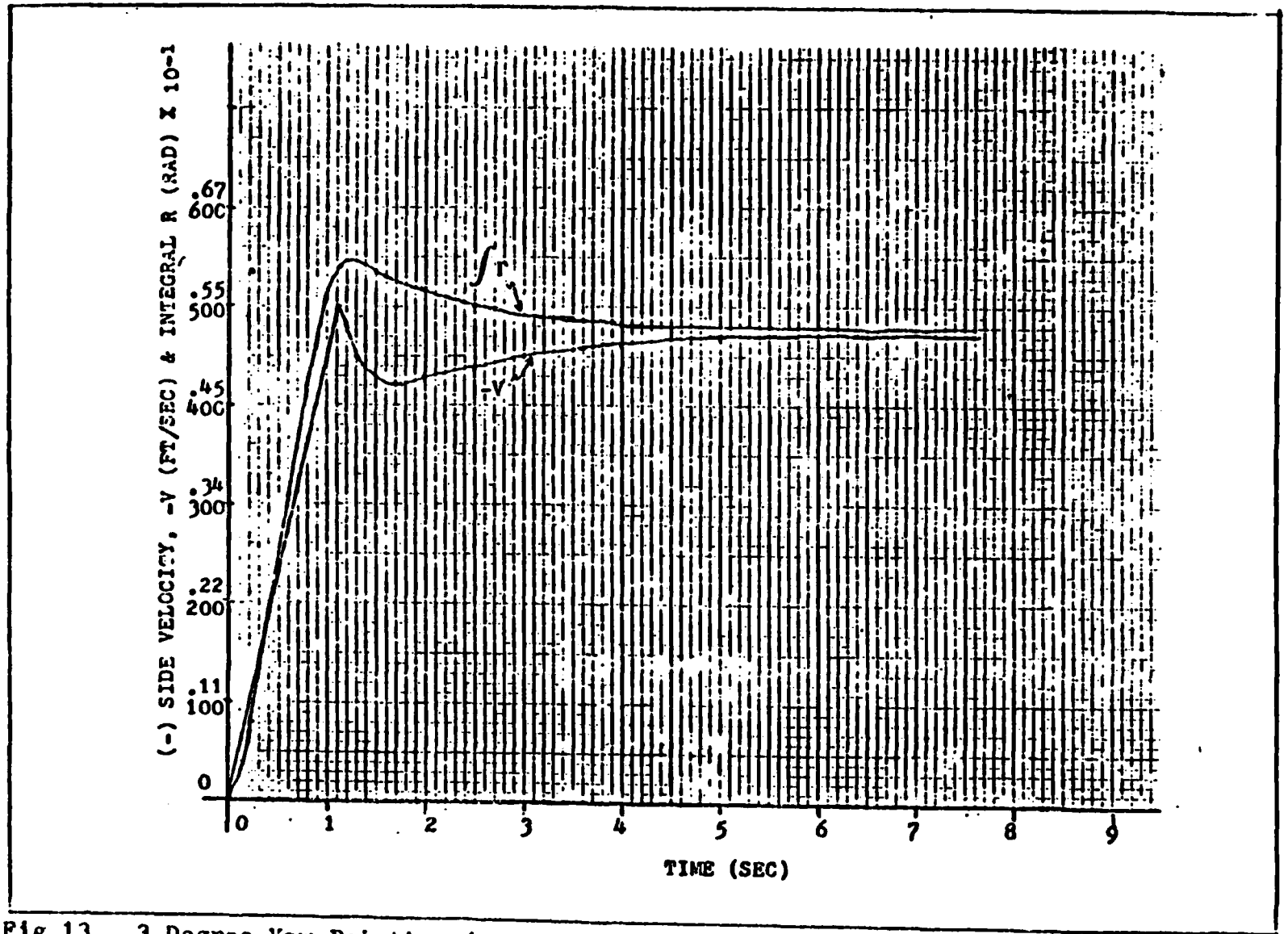



Fig 13. 3 Degree Yaw Pointing (.9M,30K)

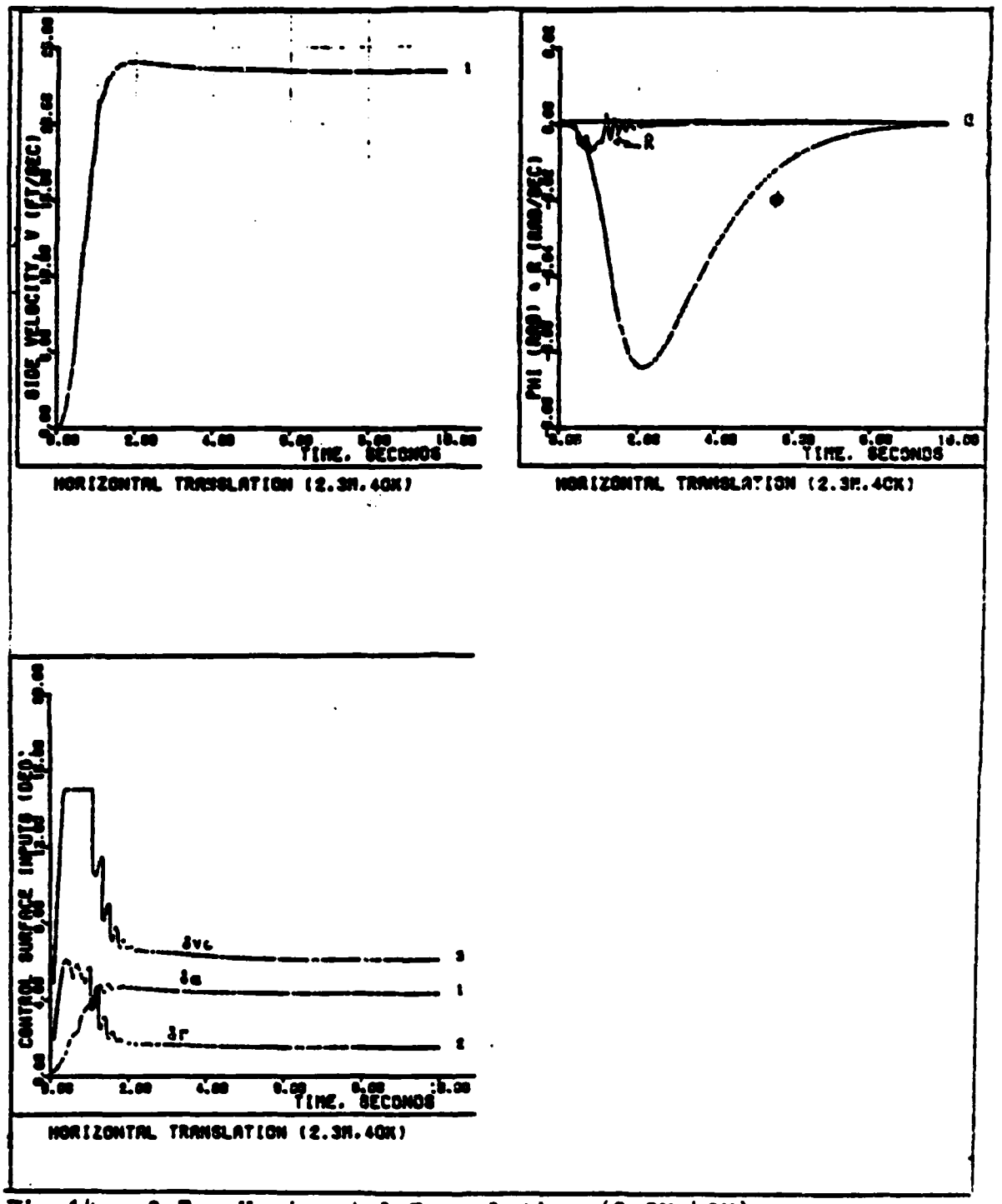



Fig 14. 0.7-g Horizontal Translation (2.3M,40K)

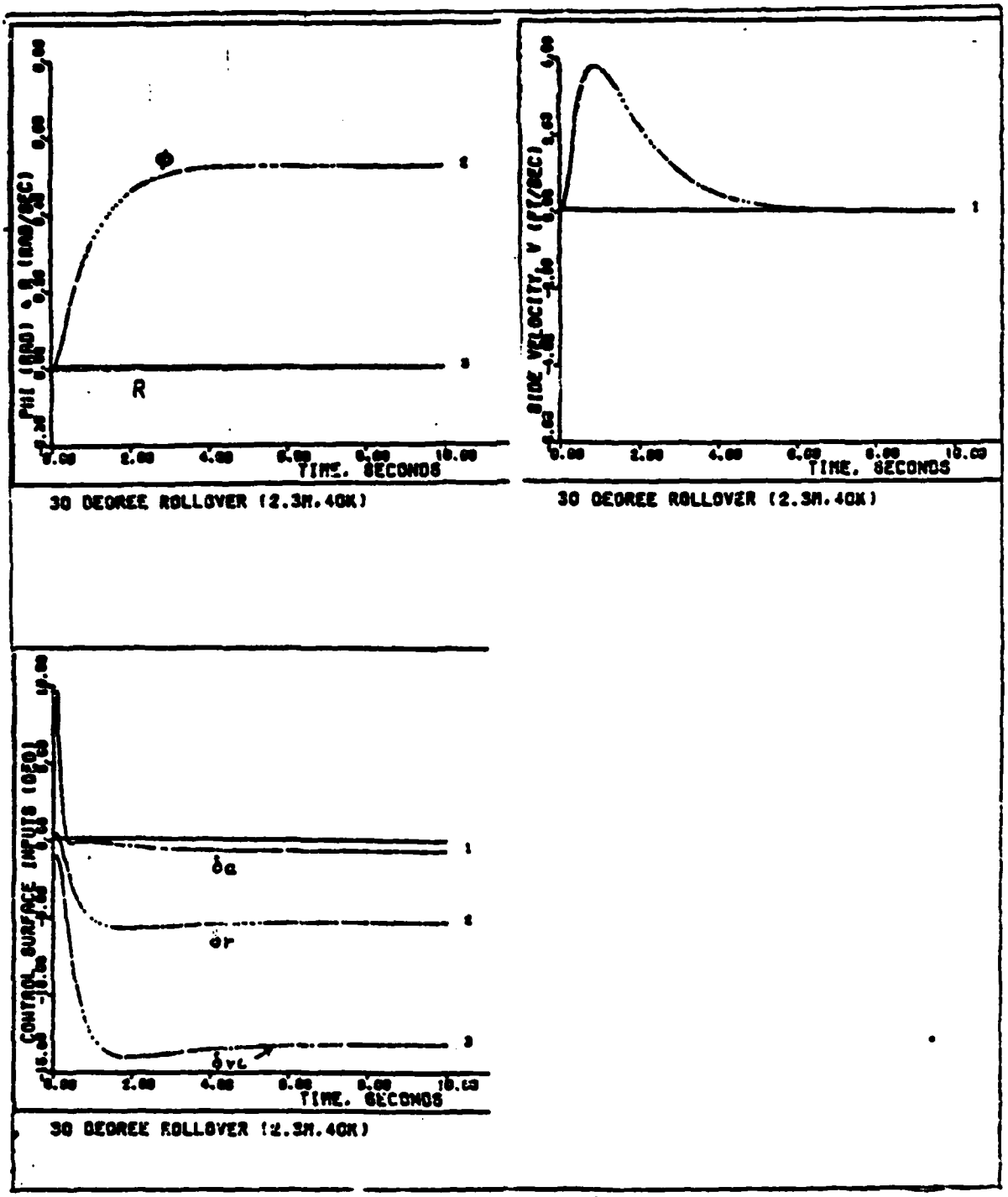



Fig 15. 30 Degree Rollover (2.3M,40K)

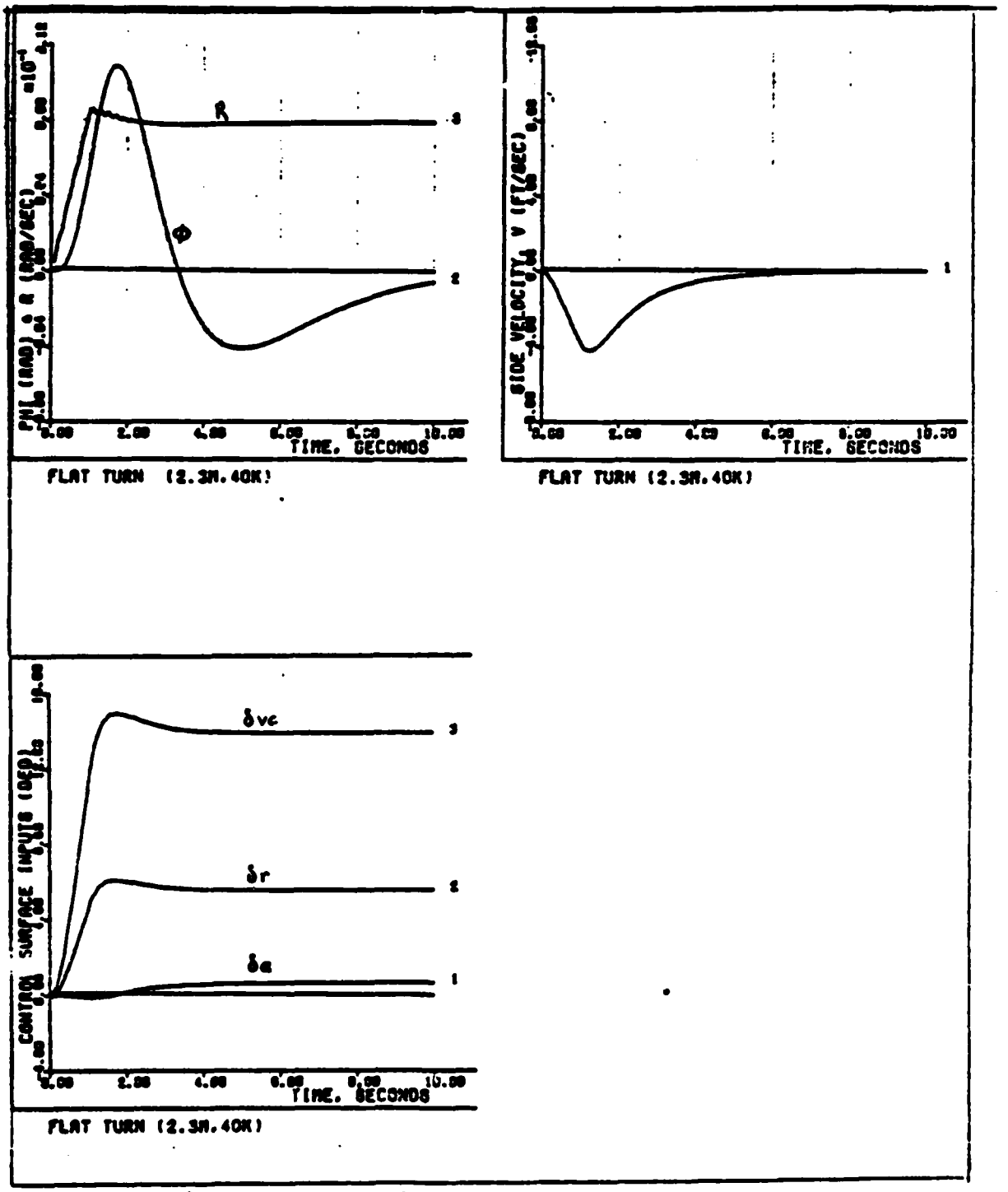
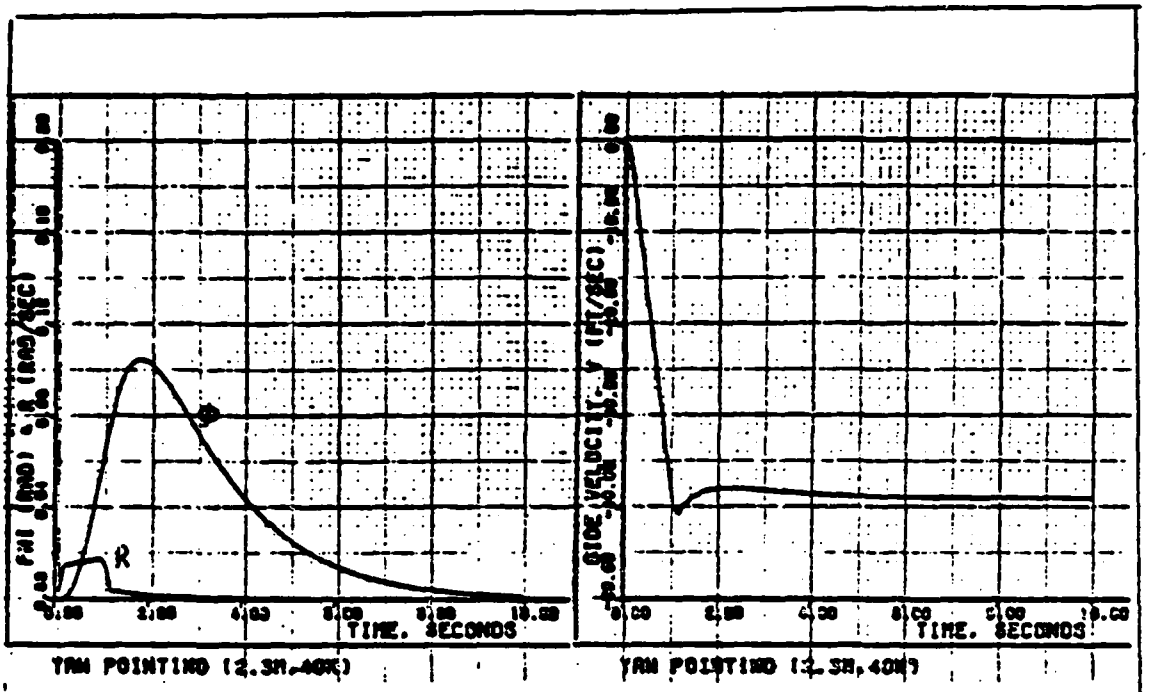



Fig 16. 0.6-g Flat Turn (2.3M,40K)



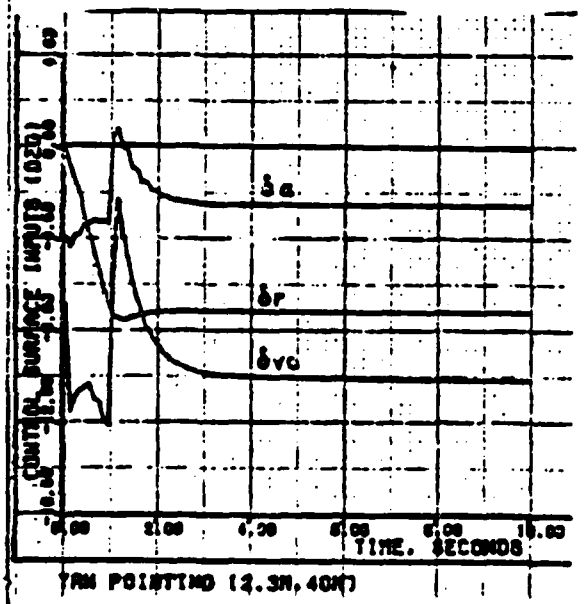




Fig 17. 1 Degree Yaw Pointing (2.3M,40K)

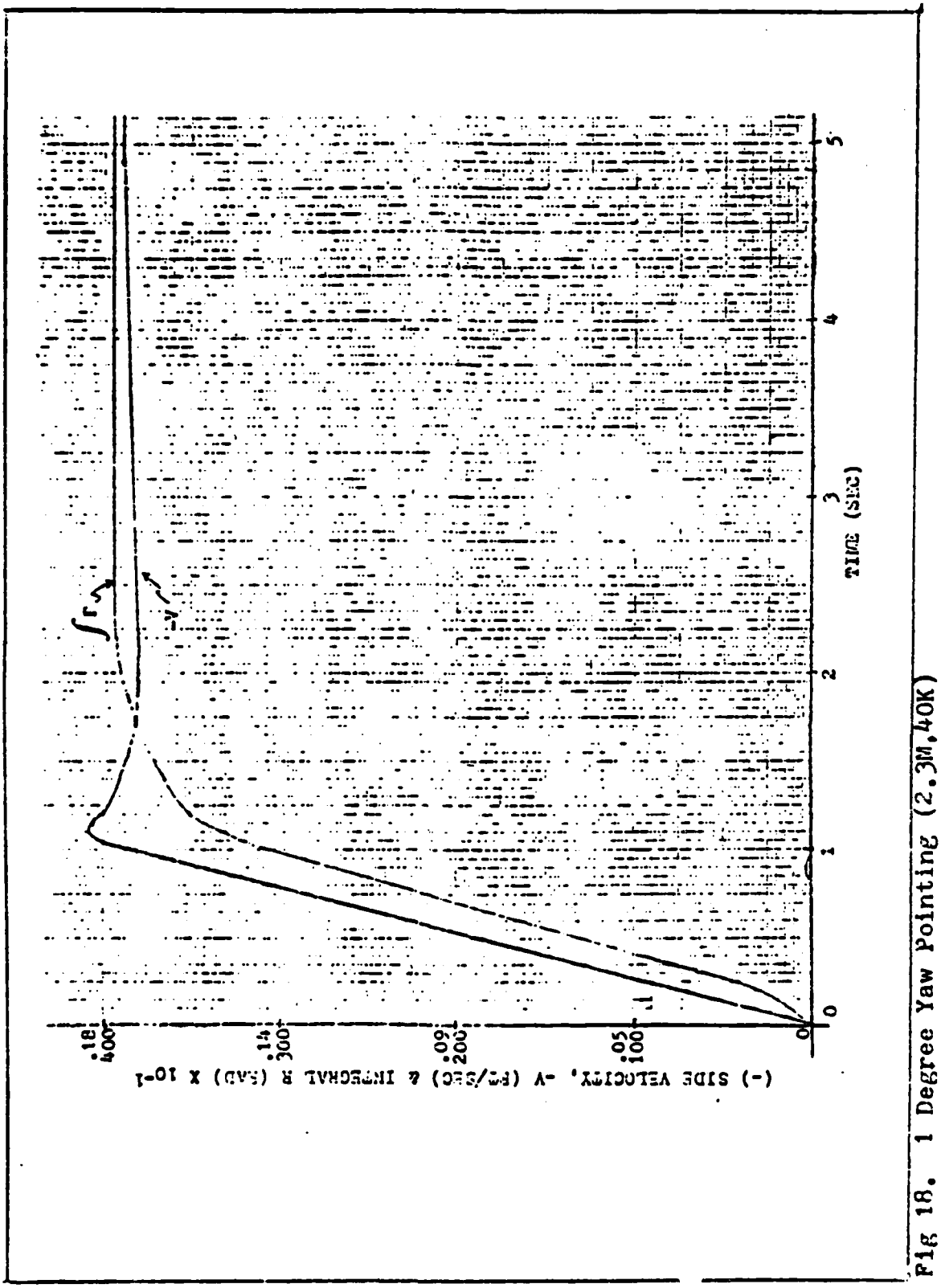



Fig 18. 1 Degree Yaw Pointing (2.3M,40K)

TABLE VI

SUMMARY OF TIME RESPONSES FOR LATERAL CONTROLLER

| Flt Cond | Maneuver | Command Vector $\underline{v}^*$ | Approx Percent Overshoot | Approx Rise Time ** | Approx Settling Time(2%) |
|---|---|---|---|---|---|
| 0.6 Mach sea level | Horizontal Translation | $\begin{bmatrix}1, & 46.85, & 20, & 20\\ 0, & 0, & 0, & 0\\ 0, & 0, & 0, & 0\end{bmatrix}$ | 2.1% | 1.5 sec | 7 sec |
| | Rollover | $\begin{bmatrix}0, & 0, & 0, & 0\\ 0, & 1.047, & 20, & 20\\ 0, & 0, & 0, & 0\end{bmatrix}$ | negligable | 1.8 sec | 3 sec |
| | Flat Turn | $\begin{bmatrix}0, & 0, & 0, & 0\\ 0, & 0, & 0, & 0\\ 1, & .04802, & 20, & 20\end{bmatrix}$ | none | .8 sec | 1.8 sec |
| | Yaw Pointing | 1) $\begin{bmatrix}1, & -46.85, & 20, & 20\\ 0, & 0, & 0, & 0\end{bmatrix}$<br>2) $\begin{bmatrix}.2, & .05364, & 1, & 1.2\end{bmatrix}$ | 1) none<br>2) - | 1) 1 sec<br>2) - | 1) 5.2 sec<br>2) - |
| 0.9 Mach 30,000 ft. | Horizontal Translation | $\begin{bmatrix}1, & 32.2, & 20, & 20\\ 0, & 0, & 0, & 0\\ 0, & 0, & 0, & 0\end{bmatrix}$ | 5% | .9 sec | 5.8 sec |
| | Rollover | $\begin{bmatrix}0, & 0, & 0, & 0\\ 0, & 1.047, & 20, & 20\\ 0, & 0, & 0, & 0\end{bmatrix}$ | none | 1.8 sec | 3 sec |
| | Flat Turn | $\begin{bmatrix}0, & 0, & 0, & 0\\ 0, & 0, & 0, & 0\\ 1, & .0216, & 20, & 20\end{bmatrix}$ | negligable | .8 sec | 1.6 sec |
| | Yaw Pointing | 1) $\begin{bmatrix}1, & -46.91, & 20, & 20\\ 0, & 0, & 0, & 0\end{bmatrix}$<br>2) $\begin{bmatrix}.2, & .04, & 1, & 1.2\end{bmatrix}$ | 1) 4%<br>2) - | 1) .7 sec<br>2) - | 1) 3.8 sec |

TABLE VI

SUMMARY OF TIME RESPONSES FOR LATERAL CONTROLLER
(cont)

| Flt Cond | Maneuver | Command Vector $\underline{v}$* | Approx Percent Overshoot | Approx Rise Time ** | Approx Settling Time(2%) |
|---|---|---|---|---|---|
| 2.3 Mach 40,000 ft. | Horizontal Translation | [1, 23.43, 20, 20<br>0, 0, 0, 0<br>0, 0, 0, 0] | 4.3% | .8 sec | 3 sec |
| | Rollover | [0, 0, 0, 0<br>0, .5236, 20, 20<br>0, 0, 0, 0] | none | 1.9 sec | 3 sec |
| | Flat Turn | [0, 0, 0, 0<br>0, 0, 0, 0<br>1, .007945, 20, 20] | 7.5% | .8 sec | 1.7 sec |
| | Yaw Pointing | 1) [1, -38.9, 20, 20<br>0, 0, 0, 0<br>2) .2, .0133, 1, 1.2] | 1) none<br>2) - | 1) .8 sec<br>2) - | 1) 1.1 sec<br>2) - |

* Note: Each pulse entry in $\underline{v}$ has 4 parts:

1) The time (seconds) the input reached steady state,
2) steady-state value,
3) the time the input left steady-state and started to return to zero, and
4) the time the input returned to zero. All angles are in radians.

** Note: Rise time is based on the time required for the non-zero output to go from 10% to 90% of its steady state value

with no increase in $\alpha$. The output u is needed in this equation because with a jet flap if u is allowed to decrease, more and more control surface is needed until the control reaches the maximum surface deflection and the maneuver cannot be maintained. If u is kept at zero, or close to zero, control deflections go through a transient to a steady state and the maneuver can continue. The only maneuver where this drop in velocity is significant is direct lift. In order to maintain u at zero during direct lift, total thrust, F, must be added to the input vector $\underline{v}$ commanded by the pilot. Commanding thrust to control forward velocity u is needed more in a jet flap type aircraft than a conventional aircraft because, as the jet flap deflects to create a moment on the aircraft, thrust changes significantly, unlike non-jet flap equiped aircraft.

Longitudinal Model. As was the case in designing the lateral controller, some modifications to the data available from FPCC Sim in the form of equations (48) and (49) must be made. Again, although the modifications to the data shown in this chapter are for the flight condition 0.6 Mach at sea level, identical modifications are required to the data for the other two flight conditions tested. The results of the modifications to the other two flight conditions are in Appendix B.

The longitudinal states and inputs in equation (48) are q, w, u, $\theta$, h, x and $\delta c$, $\delta j$, $\delta mf$, $F_1$, $F_2$, $CDI_1$, and $CDI_2$, respectively. The longitudinal outputs available in equation

(49) are $\alpha$, VEL, ACGX and ACGZ. In order to accomplish the longitudinal maneuvers discussed earlier, the required outputs are $\theta$, u, $\alpha$, and total thrust ($F_1+F_2$). The CDI contribution is minimal and can be removed. The states h and x can be eliminated with no model degradation to simplify the problem. Finally, F can be added to the input/output vectors $\underline{v}/\underline{y}$ by augmenting the modified state and input matrixes, $\underline{A}$ and $\underline{B}$, with the thrust time delay characteristic:

$$\frac{F_{TOT}}{e_{FTOT}} = \frac{.574}{s+.574} \tag{69}$$

Now total thrust $F_{TOT}$ is a state and can be used as an output. Finally, to simplify $\underline{C}$, angle of attack is approximated as:

$$\alpha \cong \frac{w}{u} \tag{70}$$

After making the above modifications, the longitudinal state, input, and output equations reduce to

$$\begin{bmatrix} \dot{\theta} \\ \dot{u} \\ \dot{w} \\ \dot{q} \\ \dot{F}_{TOT} \end{bmatrix} = \begin{bmatrix} 0 & 0 & 0 & 1 & 0 \\ -32.1 & -.0297 & .105 & -12.1 & .00218 \\ -.577 & -.0568 & -2.82 & 674 & -.69\times10^{-4} \\ 0 & -.0011 & .0639 & -.463 & -4.48\times10^{-6} \\ 0 & 0 & 0 & 0 & -.574 \end{bmatrix} \begin{bmatrix} \theta \\ u \\ w \\ q \\ F_{TOT} \end{bmatrix}$$

$$+ \begin{bmatrix} 0 & 0 & 0 & 0 \\ .581 & .0198 & .000923 & 0 \\ -1.43 & -4.73 & -.616 & 0 \\ .640 & -.0966 & -.043 & 0 \\ 0 & 0 & 0 & .574 \end{bmatrix} \begin{bmatrix} \delta c \\ \delta_{...}f \\ \delta j \\ e_{FTOT} \end{bmatrix} \tag{71}$$

$$\begin{bmatrix} \theta \\ u \\ \alpha' \\ F_{TOT} \end{bmatrix} = \begin{bmatrix} 1 & 0 & 0 & 0 & 0 \\ 0 & 1 & 0 & 0 & 0 \\ 0 & 0 & .00149 & 0 & 0 \\ 0 & 0 & 0 & 0 & 1 \end{bmatrix} \begin{bmatrix} \theta \\ u \\ w \\ q \\ F_{TOT} \end{bmatrix} = \underline{y} = \underline{v} \qquad (72)$$

This longitudinal system was found to be both controllable and observable. Also, the system matrix, $\underline{P}(s)$, described by equation (54), is checked and reveals one transmission zero at $1-0.574T$ due to the engine time constant.

Since the matrix product $\underline{C}_2\underline{B}_2$ does not have full rank, a measurement matrix must be designed for the longitudinal controller as is done for the lateral controller. This allows the $\underline{C}$ matrix to be replaced by an $\underline{f}$ matrix which has an $\underline{f}_2$ element with full rank.

Measurement Matrix Development. The measurement matrix $\underline{M}$ is designed in the same manner as for the lateral controller. Equation (72) separates into two parts:

$$\underline{C}_1 = \begin{bmatrix} 1 \\ 0 \\ 0 \\ 0 \end{bmatrix} \qquad \underline{C}_2 = \begin{bmatrix} 0 & 0 & 0 & 0 \\ 1 & 0 & 0 & 0 \\ 0 & .00149 & 0 & 0 \\ 0 & 0 & 0 & 1 \end{bmatrix} \qquad (73)$$

The proper dimension for the measurement matrix $\underline{M}$ is $4 \times 1$. Therefore:

$$\underline{M} = \begin{bmatrix} m_1 \\ m_2 \\ m_3 \\ m_4 \end{bmatrix} \qquad (74)$$

where:

$$\{d_1, d_2, d_3, d_4\} = \{0, 0, 0, 0\} \tag{75}$$

and

$$\underline{B}^* = \begin{bmatrix} 0 & 0 & 1 & 0 \\ 0 & 0 & 0 & 0 \\ 0 & 0 & 0 & 0 \\ 0 & 0 & 0 & 0 \end{bmatrix} \tag{76}$$

$\underline{}_2$ is derived using equations (30) and (31):

$$\underline{f}_2 = \begin{bmatrix} 0 & 0 & m_1 & 0 \\ 1 & 0 & m_2 & 0 \\ 0 & .00149 & m_3 & 0 \\ 0 & 0 & m_4 & 1 \end{bmatrix} \tag{77}$$

Almost all the elements of $\underline{B}^*$ are zero, so to give $\underline{F}_2$ full rank and have the simplist $\underline{M}$ matrix,

$$\underline{M} = \begin{bmatrix} m_1 \\ 0 \\ 0 \\ 0 \end{bmatrix} \tag{73}$$

Examination of equation (78) along with Figure 2 reveals that states $\theta$, u, $\alpha$, and $F_{TOT}$ along with $\dot{\theta}$, or q, are being fed back in this system. Now,

$$\underline{f}_2^{-1} = \begin{bmatrix} 0 & 1 & 0 & 0 \\ 0 & 0 & 671.141 & 0 \\ \frac{1}{m_1} & 0 & 0 & 0 \\ 0 & 0 & 0 & 1 \end{bmatrix} \tag{79}$$

The discrete-time asymtotic transfer function, $\underline{\Gamma}(\lambda)$, is calculated to be:

$$\underline{\Gamma}(\lambda) = \tilde{\underline{\Gamma}}(\lambda) + \hat{\underline{\Gamma}}(\lambda) = \begin{bmatrix} \frac{T/m_1}{\lambda_1 - 1 + T/m_1} & 0 & 0 & 0 \\ 0 & \frac{\sigma_2}{\lambda_2 - 1 + \sigma_2} & 0 & 0 \\ 0 & 0 & \frac{\sigma_3}{\lambda_3 - 1 + \sigma_3} & 0 \\ 0 & 0 & 0 & \frac{\sigma_4}{\lambda_4 - 1 + \sigma_4} \end{bmatrix} \tag{80}$$

Equation (80) reveals that the longitudinal design is decoupled as T gets very small. Also, the values chosen for $m_1$, $\sigma_2$, $\sigma_3$ and $\sigma_4$ have the biggest impact on the time response of the design. Finally, the new system matrix, $\underline{P}(s)$, containing $-\underline{f}$ instead of $-\underline{C}$ reveals transmission zeroes at $1-.574T$ and $1-T/m_1$.

Controller Design. Designing the longitudinal controller is no different than designing the lateral controller. The final values selected for the longitudinal controller are listed below. As with the lateral controller, for this system these values are found to be "optimal" or very "near optimal" for all flight conditions tested. Therefore, the values of $\underline{\Sigma}$, $\underline{M}$, $\alpha$ and $\varepsilon$ are the same for all three flight conditions tested.

$$\underline{\Sigma} = \begin{bmatrix} 6 & 0 & 0 & 0 \\ 0 & .1 & 0 & 0 \\ 0 & 0 & 1 & 0 \\ 0 & 0 & 0 & 2 \end{bmatrix} \tag{81}$$

$$\alpha = 1.1 \tag{82}$$

$$\varepsilon = 0.1, \; T = 0.01 \tag{83}$$

$$M = \begin{bmatrix} .5 \\ 0 \\ 0 \\ 0 \end{bmatrix} \tag{84}$$

For the 0.6 Mach, sea level flight condition:

$$\underline{K}_0 = \begin{bmatrix} -.1334 & .02042 & .72615 & 0 \\ 6.0737 & -.06469 & -24.3627 & 0 \\ -46.3276 & .4493 & 65.5390 & 0 \\ 0 & 0 & 0 & .3833 \end{bmatrix} \tag{85}$$

$$\underline{K}_1 = \begin{bmatrix} -.1213 & .01857 & .6601 & 0 \\ 5.5215 & -.05888 & -22.1480 & 0 \\ -42.1160 & .4085 & 59.5809 & 0 \\ 0 & 0 & 0 & .3484 \end{bmatrix} \tag{86}$$

The $\underline{K}_0$, $\underline{K}_1$ pairs for the .9 Mach, 30,000 ft. and the 2.3 Mach, 40,000 ft. flight conditions are given in Appendix B.

The time responses for the three longitudinal maneuvers for the 0.6 Mach, sea level flight condition appear in Figures 19 through 21. Time responses for the 0.9 Mach, 30,000 ft. flight condition follow in Figures 22 through 24. Finally, time responses for the 2.3 Mach, 40,000 ft. flight condition appear in Figures 25 through 27. The approximate

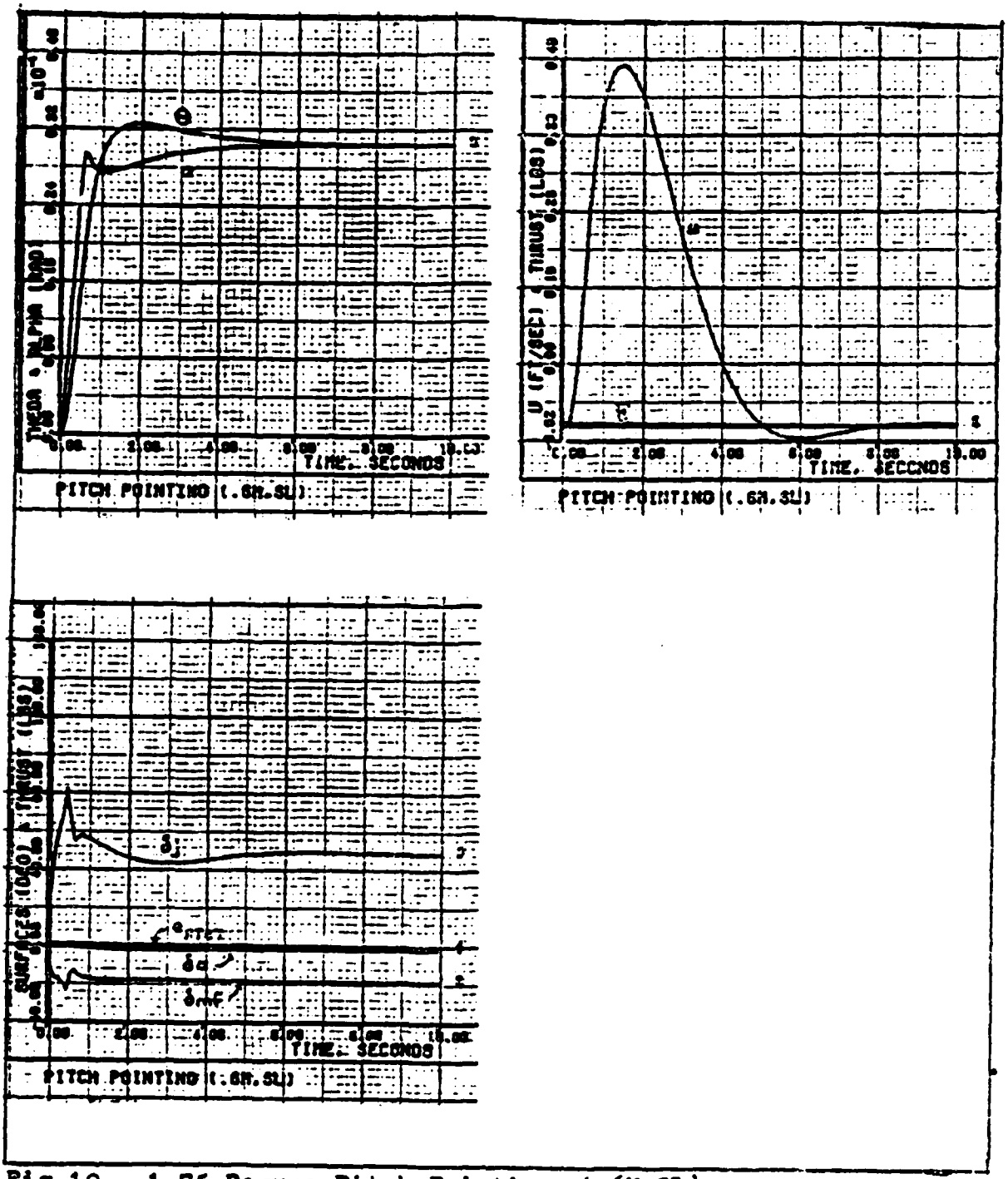



Fig 19. 1.75 Degree Pitch Pointing (.6M,SL)

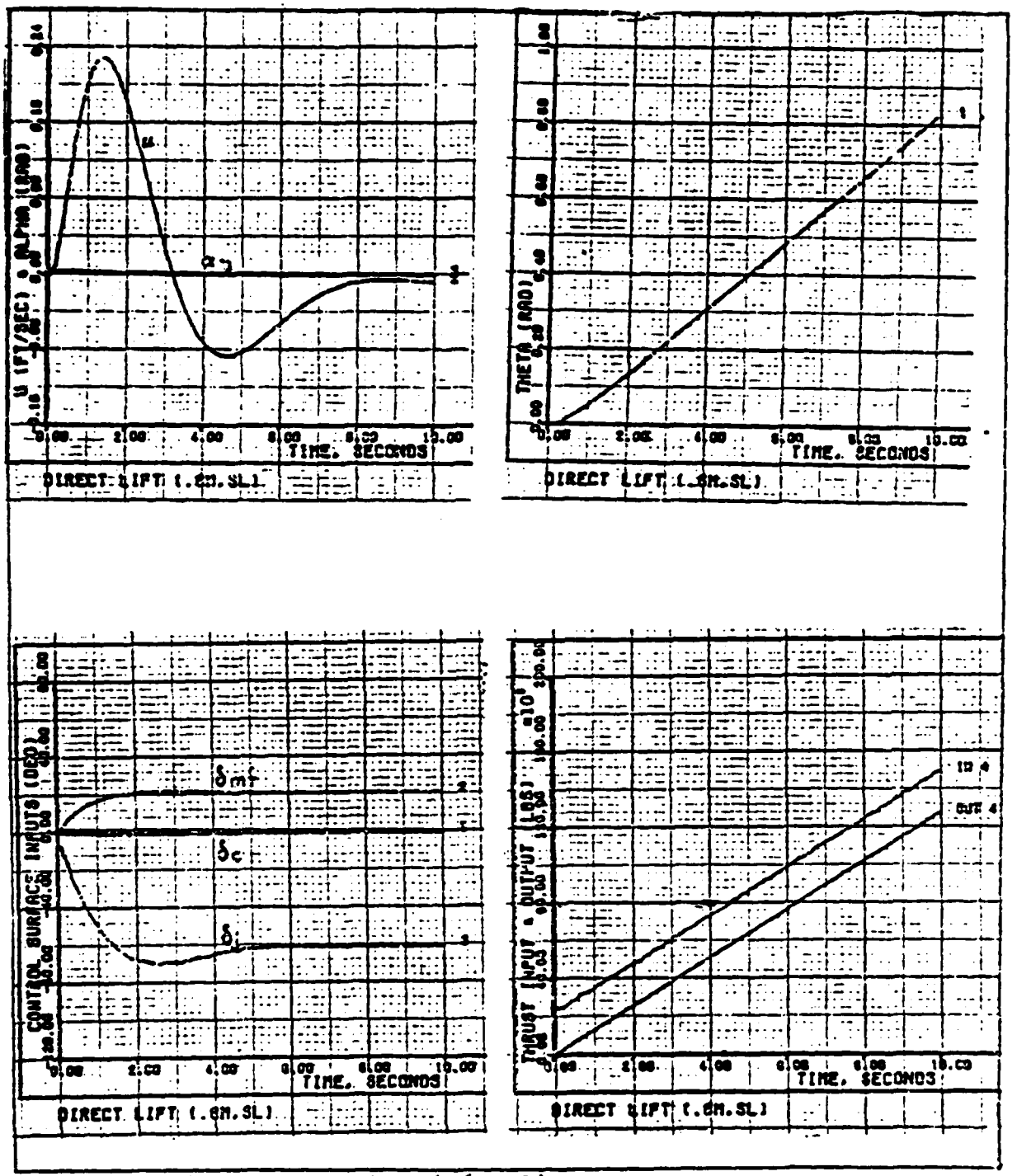



Fig 20. 1.8-g Direct Lift (.6M,SL)

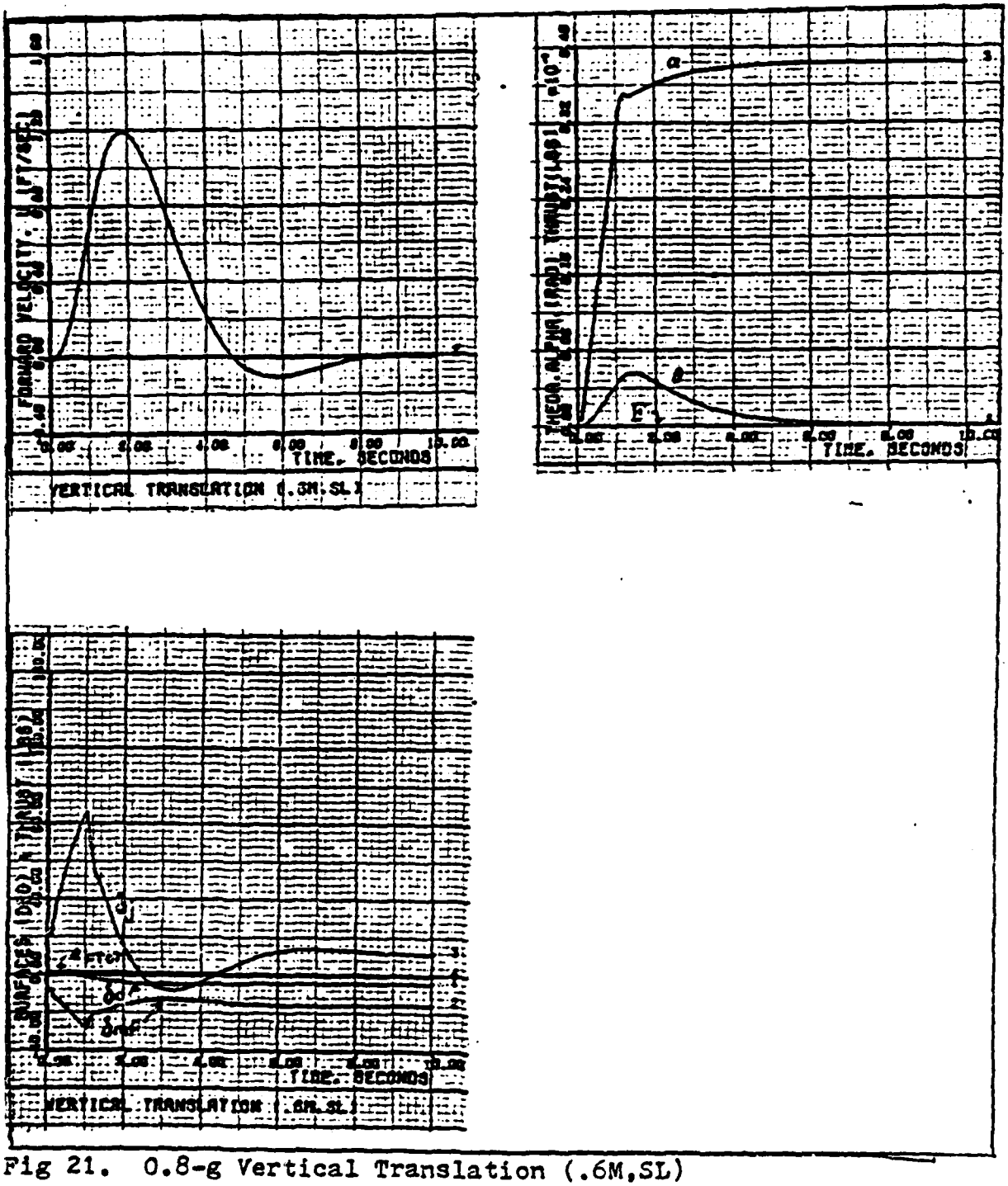



Fig 21. 0.8-g Vertical Translation (.6M,SL)

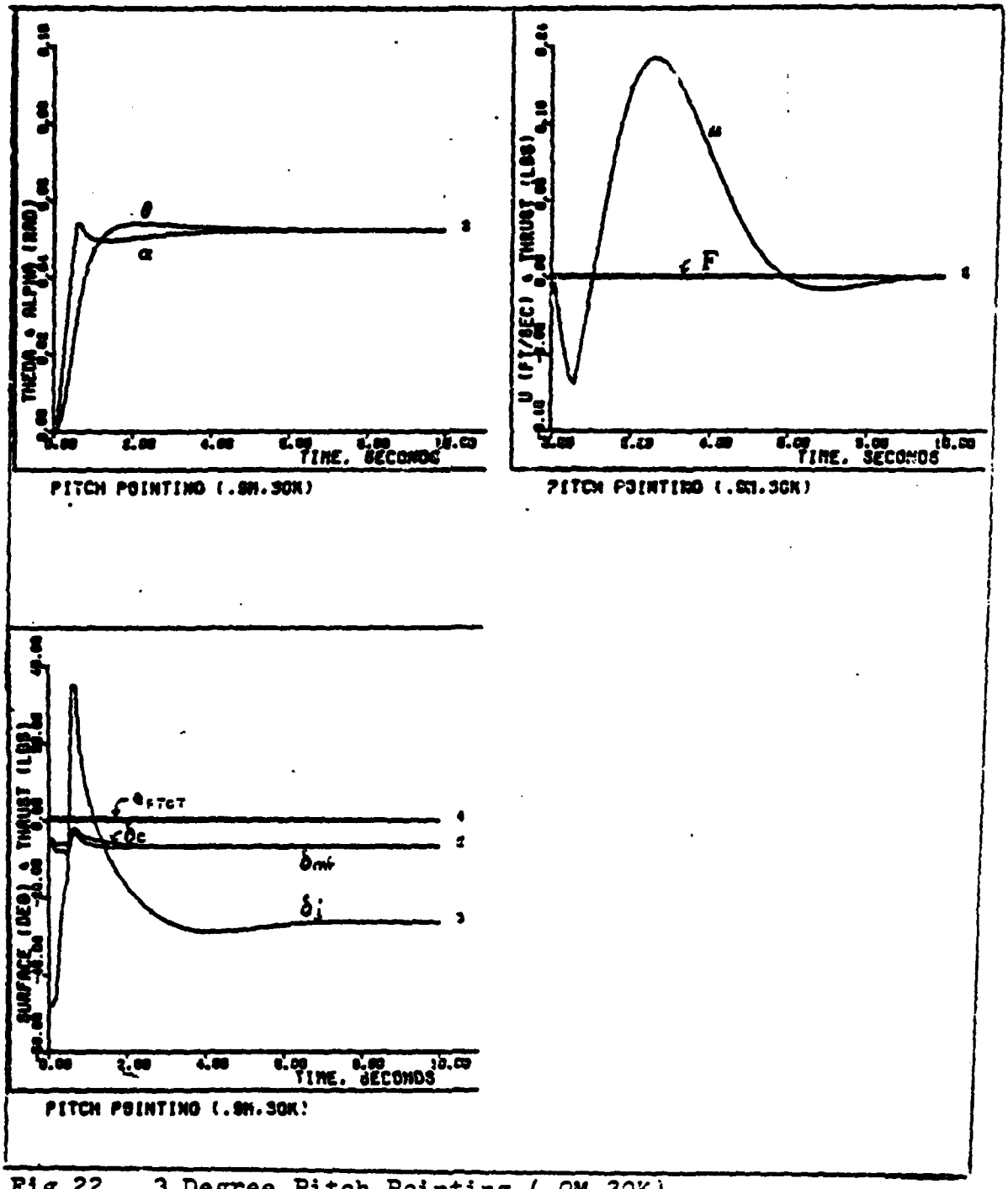



Fig 22. 3 Degree Pitch Pointing (.9M,30K)

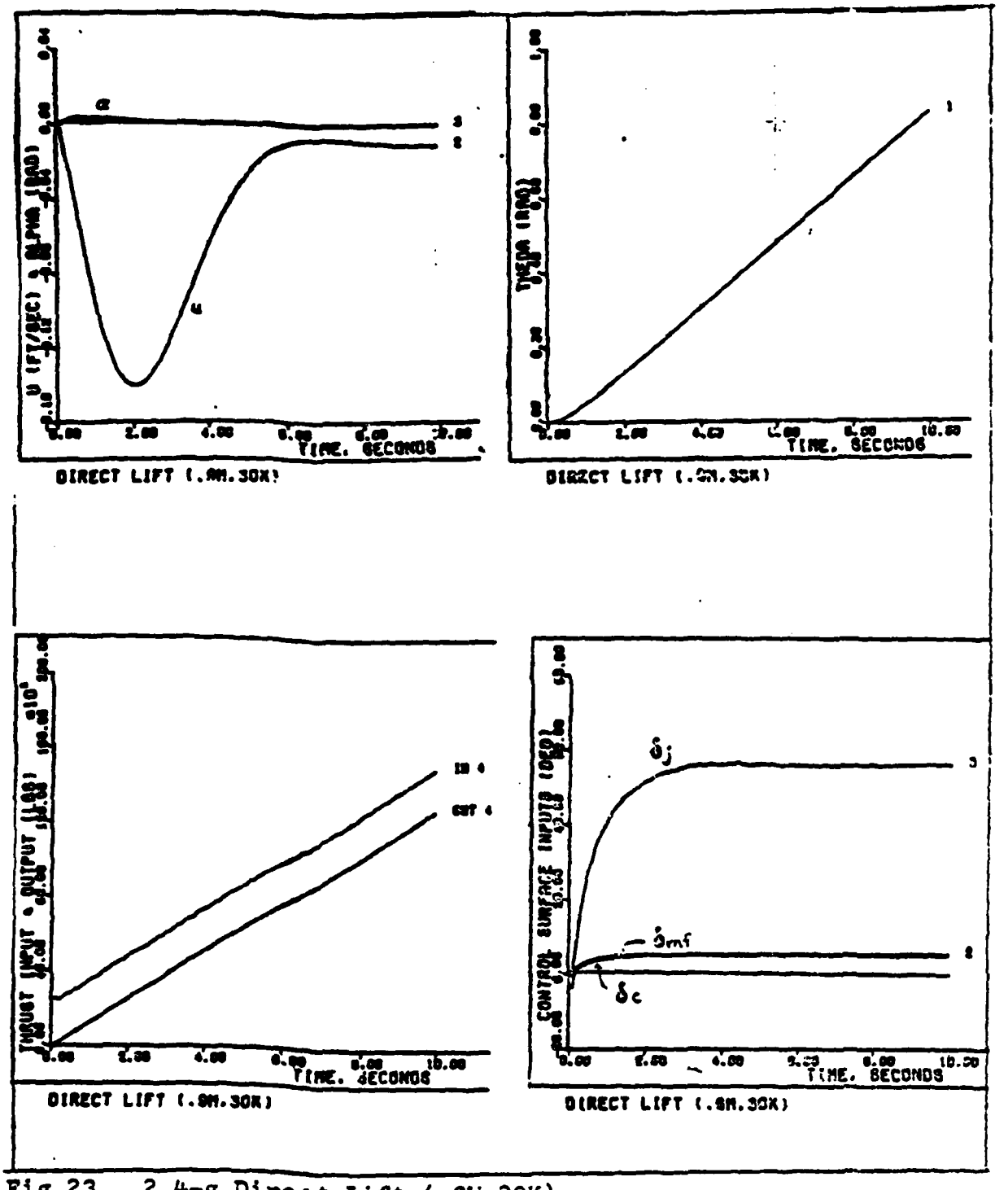



Fig 23. 2.4-g Direct Lift (.9M,30K)

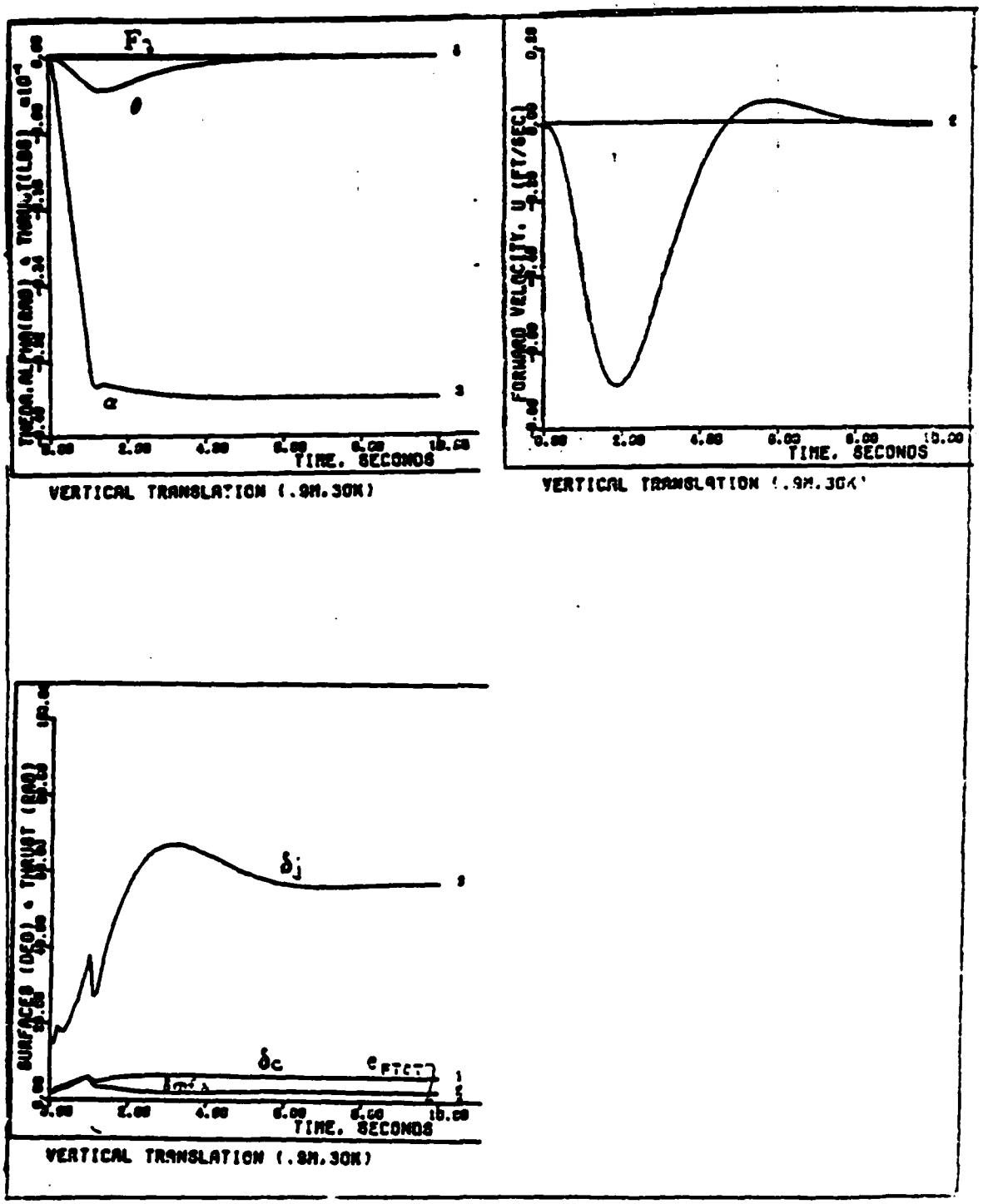



Fig 24. 1-g Vertical Translation (.9M,30K)

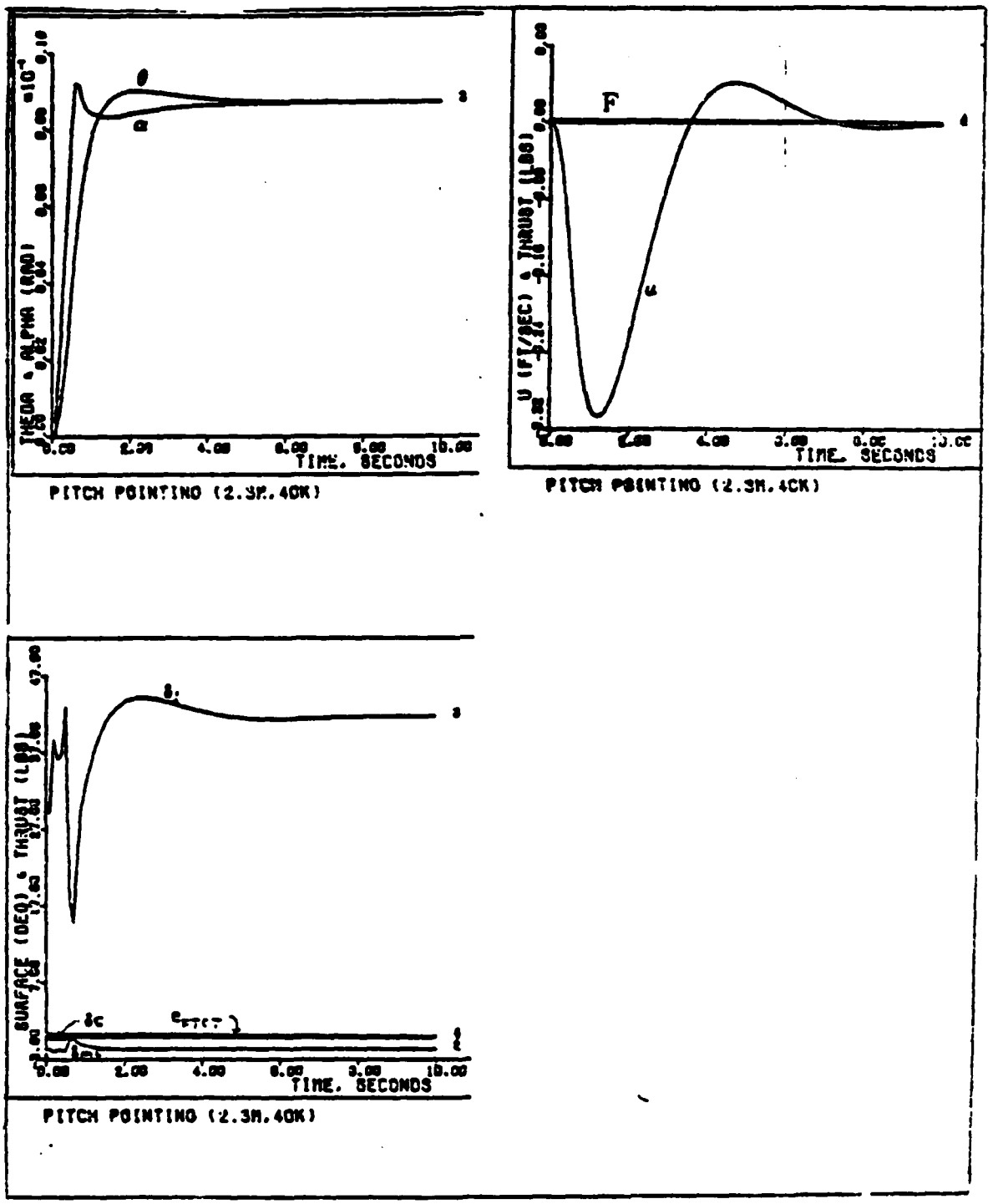



Fig 25. 0.5 Degree Pitch Pointing (2.3M,40K)

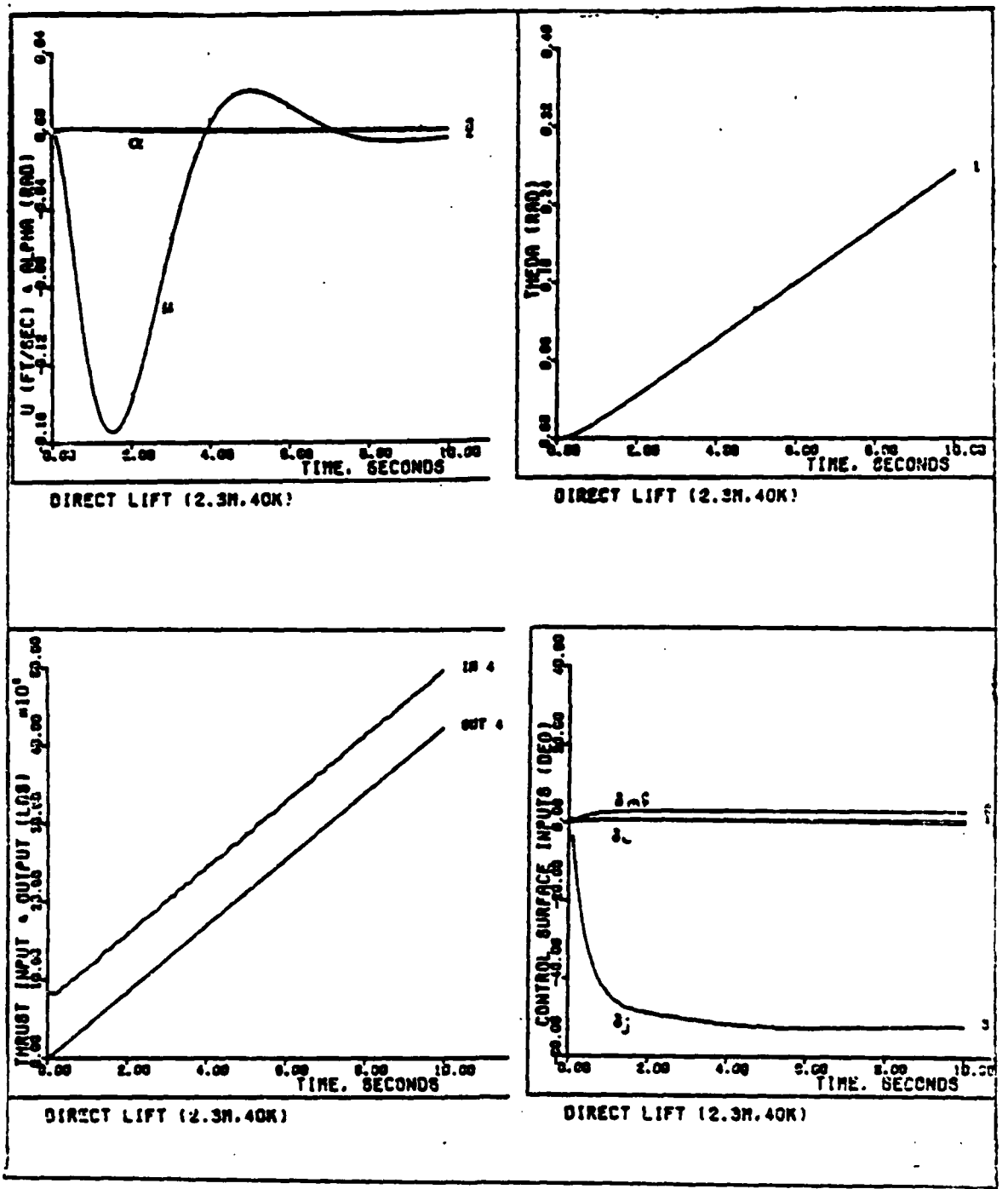



Fig 26. 2-g Direct Lift (2.3M,40K)

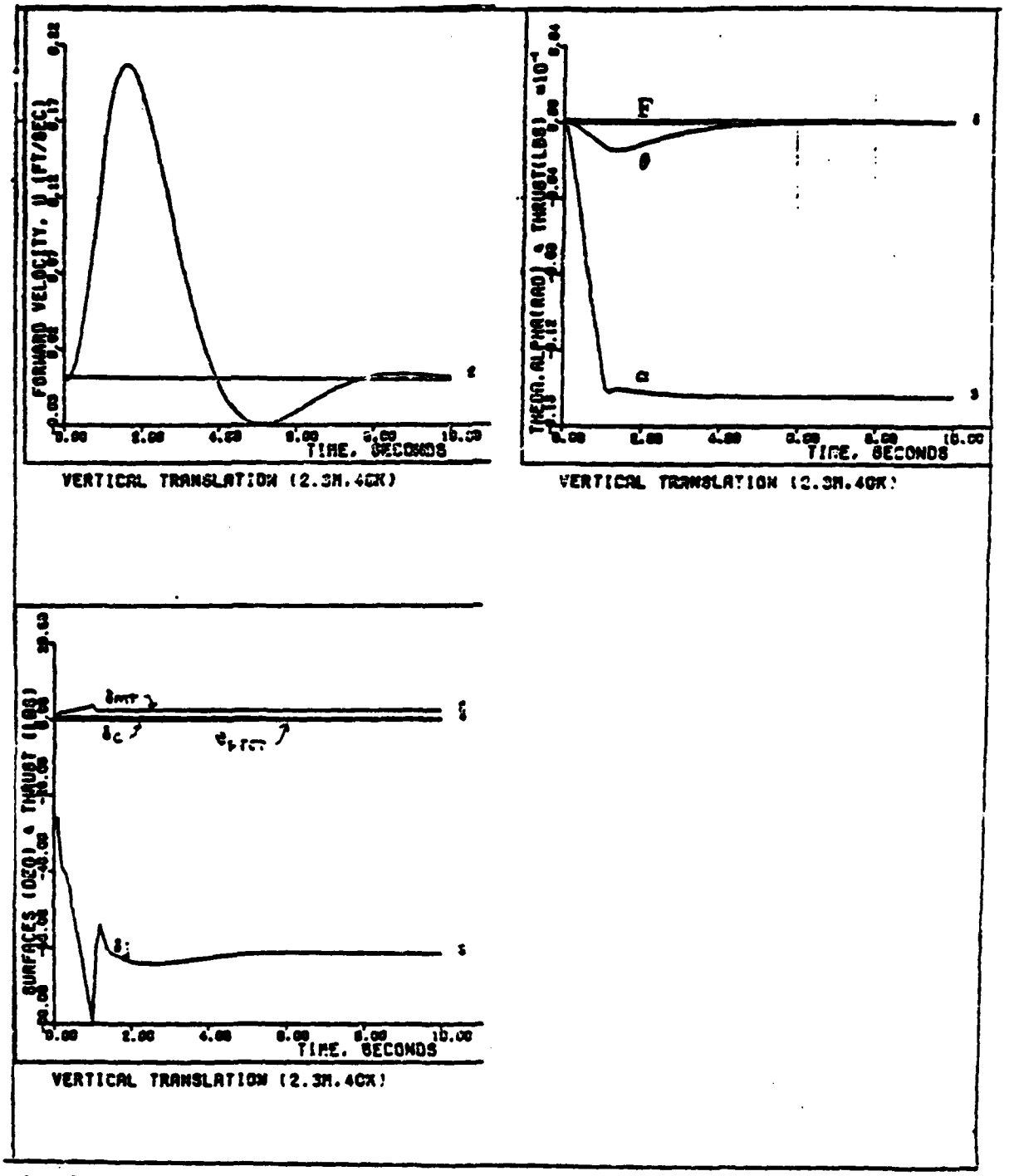



Fig 27. 1-g Vertical Translation (2.3M,40K)

figures of merit and commanded inputs for each maneuver and flight condition are summarized in Table VII.

The magnitudes of the commanded maneuvers, both lateral and longitudinal, are selected to fall in the top part of the maximum magnitude allowable at each flight condition (based on the control surface not reaching the maximum allowed at that flight condition and described in Table II). Also, the rate at which a control surface is deflected is kept at an acceptable, realizable level. Because the jet flap is a new concept and not much information on possible rate limits is available, not much was done to adjust it's rate. However, should any rate of control deflection in this report be found to be too large; it can easily be slowed by ramping up the command to its final value at a slower rate than is commanded when the rate of control deflection is unacceptable. This results in a slight lowering of rise time and settling time.

Because commands are near maximum, the reader can get a good idea of the capabilities of both this aircraft and the controllers. These controllers are the best this author could design in the time allowed for this study. They could probably be improved to achieve still better performance by engineers experienced in aircraft controller design. Never the less, responses of this controller are close to (some slightly exceed, some are slightly less than) the published capabilities of the CCV aircraft - the predecessor to the AFTI-16.

TABLE VII

SUMMARY OF TIME RESPONSES FOR LONGITUDINAL CONTROLLER

| Flt Cond | Maneuver | Command Vector $\underline{v}^*$ | Approx Percent Overshoot | Approx Rise Time ** | Approx Settling Time(2%) |
|---|---|---|---|---|---|
| 0.6 Mach sea level | Pitch Pointing | 1) $\begin{bmatrix} .5, & .0305, & 20, & 20 \\ 0, & 0, & 0, & 0 \end{bmatrix}$ 2) $\begin{bmatrix} .5, & .0305, & 20, & 20 \\ 0, & 0, & 0, & 0 \end{bmatrix}$ | 1) 6% 2) none | 1) 0.7 sec 2) 0.4 sec | 1) 3.8 sec 2) 2.6 sec |
| | Direct Lift | $\begin{bmatrix} 10, & .8725, & 20, & 20 \\ 0, & 0, & 0, & 0 \\ 0, & 0, & 0, & 0 \\ 10, & 12800, & 0, & 0 \end{bmatrix}$ | - | - | - |
| | Vertical Translation | $\begin{bmatrix} 0, & 0, & 0, & 0 \\ 0, & 0, & 0, & 0 \\ 1, & .03838, & 20, & 20 \\ 0, & 0, & 0, & 0 \end{bmatrix}$ | none | 0.9 sec | 2.5 sec |
| 0.9 Mach 30,000 ft | Pitch Pointing | 1) $\begin{bmatrix} .5, & .052356, & 20, & 20 \\ 0, & 0, & 0, & 0 \end{bmatrix}$ 2) $\begin{bmatrix} .5, & .052356, & 20, & 20 \\ 0, & 0, & 0, & 0 \end{bmatrix}$ | 1) 3.8% 2) 3.8% | 1) 0.9 sec 2) 0.4 sec | 1) 4 sec 2) 2.5 sec |
| | Direct Lift | $\begin{bmatrix} 10, & .8725, & 20, & 20 \\ 0, & 0, & 0, & 0 \\ 0, & 0, & 0, & 0 \\ 10, & 12800, & 20, & 20 \end{bmatrix}$ | - | - | - |
| | Vertical Translation | $\begin{bmatrix} 0, & 0, & 0, & 0 \\ 0, & 0, & 0, & 0 \\ 1, & -.03592, & 20, & 20 \\ 0, & 0, & 0, & 0 \end{bmatrix}$ | none | 0.8 sec | 2.2 sec |

TABLE VII

SUMMARY OF TIME RESPONSES FOR LONGITUDINAL CONTROLLER
(Cont.)

| Flt Cond | Maneuver | Command Vector $\underline{v}$* | Approx Percent Overshoot | Approx Rise Time ** | Approx Settling Time(2%) |
|---|---|---|---|---|---|
| 2.3 Mach 40,000 ft | Pitch Pointing | 1) [.5, .008726, 20, 20; 0, 0, 0, 0] 2) [.5, .008726, 20, 20; 0, 0, 0, 0] | 1) 3% 2) 5% | 1) 0.8 sec 2) 0.4 sec | 1) 3.2 sec 2) 2.4 sec |
| | Direct Lift | [10, .2889, 20, 20; 0, 0, 0, 0; 0, 0, 0, 0; 10, 4240, 20, 20] | - | - | - |
| | Vertical Translation | [0, 0, 0, 0; 0, 0, 0, 0; 1, -.01444, 20, 20; 0, 0, 0, 0] | none | 0.8 sec | 1.6 sec |

* Note: Each pulse entry $\underline{v}$ has 4 parts:

1) the time the input reached steady state,
2) steady-state value,
3) the time the input left steady state and started to return to zero, and
4) the time the input returned to zero. All angles are in radians.

** Note: Rise time is based on the time required for the non-zero output to go from 10% to 90% of its steady-state value.

Combining Lateral and Longitudinal Controllers. A close examination of equations (48) and (49) reveals that the A matrix is completely decoupled laterally and longitudinally. The B matrix becomes decoupled into controls which affect only the lateral or longitudinal mode after $CDI_1$ and $CDI_2$ are dropped and $F_1$ and $F_2$ are combined to form only one thrust input, $F_{TOT}$. As a result of combining thrust into one control rather than allowing differential thrust, the $\delta_j$ contribution to states p and r disappears, since jet flaps deflect symmetrically. Thus, the system is completely decoupled. Most aircraft are not quite as decoupled as this one, but they are close. While preceeding through this design, the effect of coupling is discussed as it affects each step of the design.

The lateral and longitudinal state equations (52), (53), (71) and (72) are combined to yield:

$$\begin{bmatrix} \dot{\theta} \\ \dot{\phi} \\ \dot{u} \\ \dot{w} \\ \dot{q} \\ \dot{F}_{TOT} \\ \dot{v} \\ \dot{r} \\ \dot{p} \end{bmatrix} = \begin{bmatrix} 0 & 0 & 0 & 0 & 1 & 0 & 0 & 0 & 0 \\ 0 & 0 & 0 & 0 & 0 & 0 & 0 & .018 & 1 \\ -32.1 & 0 & -.0297 & .105 & -12.1 & 2.18\times10^{-3} & 0 & 0 & 0 \\ -.577 & 0 & -.0568 & -2.82 & 674 & -.69\times10^{-4} & 0 & 0 & 0 \\ 0 & 0 & -.11\times10^{-2} & .0639 & -.463 & -4.48\times10^{-6} & 0 & 0 & 0 \\ 0 & 0 & 0 & 0 & 0 & -.574 & 0 & 0 & 0 \\ 0 & 32.1 & 0 & 0 & 0 & 0 & -.687 & -666 & 13.2 \\ 0 & 0 & 0 & 0 & 0 & 0 & .019 & -.389 & .256 \\ 0 & 0 & 0 & 0 & 0 & .0 & -.0103 & 1.47 & -2.35 \end{bmatrix} \begin{bmatrix} \theta \\ \phi \\ u \\ w \\ q \\ F_{TOT} \\ v \\ r \\ p \end{bmatrix}$$

$$+\begin{bmatrix} 0 & 0 & 0 & 0 & 0 & 0 & 0 \\ 0 & 0 & 0 & 0 & 0 & 0 & 0 \\ .581 & .0198 & .923\times10^{-3} & 0 & 0 & 0 & 0 \\ -1.43 & -4.73 & -.616 & 0 & 0 & 0 & 0 \\ .640 & -.0966 & -.043 & 0 & 0 & 0 & 0 \\ 0 & 0 & 0 & .574 & 0 & 0 & 0 \\ 0 & 0 & 0 & 0 & 0 & 1.78 & .581 \\ 0 & 0 & 0 & 0 & .00727 & -.188 & .0368 \\ 0 & 0 & 0 & 0 & .198 & .166 & -.0275 \end{bmatrix} \begin{bmatrix} \delta c \\ \delta mf \\ \delta j \\ e_{TOT} \\ \delta a \\ \delta r \\ \delta vc \end{bmatrix} \tag{87}$$

$$\begin{bmatrix} \theta \\ u \\ \alpha \\ F_{TOT} \\ v \\ \phi \\ r \end{bmatrix} = \begin{bmatrix} 1 & 0 & 0 & 0 & 0 & 0 & 0 & 0 & 0 \\ 0 & 0 & 1 & 0 & 0 & 0 & 0 & 0 & 0 \\ 0 & 0 & 0 & .00149 & 0 & 0 & 0 & 0 & 0 \\ 0 & 0 & 0 & 0 & 0 & 1 & 0 & 0 & 0 \\ 0 & 0 & 0 & 0 & 0 & 0 & 1 & 0 & 0 \\ 0 & 1 & 0 & 0 & 0 & 0 & 0 & 0 & 0 \\ 0 & 0 & 0 & 0 & 0 & 0 & 0 & 1 & 0 \end{bmatrix} \begin{bmatrix} \theta \\ \phi \\ u \\ w \\ q \\ F_{TOT} \\ v \\ r \\ p \end{bmatrix} \tag{88}$$

This composite system, is both controllable and observable and has one transmission zero at 1-0.574T. The $\underline{C}$ matrix, when broken down into $\underline{C}_1$ and $\underline{C}_2$, displays an interesting trait that makes combining the lateral and longitudinal controllers an easy task. $\underline{C}_1$ and $\underline{C}_2$ are both simply block diagonal matrixes with the upper block composed of the $\underline{C}_1/\underline{C}_2$ matrix from the longitudinal controller and the lower block composed of the $\underline{C}_1/\underline{C}_2$ matrix from the lateral controller. The $\underline{F}$, $\underline{\Sigma}$, $\underline{M}$, $\underline{\alpha}$, $\underline{\varepsilon}$, and $\underline{\Gamma}$ matrixes all follow the same pattern:

$$\underline{C}_1 = \left[\begin{array}{c|c} 1 & 0 \\ 0 & 0 \\ 0 & 0 \\ 0 & 0 \\ \hline 0 & 0 \\ 0 & 1 \\ 0 & 0 \end{array}\right] \qquad \underline{C}_2 = \left[\begin{array}{cc|ccc} 0 & 0 & 0 & 0 & 0 \\ 1 & 0 & 0 & 0 & 0 \\ 0 & .00149 & 0 & 0 & 0 \\ 0 & 0 & 0 & 1 & 0 \\ \hline 0 & 0 & 0 & 0 & 1 \\ 0 & 0 & 0 & 0 & 0 \\ 0 & 0 & 0 & 0 & 0 \end{array}\right] \tag{89}$$

$$\underline{M}_1 = \left[\begin{array}{c|c} m_{11} & 0 \\ 0 & 0 \\ 0 & 0 \\ 0 & 0 \\ \hline 0 & 0 \\ 0 & m_{62} \\ 0 & 0 \end{array}\right] \tag{90}$$

$$\{d_1, d_2, d_3, d_4, d_5, d_6, d_7\} = \{0,0,0,0,0,0,0\} \tag{91}$$

$$\underline{B}^* = \left[\begin{array}{cccc|cc} 0 & 0 & 1 & 0 & 0 & 0 \\ 0 & 0 & 0 & 0 & 0 & 0 \\ 0 & 0 & 0 & 0 & 0 & 0 \\ 0 & 0 & 0 & 0 & 0 & 0 \\ \hline 0 & 0 & 0 & 0 & 0 & 0 \\ 0 & 0 & 0 & 0 & .018 & 1 \\ 0 & 0 & 0 & 0 & 0 & 0 \end{array}\right] \tag{92}$$

$$f_2 = \begin{bmatrix} 0 & 0 & m_{11} & 0 & 0 & 0 & 0 \\ 1 & 0 & 0 & 0 & 0 & 0 & 0 \\ 0 & .00149 & 0 & 0 & 0 & 0 & 0 \\ 0 & 0 & 0 & 1 & 0 & 0 & 0 \\ 0 & 0 & 0 & 0 & 1 & 0 & 0 \\ 0 & 0 & 0 & 0 & 0 & .018m_{62} & m_{62} \\ 0 & 0 & 0 & 0 & 0 & 1 & 0 \end{bmatrix} \tag{93}$$

$$\underline{r}(\lambda) = \begin{bmatrix} \frac{T/m_{11}}{\lambda_1 - 1 + T/m_{11}} & 0 & 0 & 0 & 0 & 0 & 0 \\ 0 & \frac{\sigma_2}{\lambda_2 - 1 + \sigma_2} & 0 & 0 & 0 & 0 & 0 \\ 0 & 0 & \frac{\sigma_3}{\lambda_3 - 1 + \sigma_3} & 0 & 0 & 0 & 0 \\ 0 & 0 & 0 & \frac{\sigma_4}{\lambda_4 - 1 + \sigma_4} & 0 & 0 & 0 \\ 0 & 0 & 0 & 0 & \frac{\sigma_5}{\lambda_5 - 1 + \sigma_5} & 0 & 0 \\ 0 & 0 & 0 & 0 & 0 & \frac{T/m_{62}}{\lambda_6 - 1 + T/m_{62}} & 0 \\ 0 & 0 & 0 & 0 & 0 & 0 & \frac{\sigma_7}{\lambda_7 - 1 + \sigma_7} \end{bmatrix} \tag{94}$$

$$\underline{\alpha} = \left[\begin{array}{cccc:ccc} 1.1 & 0 & 0 & 0 & 0 & 0 & 0 \\ 0 & 1.1 & 0 & 0 & 0 & 0 & 0 \\ 0 & 0 & 1.1 & 0 & 0 & 0 & 0 \\ 0 & 0 & 0 & 1.1 & 0 & 0 & 0 \\ \hdashline 0 & 0 & 0 & 0 & 1.5 & 0 & 0 \\ 0 & 0 & 0 & 0 & 0 & 1.5 & 0 \\ 0 & 0 & 0 & 0 & 0 & 0 & 1.5 \end{array}\right] \tag{95}$$

$$\underline{\Sigma} = \left[\begin{array}{cccc:ccc} 6 & 0 & 0 & 0 & 0 & 0 & 0 \\ 0 & .1 & 0 & 0 & 0 & 0 & 0 \\ 0 & 0 & 1 & 0 & 0 & 0 & 0 \\ 0 & 0 & 0 & 2 & 0 & 0 & 0 \\ \hdashline 0 & 0 & 0 & 0 & .2 & 0 & 0 \\ 0 & 0 & 0 & 0 & 0 & .5 & 0 \\ 0 & 0 & 0 & 0 & 0 & 0 & 3 \end{array}\right] \tag{96}$$

$$\varepsilon = 0.1;\ m_{11} = 0.5;\ m_{62} = 1,\ T = 0.01 \tag{97}$$

(Note that $\alpha$ is a scaler when designing the individual lateral and longitudinal controllers, and is a matrix now. The same can be done with $\varepsilon$ if it differed from the lateral to the longitudinal case, or $\varepsilon$ could be absorbed by the elements of the $\underline{\Sigma}$ matrix). The block diagonal form of these matrixes holds, regardless of the amount of coupling in the combined state equations. However, the degree of coupling does affect the rest of the design.

Since there is no coupling whatsoever in the system examined here, equations (89) through (97) stand as a final design for the complete system. Again, $\underline{K}_0$ and $\underline{K}_1$ follow the block diagonal construction displayed so far throughout this design. For the 0.6 Mach, sea level flight condition:

$$\underline{K}_0 = \left[\begin{array}{cccc:ccc} -.1334 & .02042 & .7261 & 0 & 0 & 0 & 0 \\ 6.0737 & -.06469 & -24.3628 & 0 & 0 & 0 & 0 \\ -46.3276 & .4493 & 65.5390 & 0 & 0 & 0 & 0 \\ 0 & 0 & 0 & .3833 & 0 & 0 & 0 \\ \hdashline 0 & 0 & 0 & 0 & -.000790 & .3676 & 1.795 \\ 0 & 0 & 0 & 0 & .006299 & .00888 & -1.453 \\ 0 & 0 & 0 & 0 & .03234 & -.02722 & 4.451 \end{array}\right] \quad (98)$$

$$\underline{K}_1 = \left[\begin{array}{cccc:ccc} -.1213 & .0186 & .6601 & 0 & 0 & 0 & 0 \\ 5.5215 & -.0589 & -22.1480 & 0 & 0 & 0 & 0 \\ -42.1160 & .4085 & 59.5809 & 0 & 0 & 0 & 0 \\ 0 & 0 & 0 & .3484 & 0 & 0 & 0 \\ \hdashline 0 & 0 & 0 & 0 & -.000527 & .2450 & 1.1969 \\ 0 & 0 & 0 & 0 & .004199 & .00592 & -.9686 \\ 0 & 0 & 0 & 0 & .0215 & -.0181 & 2.9675 \end{array}\right] \quad (99)$$

The $\underline{K}_0$, $\underline{K}_1$ pairs for the 0.9 Mach, 30,000 ft. and 2.3 Mach, 40,000 ft. flight conditions have a form identical to equations (98) and (99) and are presented in Appendix B. Because of this form, any input to this combined system has a time response identical to that resulting from the same input into the lateral and longitudinal controllers separately. An example of this is shown in Figures 28 and 29 where the same inputs used for the horizontal translation maneuver laterally and the vertical translation maneuver longitudinally are combined and serve as inputs to the combined system (Fig 28) resulting in a response identical to those achieved separately in Figures 9 and 24.

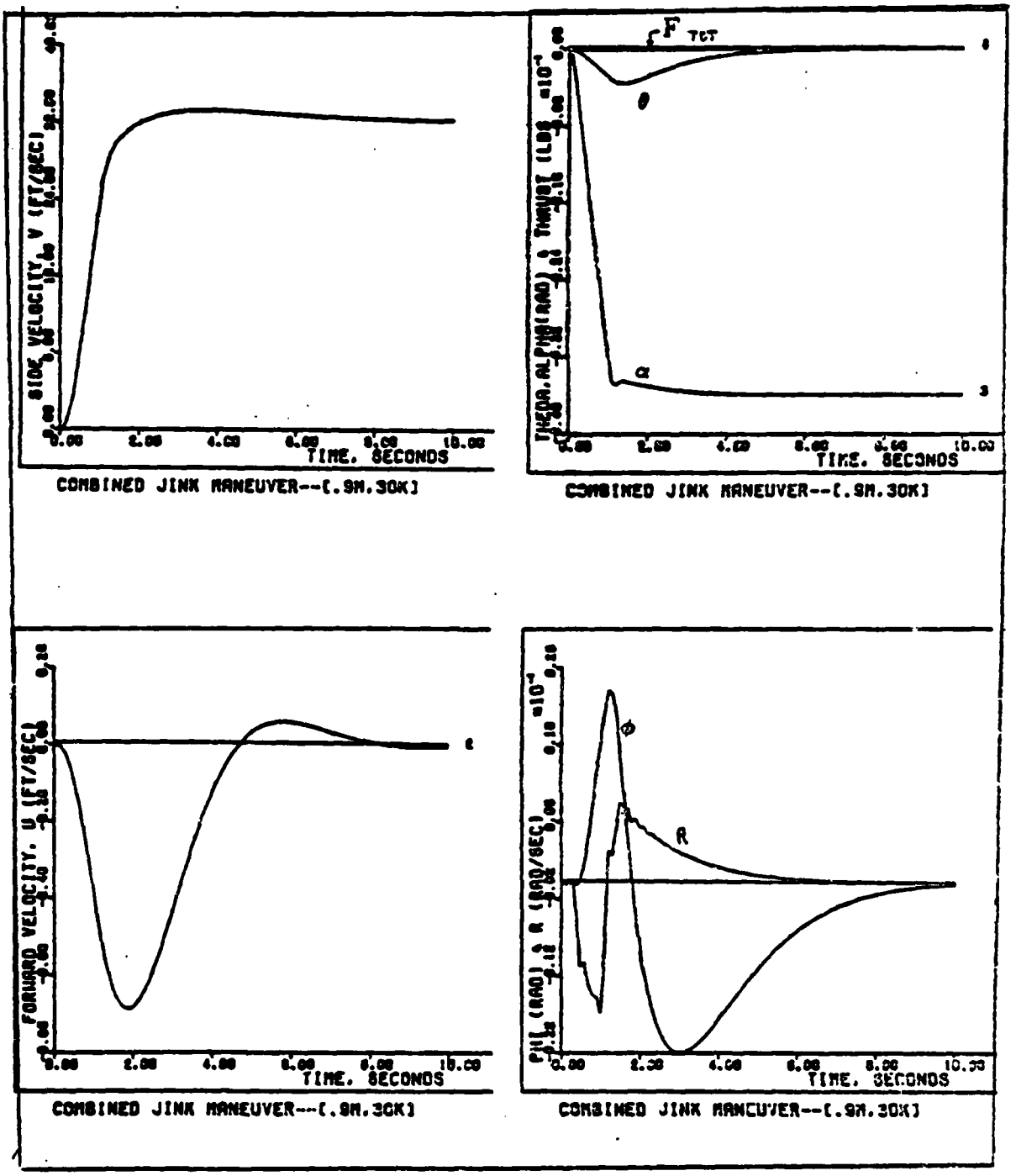



Fig 28. "Jink " Maneuver (.9M,30K)

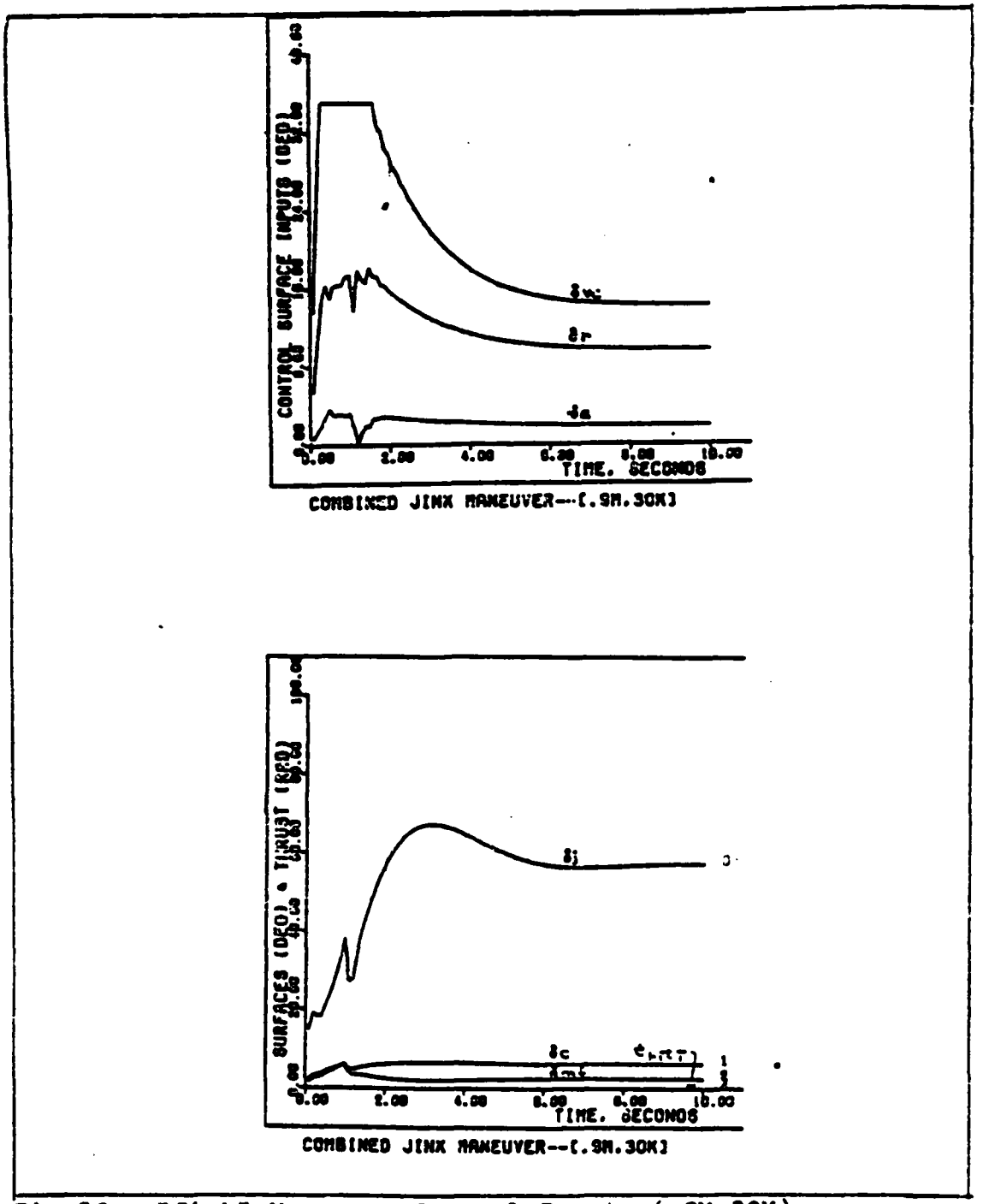



Fig 29. "Jink" Maneuver Control Inputs (.9M,30K)

This is not the case if there is any coupling between the lateral and longitudinal modes. First, if there is some coupling, the $\underline{K}_0$, $\underline{K}_1$ pair do not have the block diagonal form of equations (98) and (99). If the initial design uses $\underline{\varepsilon}$, $\underline{\Sigma}$, and $\underline{\alpha}$ as constructed in equations (95), (96), and (97) from the $\underline{\varepsilon}$, $\underline{\Sigma}$, and $\underline{\alpha}$ designs of the lateral and longitudinal controllers, the main block diagonal terms consists of the $\underline{K}_0$, $\underline{K}_1$ pair of the original controller, as in equations (98) and (99). However, if there is coupling in the $\underline{B}$ matrix, off diagonal terms appear (see Eqs (34) and (35)). The magnitude of these terms depends on the degree of coupling. The response to a given input is no longer identical to that obtained when the same input is put into the separate lateral or longitudinal system, and some more tuning of the $\underline{\Sigma}$ matrix may be required if the response is inadequate for the combined system. The same tuning may be required if the $\underline{A}$ matrix for the combined system is not fully decoupled. Although the $\underline{K}_0$, $\underline{K}_1$ pair is not affected by coupling in the $\underline{A}$ matrix, the time response to a given input is. However, since on many aircraft this coupling is minimal, very little adjustment is required on the initial design acquired after combining the controllers.

The final maneuver tested on the combined controller in this chapter is a 60 degree banked coordinated turn. The perturbation angle of attack for a level 60 degree banked turn at 0.9 Mach and 30,000 ft. is estimated to be 1.5 degrees. Yaw rate r is determined from the equation:

$$r = \frac{g}{u} \sin \phi \qquad (100)$$

If this controller was implemented on an aircraft, the proper blending of r, $\phi$, and $\alpha$ (as well as $F_{TOT}$, $\theta$, u, and v) for this and other "coupled" maneuvers would be computed according to what the pilot commands prior to being input into the controller. This function is performed by the on board computer.

The controller's response to the 60 degree bank, level, coordinated turn command is shown in Figures 30, 31, and 32. The responses are very good and demonstrate the ability of the controller designed to perform coupled as well as decoupled maneuvers.

## Conclusion

Although each maneuver is not tested on the combined controllers for each flight condition as it was on the separate lateral and longitudinal controller designs, the maneuvers are tested individually on each combined controller in the next chapter during robustness testing. What is achieved in this chapter is very significant. The combined controllers designed here have only one set of gain values needed to accomplish any combination of the seven maneuvers tested in this chapter with satisfactory results. This is contrary to what is presently done on-board other aircraft which basically gain schedule for every maneuver and flight condition. This new flight controller would thus require less computer time to accomplish gain scheduling resulting in the on-board computer having more time to accomplish other necessary tasks. Also, it can be seen by examining all $\underline{K}_0$, $\underline{K}_1$ matrix pairs

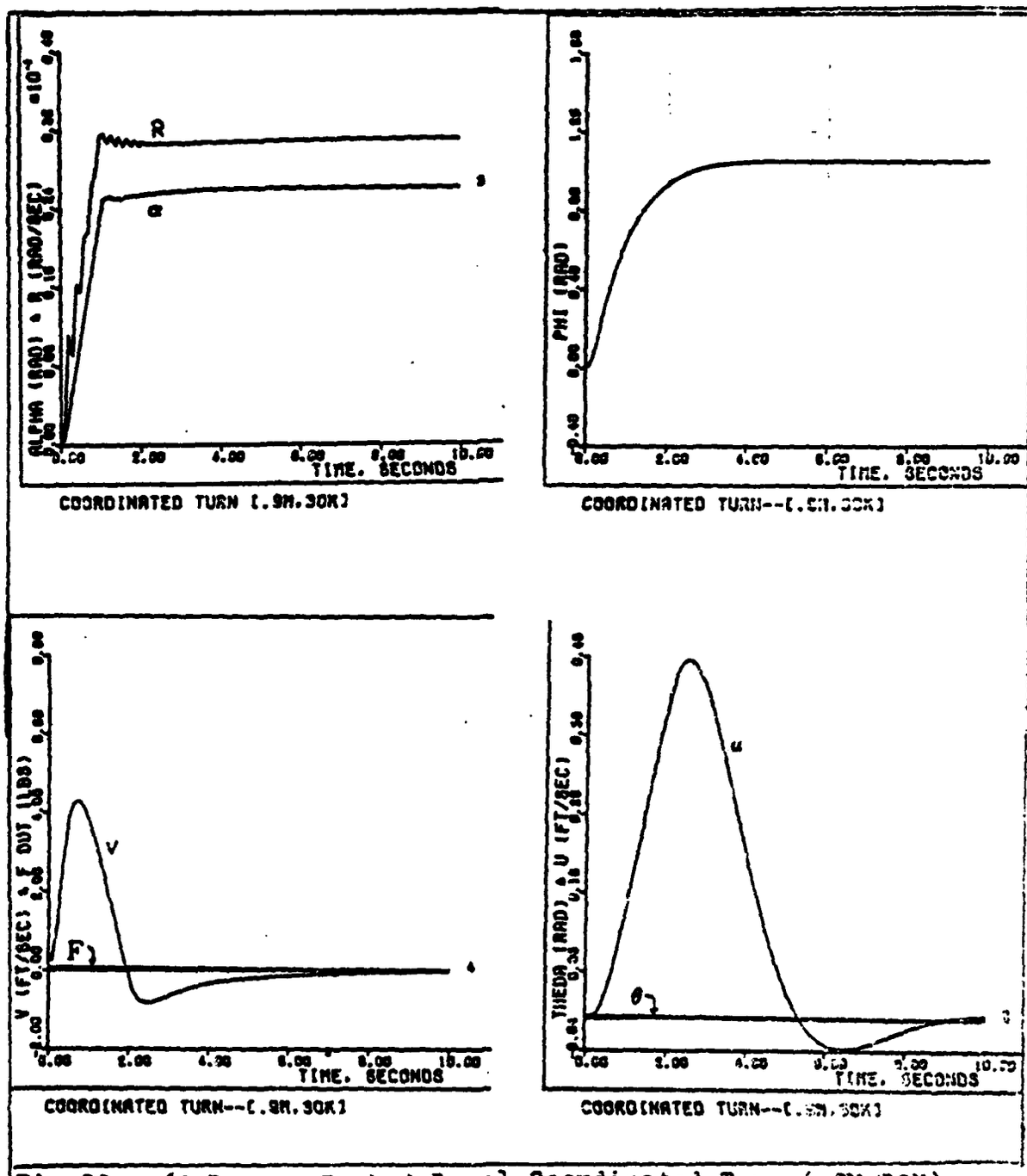



Fig 30. 60 Degree Banked Level Coordinated Turn (.9M,30K)

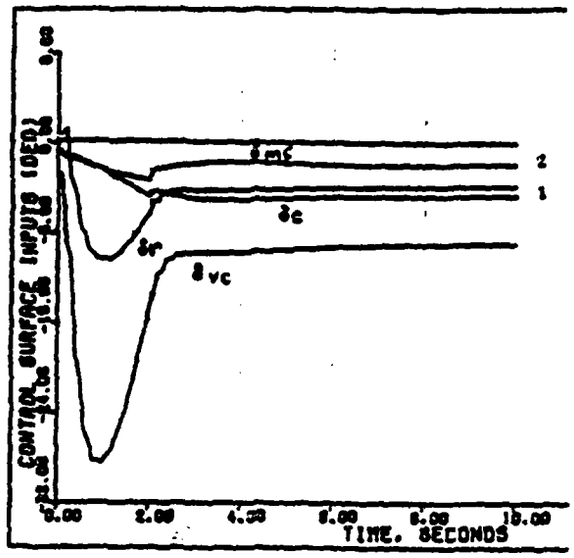



Fig 31. 60 Degree Banked Level Coordinated Turn (.9M,30K)

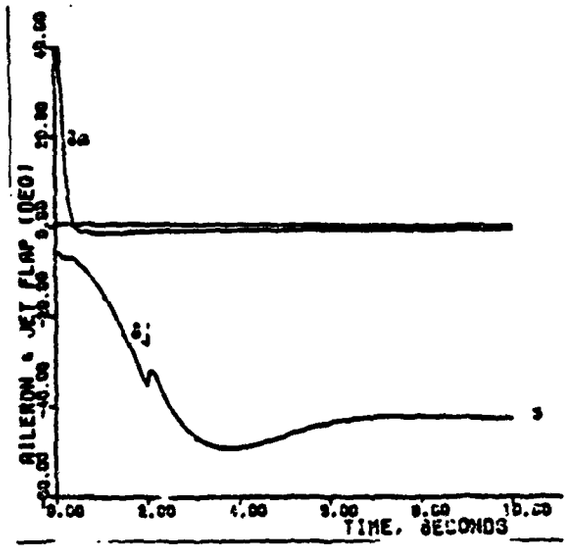



Fig 32. 60 Degree Banked Level Coordinated Turn (.9M,30K)

that the gains used by this system are relatively low and thus the system is less likely to be affected by noise. An even more significant aspect, the robustness of this the controller design, is brought out in the following chapter which further points out the advantages of using this design technique over classical methods.

# CHAPTER V

# ROBUSTNESS TESTING ON COMPLETE CONTROLLER

## Introduction

Presently on aircraft with digital flight control systems, gain scheduling is used extensively to maximize aircraft performance in accomplishing different maneuvers at different flight conditions. As a result, the on-board computer spends much of its time simply loading and unloading different gain values into its core memory to perform the necessary calculations required for flight control.

Throughout the literature published on his design technique (Ref 27, for example) Professor Porter makes the claim that the controller design using this method is very robust. In terms of an aircraft flight control system, this would mean a single controller capable of giving satisfactory performance over a wide range of flight conditions. A small set of robust controllers can eliminate much of the gain scheduling required on present digital flight control systems thus leaving the on-board computer free to accomplish other tasks.

This chapter describes how the flight controllers devised in this study are tested for robustness. A very limited amount of data from the modified version of FPCC Sim (Ref 8) is available for testing. This results in the tests being performed on only three flight conditions, but for a very wide range of dynamic pressure. For the three flight conditions examined, dynamic pressure varies from a low of 356 psf at

the 0.9 Mach, 30,000 ft. flight condition, to a high of 1450 psf for the 2.3 Mach, 40,000 ft. flight condition. As a result of this restriction on the number of flight conditions examined, the resulting "universal" controller is capable of producing stable results over a very wide range of flight conditions, but the results are not as good as they are when the controller is designed for a specific flight condition.

Universal Controller

The "universal" controller devised here consists of the lateral controller for the 2.3 Mach, 40,000 ft. flight condition and the longitudinal controller for the 0.9 Mach, 30,000 ft. flight condition. These controllers are found to give the best maneuver performance over the range of all flight conditions tested (0.6 Mach, sea level, 0.9 Mach, 30,000 ft., and 2.3 Mach, 40,000 ft.). The lateral and longitudinal parts of the "universal" controller are combined in the same manner as described in Chapter IV when combining the lateral and longitudinal controllers to achieve a complete controller for a particular flight condition. The resulting controller matrixes are:

$$\underline{K}_0 = \begin{bmatrix} 1.120 & .0157 & -6.051 & 0 & 0 & 0 & 0 \\ 1.500 & -.0198 & -7.544 & 0 & 0 & 0 & 0 \\ -31.450 & .3743 & -52.852 & 0 & 0 & 0 & 0 \\ 0 & 0 & 0 & .3833 & 0 & 0 & 0 \\ 0 & 0 & 0 & 0 & .0011 & .2737 & .8679 \\ 0 & 0 & 0 & 0 & .0094 & .0122 & -2.114 \\ 0 & 0 & 0 & 0 & .0235 & -.0186 & 3.238 \end{bmatrix} \quad (101)$$

$$\underline{K}_1 = \begin{bmatrix} 1.018 & .0143 & -5.501 & 0 & 0 & 0 & 0 \\ 1.363 & -.0180 & -6.858 & 0 & 0 & 0 & 0 \\ -28.591 & .3402 & -48.047 & 0 & 0 & 0 & 0 \\ 0 & 0 & 0 & .3484 & 0 & 0 & 0 \\ 0 & 0 & 0 & 0 & .0008 & .1825 & .5786 \\ 0 & 0 & 0 & 0 & .0063 & .0081 & -1.409 \\ 0 & 0 & 0 & 0 & .0157 & -.0124 & 2.159 \end{bmatrix} \quad (102)$$

The next task is to use this controller at different flight conditions and attempt the same maneuvers tested in Chapter IV. The results are then compared with those achieved by the controller designed specifically for that particular flight condition. In Figures 33 through 78 each output variable is plotted for the "universal" or "robust" controller verses the same output from the controller designed at the specific flight condition tested. Outputs not shown remain at zero.

0.6 Mach, Sea Level Flight Condition

The results of tests performed on the "universal" controller at the 0.6 Mach, sea level flight condition are perhaps the most interesting because neither the lateral nor longitudinal parts of the "universal" controller are designed for the 0.6 Mach, sea level flight condition. Each of the seven maneuvers tested is summarized in Figures 33 through 46. The figures of merit for the "universal" controller are summarized in Table VIII and can be compared with those of Table VI and VII for the 0.6 Mach sea level flight condition. The figures of merit for the Horizontal Translation maneuver actually improve when using the universal controller compared

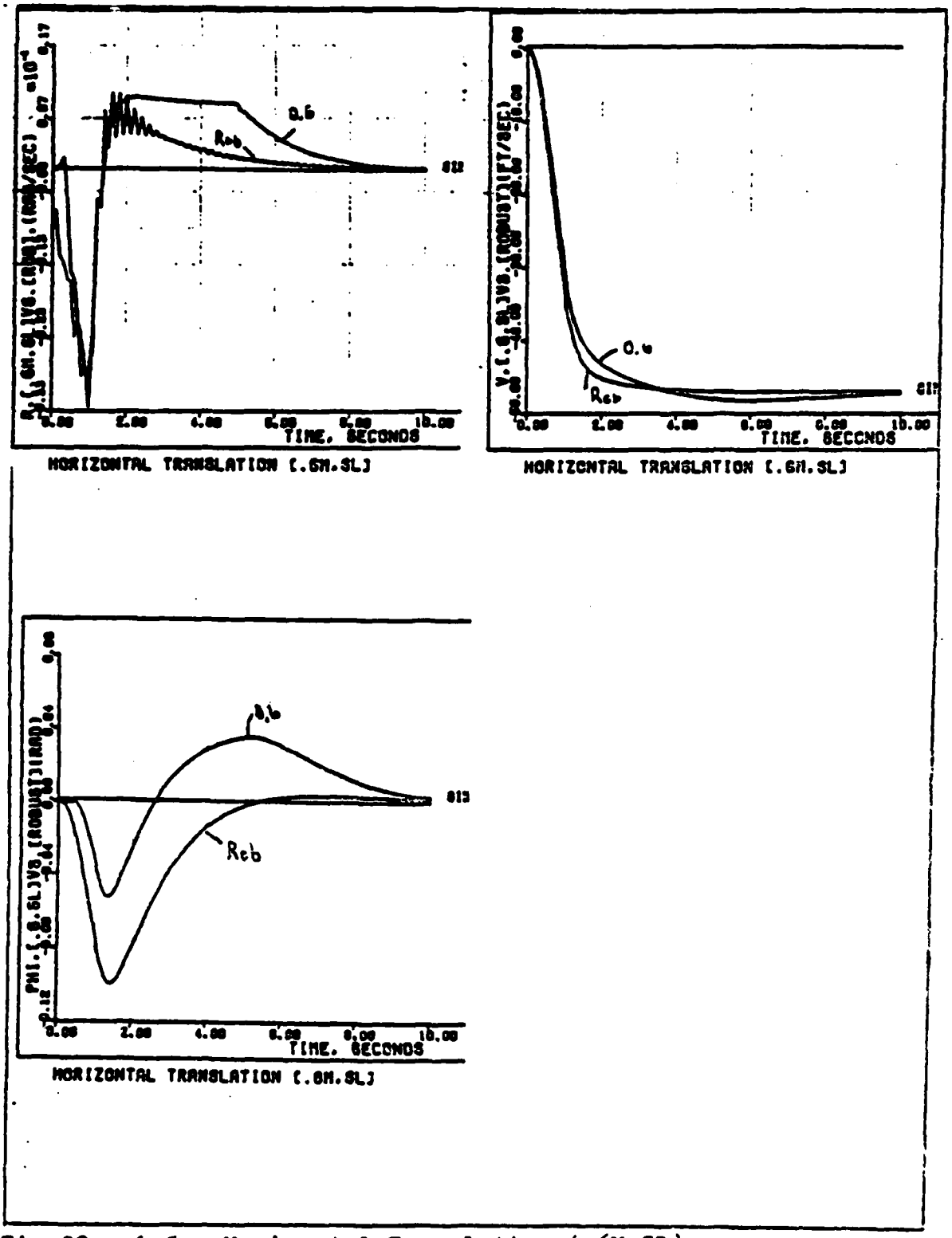



Fig 33. 1.5-g Horizontal Translation (.6M,SL)

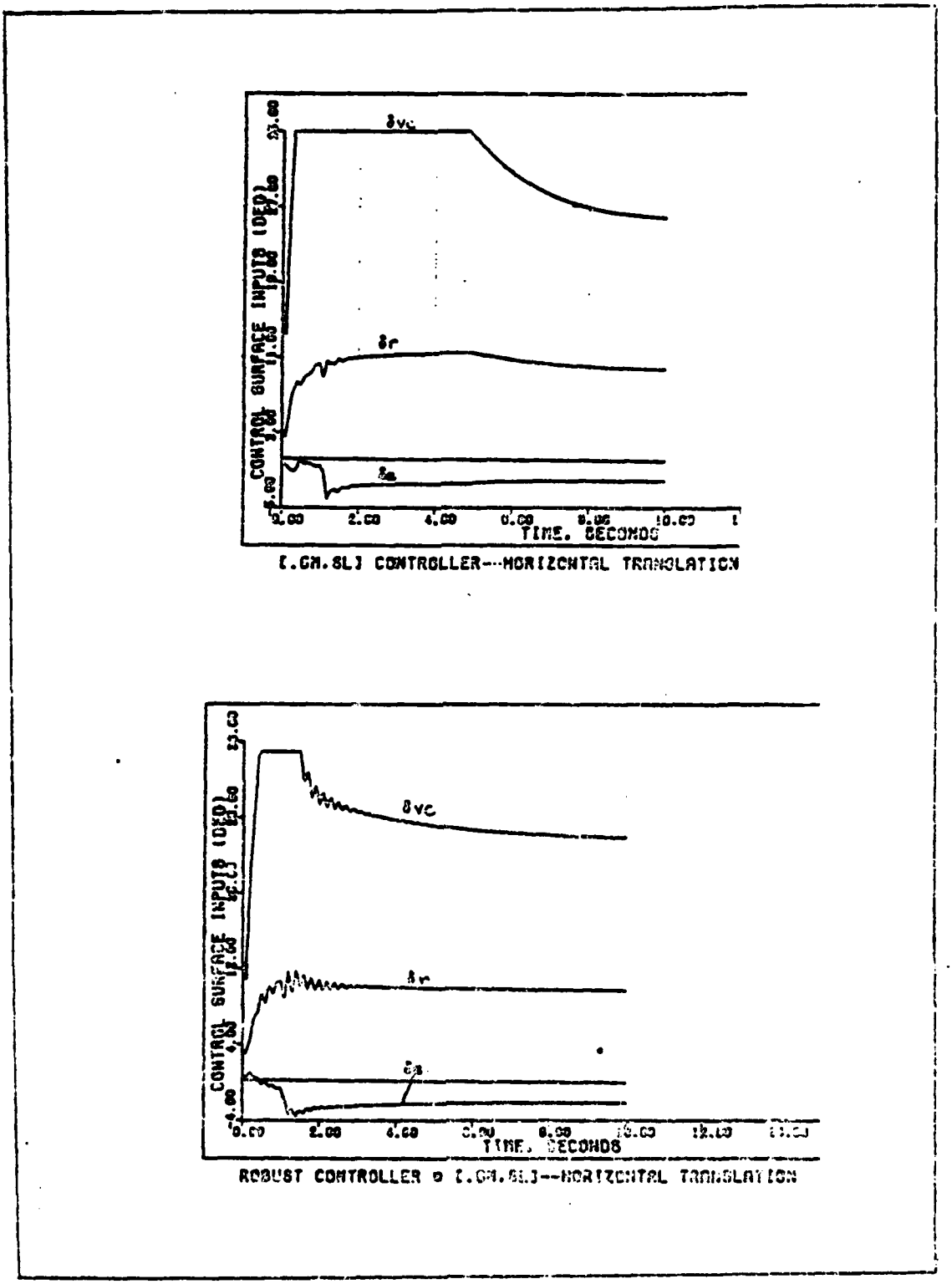



Fig 34. 1.5-g Horizontal Translation (.6M,SL)

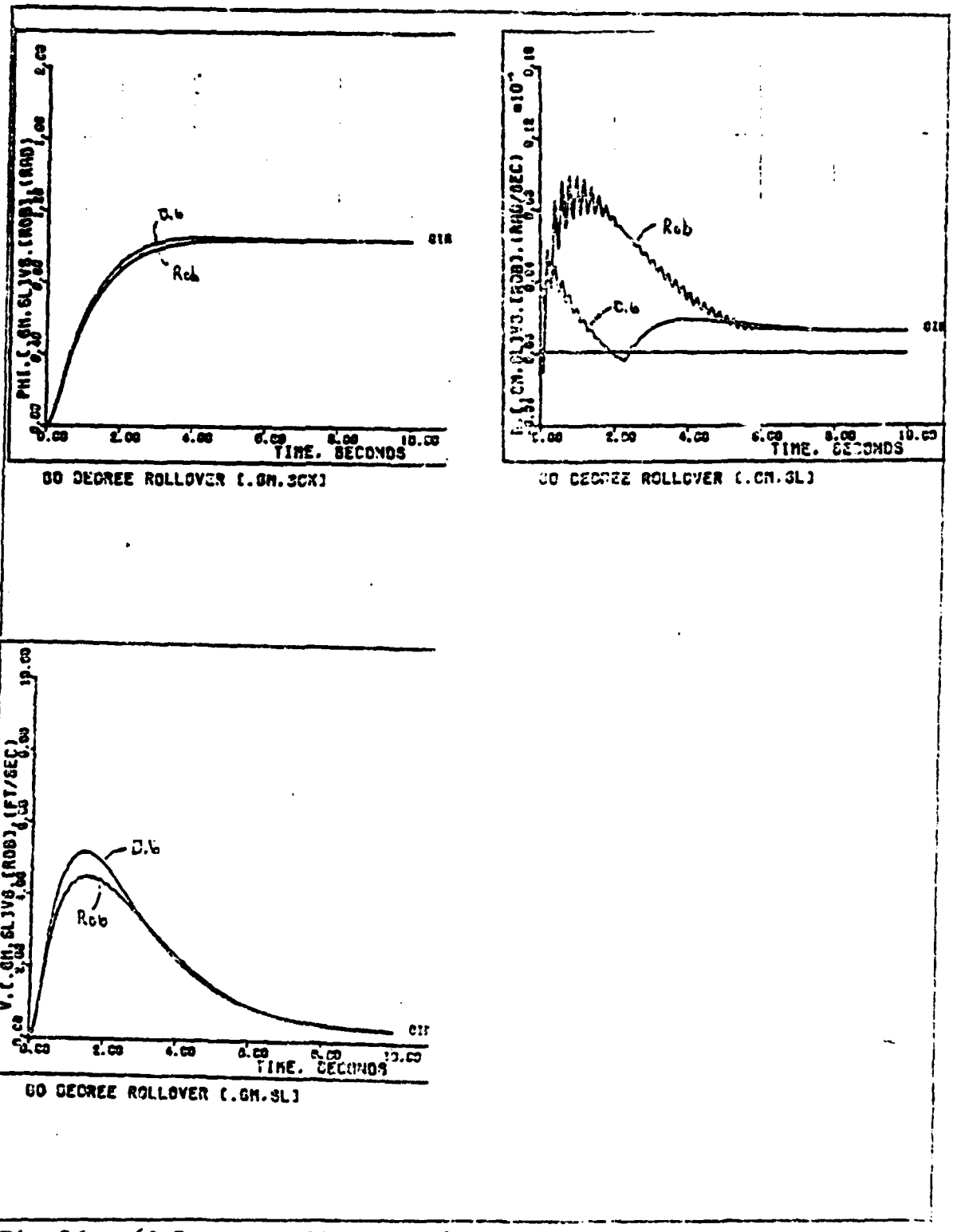
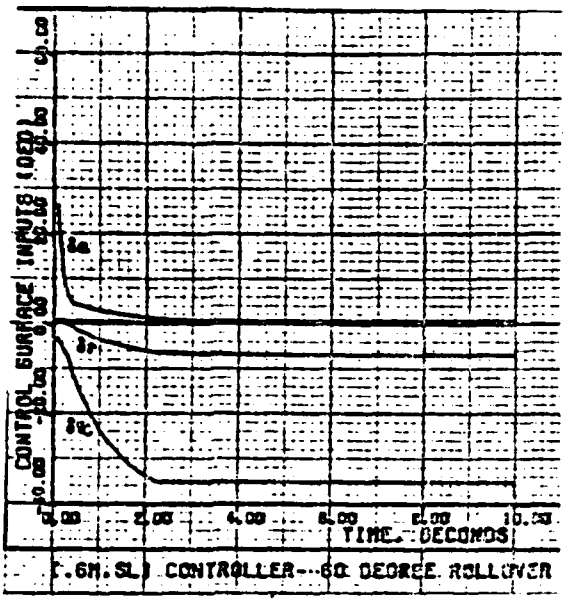



Fig 35. 60 Degree Rollover (.6M,SL)



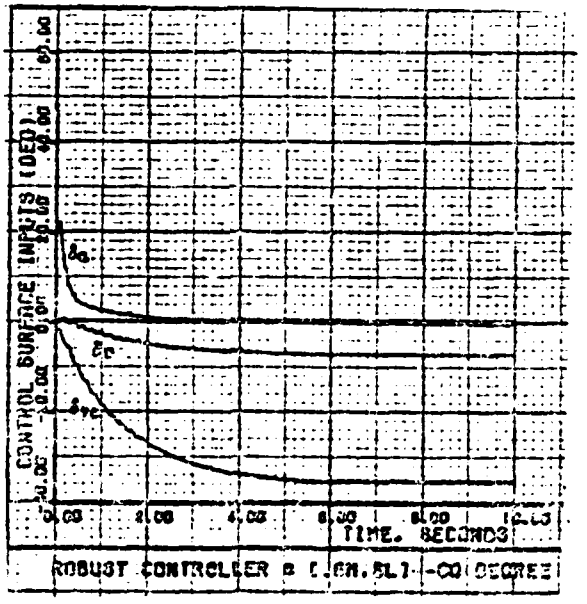




Fig 36. 60 Degree Rollover (.6M,SL)

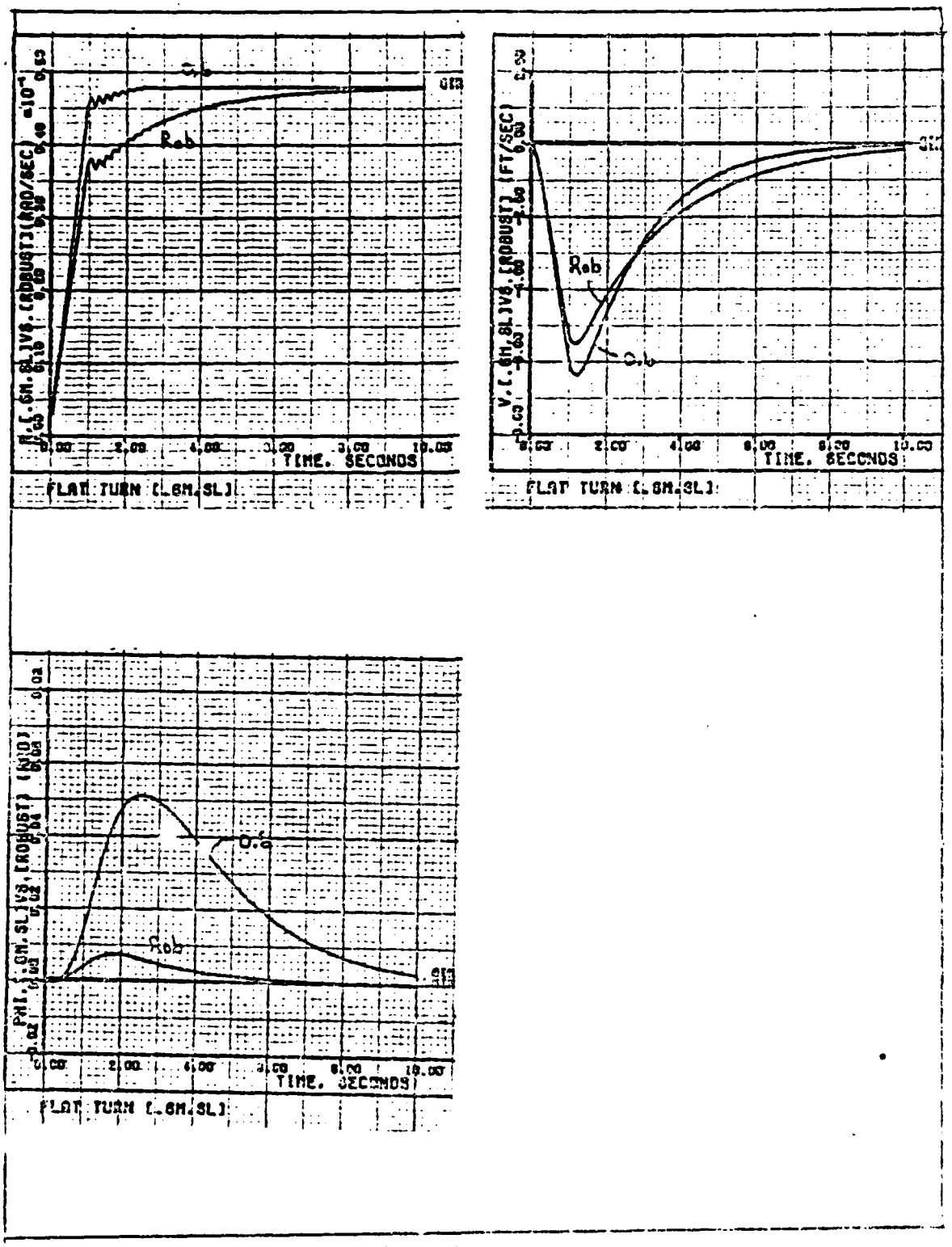
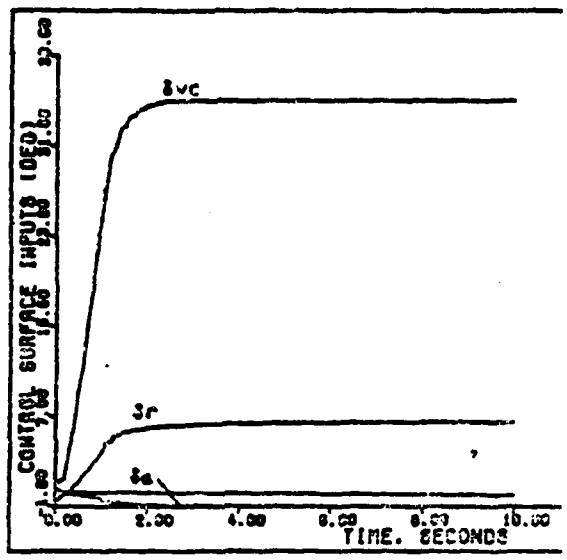
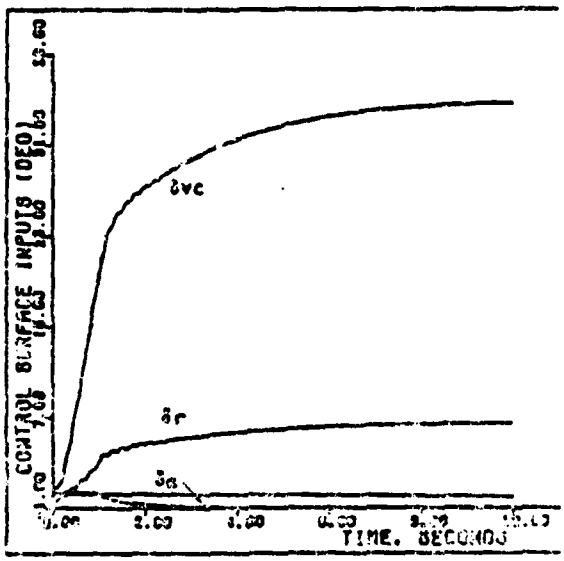



Fig 37. 1-g Flat Turn (.6M,3L)




[.6M,SL] CONTROLLER--FLAT TURN




ROBUST CONTROLLER o [.6M,SL]--FL T TURN

Fig 38. 1-g Flat Turn (.6M,SL)

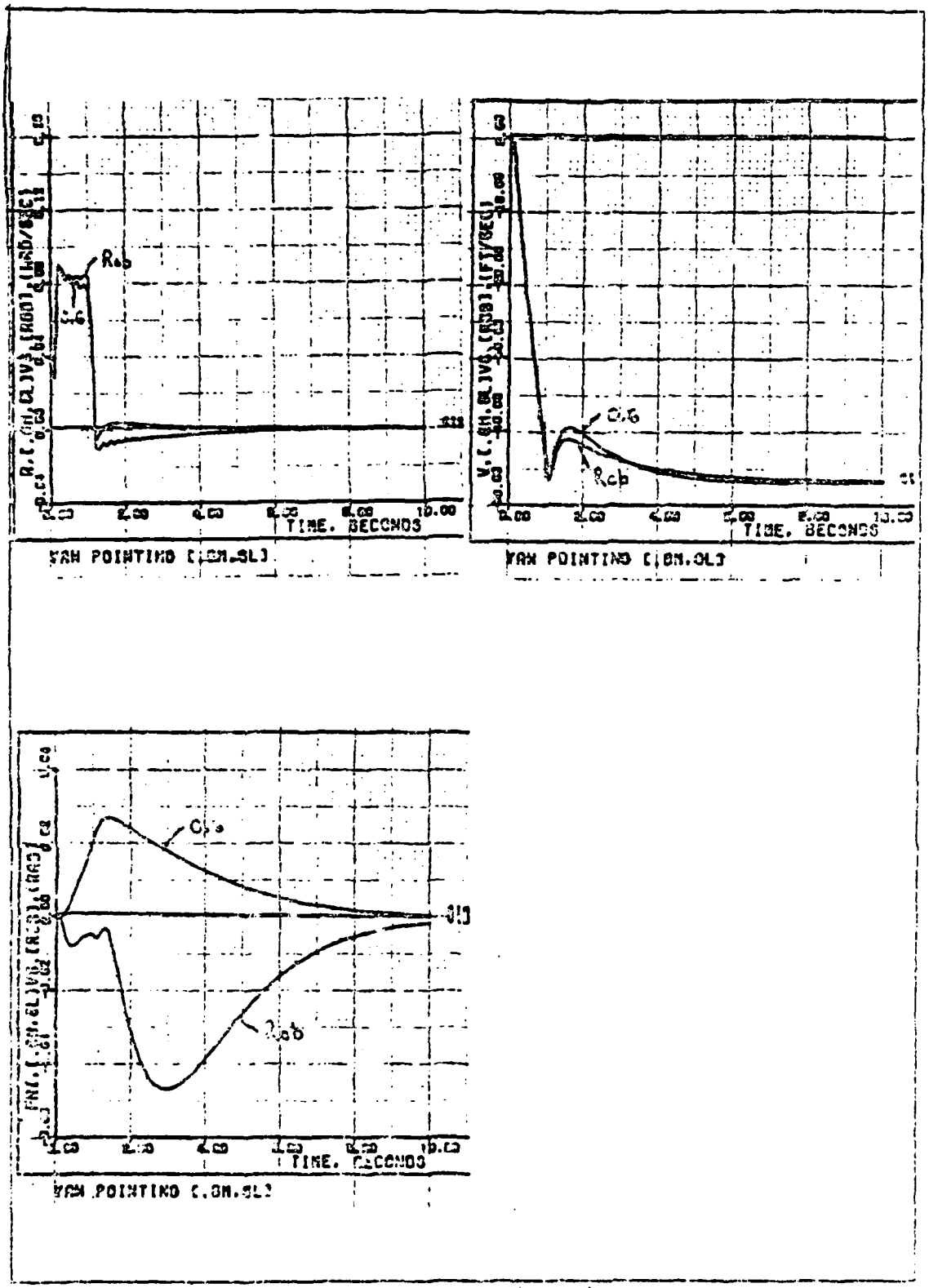



Fig 39. 4 D gree Yaw Pointing (.6M,SL)

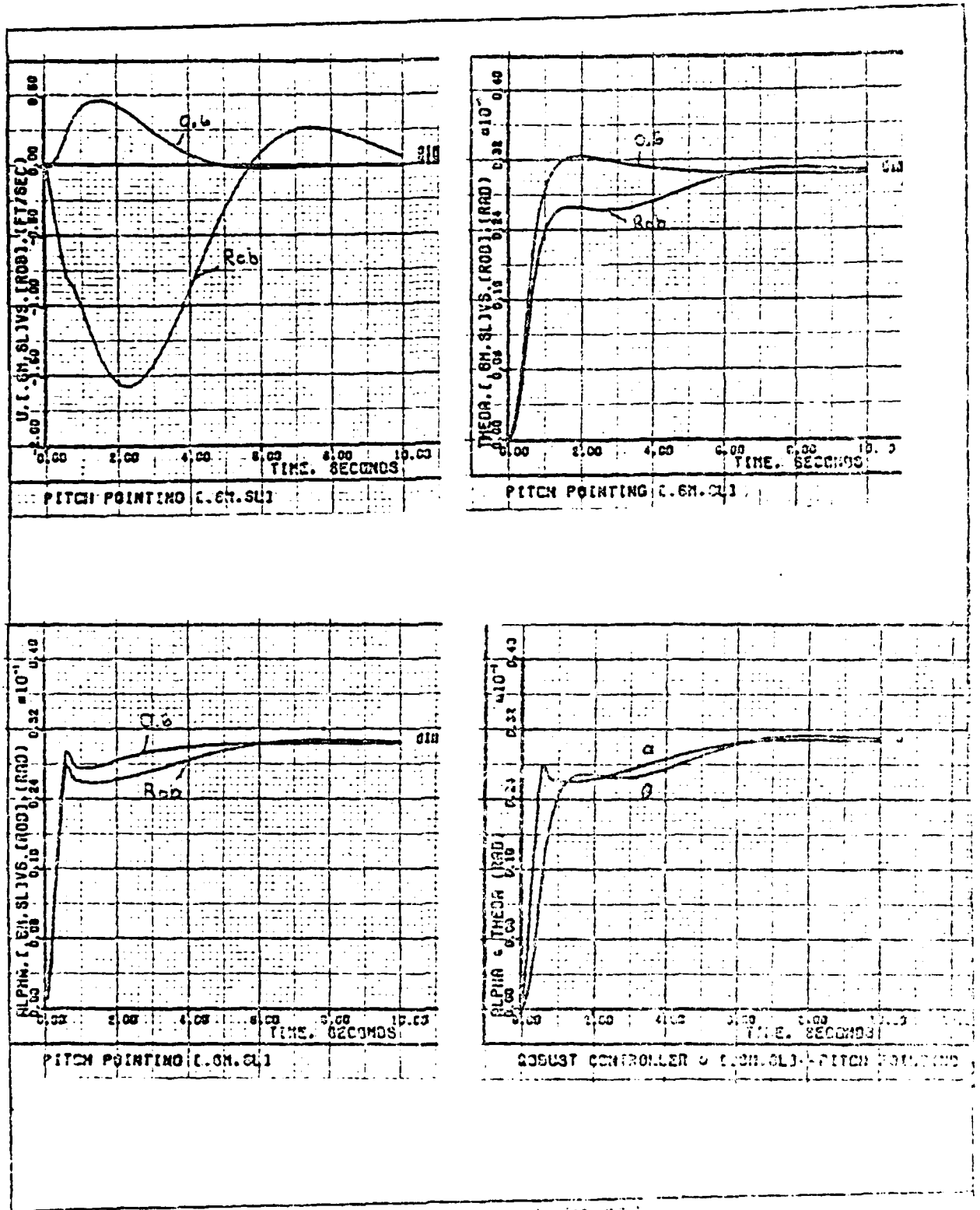
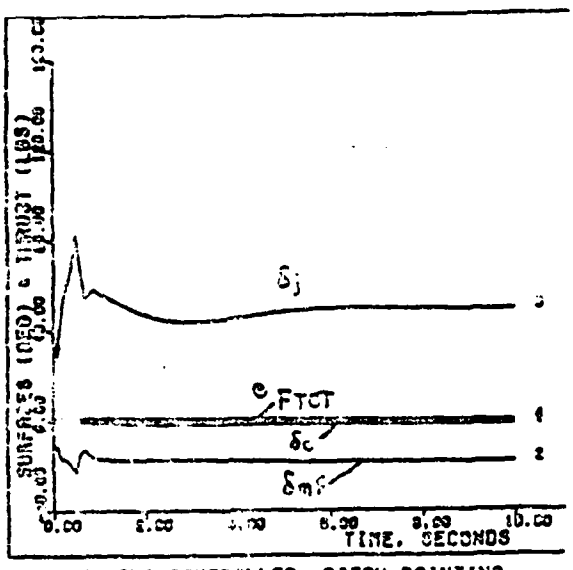
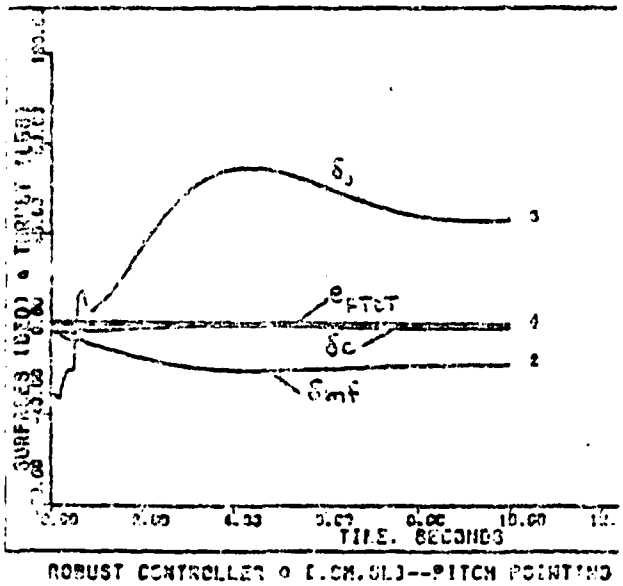



Fig 41. 1.75 Degree Pitch Pointing (.6M.SL)




(.6M,SL) CONTROLLER--PITCH POINTING




ROBUST CONTROLLER @ (.6M,SL)--PITCH POINTING

Fig 42, 1.75 Degree Pitch Pointing (.6M,SL)

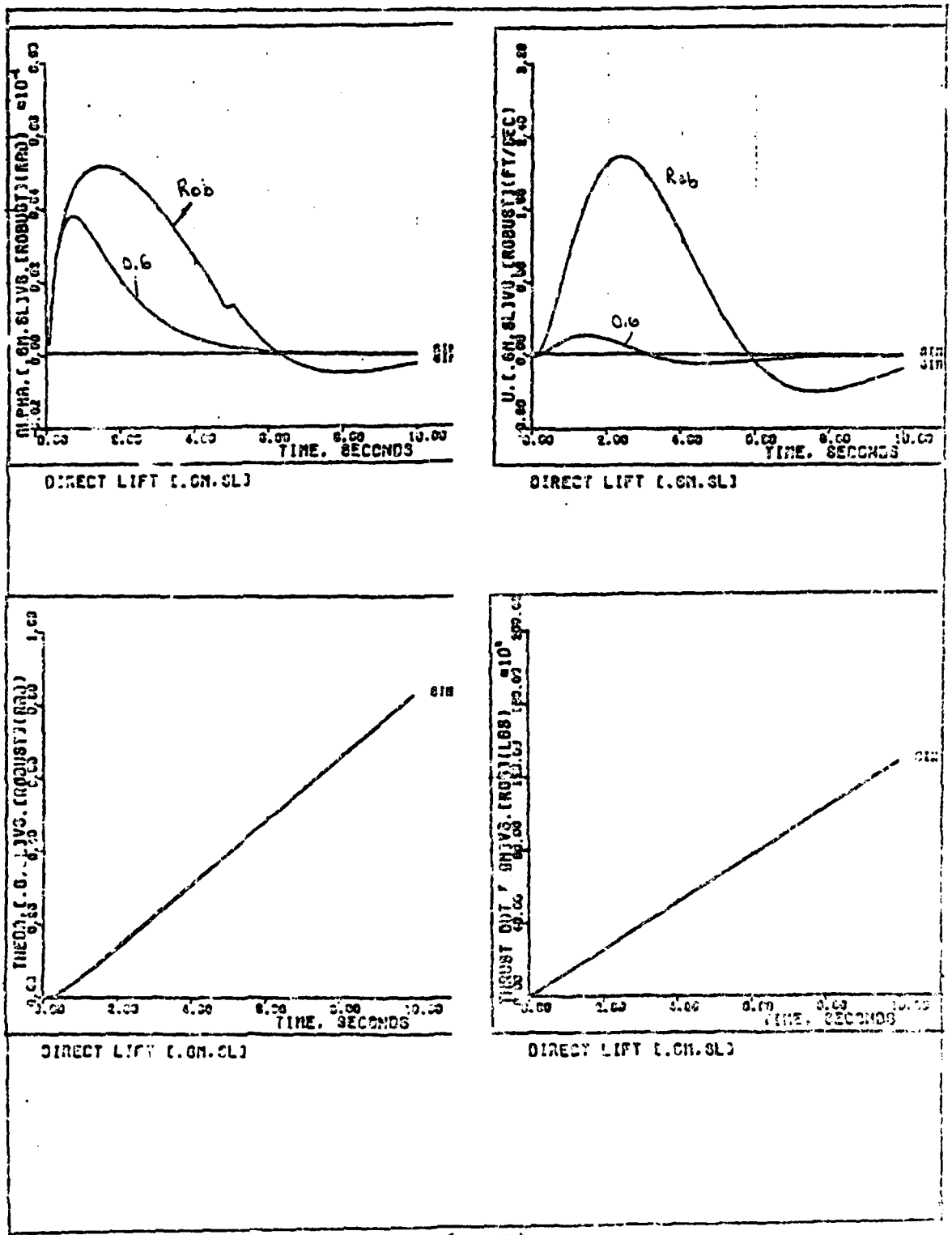



Fig 43. 1.8-g Direct Lift (.6M SL)

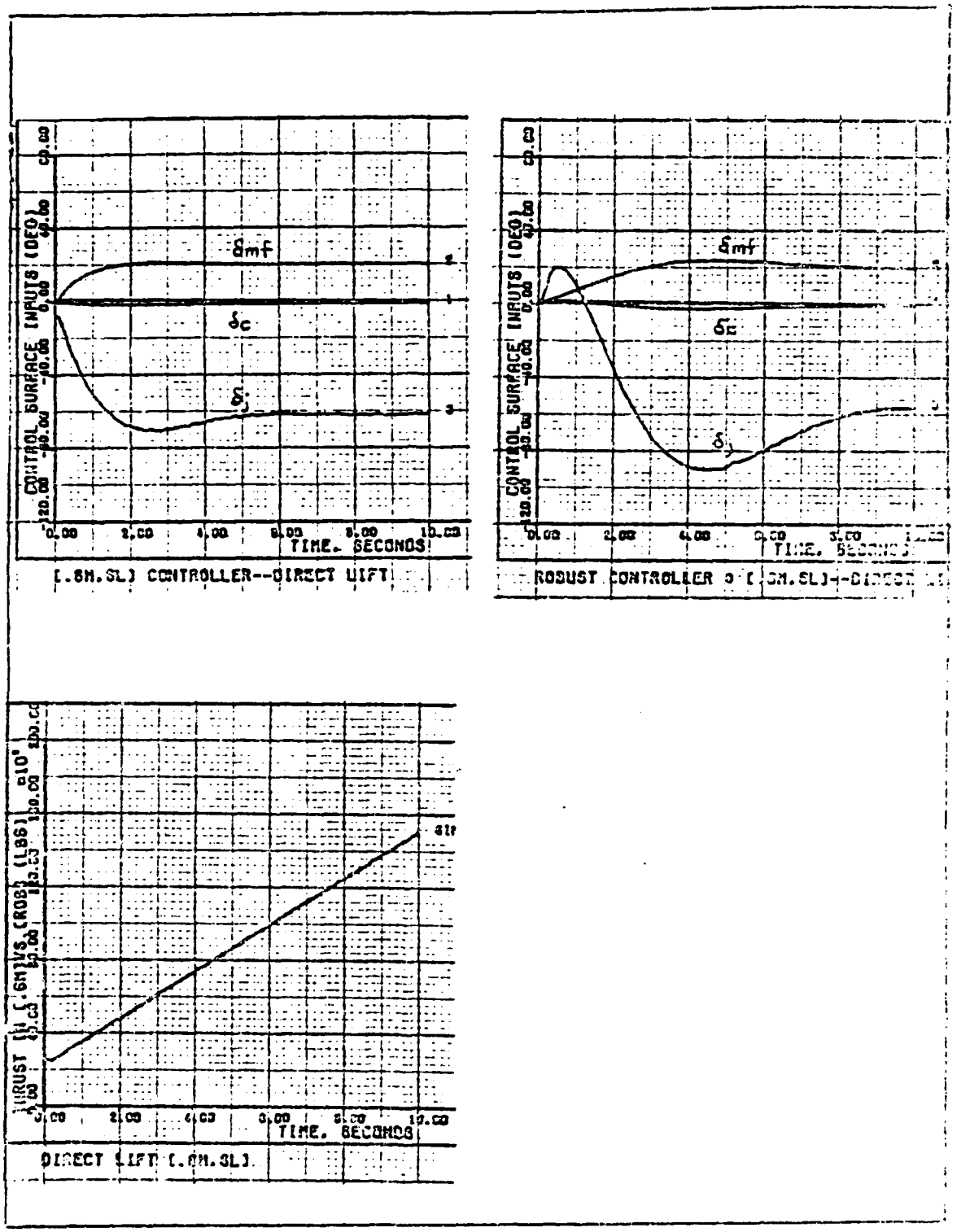



Fig 44. 1.8-g Direct Lift (.6M,SL)

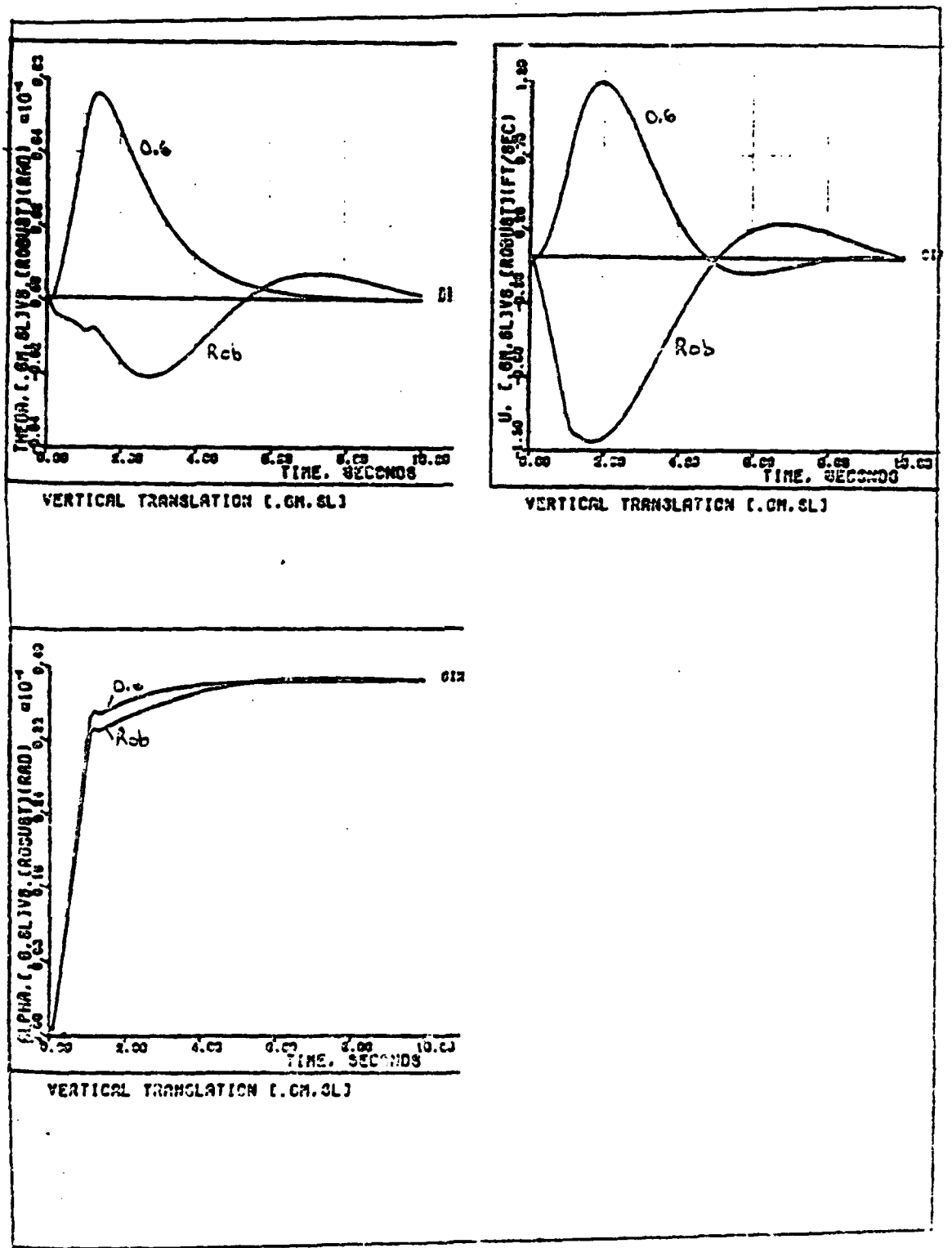



Fig 45. 0.8-g Vertical Translation (.6M,SL)

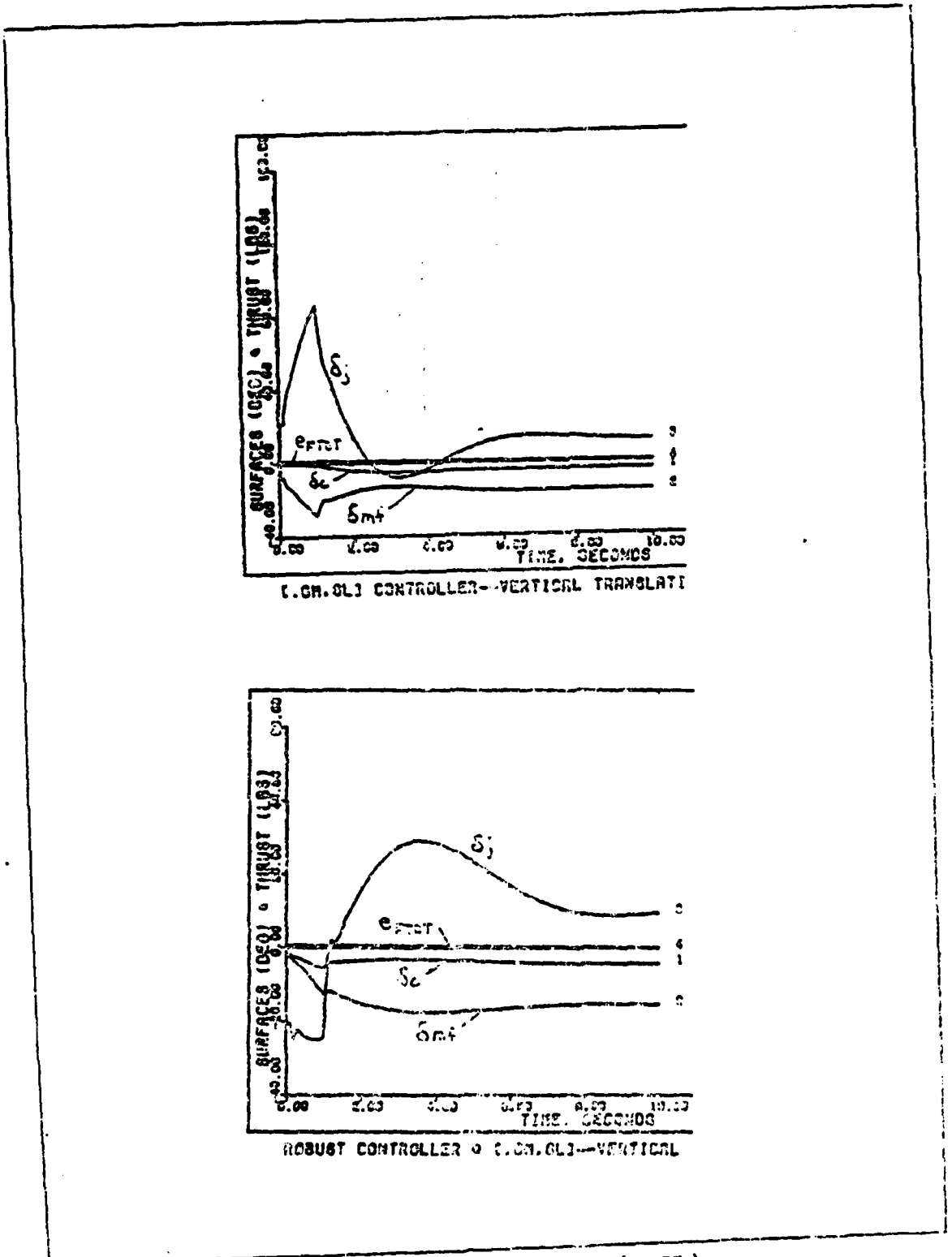



Fig 46. 0.8-g Vertical Translation (.6M,3L)

to the 0.6 Mach controller. This is the only case where this occurs in the robustness testing. Performance of the rollover, yaw pointing, and direct lift maneuvers is approximately the same when performed by the "universal" or 0.6 Mach controller. Vertical translation, horizontal translation and pitch pointing maneuver performance is down-graded somewhat to a level which may or may not be unacceptable when using the "universal" controller. The flat turn maneuver performance when using the "universal" controller is stable but unacceptable in most instances due to the long settling time.

0.9 Mach, 30,000 ft. Flight Condition

The "universal" controller contains the longitudinal part of the controller designed to operate at the 0.9 Mach, 30,000 ft. condition. Because of this, performance of the longitudinal maneuvers (pitch pointing, direct lift, and horizontal translation) is identical for both the "universal" and 0.9 Mach controllers, as shown in Figures 47 through 64. Laterally, the yaw pointing, rollover and flat turn maneuver performance is approximately the same for both the "universal" controller and the 0.9 Mach controller. The flat turn maneuver performance when using the "universal" controller can be further improved over the 0.9 Mach controller by decreasing the rise time in the command input (see Table VIII). When this is attempted on the 0.9 controller, unacceptably large oscillations occur in the body axis yaw rate output r. Horizontal translation maneuver performance is degraded when using the "universal" controller compared with that when using the 0.9

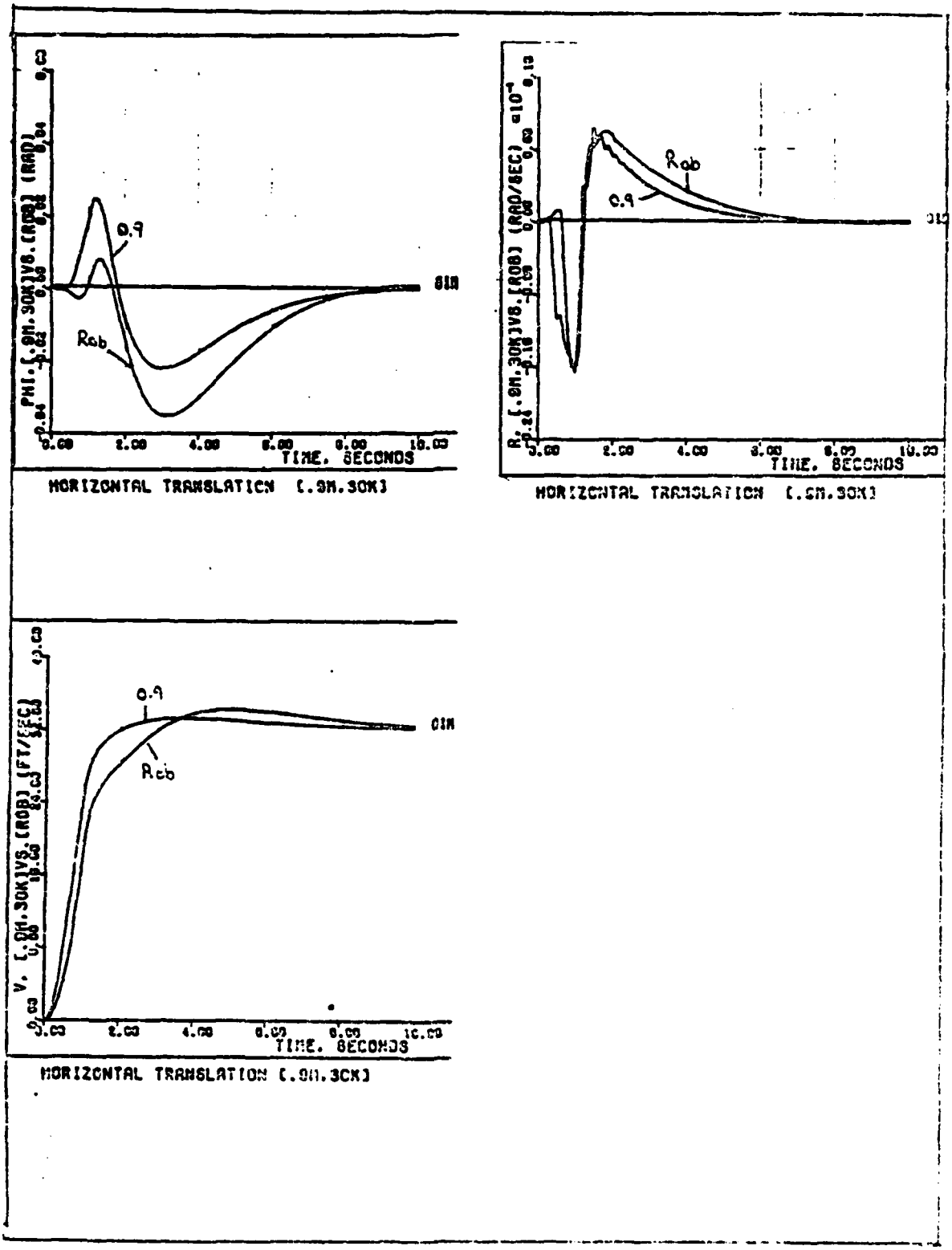



Fig 47. 1-g Horizontal Translation (.9M,30K)

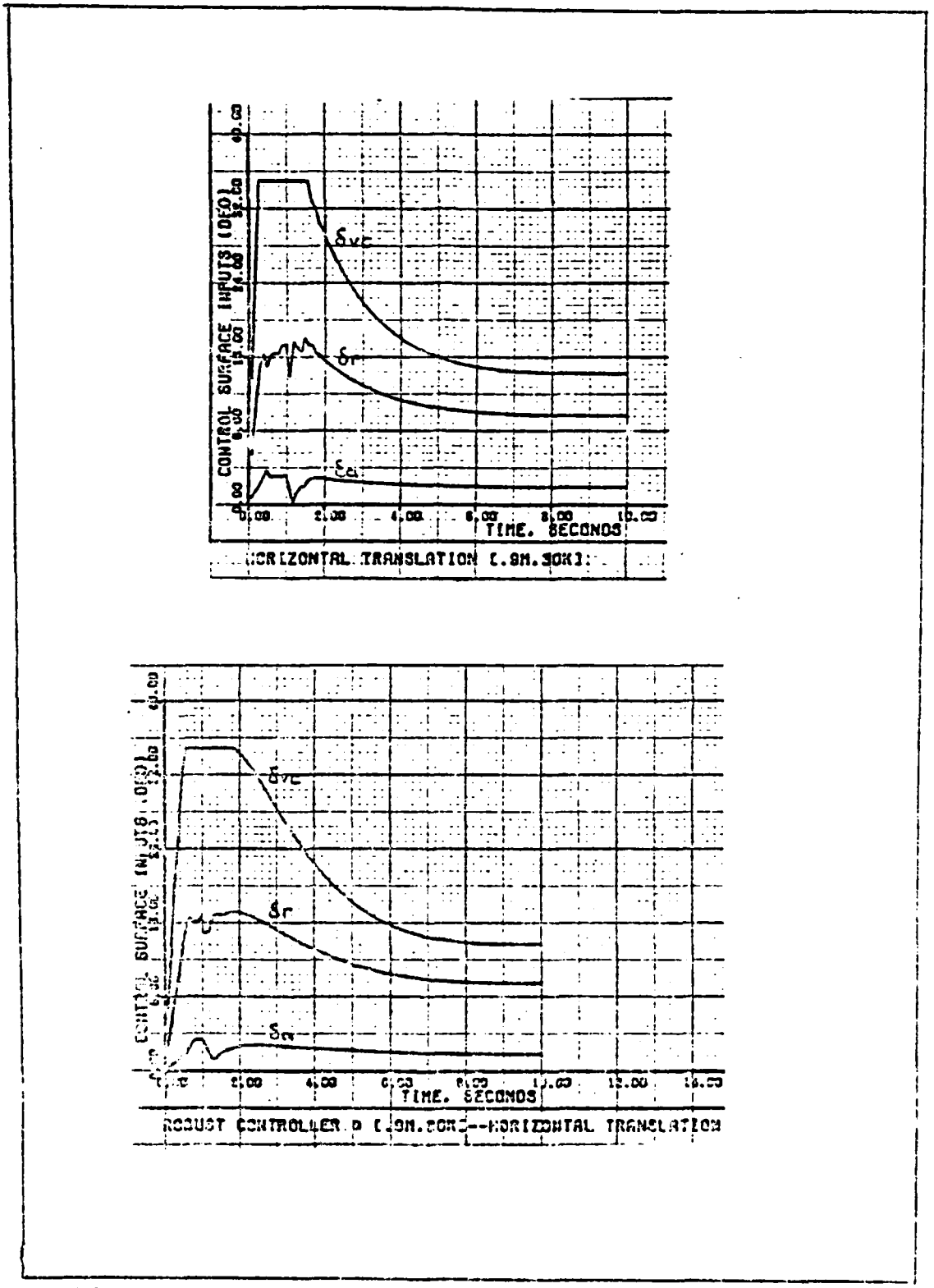



Fig 48. 1-g Horizontal Translation (.9M,30K)

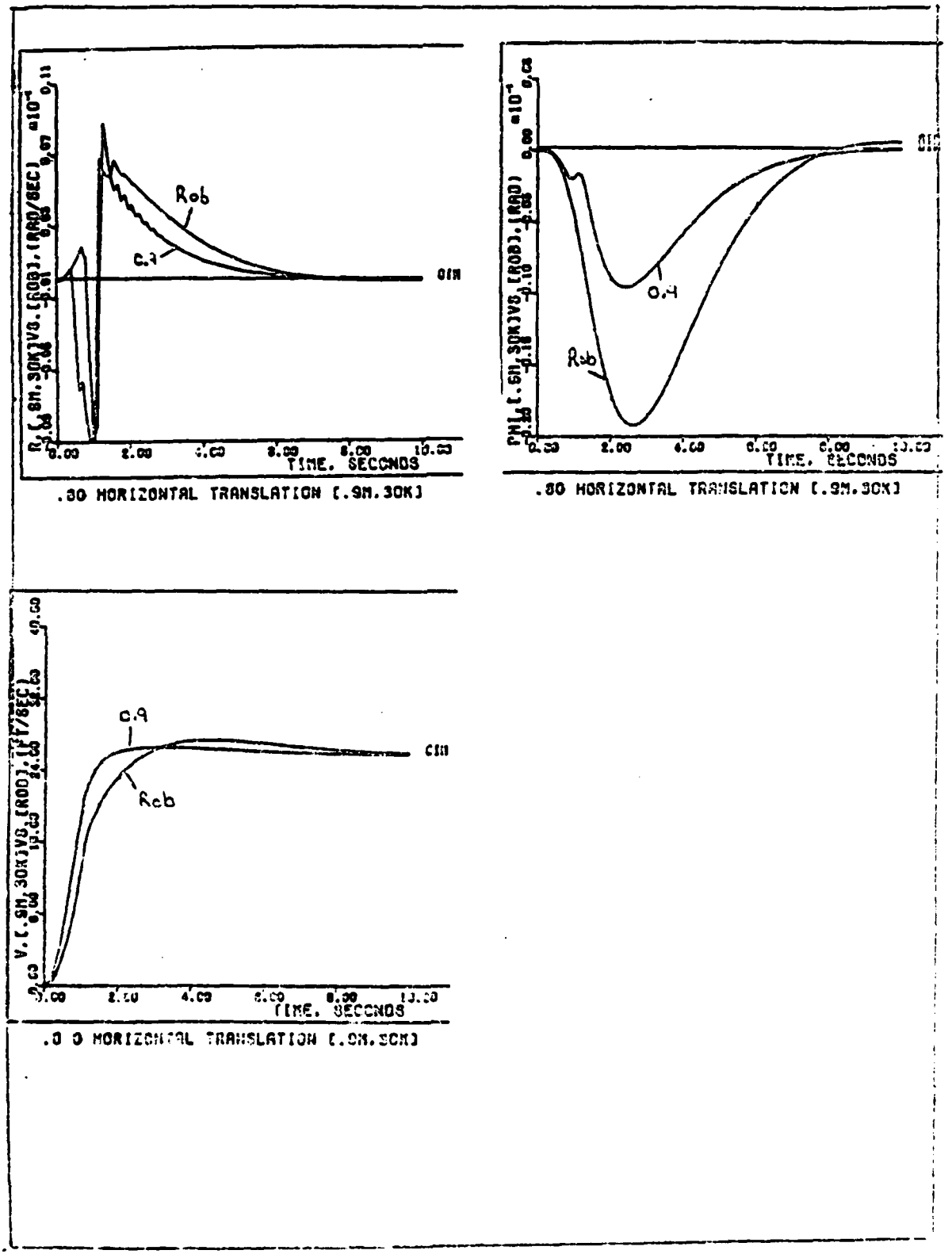



Fig 49. 0.8-g Horizontal Translation (.9M,30K)

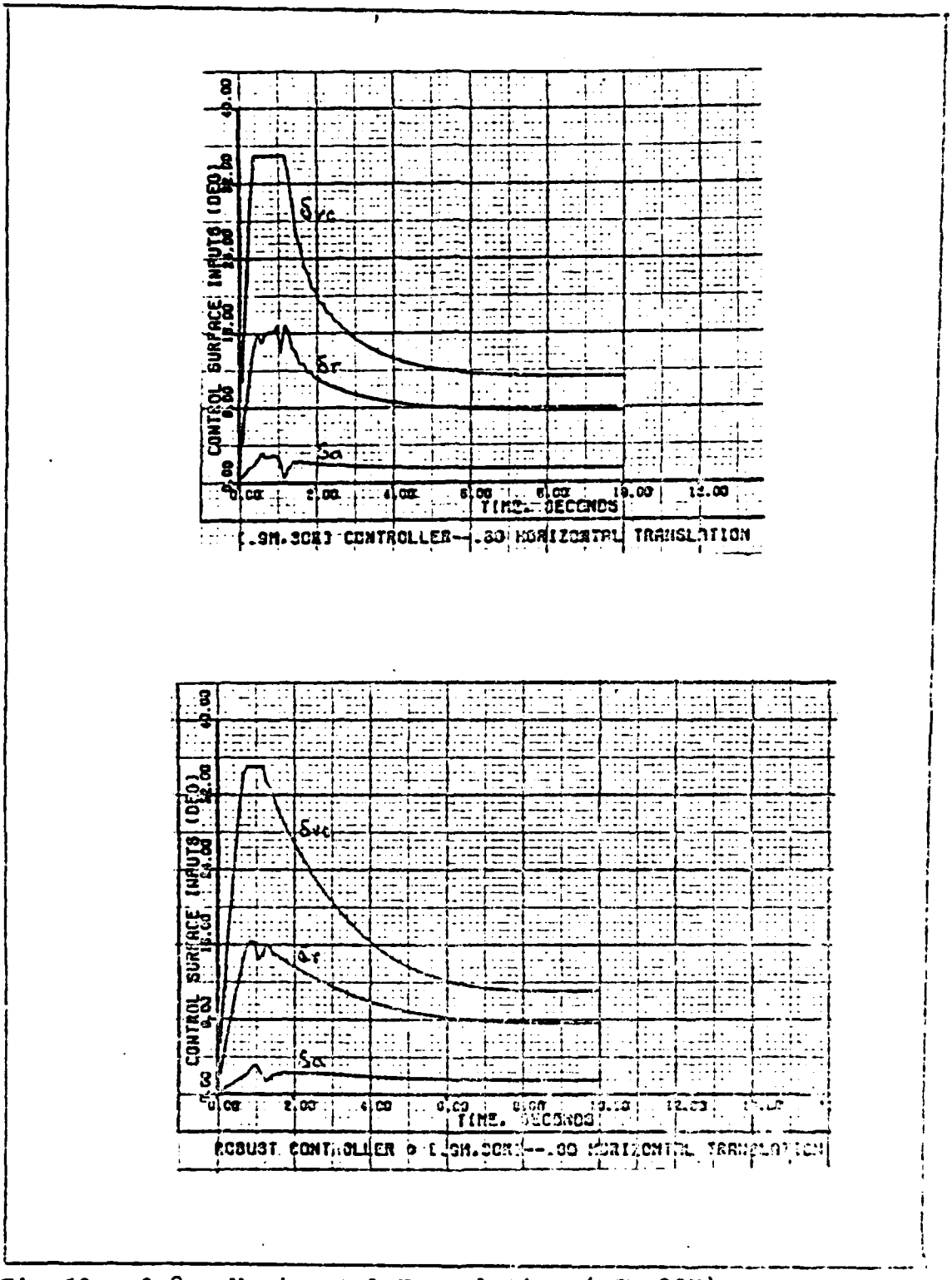



Fig 50. 0.8-g Horizontal Trnaslation (.9M,30K)

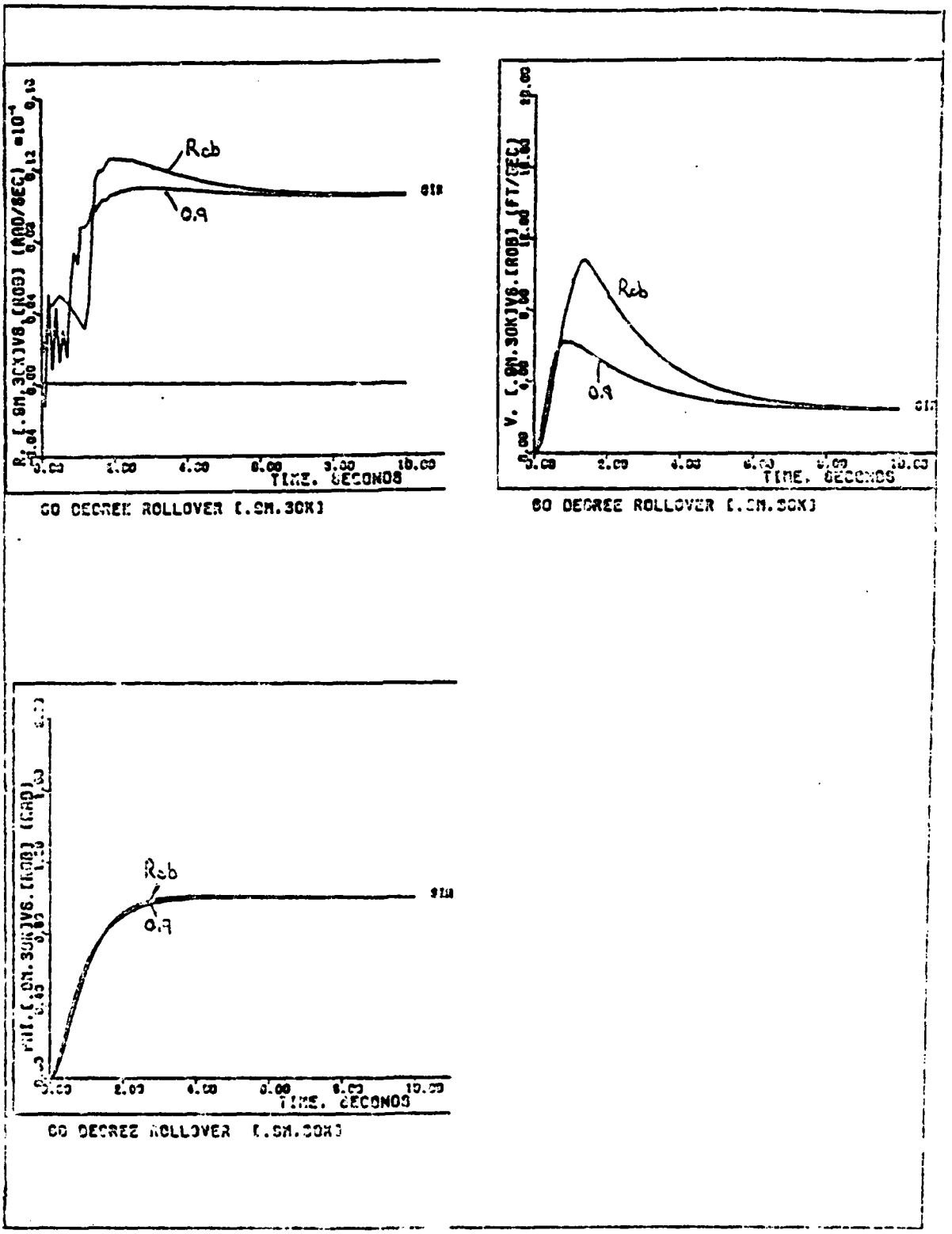



Fig 51. 60 Degree Rollover (.9M.30K)

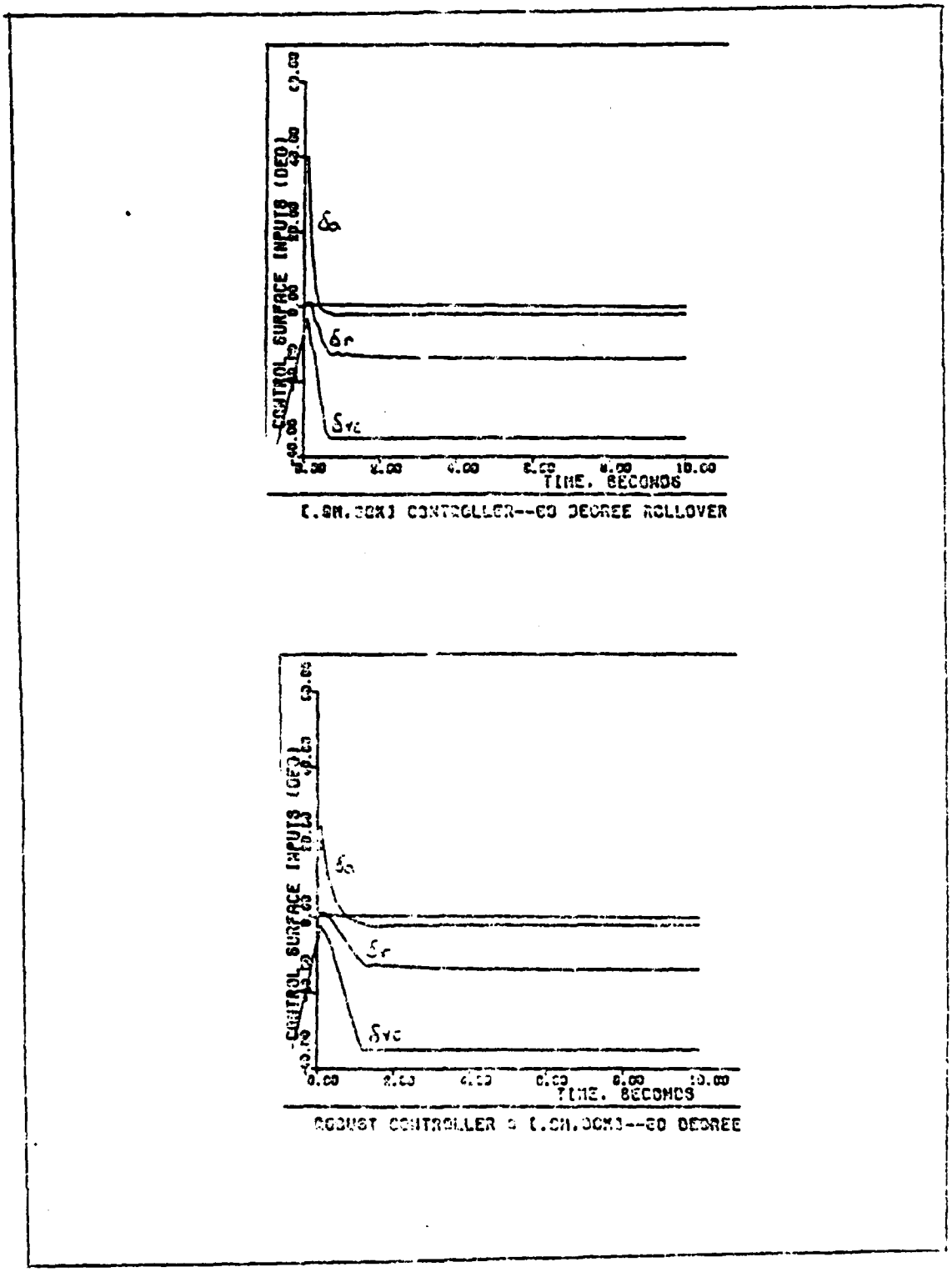



Fig 52. 60 Degree Rollover (.9M,30K)

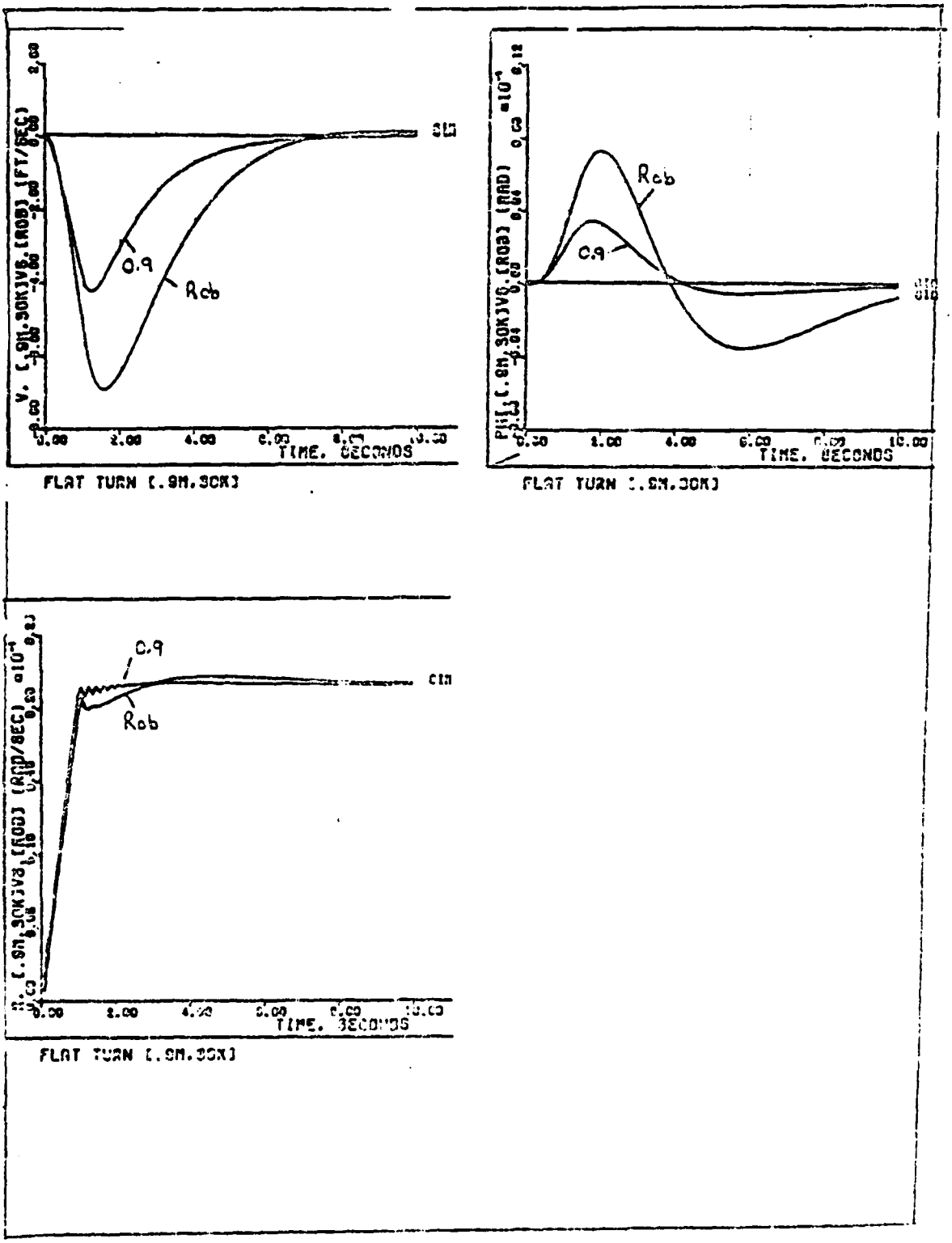
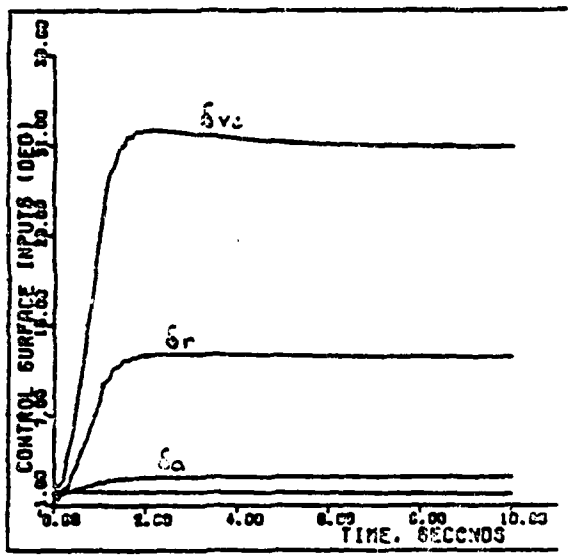
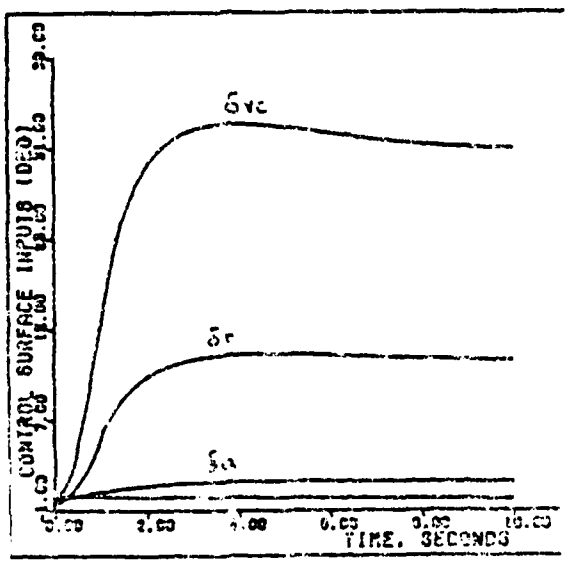



Fig 53. 0.6-g Flat Turn (.9M,30K)




(.9M,30K) CONTROLLER--FLAT TURN




ROBUST CONTROLLER @ (.9M,30K)--FLAT TURN

Fig 54. 0.6-g Flat Turn (.9M,30K)

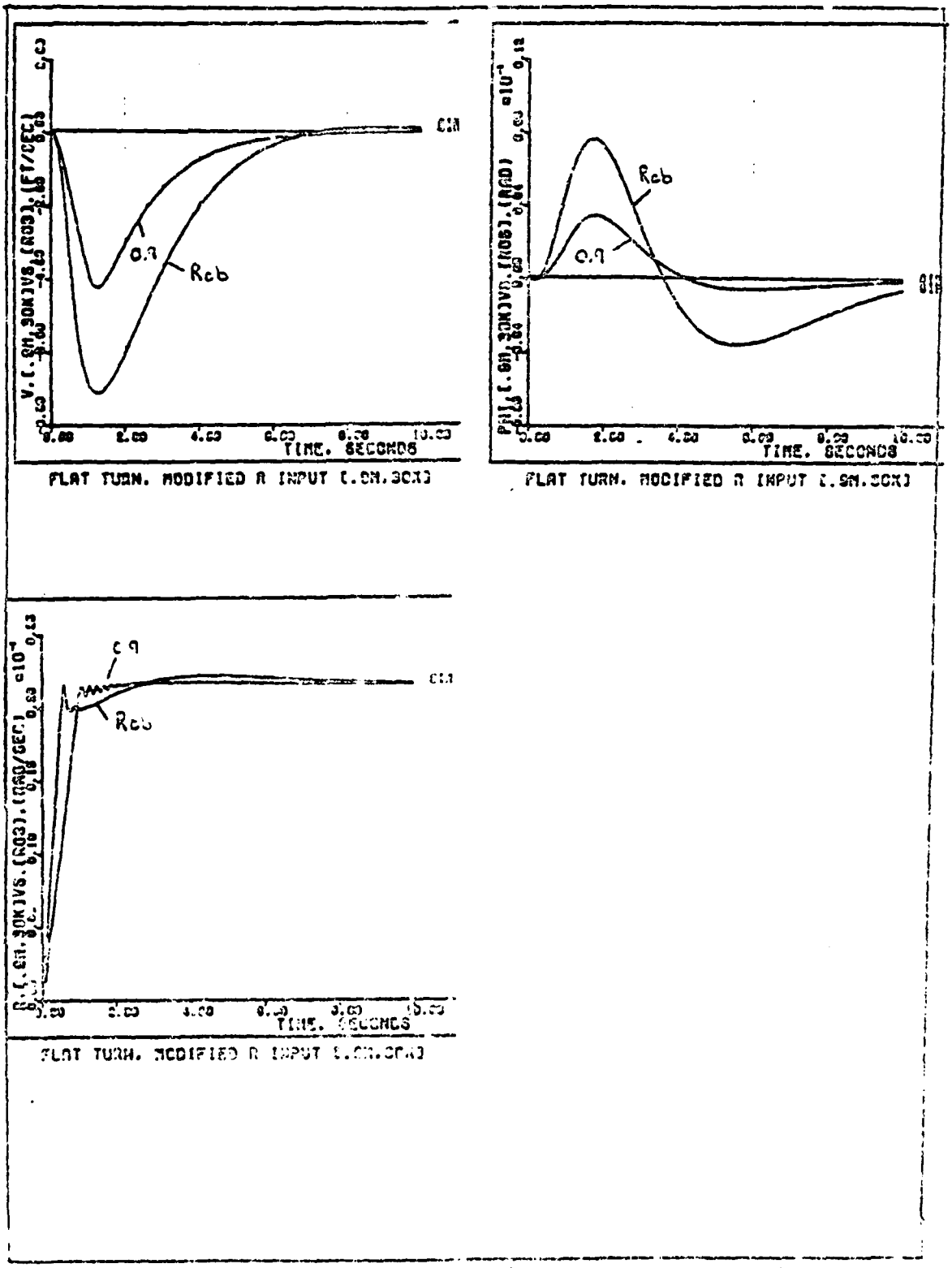
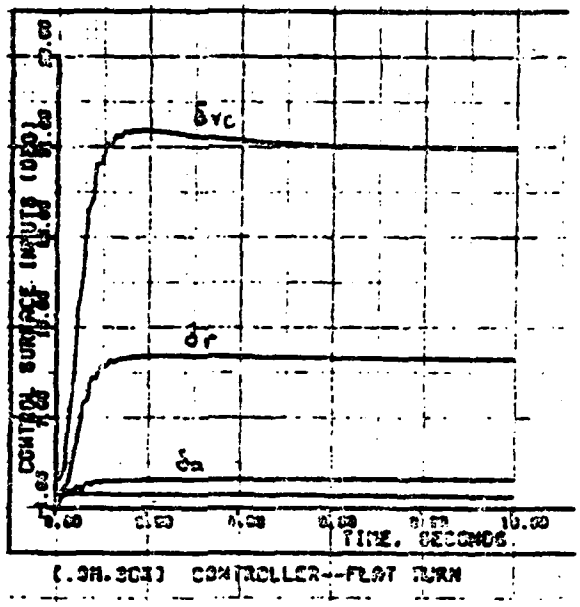



Fig 55. 0.6-g Flat Turn, Modified R Input (.9M.30K)



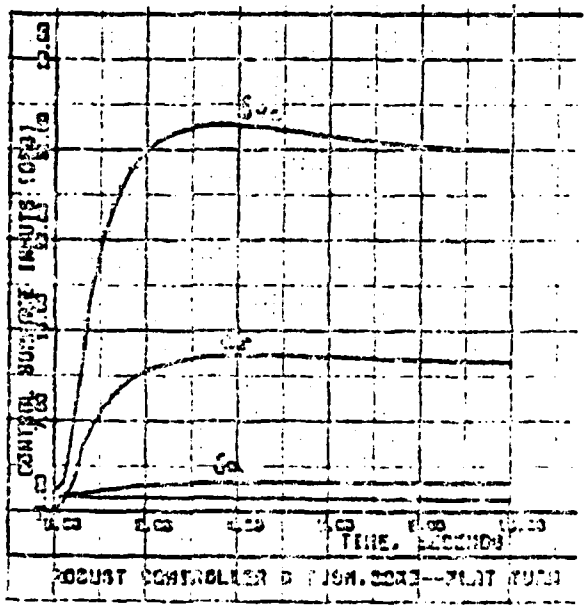




Fig 56. 0.6-g Flat Turn, Modified R Input (.9M,30K)

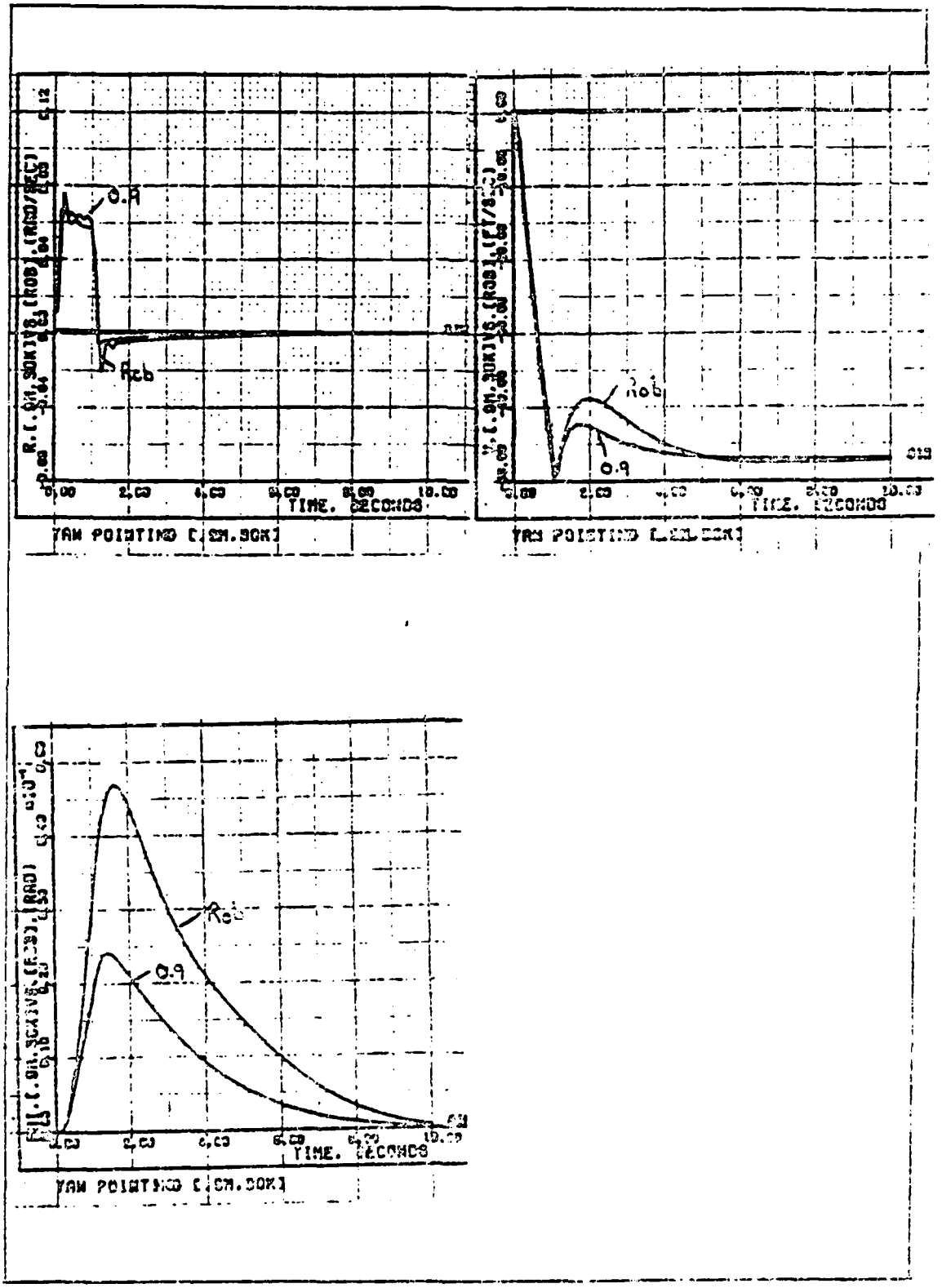
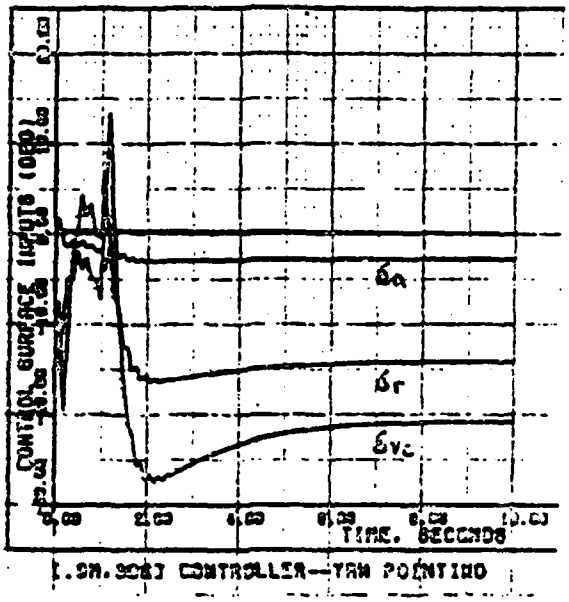
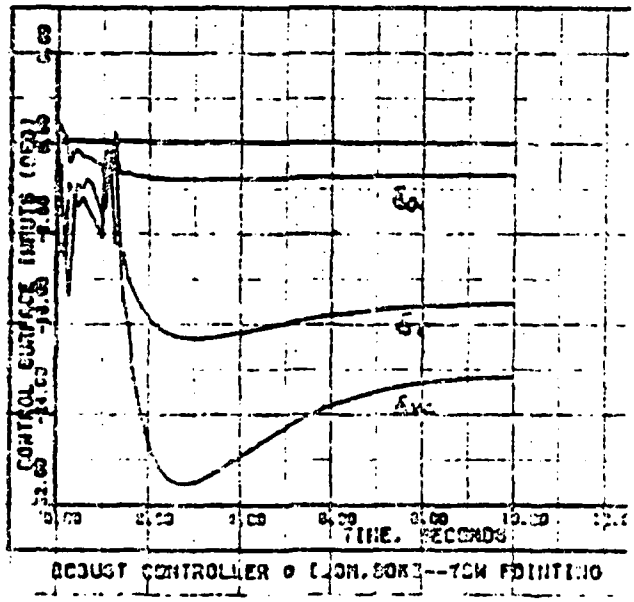



Fig 57. 3 Degree Yaw Pointing (.9M,30K)

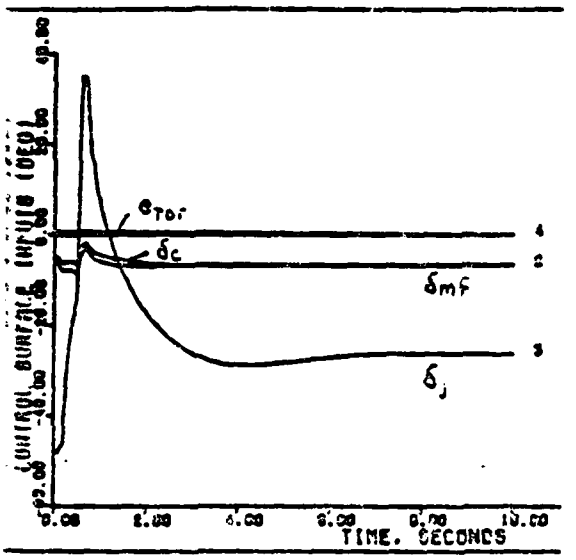



[.9M,30K] CONTROLLER--YAW POINTING

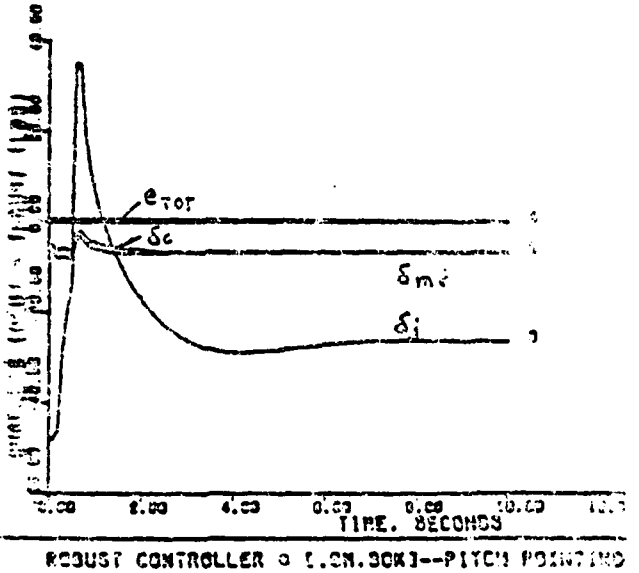



ADJUST CONTROLLER @ [.9M,30K]--YAW POINTING

Fig 58. 3 Degree Yaw Pointing (.9M,30K)




[.9,30K] CONTROLLER--YAW POINTING




ROBUST CONTROLLER @ [.9N,30K]--PITCH POINTING

Fig 59. 3 Degree Pitch Pointing (.9M,30K)

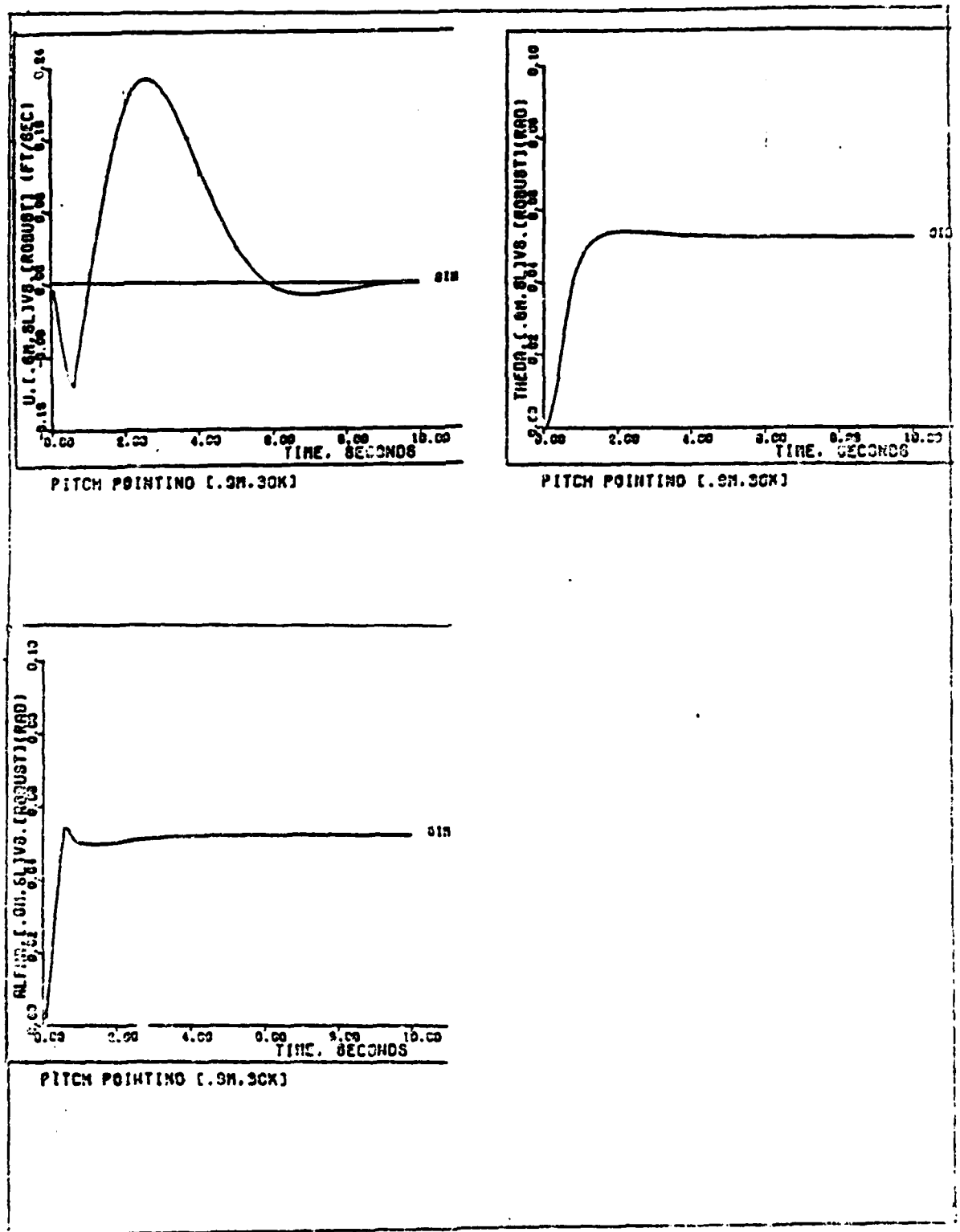



Fig 60. 3 Degree Pitch Pointing (.9M,3CK)

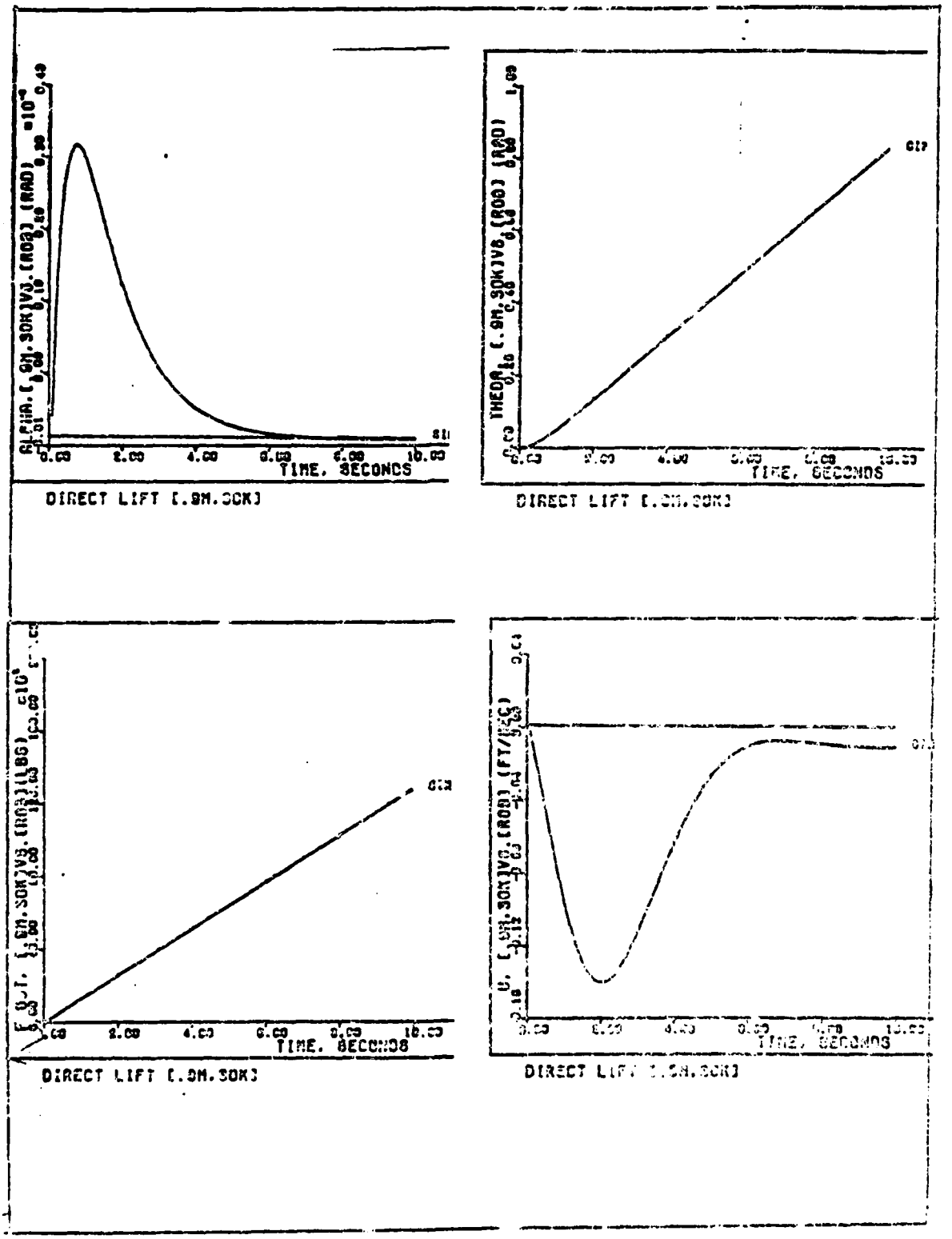



Fig 61. 2.4-g Direct Lift (.9M,30K)

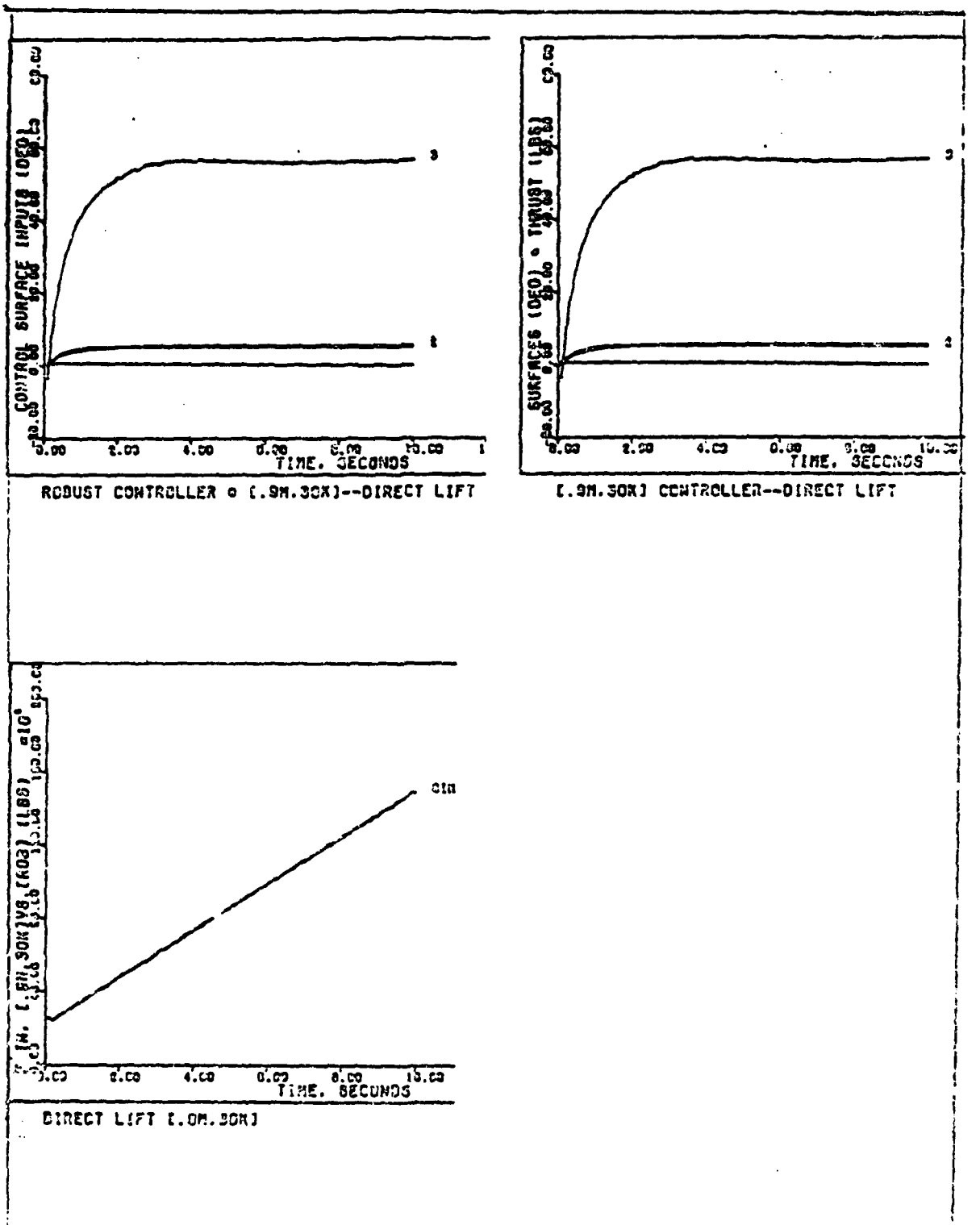



Fig 62. 2.4-g Direct Lift (.9M,30K)

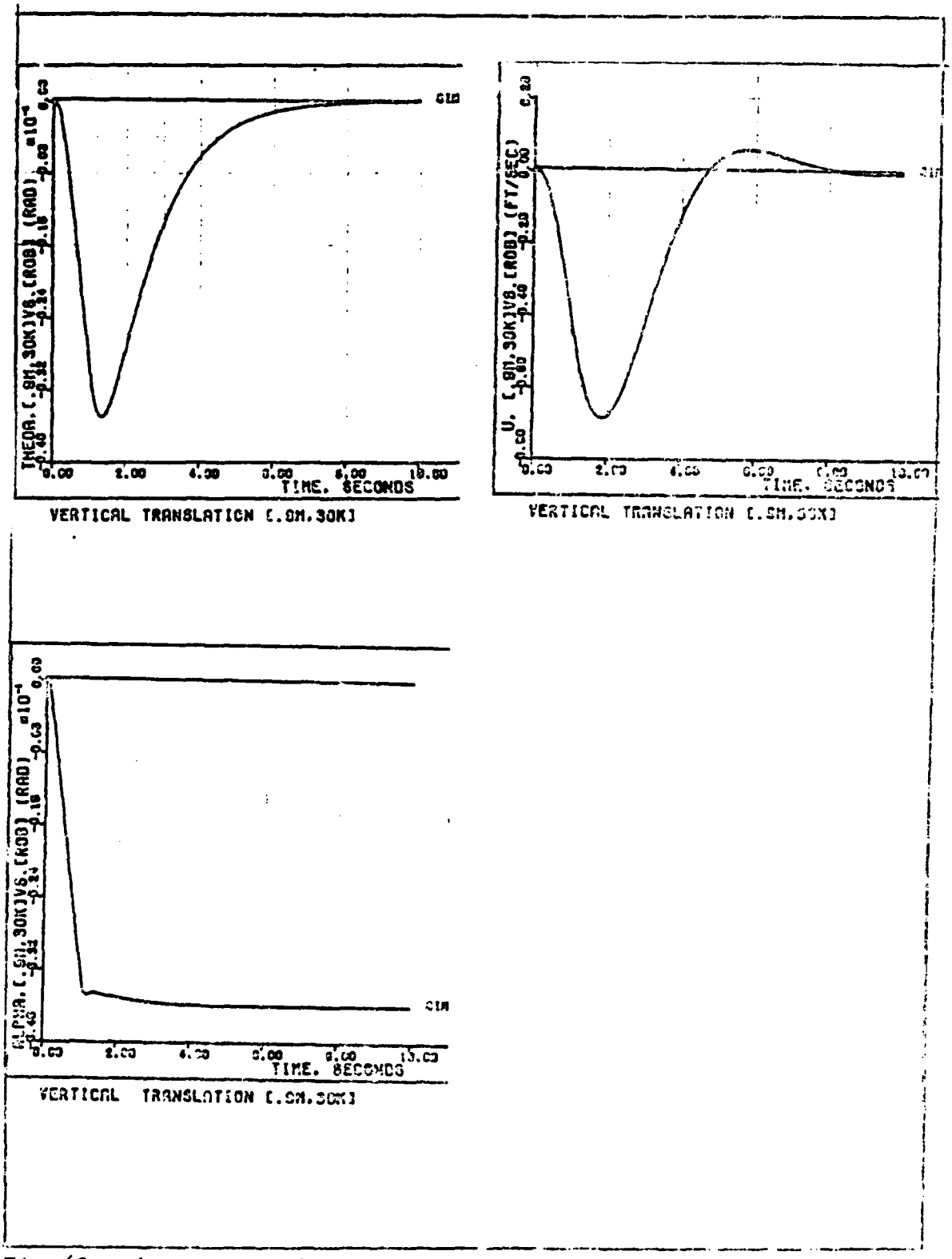
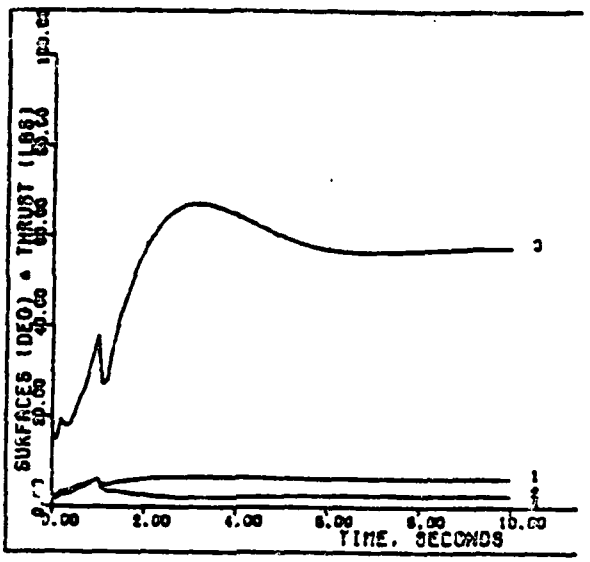
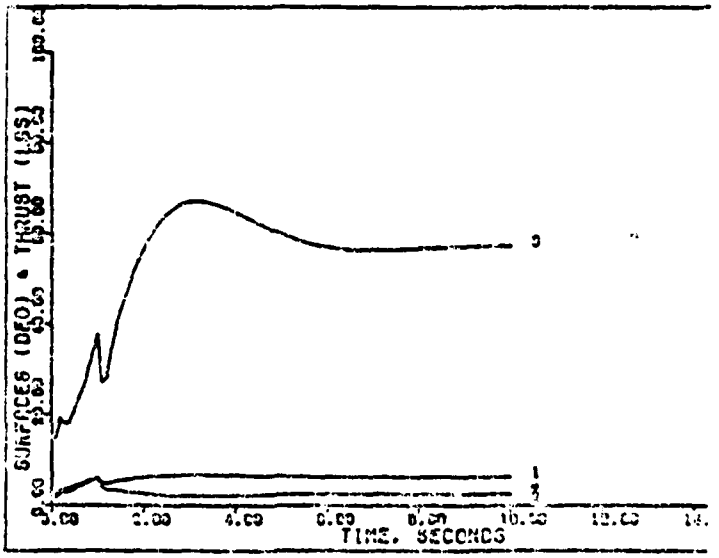



Fig 63. 1-g Vertical Translation (.8M,30K)




[.9,30K] CONTROLLER--VERTICAL TRANSLATION




ROBUST CONTROLLER 9 [.9M,30K]--VERTICAL TRANSLATION

Fig 64. 1-g Vertical Translation (.9M,30K)

Mach controller. This is mostly due to the fact that the vertical canards reach their limits sooner when using the "universal" controller than when using the 0.9 Mach controller (see figures 48 and 50). When a smaller magnitude of the side velocity v is commanded, the difference in maneuver performance between the "universal" and the 0.9 Mach controllers decreases (see Tables VII and VIII).

2.3 Mach, 40,000 ft. Flight Condition

The "universal" controller contains the lateral part of the controller designed to operate at the 2.3 Mach, 40,000 ft. flight condition. Because of this, performance of the lateral maneuvers (horizontal translation, rollover, flat turn, and yaw pointing) is identical for both the "universal" and the 2.3 Mach controllers, as shown in Figures 65 through 78. Longitudinally, pitch pointing and direct lift maneuver performance is approximately the same for both the "universal" controller and the 2.3 Mach controller. Vertical translation maneuver performance is degraded somewhat when using the "universal" controller over that achieved using the 2.3 controller due to the oscillations in the output $\alpha$ (see Figure 77). This degradation is not extreme and may be acceptable in most instances.

Conclusions

Table VIII summarizes maneuver performance using the "universal" or "robust" controller for each flight condition tested. Comparing Table VIII to Tables VI and VI along with

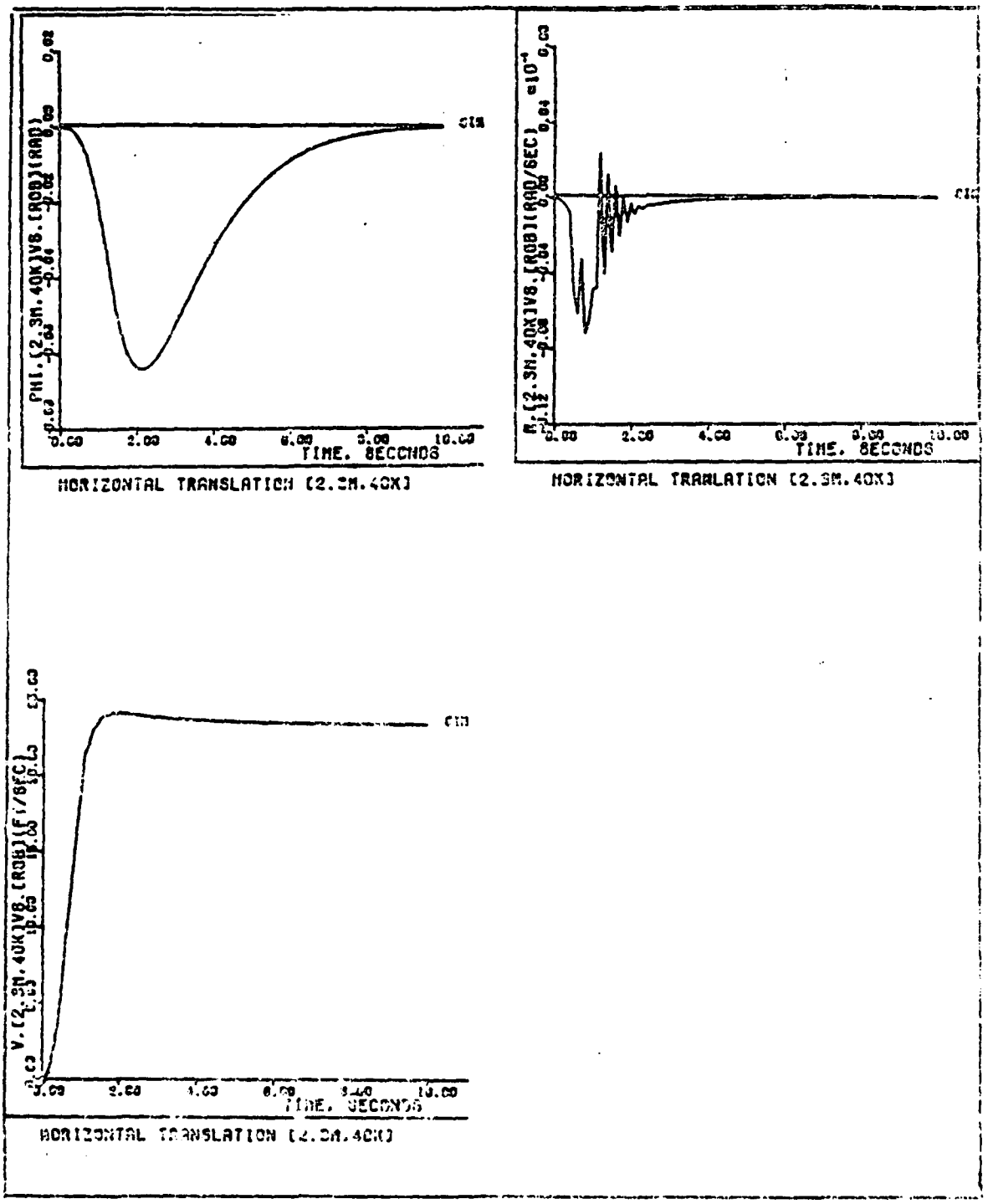



Fig 65. 0.7-g Horizontal Translation (2.3M,40X)

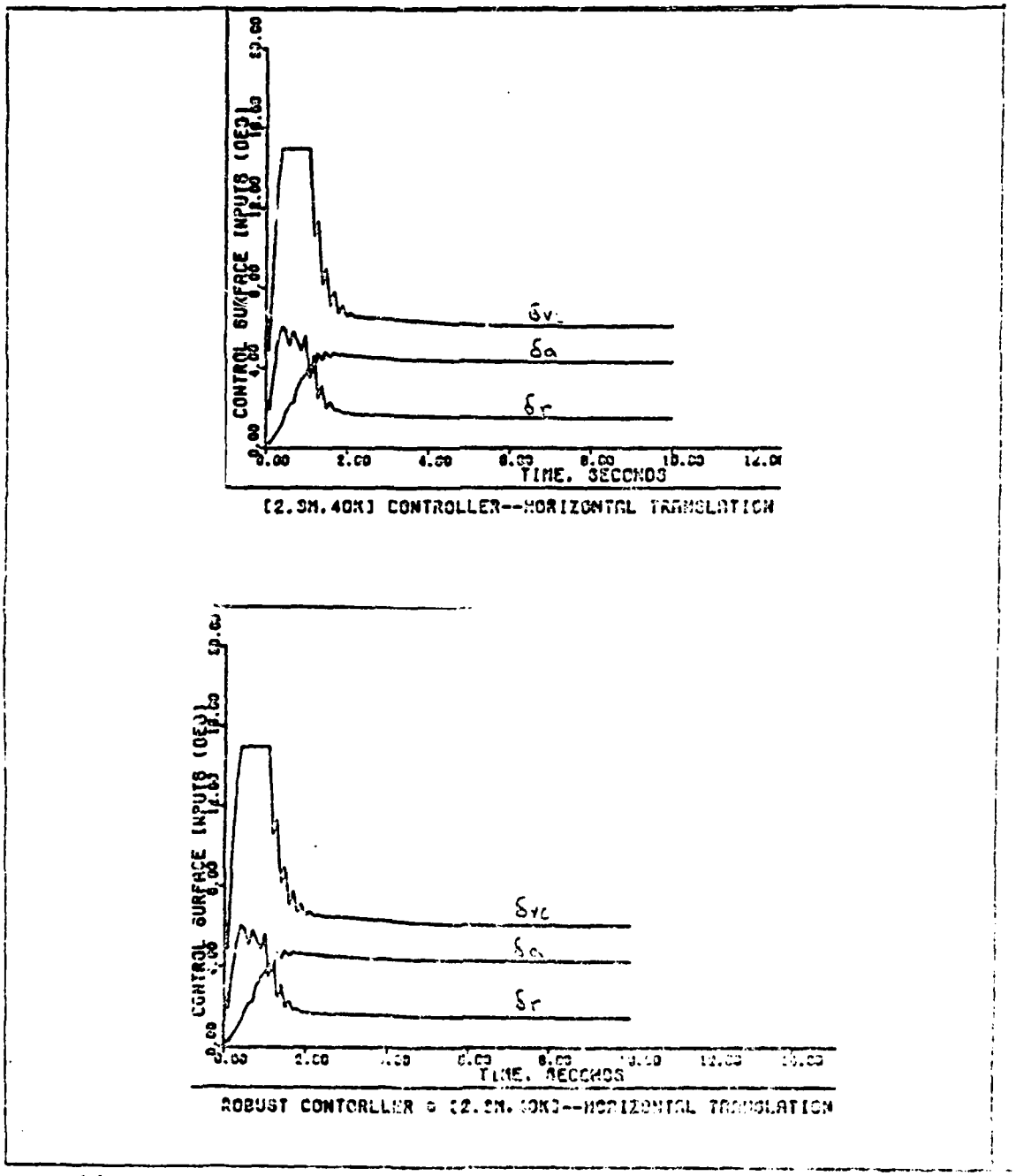



Fig 66. 0.7-g Horizontal Translation (2.3M,40K)

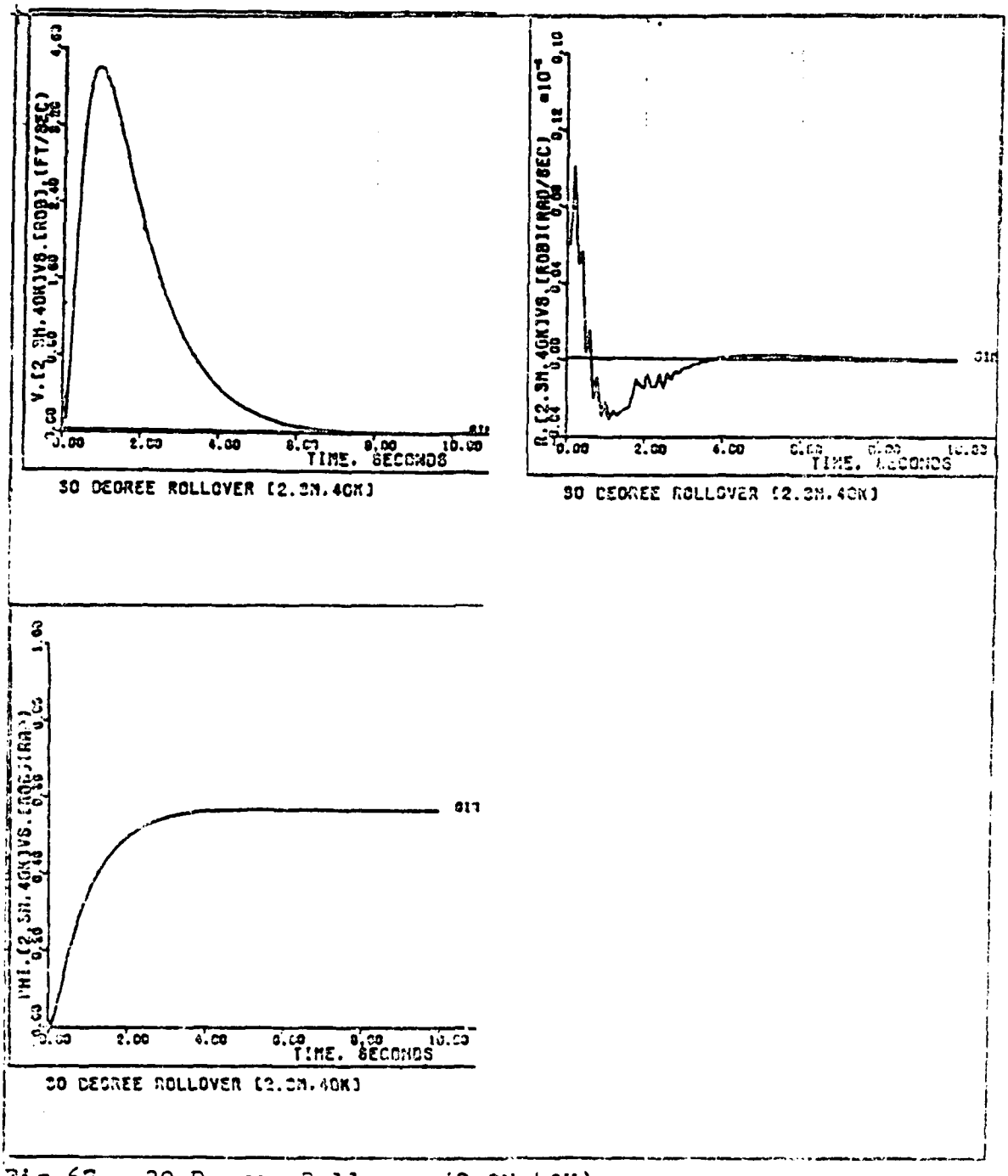
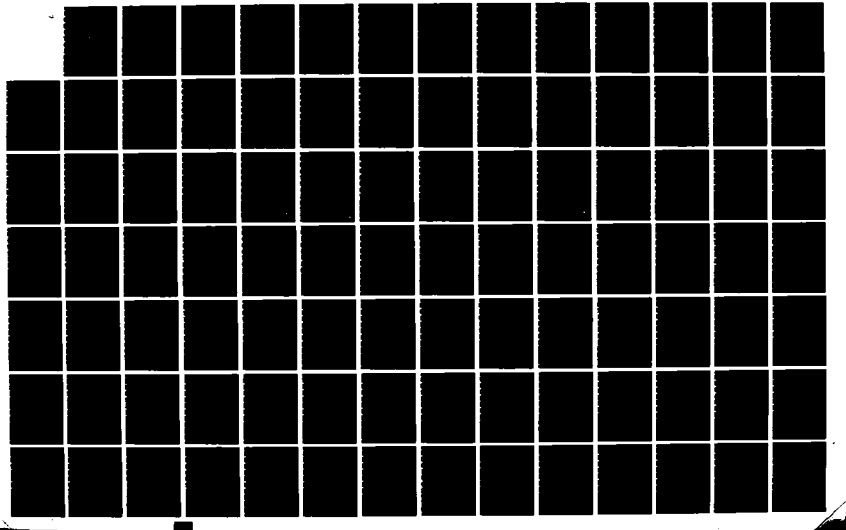
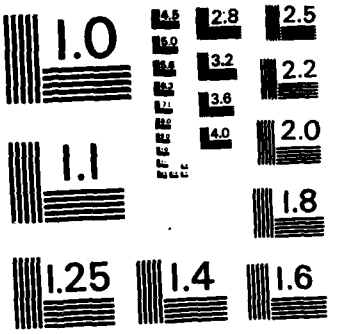



Fig 67. 30 Degree Rollover (2.3M,40K)

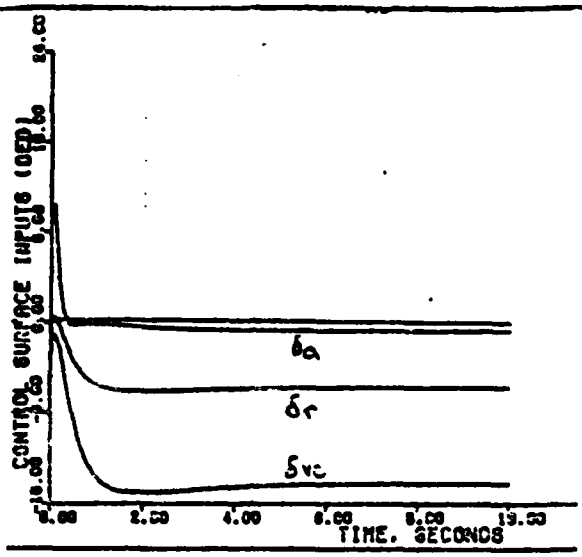
AD-A139 050 PROCEEDINGS OF THE WORKSHOP ON MULTIVARIABLE CONTROL SYSTEMS HELD AT WRIG..(U) AIR FORCE WRIGHT AERONAUTICAL LABS WRIGHT-PATTERSON AFB OH M A MASI ET AL. SEP 83 5/7

UNCLASSIFIED AFWAL-TR-83-3093 FFG 1/3 NL

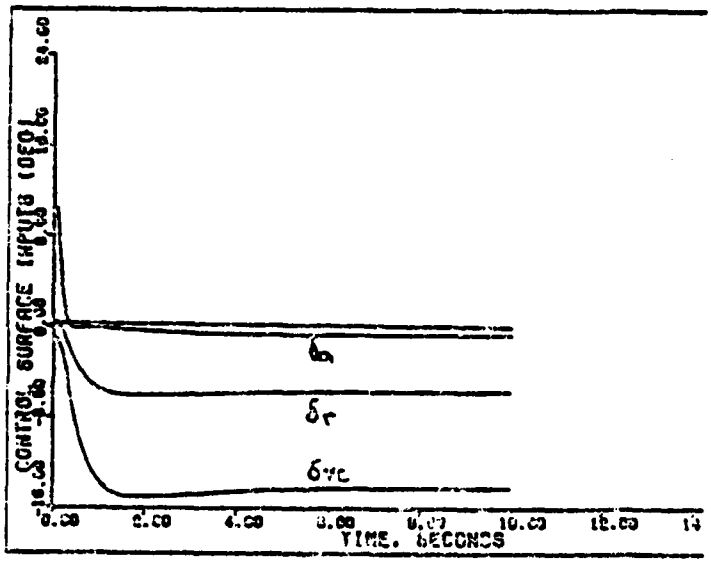





MICROCOPY RESOLUTION TEST CHART
NATIONAL BUREAU OF STANDARDS-1963-A




[2.3M,40K] CONTROLLER--30 DEGREE ROLLOVER




ROBUST CONTROLLER @ [2.3M,40K]--30 DEGREE ROLLOVER

Fig 68. 30 Degree Rollover (2.3M,40K)

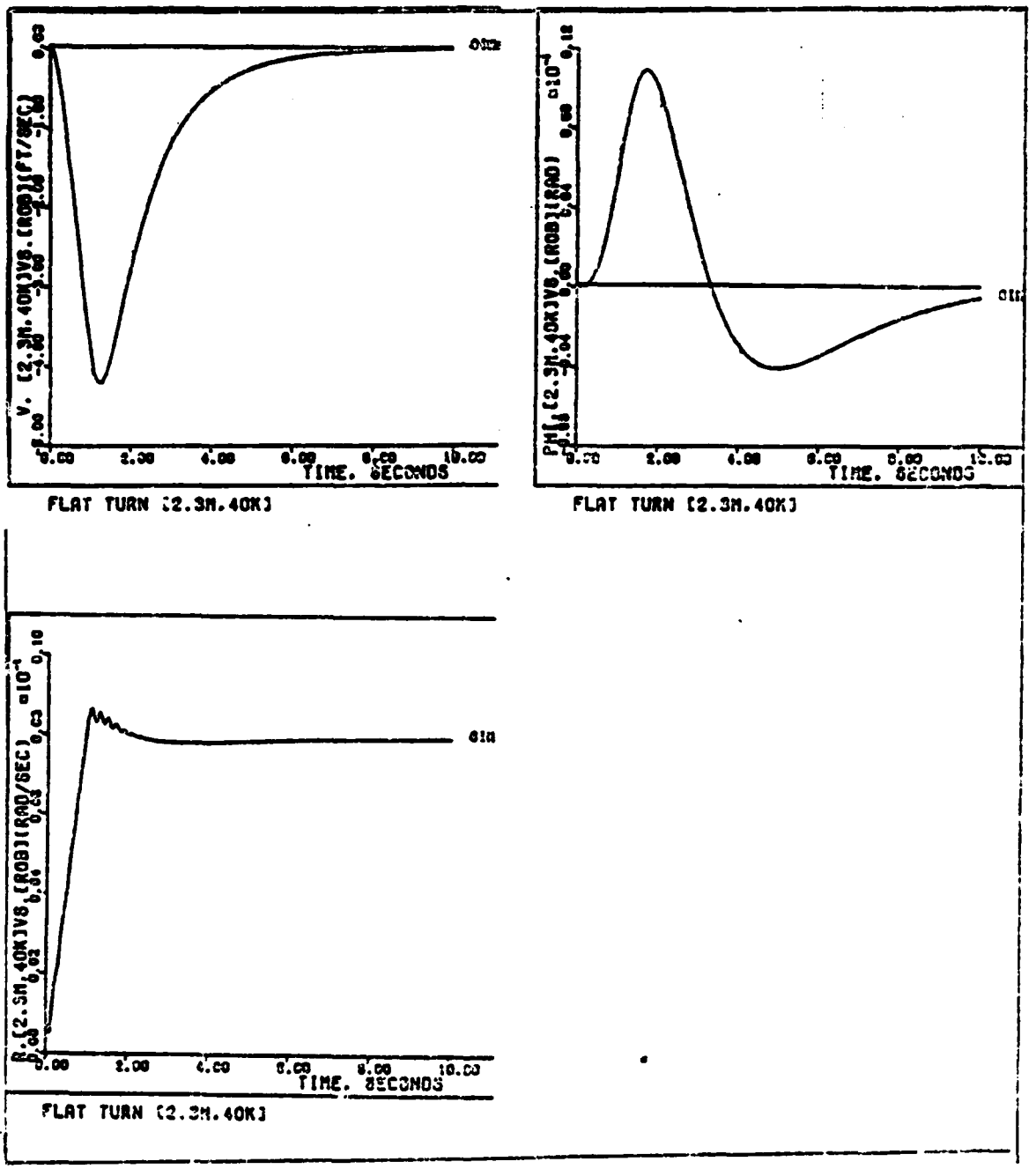



Fig 69. 0.6-g Flat Turn (2.3M,40K)

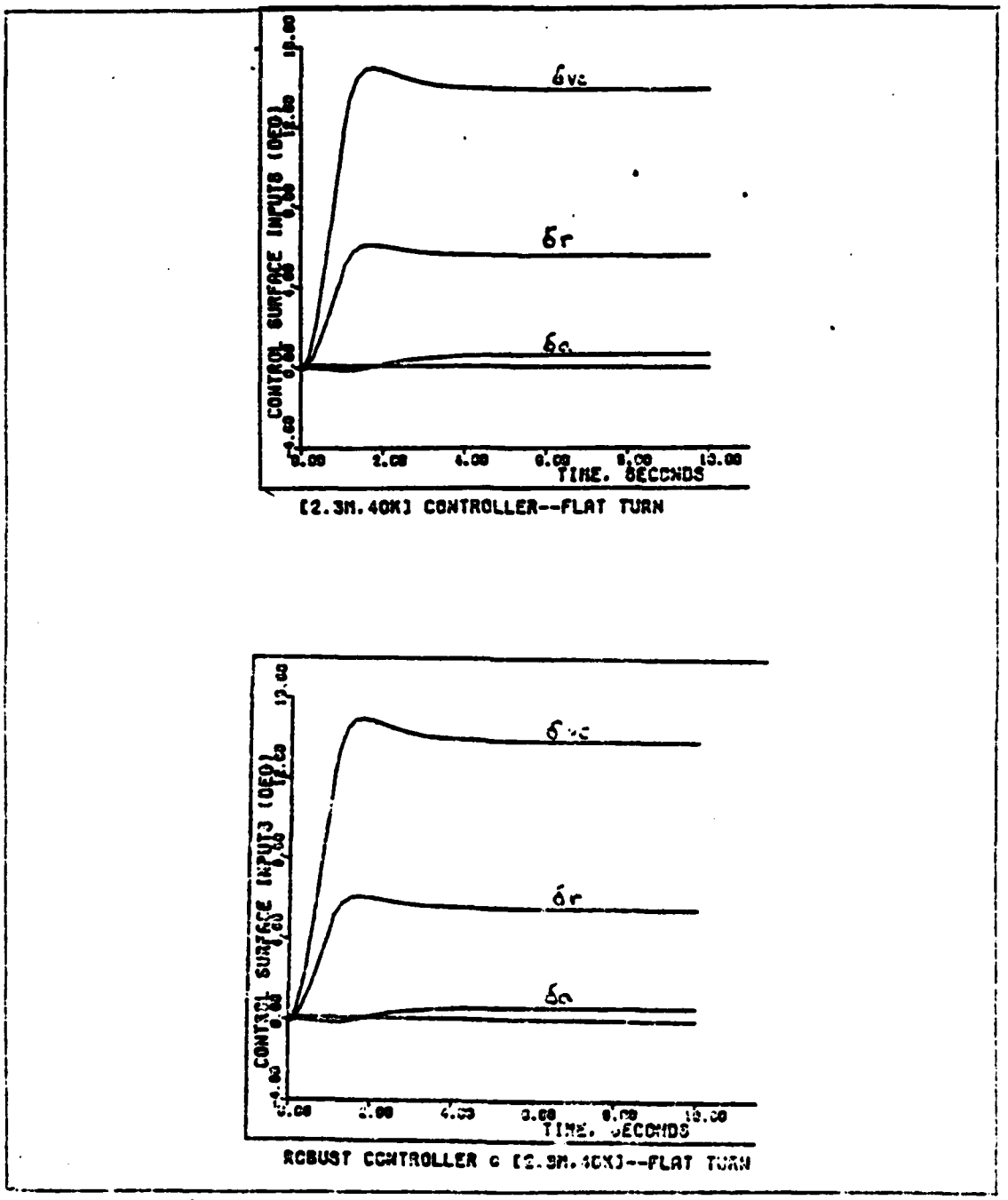



Fig 70. 0.6-g Flat Turn (2.3M,40K)

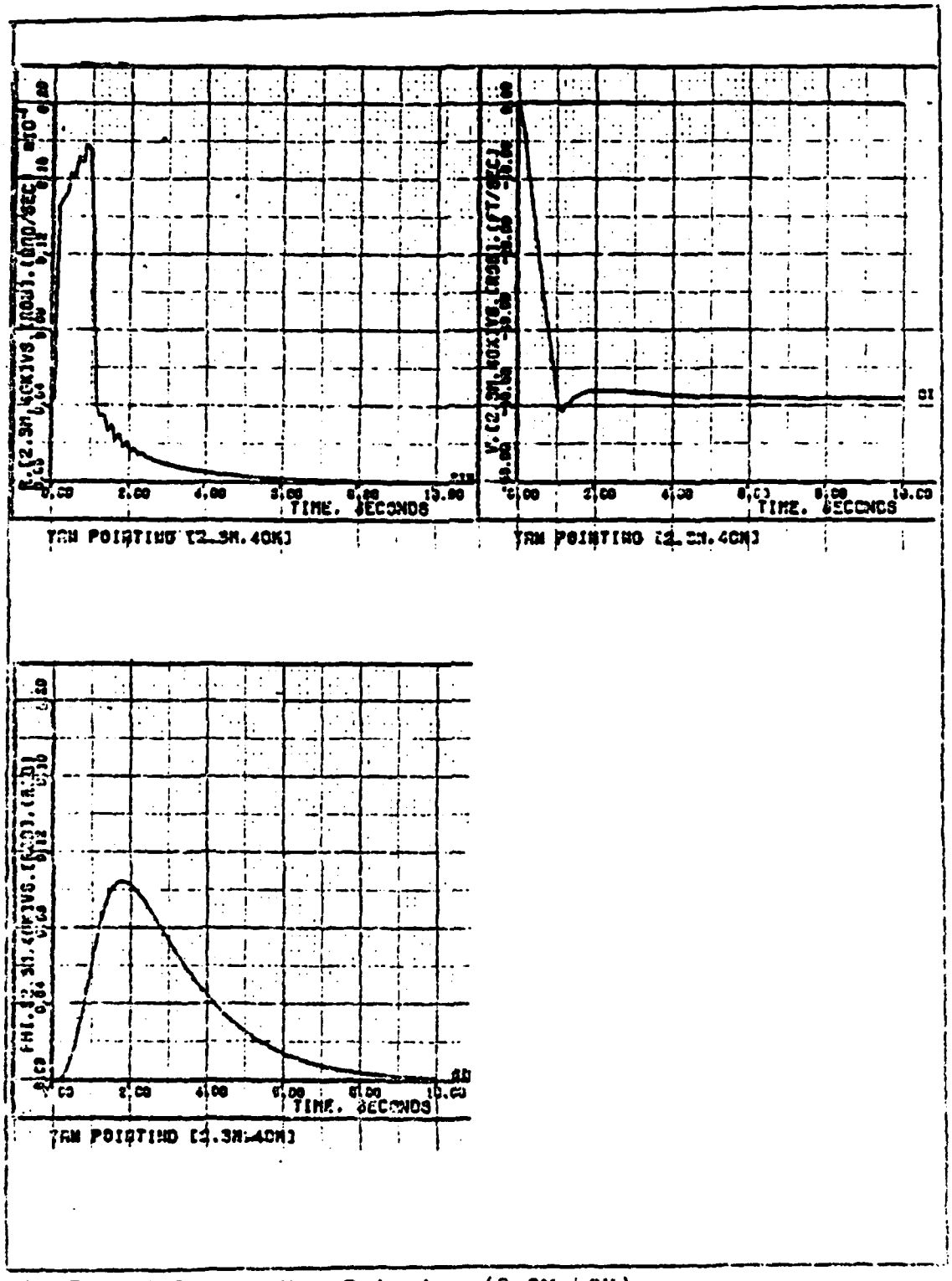
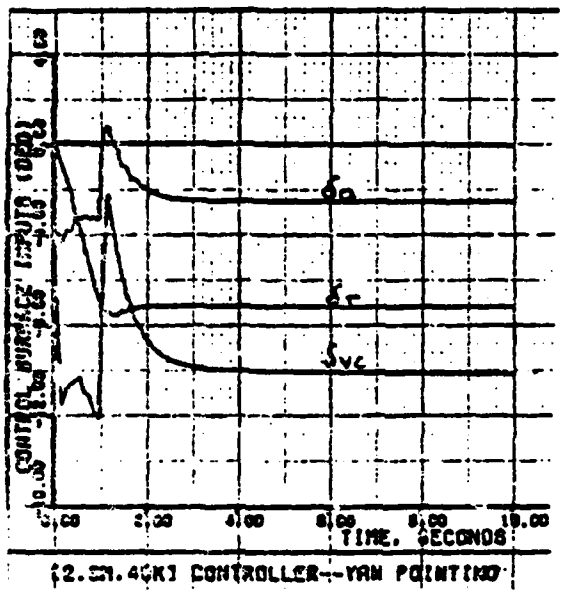
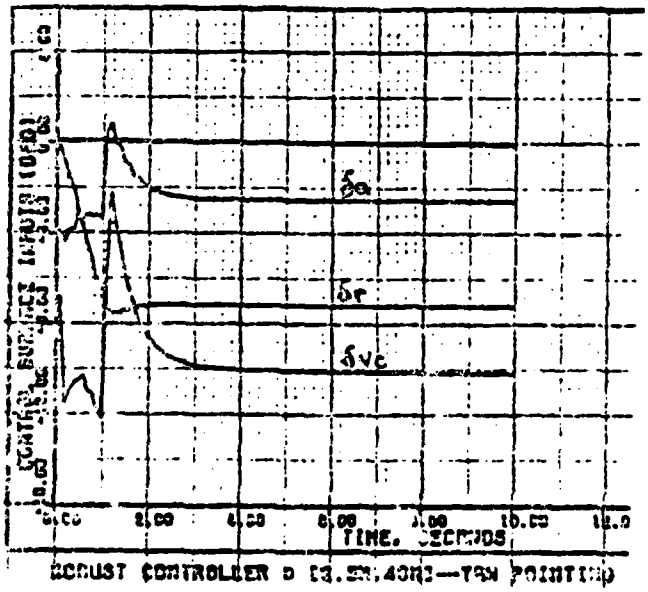



Fig 71. 1 Degree Yaw Pointing (2.3M,40K)




(2.3M,40K) CONTROLLER--YAW POINTING




ADJUST CONTROLLER D (2.3M,40K)--YAW POINTING

Fig 72. 1 Degree Yaw Pointing (2.3M,40K)

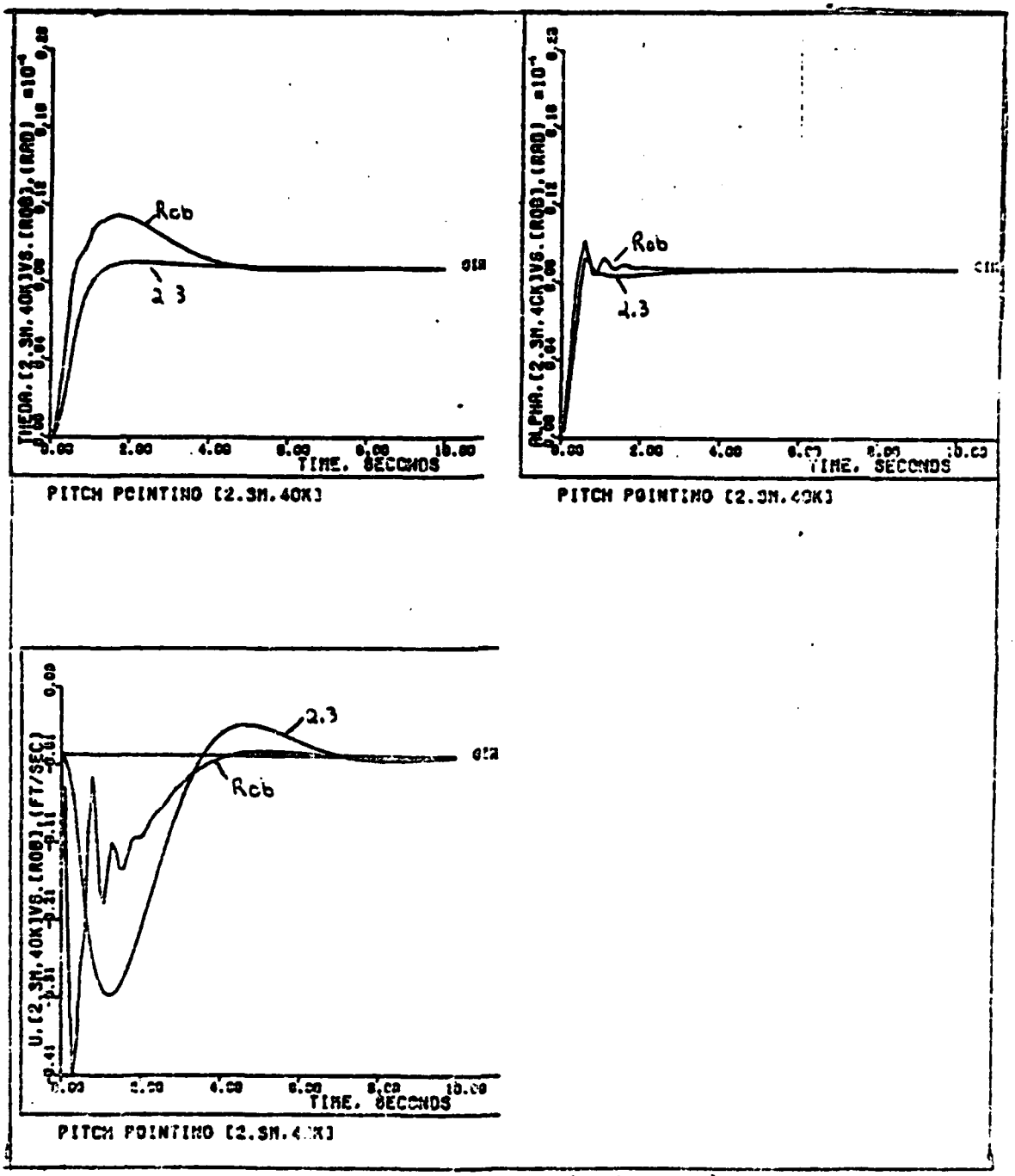
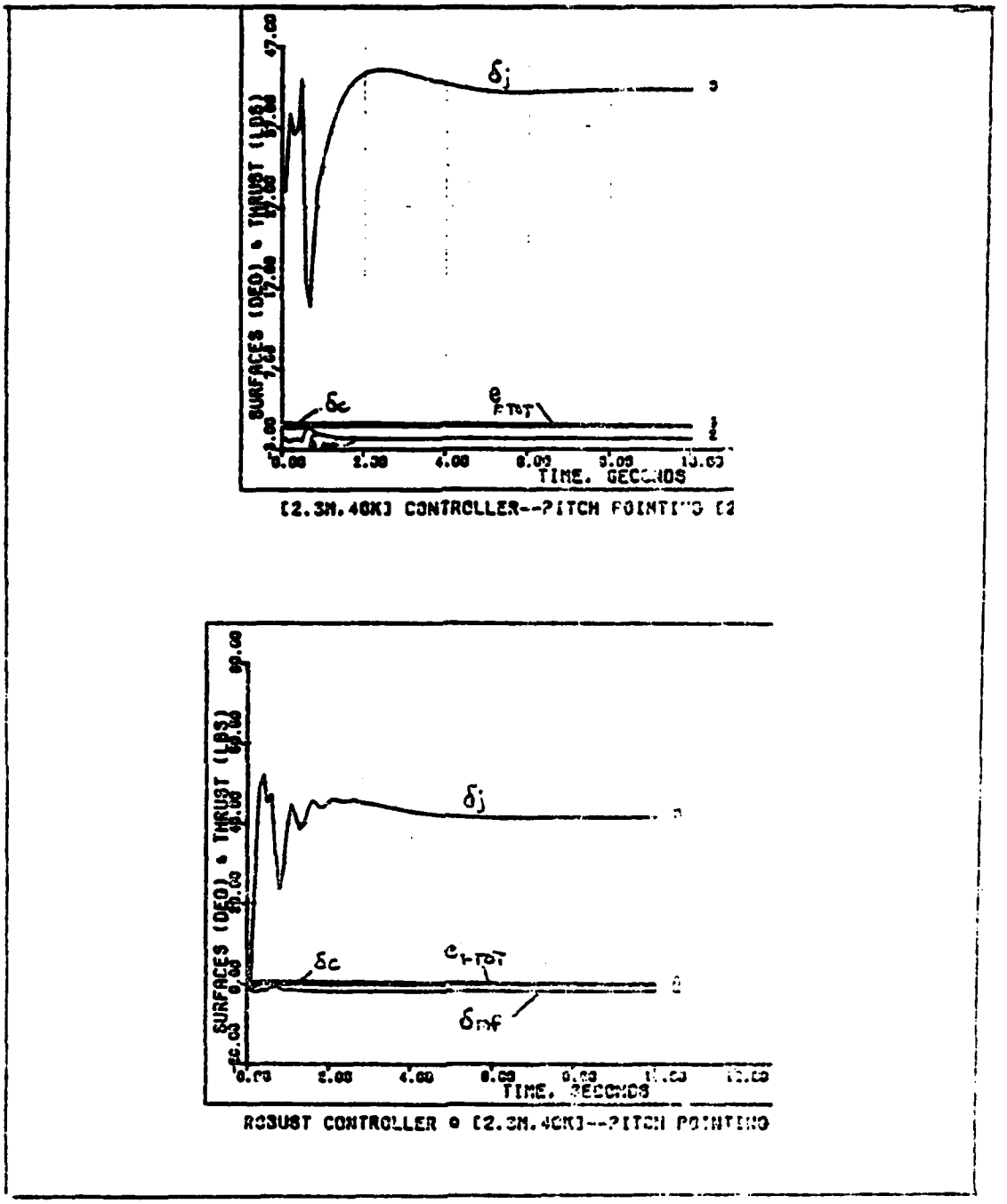



Fig 73. 0.1 Degree Pitch Pointing (2.3M,40K)




[2.3M,40K] CONTROLLER--PITCH POINTING [2

ROBUST CONTROLLER @ [2.3M,40K]--PITCH POINTING

Fig 74. 0.5 Degree Pitch Pointing (2.3M,40K)

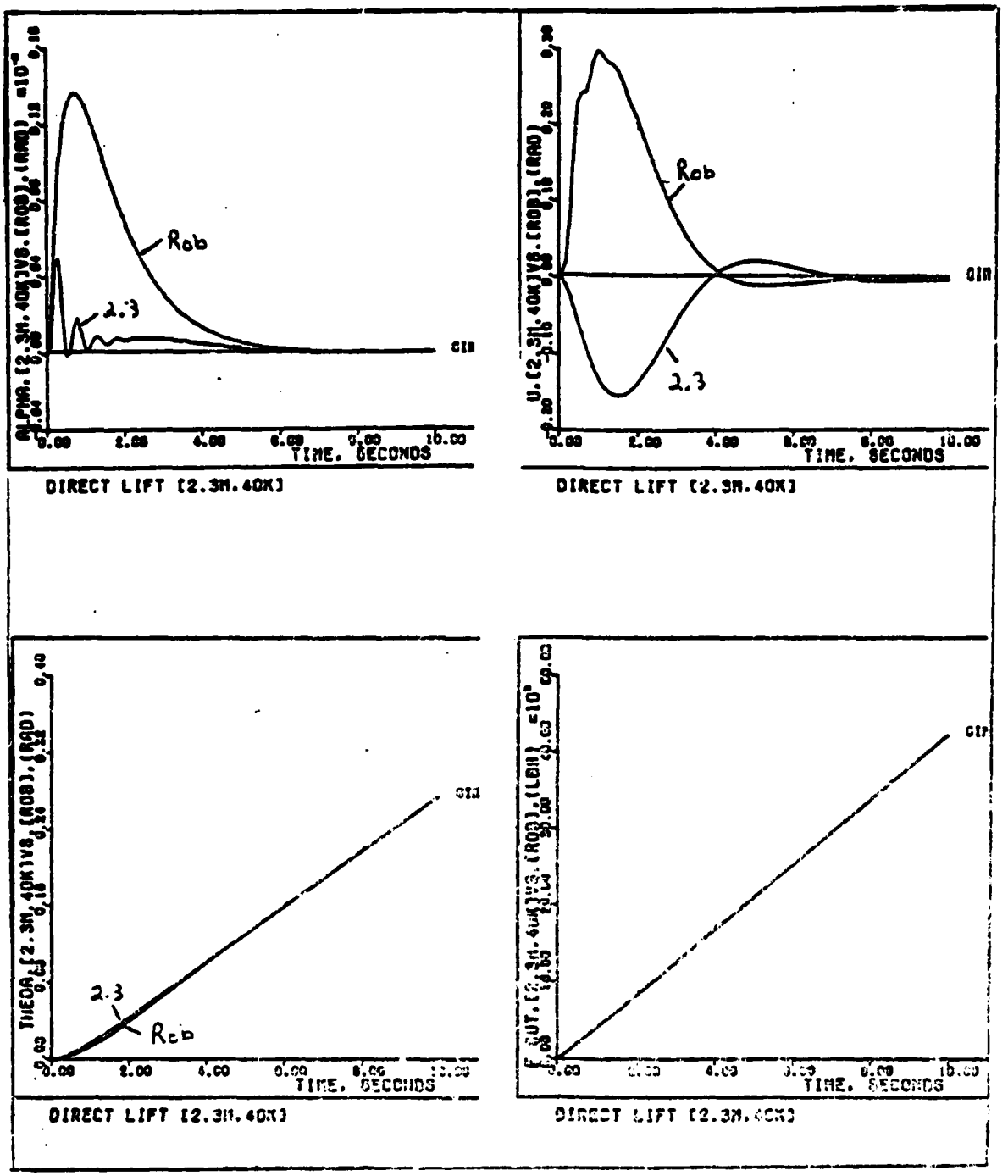



Fig 75. 2-g Direct Lift (2.3M,40K)

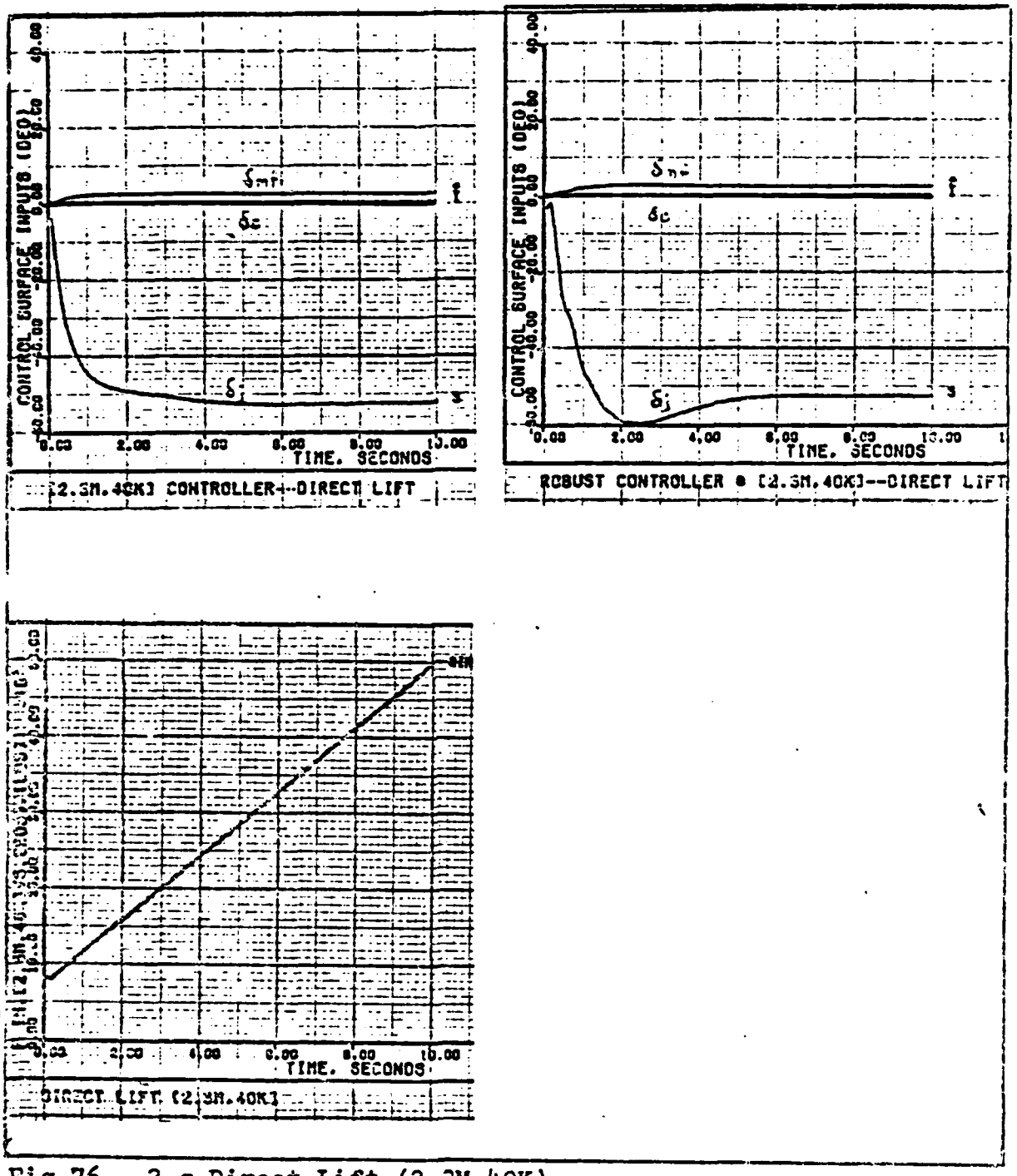



Fig 76. 2-g Direct Lift (2.3M,40K)

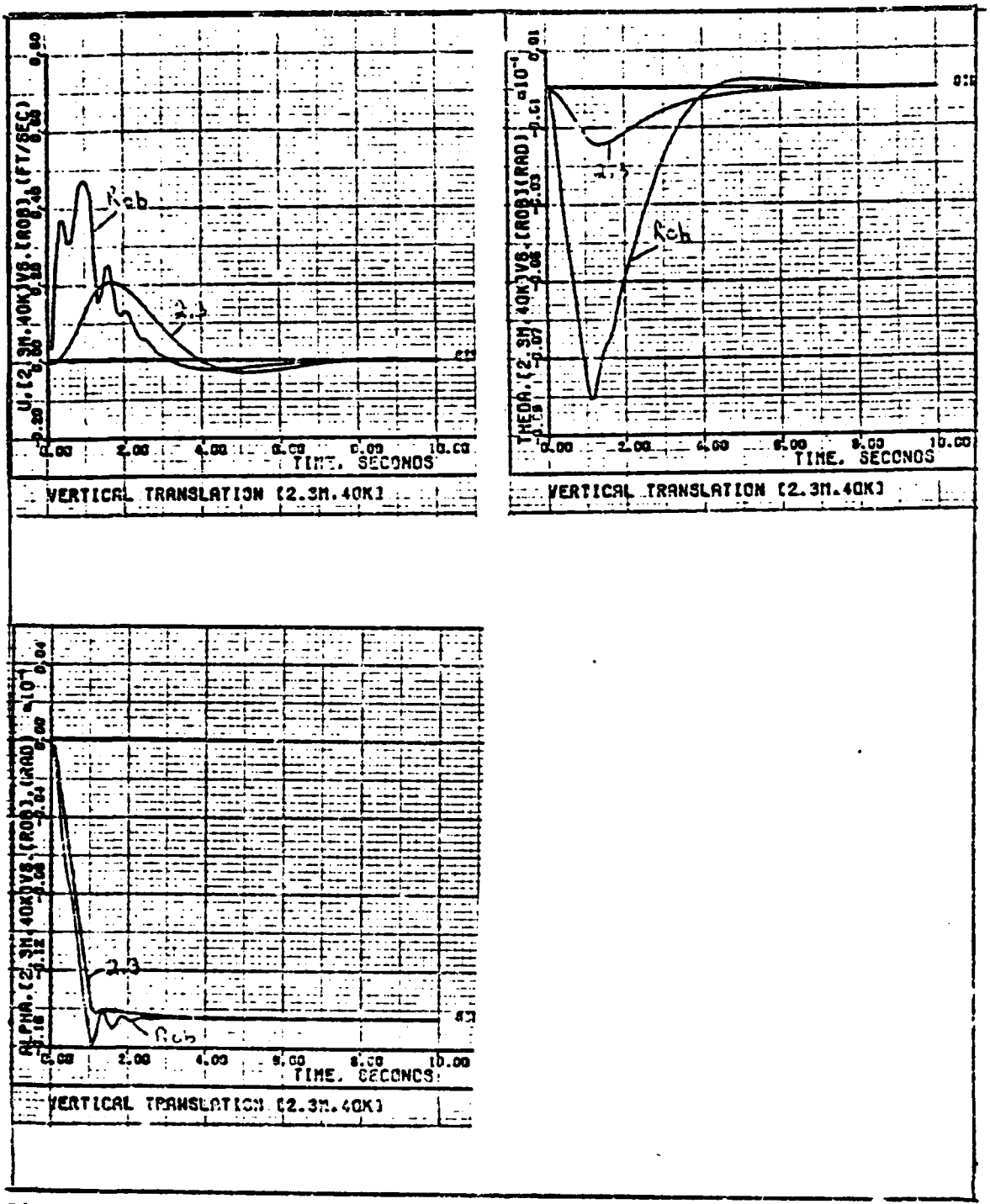



Fig 77. 1-g Vertical Translation (2.3M,40K)

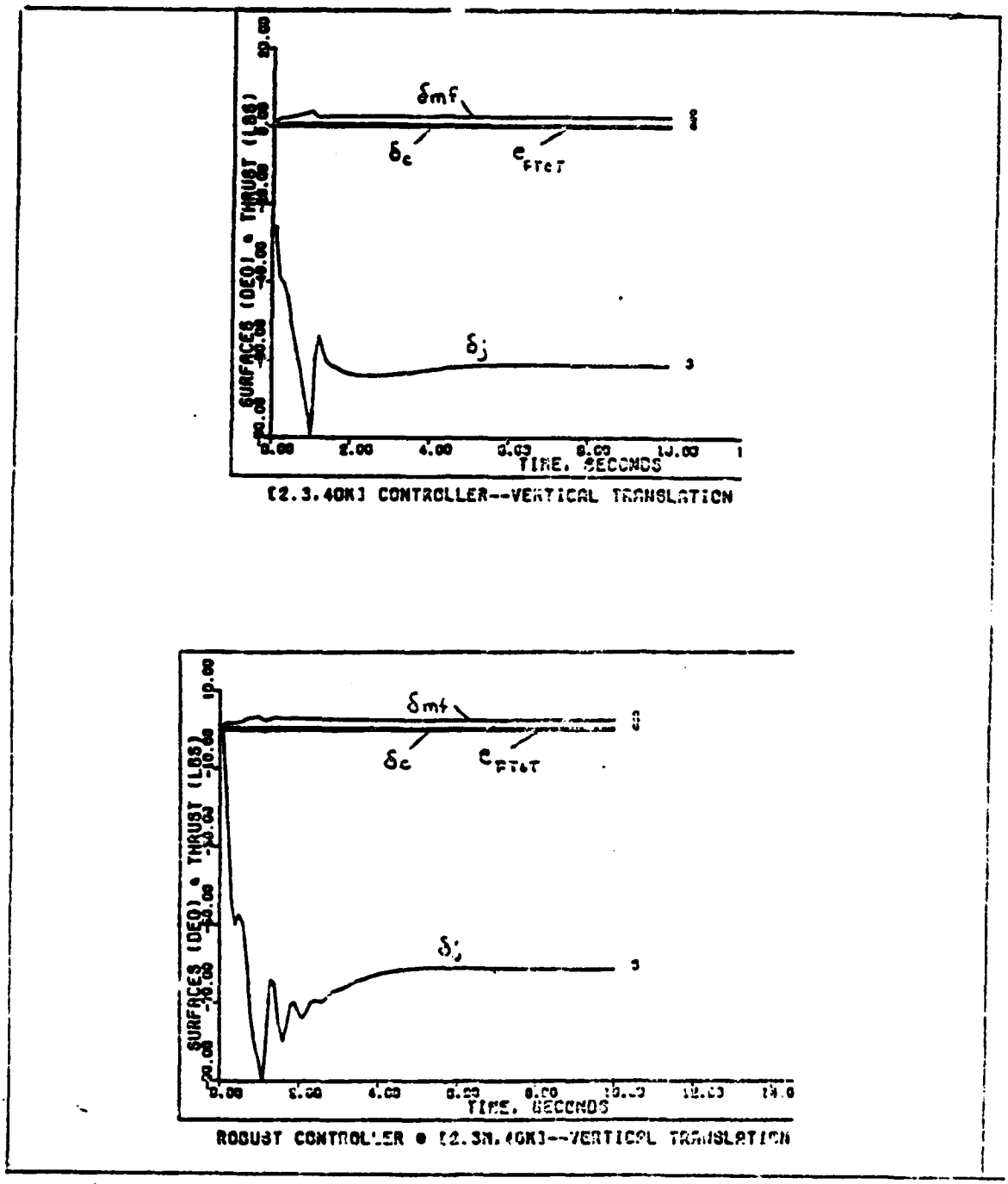



Fig 78. 1-g Vertical Translation (2.3M,40K)

TABLE VIII

SUMMARY OF TIME RESPONSES FOR UNIVERSAL CONTROLLER

| Flt Cond | Maneuver | Command Vector $\underline{v}^*$ | Approx Percent Overshoot | Approx Rise Time ** | Approx Settling Time(2%) |
|---|---|---|---|---|---|
| 0.6 Mach sea level | Horizontal Translation | $\begin{bmatrix} 0, & 0, & 0, & 0 \\ 0, & 0, & 0, & 0 \\ 0, & 0, & 0, & 0 \\ 0, & 0, & 0, & 0 \\ 1, & 46.85, & 20, & 20 \\ 0, & 0, & 0, & 0 \\ 0, & 0, & 0, & 0 \end{bmatrix}$ | none | 1.2sec | 2.8sec |
| | Rollover | $\begin{bmatrix} 0, & 0, & 0, & 0 \\ 0, & 0, & 0, & 0 \\ 0, & 0, & 0, & 0 \\ 0, & 0, & 0, & 0 \\ 0, & 0, & 0, & 0 \\ 0, & 1.047, & 20, & 0 \\ 0, & 0, & 0, & 0 \end{bmatrix}$ | none | 2.2sec | 3.8sec |
| | Flat Turn | $\begin{bmatrix} 0, & 0, & 0, & 0 \\ 0, & 0, & 0, & 0 \\ 0, & 0, & 0, & 0 \\ 0, & 0, & 0, & 0 \\ 0, & 0, & 0, & 0 \\ 0, & 0, & 0, & 0 \\ 1, & .04802, & 20, & 20 \end{bmatrix}$ | none | 2.8sec | 6.8sec |
| | Yaw Pointing | $\begin{bmatrix} 0, & 0, & 0, & 0 \\ 0, & 0, & 0, & 0 \\ 0, & 0, & 0, & 0 \\ 0, & 0, & 0, & 0 \\ 1) \ 1, & -46.85, & 20, & 20 \\ 0, & 0, & 0, & 0 \\ 2) \ .2, & .090, & 1, & 1.2 \end{bmatrix}$ | 1) none<br>2) - | 1) 0.8sec<br>2) - | 1) 4.2sec<br>2) - |

TABLE VIII

SUMMARY OF TIME RESPONSES FOR UNIVERSAL CONTROLLER
(cont)

| Flt Cond | Maneuver | Command Vector $\underline{v}$* | Approx Percent Overshoot | Approx Rise Time ** | Approx Settling Time(2%) |
|---|---|---|---|---|---|
| 0.6 Mach sea level (cont) | Pitch Pointing | 1 [5, .0305, 20, 20; 0, 0, 0, 0] | 1) neg<br>2) neg | 1) 3.6sec<br>2) 0.4sec | 1)5sec<br>2)4.4sec |
| | | 2) [.5, .0305, 20, 20; 0, 0, 0, 0; 0, 0, 0, 0; 0, 0, 0, 0] | | | |
| | Direct Lift | [10, .8725, 20, 20; 0, 0, 0, 0; 0, 0, 0, 0; 10, 12800, 20, 20; 0, 0, 0, 0; 0, 0, 0, 0; 0, 0, 0, 0] | - | - | - |
| | Vertical Translation | [0, 0, 0, 0; 0, 0, 0, 0; 1, .03838, 20, 20; 0, 0, 0, 0; 0, 0, 0, 0; 0, 0, 0, 0; 0, 0, 0, 0] | negligable | 1.7sec | 3.8sec |

TABLE VIII

SUMMARY OF TIME RESPONSES FOR UNIVERSAL CONTROLLER
(cont)

| Flt Cond | Maneuver | Command Vector $\underline{v}^*$ | Approx Percent Overshoot | Approx Rise Time ** | Approx Settling Time(2%) |
|---|---|---|---|---|---|
| 0.9 Mach 30,000 ft. | Horizontal Translation (1G) | $\begin{bmatrix} 0, & 0, & 0, & 0 \\ 0, & 0, & 0, & 0 \\ 0, & 0, & 0, & 0 \\ 0, & 0, & 0, & 0 \\ 1, & 32.2, & 20, & 20 \\ 0, & 0, & 0, & 0 \\ 0, & 0, & 0, & 0 \end{bmatrix}$ | 6.2% | 1.8sec | 8.1sec |
| | Horizontal Translation (0.86) | $\begin{bmatrix} 0, & 0, & 0, & 0 \\ 0, & 0, & 0, & 0 \\ 0, & 0, & 0, & 0 \\ 0, & 0, & 0, & 0 \\ 1, & 25.76, & 20, & 20 \\ 0, & 0, & 0, & 0 \\ 0, & 0, & 0, & 0 \end{bmatrix}$ | 6% | 1.5sec | 7.2sec |
| | Rollover | $\begin{bmatrix} 0, & 0, & 0, & 0 \\ 0, & 0, & 0, & 0 \\ 0, & 0, & 0, & 0 \\ 0, & 0, & 0, & 0 \\ 0, & 0, & 0, & 0 \\ 0, & 1.047, & 20, & 20 \\ 0, & 0, & 0, & 0 \end{bmatrix}$ | none | 2.1sec | 3.2sec |

TABLE VIII

SUMMARY OF TIME RESPONSES FOR UNIVERSAL CONTROLLER
(cont)

| Flt Cond | Manuever | Command Vector $\underline{v}^*$ | Approx Percent Overshoot | Approx Rise Time ** | Approx Settling Time(2%) |
|---|---|---|---|---|---|
| 0.9 Mach 30,000 ft. (cont) | Flat Turn | $\begin{bmatrix} 0, & 0, & 0, & 0 \\ 0, & 0, & 0, & 0 \\ 0, & 0, & 0, & 0 \\ 0, & 0, & 0, & 0 \\ 0, & 0, & 0, & 0 \\ 0, & 0, & 0, & 0 \\ 1, & .0216, & 20, & 20 \end{bmatrix}$ | 1.9% | .9sec | 2.4sec |
| | (r→1s) | | | | |
| | Flat Turn | $\begin{bmatrix} 0, & 0, & 0, & 0 \\ 0, & 0, & 0, & 0 \\ 0, & 0, & 0, & 0 \\ 0, & 0, & 0, & 0 \\ 0, & 0, & 0, & 0 \\ 0, & 0, & 0, & 0 \\ .5, & .0216, & 20, & 20 \end{bmatrix}$ | 1.9% | 4sec | 2.2sec |
| | (r→0.5s) | | | | |
| | Yaw Pointing | $\begin{bmatrix} 0, & 0, & 0, & 0 \\ 0, & 0, & 0, & 0 \\ 0, & 0, & 0, & 0 \\ 0, & 0, & 0, & 0 \end{bmatrix}$ 1) $\begin{bmatrix} 1, & -46.91, & 20, & 20 \\ 0, & 0, & 0, & 0 \end{bmatrix}$ 2) $\begin{bmatrix} .2, & .0675, & 1, & 1.2 \end{bmatrix}$ | 1) 2% 2) - | 1) 0.7sec 2) - | 1) 4.6 2) - |

TABLE VIII

SUMMARY OF TIME RESPONSES FOR UNIVERSAL CONTROLLER
(cont)

| Flt Cond | Ma[illegible] | Command Vector $\underline{v}^*$ | Approx Percent Overshoot | Approx Rise Time ** | Approx Settling Time(2%) |
|---|---|---|---|---|---|
| 0.9 Mach 30,000 ft. (cont) | [illegible] | 1) $\begin{bmatrix} .5, & .052356, & 20, & 20 \\ 0, & 0, & 0, & 0 \end{bmatrix}$ | 1) 3.8% | 1)0.9sec | 1) 4sec |
| | [illegible] | 2) $\begin{bmatrix} .5, & .052356, & 20, & 20 \\ 0, & 0, & 0, & 0 \\ 0, & 0, & 0, & 0 \\ 0, & 0, & 0, & 0 \\ 0, & 0, & 0, & 0 \end{bmatrix}$ | 2) 3.8% | 2) 0.4sec | 2) 2.5sec |
| | Direct Lift | $\begin{bmatrix} 10, & .8725, & 20, & 20 \\ 0, & 0, & 0, & 0 \\ 0, & 0, & 0, & 0 \\ 10, & 12800, & 20, & 20 \\ 0, & 0, & 0, & 0 \\ 0, & 0, & 0, & 0 \\ 0, & 0, & 0, & 0 \end{bmatrix}$ | - | - | - |
| | Vertical Translation | $\begin{bmatrix} 0, & 0, & 0, & 0 \\ 0, & 0, & 0, & 0 \\ 1, & -.03592, & 20, & 20 \\ 0, & 0, & 0, & 0 \\ 0, & 0, & 0, & 0 \\ 0, & 0, & 0, & 0 \\ 0, & 0, & 0, & 0 \end{bmatrix}$ | none | 0.8 sec | 2.2 sec |

TABLE VIII

SUMMARY OF TIME RESPONSES FOR UNIVERSAL CONTROLLER
(cont)

| Flt Cond | Maneuver | Command Vector $\underline{v}$* | Approx Percent Overshoot | Approx Rise Time ** | Approx Settling Time(2%) |
|---|---|---|---|---|---|
| 2.3 Mach 40,000 ft. | Horizontal Translation | 0, 0, 0, 0<br>0, 0, 0, 0<br>0, 0, 0, 0<br>0, 0, 0, 0<br>1, 23.43, 20, 20<br>0, 0, 0, 0<br>0, 0, 0, 0 | 4.3% | 0.8 sec | 3 sec |
| | Rollover | 0, 0, 0, 0<br>0, 0, 0, 0<br>0, 0, 0, 0<br>0, 0, 0, 0<br>0, 0, 0, 0<br>0, .5236, 20, 20<br>0, 0, 0, 0 | none | 1.9 sec | 3 sec |
| | Flat Turn | 0, 0, 0, 0<br>0, 0, 0, 0<br>0, 0, 0, 0<br>0, 0, 0, 0<br>0, 0, 0, 0<br>0, 0, 0, 0<br>1, .007945, 20, 20 | 7.5% | 0.8 sec | 1.7 sec |
| | Yaw Pointing | 0, 0, 0, 0<br>0, 0, 0, 0<br>0, 0, 0, 0<br>0, 0, 0, 0<br>1) 1, -38.9, 20, 20<br>0, 0, 0, 0<br>2) .2, .010, 1,1.2 | 1) none<br>2) - | 1) .8<br>2) - | 1) 1.1<br>2) - |

TABLE VIII

SUMMARY OF TIME RESPONSES FOR UNIVERSAL CONTROLLER
(cont)

| Flt Cond | Maneuver | Command Vector $\underline{v}$* | Approx Percent Overshoot | Approx Rise Time ** | Approx Settling Time(2%) |
|---|---|---|---|---|---|
| 2.3 Mach 40,000 ft. (cont) | Pitch Pointing | 1) [.5, .008726, 20, 20]<br>[0, 0, 0, 0]<br>2) [.5, .008726, 20, 20]<br>[0, 0, 0, 0]<br>[0, 0, 0, 0]<br>[0, 0, 0, 0]<br>[0, 0, 0, 0] | 1) 30.6%<br>2) 14.6% | 1) .4sec<br>2) .25 | 1) 4sec<br>2) 1.6sec |
| | Direct Lift | [10, .2889, 20, 20]<br>[0, 0, 0, 0]<br>[0, 0, 0, 0]<br>[0, 4240, 20, 20]<br>[0, 0, 0, 0]<br>[0, 0, 0, 0]<br>[0, 0, 0, 0] | - | - | - |
| | Vertical Translation | [0, 0, 0, 0]<br>[0, 0, 0, 0]<br>[1, -.01444, 20, 20]<br>[0, 0, 0, 0]<br>[0, 0, 0, 0]<br>[0, 0, 0, 0]<br>[0, 0, 0, 0] | 10.8% | .7sec | 1.7sec |

* Note: Each entry in v has four parts:

1) the time (seconds) the input reached steady-state,
2) steady-state value,
3) the time the input left steady-state and started to return to zero, and
4) the time the input returned to zero. All angles are in radians.

** Note: Rise time is based on the time required for the non-zero output to go from 10% to 90% of its steady-state value.

the figures in this chapter and Chapter IV gives a good feel for the amount of performance degradation, if any, when using the "universal" controller.

The ability of the single controller designed here to perform in a stable manner over such a wide range of flight conditions may be attractive to a large transport aircraft. However, on a air-to-air or ground-attack aircraft such as the one examined here, the degradation in performance over a controller designed to perform at a specific flight condition for some of the maneuvers tested here in unacceptable (see Tables VI, VII and VIII). The deficiencies can be easily corrected by designing a set of controllers, with new controller gain values being loaded into the on-board computer's central memory before maneuver performance becomes unacceptable. The result would be an aircraft capable of maximum performance over an extremely large range of flight conditions. The robustness of each controller still results in a large savings of computer time by decreasing significantly the amount of gain scheduling required by present digital control designs.

As a final note, it can be seen throughout the figures displayed in this chapter that the responses of the 0.6 Mach, the 0.9 Mach, and the 2.3 Mach complete controllers are identical for identical inputs to the separate lateral and longitudinal controllers designed in Chapter IV for the 0.6 Mach, 0.9 Mach, and 2.3 Mach flight conditions.

# CHAPTER VI

# RESULTS, CONCLUSIONS AND RECOMMENDATIONS

## Introduction

This study examines Professor Porter's multivariable design technique in the design of a flight control system for an advanced aircraft with augmented flight controls. In this thesis, first, the theory and aircraft model are briefly studied. Next, both the lateral and longitudinal controllers are designed and tested separately on decoupled six degree-of-freedom maneuvers. Then, the lateral and longitudinal controllers are combined for each flight condition studied. These combined controllers for each of the three flight conditions explored are tested against a "universal" controller composed of the lateral controller from the 2.3 Mach flight condition and the longitudinal controller from the 0.9 Mach flight condition. Also, while completing the controller designs, several modifications are made to MULTI, the basic computer tool designed by AFIT students to aid in applying Professor Porter's method of controller design. While accomplishing these tasks, several advantages and disadvantages of the design technique were uncovered.

## Results

The aircraft's response to the four lateral maneuvers tested is shown in Figures 4 through 13 and is summarized in Table VI. These results show that one lateral controller is sufficient at each flight condition to command all four maneu-

vers with excellent results. The same is true of the longitudinal controller design. The results of the longitudinal maneuver tests are shown in Figures 19 through 27 and are summarized in Table VII. Although the responses to both lateral and longitudinal commands are excellent, they can be further improved (for example, removing some of the small oscillations in the r and $\alpha$ responses) by more "tuning" of the elements contained in the $\underline{\Sigma}$ and $\underline{\alpha}$. Time does not permit improving the outputs beyond what is contained in this thesis. Also, the ability of the controllers to perform standard coupled maneuvers, such as a level 60 degree banked coordinated turn is confirmed in Figures 30, 31, and 32.

Finally, it is shown in Chapter 5 that one controller containing both the lateral controller designed for the 2.3 Mach, 40,000 ft. flight condition, and the longitudinal controller designed for the 0.9 Mach and 30,000 ft. altitude flight condition, can produce very good results at flight conditions ranging from 0.6 Mach, sea level to 2.3 Mach and 40,000 ft. altitude. The results of these robustness tests are shown in Table VIII. As expected, there is some degradation in performance when comparing the robust controller results to those attained by a controller designed for a specific flight condition, but the degradation is small when looking at the wide range of flight conditions tested (0.6 Mach, sea level; 0.9 Mach, 30,000 ft.; and 2.3 Mach, 40,000 ft.). Although there are many places in the flight envelope which have not been explored, these results are very encouraging and certainly

warrent more exhaustive study into this feature of the design technique.

A brief listing of the advantages and disadvantages of this design technique when compared to today's classical and LQG techniques follows. This list pertains to those advantages and disadvantages found while designing the controller for aircraft (irregular plant), and may not consider all the advantages and disadvantages of using the design technique on other systems.

Advantages.

1) Dr. Porter's technique is straight-forward and fast. Rather than dealing with the inner most loop of an aircraft model and working outward to a final design as is presently done using classical methods, the design is done all at once with the entire system. Feedback loops are determined by the outputs and the measurement matrix M (see Fig 2). Changes are made to the feedback loops without having to go back and redesign the entire system. This results in a large time and manpower savings over classical techniques.

2) Although some advanced knowledge of aircraft controller design is benefical, it is not required to use Porter's design technique. A thorough understanding of Porter's method is desirable. After this understanding is acquired, an engineer is well equiped to design a controller for aircraft flight control or a controller for any other system completely unrelated to aircraft. Specifications and limits are all that are really needed to accomplish any design.

3) In aircraft flight controller design, both the lateral and longitudinal controllers can be designed separately and then a minimum amount of tuning is required when both controllers are combined (see Chapter IV). Thus, two completely separate engineering teams can come up with either a lateral or longitudinal controller independently and they can then be combined in a short time to produce the overall aircraft controller.

4) Using Porter's technique has resulted in believable realistic aircraft controllers. The requirement that all states be accessable, such as in LQG controller design, is not a requirement of Porter's method. No observer or state estimator is required unless desired outputs are difficult to measure or are corrupted by noise.

5) The design method is capable of synthesizing some controllers capable of performing well not only at the flight conditions for which they are designed, but for a very wide range of other flight conditions with some small degradation of performance (see Chapter V). As a result, gain scheduling is minimized, thereby reducing the load on the flight computer.

Disadvantages.

1) Controlling rates and accelerations directly, if the integral of those rates and accelerations is an element of the state vector $\underline{x}$, results in a transmission zero at the origin in the multi-dimensional s-domain or on the unit circle in the discrete z-domain. At high gains or low sampling times, this can result in slow time responses (although systems can be designed using this method which do control rates, and accelera-

tions directly and effectively (see Ref 29). This requires a good knowledge of modelling techniques for aircraft).

2) Flight control inputs, such as aileron or elevator deflection, cannot be controlled directly and independently by the designer. Increasing or decreasing an element of the $\underline{\Sigma}$ matrix affects all control surfaces commanded by the controller to perform a specific maneuver - not only one. For an aircraft with both a jet flap and a horizontal tail, it may be desirable to use full elevator effectiveness to create a moment before using the jet flap. Achieving this "desired blend" of control inputs needs to be investigated in using the design technique.

Recommendations.

Initial studies such as this one show that Professor Porter's design technique is a very promising method of aircraft multivariable flight controller design. Like any new design technique, there is still more to learn about the method and there are some additional improvements that could be incorporated into the primary design tool, MULTI. Some of the most promising areas that need to be explored concerning the design method itself and MULTI are listed here.

Design Method.

1) Using a "ramped-up" input to a steady state value gives the designer a means of inputing rates into a problem where only angles are available as inputs/outputs (the slope of the ramp equals the time rate-of-change of the angle). Because the method presently uses only one integrator in the

controller (see Figures 1 and 2), the system acts as a type one system. There is therefore some steady-state error when using a ramp input. Studies should be made into the advantages and disadvantages of reducing this steady-state error by adding a second integrator and third controller matrix $\underline{K}_2$ to the controller. While the basic theory has been developed, the synthesis procedure needs to be refined and incorporated into the computer program MULTI.

2) The present design method for irregular plants is based on the number of inputs m equaling the number of outputs ℓ. Due to this restriction for the aircraft examined here some inputs, such as differential thrust and drag induced by engine inlets, could not be used as flight control inputs to increase aircraft performance. On conventional aircraft without augmented flight controls (without, say, horizontal or vertical canards - therefore, a smaller value for m), the number of outputs ℓ which can be directly controlled is severely curtailed. The basic theory underlying the design method permits more inputs than outputs (Ref 20), but this has not been put into the simplified form of Ref 14. The use of combined inputs to command an output should be investigated.

3) A more thorough study should be made on the robustness issue. Included in such a study should be what factors of the controller design and aircraft flight conditions determine whether a controller designed at one flight condition will work at others, and where in the flight envelope this one controller should be designed to give optimal

performance at other flight conditions.

4) Professor Porter has proposed a solution to the problem of actuator caused instabilities (Ref 31). It provides for incorporating compensators, when necessary, into the design. This solution should be tested for performance and feasibility and incorporated into MULTI. When sensors and actuators are added to this controller design, a redesign of the controller is necessary and produces good results. No compensators are required to achieve excellent flight performance.

5) The idea of using a jet flap on an aircraft to augment already existing flight control surfaces should be further explored. Included in any such study should be an examination of the advantages and disadvantages of having a jet flap available with and without an elevator.

MULTI.

1) MULTI can be expanded to give it all the capabilities when run interactively that it has when run in batch. Keeping the memory required below 70 K can be achieved by further subdivision of the program into more overlays than already exist.

2) An option should be added to MULTI to compute the figures of merit for any output.

3) MULTI needs an option for finding the location of the transmission and decoupling zeroes, if any, of a system. Such a routine has been developed at AFIT (Ref 30) and just needs to be incorporated into MULTI.

4) The option of entering rate limits to any element of the control input matrix $\underline{u}$ could be added to MULTI.

5) MULTI needs an option to assist the designer in developing a measurement matrix $\underline{M}$ using the technqiues of Reference 27. At present this is handled as a separate operation.

BIBLIOGRAPHY


1. ASD Computer Center, CALCOMP Plotter Guide Revision D. ASD Computer Center, Wright-Patterson AFB OH, August 1978.

2. Bradshaw A. and Porter, B. "Asymptotic Properties of Linear Multivariable Discrete-Time Tracking Systems Incorporating Fast-Sampling Error-Actuated Controllers" International Journal of Systems Science, Vol. 11, No. 11: pp. 1279-1293 (1980).

3. Bradshaw, A. and Porter, B. "Design of Linear Multivariable Discrete Time Tracking Systems Incorporating Fast-Sampling Error-Actuated Controllers", International Journal of Systems Science, Vol. 11, No. 7: pp 817-826 (1980).

4. D'Azzo, J., Professor of Electrical Engineering. Lecture materials distributed in EE 7.08, Advanced Multivariable Control. School of Engineering, Air Force Institute of Technology. Wright-Patterson AFB OH, 1982.

5. Falb, P. L. and Wolovich, W. A. "Decoupling in the Design and Synthesis of Multivariable Control Systems", IEEE Trans. Automatic Control, Vol. AC-12, No. 6, pp 651-659, 1967.

6. Heimbold, R. L., et al. Flight Propulsion Control Coupling (FPCC) and Dynamic Interaction Investigation, Flight Dynamics Laboratory, Wright-Patterson AFB OH, September 1975.

7. Heimbold, R. L., et al. Flight Propulsion Control Coupling (FPCC) and Dynamic Interaction Investigation, Volume III. AFFDL-TR-77-41, Air Force Flight Dynamics Laboratory, Wright-Patterson AFB OH, June 1977.

8. Honeywell, Inc. Systems and Research Center. Users Manual for the Program FPCCSIM. MR-12369, Minneapolis, Minnesota, July 1975.

9. Houtz, J. E. FPCC Linear Analysis Digital Computer Program. AFFDL/FGL-TM-77-82-FGL, Air Force Flight Dynamics Laboratory, Wright-Patterson AFB OH, November 1977.

10. Kenned[illegible], T. A. The Design of Digital Controllers for the C-141 Aircraft Using Entire Eigenstructure Assignment and the Development of an Interactive Computer Design Program. Master Thesis, Air Force Institute of Technology, Wright-Patterson AFB OH, December 1980.

11. Paschall, R. Design of a Multivariable Tracker Control Law for the A-7D Digital II Aircraft. Master Thesis, Air Force Institute of Technology, Wright-Patterson AFB OH, December 1981.

12. Porter, B. "Design of Error-Actuated Controllers for Unknown Multivariable Plants", Electronics Letters, Vol. 17, No. 3 (5 February 1981).

13. Porter, B. "Design of High-Gain State-Feedback Controllers for Linear Multivariable Systems", Electronics Letters, Vol. 14, No. 8, (13 April 1978).

14. Porter, B. Design of High-Performance Tracking Systems. USAME/DC/120/81. Air Force Flight Dynamics Laboratory, Wright-Patterson AFB OH, November 1981.

15. Porter, B. "Singular Perturbation Methods in the Design of Observers and Stabilizing Feedback Controllers for Multivariable Linear Systems", Electronics Letters, Vol. 10, No. 23, (14 November 1974).

16. Porter, B. "Singular Perturbation Methods in the Design of Stabilizing Feedback Controllers for Multivariable Linear Systems", International Journal of Control, Vol. 20, No. 4: pp. 689-692 (1974).

17. Porter, B. "Singular Perturbation Methods in the Synthesis of Feedback-Control Laws for Eigenvalue-Assignment in Multivariable Linear Systems", International Journal of Systems Science, Vol. 7, No. 5: pp. 597-601 (1976).

18. Porter, B. and Bradshaw, A. "Asymtotic Properties of Linear Multivariable Continuous-Time Tracking Systems Incorporating High-Gain Error-Actuated Controllers", International Journal of Systems Science, Vol. 10, No. 12: pp. 1433-1444 (1979).

19. Porter, B. and Bradshaw, A. "Design of Linear Multivariable Continuous-Time Output-Feedback Regulators", International Journal of Systems Science, Vol. 10, No. 2: pp. 113-121 (1979).

20. Porter, B. and Bradshaw, A. "Design of Linear Multivariable Continuous-Time Tracking Systems Incorporating High-Gain Error-Actuated Controllers", International Journal of Systems Science, Vol. 10, No. 4: pp. 461-469 (1979).

21. Porter, B. and Bradshaw, A. "High Gain Error-Actuated Controllers for a Class of Linear Multivariable Plants", 18th IEEE Conference on Decision and Control, Fort Lauderdale Florida, December 1979. Report No. WP6-9:00: pp. 322-325.

22. Porter, B. and D'Azzo, J. "Transmission Zeros of Linear Multivariable Continuous-Time Systems", Electronics Letters, Vol. 13, No. 24, (24 November 1977).

23. Porter, B. and Shenton, A. "Singular Perturbation Methods of Asymptotic Eiganvalue Assignment in Multivariable Linear Systems", International Journal of Systems Science, Vol. 6, No. 1: pp. 33-37 (1975).

24. Porter, B. and Shenton, A. "Singular Perturbation Analysis of the Transfer Function Matrices of a Class of Multivariable Linear Systems", International Journal of Control, Vol. 21, No. 4: pp. 655-660, (1975).

25. Porter, D. Design and Analysis of a Multivariable, Digital Controller for the A-7D Digital II Aircraft and the Development of an Interactive Computer Design Program. Master Thesis, Air Force Institute of Technology, Wright-Patterson AFB OH, December 1981.

26. Ridgely, D. B. Use of Entire Eiganstructure Assignment With High Gain Error Actuated Flight Control Systems. Master Thesis, Air Force Institute of Technology, Wright-Patterson AFB OH, December 1981.

27. Ridgely, B., Banda, S., and D'Azzo, J. "Decoupling of High Gain Multivariable Tracking Systems" report to be given at AIAA 21st Aerospace Sciences Conference. Reno, Nevada, January 1983. AIAA Paper No. 83-0280.

28. Smyth, J. Digital Flight Control System Design Using Singular Perturbation Methods. Master Thesis, Air Force Institute of Technology, Wright-Patterson AFB OH, December 1981.

29. Barfield, F. Multivariable Control Law Development for AFTI/F-16. Master Thesis, Air Force Institute of Technology, Wright-Patterson AFB OH, December 1982.

30. Lewis, T. High Gain Error Actuated Flight Control for Continuous Linear Multivariable Plants. Master Thesis, Air Force Institute of Technology, Wright-Patterson AFB OH, December 1982.

31. Porter, B. "High-Gain Error-Actuated Controllers for Linear Multivariable Plants With Explicit Actuator Dynamics", report given at IFAC Symposium on Computer Aided Design of Multivariable Technological Systems, West Lafayette, Indiana, September 1982, pp. 61-66.

Appendix C

PREVIOUS PAGE
IS BLANK

AFIT/GE/EE/82D-47

# DIGITAL MULTIVARIABLE TRACKER CONTROL LAWS FOR THE C-141-A STARLIFTER AIRCRAFT

THESIS

Presented to the Faculty of the School of Engineering
of the Air Force Institute of Technology
Air University
in Partial Fulfillment of the
Requirements for the Degree of
Master of Science

by

Michael A. Masi, B.S.E.E.
Capt USAF
Graduate Electrical Engineer

December 1982

Approved for public release; distribution unlimited.



PREVIOUS PAGE IS BLANK

## Preface

This thesis topic was chosen for two main reasons. First, it is in an area which parallels my graduate studies in flight control. Second, I wanted a topic which would, hopefully, hold my interest and enthusiasm. I would like to thank Duane P. Rubertus of the Flight Dynamics Laboratory, Wright-Patterson AFB, Ohio for generating and sponsoring this thesis topic. I was given the latitude to choose any large aircraft for this study. Having flown the C-141, I choose the aircraft that I am familiar with.

The theoretical background is based on techniques developed, under USAF contract, by Professor Brian Porter from the University of Salford, England. I would like to express my appreciation to Professors John J. D'Azzo and Constantine H. Houpis of the Department of Electrical Engineering at the Air Force Institute of Technology. This thesis effort would have been unachievable without their guidance and suggestions throughout. I also wish to acknowledge committee member, Capt. Aaron DeWispelare, Department of Aeronautics and Astronautics, for his assistance and suggestions.

This thesis was accomplished in parallel with four other fellow students. I would especially like to thank Mr. A. Finley Barfield and Lt. Daniel E. Russ for their assistance in the development of the aircraft model.

Numerous discussions with them and Capt. Jon Bauschlicher and Lt. Tom Lewis aided in accomplishing my objectives.

Finally, but most of all, I want to express my love and adoration to my wife, Annette B. Masi, for her patience and understanding during the production of this thesis. I especially wish to acknowledge the countless hours she spent as my personal typist. To my children, Peter and Anthony, I love you. And to my parents, I wish to express my love for your support.

Captain Michael A. Masi

## Contents


Preface .....

List of Figures .....

List of Tables .....

List of Symbols .....

Abstract .....

I. Introduction .....

- Background .....
- Problem .....
- Approach .....
- Assumptions .....
- Presentation .....

II. Aircraft Models .....

- Introduction .....
- Aircraft Description .....
- System Models .....
- Summary .....

III. Control Law Theory .....

- Introduction .....
- Unknown Plants .....
- Regular Plants .....
- Irregular Plants .....
- B* Plants .....
- Summary .....

IV. Computer Program Modification .....

- Introduction .....
- Addition of B* Design Method .....
- Modification for Batch Use .....
- Summary .....

Contents

V. Multivariable Control Law Design .....

Introduction .....
C-141-A Input/Output Model .....
Manuevers .....
Design Procedure .....
Tracker Control Laws .....
MACH 0.18 Lateral Controller .....
MACH 0.18 Longitudinal Controller .....
MACH 0.65 Controllers .....
MACH 0.76 Controllers .....
Robustness .....
Model Change .....
Summary .....

VI. Conclusions and Recommendations .....

Thesis Summary .....
Conclusions .....
Recommendations .....

Bibliography .....

Appendix A: Aircraft Equations of Motion .....

Appendix B: Additional Simulation Data .....

Appendix C: User's Guide for Batch MULTI .....

VITA .....

Reproduced from best available copy.

## List of Figures


Figure

1 Flowchart for Option #15 of MULTI .....

2 MACH 0.13 Design Condition, Coordinated Turn ..

3 MACH 0.13 Design Condition, Sideslip .....

4 MACH 0.13 Design Condition, Vertical Translation .....

5 MACH 0.13 Design Condition, Pitch Pointing ....

6 MACH 0.65 (Design MACH 0.13), Coordinated Turn .....

7 MACH 0.76 (Design MACH 0.13), Coordinated Turn .....

8 MACH 0.65 (Design MACH 0.13), Sideslip .....

9 MACH 0.76 (Design MACH 0.13), Sideslip .....

10 MACH 0.65 (Design MACH 0.13), Vertical Translation .....

11 MACH 0.76 (Design MACH 0.13), Vertical Translation .....

12 MACH 0.65 (Design MACH 0.13), Pitch Pointing ..

13 MACH 0.76 (Design MACH 0.13), Pitch Pointing ..

14 MACH 0.13 Design Condition, Normal Climb .....

B-1 MACH 0.65 Design Condition, Coordinated Turn ..

B-2 MACH 0.65 Design Condition, Sideslip .....

B-3 MACH 0.65 Design Condition, Vertical Translation .....

B-4 MACH 0.65 Design Condition, Pitch Pointing ....

B-5 MACH 0.76 Design Condition, Coordinated Turn ..

## List of Figures


Figure

B-6 MACH 0.76 Design Condition, Sideslip .....

B-7 MACH 0.76 Design Condition, Vertical Translation .....

B-8 MACH 0.76 Design Condition, Pitch Pointing ....

C-1 Example -- Irregular Plant .....

## List of Tables


Table

I Coordinated Turn Results for MACH 0.18, 1000 ft Design Condition .....

II Sideslip Results for MACH 0.18, 1000 ft Design Condition .....

III Vertical Translation Results for MACH 0.18, 1000 ft Design Condition .....

IV Pitch Pointing Results for MACH 0.18, 1000 ft Design Condition ..... .....

V Coordinated Turn Results for MACH 0.65, 25000 ft (Designed at MACH 0.18) .....

VI Coordinated Turn Results for MACH 0.76, 40000 ft (Designed at MACH 0.18) .....

VII Sideslip Results for MACH 0.65, 25000 ft (Designed at MACH 0.18) .....

VIII Sideslip Results for MACH 0.76, 40000 ft (Designed at MACH 0.18) .....

IX Vertical Translation Results for MACH 0.65, 25000 ft (Designed at MACH 0.18) .....

X Vertical Translation Results for MACH 0.76, 40000 ft (Designed at MACH 0.18) .....

XI Pitch Pointing Results for MACH 0.65, 25000 ft (Designed at MACH 0.18) .....

XII Pitch Pointing Results for MACH 0.76, 40000 ft (Designed at MACH 0.18) .....

XIII Normal Climb Results for MACH 0.18, 1000 ft Design Condition .....

## List of Tables


Table

A-I State Variables and Control Inputs .....

A-II Aircraft Data at Different MACH Numbers .....

A-III Non-dimensional Stability Axis Derivatives for MACH 0.13 .....

A-IV Non-dimensional Stability Axis Derivatives for MACH 0.65 .....

A-V Non-dimensional Stability Axis Derivatives for MACH 0.76 .....

A-VI Dimensional A and B Matrix Coefficients for MACH 0.13 .....

A-VII Dimensional A and B Matrix Coefficients for MACH 0.65 .....

A-VIII Dimensional A and B Matrix Coefficients for MACH 0.76 .....

## List of Symbols

| | |
|---|---|
| $\underline{A}$ | Continuous-time plant matrix |
| $\alpha$ | Perturbation angle of attack |
| $\alpha_0$ | Equilibrium (trim) angle of attack |
| $\alpha_r$ | Ratio of proportional to integral feedback |
| $\underline{B}$ | Continuous-time control input matrix |
| $\beta$ | Sideslip angle |
| b | Wing span |
| $\underline{C}$ | Continuous-time output matrix |
| c | Wing mean aerodynamic (geometric) chord |
| $\underline{D}$ | Continuous-time disturbance matrix |
| $\underline{D}'$ | Continuous-time direct feedforward output matrix |
| d | Disturbance vector |
| $\delta_a$ | Total aileron surface deflection from trim |
| $\delta_e$ | Elevator surface deflection from trim |
| $\delta_r$ | Rudder surface deflection from trim |
| $\delta_{sp}$ | Spoiler surface deflection from trim |
| $\delta_T$ | Percent engine thrust change from trim |
| $\underline{e}$ | Error vector |
| $\sigma$ | Sigma ($\Sigma$) scalar multiplier |
| $\underline{F}$ | Augmented continuous-time output matrix |
| $\underline{G}(0)$ | Steady-state transfer function matrix |
| g | Acceleration of gravity |
| h | Perturbation altitude from trim |

## List of Symbols

| | |
|---|---|
| $I_{xx}$ | Moment of inertia about X body axis |
| $I_{yy}$ | Moment of inertia about Y body axis |
| $I_{zz}$ | Moment of inertia about Z body axis |
| $I_{xz}$ | Product of inertia about XZ body axes |
| $\underline{K}_0$ | Proportional control law feedback matrix |
| $\underline{K}_1$ | Integral control law feedback matrix |
| $L_\beta$ | Dimensional variation of rolling moment with sideslip angle |
| $L_p$ | Dimensional variation of rolling moment with roll rate |
| $L_r$ | Dimensional variation of rolling moment with yaw rate |
| $L_\delta$ | Dimensional variation of rolling moment with ailerons ($\delta_a$) or rudder ($\delta_r$) |
| $l_t$ | Distance from 25% wing mean aerodynamic chord to 25% horizontal tail mean aerodynamic chord |
| $\underline{M}$ | Transducer (measurement) matrix |
| $M_u$ | Dimensional variation of pitching moment with speed |
| $M_\alpha$ | Dimensional variation of pitching moment with angle of attack |
| $M_{\dot{\alpha}}$ | Dimensional variation of pitching moment with rate of change of angle attack |
| $M_q$ | Dimensional variation of pitching moment with pitch rate |
| $M_\delta$ | Dimensional variation of pitching moment with elevator ($\delta_e$) or spoiler ($\delta_{sp}$) |
| $N_\beta$ | Dimensional variation of yawing moment with sideslip angle |

## List of Symbols

| | |
|---|---|
| $N_p$ | Dimensional variation of yawing moment with roll rate |
| $N_r$ | Dimensional variation of yawing moment with yaw rate |
| $N_\delta$ | Dimensional variation of yawing moment with aileron ($\delta_a$) or rudder ($\delta_r$) |
| $p$ | Perturbation roll rate |
| $\phi$ | Perturbation roll angle |
| $\bar{q}$ | Dynamic pressure |
| $q$ | Perturbation pitch rate |
| $r$ | Perturbation yaw rate |
| $S$ | (Wing referenced) surface area of aircraft |
| $\underline{z}$ | Output weighting matrix |
| $T$ | Sampling period |
| $\theta$ | Perturbation pitch angle |
| $\theta_0$ | Equilibrium (trim) pitch angle |
| $U_0$ | Equilibrium (trim) forward velocity |
| $u$ | Perturbation forward velocity |
| $\underline{u}$ | Control surface input vector |
| $V_0$ | Equilibrium (trim) vertical velocity |
| $v$ | Perturbation vertical velocity |
| $\underline{y}$ | Command input vector |
| $W$ | Weight of the aircraft |
| $W_0$ | Equilibrium (trim) horizontal velocity |
| $w$ | Perturbation horizontal velocity |
| $\underline{w}$ | Controlled output vector |

## List of Symbols

| | |
|---|---|
| $X_u$ | Dimensional variation of X-force with forward velocity |
| $X_\alpha$ | Dimensional variation of X-force with angle of attack |
| $X_{\dot{\alpha}}$ | Dimensional variation of X-force with rate of change of angle of attack |
| $X_q$ | Dimensional variation of X-force with pitch rate |
| $X_\delta$ | Dimensional variation of X-force with elevator ($\delta_e$), spoiler ($\delta_{sp}$), or thrust ($\delta_T$) |
| $\underline{x}$ | State vector |
| $Y_\beta$ | Dimensional variation of Y-force with sideslip angle |
| $Y_p$ | Dimensional variation of Y-force with roll rate |
| $Y_r$ | Dimensional variation of Y-force with yaw rate |
| $Y_\delta$ | Dimensional variation of Y-force with ailerons ($\delta_a$) or rudder ($\delta_r$) |
| $\underline{y}$ | Output vector |
| $Z_u$ | Dimensional variation of Z-force with forward velocity |
| $Z_\alpha$ | Dimensional variation of Z-force with angle of attack |
| $Z_{\dot{\alpha}}$ | Dimensional variation of Z-force with rate of change of angle of attack |
| $Z_q$ | Dimensional variation of Z-force with pitch rate |
| $Z_\delta$ | Dimensional variation of Z-force with elevator ($\delta_e$) or spoiler ($\delta_{sp}$) |
| $\underline{z}$ | Integral of error vector |

## Abstract

This thesis investigates the design of digital, multivariable tracker control laws for the C-141-A Starlifter aircraft. The thesis develops controllers for the aircraft at three diverse flight conditions. The study includes additions and modifications to the computer package MULTI.

A six degree-of-freedom aircraft model is developed. The equations of motion assume linearized aircraft models which make only small perturbations about each nominal flight condition.

The techniques developed by Professor Brian Porter, University of Salford, England, are used to design the tracker control laws. The thesis includes a discussion of robustness of the control laws determined. Robustness is considered by applying the controller at other than the flight condition for which it is specifically designed.

The thesis concludes that digital tracker control laws can be designed for this aircraft. A more accurate fully-coupled aircraft model should be derived in order to further tune the control laws.

MULTI, the computer design and simulation program, is available from the Air Force Institute of Technology.

# DIGITAL MULTIVARIABLE TRACKER CONTROL LAWS FOR THE C-141-A STARLIFTER AIRCRAFT

## I Introduction

Many aircraft use digital computers for navigation and instrumentation. An important extension in modern aircraft has been the use of computer generated digital signals for transforming command inputs into movement of the flight control surfaces. These digital flight control systems (DFCS) have resulted in faster response times to inputs, which means better controllability from a pilot's perspective.

This thesis addresses the development of digital multivariable tracker control laws for the C-141-A Starlifter aircraft. This first chapter presents the background, problem statement, approach, assumptions, and sequence of presentation.

### Background

Aircraft are now being designed with closed-loop fly-by-wire flight control systems. Such electronic controllers have generated new possibilities for multiple input/multiple output (MIMO) systems. Classical methods, which worked well for single input/single output control systems, are no longer easily applied (Ref 1).

Professor Porter and his associates have suggested four direct design methods for a DFCS (Ref 2). These techniques provide for the design of fast-sampling error-actuated digital controllers for highly-interactive linear multivariable systems. Porter has suggested that such proportional plus integral feedback DFCS's result in greater decoupling of commanded outputs than is possible using previous techniques.

Previous theses used the methods of Professor Porter to develop digital control laws for fighter type aircraft (Refs 3 & 4). These investigations found the techniques to be fairly straightforward. They found that computer simulations showed fairly good decoupling of the outputs as desired.

## Problem

The purpose of this thesis is to investigate the development of tracker control laws for a large transport aircraft, specifically the C-141-A Starlifter. The resultant designs are then checked for robustness by checking responses at flight conditions other than the designed condition. These controllers are developed and simulated by computer through the use of an existing interactive software package, MULTI (Ref 3).

## Approach

This thesis is limited to the design of digital multivariable tracker control laws for the C-141-A. It strictly

uses the techniques proposed, under U. S. Government contract, by Professor Porter and implemented via the interactive computer program MULTI. Four steps are taken in completion of this thesis:

1. Development of the aircraft equations of motion for three separate flight conditions;
2. Addition to MULTI of the fourth design method and implementation of MULTI as a batch program in order to expand its capabilities;
3. Design of digital, multivariable tracker control laws using the appropriate method (see Chapter III); and
4. Validation of robustness for the designed control laws.

## Assumptions

The assumptions in this thesis deal primarily with the aircraft. First, only small perturbations about a trimmed straight and level flight condition are assumed. Second, the aircraft equations of motion are developed for each flight condition. Third, the equations of motion are modeled as linearized, constant coefficient state equations.

It is also assumed that computer simulations approximate a realistic indication of aircraft motions.

## Presentation

Six chapters are included in this thesis. Chapter II presents the aircraft model and Appendix A details the development of the necessary aircraft equations. Professor

Porter's four design approaches for multivariable control laws are summarized in Chapter III. The computer program MULTI is introduced in Chapter IV which discusses additions and changes made by this author. Chapter V describes the development of tracker control laws for the C-141-A for three different flight conditions. This includes discussion of the results. Robustness is also considered by simulation of control laws at other than the designed flight condition. Finally, Chapter VI is the conclusion and offers recommendations for further studies and suggestions for possible improvements and/or additions to MULTI.

# II Aircraft Model

## Introduction

This thesis used the C-141-A aircraft. A linear six degree-of-freedon (D-O-F) model is generated for each of three flight conditions. As linearized constant-coefficient equations of motion, the three models represent the aircraft operating within small perturbations about each of the three sets of equilibrium conditions. The selection of three diverse standard flight conditions permits the determination of the robustness of a control law that is designed for a particular flight condition. Thus, the flight conditions chosen include a heavy weight landing configuration of MACH 0.18 at 1000 feet, a medium altitude simulated refueling cruise of MACH 0.65 at 25000 feet, and a high-speed high altitude cruise of MACH 0.76 at 40000 feet.

This chapter presents a basic description of the C-141-A Starlifter aircraft and overviews a general discussion of the linearized equations of motion.

## Aircraft Description

The C-141-A Starlifter is a four engine cargo aircraft. The aircraft has a basic weight of approximately 140,000 pounds and a maximum gross weight of 325,000 pounds. The high wings are moderately swept and the horizontal stabilizer

forms a "T-tail" with the vertical stabilizer. The four Pratt and Whitney TF33-P-7 engines are each rated at 20,250 pounds-thrust (Ref 5) for a standard day at sea level (15°C, 29.92 in. mg). Other relative geometric data, as found in Reference 6, is as follows:

| Characteristic | Symbol | Dimension |
|---|---|---|
| Fuselage | F | 145 ft |
| Wing area | S | 3228 sq ft |
| Wing span | b | 159.6 ft |
| Wing M.A.C. | c | 22.2 ft |
| Distance from 25% wing M.A.C to 25% horizontal tail M.A.C. | $l_t$ | 74.534 ft |

The abbreviation, M.A.C., stands for mean aerodynamic chord. Further data for the C-141 aircraft can be found in Reference 7.

## System Models

The aircraft models in this thesis are developed using 6 D-O-F equations of motion. The equations assume decoupling of the lateral and longitudinal modes of the aircraft. Appendix A presents the development of the equations of motion in state form.

The five control inputs available include two lateral controls — the ailerons $\delta_a$ and the rudder $\delta_r$ — and three

longitudinal controls — the elevator $\delta_e$, the spoilers $\delta_{sp}$, and the thrust $\delta_T$. Since the equations are decoupled and the theory requires that the number of inputs equals the number of outputs, two lateral and three longitudinal outputs are chosen. The lateral outputs are the roll angle $\phi$ and the sideslip $\beta$; the longitudinal outputs are the vertical height h, the pitch angle $\theta$, and the forward velocity u.

The stability derivatives that are needed are given in Appendix A. These are given in non-dimensional stability axes form. The decision has been made to convert the aircraft equations to dimensional body axes because that is what the pilot "feels."

Summary

This chapter presents a physical description of the C-141-A aircraft. The system models, as developed in Appendix A, are overviewed. With the models developed, the next chapter presents the digital theory by which the multivariable tracker control laws are designed.

Chapter 3. [illegible] Omitted

[illegible] Proceedings

# IV Computer Program Modification

## Introduction

The computer program MULTI (Ref 3) was developed to design and simulate the techniques of Professor Brain Porter. Chapter III discusses the discrete-time domain representation of the system. The design is implemented using MULTI which is a totally interactive program. Being interactive, the program provides iterative tuning of appropriate tracker control laws for linear multivariable plants.

This chapter presents the additions and modifications made to MULTI by this author. This discussion just adds to the original program. For an understanding of the program's development and structure, as well as the basic User's and Programmer's Manuals, the thesis by Captain Douglas Porter should be referenced (Ref 3).

## Addition of B* Design Method

MULTI already implemented the control laws for unknown, regular, and irregular plants (Ref 3). The expansion of the program to include $\underline{B}^*$ designs requires calculation of the control laws using Eqs. 34 and 35 from Chapter III:

$$\underline{K}_0 = [\underline{B}^*]^{-1}\Sigma_1 \tag{34}$$

$$\underline{K}_1 = [\underline{G}(0)]^{-1}\Sigma_2 \tag{35}$$

Once $\underline{K}_0$ and $\underline{K}_1$ are determined, the simulation run remains the same as before. Use of these control laws eliminates undershoots in the response by assuring decoupling of the outputs.

The first step in the B* design is to select and to enter the weighting matrices, $\Sigma_1$ and $\Sigma_2$. It should be noted that the $\Sigma$ weighting matrix, which is in memory as determined by a previous procedure, may be used for $\Sigma_1$ and/or $\Sigma_2$. If $\Sigma_1$ and $\Sigma_2$ are not both selected equal to $\Sigma$, it may still be desirable that $\Sigma_2$ equal $\Sigma_1$. Thus, $\Sigma_1$ and $\Sigma_2$ are entered via MULTI Option #15 as shown by the flowchart of Figure 1.

Once the weighting matrices have been entered, Option #14BSTAR calculates the control laws $\underline{K}_0$ and $\underline{K}_1$. This is done first by determining the $\underline{B}^*$ matrix from the plant $\underline{A}$, $\underline{B}$, and $\underline{C}$ matrices. Then $\underline{G}(0)$ is accepted if it has been entered directly, otherwise $\underline{G}(0)$ is determined from the plant matrices. Finally, $[\underline{B}^*]^{-1}$ and $[\underline{G}(0)]^{-1}$ are calculated and multiplied by $\Sigma_1$ and $\Sigma_2$, respectively. The option terminates with error if $\underline{B}^*$ and/or $\underline{G}(0)$ are singular and thus not invertable.

## Modification for Batch Use

The interactive version of MULTI is designed to operate within the constraints of $70000_8$ words of computer core memory. This is a restriction imposed on INTERCOM users of the ASD CYBER computer. This requires the limiting of the number of time response data points. Thus, when a

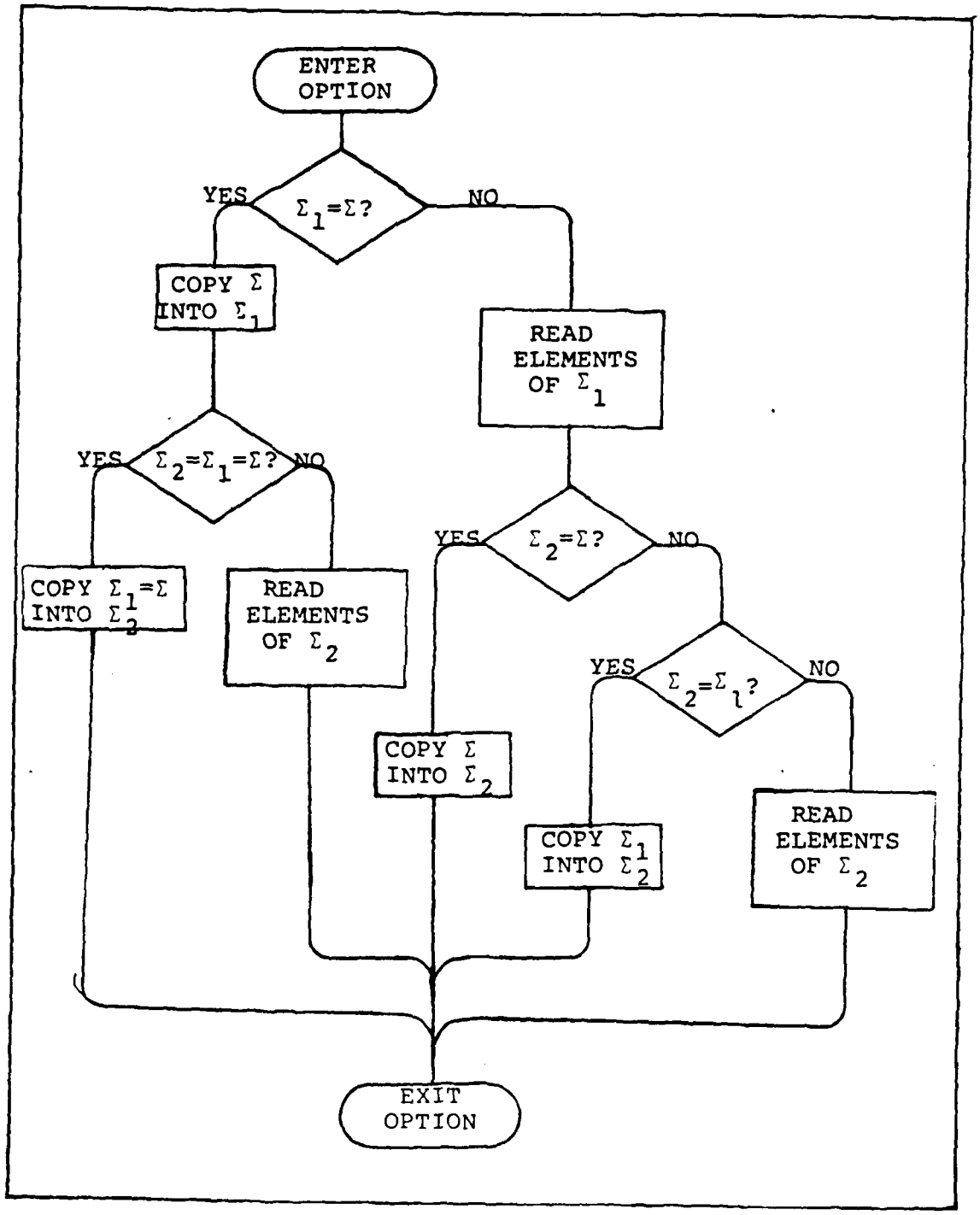



Fig. 1 Flowchart for Option #15 of MULTI

simulation is run, a maximum of 100 data points, evenly spaced throughout the total simulation time, are stored.

The limitation in the number of data points may hide transients. As an example, this can occur if the simulation produces 500 points since the interactive program would store and plot only every fifth point.

By using a batch program, the programmer is not limited to a specific core memory. MULTI is therefore modified for batch use to allow up to 500 data points.

This conversion to batch also requires elimination of the prompt commands which are used interactively. The batch version reads the data and prints back what has been read. All basic functions of "batch" MULTI remain the same as for "intercom" MULTI.

Appendix C is a User's Guide for "batch" MULTI. It is suggested that the user become familiar with the intercom version before using the batch version.

## Summary

This chapter summarizes the major additions and modifications of the MULTI computer program as made by this author. Other minor modifications have been made in trying to help improve and/or streamline the program. For a complete program listing of either the intercom or batch version, the reader should contact the AFIT Department of Electrical Engineering.

# V Multivariable Control Law Design

## Introduction

The procedures used to develop the digital multivariable tracker control laws for the C-141-A Starlifter are presented in this chapter. Controllers are designed for each of the three flight conditions. The chapter discusses the state space representation of the aircraft model used in the design of the control laws. This discussion addresses the reasons for separation of the lateral and longitudinal modes of the aircraft for the design of controllers. The manuevers used to illustrate controller performance follows. This includes enumeration of the reasons for the selection of certain manuevers. Next, the procedure used to obtain relatively "good" controllers is presented. This is followed by a discussion of the results for controllers designed at the MACH 0.18 flight condition. Robustness is tested by applying the MACH 0.18 control laws at each of the other two flight conditions. Sample controllers for the MACH 0.65 and MACH 0.76 flight conditions are also presented; simulation data for these two conditions are compiled in Appendix B. Finally, this chapter suggests consideration of a change in the output model. The reasons for this change and a sample controller are suggested.

C-141-A Input/Output Model

The design of multivariable digital control laws in this thesis is limited to the theory of Professor Brian Porter as discussed in Chapter III. Accordingly, the computer program MULTI requires that the number of outputs, which one wishes to command, must equal the number of surface inputs available. The design of controllers in this chapter uses the C-141-A state space models as developed in Chapter II and Appendix A.

The models represented by Equation (A-60) show the $\underline{A}$ and $\underline{B}$ matrices to be block diagonal. This is due to the assumption that the lateral and longitudinal modes are decoupled. Thus, in order to reduce complexity, the lateral and longitudinal control laws are designed separately. For the design of lateral controllers, the state and input vectors are:

$$\underline{x} = \begin{bmatrix} \phi \\ \beta \\ p \\ r \end{bmatrix} \quad \text{and} \quad \underline{u} = \begin{bmatrix} \delta_r \\ \delta_a \end{bmatrix} \tag{61}$$

Since there are only two lateral control surfaces, the two outputs chosen are roll angle, $\phi$, and sideslip angle, $\beta$.

Correspondingly, the longitudinal control laws are developed using the state, input, and output vectors:

$$\underline{x} = \begin{bmatrix} h \\ \theta \\ u \\ \alpha \\ q \end{bmatrix} \text{ and } \underline{u} = \begin{bmatrix} \delta_e \\ \delta_{sp} \\ \delta_T \end{bmatrix} \text{ and } \underline{y} = \begin{bmatrix} h \\ \theta \\ u \end{bmatrix} \qquad (62)$$

The system model includes the actuator and sensor dynamics as defined in Appendix A. Also included in the design are deflection limitations of the control surfaces as defined by Equation (63) below (Ref 6). It should be noted, however, that rate limitations of control surface movements are not considered.

$$\begin{aligned} -35° \leq \delta_r &\leq 35° \\ -40° \leq \delta_a &\leq 40° \\ -25° \leq \delta_e &\leq 15° \\ -30° \leq \delta_{sp} &\leq 30° \\ -50\%RPM \leq \delta_T &\leq 50\%RPM \end{aligned} \qquad (63)$$

Positive rudder is defined as the trailing edge deflected left. For the ailerons, positive deflection implies right aileron down and left aileron up. The ailerons also deflect asymmetrically such that the aileron that moves down receives 37.5% of the signal while the aileron that moves up receives the other 62.5%. Thus, 40° deflection would result in 15° down for one aileron and 25° up for the other.

Elevator deflection is defined as positive down. Positive spoilers indicate upper wing panels in use, while negative spoilers indicates lower panels. Finally, the thrust required for trimmed flight is approximately 50% of the maximum available. Thus, a "subjective" limit of $\pm$ 50% from trimmed RPM is imposed.

Manuevers

In order to illustrate performance of the digital controllers, four manuevers —— two lateral and two longitudinal —— are simulated. The four manuevers are:

1. Coordinated Turn ($\phi \leq 30°$ , $\beta = 0$)
2. Sideslip ( $\beta \leq 5°$ , $\phi = 0$)
3. Vertical Translation (h = change of altitude , $\theta = 0$ , $u = 0$)
4. Pitch Pointing ($\theta \leq 5°$ , $h = 0$ , $u = 0$)

The first two manuevers are intended to demonstrate the performance of lateral controllers; manuevers three and four correspondingly demonstrate longitudinal control capability.

The coordinated turn is a basic flight manuever for any conventional aircraft; however, the question arises as to reasons for the other three manuevers. During an approach to landing, the aircraft may be left or right of the desired flight path defined by a localizer or some other source. It may be advantageous to use sideslip to "slide" the aircraft to the desired position. The sideslip is also useful during

the touchdown in order to preclude drift while maintaining runway alignment. Similar reasons make this a useful manuever in order to get and maintain position during refueling, as simulated by the MACH 0.65 flight condition.

The vertical translation (direct lift) might also be used during approach or refueling. It could be useful for moving up or down to the desired glide slope for landing approaches or for moving vertically into position for refueling. Finally, during a landing condition in which the flaps are inoperative, the C-141 aircraft attitude is such that there is the possibility of dragging the tail during landing. Thus, pitch pointing is chosen in order to alleviate this occurrence.

Design Procedure

The generation of control laws is accomplished using the interactive computer program MULTI. The following is a condensation of the steps used in finding digital controllers which achieve "good" performance characteristics.

To begin, it must first be determined which of the four design methods discussed in Chapter III is to be used. This simply becomes a process of elimination. Neither the unknown nor the B* techniques can be used because both the steady-state transfer function matrix, $\underline{G}(0)$, and the $\underline{B}^*$ matrix are singular. Similarly, the regular plant design can not be used because the first Markov parameter, $\underline{CB}$, does not have

full rank. Therefore, the irregular technique is used in the design of all control laws.

Since irregular plant design is to be used, measurement matrices must be selected for the lateral and longitudinal systems, respectively. It is desirable to choose each measurement matrix, $\underline{M}$, as sparse as possible. This is done by using the procedures outlined by D. Brett Ridgely and others (Ref 12). All necessary elements of the measurement matrices are chosen as 0.25.

A sampling time, T, must also be selected for the digital simulations. In discussion with computer engineers, current digital computers can probably handle sampling frequencies up to 60 Hertz. Therefore, something less than 60 Hertz should be considered. The sampling time of 0.05 second (20 Hertz) is chosen as being very reasonable for aircraft computers.

With $\underline{M}$ and T chosen, all other design parameters are initially set to unity values. Each manuever is attempted with the resultant control laws and all responses are found to be unstable and highly oscillatory.

The parameter, $\alpha_r$, which sets the ratio of proportional to integral error feedback, is varied until a stable response is obtained. It is found in both the lateral and longitudinal cases that $\alpha_r > 5$ is necessary for stability; $\alpha_r = 10$ is chosen as an "optimum." This optimum value is justified by

the fact that current classical controllers for most large aircraft are also implemented with a similar 10:1 ratio.

Having selected $\alpha_r$, the $\varepsilon$ scalar parameter is varied next. Trials are made with $\varepsilon$ varying from 0.001 to 2.0. Considering trade-off in peak values, settling times, and rise times, separate $\varepsilon$ values are selected for the lateral and longitudinal designs.

At this point, the individual elements, $\sigma_i$'s, of the weighting matrix, $\Sigma$, are varied. Since, in the limiting case, these high-gain controllers achieve decoupling of the commanded outputs, the individual $\sigma_i$'s are first assumed to affect only each corresponding particular output. Various combinations of $\sigma_i$ values are then used in an attempt to find the "best" single combination.

Finally, all parameters are again varied in an attempt to "fine-tune" the appropriate controllers. Thus, the entire procedure is a repetitive one from which the desired control law is obtained.

Tracker Control Laws

The above design procedure is a straightforward process. The final selection of design parameters is intended to result in an "optimal" controller. Controllers are thus developed for each of the three flight conditions as established in Chapter II. Results of the lateral and longitudinal controllers designed for the MACH 0.18 flight condition are

discussed on the following pages. Control laws are also presented for the *MACH 0.65 and MACH 0.76 flight conditions;* simulations for these controllers are compiled in Appendix B.

MACH 0.18 Lateral Controller. The control law selected for the MACH 0.18 lateral controller is defined by the parameters:

$$T = 0.05 \text{ sec (20 Hz)} \tag{64}$$

$$\alpha_r = 10.0 \tag{65}$$

$$\varepsilon = 0.01 \tag{66}$$

$$\Sigma = \text{diag } [0.5 \ , \ 0.5] \tag{67}$$

$$\underline{M} = \begin{bmatrix} 0.25 & 0. \\ 0. & 0.25 \end{bmatrix} \tag{68}$$

which yields:

$$\underline{K}_0 = \begin{bmatrix} 0.07466 & 1.193 \\ -0.8531 & 0.2293 \end{bmatrix} \tag{69}$$

$$\underline{K}_1 = \begin{bmatrix} 0.007466 & 0.1193 \\ -0.08531 & 0.02293 \end{bmatrix} \tag{70}$$

Figure 2 shows the simulation data for this designed controller for a 15° coordinated turn. The command input vector is given by Figure 2(b). As seen in Figure 2(a), the roll angle, $\phi$, tracks the command as desired. The peak value of $\phi$, 16.6°, occurs at 5.95 sec, which is less than 1 sec

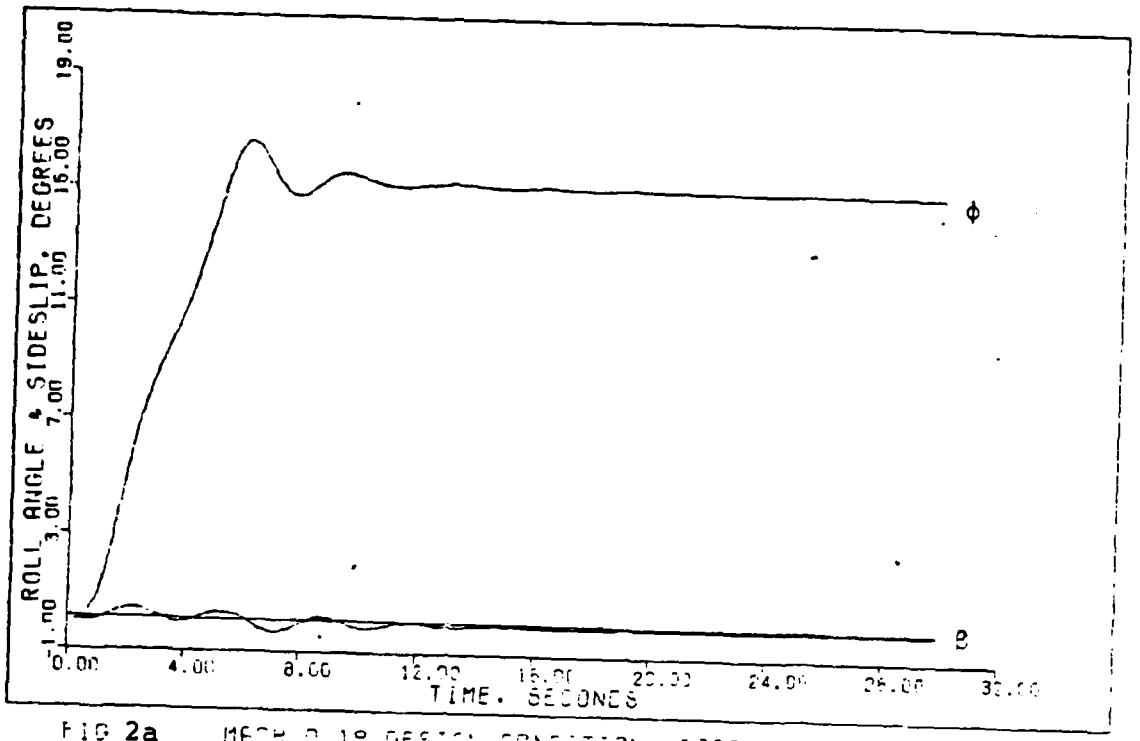



FIG 2a MACH 0.18 DESIGN CONDITION, COORDINATED TURN

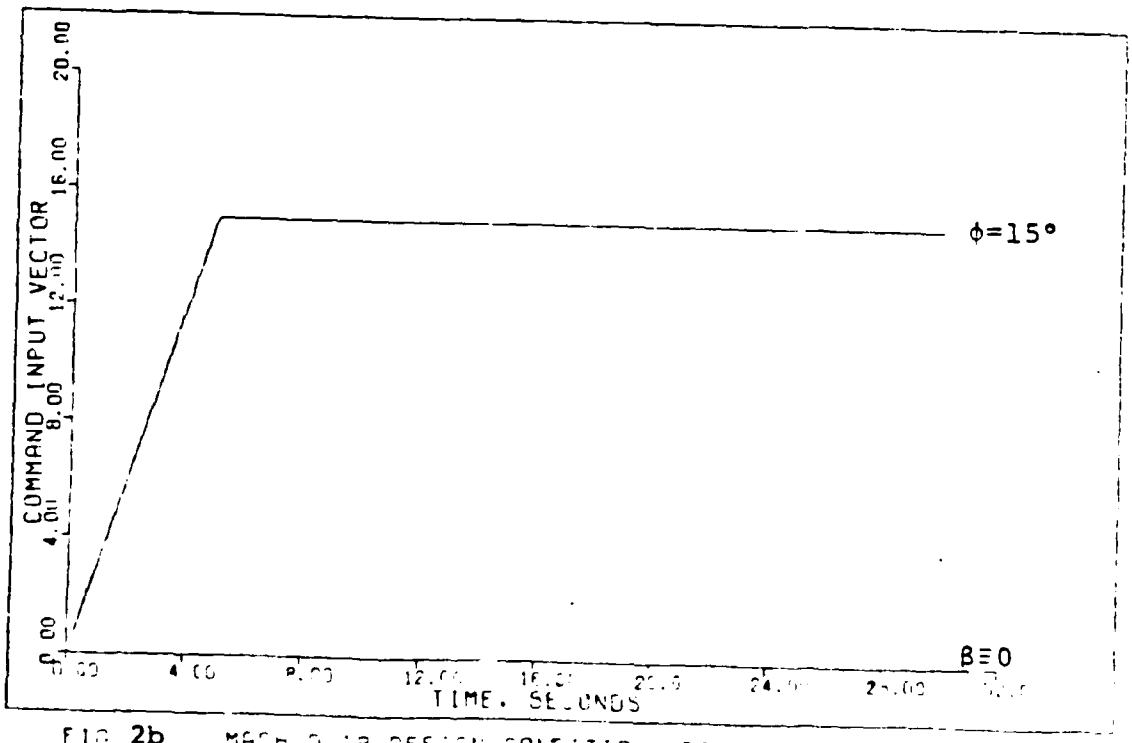



FIG 2b MACH 0.18 DESIGN CONDITION, COORDINATED TURN



Copy available to DTIC does not permit fully legible reproduction

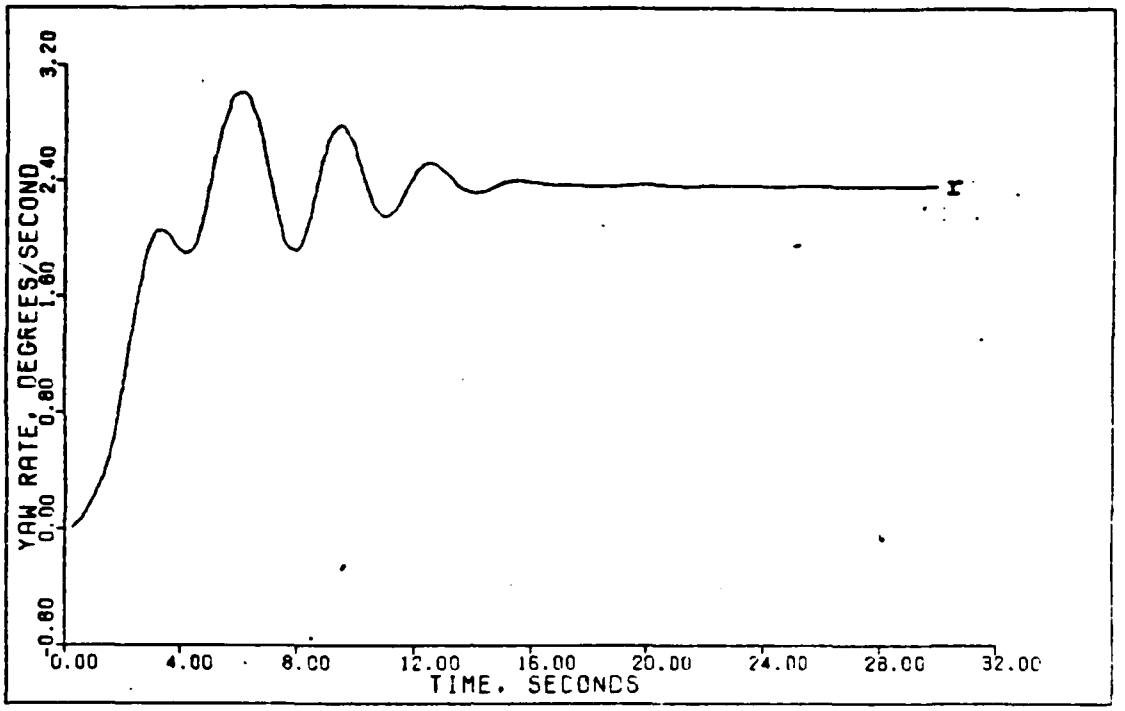



FIG 2c MACH 0.18 DESIGN CONDITION, COORDINATED TURN

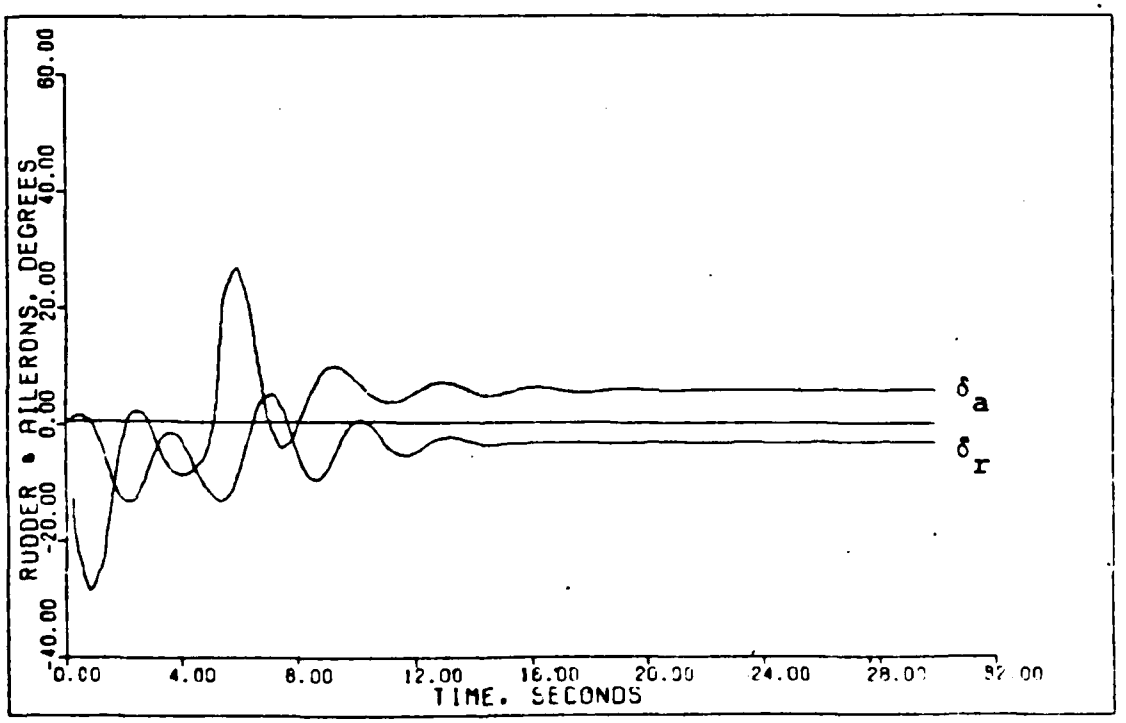



FIG 2d MACH 0.18 DESIGN CONDITION, COORDINATED TURN

after the command to steady-state. Sideslip is almost negligible as it peaks at less than one-half degree. Settling time occurs at approximately 10 sec which is 5 sec after the commanded time to steady-state.

Additionally, based on the assumptions used in Appendix A, Blakelock (Ref 13) requires that a constant yaw rate, r, be achieved in a coordinated turn. This yaw rate is defined by:

$$r = 57.3 \frac{g}{U_0} \sin\phi \qquad \frac{\text{deg}}{\text{sec}} \qquad (71)$$

Figure 2(c) shows that the state r does, in fact, reach the steady-state value of 2.38 deg/sec as computed.

Figure 2(d) shows the control surface deflections. Based on this figure, rudder and ailerons both remain within the limits set by Equation (63).

Table I summarizes the response in this simulation of the controller designed and used at MACH 0.18.

Next, the control laws previously defined by Equations (64) thru (70) are used to simulate the sideslip manuever. The outputs for this manuever are shown in Figure 3(a) for the command vector of Figure 3(b). The sideslip, $\beta$, peaks at only 5.08° (i.e., less than 2% overshoot). Peak value of $\beta$ occurs at 8.95 sec or 0.95 sec after command. Peak value of roll angle is negligible (only 0.65°), occurring at 8.65 sec.

TABLE I

Coordinated Turn Results for MACH 0.18,
1000 ft Design Condition

| INPUT/ OUTPUT | $t_p$(sec) | $t_s$(sec) | PEAK VALUE | FINAL VALUE |
|---|---|---|---|---|
| $\phi$(deg) | 5.95 | 10.45 | 16.6 | 15.0 |
| $\beta$(deg) | 2.35 | —— | 0.44 | 0. |
| r(deg/sec) | 6.25 | 13.45 | 3.0 | 2.38 |
| $\delta_r$(deg) | —— | —— | -13.07 | —— |
| $\delta_a$(deg) | —— | —— | -29.41 | —— |

Settling time is only 3 sec after steady-state command at 11 sec.

These results for a 5° sideslip manuever are summarized in Table II. This table and Figure 3(d) show that the control surfaces again remain within limits. The small offsets of $\phi$ and r shown in Figures 3(a) and (c) reach the desired steady-state value of zero at approximately one minute.

The above results of the lateral controller show it to define a decent tracker at its MACH 0.18 designed condition. Decoupling of the outputs is also good. The same controller is able to perform both manuevers.

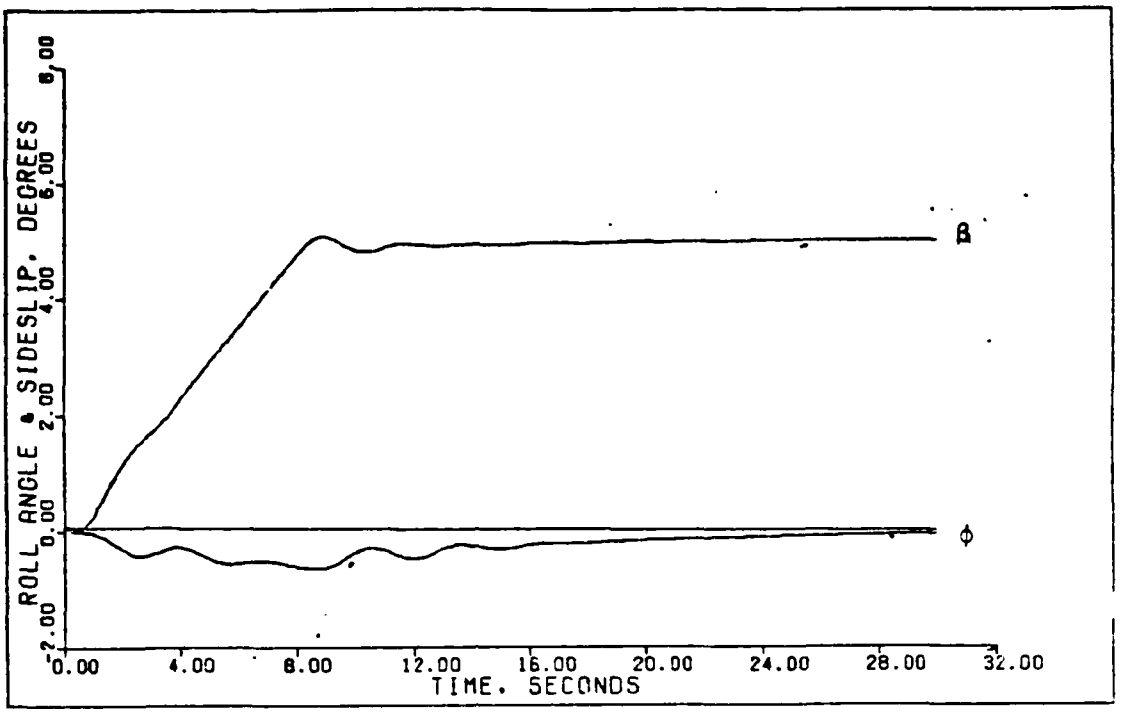



FIG 3a MACH 0.18 DESIGN CONDITION, SIDESLIP

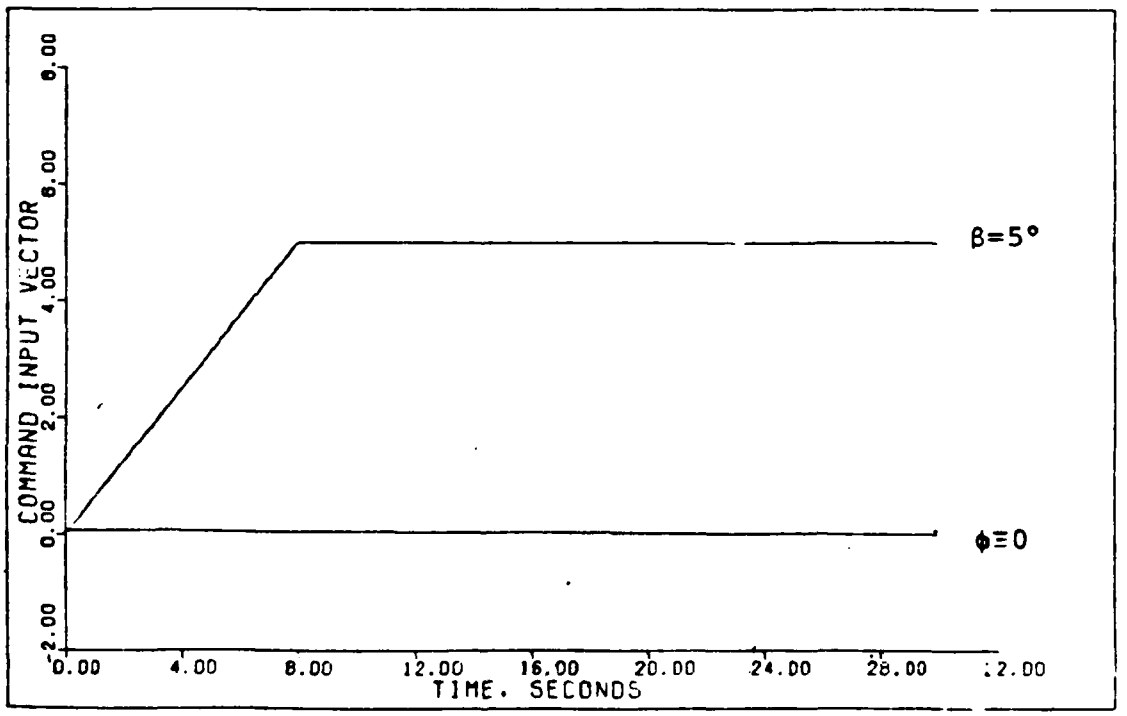



FIG 3b MACH 0.18 DESIGN CONDITION, SIDESLIP

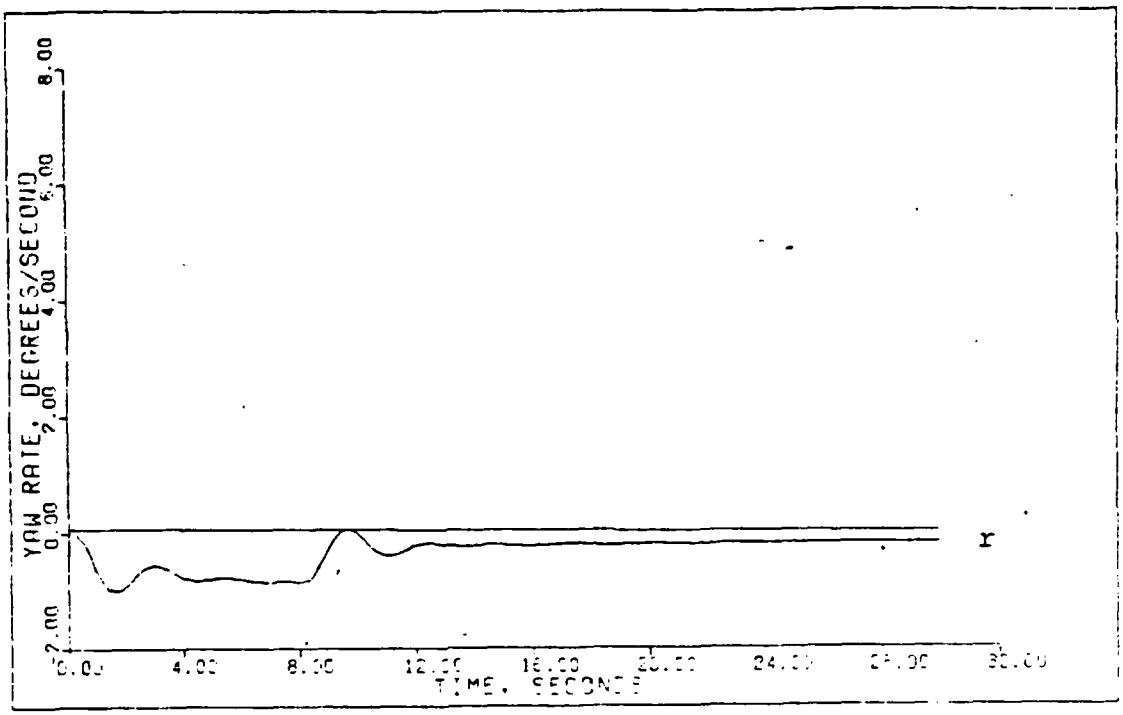



FIG 3c MACH 0.18 DESIGN CONDITION, SIDESLIP

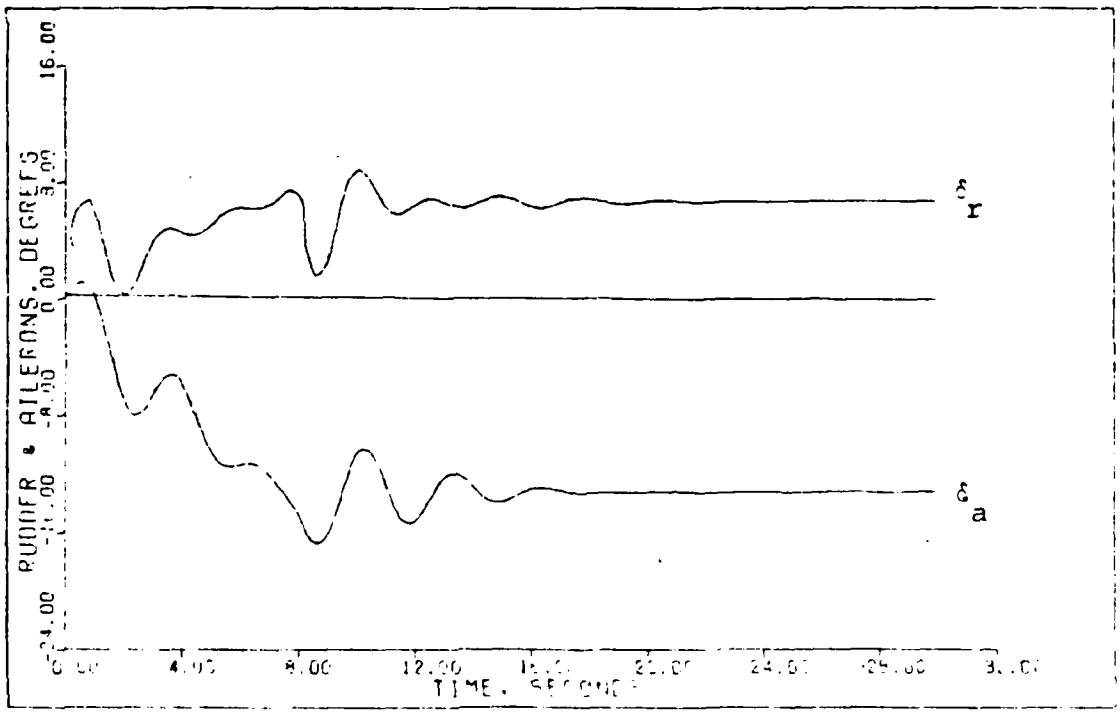



FIG 3d MACH 0.18 DESIGN CONDITION, SIDESLIP

TABLE II

Sideslip Results for MACH 0.18,
1000 ft Design Condition

| INPUT/ OUTPUT | $t_p$(sec) | $t_s$(sec) | PEAK VALUE | FINAL VALUE |
|---|---|---|---|---|
| $\beta$(deg) | 8.95 | 11.0 | 5.08 | 5.0 |
| $\phi$(deg) | 8.65 | —— | -0.65 | 0. |
| r(deg/sec) | 1.75 | —— | -0.99 | 0. |
| $\delta_r$(deg) | —— | —— | 8.93 | —— |
| $\delta_a$(deg) | —— | —— | -16.74 | —— |

MACH 0.18 Longitudinal Controller. A longitudinal controller is also designed for the MACH 0.18 flight condition. Using the longitudinal equations for MACH 0.18, the design procedure produces a controller characterized by the design parameters:

$$T = 0.05 \text{ sec (20 Hz)} \tag{72}$$

$$\alpha_r = 10.0 \tag{73}$$

$$\varepsilon = 0.005 \tag{74}$$

$$\underline{M} = \begin{bmatrix} 0.25 & 0. \\ 0. & 0.25 \\ 0. & 0. \end{bmatrix} \tag{75}$$

$$\Sigma = \text{diag } [0.1 \ , \ 1.0 \ , \ 0.2] \tag{76}$$

These parameters yield the digital control law matrices, $\underline{K}_0$ and $\underline{K}_1$, for the irregular longitudinal plant as:

$$\underline{K}_0 = \begin{bmatrix} -0.01066 & -0.2976 & 0. \\ -0.03822 & -0.04902 & 0. \\ 0.06651 & 0.04823 & -0.1352 \end{bmatrix} \quad (77)$$

$$\underline{K}_1 = \begin{bmatrix} -0.001066 & -0.02976 & 0. \\ -0.003822 & -0.004902 & 0. \\ 0.006651 & 0.004823 & -0.01352 \end{bmatrix} \quad (78)$$

Figure 4 shows the simulation of the above longitudinal control law to a commanded vertical translation manuever of h = 50 ft. These plots indicate deviations from the original trimmed flight condition as do all simulations. Table III summarizes the results of this simulation. For this simulation, the desired 50 foot change of altitude overshoots by about 13%. Excellent decoupling occurs for pitch angle and velocity. Maximum pitch change is less than one-half degree from the 6.1° trim condition. Velocity drops less than 2% below trim velocity, $U_0$, of 201 ft/sec.

The fourth manuever, pitch pointing, is also accomplished with the designed control laws. Figure 5 illustrates the system response for this manuever command as shown in Figure 5(b). The fact that the settling time for pitch angle is 30 sec is not an undesirable characteristic. This suggests that the stability of the system results in the desired pitch change without changing altitude, velocity, or flight path angle.

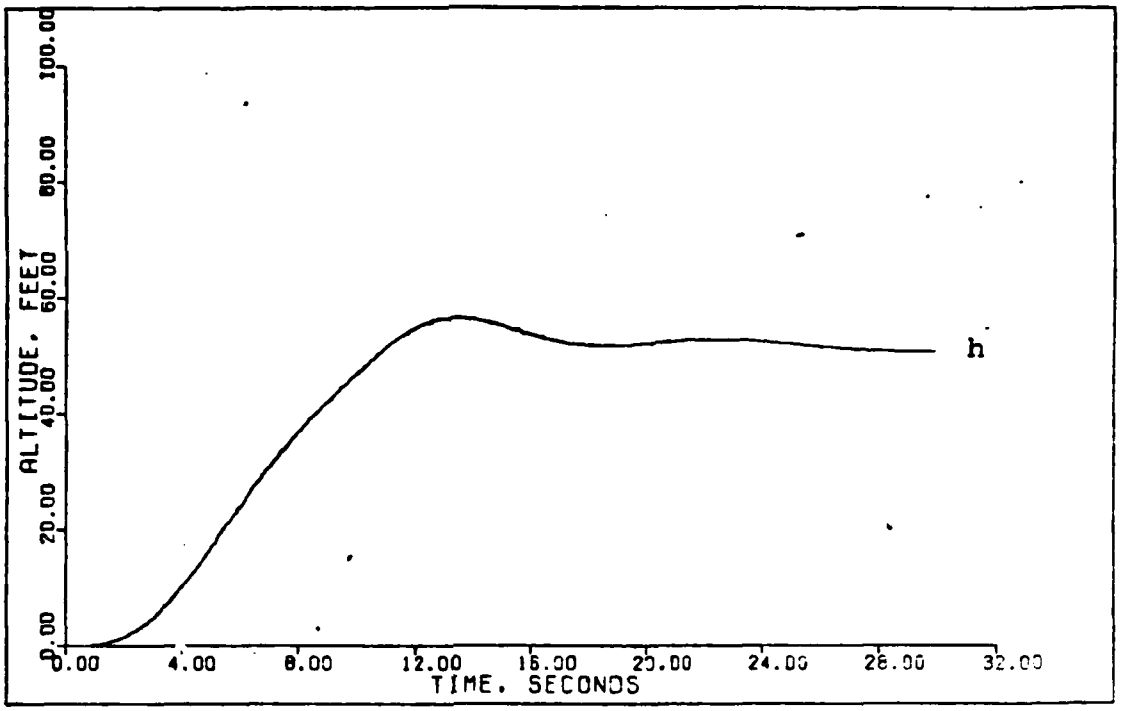



FIG 4a MACH 0.18 DESIGN CONDITION, VERTICAL TRANSLATION

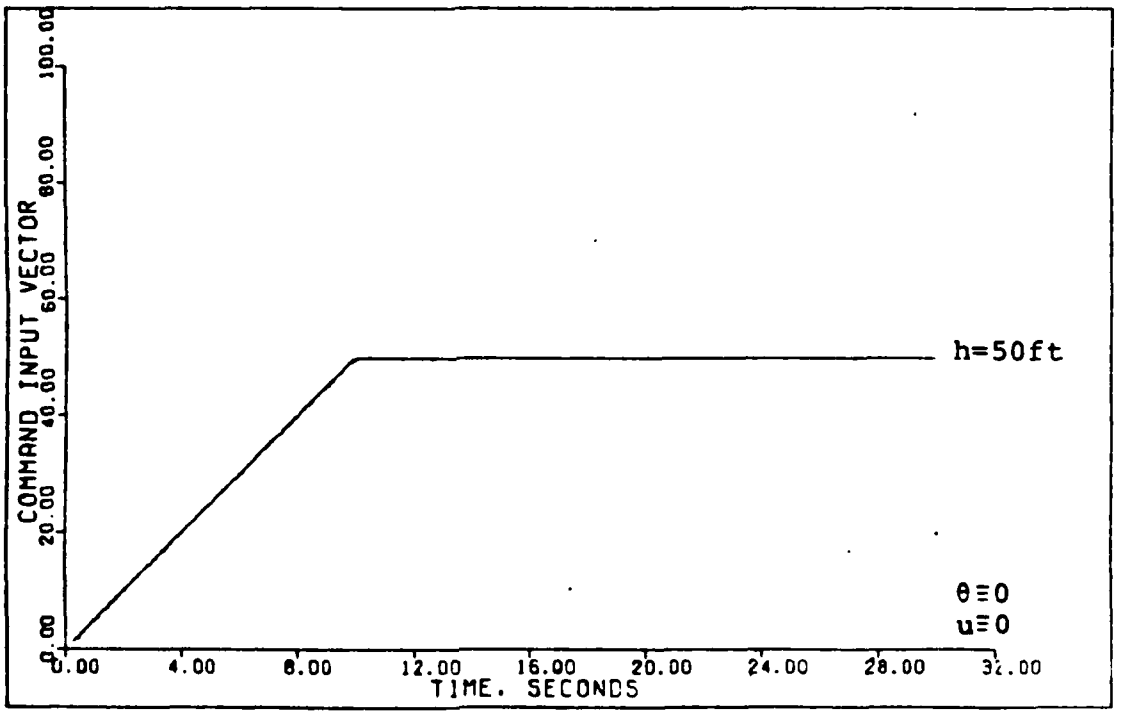



FIG 4b MACH 0.18 DESIGN CONDITION, VERTICAL TRANSLATION

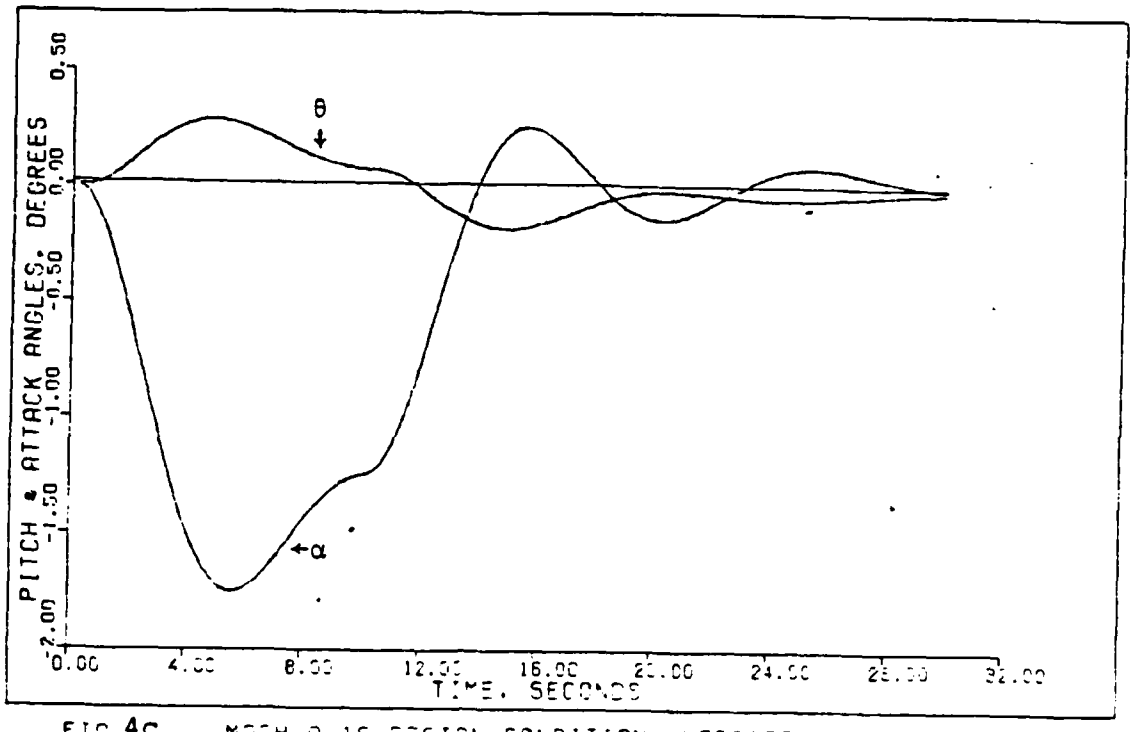



FIG 4c MACH 0.18 DESIGN CONDITION, VERTICAL TRANSLATION

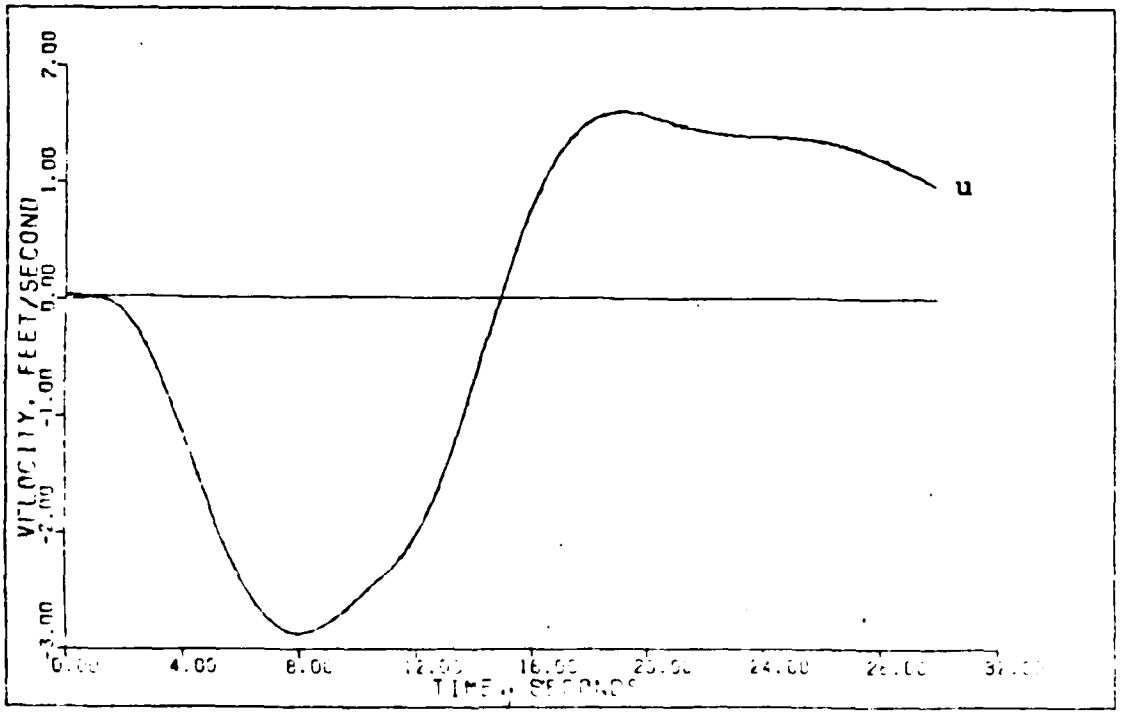



FIG 4d MACH 0.18 DESIGN CONDITION, VERTICAL TRANSLATION

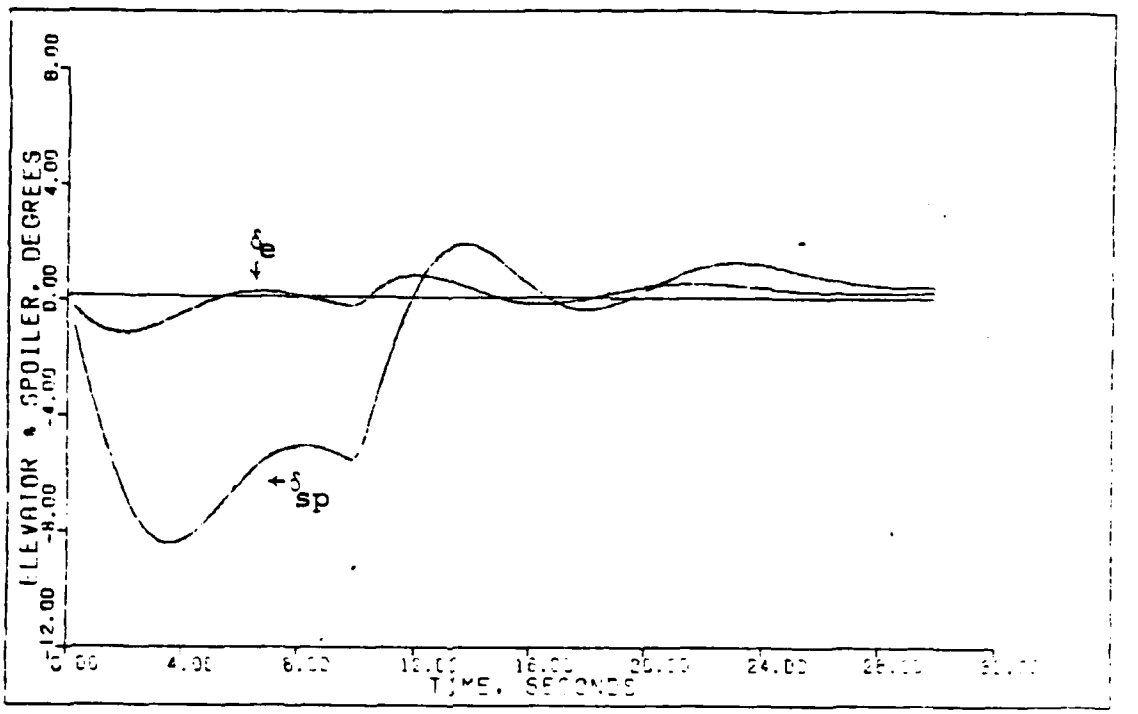



FIG 4e MACH 0.18 DESIGN CONDITION, VERTICAL TRANSLATION

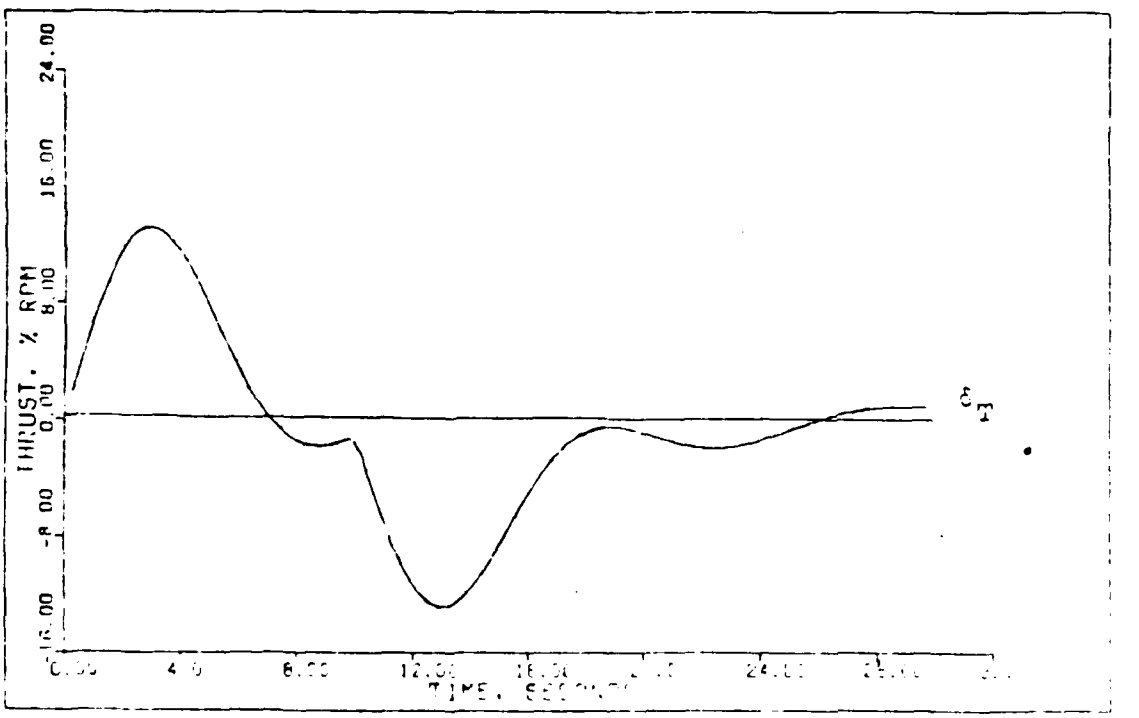



FIG 4f MACH 0.18 DESIGN CONDITION, VERTICAL TRANSLATION



Copy available to DTIC does not permit fully legible reproduction

TABLE III

Vertical Translation Results for MACH 0.18, 1000 ft Design Condition

| INPUT/ OUTPUT | $t_p$(sec) | $t_s$(sec) | PEAK VALUE | FINAL VALUE |
|---|---|---|---|---|
| h(ft) | 13.45 | 27.0 | 56.0 | 50. |
| $\theta$(deg) | 4.75 | —— | 0.28 | 0. |
| $\alpha$(deg) | 5.65 | —— | -1.75 | 0. |
| u(ft/sec) | 8.05 | —— | -2.86 | 0. |
| $\delta_e$(deg) | —— | —— | -1.16 | —— |
| $\delta_{sp}$(deg) | —— | —— | -8.41 | —— |
| $\delta_T$(% RPM) | —— | —— | 13.1 | —— |

Figures 5(c) and (d) show that altitude varies by less than 10 ft and velocity a maximum of only about 1.5 ft/sec. Figures 5(e) and (f) illustrate the control surface deflections for the system. These deflections, as in all previous simulations, remain well within the permissable values. The results of the pitch pointing manuever at MACH 0.18 are summarized in Table IV.

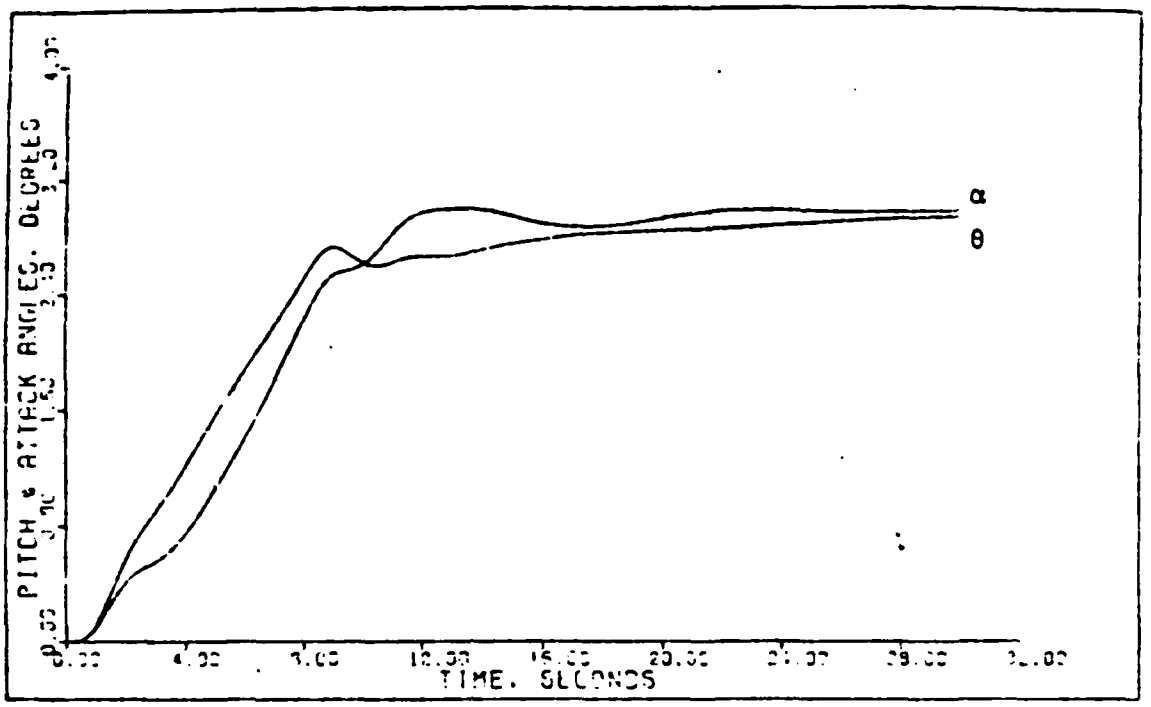



FIG 5a MACH 0.19 DESIGN CONDITION. PITCH POINTING

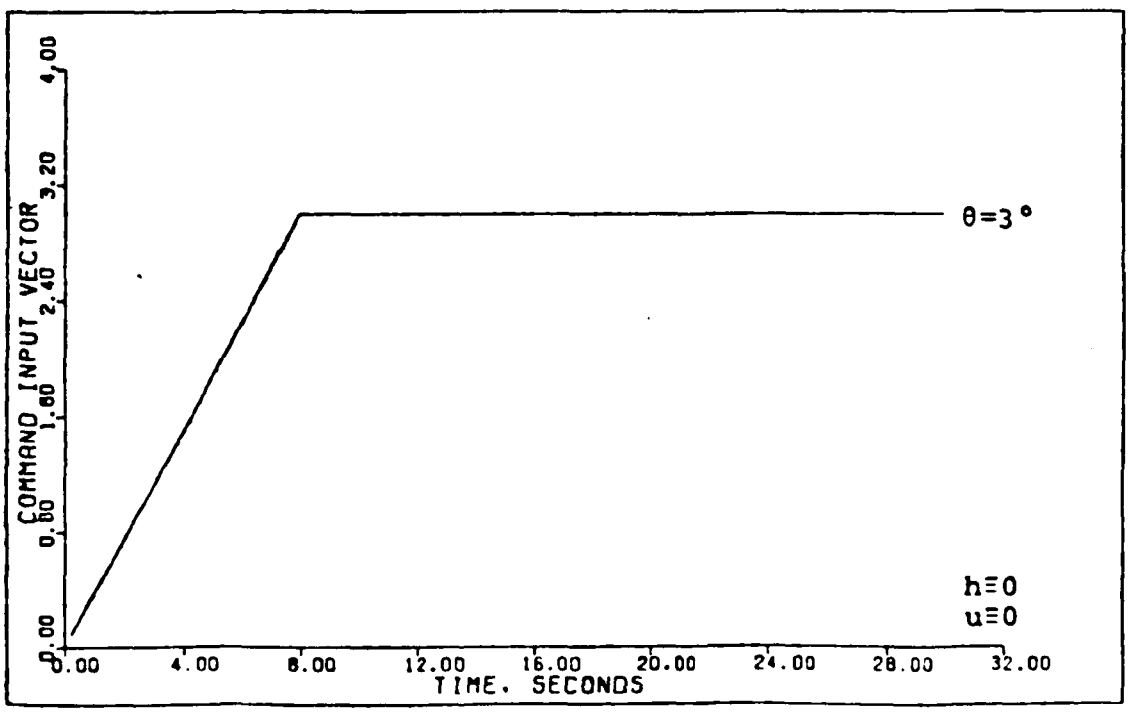



FIG 5b MACH 0.18 DESIGN CONDITION. PITCH POINTING

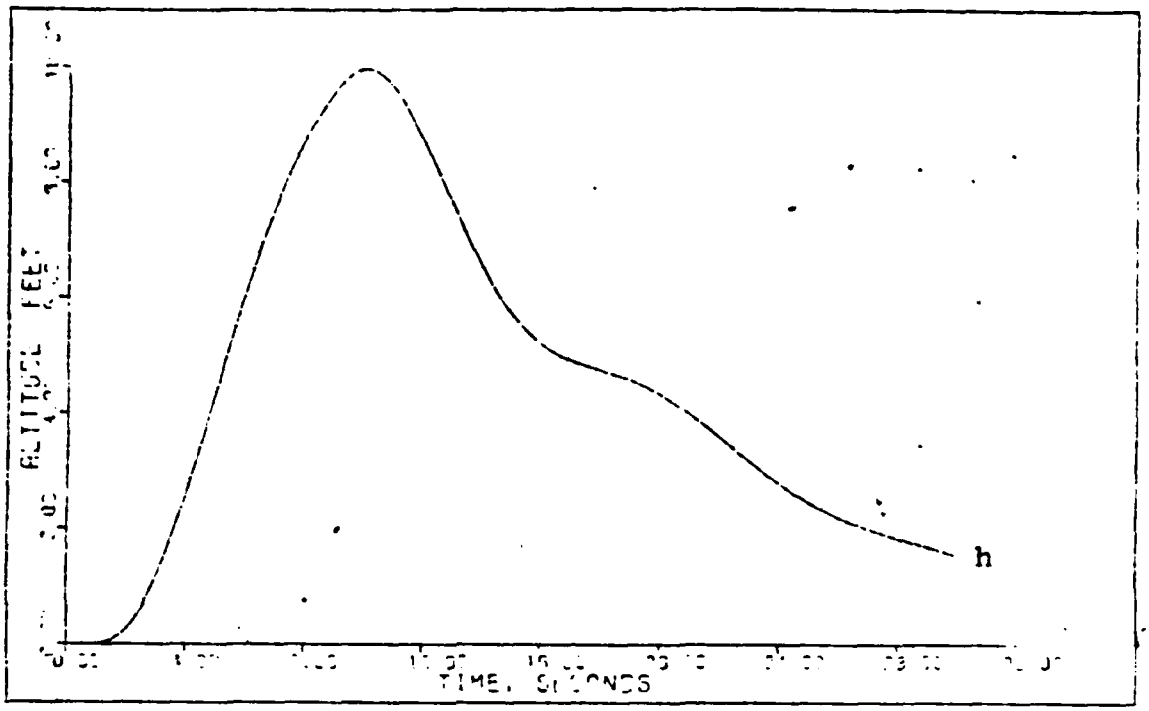



FIG 5c MACH 0.10 DESIGN CONDITION, PITCH POINTING

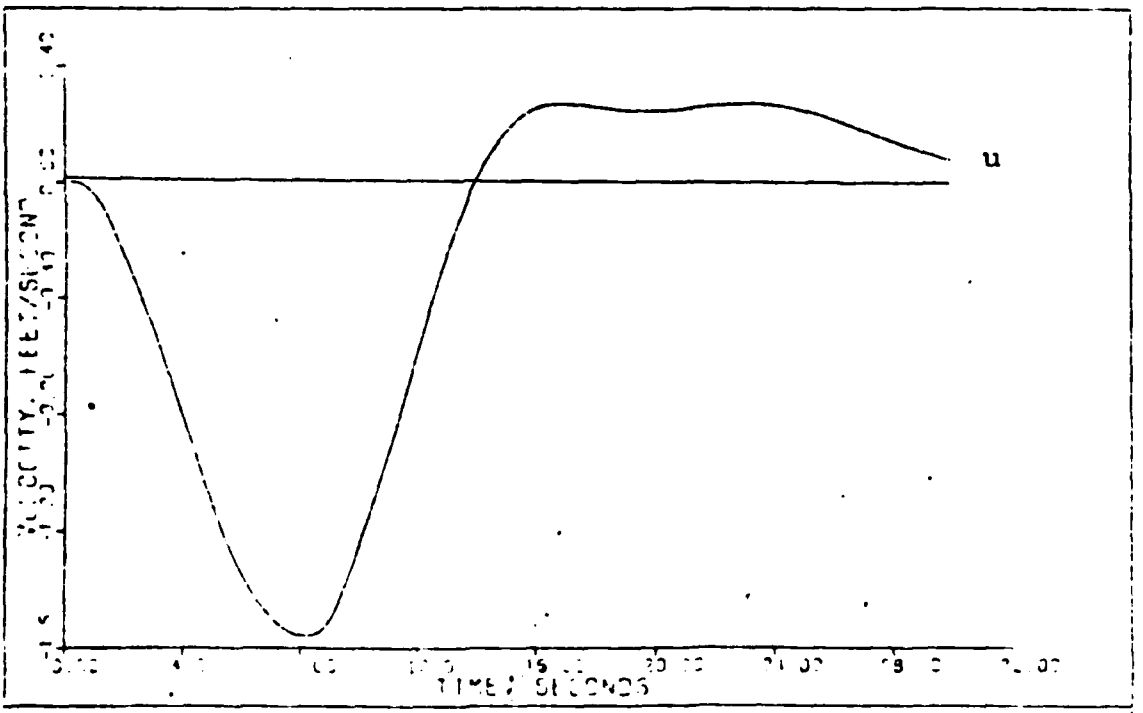



FIG 5d MACH 0.10 DESIGN CONDITION, PITCH POINTING

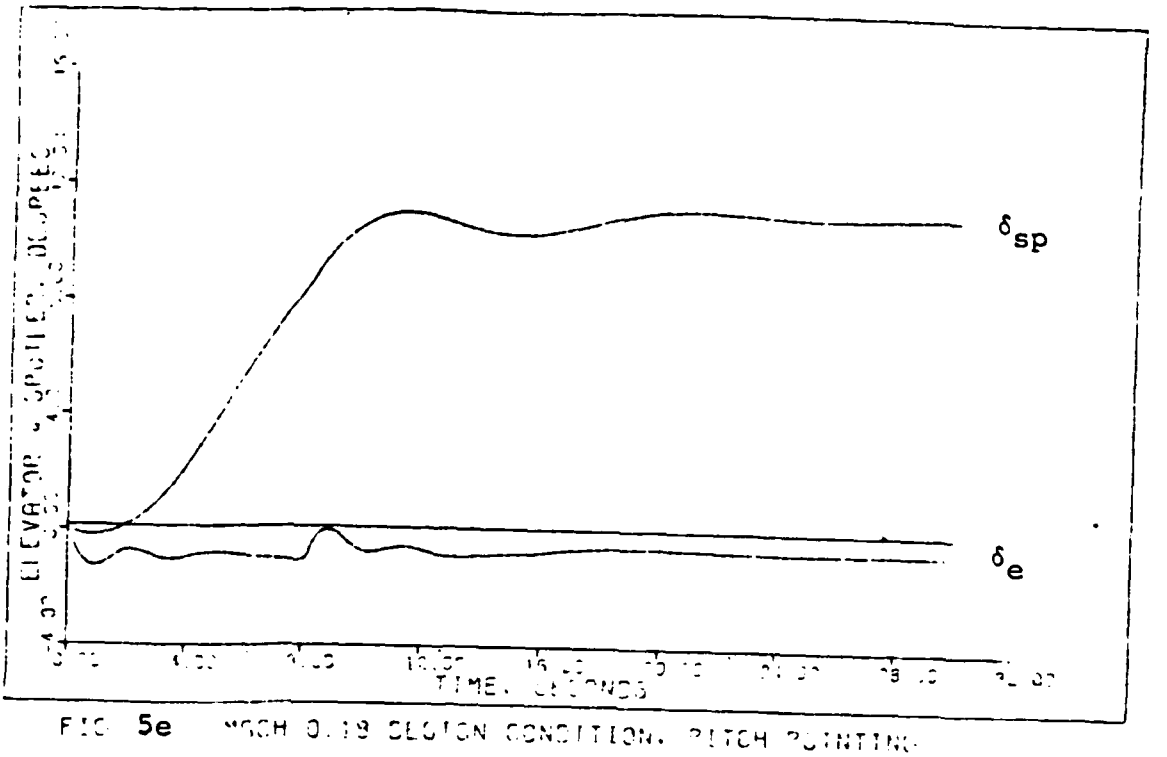



FIG 5e MACH 0.18 CLIMB CONDITION, PITCH POINTING

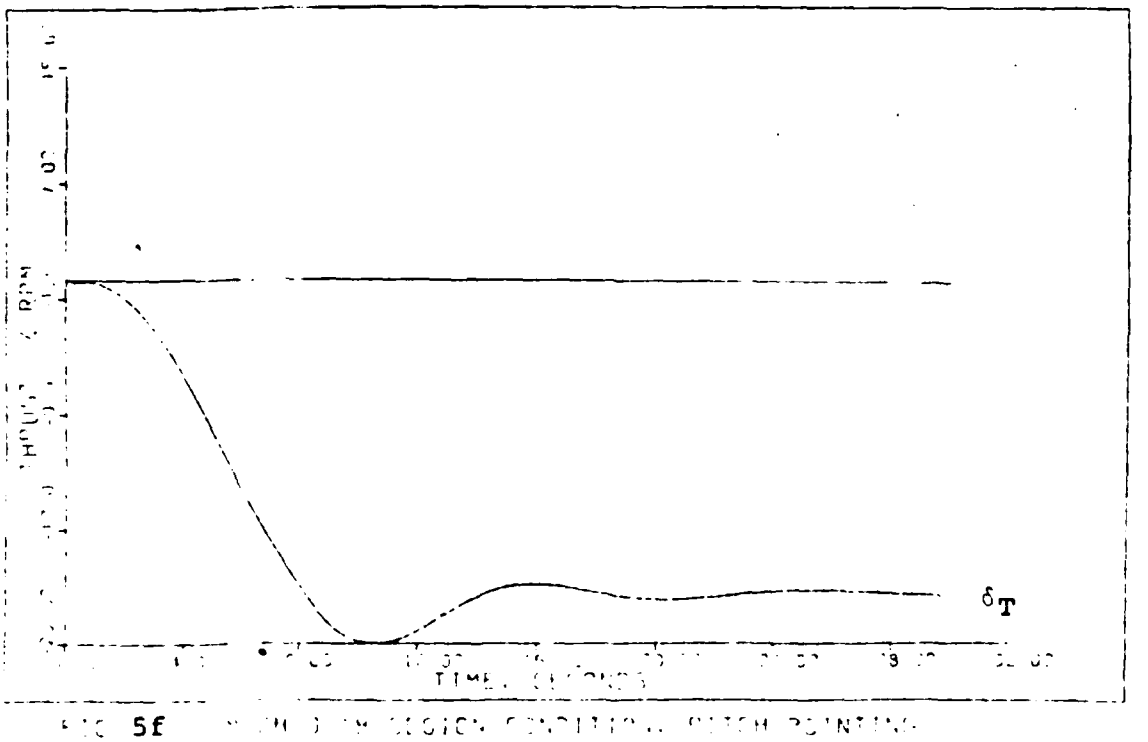



FIG 5f MACH 0.18 CLIMB CONDITION, PITCH POINTING

TABLE IV

Pitch Pointing Results for MACH 0.18, 1000 ft Design Condition

| INPUT/ OUTPUT | $t_p$(sec) | $t_s$(sec) | PEAK VALUE | FINAL VALUE |
|---|---|---|---|---|
| $\theta$(deg) | — | 60 | 3.0 | 3.0 |
| $\alpha$(deg) | — | 60 | 3.0 | 3.0 |
| h(ft) | 10.15 | — | 9.97 | 0. |
| u(ft/sec) | 8.35 | — | -1.56 | 0. |
| $\delta_e$(deg) | — | — | -1.27 | — |
| $\delta_{sp}$(deg) | — | — | 11.1 | — |
| $\delta_T$(% RPM) | — | — | -25.0 | — |

MACH 0.65 Controllers. Using the design procedures outlined, controllers can also be designed at other flight conditions. A sample lateral controller for the MACH 0.65 flight condition is defined by the parameters:

$$T = 0.05 \text{ sec (20 Hz)} \tag{79}$$

$$\alpha_r = 10.0 \tag{80}$$

$$\varepsilon = 0.01 \tag{81}$$

$$\underline{M} = \begin{bmatrix} 0.25 & 0. \\ 0. & 0.25 \end{bmatrix} \tag{82}$$

$$\Sigma = \text{diag } [2.0 \ , \ 2.0] \tag{83}$$

which yields the control law matrices:

$$\underline{K}_0 = \begin{bmatrix} 0.03270 & 0.8596 \\ -0.9285 & 0.2534 \end{bmatrix} \quad (84)$$

$$\underline{K}_1 = \begin{bmatrix} 0.003270 & 0.08596 \\ -0.09285 & 0.02534 \end{bmatrix} \quad (85)$$

A corresponding longitudinal controller produced from the parameter values:

$$T = 0.05 \text{ sec } ( 20 \text{ Hz}) \quad (86)$$

$$\alpha_r = 10.0 \quad (87)$$

$$\varepsilon = 0.005 \quad (88)$$

$$\underline{M} = \begin{bmatrix} 0.25 & 0. \\ 0. & 0.25 \\ 0. & 0. \end{bmatrix} \quad (89)$$

$$\Sigma = \text{diag } [0.05 , 2.0 , 0.001] \quad (90)$$

yields the control law matrices:

$$\underline{K}_0 = \begin{bmatrix} -0.001431 & -0.1218 & 0. \\ -0.005965 & -0.03237 & 0. \\ 0.05655 & 0.30 & -0.001293 \end{bmatrix} \quad (91)$$

$$\underline{K}_1 = \begin{bmatrix} -0.0001431 & -0.01218 & 0. \\ -0.0005965 & -0.003237 & 0. \\ 0.005655 & 0.030 & -0.0001293 \end{bmatrix} \quad (92)$$

Simulations are accomplished for these control laws at MACH 0.65 using all four manuevers. Rather than discuss

these simulations in detail, they are simply compiled in Appendix B for observation.

MACH 0.76 Controllers. Digital tracker control laws can also be designed at the MACH 0.76 flight condition. An "optimal" lateral controller thus designed is based on the parameter values:

$$T = 0.05 \text{ sec (20 Hz)} \tag{93}$$

$$\alpha_r = 10.0 \tag{94}$$

$$\varepsilon = 0.01 \tag{95}$$

$$\underline{M} = \begin{bmatrix} 0.25 & 0. \\ 0. & 0.25 \end{bmatrix} \tag{96}$$

$$\Sigma = \text{diag } [1.0 \ , \ 1.0] \tag{97}$$

and yields the control law matrices:

$$\underline{K}_0 = \begin{bmatrix} 0.02643 & 0.5493 \\ -0.4614 & 0.1211 \end{bmatrix} \tag{98}$$

$$\underline{K}_1 = \begin{bmatrix} 0.002643 & 0.05493 \\ -0.04614 & 0.01211 \end{bmatrix} \tag{99}$$

Similarly, longitudinal control laws are defined by the parameter values:

$$T = 0.05 \text{ sec (20 Hz)} \tag{100}$$

$$\alpha_r = 10.0 \tag{101}$$

$$\varepsilon = 0.005 \tag{102}$$

$$\underline{M} = \begin{bmatrix} 0.25 & 0. \\ 0. & 0.25 \\ 0. & 0. \end{bmatrix} \tag{103}$$

$$\Sigma = \text{diag}\,[0.05\ ,\ 0.5\ ,\ 0.01] \tag{104}$$

which yield the controller matrices:

$$\underline{K}_0 = \begin{bmatrix} -0.001364 & -0.03410 & 0. \\ -0.006595 & -0.01058 & 0. \\ 0.07686 & 0.120 & -0.01747 \end{bmatrix} \tag{105}$$

$$\underline{K}_1 = \begin{bmatrix} -0.0001364 & -0.003410 & 0. \\ -0.0006595 & -0.001058 & 0. \\ 0.007686 & 0.0120 & -0.001747 \end{bmatrix} \tag{106}$$

These multivariable control laws are also simulated for all four manuevers at the design condition. Appendix B contains these simulations for viewing.

Robustness

Although control laws are designed at each flight condition, it is desirable that a single controller should result in satisfactory performance at all flight conditions. A robust controller would preclude gain scheduling as is now required for classically designed controllers. Thus, robustness of the control laws designed at the MACH 0.18 flight condition is tested at the other two flight conditions. Again, each of the four manuevers are attempted at MACH 0.65 and MACH 0.76 using the control laws defined by Equations (64) thru (70) and Equations (72) thru (78).

TABLE V

Coordinated Turn Results for MACH 0.65, 25000 ft (Designed at MACH 0.18)

| INPUT/ OUTPUT | $t_p$(sec) | $t_s$(sec) | PEAK VALUE | FINAL VALUE |
|---|---|---|---|---|
| $\phi$(deg) | 5.65 | 5.95 | 31.2 | 30.0 |
| $\beta$(deg) | 0.85 | —— | 0.15 | 0. |
| r(deg/sec) | 6.85 | 25.0 | 1.8 | 1.4 |
| $\delta_r$(deg) | —— | —— | -3.8 | —— |
| $\delta_a$(deg) | —— | —— | -28.6 | —— |

*Commanding* a 30° coordinated turn at MACH 0.65, the responses are presented in Figure 6. The roll angle tracks very well as shown in Figure 6(a). Sideslip is highly decoupled and is almost negligible. Yaw rate, r, in Figure 6(c) reaches the desired steady-state value of 1.4 deg/sec as defined by Equation (71). These results are summarized in Table V.

A 30° coordinated turn at MACH 0.76 is also command using the MACH 0.18 lateral control laws. The simulations are shown in Figure 7 and the results are summarized in Table VI. This simulation tracks the command as desired and produces a yaw rate of 1.4 deg/sec.

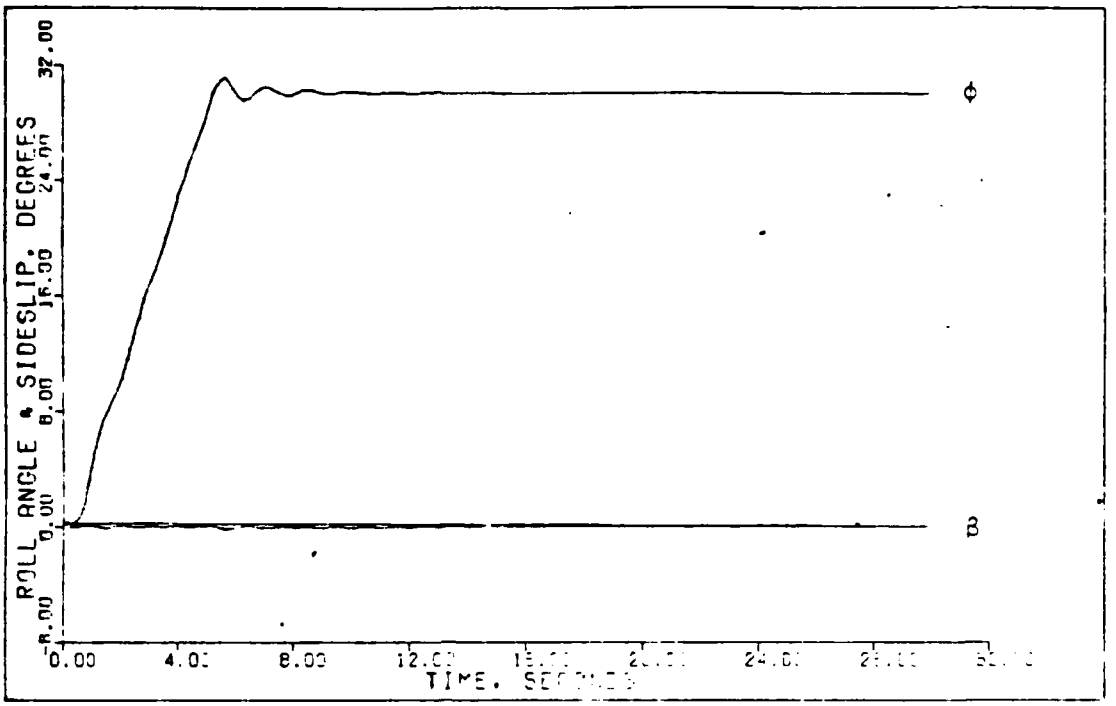



FIG 6a MACH 0.65 (DESIGN MACH 0.18), COORDINATED T.R.

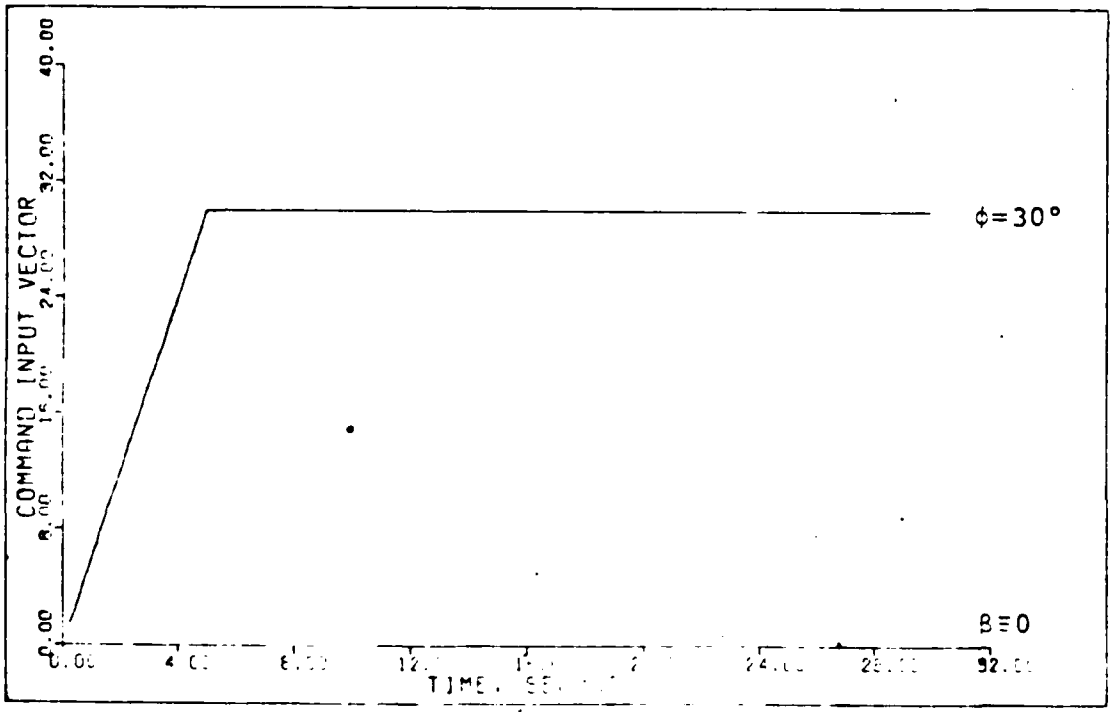



FIG 6b MACH 0.65 (DESIGN MACH 0.18), COORDINATED T.R.



Copy available to DTIC does not permit fully legible reproduction

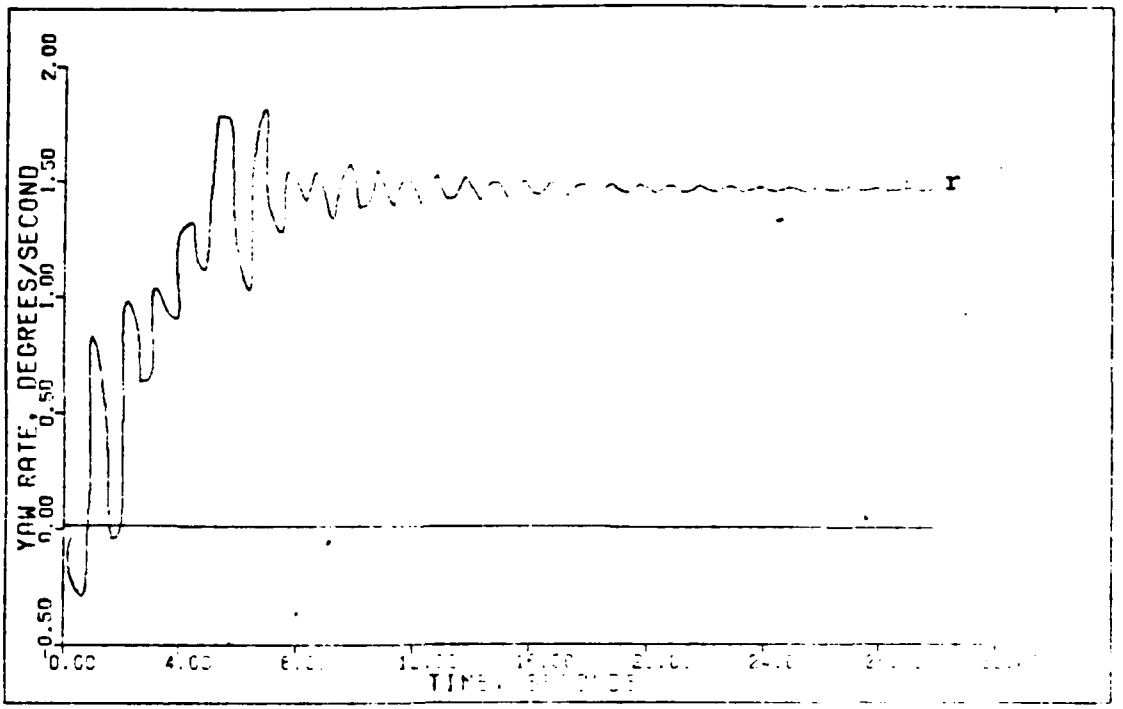



FIG 6c MACH 0.85 ICBEIA/ MACH 0.15 , CONFIGURATION 1.3

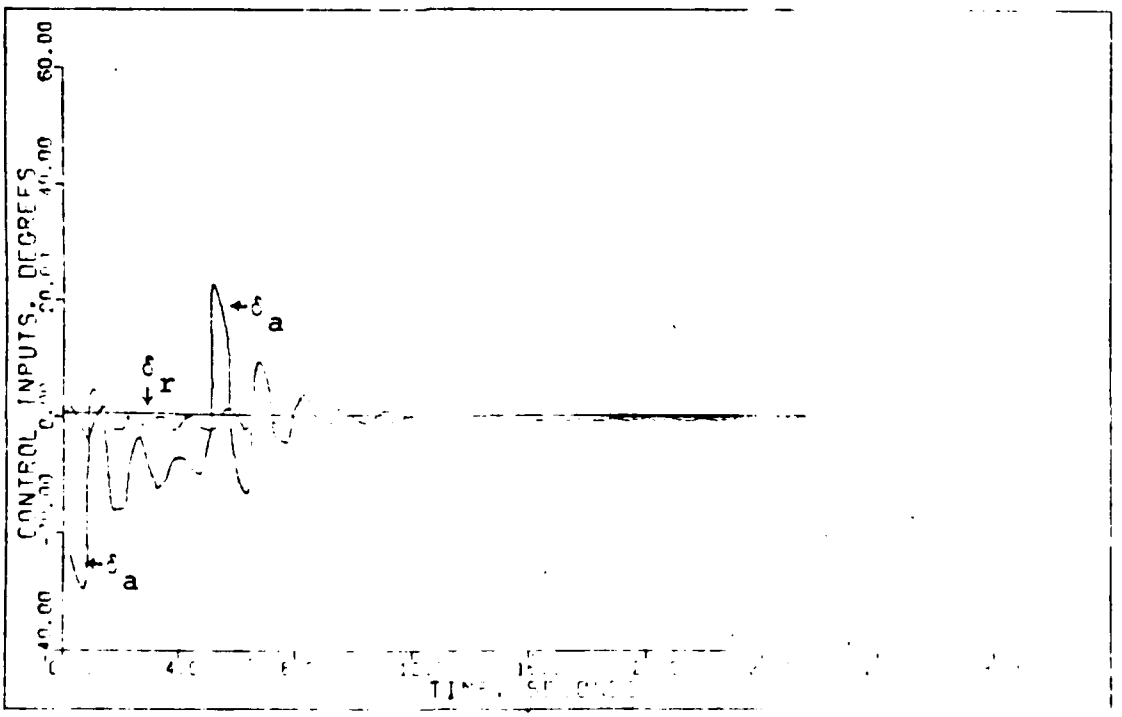



FIG 6d MACH 0.85 ICBEIA/ MACH 0.15 , CONFIGURATION 1.3

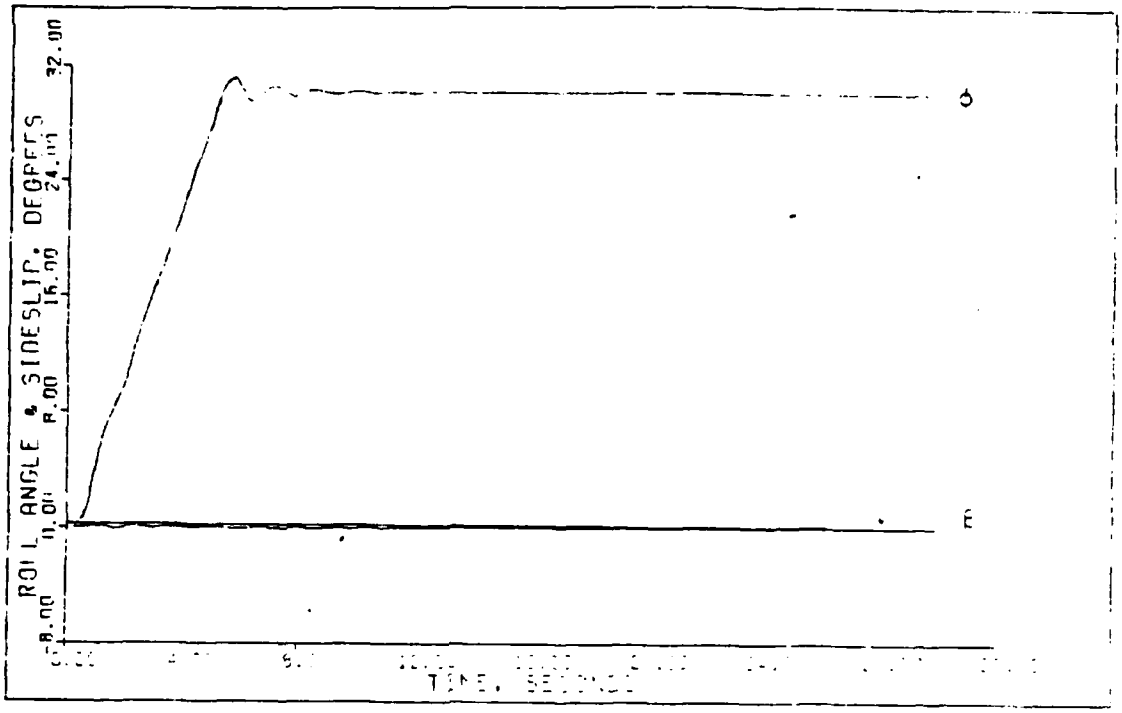



FIG 7a MACH 0.75 DESIGN MACH 0.8 , CORRECTED TURN

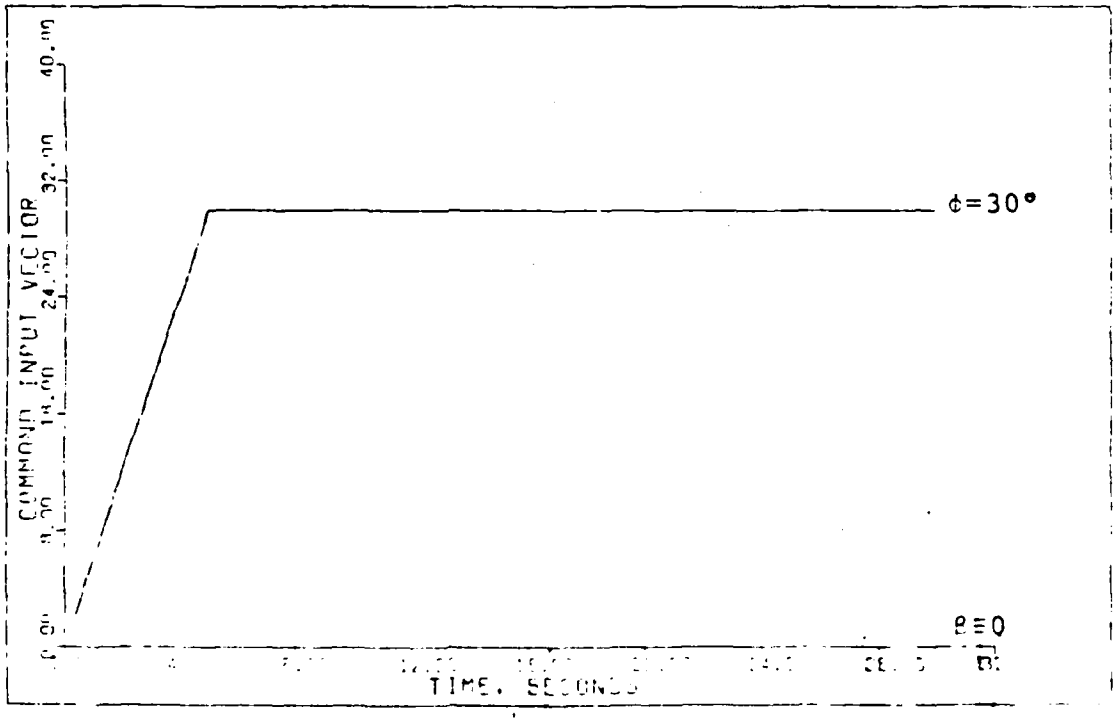



FIG 7b MACH 0.75 DESIGN MACH 0.8 , COORDINATED TURN



Copy available to DTIC does not permit fully legible reproduction

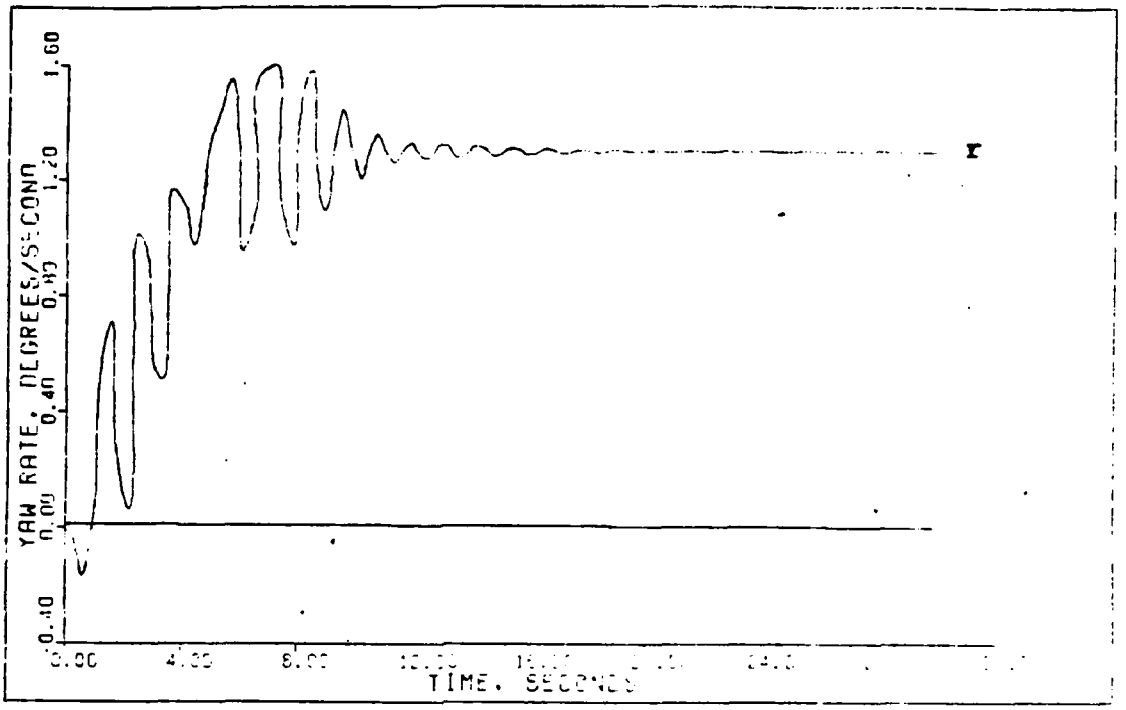



FIG 7c MACH 0.76 (DESIGN MACH 0.80), COORDINATED

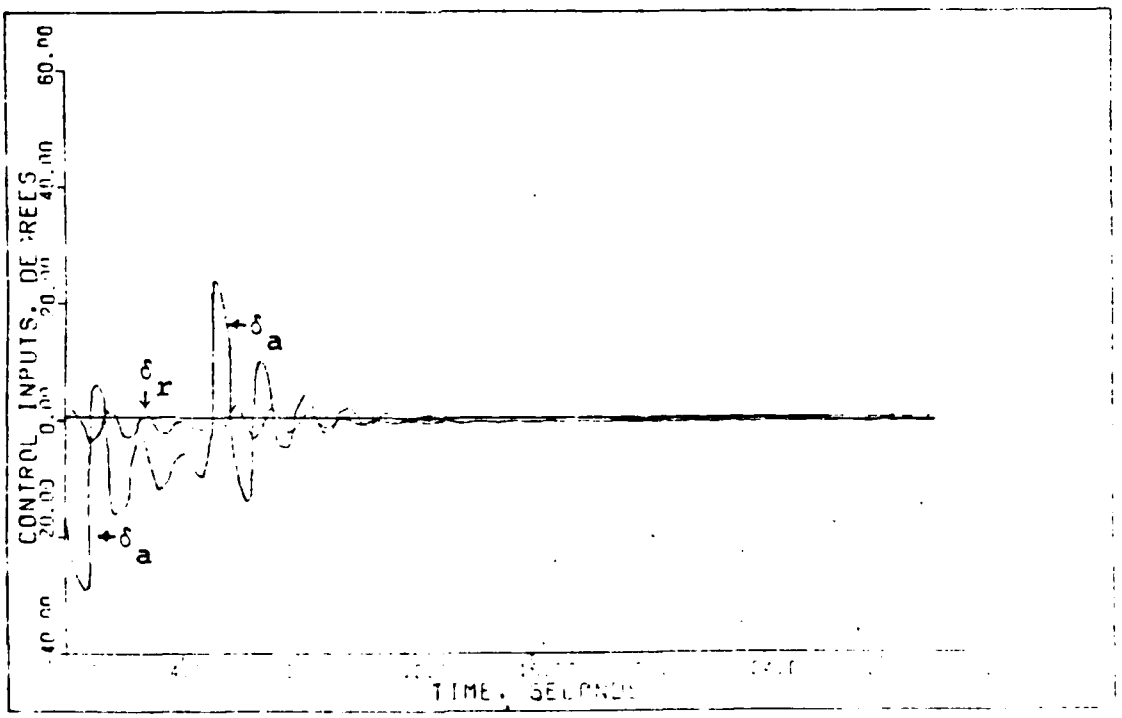



FIG 7d MACH [illegible] DESIGN MACH [illegible], COORDINATED

TABLE VI

Coordinated Turn Results for MACH 0.76, 40000 ft (Designed at MACH 0.18)

| INPUT/ OUTPUT | $t_p$ (sec) | $t_s$ (sec) | PEAK VALUE | FINAL VALUE |
|---|---|---|---|---|
| $\phi$ (deg) | 5.65 | 5.95 | 31.2 | 30.0 |
| $\beta$ (deg) | 2.35 | —— | 0.13 | 0. |
| r (deg/sec) | 7.15 | 20.0 | 1.6 | 1.24 |
| $\delta_r$ (deg) | —— | —— | -3.6 | —— |
| $\delta_a$ (deg) | —— | —— | -28.0 | —— |

Similar comparisons are made when simulating the sideslip manuever for both the MACH 0.65 and MACH 0.76 conditions using the MACH 0.18 controller. These simulations are given in Figures 8 and 9, respectively. The corresponding results are summarized in Tables VII and VIII. In both cases, tracking is good for sideslip. Further, the roll angle is greatly decoupled from the sideslip, and the yaw rate steady-state is zero as predicted.

For the four lateral simulations (Figures 6 thru 9), neither rudder nor ailerons reach their limiting values throughout the simulation. The MACH 0.18 laterally designed digital multivariable tracker control laws show good responses for three diverse flight conditions. Robustness of the lateral controller is excellent.

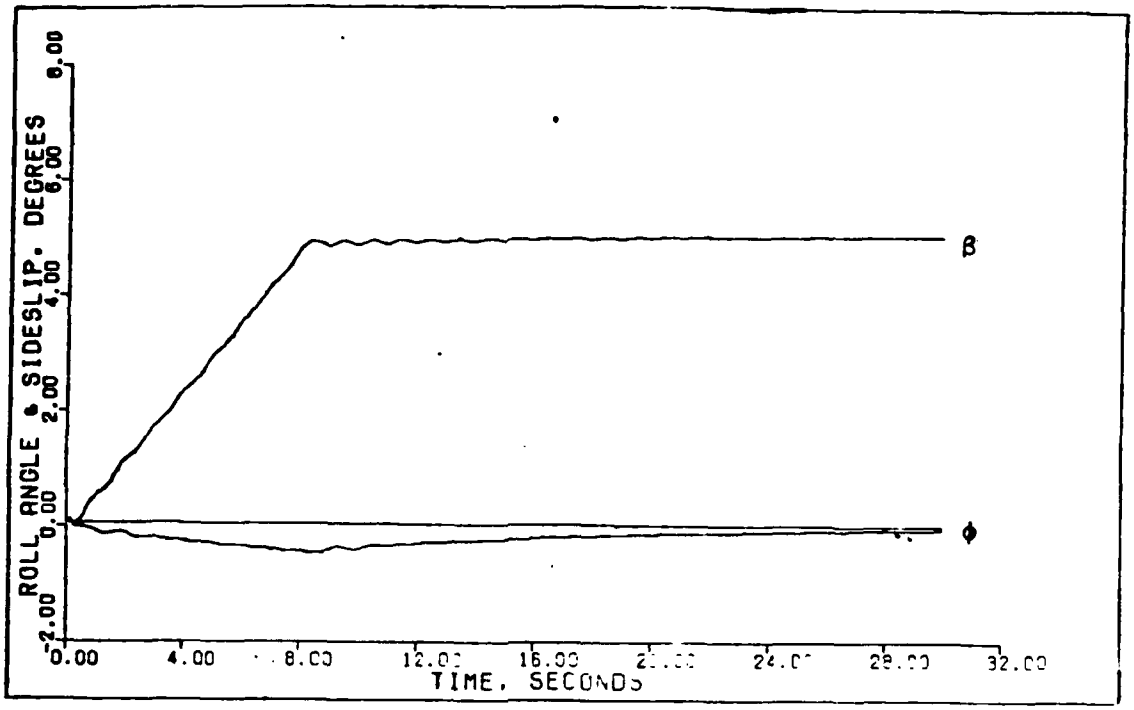



FIG 8a MACH 0.65 (DESIGN MACH 0.18), SIDESLIP

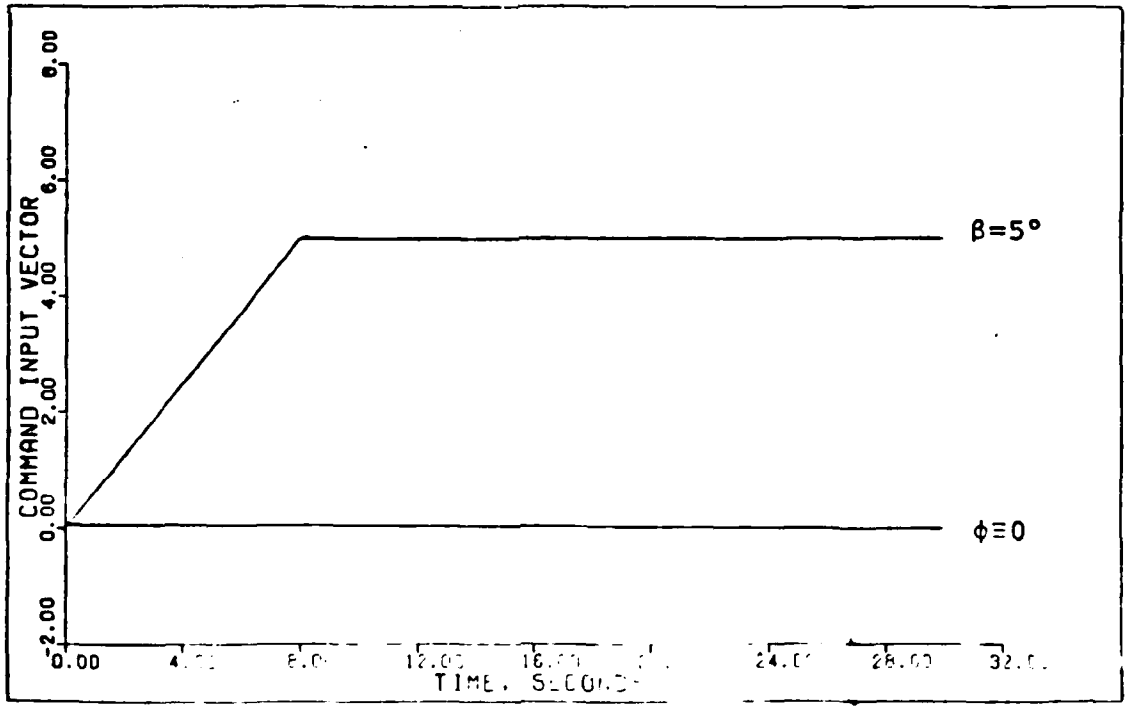



FIG 8b MACH 0.65 (DESIGN MACH 0.18), SIDESLIP

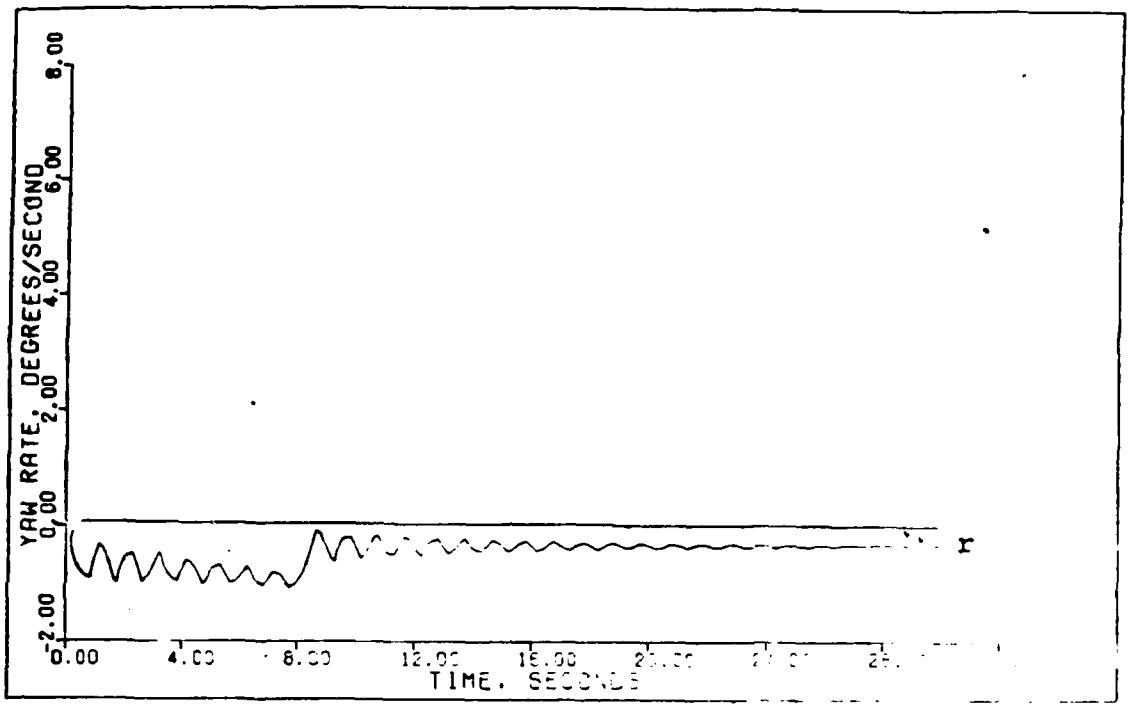



FIG 8c MACH 0.85 (DESIGN MACH 0.18 ...

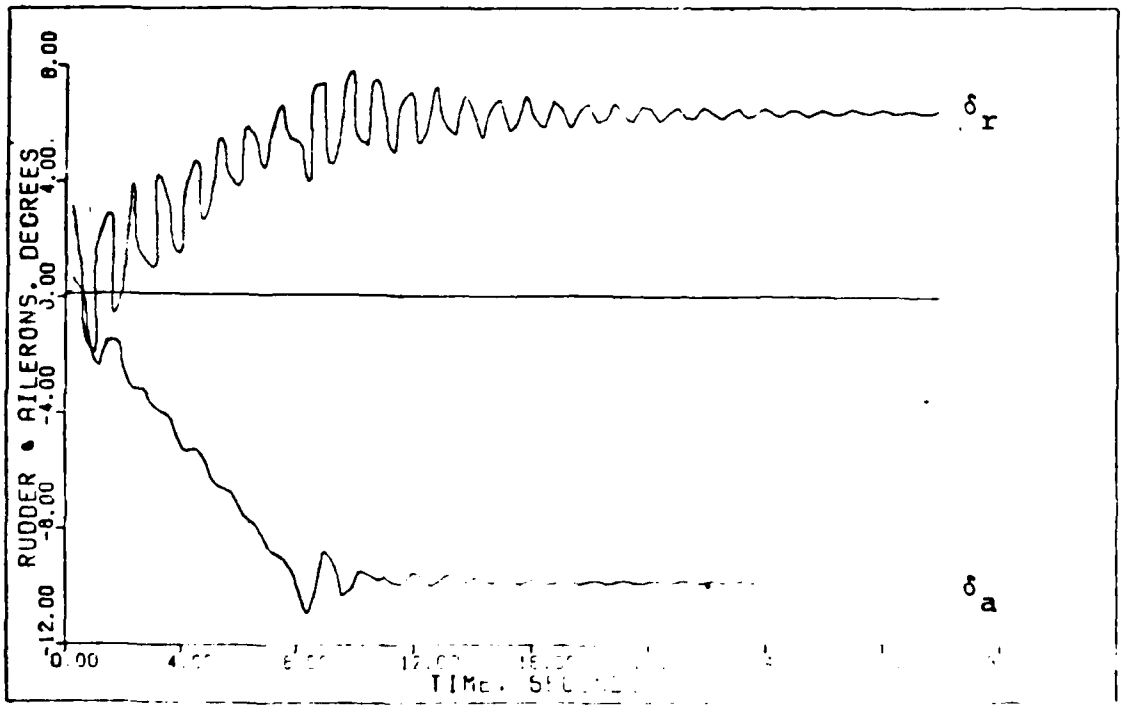



FIG 8d MACH ...



Copy available to DTIC does not permit fully legible reproduction

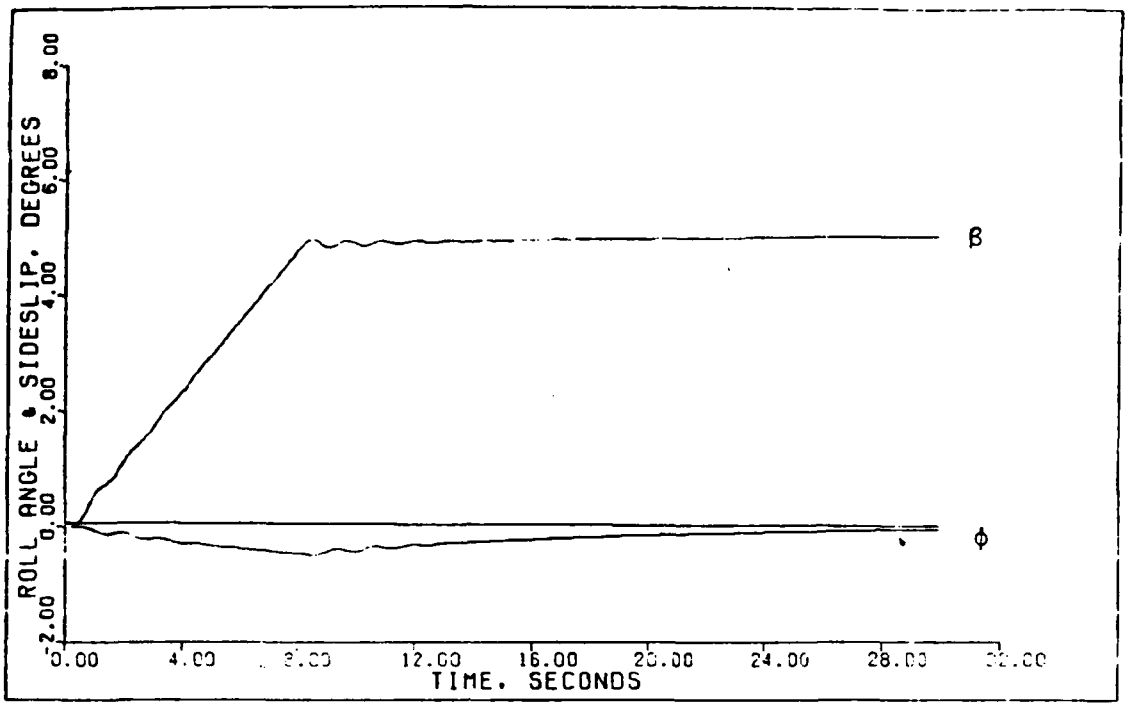



FIG 9a MACH 0.76 (DESIGN MACH 0.18). SIDESLIP

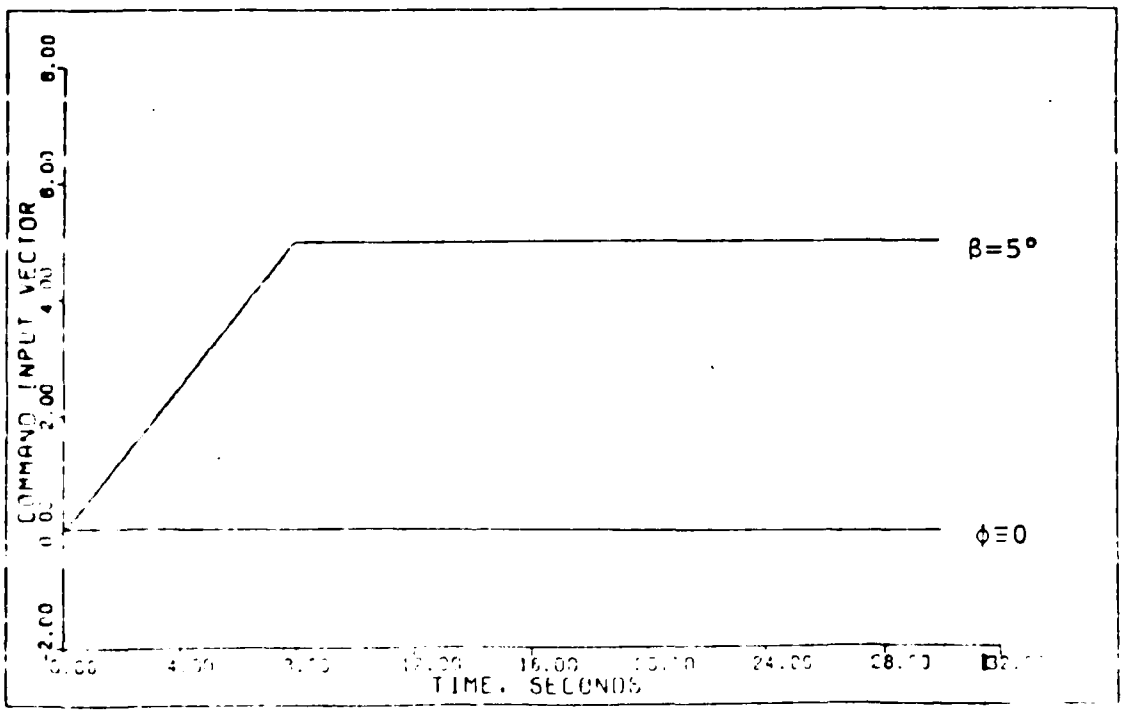



FIG 9b MACH 0.76 (DESIGN MACH 0.18). SIDESLIP

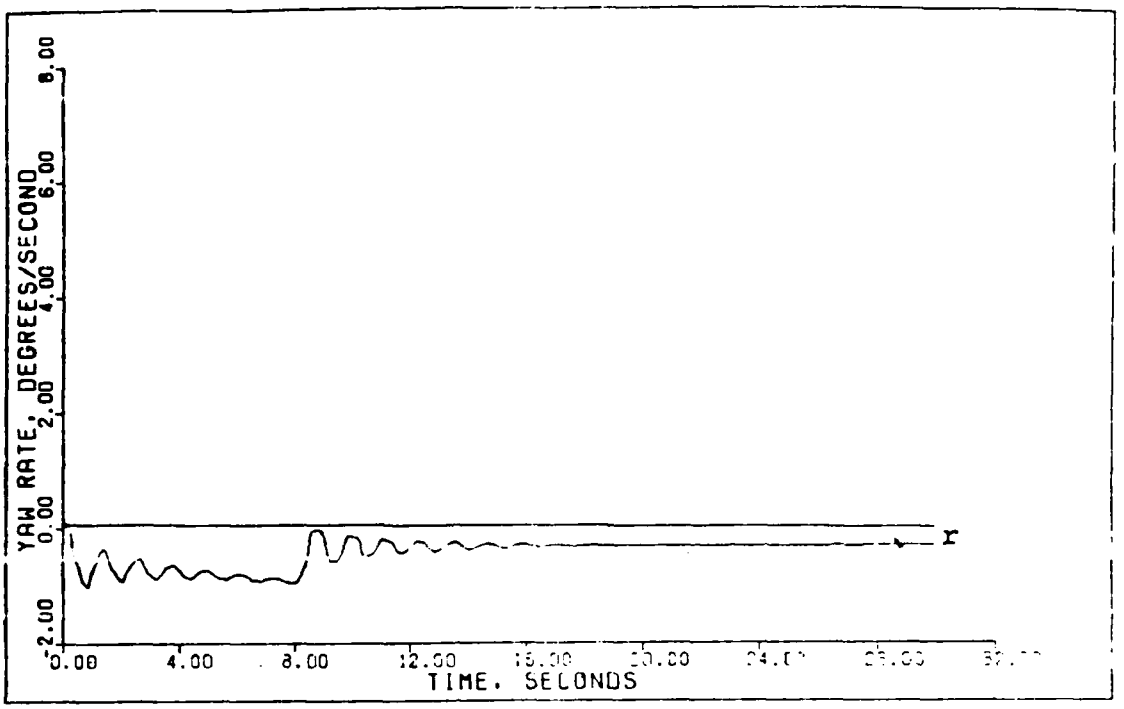



FIG 9c MACH 0.76 (DESIGN MACH 0.18), SIDESLIP

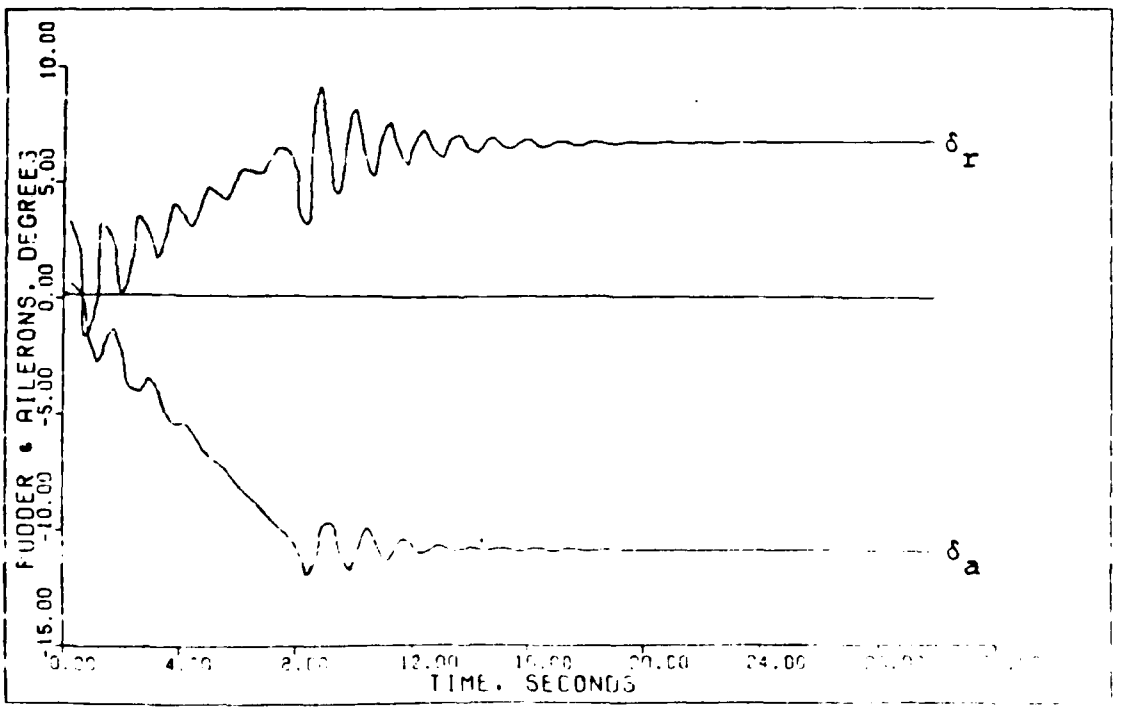



FIG 9d MACH 0.76 (DESIGN MACH 0.18), SIDESLIP

TABLE VII

Sideslip Results for MACH 0.65,
25000 ft (Designed at MACH 0.18)

| INPUT/ OUTPUT | $t_p$(sec) | $t_s$(sec) | PEAK VALUE | FINAL VALUE |
|---|---|---|---|---|
| $\beta$(deg) | —— | 11.3 | 5.0 | 5.0 |
| $\phi$(deg) | 8.65 | —— | -0.45 | 0. |
| r(deg/sec) | 7.75 | —— | -1.1 | 0. |
| $\delta_r$(deg) | —— | —— | 7.9 | —— |
| $\delta_a$(deg) | —— | —— | -10.1 | —— |

TABLE VIII

Sideslip Results for MACH 0.76,
40000 ft (Designed at MACH 0.18)

| INPUT/ OUTPUT | $t_p$(sec) | $t_s$(sec) | PEAK VALUE | FINAL VALUE |
|---|---|---|---|---|
| $\beta$(deg) | 11.65 | 11.0 | 5.01 | 5.0 |
| $\phi$(deg) | 8.65 | —— | -0.49 | 0. |
| r(deg/sec) | 0.85 | —— | -1.0 | 0. |
| $\delta_r$(deg) | —— | —— | 9.1 | —— |
| $\delta_a$(deg) | —— | —— | -12.0 | —— |

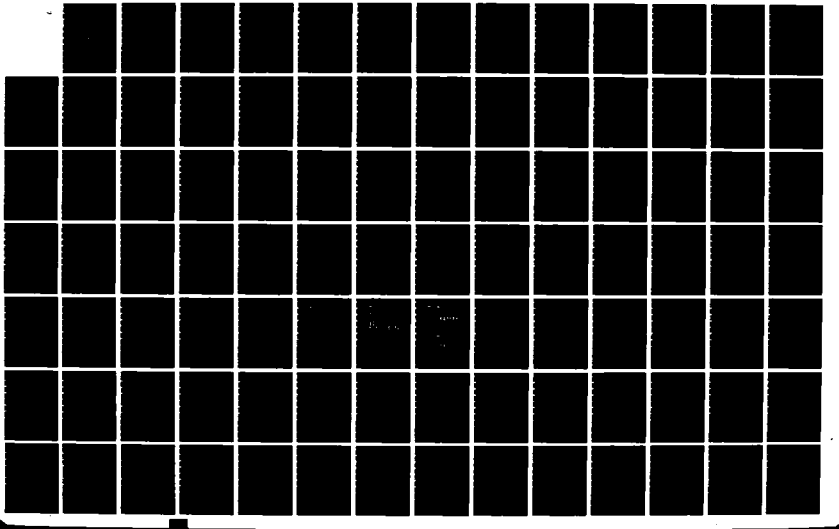
The MACH 0.18 longitudinal control laws are correspondingly used at the other two flight conditions for vertical translation and pitch pointing manuevers. The robustness of this controller is demonstrated in Figures 10 thru 13. Figures 10 and 11 illustrate vertical translation at MACH 0.65 and MACH 0.76, respectively. Tables IX and X, likewise, summarize these results.

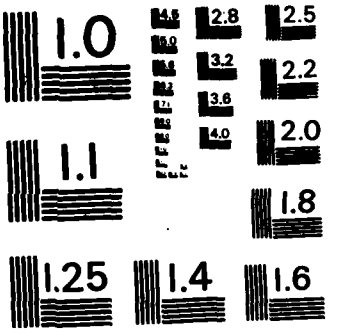
Pitch pointing is demonstrated in Figures 12 and 13. Tables XI and XII give the corresponding results for the MACH 0.65 and MACH 0.76 flight conditions. In all manuevers attempted, thrust control for these last two pitch pointing conditions is the only control input which exceeds any limit as set by Equation (63). This can be seen in Figures 12(f) and 13(f).

Overall, all controllers designed at MACH 0.18 show good robustness at MACH 0.65 and MACH 0.76. All responses are stable and track the commanded input as desired. An examination of the three flight conditions used show them to cover diverse phases of the flight envelope. Further designs and simulations should be investigated using more flight conditions and non-linear simulations.

AD-A139 050 PROCEEDINGS OF THE WORKSHOP ON MULTIVARIABLE CONTROL SYSTEMS HELD AT WRIG..(U) AIR FORCE WRIGHT AERONAUTICAL LABS WRIGHT-PATTERSON AFB OH M A MASI ET AL. SEP 83 6/7

UNCLASSIFIED AFWAL-TR-83-3093 FFG 1/3 NL






MICROCOPY RESOLUTION TEST CHART
NATIONAL BUREAU OF STANDARDS-1963-A

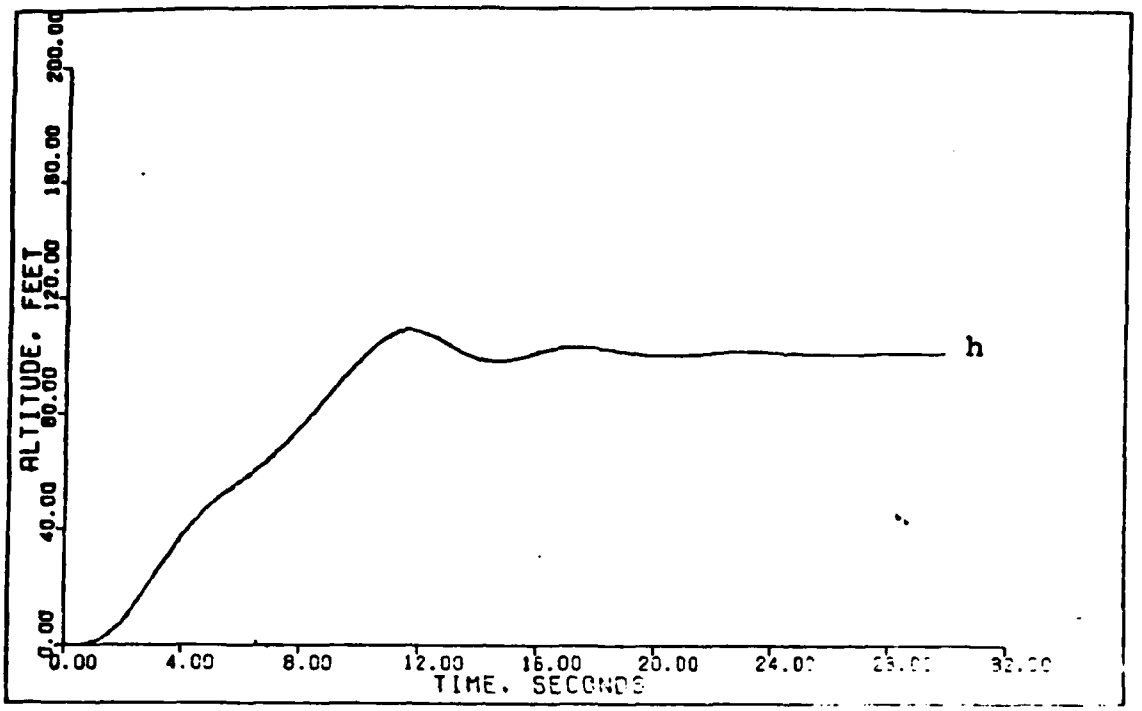



FIG 10a MACH 0.65 (DESIGN MACH 0.16), VERTICAL TRANSLATION

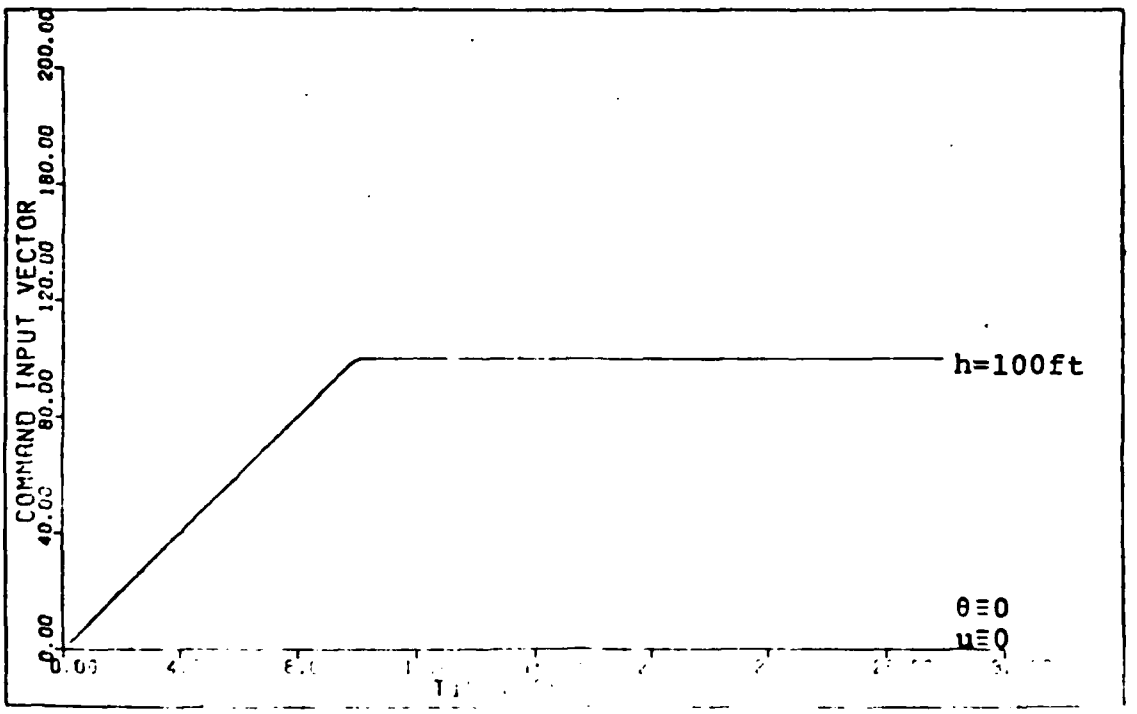



FIG 10b MACH 0.65 (DESIGN MACH 0.16), VERTICAL TRANSLATION

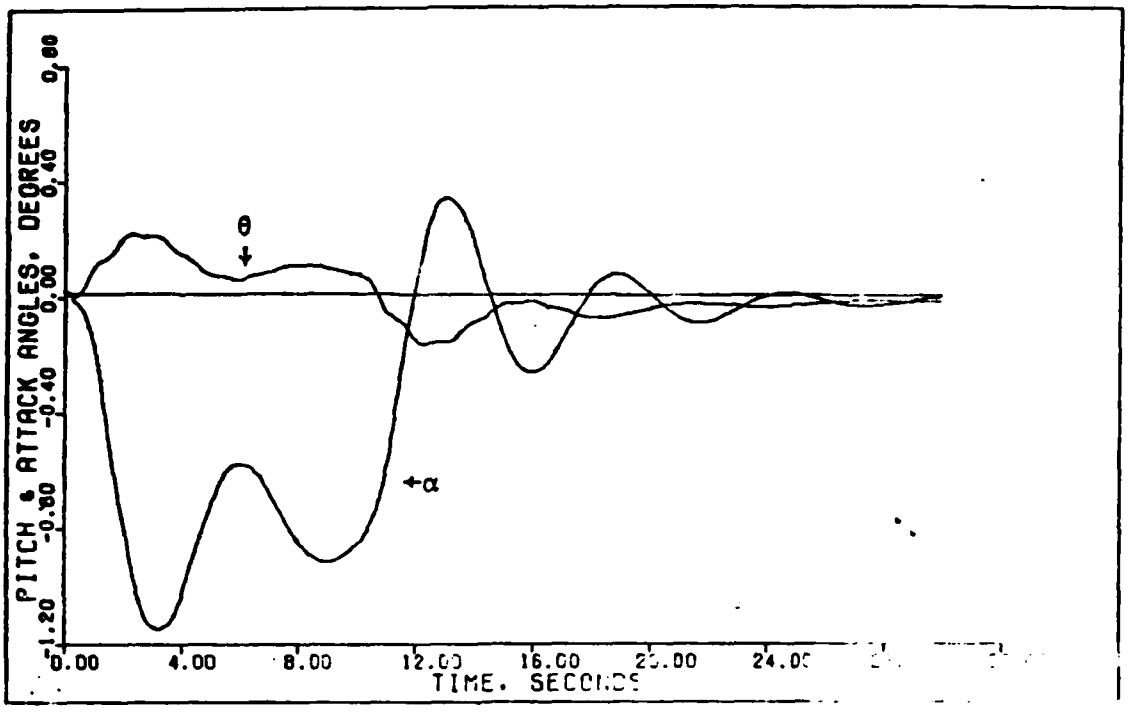



FIG 10c MACH 0.65 (DESIGN MACH 0.18). VERTICAL [illegible]

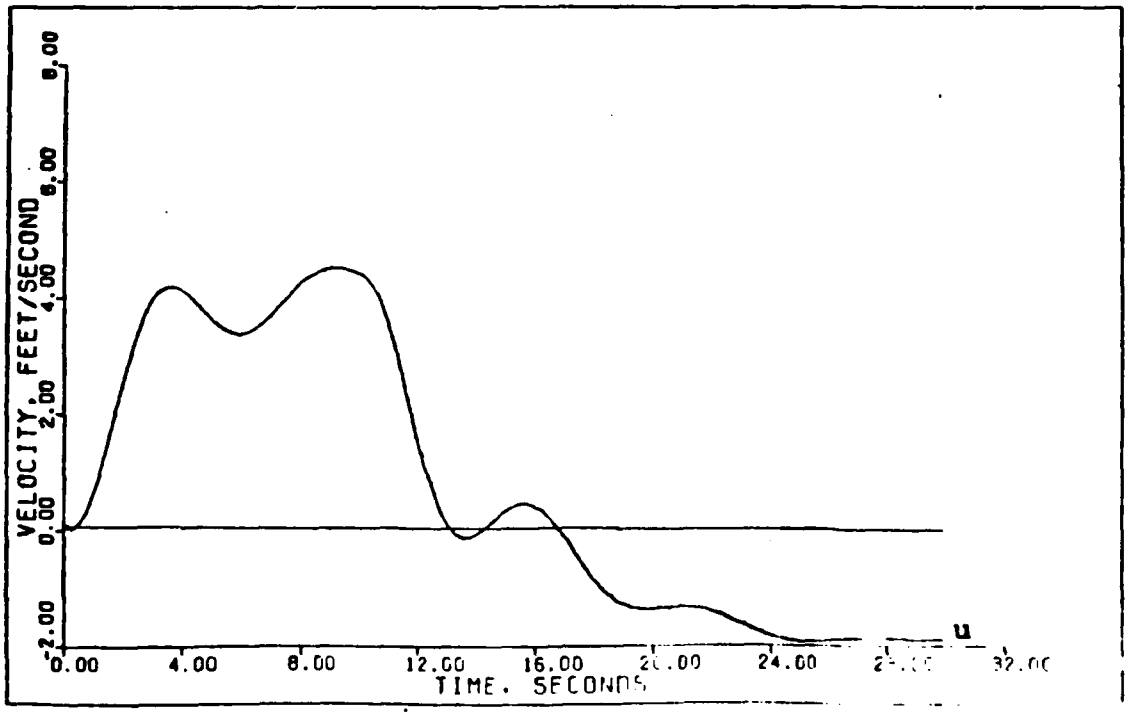



FIG 10d MACH 0.65 (DESIGN MACH 0.18). VERTICAL [illegible]

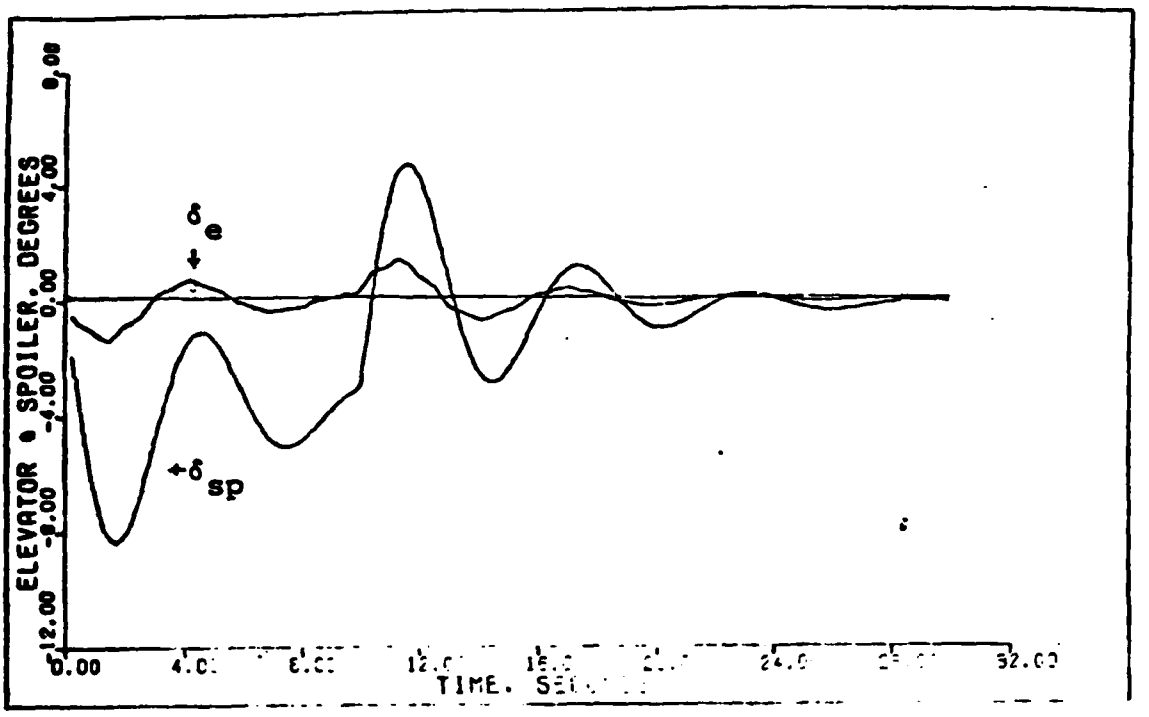



FIG 10e MACH 0.65 (DESIGN MACH 0.18), VERTICAL TRANSLATION

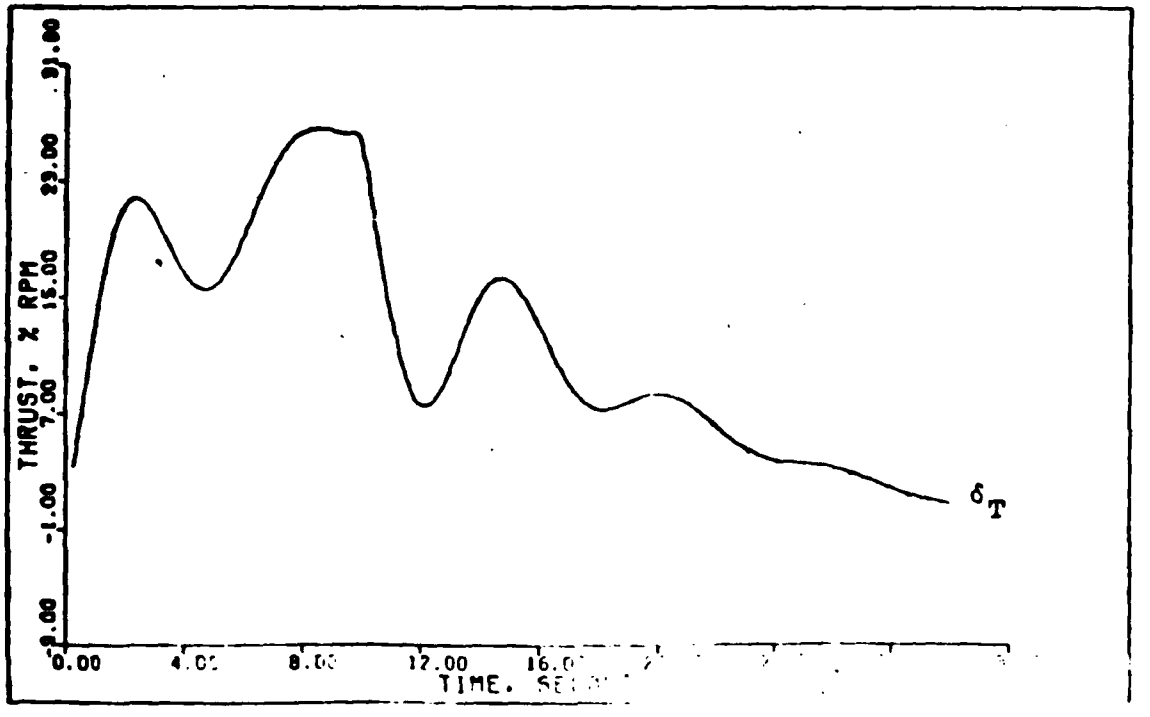



FIG 10f MACH 0.65 (DESIGN MACH 0.1

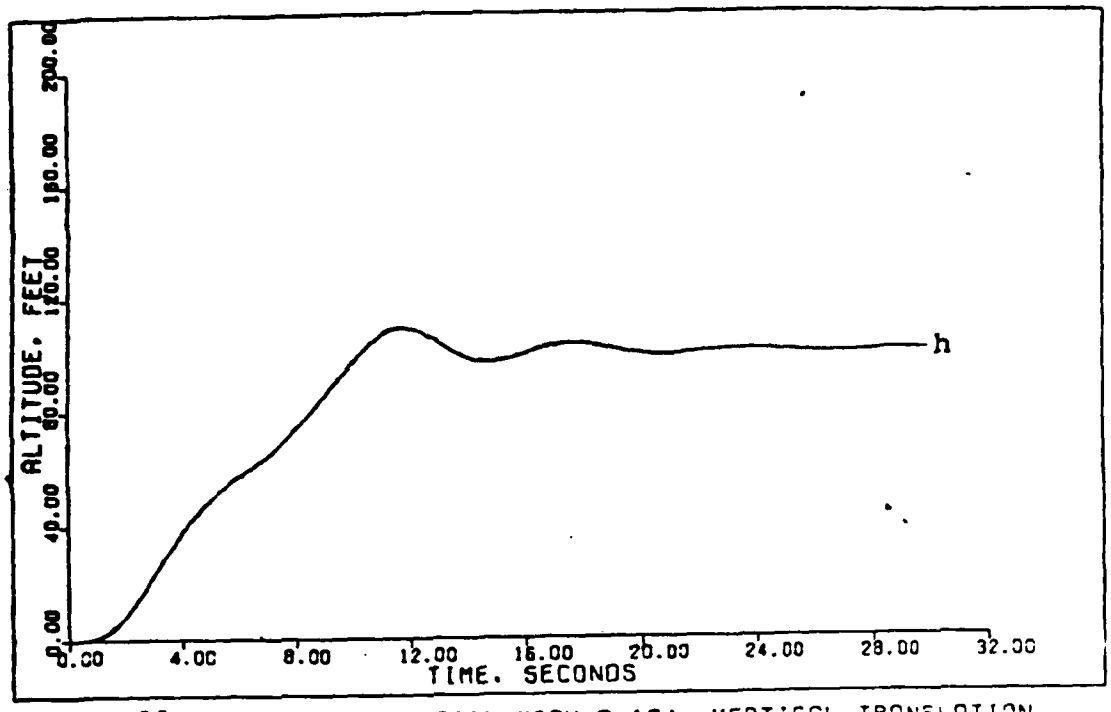



FIG 11a MACH 0.75 (DESIGN MACH 0.18). VERTICAL TRANSLATION

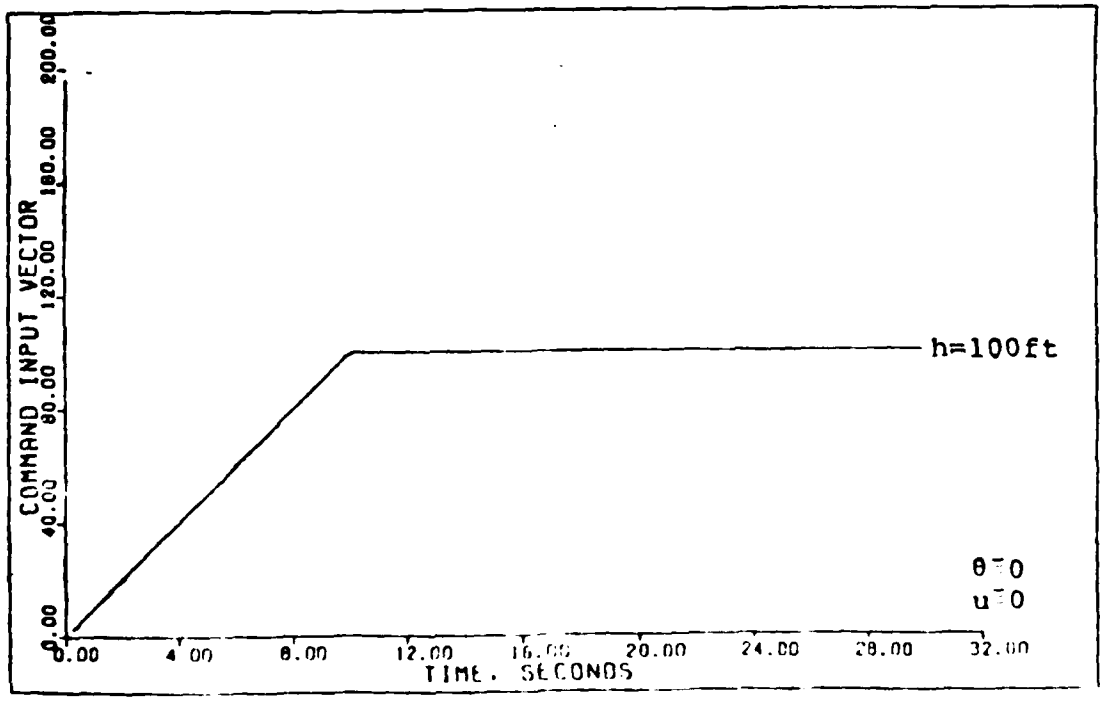



FIG 11b MACH 0.76 (DESIGN MACH 0.18). VERTICAL TRANSLATION

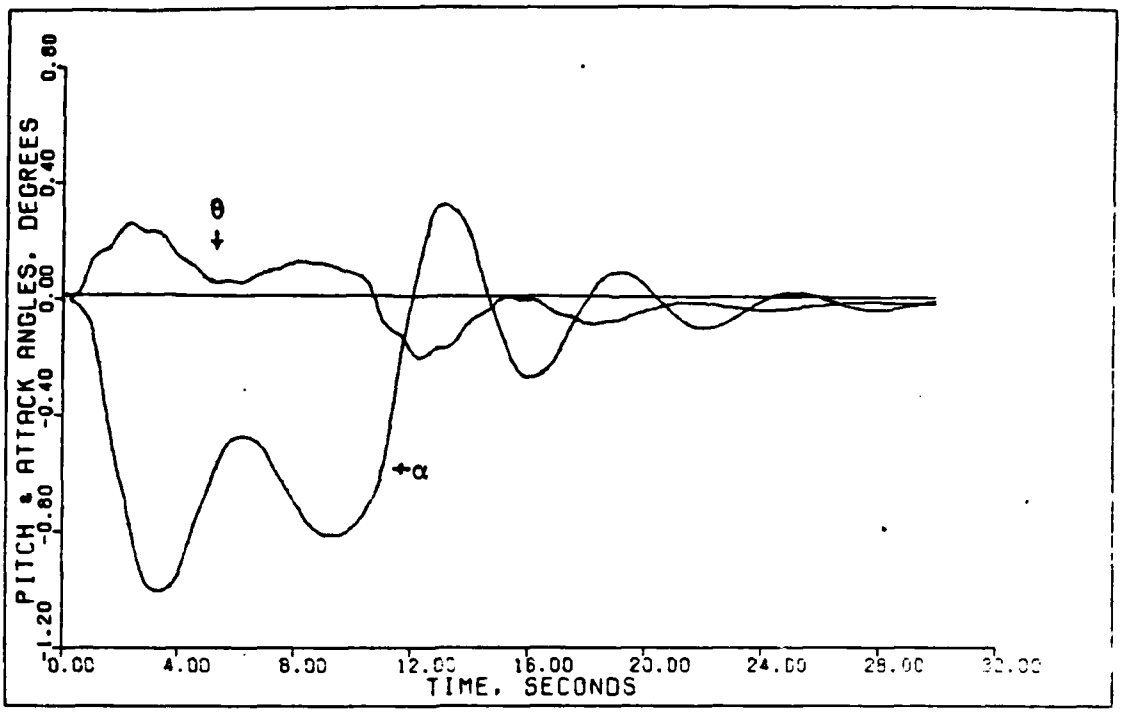



FIG 11c MACH 0.76 (DESIGN MACH 0.18), VERTICAL TRANSLATION

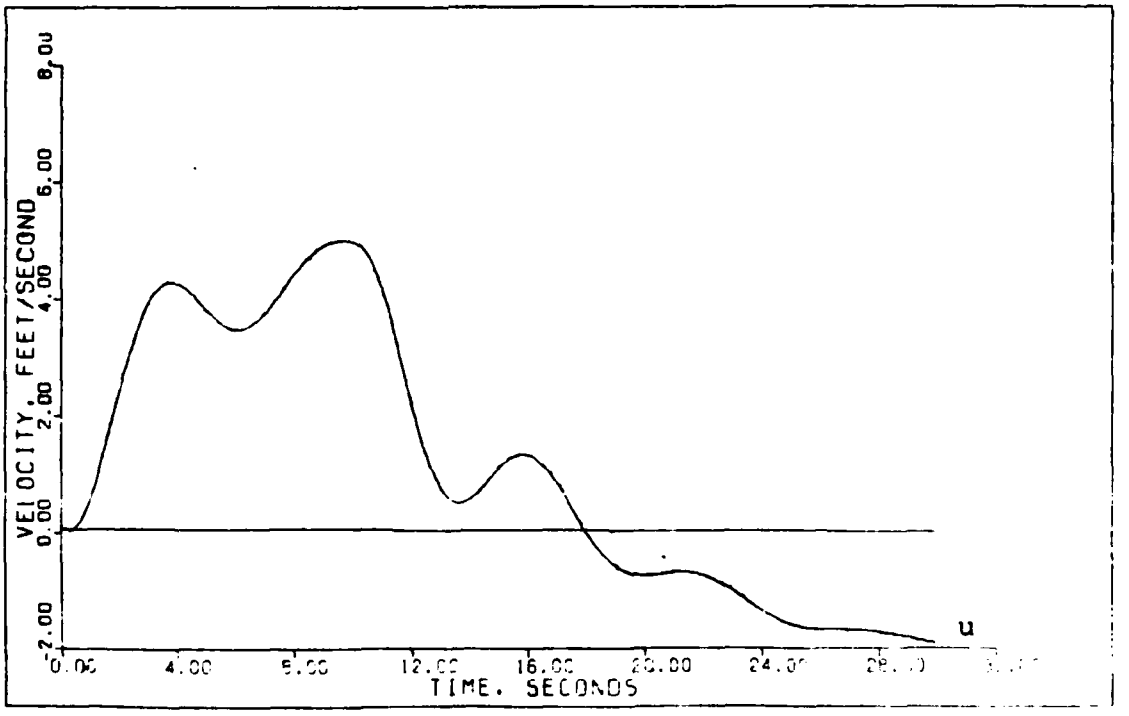



FIG 11d MACH 0.76 (DESIGN MACH 0.18), VERTICAL TRANSLATION

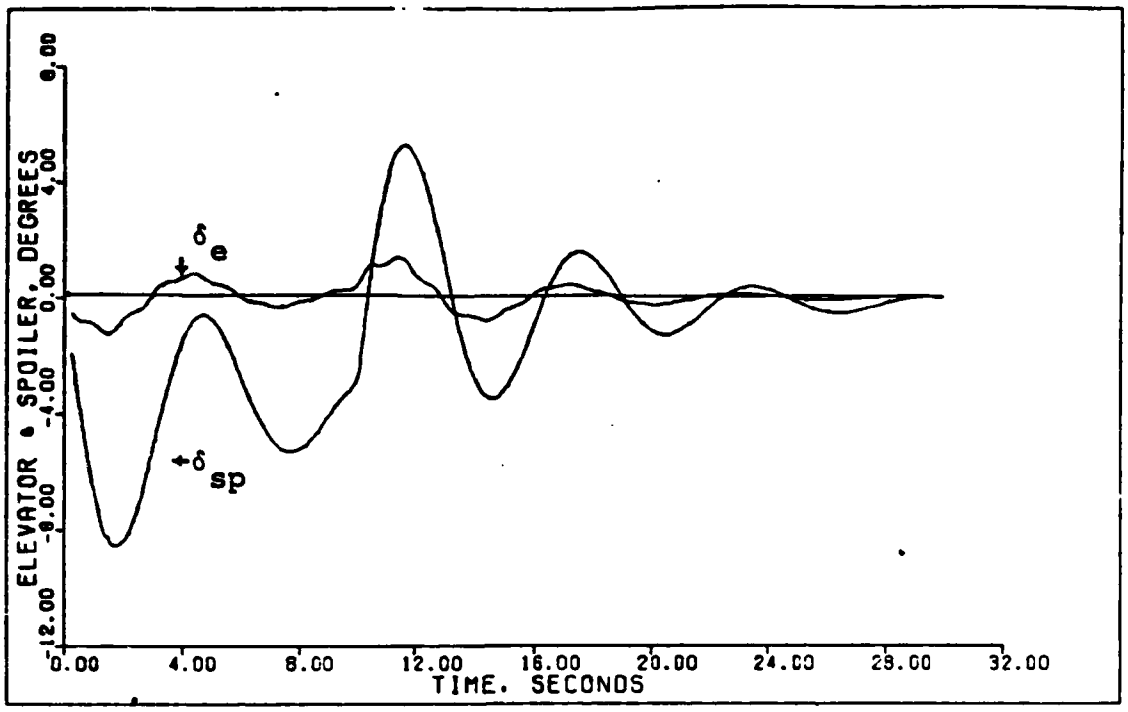



FIG 11e MACH 0.75 (DESIGN MACH 0.18), VERTICAL TRANSLATION

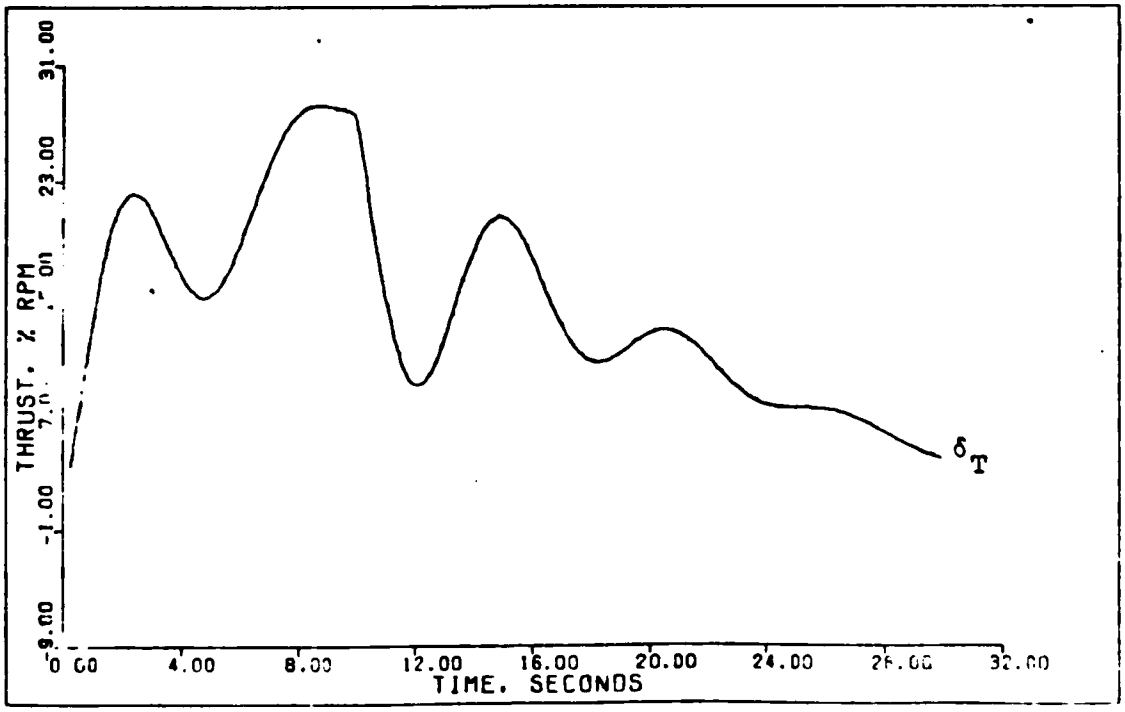



FIG 11f MACH 0.78 (DESIGN MACH 0.18), VERTICAL TRANSLATION

TABLE IX

Vertical Translation Results for MACH 0.65, 25000 ft (Designed at MACH 0.18)

| INPUT/ OUTPUT | $t_p$(sec) | $t_s$(sec) | PEAK VALUE | FINAL VALUE |
|---|---|---|---|---|
| h(ft) | 11.65 | 13.45 | 109. | 100. |
| $\theta$(deg) | 2.35 | — | 0.22 | 0. |
| $\alpha$(deg) | 3.25 | — | -1.15 | 0. |
| u(ft/sec) | 9.25 | — | 4.5 | 0. |
| $\delta_e$(deg) | — | — | 1.4 | — |
| $\delta_{sp}$(deg) | — | — | -8.4 | — |
| $\delta_T$(% RPM) | — | — | 26.7 | — |

TABLE X

Vertical Translation Results for MACH 0.76, 40000 ft (Designed at MACH 0.18)

| INPUT/ OUTPUT | $t_p$(sec) | $t_s$(sec) | PEAK VALUE | FINAL VALUE |
|---|---|---|---|---|
| h(ft) | 11.65 | 15.55 | 110. | 100. |
| $\theta$(deg) | 2.35 | — | 0.25 | 0. |
| $\alpha$(deg) | 3.25 | — | -1.0 | 0. |
| u(ft/sec) | 9.55 | — | 5.0 | 0. |
| $\delta_e$(deg) | — | — | 1.5 | — |
| $\delta_{sp}$(deg) | — | — | -8.6 | — |
| $\delta_T$(% RPM) | — | — | 28.3 | — |

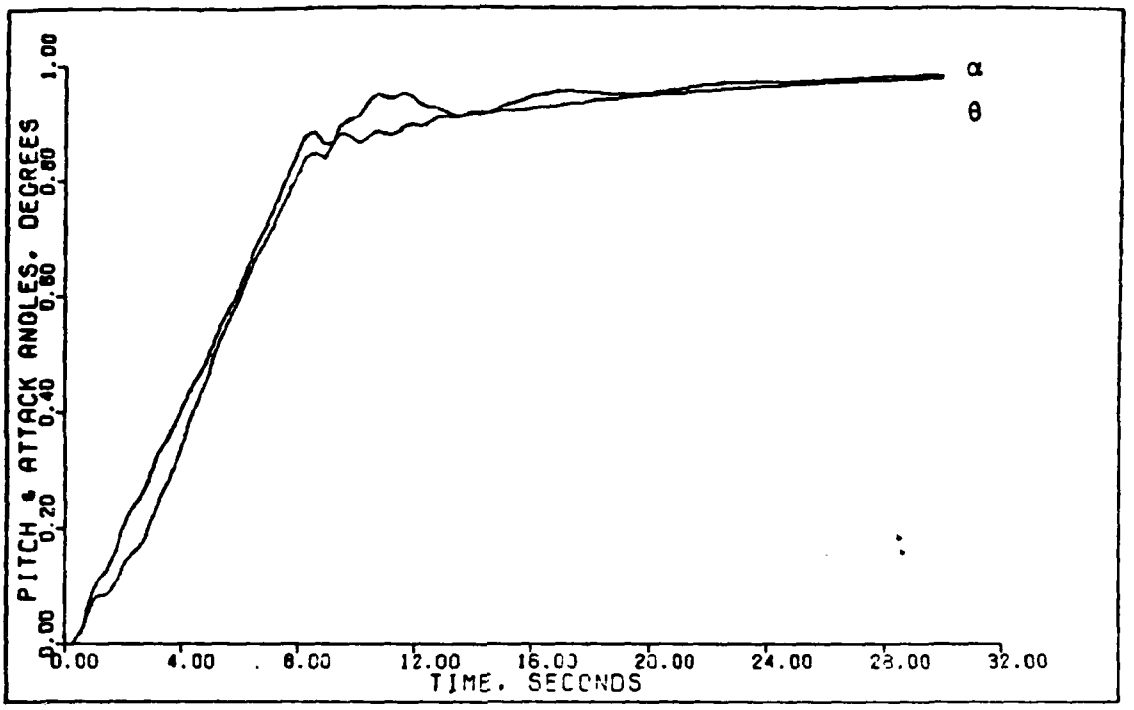



FIG 12a MACH 0.65 (DESIGN MACH 0.18), PITCH POINTING

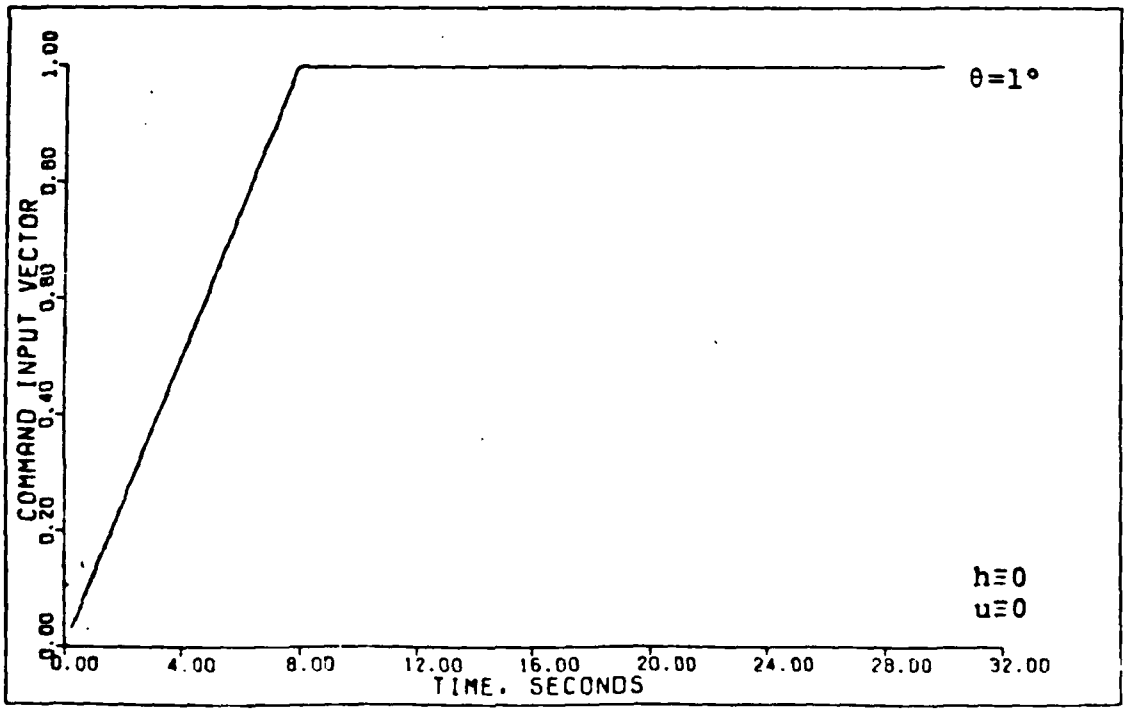



FIG 12b MACH 0.65 (DESIGN MACH 0.18), PITCH POINTING

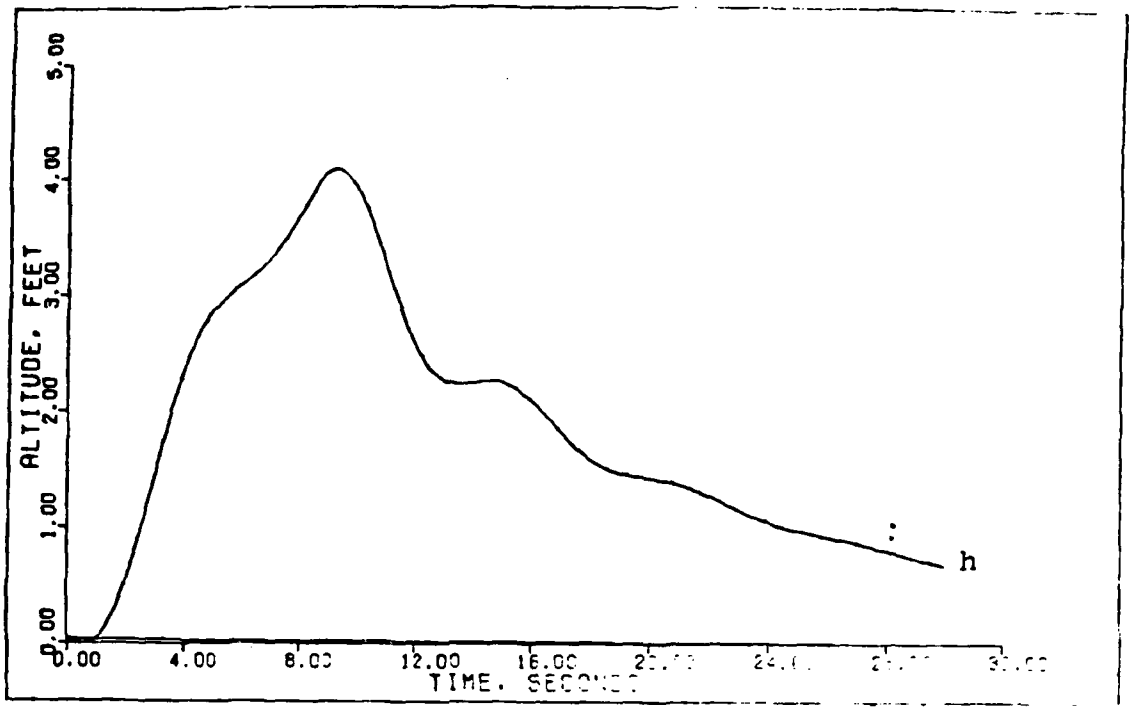



FIG 12c MACH 0.55 (DESIGN MACH 0.[illegible] . PITCH [illegible]

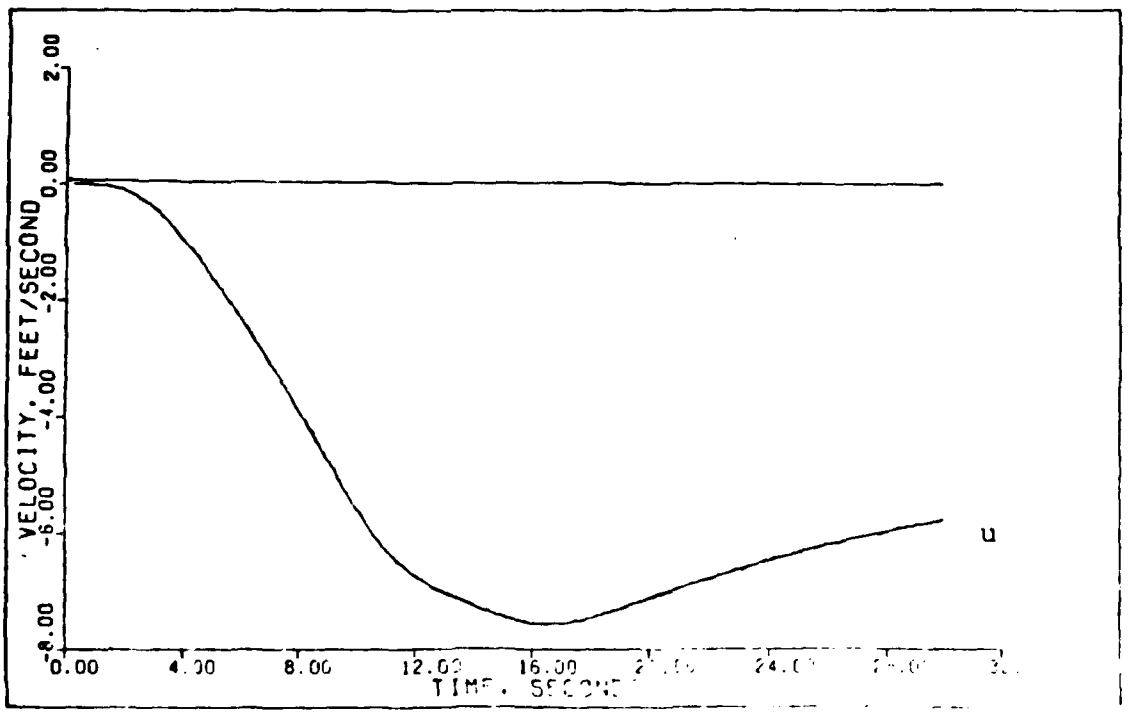



FIG 12d MACH 0.55 (DESIGN MACH 0.[illegible]. PITCH [illegible]

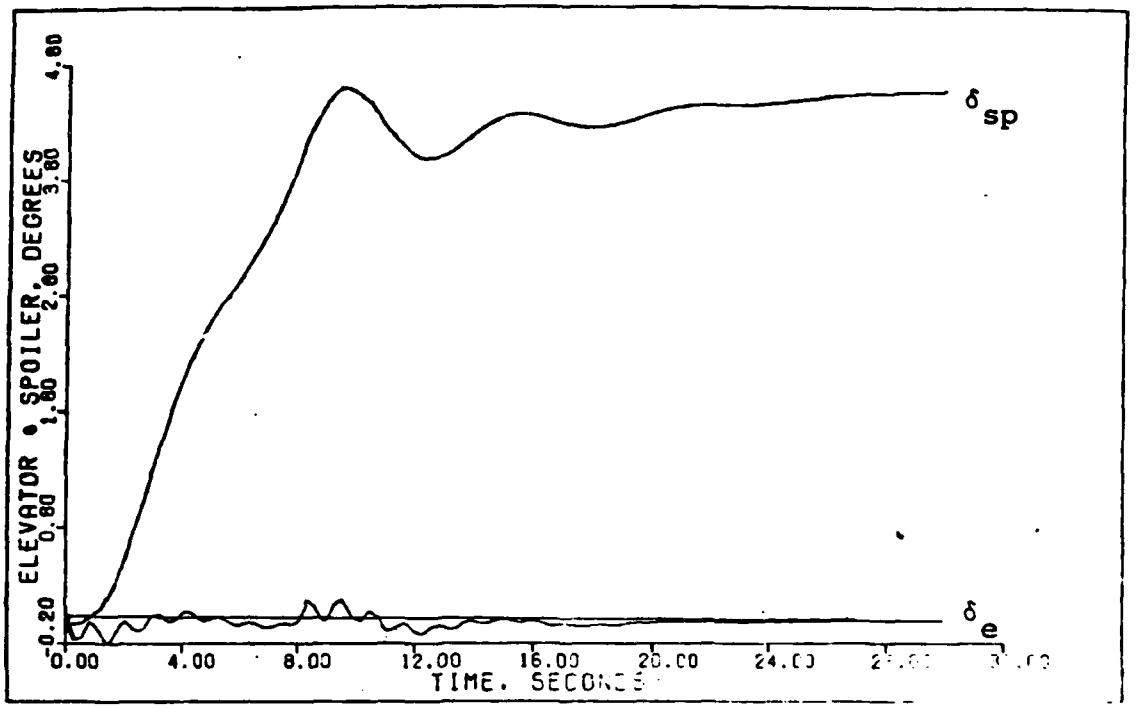



FIG 12e MACH 0.65 (DESIGN MACH 0.18), PITCH POINTING

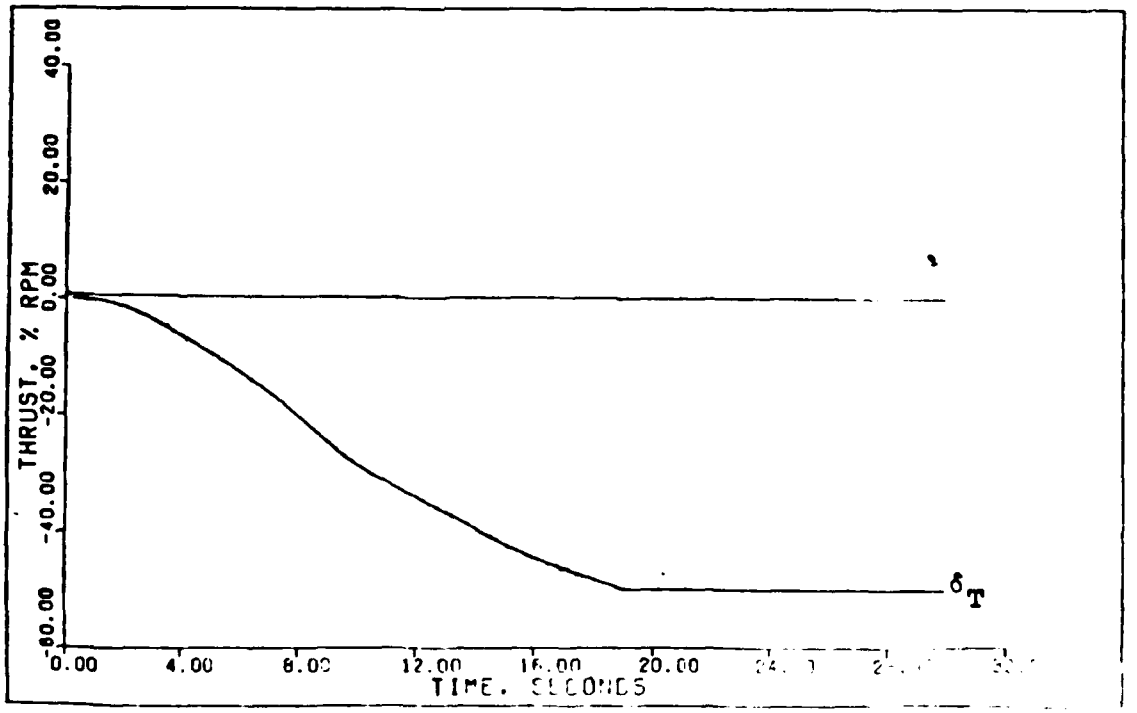



FIG 12f MACH 0.65 (DESIGN MACH 0.18), PITCH POINTING

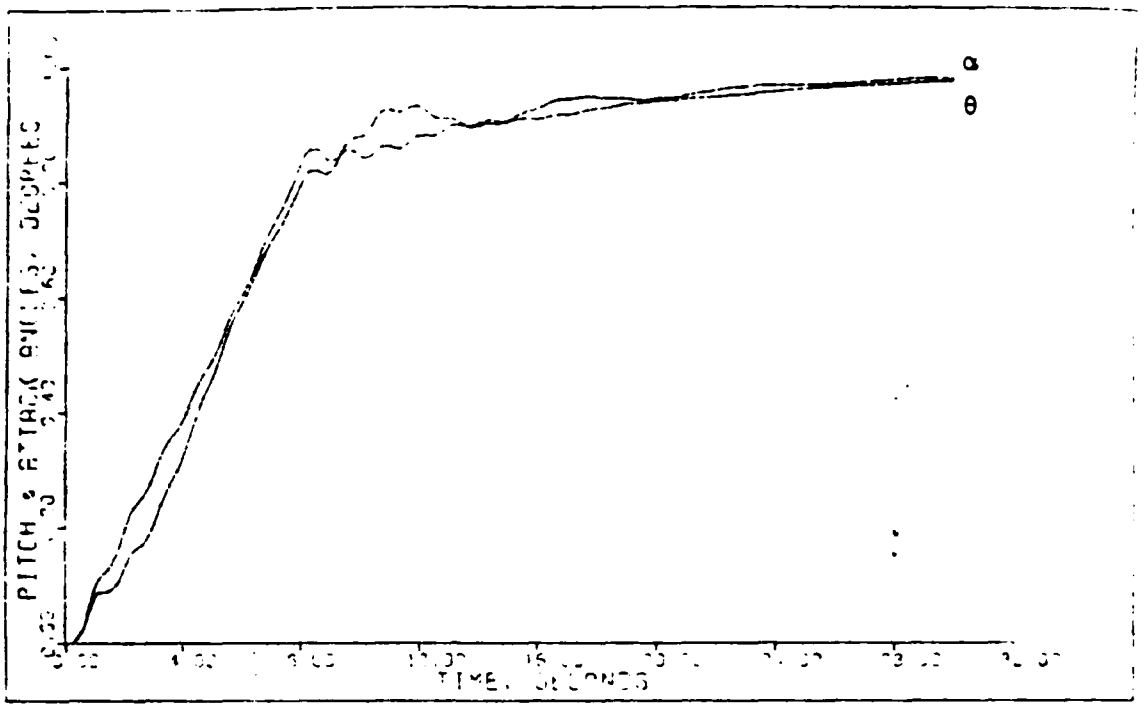



FIG 13a MACH 0.76 (DESIGN MACH 0.18). PITCH POINTING

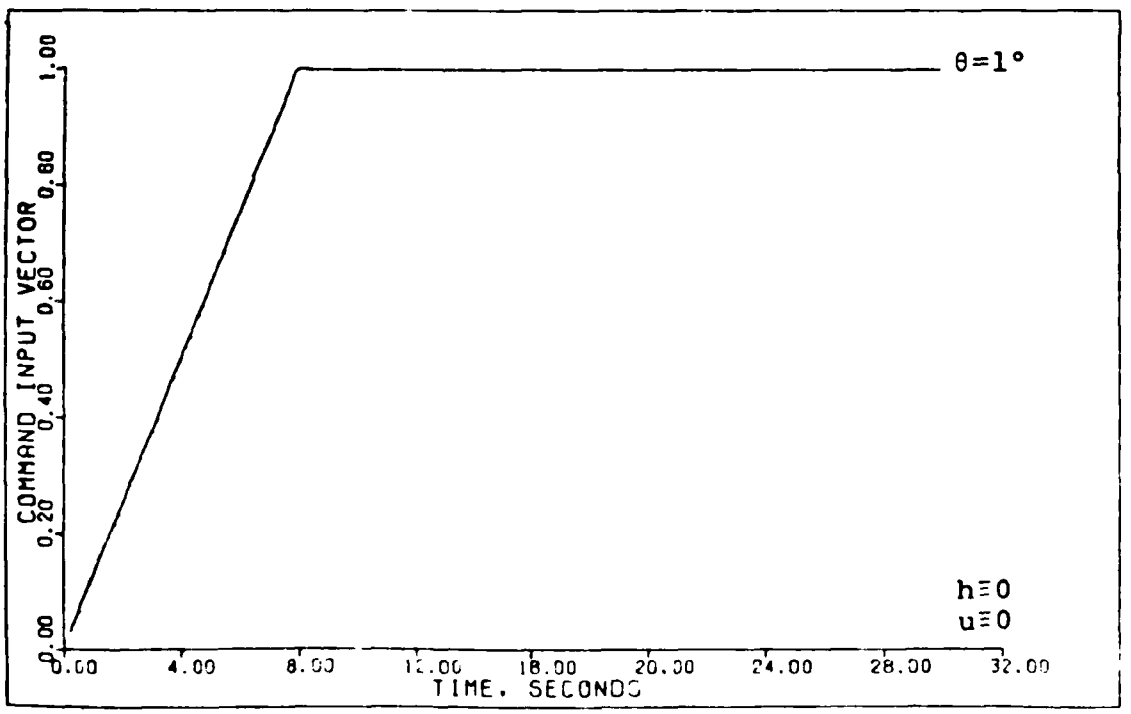



FIG 13b MACH 0.76 (DESIGN MACH 0.18). PITCH POINTING

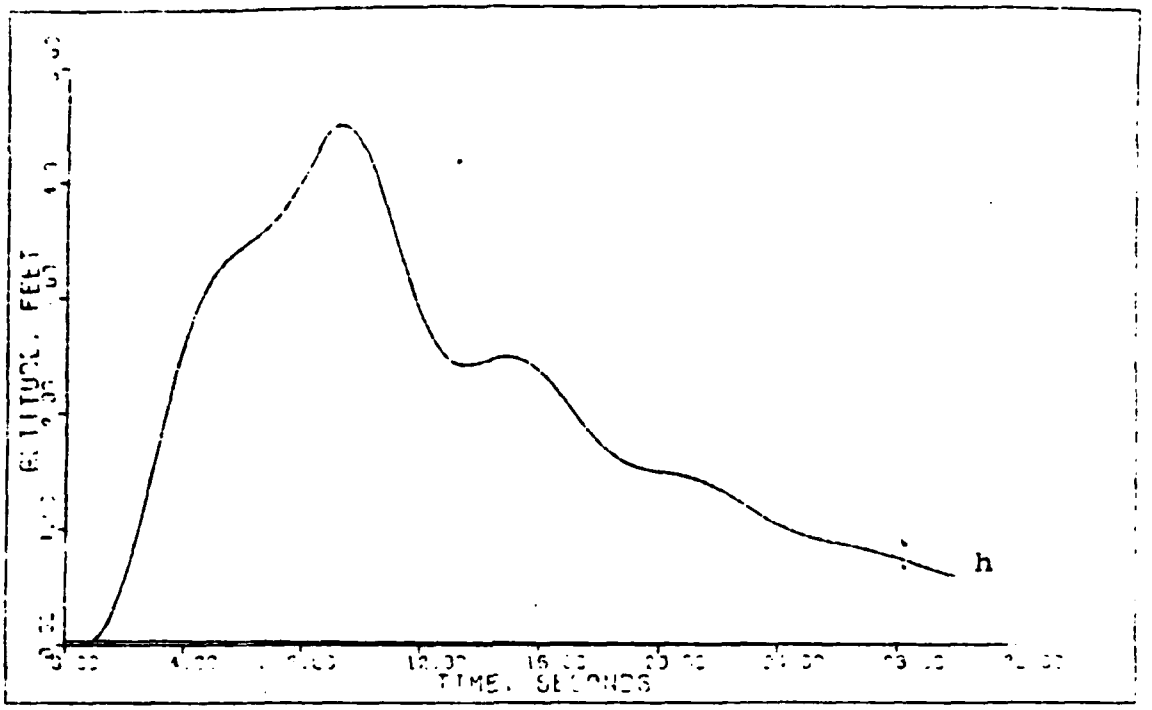



FIG. 13c MACH 0.95 (DESIGN MACH 0.10), PITCH POINTING

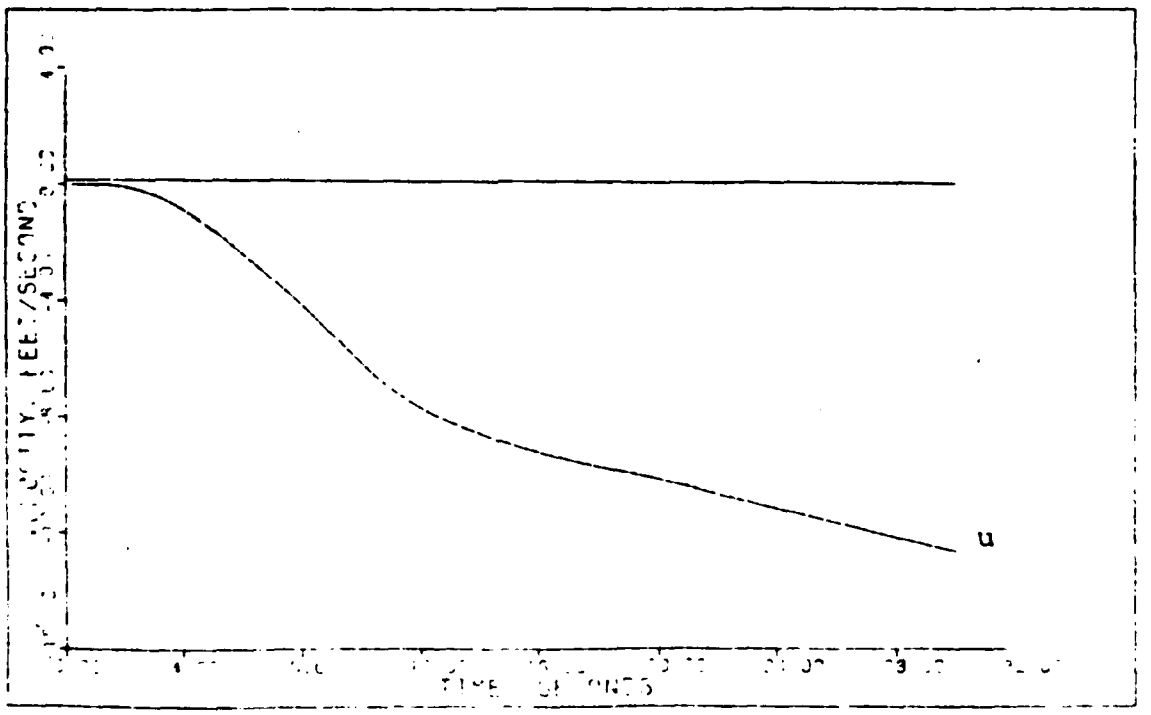



FIG. 13d MACH 0.95 (DESIGN MACH 0.10), PITCH POINTING



Copy available to DTIC does not permit fully legible reproduction

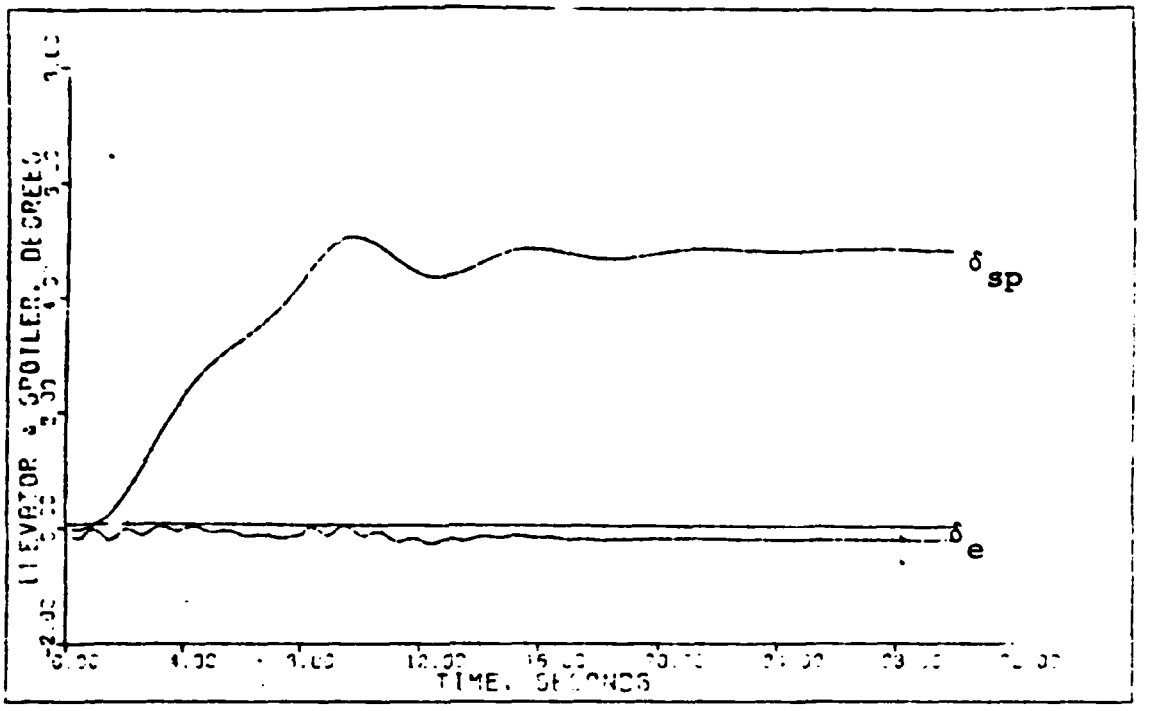



FIG 13e MACH 0.75 (DESIGN MACH 0.13).. PITCH POINTING

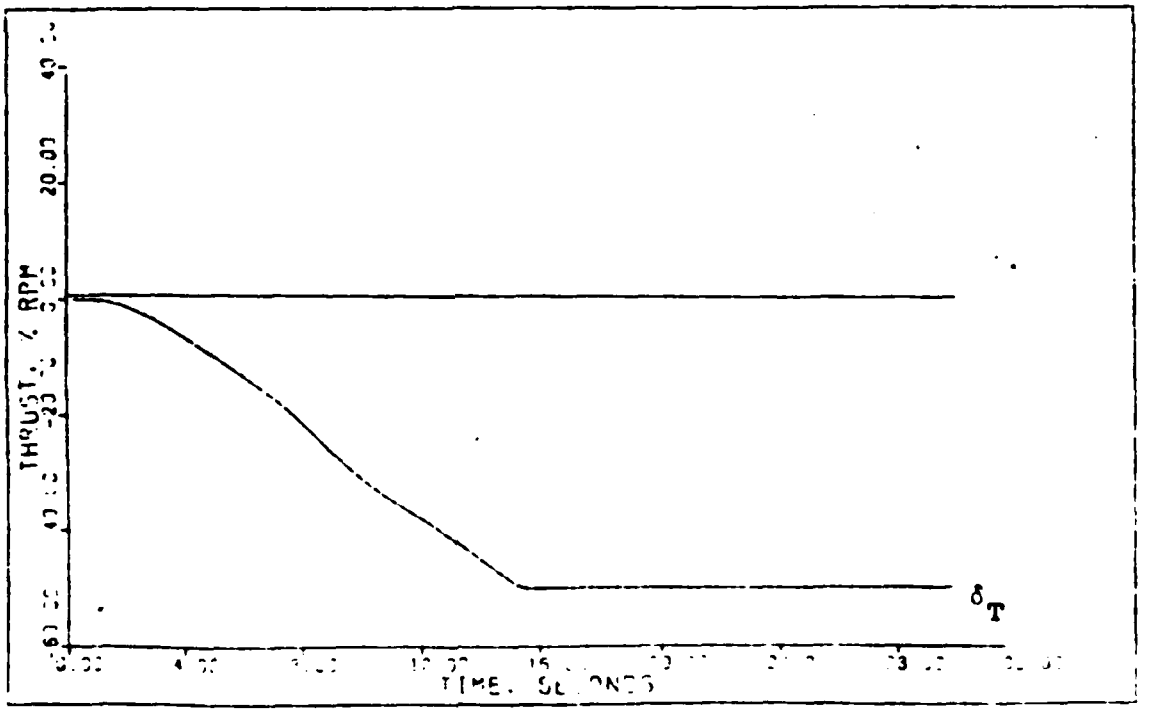



FIG 13f MACH 0.75 (DESIGN MACH 0.13). PITCH POINTING

TABLE XI

Pitch Pointing Results for MACH 0.65,
25000 ft (Designed at MACH 0.18)

| INPUT/ OUTPUT | $t_p$(sec) | $t_s$(sec) | PEAK VALUE | FINAL VALUE |
|---|---|---|---|---|
| $\vartheta$(deg) | —— | 60 | 1.0 | 1.0 |
| $\alpha$(deg) | —— | 60 | 1.0 | 1.0 |
| h(ft) | 9.25 | —— | 4.1 | 0. |
| u(ft/sec) | 16.0 | —— | -7.6 | 0. |
| $\delta_e$(deg) | —— | —— | -0.2 | —— |
| $\delta_{sp}$(deg) | —— | —— | 4.6 | —— |
| $\delta_T$(% RPM) | —— | —— | -50.0 | —— |

TABLE XII

Pitch Pointing Results for MACH 0.76, 40000 ft (Designed at MACH 0.18)

| INPUT/ OUTPUT | $t_p$(sec) | $t_s$(sec) | PEAK VALUE | FINAL VALUE |
|---|---|---|---|---|
| $\theta$(deg) | —— | 60 | 1.0 | 1.0 |
| $\alpha$(deg) | —— | 60 | 1.0 | 1.0 |
| h(ft) | 9.25 | —— | 4.5 | 0. |
| u(ft/sec) | 180 | —— | -24.6 | 0. |
| $\delta_e$(deg) | —— | —— | -0.27 | —— |
| $\delta_{sp}$(deg) | —— | —— | 5.0 | —— |
| $\delta_T$(% RPM) | —— | —— | 50.0 | —— |

Model Change

At this point, the question arises as to how to perform a normal climb manuever when both altitude, h, and pitch angle, $\theta$, have to be commanded as part of the output vector. Altitude is related to pitch angle by the question:

$$\dot{h} = U_0 (\theta - \alpha) \tag{107}$$

where $\dot{h}$ is the rate of change of altitude, or vertical velocity. However, pitch angle in a normal climb is not related to the altitude, h, through a simple relationship. Thus, it is desirable to remove $\theta$ from the output equation.

Additionally, it is also desirable to command the spoilers, $\delta_{sp}$, to insure that they reach zero deflection in the steady state. There are two ways to accomplish this. First, the spoiler actuator can be incorporated into the state model; thus, spoiler position becomes a state and is commanded through the output matrix, $\underline{C}$. However, this increases the size of the state model and thus adds complexity.

The second way to add $\delta_{sp}$ to the output is to add a direct feedforward matrix. The new output equation for the longitudinal model becomes:

$$\underline{Y} = \begin{bmatrix} h \\ \delta_{sp} \\ u \end{bmatrix} = \underline{C}\underline{x} + \underline{D}'\underline{u} \tag{108}$$

where

$$\underline{C} = \begin{bmatrix} 1 & 0 & 0 & 0 & 0 \\ 0 & 0 & 0 & 0 & 0 \\ 0 & 0 & 1 & 0 & 0 \end{bmatrix}$$

$$\underline{D}' = \begin{bmatrix} 0 & 0 & 0 \\ 0 & 1 & 0 \\ 0 & 0 & 0 \end{bmatrix}$$

Using this change in the model a new longitudinal controller is designed at the MACH 0.18 flight condition. The resultant control laws are defined by the parameters:

$$T = 0.05 \text{ sec (20 Hz)} \tag{109}$$

$$\alpha_r = 10.0 \tag{110}$$

$$\varepsilon = 0.005 \tag{111}$$

$$\underline{M} = \begin{bmatrix} 0.25 & 0. \\ 0. & 0.25 \\ 0. & 0. \end{bmatrix} \tag{112}$$

$$\Sigma = \text{diag } [0.2 , 10.0 , 5.0] \tag{113}$$

These parameters yield the control laws given by:

$$\underline{K}_0 = \begin{bmatrix} -0.02132 & -2.967 & 0. \\ -0.07643 & -0.4902 & 0. \\ 0.1330 & 0.4823 & -3.379 \end{bmatrix} \tag{114}$$

$$\underline{K}_1 = \begin{bmatrix} -0.002132 & -0.2967 & 0. \\ -0.007643 & -0.04902 & 0. \\ 0.01330 & 0.04823 & -0.3379 \end{bmatrix} \tag{115}$$

This new controller produces the simulation shown in Figure 14. The command vector is given by Figure 14(b). Altitude tracks the commanded input fairly good as shown by Figure 14(a). Figure 14(c) shows that pitch angle and angle of attack reach zero steady-state, but this will not occur for a non-linear simulation. Velocity changes are negligible as shown by Figure 14(d).

Figure 14(e) shows that spoilers are still used to help initiate and terminate the climb. However, due to the command, spoiler position is pushed to zero in the steady-state, as desired.

Table XIII summarizes these results. These appear to be good tracker control laws, but more data needs to be obtained using this type of direct feedforward output matrix.

## Summary

This chapter presents digital multivariable tracker control laws for the C-141-A Starlifter aircraft. The actual design procedure is outlined and the decoupled lateral and longitudinal control laws are presented separately. Controllers for the MACH 0.18 flight condition are discussed and robustness is considered, using these controllers at the two other flight conditions. Robustness is determined to be acceptable when using the MACH 0.18 designed laws for the complete range of flight conditions.

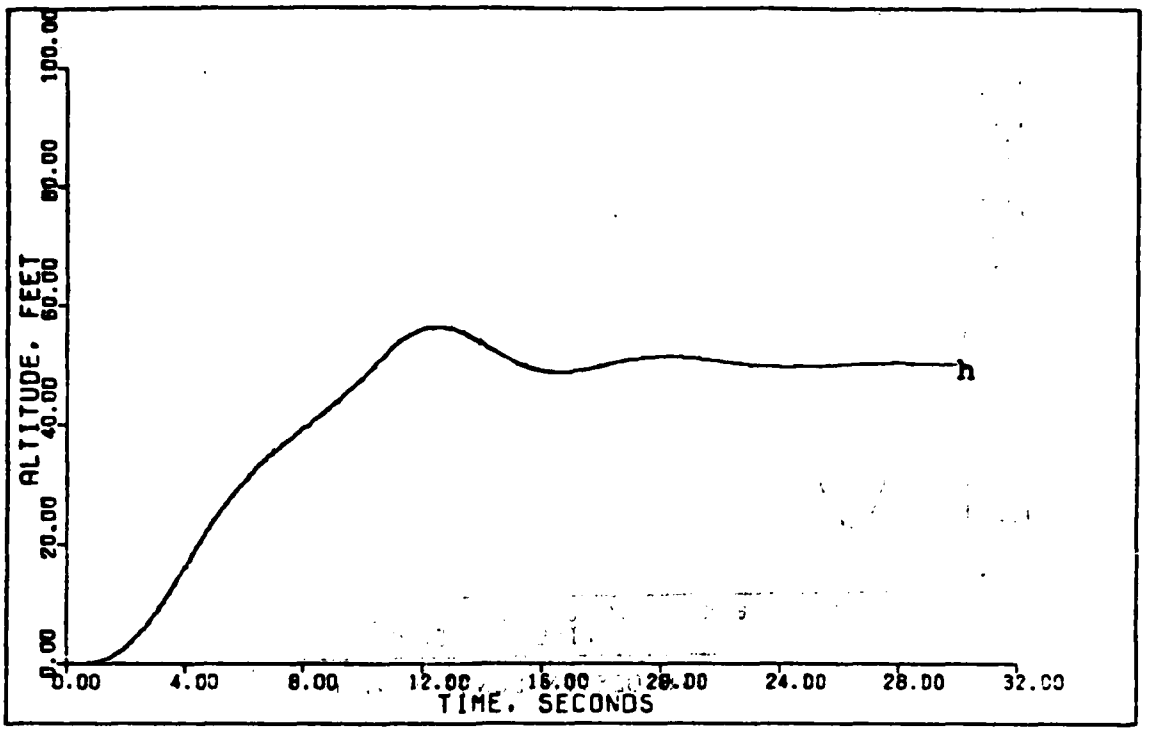



FIG 14a MACH 0.18 DESIGN CONDITION. NORMAL CLIMB

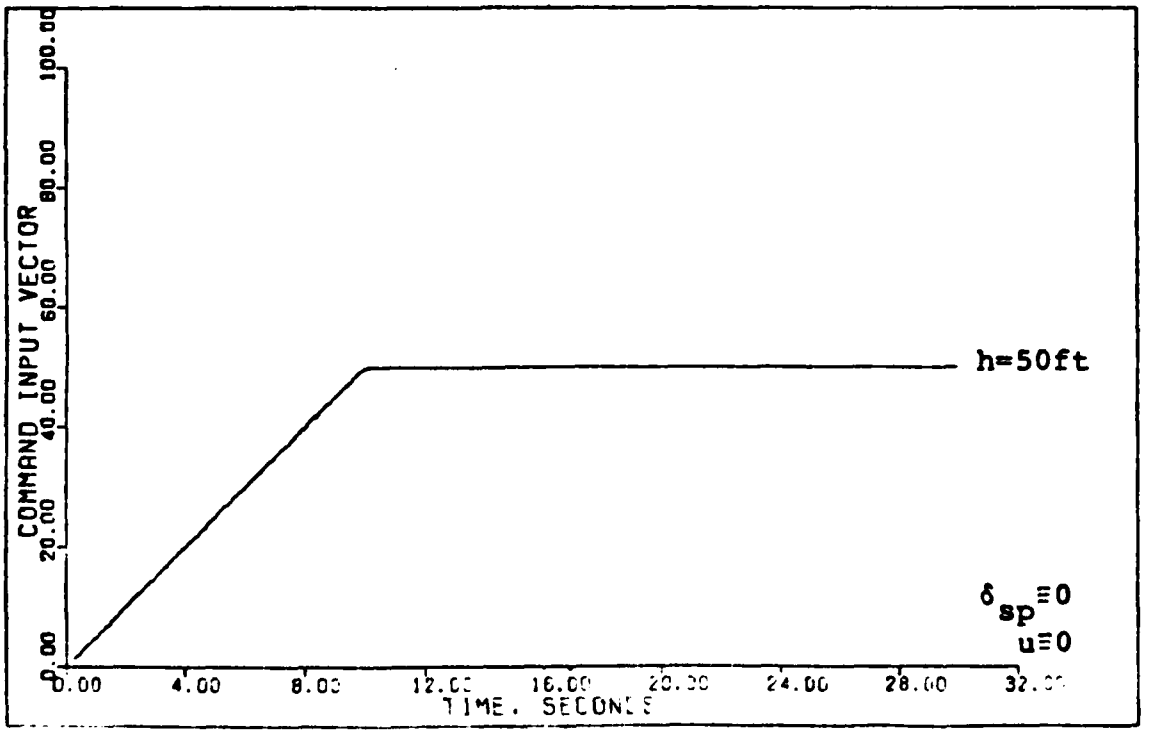



FIG 14b MACH 0.18 DESIGN CONDITION. NORMAL CLIMB

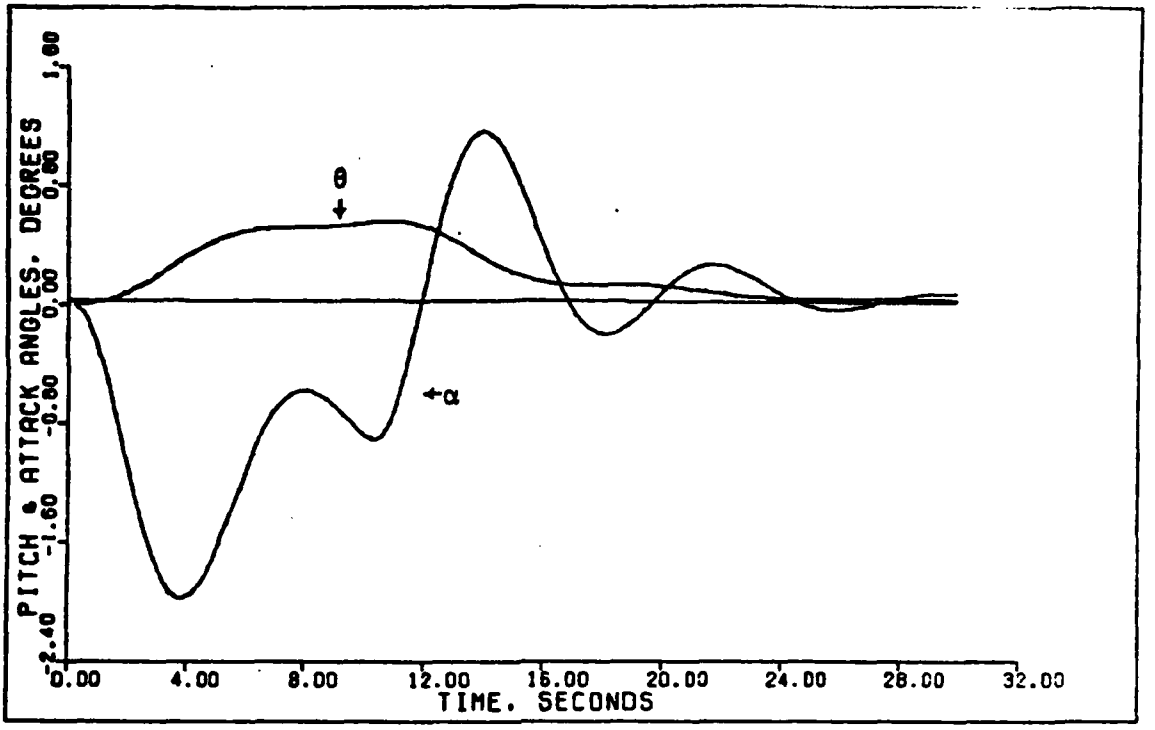



FIG 14c MACH 0.18 DESIGN CONDITION. NORMAL CLIMB

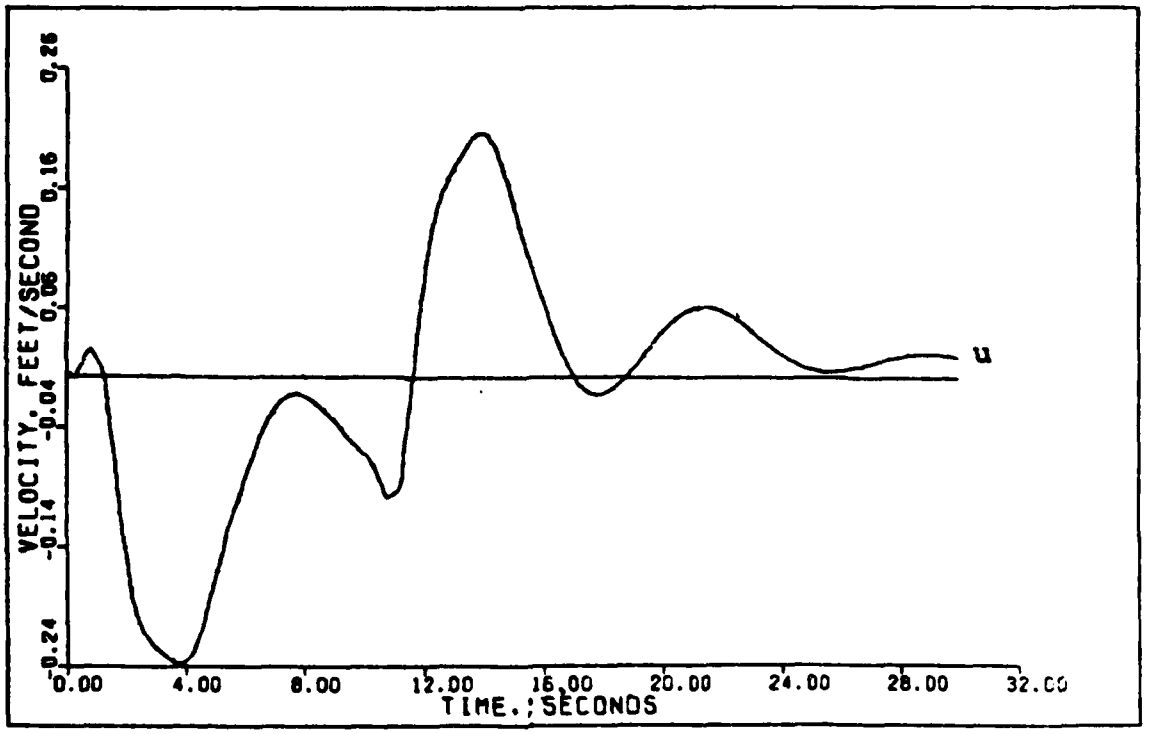



FIG 14d MACH 0.18 DESIGN CONDITION. NORMAL CLIMB

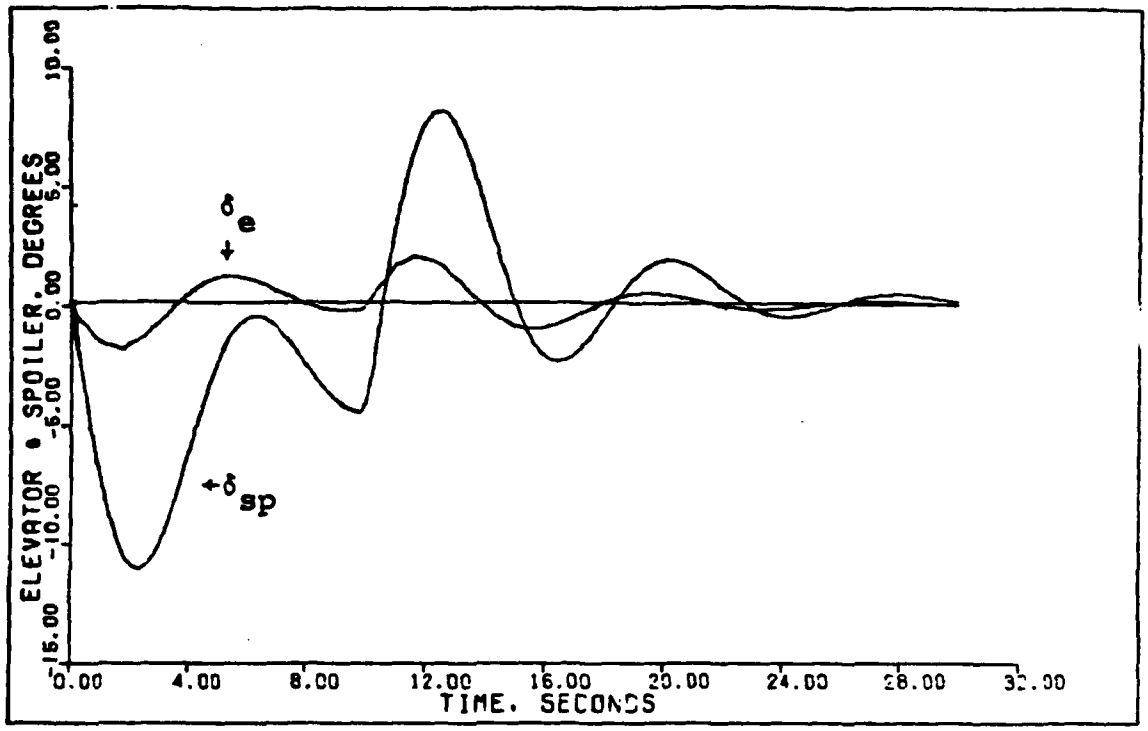



FIG 14e MACH 0.18 DESIGN CONDITION, NORMAL CLIMB

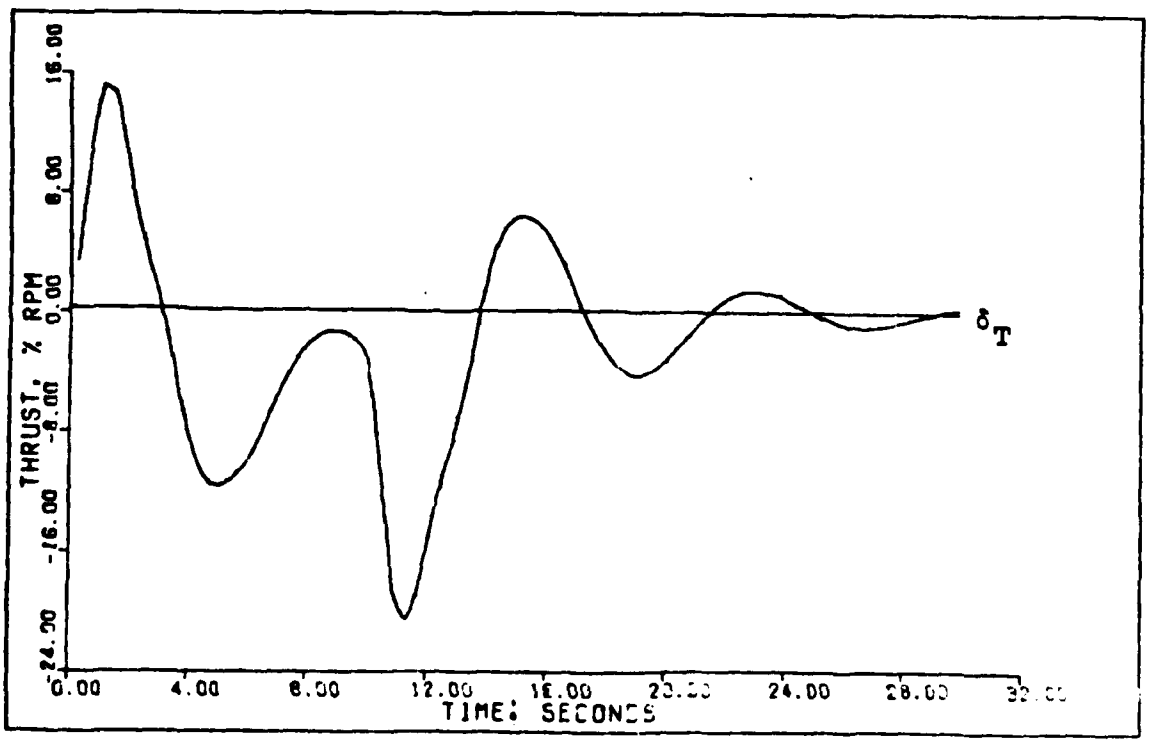



FIG 14f MACH 0.18 DESIGN CONDITION, NORMAL CLIMB

TABLE XIII

Normal Climb Results for MACH 0.18,
1000 ft Design Condition

| INPUT/ OUTPUT | $t_p$(sec) | $t_s$(sec) | PEAK VALUE | FINAL VALUE |
|---|---|---|---|---|
| h(ft) | 12.55 | 21.25 | 56.3 | 50.0 |
| $\delta_{sp}$(deg) | 2.35 | —— | -11.0 | 0. |
| $\beta$(deg) | 10.75 | —— | 0.55 | 0. |
| $\alpha$(deg) | 3.85 | —— | -1.973 | 0. |
| u(ft/sec) | 3.85 | —— | -0.23 | 0. |
| $\delta_e$(deg) | —— | —— | 2.1 | —— |
| $\delta_T$(% RPM) | —— | —— | -20.5 | —— |

A suggested change in the system model is presented using a direct feedforward matrix. This matrix allows a control input to be commanded in the steady state. A controller is presented for this new model for MACH 0.18. This results in a stable system and suggests that this new model should be investigated further.

The final chapter presents the conclusions formulated as a result of this thesis and suggests recommendations for further studies and improvements/additions to MULTI.

# VI Conclusions and Recommendations

## Thesis Summary

This thesis effort is designed to show the applicability of Professor Brian Porter's control techniques as applied to a large aircraft, specifically the C-141-A Starlifter. Development of digital control laws at three diverse flight conditions are considered and robustness is considered for controllers designed at the MACH 0.18 flight condition when it is used at other flight conditions.

Chapter I presents an introduction to the need for thesis study in this area. Chapter II describes the aircraft and discusses the required state space representation for the system models. A brief summary of control law theory for unknown, regular, irregular, and B* design techniques is presented in Chapter III. Chapter IV discusses modifications of the computer program MULTI made in conjunction with this thesis. Chapter V describes the actual development and analysis of control laws for the C-141-A aircraft.

Appendices in this thesis contain a development of the aircraft equations of motion (Appendix A), simulation data for the MACH 0.65 and MACH 0.76 designed controllers (Appendix B), and a User's Guide for the batch processing version of MULTI ( Appendix C).

The associate theses by Barfield (Ref 14), Bauschlicher (Ref 15), Russ (Ref 16), and Lewis (Ref 17) should be referenced for other studies of Porter's techniques and concurrent changes in MULTI. The thesis by Lewis analyzes control laws designed using continuous-time domain techniques.

## Conclusions

This thesis concludes that digital tracker control laws can indeed be very successfully designed for the C-141-A Starlifter aircraft. Controllers designed at specific flight conditions are found to tightly track the commanded inputs.

Theory provides that total decoupling of the outputs is achievable. However, the high-gain nature of the design technique would require large control surface deflections, unless the command input is shaped to meet performance specifications. Thus, the control law parameter is adjusted to reduce the control surface commands and still meet overall tracking requirements in a very satisfactory manner. There is some small acceptable interaction between outputs.

Robustness of the control laws design for the MACH 0.18 condition is demonstrated. Robustness is defined as the ability of a constant gain controller, designed for manuevers at a particular flight condition, to adequately perform similar manuevers at other flight conditions. This robustness is very desirable for avoiding gain scheduling requirements over a wide range of flight conditions.

Implementation of a direct feedforward matrix in the output equation is suggested as an extension of system designs. This type of model allows for command of control surface inputs to insure a desired steady-state deflection. Further investigation should be conducted in this area.

Overall, the conclusion is that a robust set of lateral and longitudinal digital tracker control laws can be designed for the C-141-A Starlifter, or any large aircraft.

## Recommendations

There are several areas of interest which should be investigated in the future. A more complete aircraft model should be derived to include coupling of the lateral and longitudinal modes. A "complete" aircraft controller should then be designed and tested.

Another area to be researched is the possible real-time simulation of a non-linear aircraft model using digital control laws designed by this method. Thus, a full analysis of the design techniques should be investigated.

Final recommendations suggest improvements in the computer program MULTI. These include, but are not limited to:

1. A major modification of the program to provide for more efficient use of memory allocations. This is a must for future additions to the program.
2. The addition of a continuous-time simulation option

to the program as the theory also applies to continuous-time controllers.

3. The inclusion of time response figures of merit for determining response acceptability.

## Bibliography


1. Rubertus, Duane P. "Proposed AFIT Thesis Topic #2" Handout. Wright-Patterson AFB, Ohio: Flight Dynamics Laboratory, April 1982.

2. Porter, B. and A. Bradshaw. "Singular Perturbation Methods in the Design of Tracking Systems Incorporating Fast-Sampling Error-Actuated Controllers," International Journal of Systems Science, 12(10): 1181-1192 (October 1981).

3. Porter, Douglas S. Design and Analysis of a Multivariable Digital Controller for the A-7D DIGITAC II Aircraft and the Development of an Interactive Computer Design Program. MS thesis. Air Force Institute of Technology, Wright-Patterson AFB, OH; December 1981. (AFIT/GE/EE/81D-48)

4. Paschall, Randall N. Design of a Multivariable Control Law for the A-7D DIGITAC II Aircraft. MS thesis. Air Force Institute of Technology, Wright-Patterson AFB, OH; December 1981. (AFIT/GE/EE/81D-47)

5. "Engine General" Training Manual for C-141 Instruction. Altus AFB, Oklahoma: 443 Technical Training Squadron, September 1975.

6. Larson, H. B. et. al. Military Transport (C-141) Fly-by-Wire Program, Vol I. AFFDL-TR-74-52, Minneapolis: Honeywell, Inc., April 1974.

7. Lockheed-Georgia Company. C-141B Stability and Control Characteristics. Report Number LG81ER0079, Marietta, Georgia: Lockheed Aircraft Corporation, January 1981.

8. Porter, B. Design of Set Point Tracking and Disturbance Rejection Controllers for Unknown Multivariable Plants. Progress Report for period 15 November 1980 to 31 December 1980. USAME/DC/101/81. Aif Force Flight Dynamics Laboratory, Wright-Patterson AFB, OH. January 1981.

9. Porter, B. Design of High Performance Tracking Systems. USAME/DC/120/81. Air Force Flight Dynamics Laboratory, Wright-Patterson AFB, OH. October 1981.

10. Porter, B. "Design of Tunable Non-Undershooting Servomechanisms," Corespondence with Dr. J. J. D'Azzo, Wright-Patterson AFB, Ohio: Air Force Institute of Technology, 1981.

11. Lewis, Tom. "High-Gain Error Actuated Flight Control Systems for Continuous Multivariable Plants." Unpublished MS thesis. School of Engineering, Air Force Institute of Technology, Wright-Patterson AFB, Ohio, December 1982.

12. Ridgely, D. B., S. Banda, and J. J. D'Azzo. "Decoupling of High-Gain Multivariable Tracking Systems." Paper No. 83-0280 scheduled for presentation to the AIAA 21st Aerospace Sciences Meeting at Reno, Nevada, in January, 1983. Wright-Patterson AFB, OH. June 1982.

13. Blakelock, John H. Automatic Control of Aircraft and Missiles. New York: John Wiley and Sons, Inc., 1965.

14. Barfield, A. Finley. "Multivariable Control Laws for the AFTI/F-16." Unpublished MS thesis. School of Engineering, Air Force Institute of Technology, Wright-Patterson AFB, OH, December 1982.

15. Bauschlicher, Jon M. "Design of a Complete Multivariable Digital Flight Control Systems." Unpublished MS thesis. School of Engineering, Air Force Institute of Technology, Wright-Patterson AFB, OH, December 1982.

16. Russ, Daniel E. "Reconfigurable Digital Control Laws for the A-7D Digitac Aircraft with Failed Primary Control Surfaces." Unpublished MS thesis. School of Engineering. Air Force Institute of Technology, Wright-Patterson AFB, Oh, December 1982.

17. Roskam, J. Airplane Flight Dynamics and Automatic Flight Controls. Lawerence, Kansas: Roskam Aviation and Engineering Corporation, 1976.

18. D'Azzo, John J. and Constantine H. Houpis. Linear Control Systems Analysis and Design, Second Edition. New York: McGraw-Hill Book Company, 1981.

19. Balfour, A. and D. H. Marwick. Programming in Standard FORTRAN 77. New York: North-Holland Inc., 1979.

20. Porter, B. "High-Gain Error-Actuated Controllers for Linear Multivariable Plants with Explicit Actuator Dynamics," Proceedings of the 2nd IFAC Symposium on Computer Aided Design of Multivariable Technological Systems. 61-65. West Lafayette, IN, September 15-17, 1982.

21. Porter, B. "Computation of the Zeros of Linear Multivariable Systems," International Journal of Systems Science, 10(12): 1427-1432 (December 1979).

22. Porter, B., and J. J. D'Azzo. "Transmission Zeros of Linear Multivariable Continuous-Time Systems," Electronics Letters, 13(24): 753-755 (November 24, 1977).

23. Porter, B. "Asymptotic Properties of Linear Multivariable Continuous-Time Tracking Systems Incorporating High-Gain Error-Actuated Controllers," International Journal of Systems Science, 10(12): 1433-1444 (December 1979).

24. Porter, B., and A. Bradshaw. "Design of Linear Multivariable Discrete-Time Tracking Systems Incorporating Fast-Sampling Error-Actuated Controllers," International Journal of Systems Science, 11(7): 817-826 (July 1980).

25. Porter, B. "Asymptotic Properties of Linear Multivariable Discrete-Time Tracking Systems Incorporating Fast-Sampling Error-Actuated Controllers," International Journal of Systems Science, 11(11): 1279-1293 (November 1980).

26. Porter, B. "Singular Perturbation Methods in the Design of Tracking Systems Incorporating Error-Actuated Controllers for Plants with Explicit Actuator Dynamics," International Journal of Control, 35(2): 383-389 (October 1981).

27. Falb, P. L. and W. A. Wolovich. "Decoupling in the Design and Synthesis of Multivariable Control Systems," IEEE Transaction on Automatic Control, AC-12(6): 651-659 (December 1967).

Appendix D

PREVIOUS PAGE
IS BLANK

AFIT/GAE/EE/82D-1

# HIGH-GAIN ERROR ACTUATED FLIGHT CONTROL SYSTEMS FOR CONTINUOUS LINEAR MULTIVARIABLE PLANTS

THESIS

Presented to the Faculty of the School of Engineering

of the Air Force Institute of Technology

Air University

in Partial Fulfillment of the

Requirements for the Degree of

Master of Science

by

Thomas Lewis, B.S.A+AE.

2Lt USAF

Graduate Aeronautical Engineering

December 1982

Approved for public release; distribution unlimited

## Acknowledgements

I would like to thank my thesis advisors, Dr. John D'Azzo and Dr. Constantine Houpis, for all their encouragement and guidance. I would also like to thank the Flight Dynamics Laboratory for sponsoring my thesis, especially the Control Techniques Group and Control Data Group for sharing their facilities with me.

## Dedication

I dedicate this thesis to my grandfather William Lewis, a self taught engineer, who was an inspiration throughout my engineering education.

## Contents


Preface .....

Illustrations .....

Symbols .....

Absract .....

I. Introduction .....

Backround .....

Problem Statement and Approach .....

Assumptions .....

Organization .....

II. Theoretical Development .....

III. Discussion of Results .....

Design Procedure .....

Robustness Tests .....

Actuator Dynamics .....

IV. Conclusions and Recommendations .....

Bibliography .....

Appendix A-1 Development of the Aircraft Equations of Motion

Appendix A-2 Dimensionalization Computer Program .....

Appendix B-1 Computer Program to Calculate System Zeros .....

Appendix B-2 Listing of Program ZERO and Examples .....

Appendix C Main Computer Program .....

Vita .....

## Illustrations

Figures


2-1 - Tracking System .....

2-2 - Tracking System with Actuators .....

3-1 - Figures of Merit for Output Responses .....

3-2 - Comparison of Figures of Merit

(a)- Peak Overshoot to a Step r Input .....

(b)- Steady-state Pointing Angle $\psi$ .....

(c)- Absolute Time Integral $\phi$ .....

(d)- Maximum Control Surface Deflection Error .....

(e)- Velocity Vector Pointing Angle Range .....

(f)- Steady-state Velocity Vector Pointing Angle .....

3-3 - Low Q Yaw Pointing .....

3-4 - Mid Q Yaw Pointing .....

3-5 - High Q Yaw Pointing .....

3-6 - Design 2A Additional Maneuvers .....

3-7 - Mid Q Additional Maneuvers .....

3-8 - Low Q Yaw Pointing Without Actuators .....

3-9 - Mid Q Yaw Pointing Without Actuators .....

3-10 - High Q Yaw Pointing Without Actuators .....

3-11 - Design 2 Additional Maneuvers .....

3-12 - All Constants Changed .....

3-13 - One Constant Decreased .....

3-14 - One Constant Increased .....

3-15 - Two Constants Decreased .....

3-16 - Two Constants Increased .....

3-17 - One Constant Decreased, One Constant Increased .....

B-1 - Program ZERO Flow Chart .....

C-1 - Main Computer Program Flow Chart .....


Tables


3-1 - Input Commands .....

3-2 - Design 1A Figures of Merit .....

3-3 - Design 2A Figures of Merit .....

3-4 - Design 3A Figures of Merit .....

## Illustrations

Tables

3-5 - Mid Q Designs .....

A-1 - Flight Condition Data .....

A-2 - AFTI-16 Non-Dimensional Stability Axis Data .....

A-3 - Lateral-Directional Dimensionalization Factors .....

A-4 - AFTI-16 Fixed Aircraft Parameters .....

A-5 - AFTI-16 Plant Matrices .....

B-1 - Required Input for Program LERS .....

## Symbols

$\underline{A}$ - State Matrix

$\underline{A}_c$ - Actuator Contant Matrix

$\underline{A}_{CL}$ - Closed-loop State Matrix

$\underline{AA}$ - Generalized Eigenvalue Problem Matrix

b - Wing Span

$\underline{B}$ - Input Matrix

$\underline{B}_{CL}$ - Closed-loop Input Matrix

$\underline{BB}$ - Generalized Eigenvalue Problem Matrix

$\underline{c}_i$ - $i^{th}$ Row of Output Matrix

C - Set of Complex Numbers

$\underline{C}$ - Output Matrix

$\underline{C}_{CL}$ - Closed-loop Output Matrix

$C_l$ - Roll Moment Coeficient

$C_n$ - Yaw Moment Coeficient

$C_y$ - Side Force Coeficient

$\underline{d}$ - Riccati Equation Vector Due to Tracking

dt - Time Derivitive

$\underline{e}$ - Error Vector

$\underline{F}$ - Measurement Output Matrix

g - Acceleration Due to Gravity

- Forward- oop Gain Parameter

$\underline{G}$ - Transfer Function

$\underline{G}_A$ - Transfer Function for Actuator Dynamics

$\underline{H}$ - Weighting Matrix

$I_i$ - Identity Matrix of Rank i

$I_{xx}$ - Moment of Inertia x body axis

$I_{xz}$ - Cross Product of Inertia x and z body axis

$I_{zz}$ - Moment of Inertia z body axis

J - Performance Index

$\underline{K}$ - Controller Matrix

- Feedback Gain Matrix

- Random Matrix

$\ell$ - Number of Outputs

L - Roll Moment

L' - Roll Moment with Inertia Terms

## Symbols

| | |
|---|---|
| $m$ | - Number of Inputs |
| $\underline{M}$ | - Measurement Matrix |
| $n$ | - Number of States |
| $N$ | - Yaw Moment |
| $N'$ | - Yaw Moment with Inertia Terms |
| $p$ | - Roll Rate |
| $\underline{P}$ | - Riccati Equation Solution Matrix |
| $Q$ | - Dynamic Pressure |
| $\underline{Q}$ | - Weighting Matrix |
| $r$ | - Yaw Rate |
| $R$ | - Set of Real Numbers |
| $\underline{R}$ | - Weighting Matrix |
| $s$ | - Laplace Transformation Parameter |
| $S$ | - Wing Area |
| $t$ | - Time |
| $t_f$ | - Final Time |
| $\underline{u}$ | - Input Vector |
| $\underline{u}_A$ | - Input Vector with Actuator Dynamics |
| $\underline{u}^*$ | - Optimal Input Vector |
| $U$ | - Aircraft Velocity |
| $v$ | -Pertubation Side Velocity |
| $\underline{v}$ | - Command Vector |
| $w$ | - Weight |
| $\underline{w}$ | - Measurement Vector |
| $\underline{x}$ | - State Vector |
| $\underline{y}$ | - Output Vector |
| $Y$ | - Side Force with v as a State |
| $Y^*$ | - Side Force with $\beta$ as a State |
| $\underline{z}$ | - Time Integral of Error Vector |
| | - Generalized Eigenvector |
| $z_1$ | - First Set of Slow Eigenvalues |
| $z_2$ | - Second Set of Slow Eigenvalues |
| $z_3$ | - Set of Fast Eigenvalues |

## Symbols

| | |
|---|---|
| $\alpha_o$ | - Trim Angle of Attack |
| $\beta$ | - Side-Slip Angle |
| $\gamma$ | - Flight Path Angle |
| $\underline{\Gamma}$ | - Asymptotic Transfer Function |
| $\underline{\hat{\Gamma}}$ | - Slow Asymptotic Transfer Function |
| $\underline{\tilde{\Gamma}}$ | - Fast Asymptotic Transfer Function |
| $\phi$ | - Roll Angle |
| $\delta_a$ | - Aileron Deflection |
| $\delta_c$ | - Cannard Deflection |
| $\delta_{dt}$ | - Differential Tail Deflection |
| $\delta_f$ | - Flaperon Deflection |
| $\delta_r$ | - Rudder Deflection |
| $\epsilon$ | - Pertubation Parameter |
| $\in$ | - " is a member of " |
| $\underline{\xi}$ | - Eigenvector |
| $\theta_o$ | - Trim Flight Path Angle |
| $\lambda$ | - Eigenvalue |
| $\rho$ | - Air Density |
| $\sigma$ | - Fast Pole |
| $\underline{\Sigma}$ | - Matrix of Fast Poles |
| $\tau$ | - Time Dummy Argument |
| $\underline{\omega}$ | - Portion of Null Space |
| $\psi$ | - Pointing Angle |
| $\dot{\ }$ | - Time Derivitive of a Vector |
| $\mathcal{N}$ | - Null Space |
| det | - Determinant of a Matrix |
| $\lvert\ \rvert$ | - Determinant of a Matrix |
| $[\ ]^T$ | - Transpose of a Matrix |
| $[\ ]^{-1}$ | - Inverse of a Matrix |

## Subscripts

| | |
|---|---|
| b | - Body Axis |
| s | - Stability Axis |
| ss | - Steady-State |

## Abstract

The theory of high-gain error actuated feedback control, developed by Porter and Bradshaw, is applied to the design of various lateral-directional decoupling flight control systems for an advanced aircraft. The controllers developed in this report utilize output feedback with proportional plus integral control to produce desirable closed-loop responses with minimal interactions between outputs. Because of the structure of the system, measurement variables in addition to the outputs are necessary to apply this method. The report examines controller design robustness by varying the flight conditions or maneuver commands from the ones the controller is specifically designed for, and then judges system performance. The results show that the controller is robust with respect to varying flight conditions, but is not robust with respect to varying maneuver commands. This report also examines the effect of first-order actuator dynamics in the system model. Actuator dynamics are shown to significantly affect the control system response, indicating that a simplified model, without actuators, is not desireable in one's control design scheme. Also a computer program to determine transmission zeros and decoupling zeros is developed.

# HIGH-GAIN ERROR ACTUATED FLIGHT CONTROL SYSTEMS FOR CONTINUOUS LINEAR MULTIVARIABLE PLANTS

## I. Introduction

Advanced Fighter Technology Integration (AFTI) is the culmination of the most recent technology advances in flight control and avionics. The AFTI-16 aircraft, which incorporates this technology, is presently undergoing flight tests. A new digital flight control system, along with additional control surfaces, such as vertical cannards, allow the aircraft to perform direct force, decoupled maneuvers.

This report contains an investigation of a new controller design method for the AFTI-16. Specifically, an analogue controller is designed to perform four lateral-directional decoupled maneuvers. These maneuvers are horizontal translation, wings level turn, constant altitude coordinated turn, and yaw pointing. The maneuvers can be described by three output variables: side-slip angle, $\beta$; roll angle, $\phi$; and yaw rate, r. Initially all output variables are zero. For horizontal translation the side-slip angle, $\beta$, changes, while $\phi$ and r remain unchanged. In a wings level turn the yaw rate, r, changes, while $\beta$ and $\phi$ remain unchanged. In a constant altitude coordinated turn the yaw rate, r, is proportional to the roll angle, $\phi$,

$$r = \frac{g}{U} \sin \phi, \tag{1-1}$$

while $\beta$ remains zero. For yaw pointing the time rate of change of the side-slip angle, $\beta$, must be equal in magnitude and opposite in sign to

the yaw rate, r, while $\phi$ remains zero.

## Background

Controllers have been designed for single input/single output (SISO) systems using conventional techniques for a long time. The advance of computational technology readily permits the design of controllers for multiple input/multiple output (MIMO) systems. A MIMO system design offers a greater amount of control and greater precision. Conventional control employs widely accepted design techniques, such as root-locus and frequency response analysis. Multivariable control design is still growing and a number of different theories and design methods have been developed. In this report the design method developed and proposed by Dr Brian Porter of the University of Salford, England is utilized and evaluated.

Other multivariable control methods presently available utilize optimal control, entire eigenstructure assignment, and frequency domain techniques.

In the optimal control design method (Ref.2) a control law is found by minimizing the value of the performance index or cost functional

$$J = 1/2 \int_0^{t_f} \left[ \left[ \underline{y}(t) - \underline{v}(t) \right]^T \underline{Q}(t) \left[ \underline{y}(t) - \underline{v}(t) \right] + \underline{u}^T(t) \, \underline{R}(t) \, \underline{u}(t) \right] dt + 1/2 \left[ \underline{y}(t_f) - \underline{v}(t_f) \right]^T \underline{H} \left[ \underline{y}(t_f) - \underline{v}(t_f) \right] \quad (1\text{-}2)$$

for the system described by the state and output equations

$$\dot{\underline{x}}(t) = \underline{A} \, \underline{x}(t) + \underline{B} \, \underline{u}(t)$$

$$\underline{y}(t) = \underline{C} \, \underline{x}(t) \quad (1\text{-}3)$$

where $\underline{y}(t)$ is the output vecto..

$\underline{v}(t)$ is the command vector, and $\underline{Q}(t)$, $\underline{R}(t)$, and $\underline{H}$ are symmetric positive definite quadratic weighting matrices. The optimal control law that minimizes J is

$$\underline{u}^*(t) = \underline{K}(t)\ \underline{x}(t) - \underline{R}^{-1}(t)\ \underline{B}^T\ \underline{d}(t) \tag{1-4}$$

The time varying feedback gain matrix is

$$\underline{K}(t) = -\ \underline{R}^{-1}(t)\ \underline{B}^T\ \underline{P}(t) \tag{1-5}$$

where $\underline{P}(t)$ is the solution of a nonlinear time varying matrix differential equation, commonly known as the Riccati Equation:

$$\dot{\underline{P}}(t) = -\underline{A}^T\ P(t) - \underline{P}(t)A + \underline{P}(t)\underline{B}\ \underline{R}^{-1}(t)\ \underline{B}^T\underline{P}(t)$$

$$-\underline{C}^T\ \underline{Q}(t)\ \underline{C} \tag{1-6}$$

where $P(t_f) = \underline{C}^T\ \underline{H}\ \underline{C}$.

The vector $\underline{d}(t)$ is the solution to the matrix differential equation

$$\dot{\underline{d}}(t) = \underline{A}^T\underline{d}(t) + \underline{K}(t)\ \underline{B}\ \underline{R}^{-1}(t)\underline{B}^T\underline{d}(t)$$

$$+\ \underline{C}^T\ \underline{Q}(t)\ \underline{C} \tag{1-7}$$

where $\underline{d}(t_f) = -\underline{C}^T\ \underline{H}\ \underline{C}\ \underline{v}(t_f)$.

Due to the boundary conditions on the two matrix differential equations, they must be integrated backwards in time. This requires that command input information be known in the future. The computation required for the numerical solutions to these equations are extremely costly

and difficult to achieve. Also selection of the positive definite weighting matrices, $\underline{Q}(t)$, $\underline{R}(t)$, and $\underline{H}$, must be made. This is usually accomplished by a trial and error iterative process, requiring repeated integrations of the matrix differential equations.

In the entire eigenstructure assignment design method (Ref 11), the designer selects the system closed-loop eigenvalues, $\lambda_i$, and corresponding eigenvectors, $\underline{\xi}_i$. Given the system described by eq. 1.3, a state feedback control law

$$\underline{u}(t) = \underline{K}\,\underline{x}(t) + \underline{v}(t) \tag{1-8}$$

is assumed. Substituting this control law into the state equations yields the closed-loop system

$$\dot{\underline{x}}(t) = \left[\underline{A} + \underline{B}\,\underline{K}\right]\underline{x}(t) + \underline{B}\,\underline{v}(t) \tag{1-9}$$

The feedback gain matrix, $\underline{K}$, is

$$\underline{K} = \left[\underline{\omega}_1, \underline{\omega}_2, \cdots, \underline{\omega}_n\right]\left[\underline{\xi}_1, \underline{\xi}_2, \cdots, \underline{\xi}_n\right]^{-1} \tag{1-10}$$

The feedback gain matrix of eq. 1-10 produces a closed-loop system with the selected eigenvalues and corresponding eigenvectors, provided all eigenvectors, $\underline{\xi}_i$, and vectors, $\underline{\omega}_i$, satisfy the relation

$$\begin{bmatrix}\underline{\xi}_i \\ \underline{\omega}_i\end{bmatrix} \in N\left[\underline{A} - \lambda_i I_n \;,\; \underline{B}\right] \tag{1-11}$$

Extreme care must be taken when selecting the eigenvectors from the null space of $\left[\underline{A} - \lambda_i\, I,\, B\right]$, in order that the matrix $\left[\underline{\xi}_1, \underline{\xi}_2, \ldots \underline{\xi}_n\right]^{-1}$

exists. Also, the eigenvalues and eigenvectors must be chosen to minimize the amount of interaction between outputs. Selection of the eigenvalues, $\lambda_i$, and eigenvectors, $\underline{\xi}_i$, is an art, requiring insight and a lot of trial and error iterations.

Porter's design method, described in Chapter II, often produces a successful controller design with less trial and error iterations than the two methods described above.

Problem Statement and Approach

It is desired to design and evaluate a flight controller, using Porter's design method (Ref 7), for an AFTI-16 aircraft which simulates maneuvers of horizontal translation, wings level turn, constant altitude coordinated turn, and yaw pointing. The evaluation consists of examining robustness and effect of first-order actuators in the simulation.

A robust controller design can perform satisfactorily at conditions other than the one it is specifically designed for. In this report robustness is examined by using a controller designed for a yaw pointing maneuver at a specific design flight condition, and using it without change in the simulation of a yaw pointing maneuver at other flight conditions. Also the same controller is used in the simulation of the three other maneuvers at the design flight condition. The performance of the three maneuvers is compared with the performance of controllers designed to perform the specific maneuver.

Three different controllers are designed to perform the yaw pointing maneuver. One at a low dynamic pressure, Q, design flight condition, another at a medium dynamic pressure design flight condition, and the

third at a high dynamic pressure design flight condition. Each of these controllers are then included in the simulation of a yaw pointing maneuver at nine other flight conditions, covering a spectrum of dynamic pressures.

A successful design is based on several criteria. In this report the following specifications are established: First, the closed-loop system must be stable. Second, all transient responses should be within 98% of their steady-state value in three seconds. Third, the steady-state response should achieve the commanded value with no observable error. Fourth, the control surfaces are not commanded beyond a pre-set limit.

Assumptions

The following assumptions are made to simplify the computations and analysis:

1. The earth is flat and non-rotating.
2. The atmosphere is at rest with respect to the earth.
3. The acceleration due to gravity is constant.
4. The aircraft is a rigid body.
5. The aircraft has a constant mass.
6. The aircraft performs maneuvers while flying straight with wings level, unless otherwise specified.
7. The motion of the aircraft about a straight and level trim condition can be adequately modeled by a linear dynamical system of equations.
8. The dynamics of the actuators can be adequately modeled by a first-order differential equation.
9. The side slip angle, $\beta$, can be measured.

## Organization

First, the theory used in Porter's design is described, and the method for developing a controller is discussed. Also included in Chapter II are methods for including first-order actuator dynamics in the model. Chapter III presents the results of applying this method to an aircraft model. The effects of varying flight conditions and maneuver commands are described in detail. Also the effects of actuator dynamics in the simulation are discussed. Chapter IV discusses the results and provides recommendations for further study.

Included in the Appendices are discussion of the aircraft equations of motion, a computer program to calculate system zeros, and the computer program used to perform design iterations and simulations.

Chapter 2, Design Theory, Omitted

See Proceedings

## III. Discussion of Results

### Design Procedure

As a result of this thesis it is concluded that Porter's design method is easy to apply. Satisfactory controllers are found for a specific maneuver and flight condition without many design iterations. Also a designer's "feel" is quickly obtained, making controller designs easy to obtain. A feel is when the designer knows how different parameters affect the output response. The effect of the various parameters discovered during the design iterations for the controllers of this report are now discussed.

The measurement matrix, $\underline{M}$, is selected as a sparse matrix using the second method discussed in Chapter II (Ref 9). The reciprocal of the non-zero element of the $\underline{M}$ matrix becomes the transmission zero of the system. A transmission zero of -4 is selected for all of the controller designs in this report. This value is recommended by Lt Ridgely (Ref 10).

The value of the sigma matrix, $\underline{\Sigma}$, does affect the outputs in a predictable way. To keep the outputs decoupled, and the fast asymptotic transfer function, $\hat{\underline{\Gamma}}$, diagonal, $\underline{\Sigma}$ is selected as a diagonal matrix. Each diagonal element, $\sigma_i$, affects the corresponding output (the first diagonal element affects the first output, etc.). Increasing the value of the element causes the output to track the command input closer. A large diagonal sigma element is desirable when the specific output response is commanded to zero. An adverse effect of a large diagonal element is that the magnitude of the control surface responses are increased. Decreasing the diagonal element causes an

increase in the transient response of the output. Varying the diagonal elements in the sigma matrix is the main avenue used to achieve desired output and control surface time responses for the controller's designs contained in this report. An observation made during the design iterations is that an optimal sigma matrix found for a specific maneuver and specific flight condition is very close to the optimal sigma matrix for the same maneuver at a different design flight condition. This observation is shown by comparing the sigma matrices for the three yaw pointing designs, Tables 3-2 through 3-4.

The gain value, g, is used in the design iterations for the controllers in this report, to adjust the peak value and settling time of the response to a step input. The gain can be adjusted so the output response has no noticeable peak and an acceptable settling time. For all values of gain an overshoot is found to exist. Very high gain and very low gain cause a large overshoot. The gain for a minimum overshoot is a medium value. Settling time decreases with increasing gain value.

The value of the input commands can be used to adjust the control surface time responses. Changes to the values of the input commands do not adversely affect the output responses, in that they will track the commands. The control surface responses are, naturally, sensitive to the magnitude of the input command. The value of the input command can be reduced to keep the control surface deflections within limits. This is the last parameter to be adjusted in the design procedure. The initial values of input commands are obtained from [illegible] tunnel data (Ref 12).

The control surface deflection limits for the designs of this report are:

$$\text{Rudder, } -35^\circ \leq \delta_r \leq 35^\circ$$

$$\text{Aileron, } -35^\circ \leq \delta_a \leq 35^\circ$$

$$\text{Cannard, } -30^\circ \leq \delta_c \leq 30^\circ$$

These limit values are selected by the designer and considered reasonable.

The interactive computer program, listed in Appendix C, make rapid design iterations possible.

Robustness Tests

As stated in the Introduction, the robustness tests are performed with the yaw pointing maneuver. The output matrix is

$$\left[C_1 : C_2\right] = \left[\begin{array}{c:ccc} 0 & 1 & 0 & 0 \\ 1 & 0 & 0 & 0 \\ 0 & 0 & 0 & 1 \end{array}\right] \tag{3.1}$$

The values of the input commands to produce a yaw pointing angle are shown in Table 3-1. The side-slip angle, $\beta$, is commanded as a ramp with the slope $-\beta_o$ until the value of the side-slip angle reaches minus three degrees. At this time, $\tau$, the slope is changed to zero. The ramp input is used as a way of commanding the time rate of the side-slip angle, $\dot{\beta}$. The roll angle, $\phi$, is commanded to zero. The yaw rate, r, is commanded as a pulse with a constant magnitude equal to $\beta_o$. The value of $\beta_o$ is a function of the dynamic pressure, Q, which is determined by the flight condition. At time $\tau$ the value of yaw rate is commanded to zero.

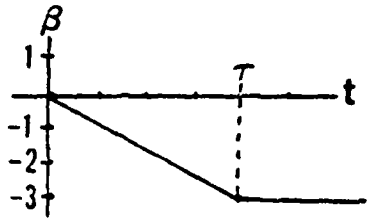
TABLE 3-1

# INPUT COMMANDS

1) Side Slip Angle, $\beta$

$\beta(t) = -\beta_0 t \quad 0 \le t \le \tau$

$= -3 \quad t > \tau$



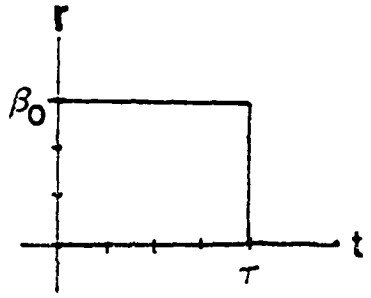

2) Roll Angle, $\phi$

$\phi(t) = 0 \quad t \ge 0$

3) Yaw Rate, r

$r(t) = \beta_0 \quad 0 \le t \le \tau$

$= 0 \quad t > \tau$




| Q CONDITION | SLOPE, $\beta_0$ | TIME CONSTANT, $\tau$ | $\int_0^\tau \beta(t)dt$ | $\int_0^\tau r(t)dt$ |
|---|---|---|---|---|
| | (deg/sec) | (seconds) | (deg·sec) | (degrees) |
| Low | -0.00 | 3.75 | 5.625 | 3.00 |
| Low-Mid | -1.00 | 3.00 | 4.500 | 3.00 |
| Mid | -3.00 | 1.00 | 1.500 | 3.00 |
| High | -4.00 | .75 | 1.125 | 3.00 |

The results of the yaw pointing robustness test for varying flight conditions are summarized in Tables 3-2 through 3-4 and Figures 3-2a through 3-2f.* In all cases, except one (Design 1A, Q = 825) the controller performs the desired yaw pointing maneuver. This is shown by the fact that the steady-state side-slip angle, $\beta_{ss}$, and the steady-state pointing angle, $\psi_{ss}$, are equal in magnitude and opposite in sign. The pointing angle, $\psi$, is the time integral of the yaw rate

$$\psi(t) = \int_0^t r(t)dt \tag{3.2}$$

The most noticeable difference, when the controller is used outside its design flight condition, is the response of the yaw rate, r. Outside the design flight condition the yaw rate has an initial overshoot and a few oscillations. This does not affect the performance of the maneuver, based on the smooth response of the side-slip angle and the pointing angle.

Figures 3-3 through 3-5 show the output and control surface time responses of all three controllers performing a yaw pointing maneuver at a specific flight condition. Figure 3-3 shows the responses of a low dynamic pressure maneuver (Q = 109). Figure 3-4 shows the responses of a medium dynamic pressure maneuver (Q = 443). Figure 3-5 shows the responses of a high dynamic pressure maneuver (Q = 825).

The controller designed at a low dynamic pressure, Design 1A, consistently overcommanded the control surfaces when performing the yaw pointing maneuver outside its design flight condition, as shown

*Figure 3-1 shows the basis for the data in Tables 3-2 through 3-4.

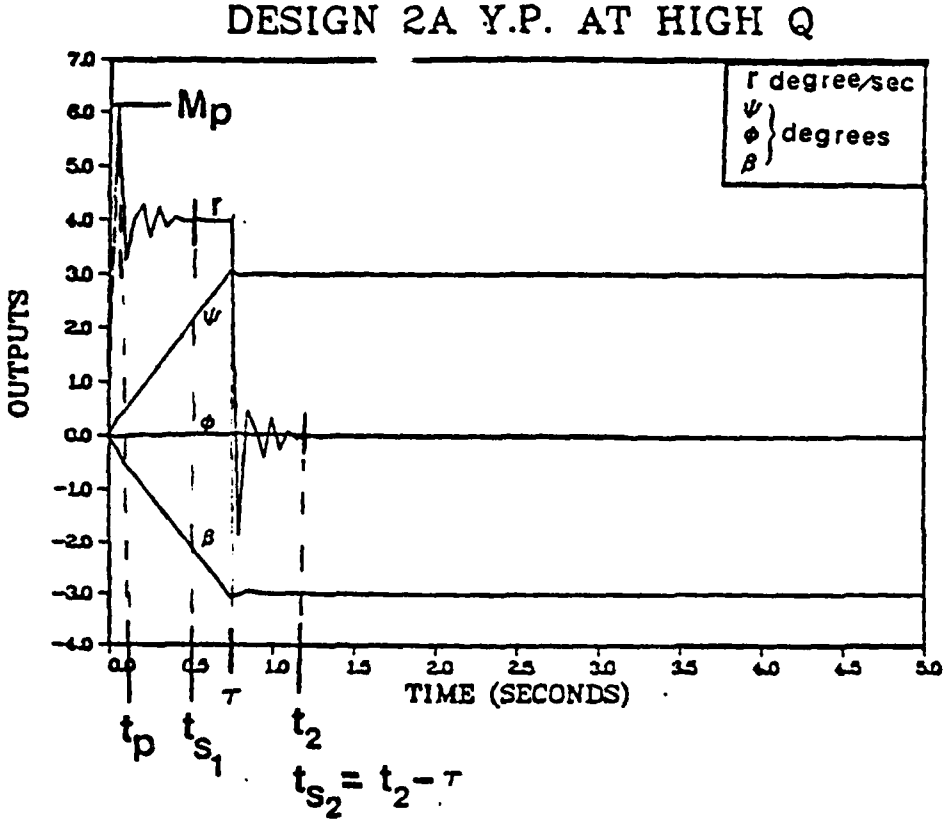
in Figure 3-2d. Controllers designed at medium dynamic pressure, Design 3A, only overcommanded the control surfaces at two of the ten flight conditions simulated, and the value of the deflection error is not great.

Figures 3-2e and 3-2f show the range of motion of the velocity vector pointing angle. The velocity vector is the sum of the side-slip angle and the pointing angle. Figure 3-2e shows the range of values that the velocity vector pointing angle moves. In the worst case (Design 1A, Q = 825) the total horizontal translation is not greater than 10 feet, during the time of the maneuver, $\tau$. In this case the steady-state velocity vector pointing angle is 0.13 degrees, resulting in a steady-state horizontal velocity of 2.2 feet/second.

Figure 3-2c shows the time integral of the roll angle. This quantity is used as a judgement of performance, and a basis for comparison. In the worst case (Design 3A, Q = 70) the value is 0.176 degree-second. This is equivalent to a roll angle of 0.06 degrees for three seconds. The magnitudes of the roll angle time integral shows that in all cases the plane remained essentially wings level.

Based on all performance criteria shown in Tables 3-2 through 3-4, and Figures 3-2a through 3-2f, the controller designed for a medium dynamic pressure flight condition, Design 2A, is the more robust design.

Another robustness test is judging the performance of a controller designed to perform a specific maneuver at a specific flight condition performing other maneuvers at the same flight condition.




$$\%\text{error} = \frac{Mp - \beta_0}{\beta_0} 100$$

Figure 3-1 Figures of Merit for Output Responses

TABLE 3-2 Design 1A Figures of Merit

DESIGN 1A LOW Q $Q = 109\ lb/ft^2$ $h = 20{,}000\ ft$ Mach = 0.4

$$\underline{M} = \begin{bmatrix} 0 \\ 0.25 \\ 0 \end{bmatrix} \quad \underline{\Sigma} = \begin{bmatrix} 1 & 0 & 0 \\ 0 & 15 & 0 \\ 0 & 0 & 30 \end{bmatrix} \quad \underline{A}_0 = \begin{bmatrix} 20 & 0 & 0 \\ 0 & 20 & 0 \\ 0 & 0 & 20 \end{bmatrix}$$

$$\underline{K}_0 = \begin{bmatrix} 29.1768 & 1.6411 & -6.4843 \\ 5.4674 & -4.3414 & -1.6377 \\ 44.6171 & 0.5608 & 20.4908 \end{bmatrix} \quad \underline{K}_1 = \underline{K}_0 \quad \varepsilon = 29.5$$

| Q | $\beta_{ss}$ | $\int_0^t r(\xi)d\xi \,/\, \psi_{ss}$ | $M_p$ | %error | $t_p$ | $t_{s_1}$ | $t_{s_2}$ | $\int_0^t \phi(\xi)d\xi$ | CONTROL SURFACE COMMENT |
|---|---|---|---|---|---|---|---|---|---|
| 70 | -2.999 | 2.993 | 1.0508 | 31.350 | 0.10 | 0.40 | 0.45 | 0.0414 | exceeds limits $\delta_c > 38.0^\circ$ |
| 109 | -2.999 | 3.012 | 0.8197 | 2.462 | 0.35 | 0.40 | 0.30 | 0.0242 | within limits |
| 163 | -2.999 | 3.005 | 1.0114 | 28.453 | 0.10 | 0.45 | 0.40 | 0.0162 | exceeds limits $\delta_c > 10.9^\circ$ |
| 223 | -2.999 | 2.992 | 1.5377 | 53.770 | 0.05 | 0.40 | 0.45 | 0.0188 | within limits |
| 436 | -2.999 | 3.018 | 3.7456 | 24.853 | 0.10 | 0.45 | 0.35 | 0.0166 | exceeds limits $\delta_c > 28.9^\circ$ |
| 443 | -2.999 | 3.037 | 3.6850 | 22.820 | 0.15 | 0.45 | 0.35 | 0.0147 | exceeds limits $\delta_c > 43.1^\circ$ |
| 532 | -2.999 | 3.007 | 4.2513 | 41.710 | 0.05 | 0.40 | 0.40 | 0.0153 | exceeds limits $\delta_c > 28.1^\circ$ |
| 652 | -2.999 | 2.9915 | 4.5565 | 51.833 | 0.05 | 0.40 | 0.40 | 0.0164 | exceeds limits $\delta_c > 33.9^\circ$ |
| 825 | -2.999 | 3.132 | 4.2150 | 5.375 | 0.60 | 0.75 | 0.10 | 0.0159 | exceeds limits $\delta_r > 10.6^\circ$ |
| 1198 | -2.999 | 2.993 | 6.3388 | 58.470 | 0.05 | 0.40 | 0.15 | 0.0171 | exceeds limits $\delta_r > 6.5^\circ$ |

TABLE 3-3 Design 2A Figures of Merit .

DESIGN 2A MID Q $Q = 443$ lb/ft$^2$ $h = 5{,}000$ Mach $= 0.6$

$$\underline{M} = \begin{bmatrix} 0 \\ 0.25 \\ 0 \end{bmatrix} \quad \underline{\Sigma} = \begin{bmatrix} 1 & 0 & 0 \\ 0 & 15 & 0 \\ 0 & 0 & 30 \end{bmatrix} \quad \underline{A}_o = \begin{bmatrix} 20 & 0 & 0 \\ 0 & 20 & 0 \\ 0 & 0 & 20 \end{bmatrix}$$

$$\underline{\Sigma}_o = \begin{bmatrix} 11.6944 & 0.1981 & -2.0615 \\ 2.7389 & -1.0522 & -0.1395 \\ 14.6517 & -0.2256 & 4.4020 \end{bmatrix} \quad \underline{K}_1 = 2\underline{K}_0 \quad s = 29.0$$

| Q | $\beta_{ss}$ | $\int_0^t r(\xi)d\xi \; \psi_{ss}$ | $M_p$ | %error | $t_p$ | $t_{s_1}$ | $t_{s_2}$ | $\int_0^t \phi(\xi)d\xi$ | CONTROL SURFACE COMMENT |
|---|---|---|---|---|---|---|---|---|---|
| 70 | -3.000 | 3.011 | 1.1771 | 47.1375 | 0.05 | 0.50 | 0.45 | 0.1069 | within limits |
| 109 | -3.000 | 3.001 | 1.3366 | 67.0750 | 0.05 | 0.45 | 0.45 | 0.0644 | within limits |
| 163 | -3.000 | 2.995 | 1.1883 | 48.5250 | 0.05 | 0.45 | 0.45 | 0.0459 | within limits |
| 223 | -3.000 | 2.9821 | 1.4072 | 40.7200 | 0.10 | 0.45 | 0.40 | 0.0463 | within limits |
| 436 | -3.000 | 3.053 | 3.0801 | 2.6700 | 0.40 | 0.30 | 0.30 | 0.0385 | within limits |
| 443 | -3.000 | 3.043 | 3.0414 | 1.3800 | 0.40 | 0.20 | 0.35 | 0.0342 | within limits |
| 532 | -3.000 | 3.020 | 3.6418 | 21.3933 | 0.15 | 0.40 | 0.40 | 0.0324 | within limits |
| 652 | -3.000 | 3.011 | 4.1880 | 39.6000 | 0.10 | 0.50 | 0.35 | 0.0368 | within limits |
| 825 | -3.000 | 2.993 | 6.0860 | 52.1500 | 0.05 | 0.40 | 0.40 | 0.0367 | exceeds limits $\delta_c > 2.0°$ |
| 1198 | -3.000 | 2.981 | 5.4505 | 36.2625 | 0.05 | 0.45 | 0.40 | 0.0365 | exceeds limits $\delta_c > 5.0°$ |

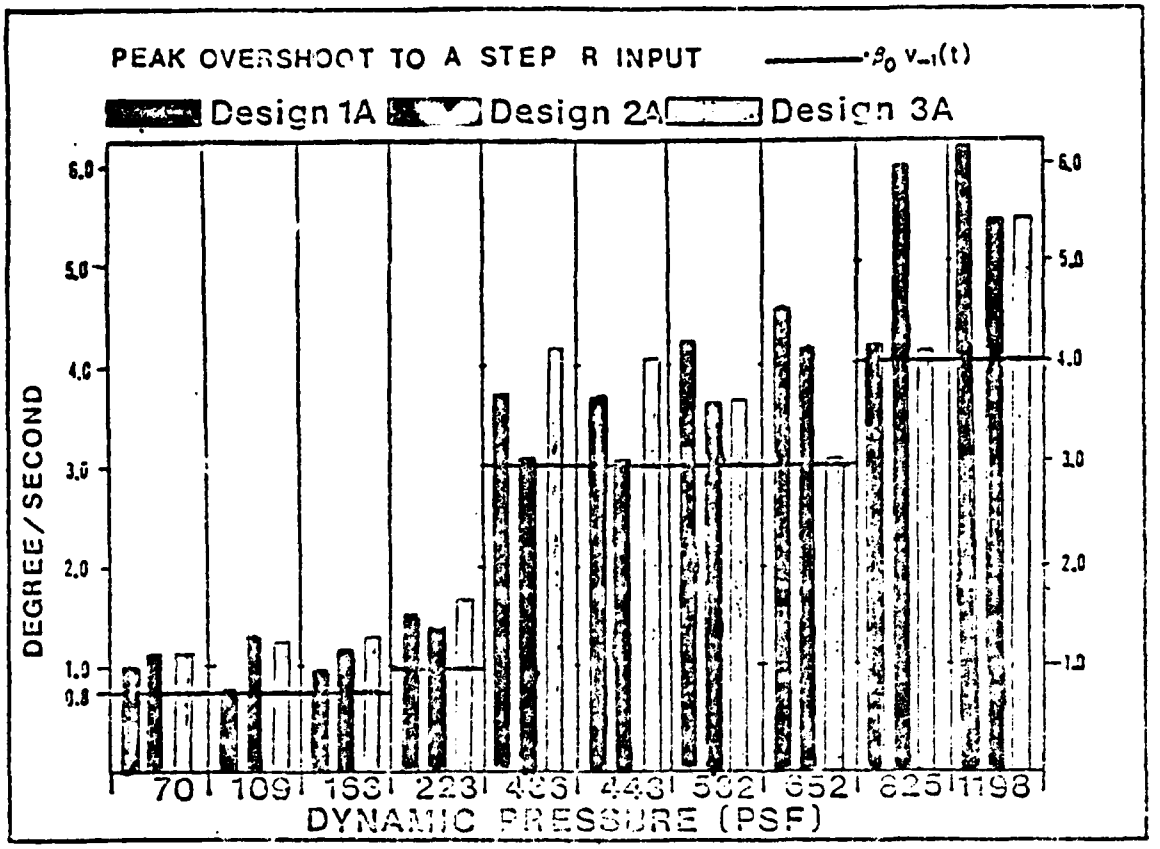
TABLE 3-4 Design 3A Figures of Merit

**DESIGN 3A HIGH Q** $Q = 825\ lb/ft^2$ $h = 10{,}000\ ft$ Mach = 0.9

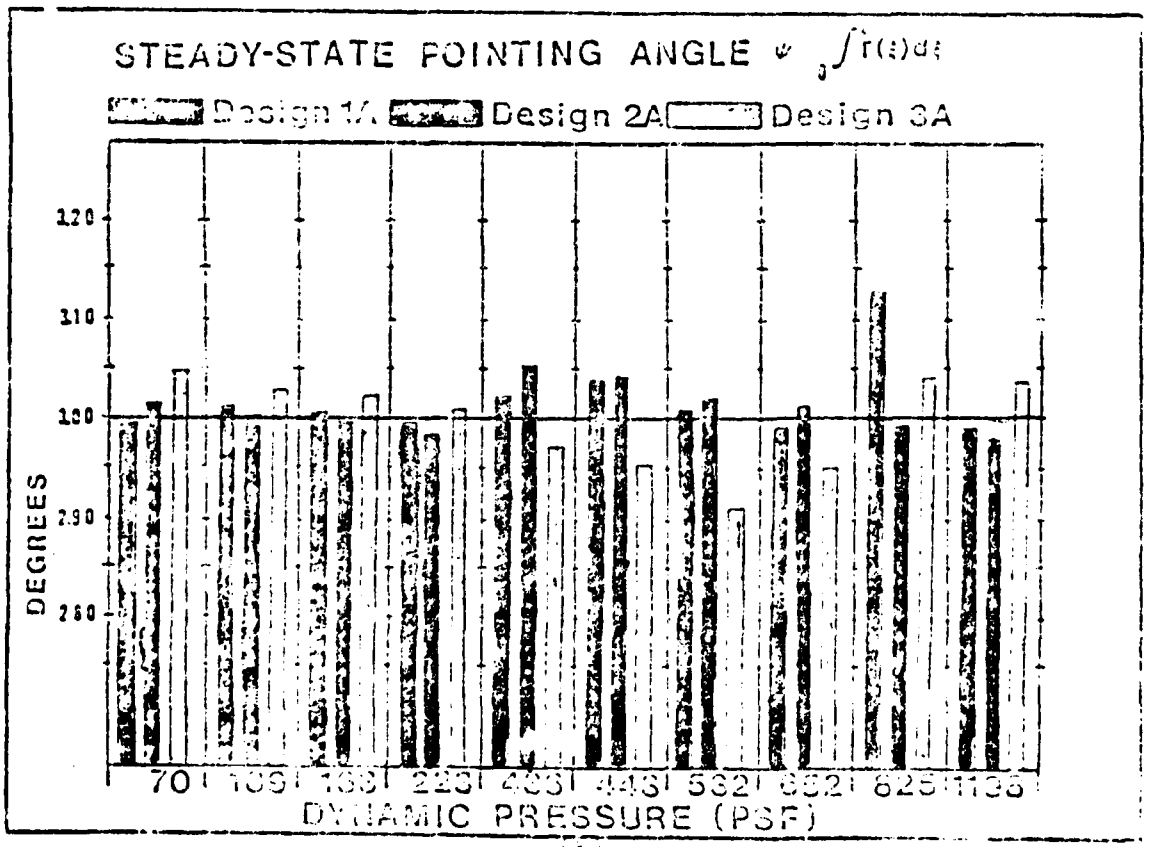
$$\underline{M} = \begin{bmatrix} 0 \\ 0.25 \\ 0 \end{bmatrix} \quad \underline{\Sigma} = \begin{bmatrix} 2 & 0 & 0 \\ 0 & 15 & 0 \\ 0 & 0 & 30 \end{bmatrix} \quad \underline{A}_a = \begin{bmatrix} 20 & 0 & 0 \\ 0 & 20 & 0 \\ 0 & 0 & 20 \end{bmatrix}$$

$$\underline{K}_0 = \begin{bmatrix} 22.5871 & 0.1857 & -1.6393 \\ 5.9893 & -0.7110 & -0.0607 \\ 22.3193 & -0.1024 & 1.9477 \end{bmatrix} \quad \underline{K}_1 = 2\underline{K}_0 \quad \varepsilon = 29.5$$

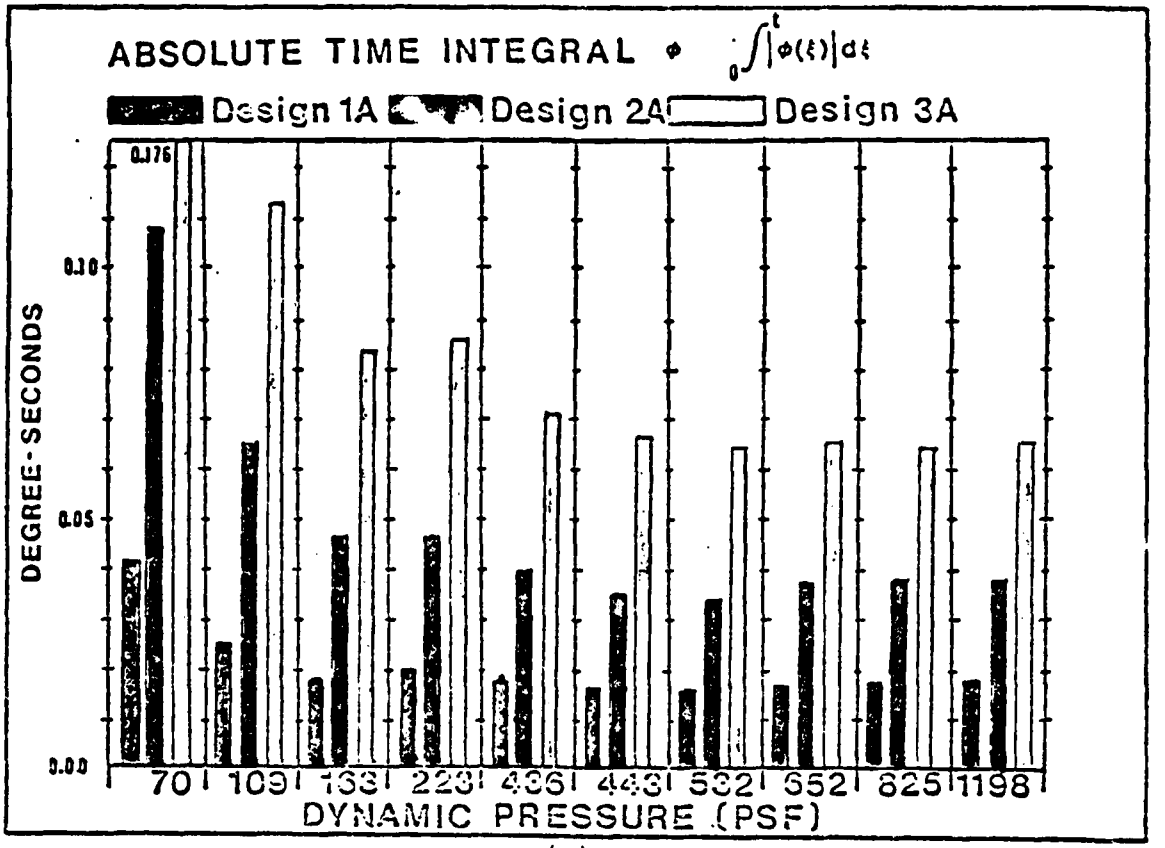
| Q | $\beta_{ss}$ | $\int_0^t r(\xi)d\xi$ / $\psi_{ss}$ | $M_p$ | %error | $t_p$ | $t_{s_1}$ | $t_{s_2}$ | $\int_0^t \phi(\xi)d\xi$ | CONTROL SURFACE COMMENT |
|---|---|---|---|---|---|---|---|---|---|
| 70 | -3.000 | 3.045 | 1.1625 | 45.312 | 0.10 | 0.80 | 0.60 | 0.1763 | within limits |
| 109 | -3.000 | 3.025 | 1.2601 | 57.512 | 0.05 | 0.50 | 0.55 | 0.1119 | within limits |
| 163 | -3.000 | 3.021 | 1.3857 | 73.212 | 0.05 | 0.50 | 0.45 | 0.0829 | within limits |
| 223 | -3.000 | 3.009 | 1.6871 | 68.710 | 0.05 | 0.45 | 0.50 | 0.1361 | within limits |
| 436 | -3.000 | 2.972 | 4.1703 | 39.010 | 0.10 | 0.50 | 0.60 | 0.0705 | exceeds limits $\sigma_c > 8.6°$ |
| 443 | -3.000 | 2.952 | 4.0944 | 36.480 | 0.10 | 0.40 | 0.65 | 0.0662 | exceeds limits $\sigma_c > 2.3°$ |
| 532 | -3.000 | 2.907 | 3.6494 | 21.646 | 0.15 | 0.95 | 0.60 | 0.0632 | within limits |
| 652 | -3.000 | 2.951 | 3.0646 | 2.153 | 0.30 | 0.40 | 0.55 | 0.0652 | within limits |
| 825 | -3.000 | 3.041 | 4.1046 | 2.615 | 0.35 | 0.45 | 0.60 | 0.0635 | within limits |
| 1198 | -3.000 | 3.045 | 5.4566 | 36.415 | 0.10 | 0.40 | 0.55 | 0.0655 | within limits |


PEAK OVERSHOOT TO A STEP R INPUT
Design 1A
Design 2A
Design 3A
DEGREE/SECOND
6.0
5.0
4.0
3.0
2.0
1.0
0.8
70
109
163
223
443
532
625
1198
DYNAMIC PRESSURE (PSF)

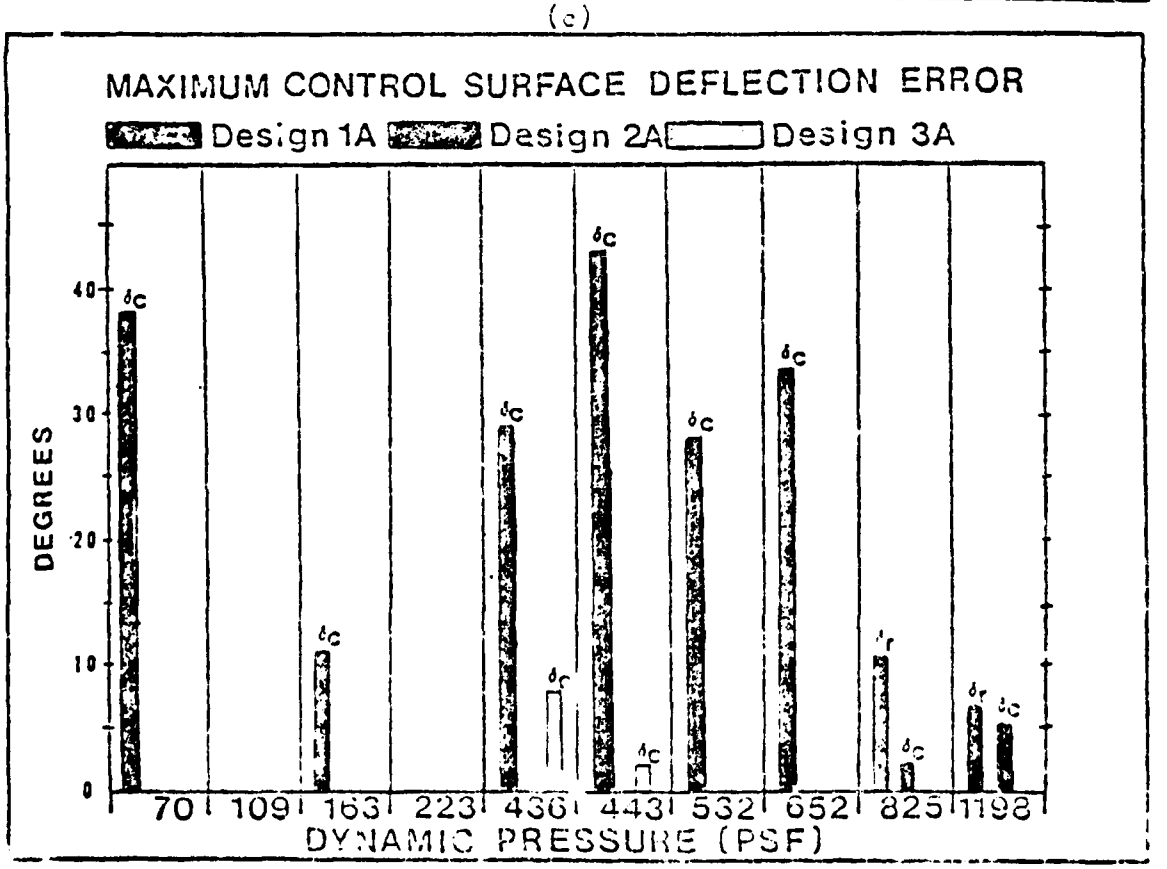
(a)

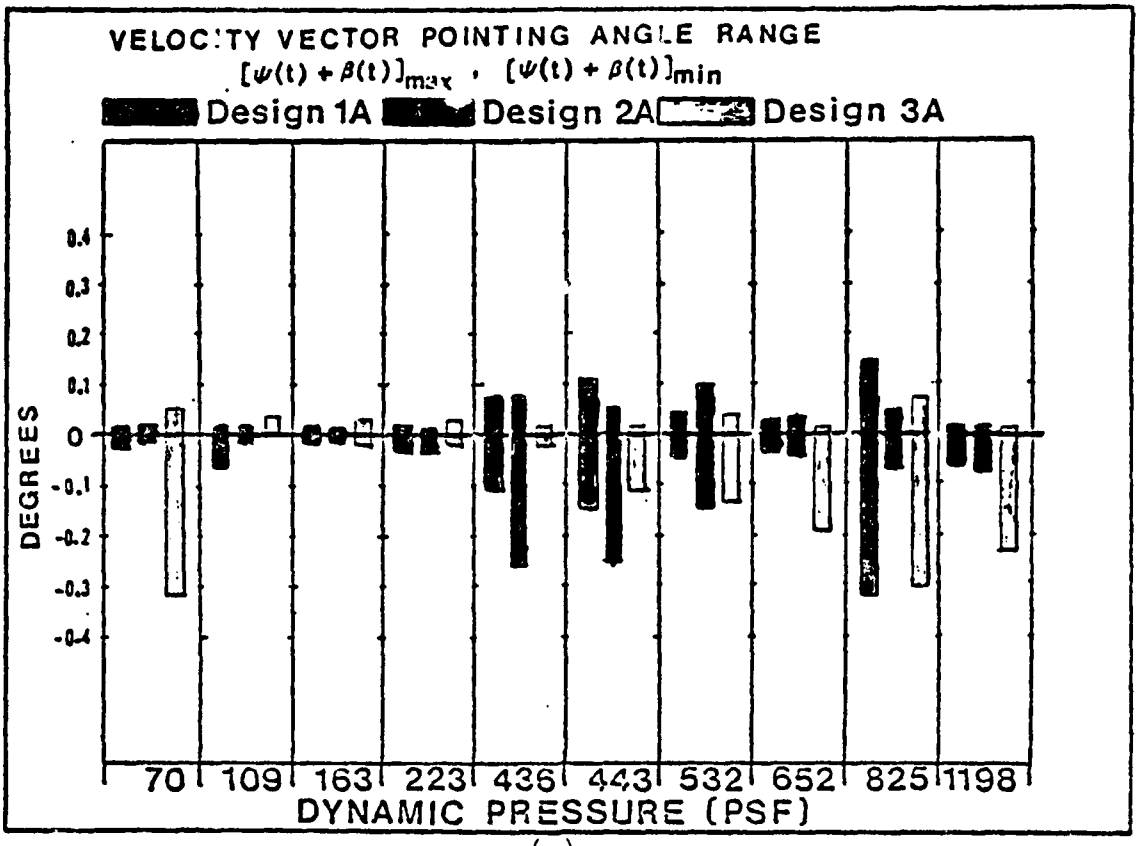

STEADY-STATE POINTING ANGLE
Design 1A
Design 2A
Design 3A
DEGREES
1.20
1.10
1.00
0.90
0.80
70
109
163
223
443
532
625
DYNAMIC PRESSURE (PSF)

(b)

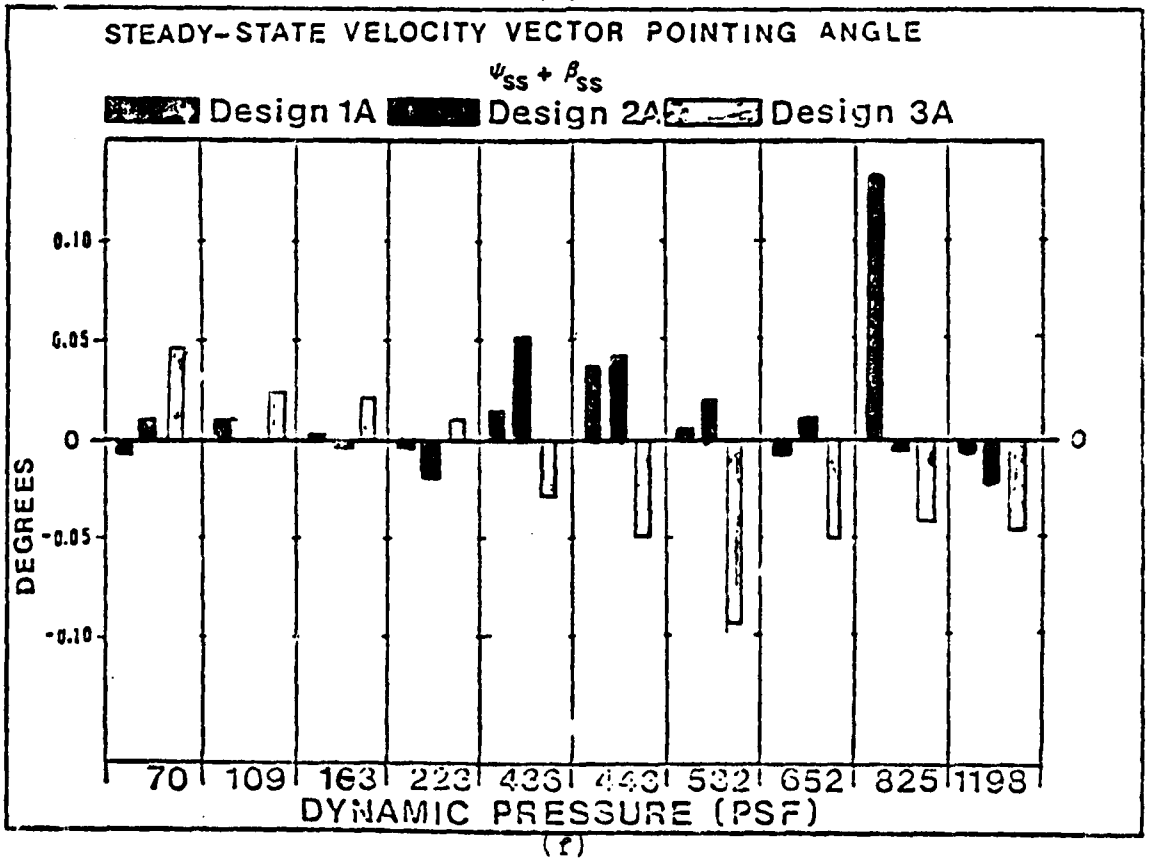

ABSOLUTE TIME INTEGRAL $\Phi \int_0^t |\phi(\xi)| d\xi$
Design 1A
Design 2A
Design 3A
0.176
0.10
0.05
0.00
DEGREE-SECONDS
70
109
163
223
436
443
532
652
825
1198
DYNAMIC PRESSURE (PSF)

(c)


MAXIMUM CONTROL SURFACE DEFLECTION ERROR
Design 1A
Design 2A
Design 3A
40
30
20
10
0
DEGREES
$\delta_C$
$\delta_T$
70
109
163
223
436
443
532
652
825
1198
DYNAMIC PRESSURE (PSF)


VELOCITY VECTOR POINTING ANGLE RANGE
$[\psi(t) + \beta(t)]_{max}$ - $[\psi(t) + \beta(t)]_{min}$
Design 1A
Design 2A
Design 3A
DEGREES
0.4
0.3
0.2
0.1
0
-0.1
-0.2
-0.3
-0.4
70
109
163
223
436
443
532
652
825
1198
DYNAMIC PRESSURE (PSF)

(e)


STEADY-STATE VELOCITY VECTOR POINTING ANGLE
$\psi_{ss} + \beta_{ss}$
Design 1A
Design 2A
Design 3A
DEGREES
0.10
0.05
0
-0.05
-0.10
70
109
163
223
436
443
532
652
825
1198
DYNAMIC PRESSURE (PSF)

(f)

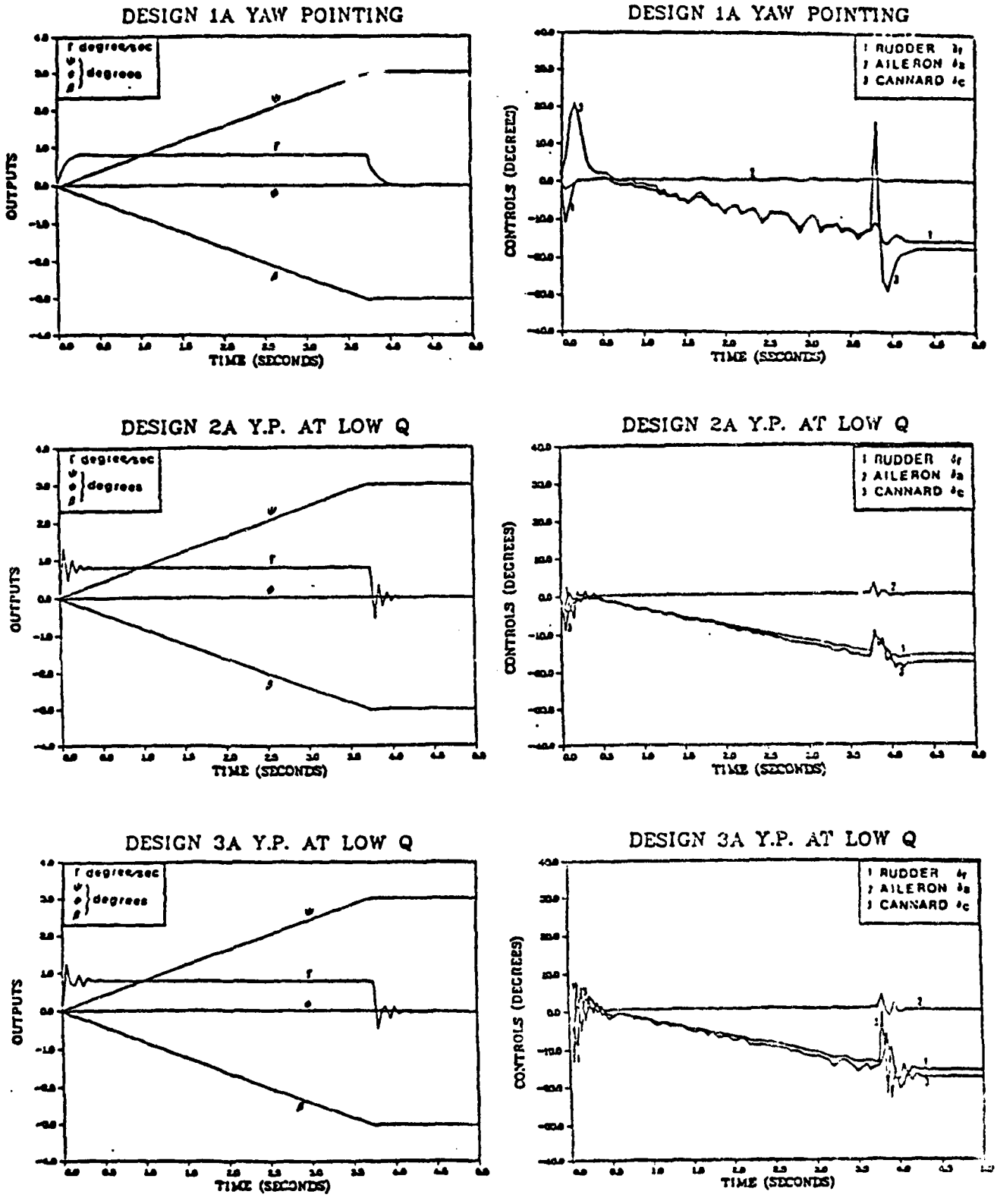
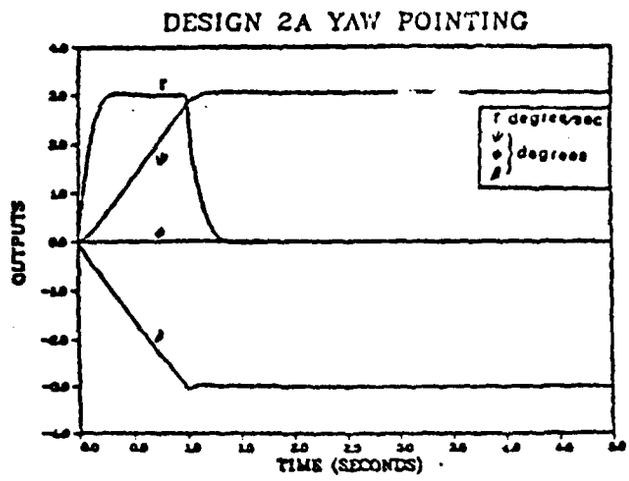
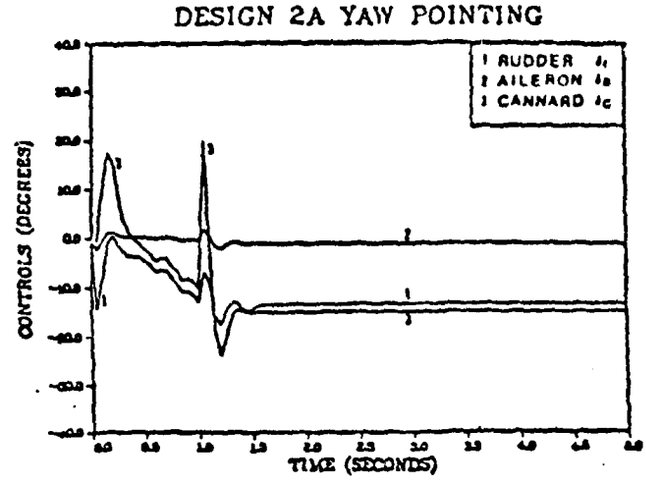
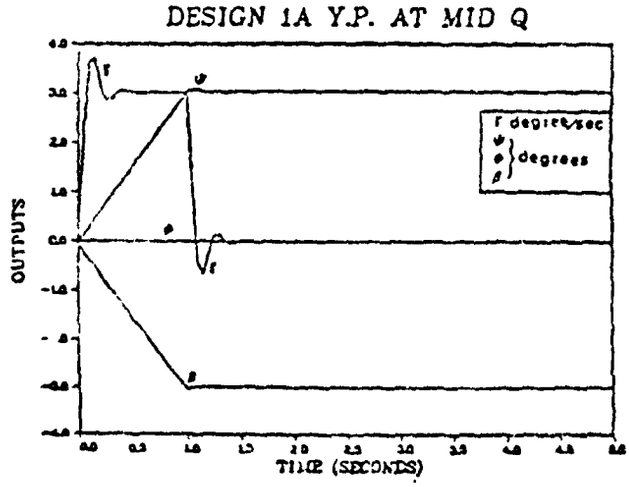
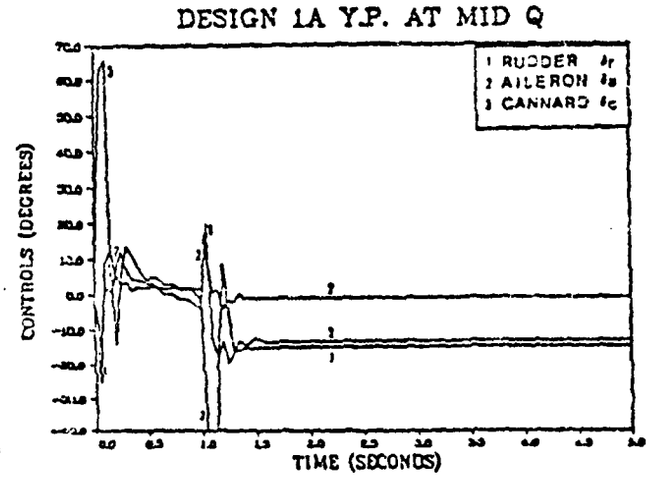


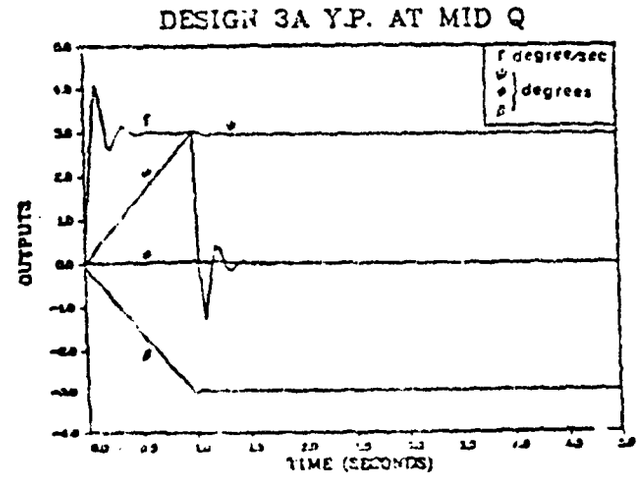

Figure 3-3 Low Q Yaw Pointing



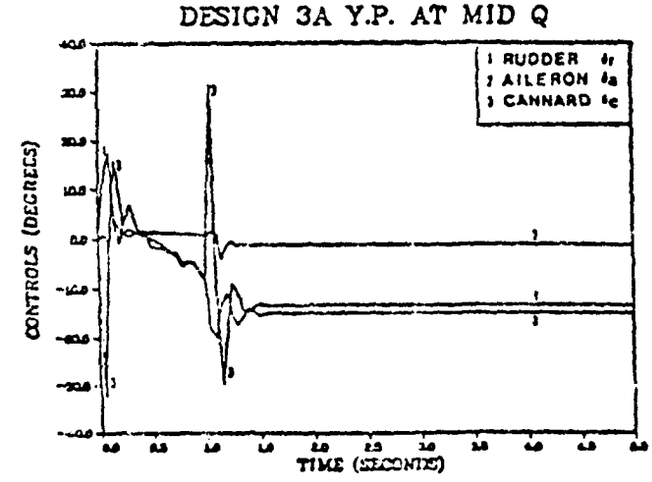




Figure [illegible] Yaw Pointing

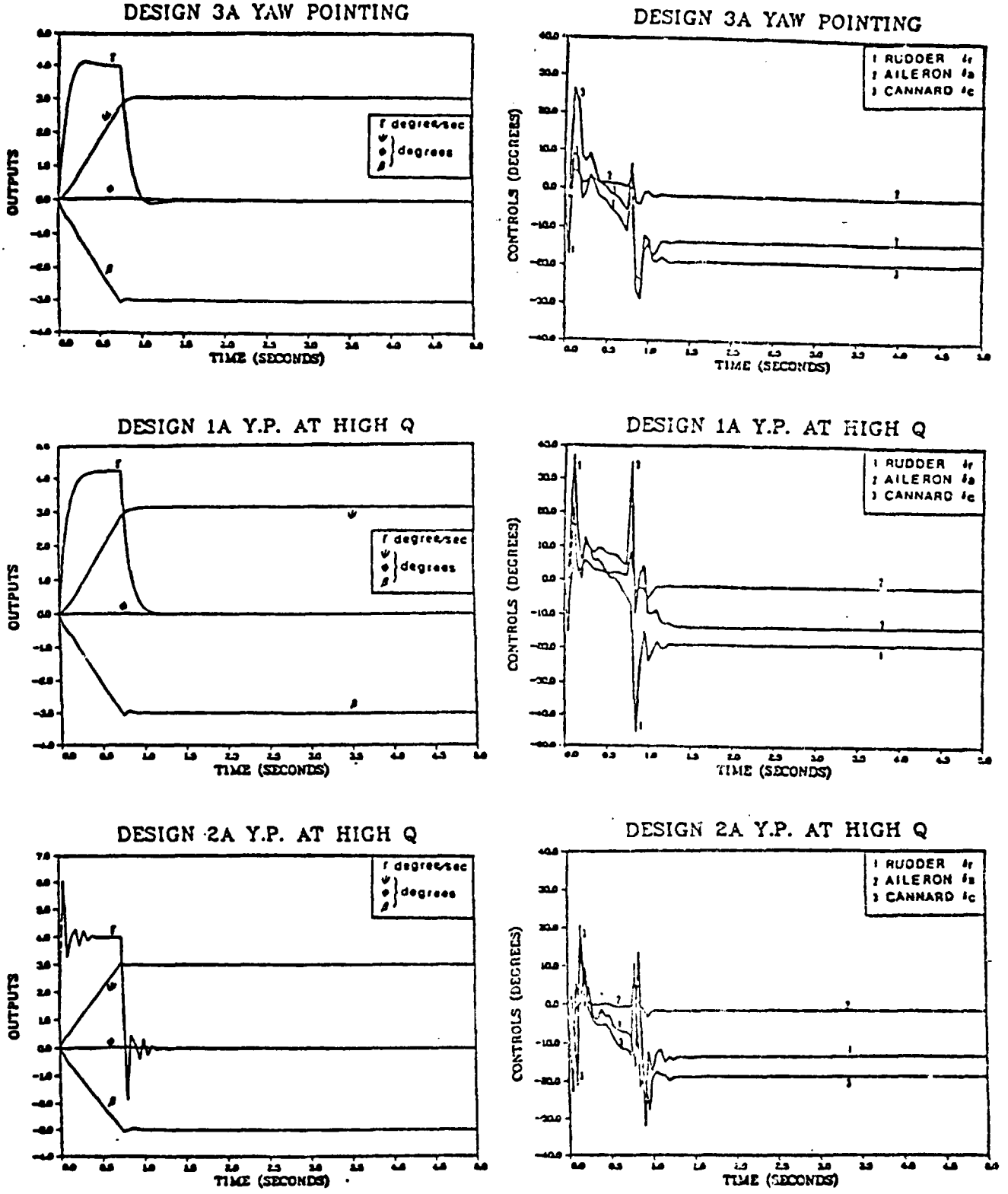



Figure 3-5 High Q Yaw Pointing

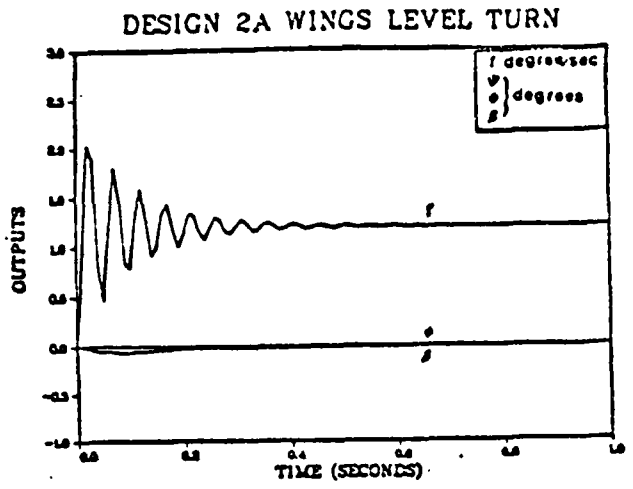
The controller design 2A is given commands to perform a wings level turn, a horizontal translation, and a constant altitude coordinated turn. The magnitudes of these commands are adjusted until the maneuver can be performed without commanding the control surfaces beyond their limits.

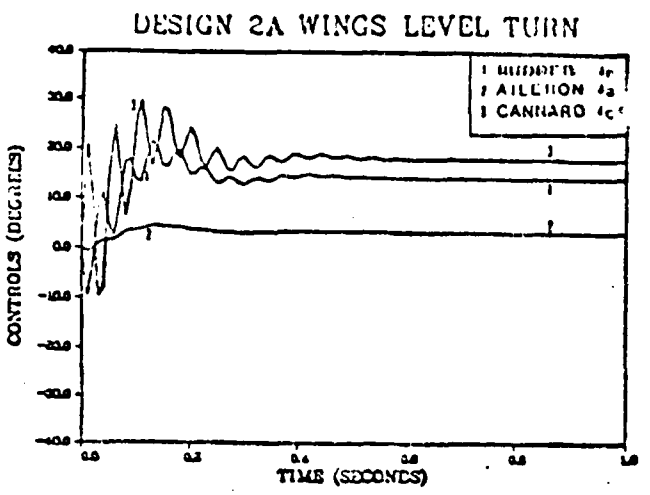
The input command for a wings level turn is a step input for yaw rate, r, while side-slip angle, $\beta$, and roll angle, $\phi$, are commanded to zero. For horizontal translation the side-slip angle is commanded as a ramp, till a side-slip angle of four degrees is reached. The roll angle and yaw rate are commanded to zero. For a coordinated turn the relation between yaw rate and roll angle is

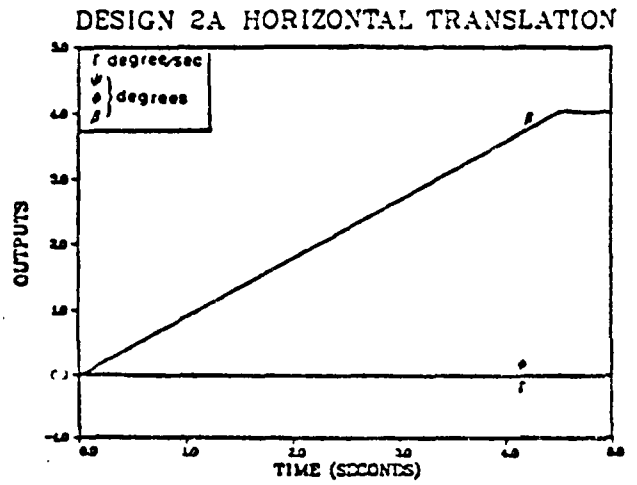
$$r = \frac{g}{U} \sin \phi \tag{3.3}$$

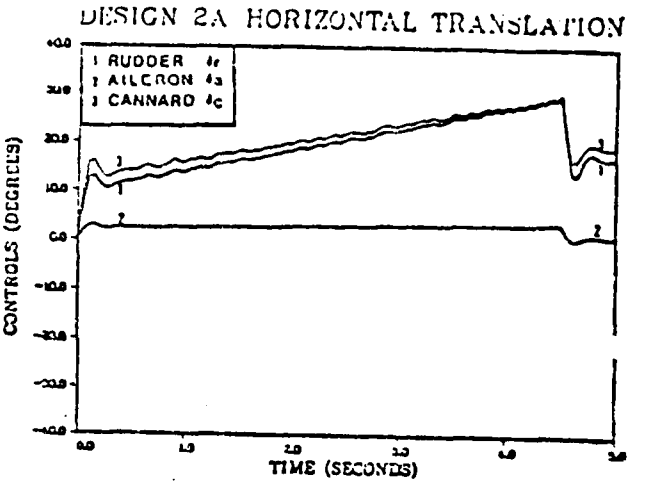
while side-slip angle is commanded to zero.

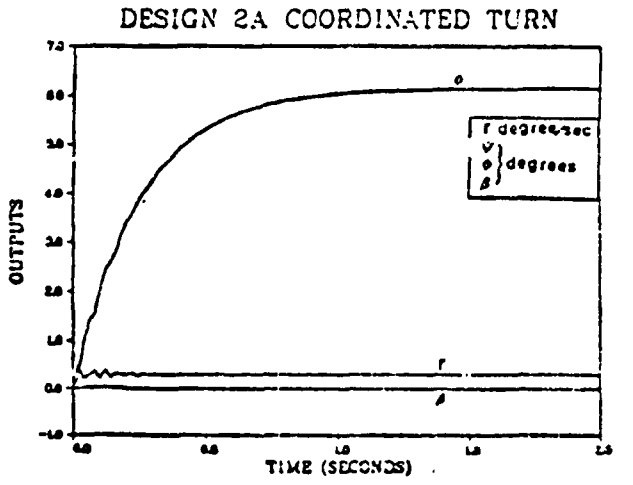
The output and control surface time responses of Design 2A perfoming the above three maneuvers are shown in Figure 3-6. These responses are compared with those of Figure 3-7 which show the responses of controllers designed to specifically perform the maneuvers at the design 2A flight condition (Q = 443). It is easily seen that Design 2A can not perform the maneuvers as well as the design for that specific maneuver. The magnitudes of the maneuvers of Design 2A are much less than the magnitudes of the Mid Q designs. For example the Mid Q design for horizontal translation can successfully command a side-slip angle of four degrees in 1.33 seconds, while the controller of Design 2A took 4.5 seconds. In this respect, the controller is not robust with respect to varying command inputs. The Mid Q



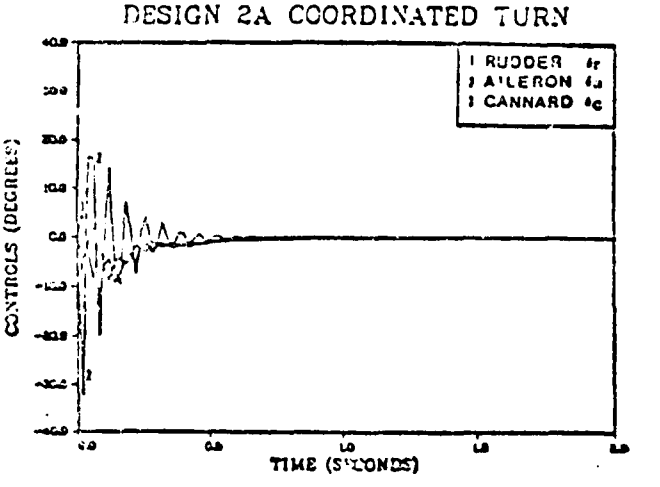




Figure [illegible] Design 2A Additional Maneuvers

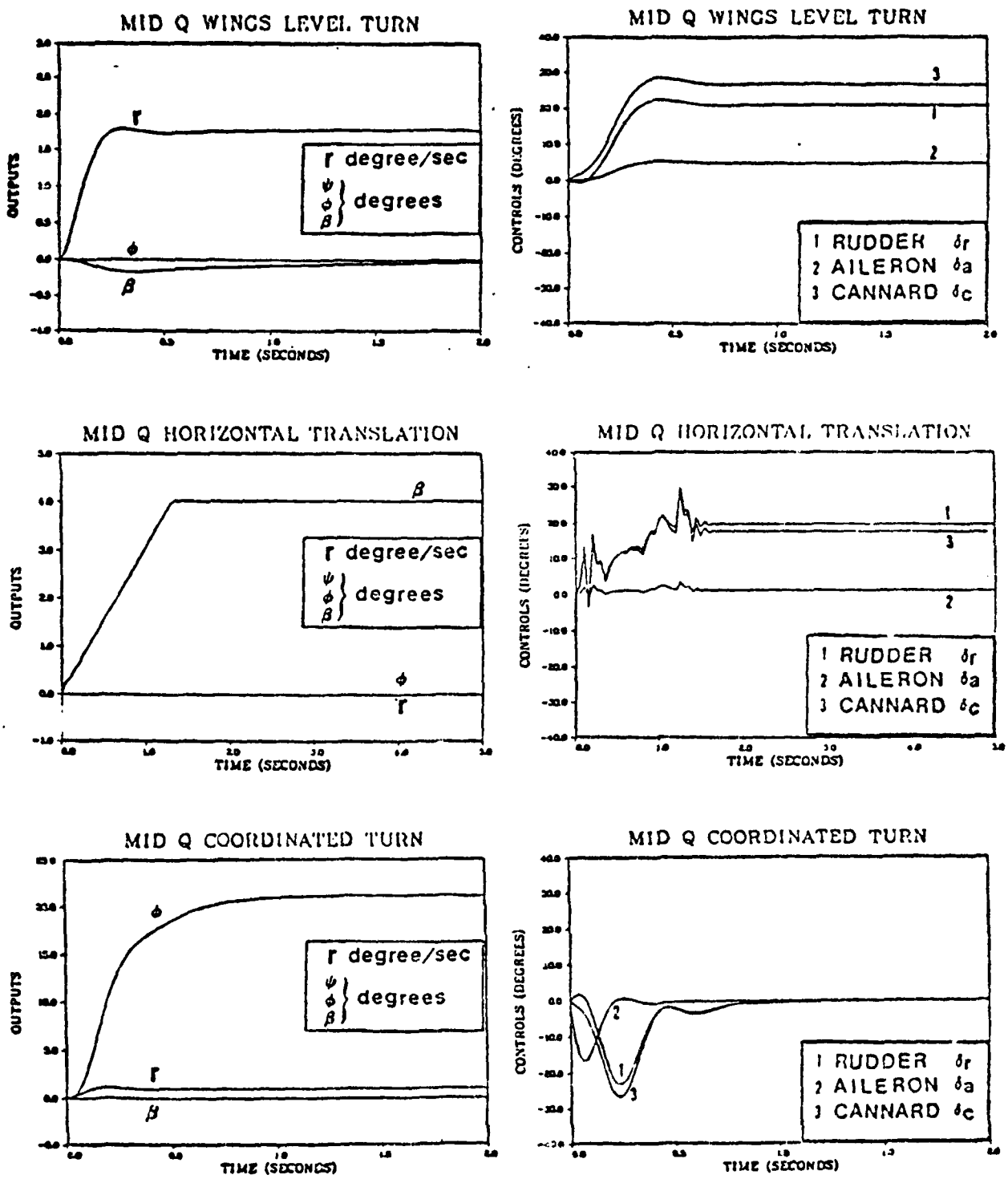



Figure 3-7 Mid Q Additional Maneuvers

Table 3-5 Mid Q designs

MID Q WINGS LEVEL TURN

$$\underline{M} = \begin{bmatrix} 0 \\ 0.25 \\ 0 \end{bmatrix} \qquad \underline{\Sigma} = \begin{bmatrix} .5 & 0 & 0 \\ 0 & 10 & 0 \\ 0 & 0 & .5 \end{bmatrix} \qquad \underline{A}_c = \begin{bmatrix} 20 & 0 & 0 \\ 0 & 20 & 0 \\ 0 & 0 & 20 \end{bmatrix}$$

$$\underline{K}_0 = \begin{bmatrix} 5.8472 & 0.1321 & -0.0344 \\ 1.3695 & -0.7015 & -0.0023 \\ 7.3259 & -0.1504 & 0.0734 \end{bmatrix} \qquad \underline{K}_1 = \underline{K}_0 \qquad g = 20$$

| | Steady-state Yaw Rate | Peak Overshoot | Settling Time |
|---|---|---|---|
| Desgign 2A | 1.30 deg/sec | 2.0 deg/sec | 0.5 sec |
| Mid Q | 1.75 deg/sec | 1.8 deg/sec | 0.5 sec |

MID Q HORIZONTAL TRANSLATION

$$\underline{M} = \begin{bmatrix} 0 \\ 0.25 \\ 0 \end{bmatrix} \qquad \underline{\Sigma} = \begin{bmatrix} .5 & 0 & 0 \\ 0 & 50 & 0 \\ 0 & 0 & 75 \end{bmatrix} \qquad \underline{A}_c = \begin{bmatrix} 20 & 0 & 0 \\ 0 & 20 & 0 \\ 0 & 0 & 20 \end{bmatrix}$$

$$\underline{K}_0 = \begin{bmatrix} [illegible] & [illegible] & -5.1539 \\ [illegible] & [illegible] & -0.3487 \\ [illegible] & [illegible] & 11.0091 \end{bmatrix} \qquad \underline{K}_1 = 2\underline{K}_0 \qquad g = 40$$

| | [illegible]-state [illegible]-slip angle | Maneuver Time | Maneuver Rate |
|---|---|---|---|
| [illegible] | [illegible] degrees | 4.50 seconds | 0.9 deg/sec |
| [illegible] | [illegible] mean | 1.33 seconds | 3.[illegible] deg/sec |

[illegible]

$$\underline{M} = \begin{bmatrix} [illegible] \\ [illegible] \\ [illegible] \end{bmatrix} \qquad \underline{\Sigma} = \begin{bmatrix} [illegible] & [illegible] & 0 \\ [illegible] & [illegible] & 0 \\ [illegible] & [illegible] & [illegible] \end{bmatrix} \qquad \underline{A}_c = \begin{bmatrix} 20 & 0 & 0 \\ 0 & 20 & 0 \\ [illegible] & [illegible] & [illegible] \end{bmatrix}$$

$$\underline{K}_0 = \begin{bmatrix} [illegible] & [illegible] & -2.1697 \\ [illegible] & [illegible] & 0.0046 \\ [illegible] & [illegible] & 0.1497 \end{bmatrix} \qquad \underline{K}_1 = \underline{K}_0 \quad [illegible]$$

| | [illegible]eady-state [illegible]ngle | Steady-state Yaw Rate |
|---|---|---|
| [illegible] | [illegible].19 degrees | 0.50 deg/sec |
| [illegible] | [illegible] degrees | 1.00 deg/sec |



Copy available to DTIC does not permit fully legible reproduction

controller designs and performance comparison summary are shown in Table 3-5.

Actuator Dynamics

As discussed in Chapter 2 there are two methods to add first-order actuator dynamics to the system. The method used in this report is to augment the closed-loop system matrix. This does not cause the size of the measurement matrix to increase. If the actuator dynamics are added by augmenting the open-loop system matrix, the size of the measurement matrix increases from a 3-by-1 matrix to a 3-by-4 matrix. When an attempt is made to add the actuator dynamics this way, the method used for selecting a measurement matrix that both stabilizes the system and diagonalizes the asymptotic transfer function fails. This leaves the selection of a measurement matrix to a trial and error iterative procedure.

The actuator dynamics are significant in the simulations. For comparison the yaw pointing robustness test is repeated for the same three controllers without actuator dynamics in the model. The results of these simulation tests are very misleading. Figures 3-8 through 3-10 show the output and control surface time responses of the three controller designs performing the yaw pointing maneuver at a specific flight condition. When these figures are compared with Figures 3-3 through 3-5 the significance of the actuator dynamics is clearly shown. Note that in all cases the outputs follow the commands exactly, with no overshoots or oscillations. Also note the smooth control surface response curves. The actuator dynamics in the model greatly affect the time responses and should not be ignored

when designing a controller. This same trend is observed when Figure 3-11 is compared with Figure 3-6.

Without actuator dynamics the output responses are much more insensitive to changes in the diagonal elements in the sigma matrix and gain values. This is another reason why the actuator dynamics should not be ignored when designing a controller.

Also studied is the effect of changing the first-order actuator dynamics time constant. The controller is designed with all actuator constants at 20. This design is used in the simulation of a yaw pointing maneuver with the actuator constants varying. The responses are shown in Figures 3-12 through 3-18. The three numbers on the title of the response correspond to the three actuator constants. The respective order is: rudder actuator constant, aileron actuator constant, and canard actuator constant. For example, (20, 10, 40) represents a rudder constant of 20, a aileron constant of 10, and a canard constant of 40.

Figure 3-12 shows the responses when all constants are decreased and increased by a factor of two. Figure 3-13 shows the responses when just one constant is decreased by a factor of two. Figure 3-14 shows the responses when just one constant is increased by a factor of two. Figure 3-15 shows the responses when two constants are decreased by a factor of two. Figure 3-16 shows the responses when two constants are increased by a factor of two. Figure 3-17 shows the responses when one constant is decreased and one constant is increased by a factor of two.

This actuator study shows:

1. The aileron has [illegible]le effect in the yaw pointing maneuver

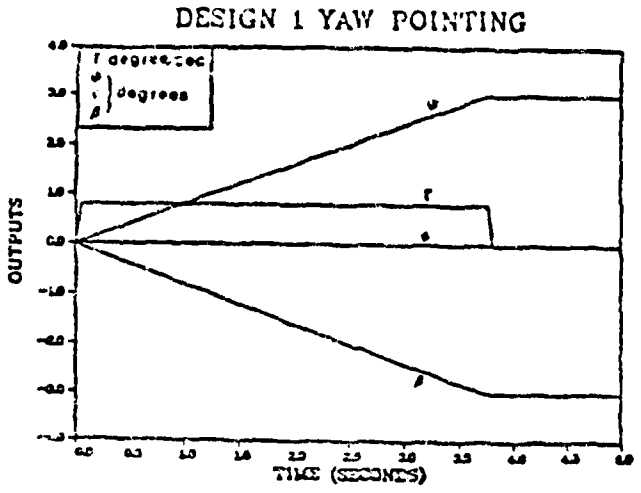
2. Decreasing the cannard constant increases settling time and increases cannard activity

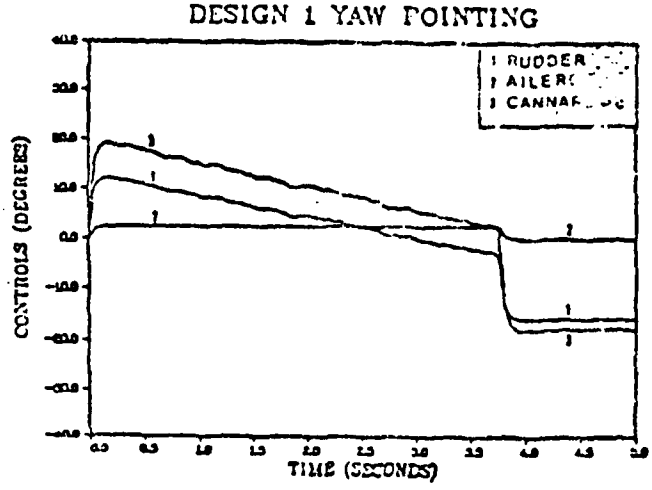
3. Increasing the rudder constant causes increased rudder activity

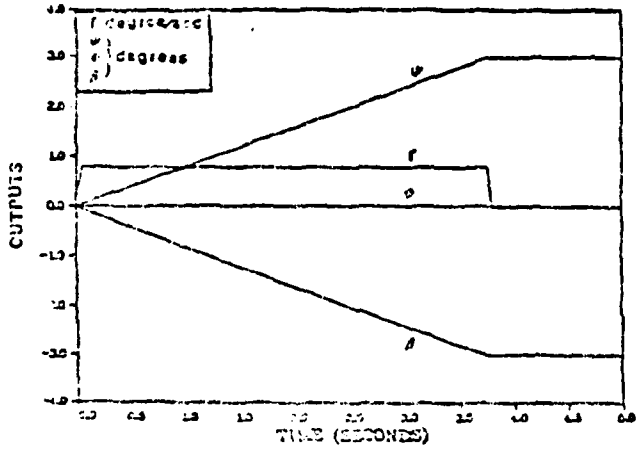
4. Increasing both rudder and cannard constants cause the magnitude of surface deflection to decrease.

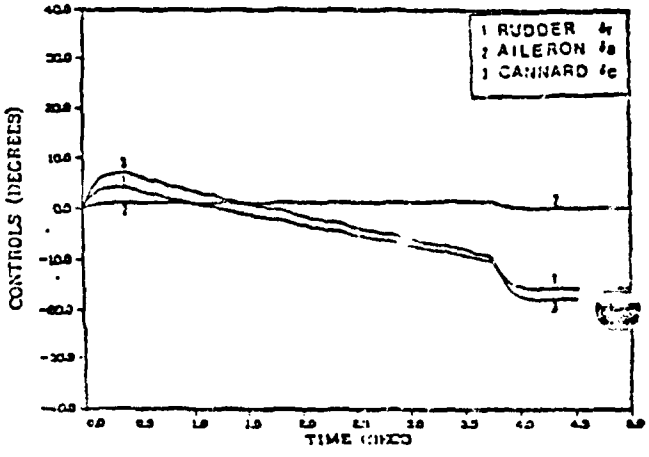
Overall this study amplifies the importance of actuator dynamics in the model, in that they significantly affect the output and control surface time responses. The actuator time constant is dependent on the physical system used in the aircraft. Varying the constants in the design can be advantageous in a preliminary design study and can be used as a basis for selecting the best actuator.

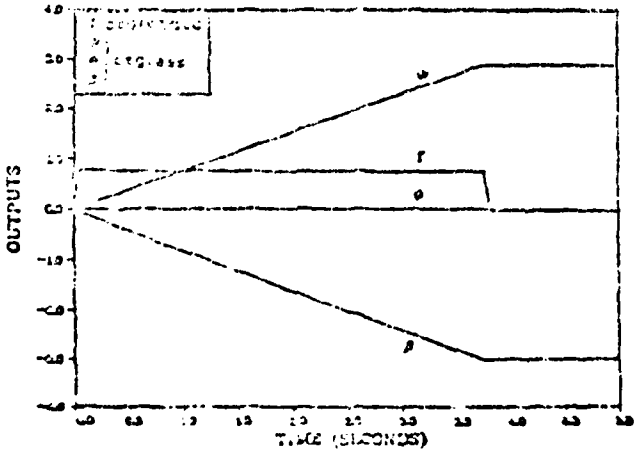
In this study there is no constraint placed on the rate of control surface deflection. As a result the control surface deflection rates were often unreasonably fast. Any further study should include this constraint.



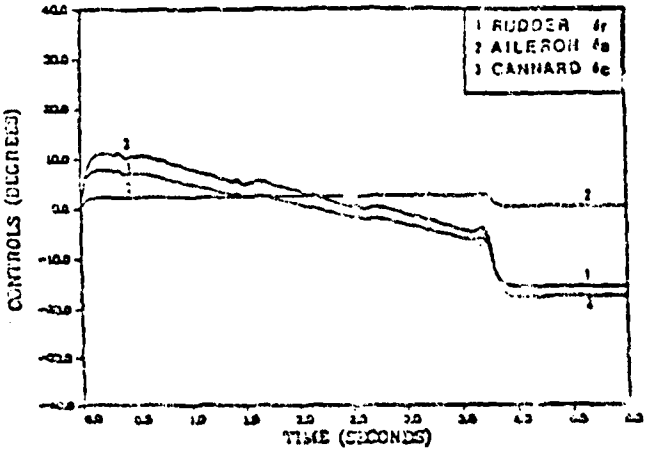




Figure 3-3 Low q Yaw Pointing Without Actuators

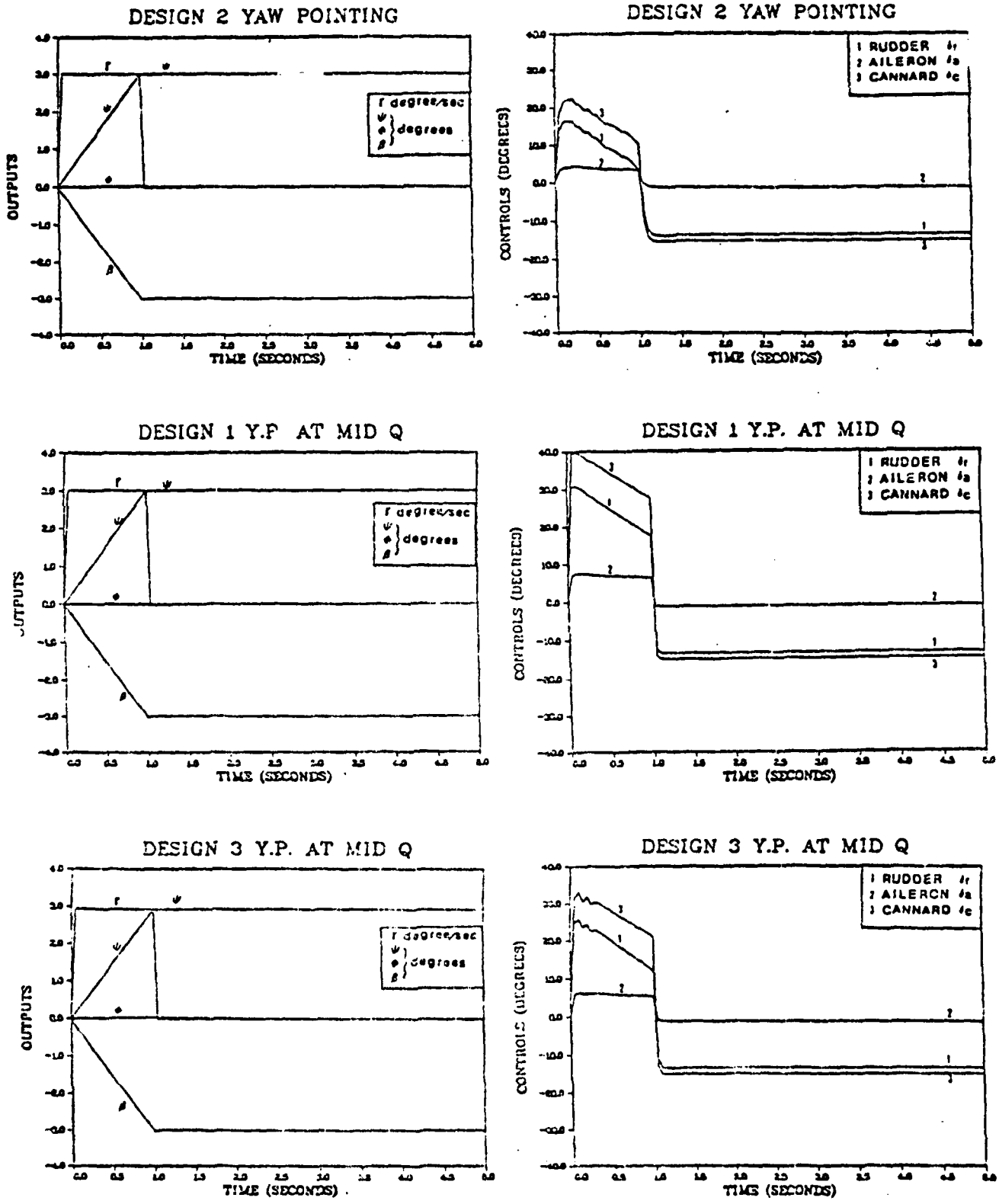



Figure 3-9 Mid Q Yaw Pointing Without Actuators

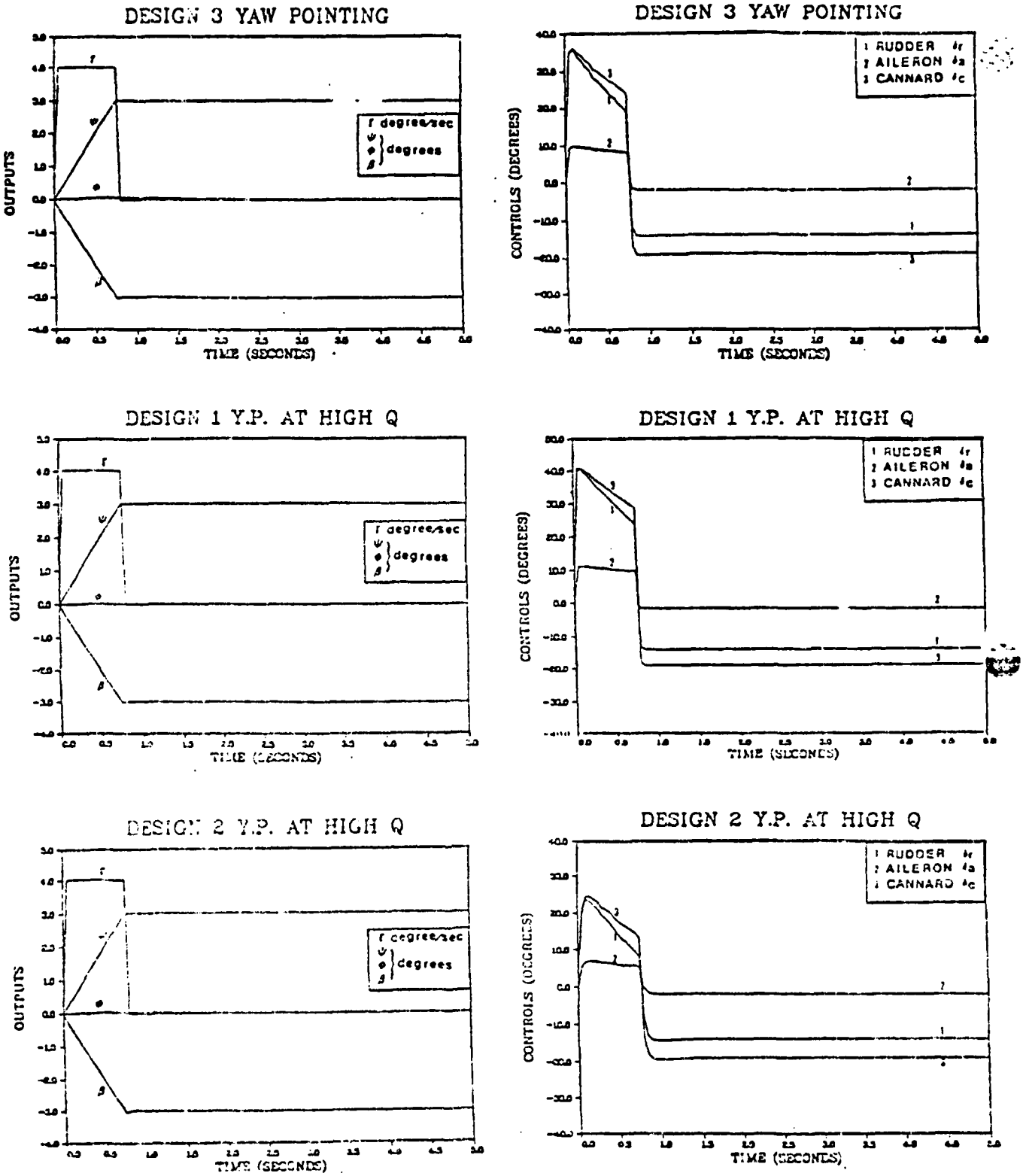



Figure 3-10 High Yaw Pointing Without Actuators

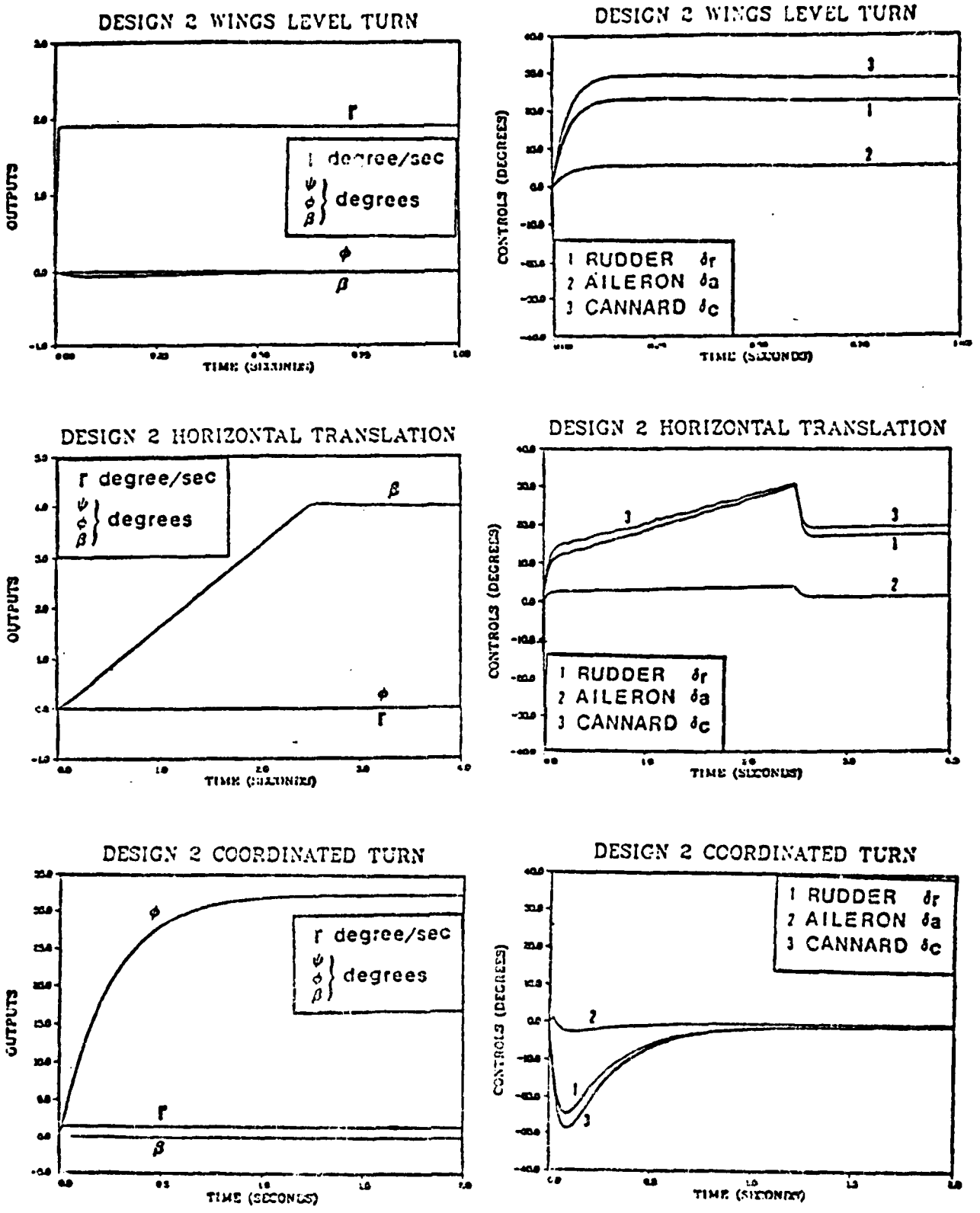



Figure 3-11 Design 2 Additional Maneuvers

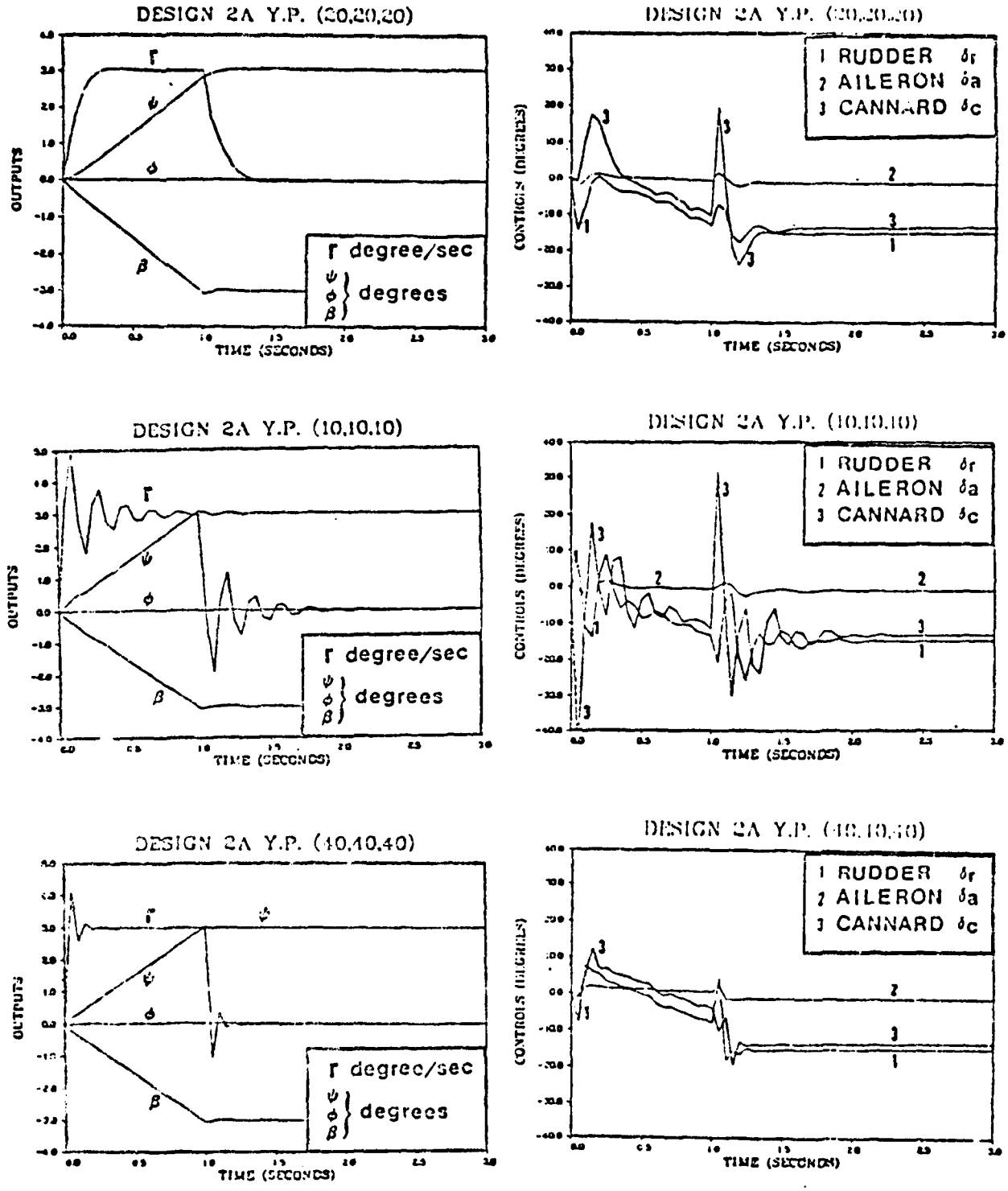



Figure 3-12 All Constants Changed

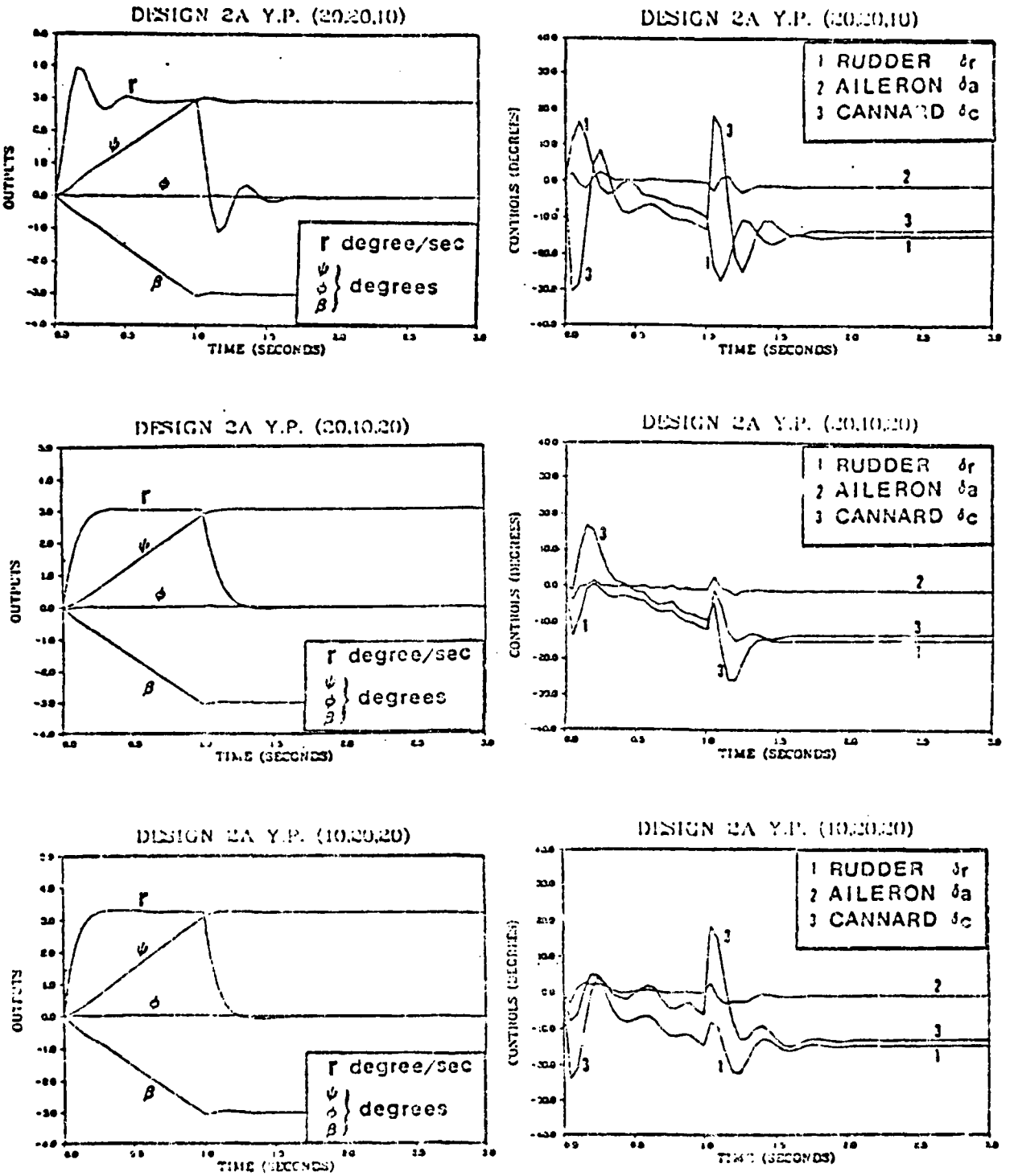



Figure 3-13 One Constant Decreased

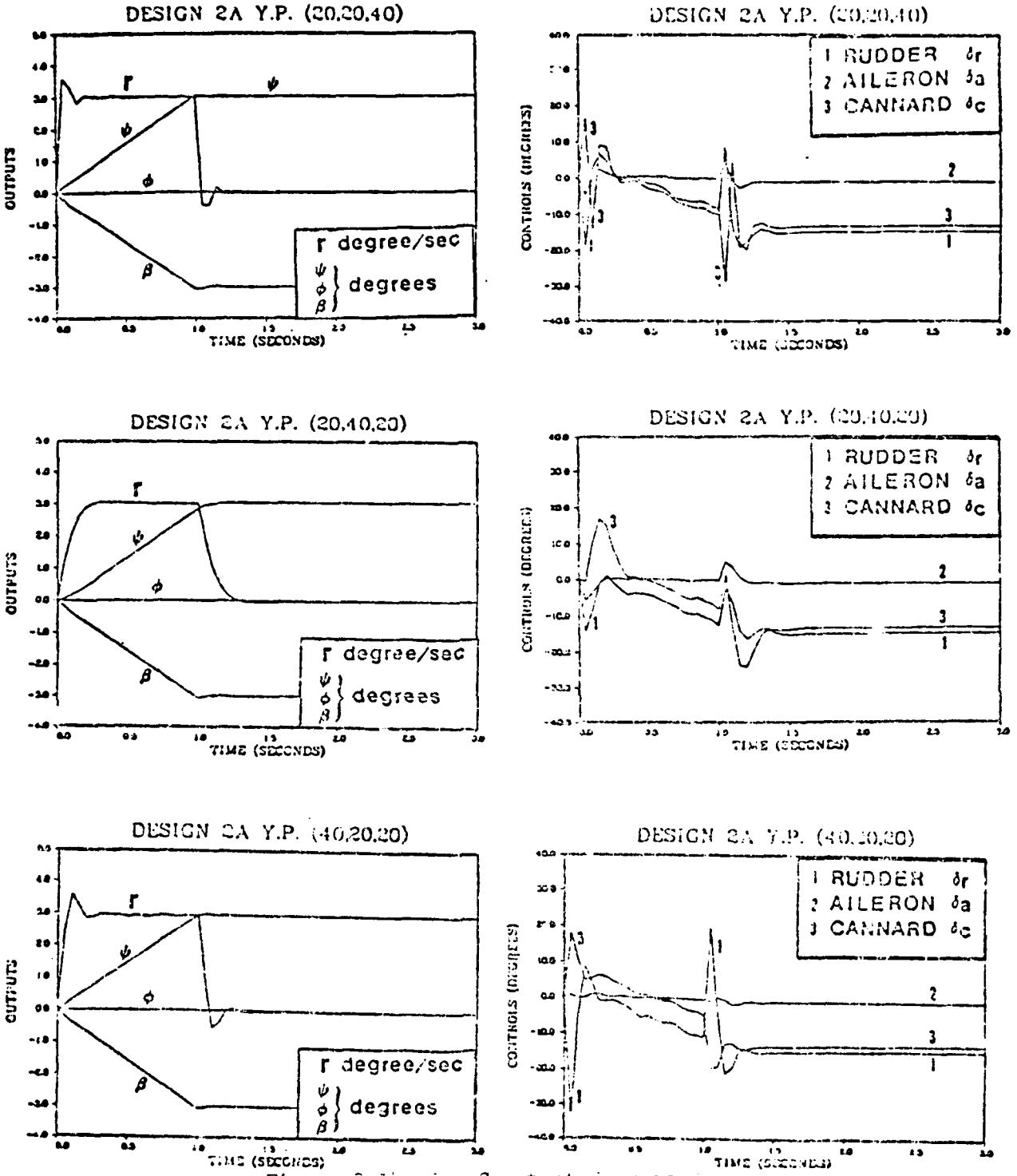



Figure 3-14 One Constant Increased

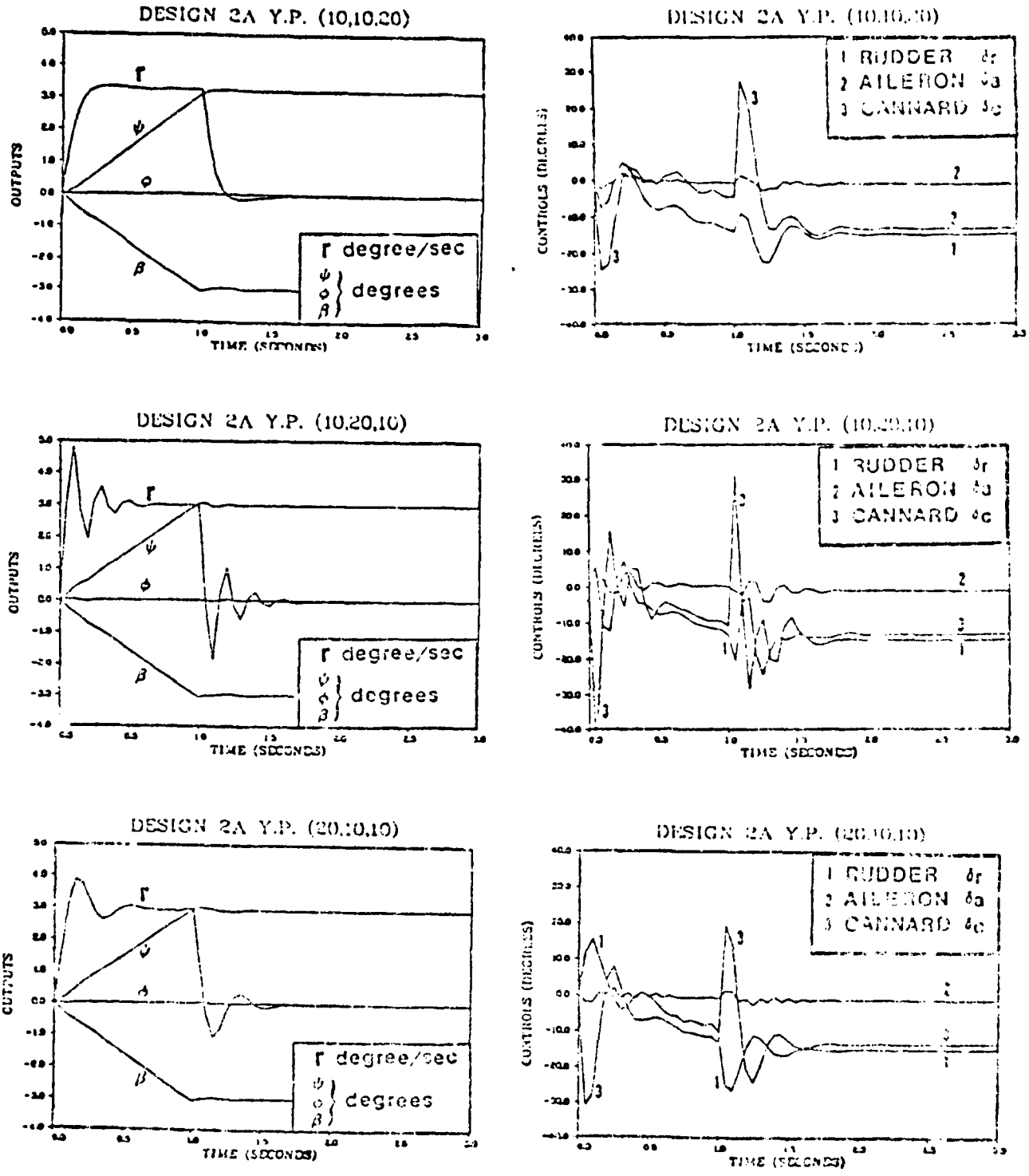



Figure 3-15 Two Constants Decreased

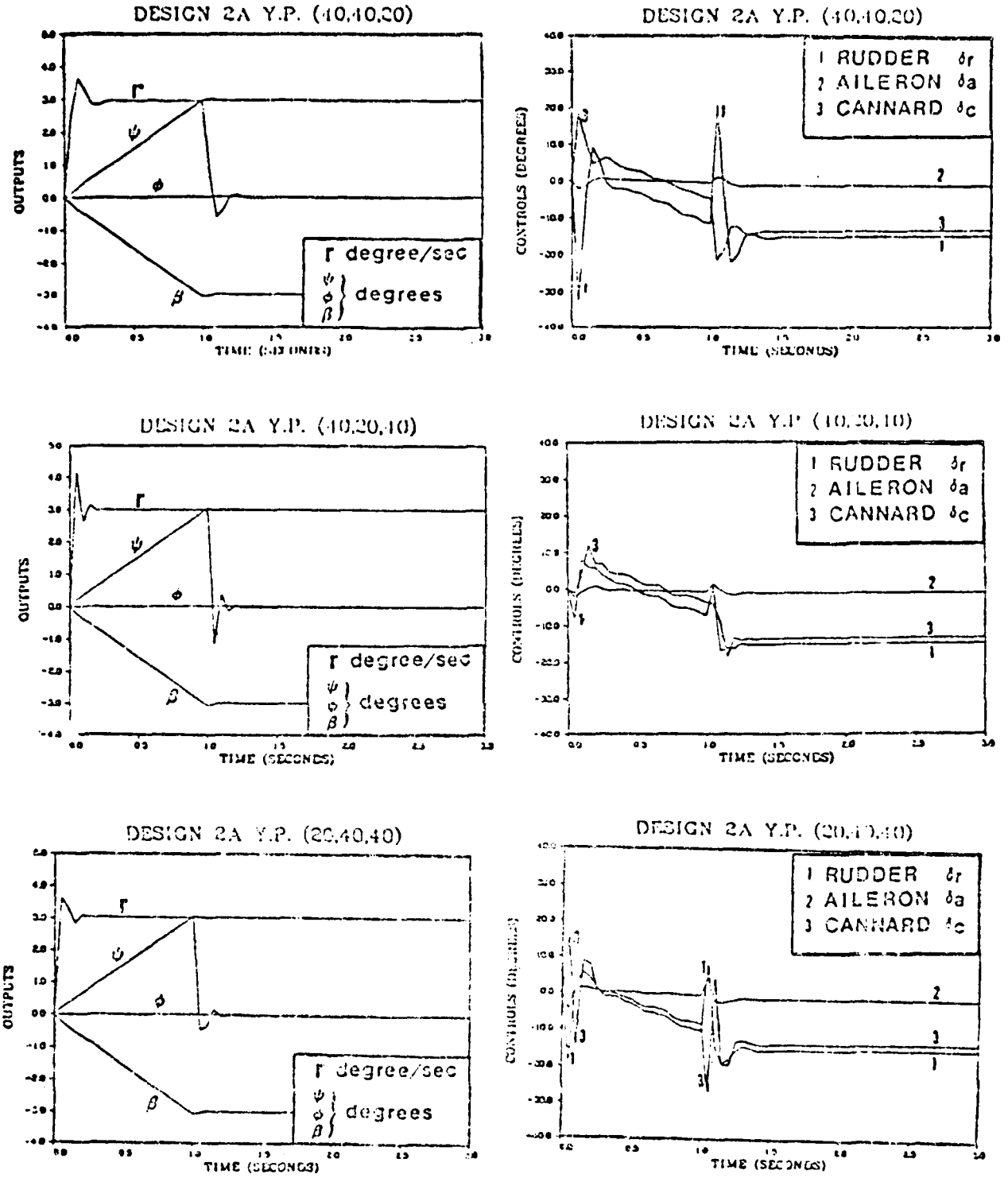



Figure 3-b Two Constants Increased

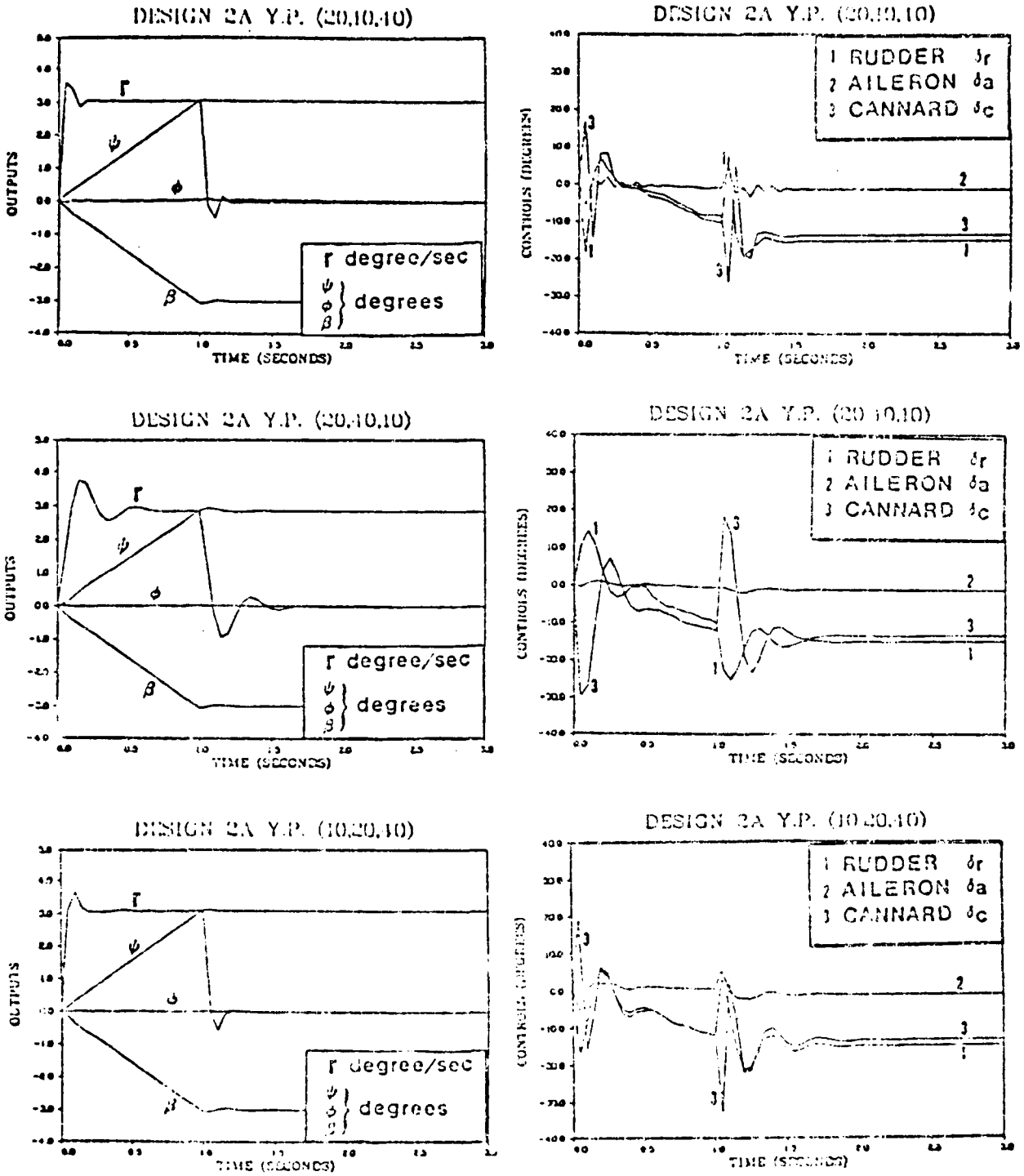
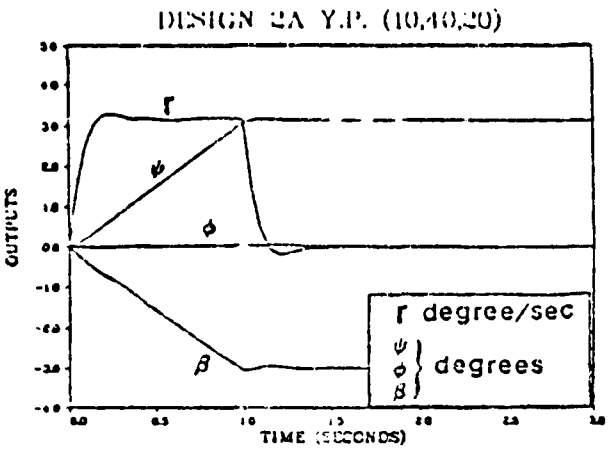
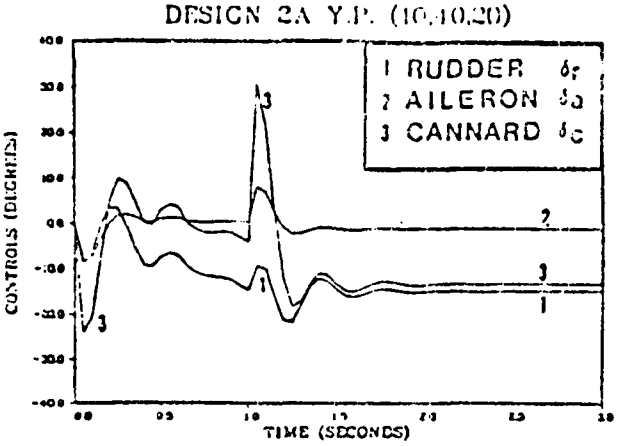
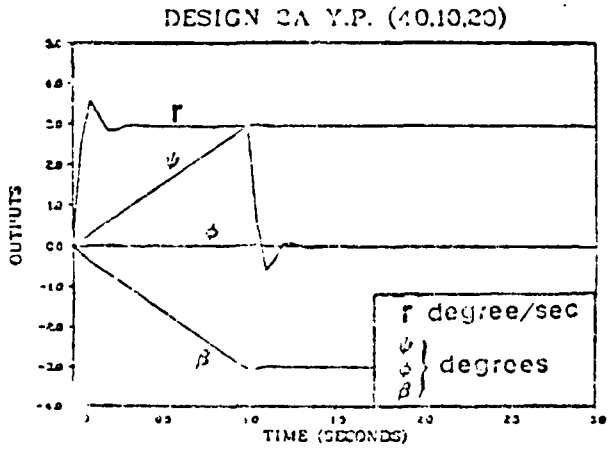
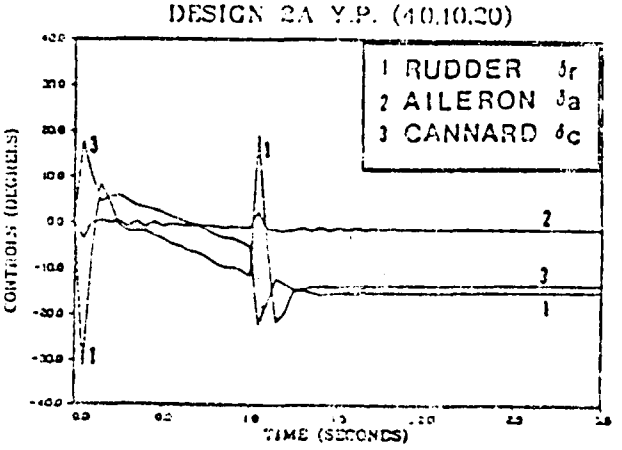


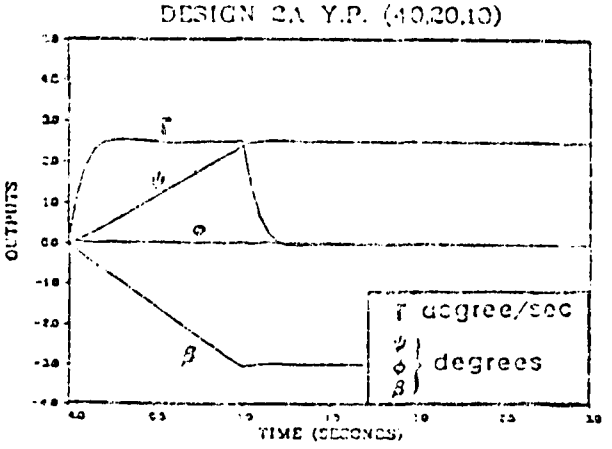

Figure 3-17 One Constant Decreased One Constant Increased

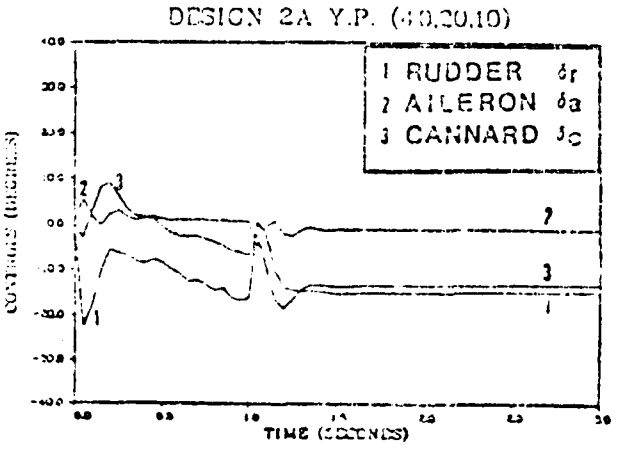

DESIGN 2A Y.P. (10,40,20)
OUTPUTS
TIME (SECONDS)
r
ψ
φ
β
r degree/sec
ψ
φ
β
degrees


DESIGN 2A Y.P. (10,10,20)
CONTROLS (DEGREES)
TIME (SECONDS)
1 RUDDER δr
2 AILERON δa
3 CANNARD δc


DESIGN 2A Y.P. (40,10,20)
OUTPUTS
TIME (SECONDS)
r
ψ
φ
β
r degree/sec
ψ
φ
β
degrees


DESIGN 2A Y.P. (40,10,20)
CONTROLS (DEGREES)
TIME (SECONDS)
1 RUDDER δr
2 AILERON δa
3 CANNARD δc


DESIGN 2A Y.P. (40,20,10)
OUTPUTS
TIME (SECONDS)
r
ψ
φ
β
r degree/sec
ψ
φ
β
degrees


DESIGN 2A Y.P. (40,20,10)
TIME (SECONDS)
1 RUDDER δr
2 AILERON δa
3 CANNARD δc

# IV. Conclusions and Recommendations

## Conclusions

Major conclusions are based on the results of this report. They are first presented in Chapter III and are now summarized.

The design method of Dr Porter is easy to apply and does produce controller designs to perform desired maneuvers. This method is relatively new and promising. Research and applications of this method should continue.

The controllers are robust with respect to varying flight conditions. They are not robust with respect to varying maneuver commands. The controller designed at a medium dynamic pressure flight condition produced the more robust controller design.

Actuator dynamics significantly affect the output and control surface time responses. Simplified models without actuator dynamics included provide misleading results. Actuator dynamics should not be ignored in the design of flight controllers with this method.

## Recommendations

This study followed the study performed by Lt Ridgely (Ref 10). His study examines the longitudinal modes of AFTI. This study examines the lateral-directional modes of AFTI. The next study should combine the two modes and examine the response of the total aircraft when performing various maneuvers.

Further robustness examination should be conducted to find if a controller can be designed that is both robust with respect to flight condition and maneuver commands. If so, what parameters affect robustness.

The computer program used for this study is limited when compared with the computer program developed for the design of digital controllers using Porter's ... od, MULTI (Ref 13). MULTI should be augmented to include the design of analogue controllers.

The precision of program ZERO should be increased from single precision to double precision to increase the program's accuracy. Also the subroutines in ZERO that check the rank of the system matrices should be changed so that complex system zeros can also be tested.

## Bibliography


1. Fortmann,T. and Hitz,K. 1977. An Introduction to Linear Control Systems. New York: Marcel Dekker Inc.

2. Kirk,D. 1970. Optimal Control Theory. New Jersey: Prentice-Hall.

3. Laub,A.J. and Moore, B.C. 1977. Calculation of Transmission Zeros Using QZ Techniques. Proceedings of the 1977 IEEE Conference on Decision and Control.

4. MacFarlane,A.G.J. and Karcanias,N. 1976. Poles and Zeros of Linear Multivariable Systems. International Journal of Control. 24 no.1 :33-74.

5. McRuer, Ashkenas, and Graham. 1973. Aircraft Dynamics and Automatic Control. New Jersey: Princeton University Press.

6. Moler, C.B. and Stewart, G.W. 1973. An Algorithm for Generalized Matrix Eigenvalue Problems. SIAM Journal of Numerical Analysis. 24 no.10: 241-255.

7. Porter, B. 1981. Design of High-Performance Tracking Systems. AFWAL/FIGL. Wright-Patterson AFB. Ohio.

8. Porter,B. 1979. Computation of the Zeros of Linear Multivariable Systems. International Journal of System Science. 10 no.12: 1427-1432.

9. Ridgely, Banda, D'Azzo. 1981. Decoupling of High-Gain Multivariable Tracking Systems. AFWAL/FIGCA. Wright-Patterson AFB. Ohio.

10. Ridgely,D. 1981. Use of Entire Eigenstructure Assignment with High-Gain Error-Actuated Flight Control Systems. Masters Thesis. Air Force Institute of Technology. Wright-Patterson AFB. Ohio.

## Bibliography


11. Silverthorn,J. and Reid,J.G. 1980. Computation of the Subspaces for Eintire Eigensructure Assignment Via Singular Value Decomposition. Proceedings of the 19th IEEE onference on Decision and Control. 12 no.10: 1206-1207.

12. Wind Tunnel Data, AFTI/F-16. AFWAL/FII. Wright-Patterson AFB. Ohio

13. Porter,D. 1981. Design and Analysis of Multivariable Digital Controler for the A-7D Digital II Aircraft and the Development of an Interactive Computer Design Program. Masters Thesis. Air Force Institute of Technology. Wright-Patterson AFB. Ohio.

Appendix E

AFIT/GE/EE/82D-59

# RECONFIGURABLE DIGITAL CONTROL LAWS FOR THE A-7D DIGITAC II AIRCRAFT WITH FAILED PRIMARY CONTROL SURFACES

THESIS

Presented to the Faculty of the School of Engineering
of the Air Force Institute of Technology
Air University
in Partial Fulfillment of the
Requirements for the Degree of
Master of Science

by

Daniel E. Russ, B.S.E.E.
2Lt USAF
Graduate Electrical Engineer

December 1982

Approved for public release; distribution unlimited.

## Preface

I would like to thank my thesis advisors, Dr. J. J. D'Azzo and Dr. C. H. Houpis, for the many hours they took out of their busy schedules to answer countless questions and provide invaluable guidance throughout the development of this thesis.

The workload, at times, seemed almost insurmountable, but the analytic abilities of fellow thesis students A. Finley Barfield, Captain Jon Bauschlicher, Lieutenant Tom Lewis, and Captain Mike Masi aided me in getting "over" those very tough "peaks".

Finally, I would like to thank the members of my family for all their love and support during this thesis effort.

Lieutenant Daniel E. Russ

## Contents


Preface . . . . .

List of Figures . . . . .

List of Tables . . . . .

List of Symbols . . . . .

Abstract . . . . .

I. Introduction . . . . .

- Background . . . . .
- Problem . . . . .
- Assumptions . . . . .
- Approach . . . . .
- Order of Presentation . . . . .

II. Aircraft Models for the A-7D . . . . .

- Introduction . . . . .
- A-7D Aircraft Description . . . . .
- System Models . . . . .
- Summary . . . . .

III. Multivariable Digital Control Theory . . . . .

- Introduction . . . . .
- Regular Plants . . . . .
- Irregular Plants . . . . .
- Unknown Plants . . . . .
- Summary . . . . .

IV. Modifications to the MULTI Computer Program . . . . .

- Introduction . . . . .
- Additions to MULTI . . . . .
- Transfer Function Matrix Option . . . . .
- Actuator/Sensor Modifications to the Simulation Option . . . . .
- Summary . . . . .

V. Design of Multivariable Control Laws . . . . .

- Introduction . . . . .

A-7D Aircraft Model . . . . . .
Maneuvers . . . . . .
Design Procedure . . . . . .
Controller Design . . . . . .
Configuration 1 . . . . . .
Control Surface Failures . . . . . .
Configuration 2 . . . . . .
Configuration 3 . . . . . .
Configuration 4 . . . . . .
Configuration 5 . . . . . .
Configuration 6 . . . . . .
Robustness . . . . . .
Summary . . . . . .

VI. Proposed Reconfiguration Strategy . . . . . .

Introduction . . . . . .
Reconfiguration . . . . . .
Transition Strategy . . . . . .
Summary . . . . . .

VII. Conclusions and Recommendations . . . . . .

Conclusions . . . . . .
Recommendations . . . . . .

Bibliography . . . . . .

Appendix A: Aircraft Equations of Motion . . . . . .

Appendix B: Simulation Data . . . . . .

Appendix C: Multi Source Code Modifications . . . .

VITA . . . . . .

## List of Figures


Figure

3-1 Functional Block Diagram for System (Regular Plant) . . . . .

3-2 Functional Block Diagram for System (Irregular Plant) . . . . .

5-1 Configuration 1, 30° Coordinated Turn Commanded . . . . .

5-2 Command Input for 10° Pitch-Up . . . . .

5-3 Configuration 2, 10° Pitch-Up Commanded . . . . .

5-4 Configuration 3, 10° Pitch-Up Commanded . . . . .

5-5 Configuration 4, 10° Pitch-Up Commanded . . . . .

5-6 Configuration 2, 30° Coordinated Turn Commanded . . . . .

5-7 Configuration 3, 30° Coordinated Turn Commanded . . . . .

5-8 Configuration 4, 30° Coordinated Turn Commanded . . . . .

5-9 Configuration 5, 30° Coordinated Turn Commanded . . . . .

5-10 Configuration 6, 30° Coordinated Turn Commanded . . . . .

B-1 Configuration 1, 5° Yaw Angle Commanded . . . . .

B-2 Configuration 1, 5° Pitch Angle Commanded . . . . .

B-3 Configuration 1, 5° Angle of Attack Commanded . . . . .

B-4 Configuration 1, 25ft/sec Forward Velocity Commanded . . . . .

Figure


B-5 Configuration 1, 5° Sideslip Angle Commanded . . . . . .

B-6 Configuration 1, 30° Roll Angle Commanded . . . . . .

B-7 Command Inputs for Maneuvers . . . . . .

B-8 Configuration 1, 5° Yaw Pointing Commanded . . . . . .

B-9 Configuration 1, 5° Pitch Pointing Commanded . . . . . .

B-10 Configuration 1, 30° Pitch-Up Commanded . . . . . .

B-11 Configuration 2, 5° Yaw Pointing Commanded . . . . . .

B-12 Configuration 2, 5° Pitch Pointing Commanded . . . . . .

B-13 Configuration 2, 30° Pitch-Up Commanded . . . . . .

B-14 Configuration 3, 5° Yaw Pointing Commanded . . . . . .

B-15 Configuration 3, 5° Pitch Pointing Commanded . . . . . .

B-16 Configuration 3, 30° Pitch-Up Commanded . . . . . .

B-17 Configuration 1, 5° Yaw Pointing Commanded . . . . . .

B-18 Configuration 1, 5° Pitch Pointing Commanded . . . . . .

B-19 Configuration 1, 30° Pitch-Up Commanded . . . . . .

B-20 Configuration 2, 5° Yaw Pointing Commanded . . . . . .

B-21 Configuration 2, 5° Pitch Pointing Commanded . . . . . .

Figure

B-22 Configuration 5, 30° Pitch-Up Commanded . . . . . .

B-23 Configuration 6, 5° Yaw Pointing Commanded . . . . . .

B-24 Configuration 6, 5° Pitch Pointing Commanded . . . . . .

B-25 Configuration 6, 30° Pitch-Up Commanded . . . . . .

## List of Tables


Table

2-1 A-7D Aircraft Data . . . . . .

2-2 A-7D Aerodynamic Data . . . . . .

5-1 Configuration 1 Results . . . . . .

5-2 Configuration 2 Results . . . . . .

5-3 Configuration 3 Results . . . . . .

5-4 Configuration 4 Results . . . . . .

5-5 Configuration 5 Results . . . . . .

5-6 Configuration 6 Results . . . . . .

A-1 Dimensional Stability Derivatives for Flight Condition 1 . . . . . .

A-2 Dimensional Stability Derivatives for Flight Condition 2 . . . . . .

A-3 Dimensional Stability Derivatives for Flight Condition 3 . . . . . .

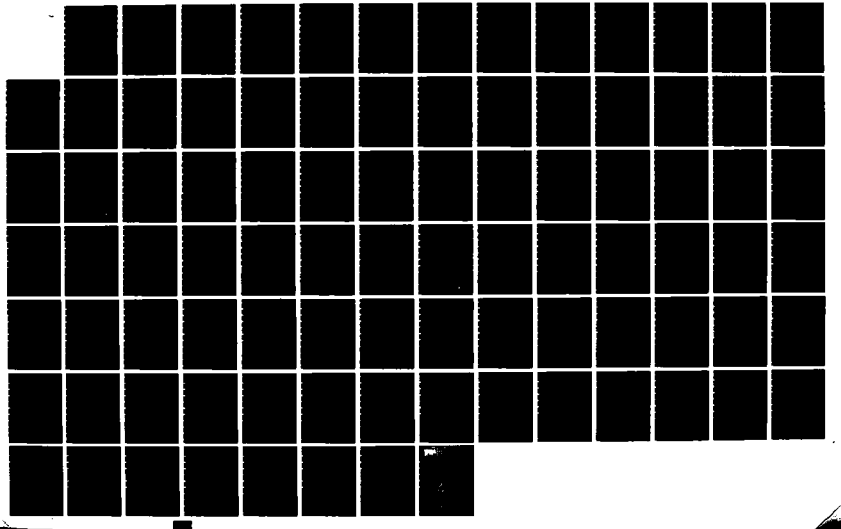
A-4 Dimensional Control Derivatives for Flight Condition 1 (Right Surface) . . . . .

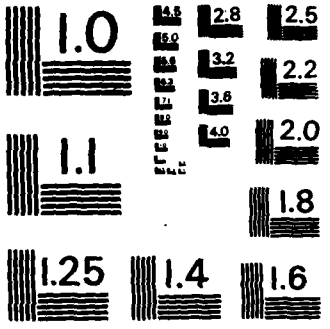
A-5 Dimensional Control Derivatives for Flight Condition 2 (Right Surface) . . . . .

A-6 Dimensional Control Derivatives for Flight Condition 3 (Right Surface) . . . . .

AD-A139 050 PROCEEDINGS OF THE WORKSHOP ON MULTIVARIABLE CONTROL SYSTEMS HELD AT WRIG..(U) AIR FORCE WRIGHT AERONAUTICAL LABS WRIGHT-PATTERSON AFB OH M A MASI ET AL. SEP 83 7/7

UNCLASSIFIED AFWAL-TR-83-3093 FFG 1/3 NL






MICROCOPY RESOLUTION TEST CHART
NATIONAL BUREAU OF STANDARDS-1963-A

## List of Symbols

| | |
|---|---|
| $\alpha$ | Angle of attack, ratio of proportional and integral feedback |
| $\beta$ | Sideslip angle |
| b | Wing span |
| $\bar{c}$ | Mean aerodynamic (geometric) chord |
| $\underline{e}$ | Error vector |
| g | Acceleration of gravity |
| $\underline{G}(0)$ | Steady state transfer function matrix |
| $\underline{G}(\lambda)$ | Transfer function matrix |
| $I_{xx}$ | Moment of inertia about X axis |
| $I_{yy}$ | Moment of inertia about Y axis |
| $I_{zz}$ | Moment of inertia about Z axis |
| $I_{xz}$ | Product of inertia in XYZ system |
| $\underline{K}$ | Control feedback matrix |
| $L_\beta$ | Dimensional variation of rolling moment about $X_s$ with sideslip angle |
| $L_p$ | Dimensional variation of rolling moment about $X_s$ with roll rate |
| $L_r$ | Dimensional variation of rolling moment about $X_s$ with yaw rate |
| $L_\delta$ | Dimensional variation of rolling moment about $X_s$ with stabilizer, aileron, flap, rudder, and spoiler where $\delta = \delta_H, \delta_a, \delta_f, \delta_r, \delta_s$, angle |
| m | Airplane mass |
| $\underline{M}$ | Measurement matrix |
| $M_u$ | Dimensional variation of pitching moment with speed |

$M_\alpha$ Dimensional variation of pitching moment with angle of attack

$M_{\dot{\alpha}}$ Dimensional variation of pitching moment with rate of change of angle attack

$M_q$ Dimensional variation of pitching moment with pitch rate

$M_\delta$ Dimensional variation of pitching moment with a stabilizer, aileron, flap, rudder, spoiler where $\delta = \delta_H, \delta_a, \delta_f, \delta_r, \delta_s$ angle

$N_\beta$ Dimensional variation of yawing moment about $Z_s$ with sideslip angle

$N_p$ Dimensional variation of yawing moment about $Z_s$ with roll rate

$N_r$ Dimensional variation of yawing moment about $Z_s$ with yaw rate

$N_\delta$ Dimensional variation of yawing moment about $Z_s$ with stabilizer, aileron, flap, rudder, and spoiler, where $\delta = \delta_H, \delta_a, \delta_f, \delta_r, \delta_s$ angle

$p$ Perturbed roll rate

$\phi$ Perturbed roll angle

$\bar{q}$ Dynamic pressure

$q$ Perturbed pitch rate (about y)

$r$ Perturbed yaw rate

$S$ Surface area, Reference (wing) area

$T$ Sampling period

$\theta$ Perturbed pitch angle

$U_1$ Forward velocity (along $X_s$) steady state

$u$ Perturbed forward velocity (along $X_s$)

$\underline{v}$ Command vector

$X_u$ Dimensional variation of $X_s$-force with speed

$X_\alpha$ Dimensional variation of $X_s$-force with angle of attack

$X_{\dot{\alpha}}$ Dimensional variation of $X_s$-force with rate of change of angle of attack

$X_\delta$ Dimensional variation of $X_s$-force with stabilizer, aileron, flap, rudder, and spoiler where $\delta = \delta_H, \delta_a, \delta_f, \delta_r, \delta_s$ angle

$\underline{x}$ State vector

$Y_\beta$ Dimensional variation of $Y_s$-force with sideslip angle

$Y_p$ Dimensional variation of $Y_s$-force with roll rate

$Y_r$ Dimensional variation of $Y_s$-force with yaw rate

$Y_\delta$ Dimensional variation of $Y_s$-force with stabilizer, aileron, flap, rudder, and spoiler where $\delta = \delta_H, \delta_a, \delta_f, \delta_r, \delta_s$ angle

$Z_u$ Dimensional variation of $Z_s$-force with speed

$Z_\alpha$ Dimensional variation of $Z_s$-force with angle of attack

$Z_{\dot{\alpha}}$ Dimensional variation of $Z_s$-force with rate of change of angle of attack

$Z_q$ Dimensional variation of $Z_s$-force with pitch rate

$Z_\delta$ Dimensional variation of $Z_s$-force with stabilizer, aileron, flap, rudder, and spoiler where $\delta = \delta_H, \delta_a, \delta_f, \delta_r, \delta_s$ angle

$X_s, Y_s, Z_s$ Stability axes coordinate system

$\underline{z}$ Error integral vector

## Abstract

This thesis develops a set of high-gain, error-actuated multivariable digital control laws for the A-7D DIGITAC II aircraft at three different flight conditions and for the aircraft with three different control surface failures. Additional modifications to the computer-aided-design package MULTI are included.

The aircraft model is based on a six degree-of-freedom model which contains separate left and right horizontal stabilizer and left and right aileron control surfaces. These split surfaces provide additional flexibility and permit the aircraft to perform both conventional and CCV maneuvers.

The design procedure used to obtain the various tracker control laws is outlined. The presentation includes a discussion of the effects of surface failures on aircraft performance and the robustness of the controllers at other flight conditions. A proposed reconfiguration strategy is also included.

The thesis concludes that further investigation is needed to determine the possible correlation between robustness and the location of transmission zeros. The development of an accurate aircraft model is also necessary.

# RECONFIGURABLE DIGITAL CONTROL LAWS FOR THE A-7D DIGITAC II AIRCRAFT WITH FAILED PRIMARY CONTROL SURFACES

## I Introduction

Advances in the size and speed of digital computers have led to the use of these sophisticated devices for a wide range of tasks in the modern aircraft of today. The use of computers in aircraft flight control systems is just one such application. A digital flight control system generates a set of electrical signals, based on pilot inputs, which actuate the primary control surfaces of the aircraft in order to achieve the desired stability and performance. Such a control system is in sharp contrast to those of older aircraft which use mechanical linkages to actuate their control surfaces.

Aircraft which employ fly-by-wire closed-loop flight control systems depend on control laws that assume each element of the control loop is performing properly. The use of redundancy management concepts ensures continual operation of each element for all reasonable failures. However, these control laws are not valid if a primary surface becomes

inoperative due to combat damage or mechanical failure. This problem is further amplified if the aircraft is statically unstable. This thesis develops the control laws used by such a digital flight control system.

The first chapter presents appropriate background material, the problem statement, the assumptions that are made, the approach taken, and the order of presentation in the thesis.

## Background

The advances in control system design techniques are many and varied. Among these is the emergence of digital control system design techniques which provide a means of trying to achieve system performance specifications that are not achievable by analog control design techniques. This is the reason for the shift in emphasis from analog to digital flight control systems. These new digital flight control systems provide faster responses and improved flexibility in maintaining a high level of aircraft performance.

The A-7D DIGITAC II aircraft serves as a test bed for the development of experimental digital flight control systems. These tests provide a technical data base for use in future development efforts. Recent programs involve detection and isolation capabilities of digital flight control systems in the event of a surface failure.

## Problem

This thesis concentrates on the development of a set of control laws for the A-7D DIGITAC I: aircraft which can accommodate control surface failures and operate over a wide range of flight conditions.

At present, the Air Force Flight Dynamics Laboratory is studying a number of different multivariable, digital control law design techniques. The design method of Professor Brian Porter of the University of Salford, United Kingdom (Ref 1; 3) shows promise in developing these robust control laws.

## Assumptions

The following assumptions are made concerning the aircraft model, and its operation, in order to simplify the analysis. First, it is assumed that the aircraft model developed by Captain David W. Potts (Ref 25) is correct. This model assumes that: (1) the aircraft equations of motion are developed using stability axes; (2) the aircraft makes only small deviations from straight and level flight; and (3) the flight control surfaces can be separated into independent left and right surfaces.

## Approach

The purpose of this thesis is to develop a set of reconfigurable multivariable digital control laws for the

A-7D DIGITAC II aircraft. This is accomplished by using the design techniques of Professor Porter and the interactive computer program MULTI.

## Order of Presentation

This thesis is comprised of seven chapters. Chapter II presents the aircraft model which is based on the equations of motion and stability derivatives contained in Appendix A. Chapter III provides a summary of the multivariable control law theory of Professor Porter. Chapter IV discusses the changes made to the computer-aided-design program MULTI. Chapter V presents the controller designs for six different flight configurations and results of the control law simulations. Chapter VI discusses a possible reconfiguration strategy necessary to transition from normal to reconfigured control laws. Chapter VII presents the conclusions which are drawn from the thesis effort as well as recommendations for further study.

# II Aircraft Models for the A-7D

## Introduction

The models used for the A-7D aircraft used in this thesis are based on those developed by Potts (Ref 25) and modified by Paschall (Ref 18). These models have six degrees-of-freedom (D-O-F) and contain split control surfaces: left and right horizontal tail, left and right ailerons, left and right spoilers, left and right flaps. The linear perturbation equations used for this study were obtained by linearizing the nonlinear equations about a nominal operating point. Three different flight conditions are studied, thus providing an opportunity to test the robustness of the control laws developed for the aircraft. The three flight conditions are:

1. Cruise - M = 0.30 at sea level.
2. Cruise - M = 0.60 at 15,000 ft.
3. Cruise - M = 0.90 at 15,000 ft.

This chapter gives a brief description of the aircraft and a development of the system models.

## A-7D Aircraft Description

The A-7D is a single-seat, light attack, fighter aircraft with moderately swept wing and tail surfaces. The aircraft is powered by a single TF41-A-1 engine (Ref 25). Tables 2-1 and 2-2 provide some pertinent data.

Table 2-1

A-7D Aircraft Data

| | |
|---|---|
| Fuselage Length | 45.4 ft |
| Wing Area | 375 $ft^2$ |
| Wing m.g.c.* | 10.8 ft |
| Horizontal Slab Area | 56.2 ft |
| Slab m.g.c. | 6.1 ft |
| Distance from 25% wing m.g.c. to 25% slab m.g.c. | 16.2 ft |
| Weight | 25,238 lbs |

* - mean geometric chord

Table 2-2

A-7D Aerodynamic Data

| Altitude | Sea Level | 15,000 | 15,000 | ft |
|---|---|---|---|---|
| M | 0.30 | 0.60 | 0.90 | |
| $U_1$ | 335.1 | 634.4 | 952.2 | ft/sec |
| m | 786.89 | 786.89 | 786.89 | slugs |
| $I_{xx}$ | 16,117 | 15,365 | 15,322 | slug-ft$^2$ |
| $I_{yy}$ | 69,528 | 69,528 | 69,528 | slug-ft$^2$ |
| $I_{zz}$ | 78,253 | 79,005 | 79,048 | slug-ft$^2$ |
| $I_{xz}$ | -7,076 | -1,664 | 125 | slug-ft$^2$ |
| b | 38.73 | 38.73 | 38.73 | ft |
| $\bar{c}$ | 10.84 | 10.84 | 10.84 | ft |
| $\bar{q}$ | 133.308 | 300.88 | 676.998 | lbs/ft$^2$ |
| C.G.(% m.g.c.) | 28.71 | 28.71 | 28.71 | |
| S | 375 | 375 | 375 | ft$^2$ |

System Models

The system models used to describe the A-7D are based on the six degree-of-freedom aircraft equations developed by Potts. The techniques used by Potts provide aircraft models which achieve lateral-directional control using longitudinal control surfaces and longitudinal control using lateral-directional control surfaces. For example, using the horizontal tail differentially can produce a rolling moment.

Also, aileron deflections in the same direction can produce a pitching moment. The ability to control the aircraft in this way is essential if the design of effective reconfigured control laws is to be achieved. These reconfigured control laws provide the ability to maintain some degree of control over the aircraft in the event that a primary control surface becomes inoperative due to actuator failure or battle damage. The state equations and the state, input, and output matrices for the three flight conditions are given in Appendix A.

The aircraft is modelled using six inputs and six outputs:

| INPUTS | OUTPUTS |
|---|---|
| Right Horizontal Tail ($\delta_{H_r}$) | Yaw Angle ($\psi$) |
| Left Horizontal Tail ($\delta_{H_l}$) | Pitch Angle ($\theta$) |
| Rudder ($\delta_r$) | Angle of Attack ($\alpha$) |
| Right Aileron ($\delta_{a_r}$) | Forward Velocity (u) |
| Left Aileron ($\delta_{a_l}$) | Sideslip Angle ($\beta$) |
| Spoiler-Flap ($\delta_{sf}$) | Roll Angle ($\phi$) |

Summary

This chapter gives a brief description of the A-7D DIGITAC II aircraft and gives a partial list of important aircraft data. The six degree-of-freedom aircraft equations used to model the A-7D are discussed. The importance of longitudinal and lateral-directional control surfaces in the

development of effective reconfigurable control laws is also noted.

The theory necessary to develop the control laws for these models is presented in the next chapter.

Chapter , Design Theory, Omitted

See Proceedings

# IV Modifications to the MULTI Computer Program

## Introduction

MULTI is an interactive, Computer-Aided-Design (CAD) program developed by Captain Douglas Porter, Lieutenant Randall Paschall, and Lieutenant Joseph Smyth (Ref 19). This program allows the user to design and simulate control laws for systems which are characterized by regular, irregular, and unknown plants.

This chapter outlines the changes to MULTI which have been implemented through the joint efforts of Captain Jon Bauschlicher (Ref 22), Captain Michael Masi (Ref 23), A. Finley Barfield (Ref 24) and this author. In particular, the addition of an option to compute the open-loop transfer function matrix, $\underline{G}(s)$, and modifications to the simulation with respect to the inclusion or exclusion of actuator and/or sensor dynamics is addressed in this thesis.

## Additions to MULTI

There are six changes to MULTI which expand the program's capabilities and usefulness to the user:

1. The addition of provisions for a "ramped-up" input which more accurately models the desired dynamics of an input to the system. That is, the ability to model the finite length of time required for an input to reach its final value (Ref 22).

2. The addition of batch capability which allows the user to simulate higher-order systems than can be done interactively. The ability to run MULTI in a batch mode also removes the limitations on file space for the time responses and permits the plots of all desired quantities to be run for longer periods of time (Ref 23).

3. The addition of an option which computes the transmission zeros and all decoupling zeros of the system. This option also determines whether the decoupling zeros are input, output, or input-output decoupling zeros (Ref 24).

4. The addition of an option using the B* design method to eliminate undesirable undershoots in system responses (Ref 23).

5. The addition of an option to compute the transfer function matrix, $\underline{G}(s)$, for the open-loop plant.

6. Modification to the simulation permitting the inclusion or exclusion of actuator or sensor dynamic models.

The last two of the six changes to MULTI are described in further detail in this chapter. Details on the development and implementation of the other modifications to MULTI are given in the ir ted references.

## Transfer Function tion

Option #6 is used to compute the open-loop transfer function matrix, $\underline{G}(s)$, for the system under consideration. This option provides to the user the ability to input the plant, input, and output matrices for the system directly or

to simply calculate $\underline{G}(s)$ immediately if these matrices have already been entered using Option #3. In either case, Option #6 informs the user of the dimension of $\underline{G}(s)$ and then requests the user to indicate which inputs and which outputs are desired in order to provide the appropriate transfer function.

The transfer function option uses two subroutines, PHOFS and CADJB, to calculate the appropriate numerator and denominator polynomials respectively. The subroutine POLYRT is also used in the option and provides a factored form of the polynomial, thus yielding the poles and zeros of the system. The subroutines PHOFS, CADJB, and POLYRT are shown in Appendix C.

## Actuator/Sensor Modifications to the Simulation Option

MULTI offers a great deal of flexibility in simulating system responses to various command inputs. One possible way is to simulate the system without actuator and/or sensor dynamics. In its original form, MULTI did not provide this choice. Instead, if a simulation without actuators and sensors was desired, it modelled them as extremely fast first-order lags (Ref 19). This resulted in the poles of the actuators/sensors being located far to the left in the s-plane, thus having little effect on the dominant poles of the system. In order to be totally accurate, and to reduce

computer operating time, the actuator and/or sensor blocks should be completely removed from the block diagram (Ref 19).

The simulation performed by MULTI is based on the solution of the plant, actuator, and sensor differential equations with the IMSL subroutine ODE. One of four externally referenced subroutines (CLPASS, CLPSS1, CLPSS2, CLPSS3) is used to form the differential equation array XDOT. The differential equations for the plant occupy the first n places in XDOT, followed by the differential equations for the actuators and then by the differential equations for the sensors. Based on the values of the character variables ACT and SEN, one of the four externally referenced subroutines is used to form XDOT by "loading" the appropriate differential equations into the array. For example, a simulation that includes both actuator and sensor dynamics would form an XDOT array with the plant, actuator, and sensor differential equations, whereas a simulation with no actuator and sensor dynamics would form an XDOT array with only the plant differential equations. The modifications to Option #26 is shown in Appendix C.

Summary

This chapter describes briefly each of the changes made to MULTI by a number of thesis students. In particular, the addition of an option to compute the open-loop transfer function matrix and modifications to the simulation are

explained in detail. Source listings of the additional code are included in Appendix C.

The next chapter outlines the procedures used in the design of multivariable digital control laws as well as the controllers that are developed.

# V Design of Multivariable Control Laws

## Introduction

This chapter presents the procedures used to develop the multivariable digital control laws for the A-7D DIGITAC II aircraft. Controllers are developed for three different flight conditions with all control surfaces operative and for the aircraft with inoperative surfaces. This chapter contains an examination of the problems encountered with the aircraft model, how these problems are overcome, and why the M=0.60 flight condition is used for the bulk of the design work. The four maneuvers used to illustrate the performance of the controllers are described next, as well as the reasons for their selection. This is followed by the control law design procedure; the discussion addresses the relative decoupling of the longitudinal and lateral-directional modes and the procedure used to vary design parameters to obtain a "good" controller. The design of a controller for the basic aircraft (M=0.60 flight condition with all surfaces operative) is then presented. Next, the effect of surface failures on controller performance is examined and the design of new controllers for the aircraft with failed surfaces is outlined. Finally, the chapter concludes with the design of basic controllers for the complete aircraft (all surfaces operative) at the other two flight

conditions and a simple robustness test of the performance of the three basic controllers at the other flight conditions.

A-7D Aircraft Model

The design of a multivariable digital controller which provides the desired performance characteristics can only be achieved if the system model is an accurate representation of the actual physical plant. During the development of the aircraft models used in this thesis, two problems arose, namely (1) how many states are necessary to accurately model the aircraft, and (2) obtaining accurate aircraft data for a realistic system model. Each of these problems is addressed separately.

Preliminary design efforts with the Paschall and Potts aircraft models (Ref 18; 25) revealed that there were difficulties in commanding certain outputs to desired values for a given maneuver. In particular, when performing a coordinated turn, it is desired to command a given roll angle, $\phi$, the appropriate yaw rate, r, and the side-slip angle, $\beta$, equal to zero; that is:

$$\phi = \phi_o$$

$$r = r_o$$

$$\beta = 0$$

However, attempts at designing a controller which adequately performed a coordinated turn with this aircraft model indicated that it is impossible to command $\beta=0$ and also to

command the appropriate yaw rate $r_o$ . Examining the relationship between r and $\beta$ (Ref 20), based on the modelling assumptions outlined in Appendix A, shows that:

$$r = \dot{\psi}$$

$$\psi = -\beta$$

Further, studying the output vector used by Paschall (Ref 18) reveals that although $\theta$ and $\phi$ are commanded, p and q are not. Thus, based on these two observations, it appears that in order to command any one output to any desired value requires that only the output, and not its derivative or integral, appear in the output vector. That is, if $\theta$ is the desired output, then q cannot appear in the output vector, $\underline{y}$.

A number of possible solutions are examined. The solution that is used involves expanding the model from eight states to nine states. This is accomplished by adding the yaw angle, $\psi$, as a state. The state-space representation is altered by adding the kinematic relation:

$$\dot{\psi} = r \qquad (5\text{-}1)$$

The resultant nine state system model is shown in Appendix A. The addition of $\psi$ accomplishes two important things, First, it permits replacing r with $\psi$ in the output vector, so that the interaction between r and $\beta$ is eliminated and $\beta$ can now be commanded to any desired value. Second, a coordinated turn can now be performed by commanding $\beta$=0 , and "ramping up" $\psi$, via the new input option available on the computer

program MULTI (Ref 22), such that the slope of $\psi$ is:

$$\dot{\psi} = \frac{g}{V_T} \tan \phi \qquad (5\text{-}2)$$

This produces the desired yaw rate, $r_o$, necessary to achieve coordination (Ref 20).

The use of accurate aircraft data to model the plant is critical in the development of a controller which yields accurate, realistic system performance. Paschall's aircraft model (Ref 18:Appendix A) was used initially; however, the accuracy of some of the control derivatives in the input matrix, $\underline{B}$, was questionable. As a result, the aircraft model developed by Potts (Ref 25:Appendices A,B) for the M=0.60 flight condition is used as the baseline since it produced results consistent with the expected performance of the A-7D. The aircraft model for the other two flight conditions, M=0.30 at sea level and M=0.90 at 15,000 ft, is based on data from the flight test evaluation report by Bender and Wolf (Ref 26) and the procedures used by Paschall and Potts. The state-space representation for the A-7D at all three flight conditions is presented in detail in Appendix A.

Maneuvers

In order to determine the capabilities of the multivariable controller, four basic maneuvers are used to illustrate the performance of the system. The four maneuvers are:

1. 5° Yaw Pointing ($\psi = -\beta$)
2. 5° Pitch Pointing ($\theta = \alpha$)
3. 30° Pitch Up ($\theta = \theta_o$ , $\alpha = \alpha_o$)
4. 30° Coordinated Turn ($\phi = \phi_o$ , $\dot{\psi} = r_o$ , $\beta = 0$)

The maneuvers, as a group, demonstrate the ability of the controller to perform both conventional (pitch up, coordinated turn) and Control Configured Vehicle or CCV (yaw pointing, pitch pointing) maneuvers. The 30° coordinated turn is used in this chapter to show the system responses to the various controller designs that are developed. The aircraft responses for the other three maneuvers can be found in Appendix B.

Design Procedure

The synthesis of a control law is accomplished using the interactive computer program MULTI. The following steps, which comprise the design procedure, proved to be successful in obtaining a control law which exhibits the desired performance characteristics.

Before beginning the actual design process, an examination of the plant matrix, $\underline{A}$, provides some meaningful insights on how to proceed. Note that the partition $\underline{A}_{22}$ in Eqs (A-12), (A-14), and (A-16) is block diagonal and that each "block" of elements is associated either with the longitudinal or lateral-directional mode. This suggests that the two modes are essentially uncoupled and that in the

process of "tuning" the controller, changes made to parameters associated with either mode do not affect the controller performance with respect to the other mode. Thus, although the design is performed with the complete aircraft model, the designer can concentrate on either the longitudinal or lateral-directional mode separately.

As an initial trial, all design parameters are set to unity values. Each variable in the command input vector, $\underline{v}$:

$$\underline{v} = \begin{bmatrix} \psi \\ \theta \\ \alpha \\ u \\ \beta \\ \phi \end{bmatrix} = \underline{y} \qquad (5\text{-}3)$$

is commanded to a positive value, and, in all cases, resulted in an unstable response. Examining the control matrices, $\underline{K}_o$ and $\underline{K}_1$, reveals matrix elements on the order of $10^3$ and greater. In order to reduce the magnitude of the majority of the elements to $10^1$ or $10^2$, the scalar multiplier, $\varepsilon$, is adjusted accordingly. A value of $\varepsilon$=0.01 is selected in this case. The resulting simulations yielded stable, highly overdamped responses.

Once a stable system is obtained, the individual $\sigma_i$ values of the output weighting matrix, $\underline{\Sigma}$, are adjusted to improve the system response so that the desired performance specifications are met. Note that variations in the $\sigma_i$'s

associated with longitudinal variables have little effect on the responses of lateral-directional variables and vice-versa. Variations in the $\sigma_i$'s associated with a given variable may or may not affect the responses of the other variables associated with the same mode.

The speed of the response to the command inputs is affected by the selection of the measurement matrix elements. Reducing the magnitude of the elements speeds up the response of those variables influenced by the measurement matrix. Increasing the magnitude of the elements slows down the response of those same variables. After the selection of the measurement matrix elements is made, further "tuning" of the $\alpha$, $\varepsilon$, and $\sigma_i$ parameters is performed until the desired response is achieved. Thus, the entire design process is an iterative one in which the variation of parameters not only dictate the results that are obtained but also illustrate what trade-offs are made in obtaining the desired performance levels.

## Controller Design

The design of a multivariable digital controller, as noted above, is a straightforward process involving the selection of values for a number of different parameters. It is desired to develop a set of control laws for the A-7D aircraft for a given flight configuration. Six different flight regimes are examined:

Configuration 1: M=0.60 at 15,000 ft, all surfaces operative

Configuration 2: M=0.60 at 15,000 ft, rudder inoperative

Configuration 3. M=0.60 at 15,000 ft, ailerons inoperative

Configuration 4: M=0.60 at 15,000 ft, spoiler-flap inoperative

Configuration 5: M=0.30 at sea level, all surfaces operative

Configuration 6: M=0.90 at 15,000 ft, all surfaces operative

The flight condition of Configuration 1 is used as the baseline of performance because its moderate dynamic pressure, $\bar{q}$, reflects a common operating point in the flight envelope. The controller designed for each of the six flight regimes is discussed below.

Configuration 1. The system model used for this regime is that outlined in Eqs (A-14), (A-19), and (A-22). The design includes the actuator and sensor dynamics described in Appendix A, but does not include control surface limitations. It should be noted, however, that "subjective" limits are placed on the control surfaces. That is, it is desired that the control surface deflections lie within the range:

$$\begin{aligned} -30^\circ \leq \delta_H \leq 30^\circ \\ -20^\circ \leq \delta_r \leq 20^\circ \\ -30^\circ \leq \delta_a \leq 30^\circ \\ -30^\circ \leq \delta_{sf} \leq 30^\circ \end{aligned} \qquad (5\text{-}1)$$

Using the design procedure outlined above, the following controller is obtained. This controller is characterized by the parameter values:

$$T = 0.02 \text{ sec } (f = 50 \text{ hz}) \tag{5-5}$$

$$\alpha = 0.5 \tag{5-6}$$

$$\varepsilon = 1.0 \tag{5-7}$$

$$\underline{\Sigma} = \text{diag}\{1.25, 0.80, 1.25, 0.10, 2.5, 0.75\} \tag{5-8}$$

These parameter values yield the irregular plant control matrices, $\underline{K}_o$ and $\underline{K}_1$, as:

$$\underline{K}_o = \begin{bmatrix} -.8928E+02 & -.7090E+00 & -.8808E+01 & -.3813E-03 & -.3060E+03 & -.1483E+01 \\ .7020E+02 & -.7090E+00 & -.8809E+00 & -.3813E-03 & .3070E+03 & .1488E+01 \\ -.8016E+01 & .4595E-14 & 0. & -.3829E-17 & -.8885E+01 & -.3674E-01 \\ -.2794E+02 & .3028E+01 & -.2851E+01 & -.2730E-02 & -.1384E+03 & -.1280E+00 \\ -.3451E+02 & -.3028E+01 & .2851E+01 & .2731E-02 & -.1457E+03 & -.1501E+00 \\ .1614E+02 & .8340E+01 & .1012E+02 & -.1341E-01 & .1799E+02 & .7398E-01 \end{bmatrix} \tag{5-9}$$

$$\underline{K}_1 = \begin{bmatrix} -.1386E+03 & -.1418E+01 & -.1722E+01 & -.7628E-03 & .6131E+03 & -.2967E+01 \\ .1404E+03 & -.1418E+01 & -.1722E+01 & -.7628E-03 & .6151E+03 & .2975E+01 \\ -.1604E+02 & .9171E-14 & 0. & -.7657E-17 & -.1777E+02 & -.7348E-01 \\ -.5589E+02 & .6055E+01 & -.5702E+01 & -.5461E-02 & -.2768E+03 & -.2560E+00 \\ -.6902E+02 & -.6055E+01 & .5702E+01 & .5461E-02 & -.2914E+03 & -.3163E+00 \\ .3229E+02 & .1668E+02 & .2025E-02 & -.2683E-01 & .3578E+02 & .1480E+00 \end{bmatrix} \tag{5-10}$$

The measurement matrix developed for this irregular plant is:



Reproduced from best available copy.

$$\underline{M} = \begin{bmatrix} 0.02 & 0 & 0 \\ 0 & 0.02 & 0 \\ 0 & 0 & 0 \\ 0 & 0 & 0 \\ 0 & 0 & 0 \\ 0 & 0 & 0.02 \end{bmatrix} \qquad (5\text{-}11)$$

Figure 5-1 shows the system response for a commanded 30° coordinated turn. Figure 5-1(a) is the command vector, $\underline{v}$, for a coordinated turn where $\phi$ and $\psi$ are in radians and are scaled by a factor of:

$$c_o = \frac{2}{57.3} = 0.0349 \qquad (5\text{-}12)$$

to account for the difference in units between the plant and control surface derivatives. Using Eq (5-2), the desired commands are:

$$\phi = 30° = 0.524 \text{ rad}$$

$$\dot{\psi} = \frac{g}{V_T} \tan \phi = 0.0293 \text{ rad/sec}$$

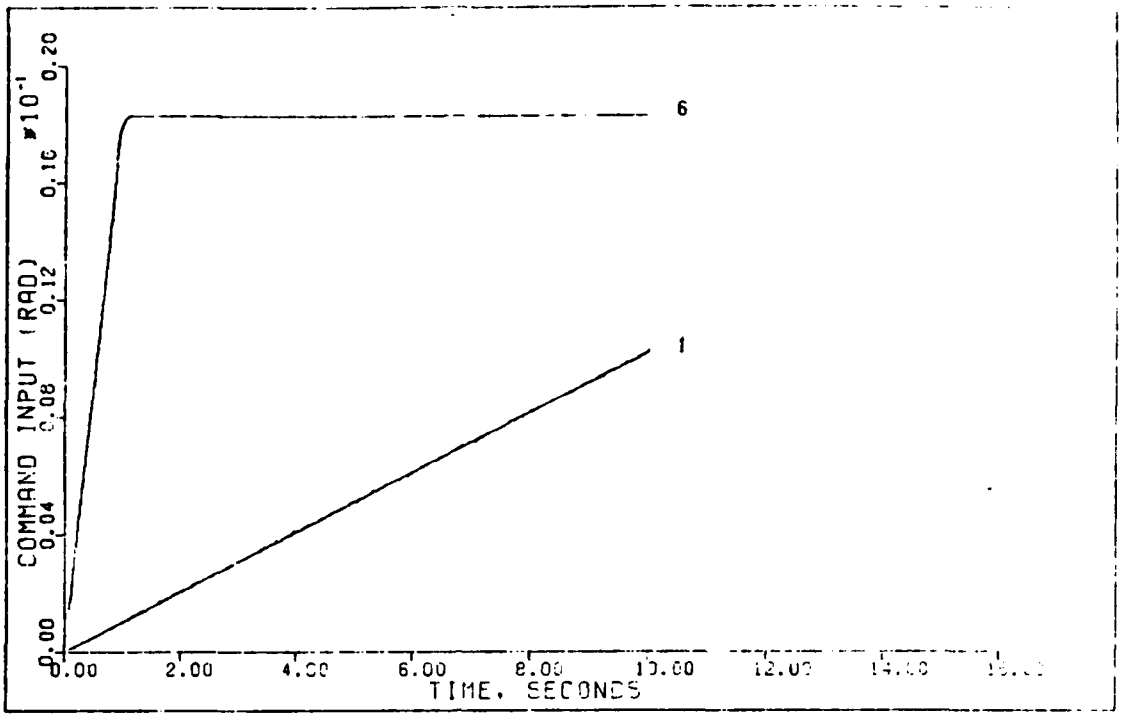
$$\beta = 0 \text{ rad}$$

and the corrected values are:

$$\phi' = C_o\phi = 0.0183 \text{ rad}$$

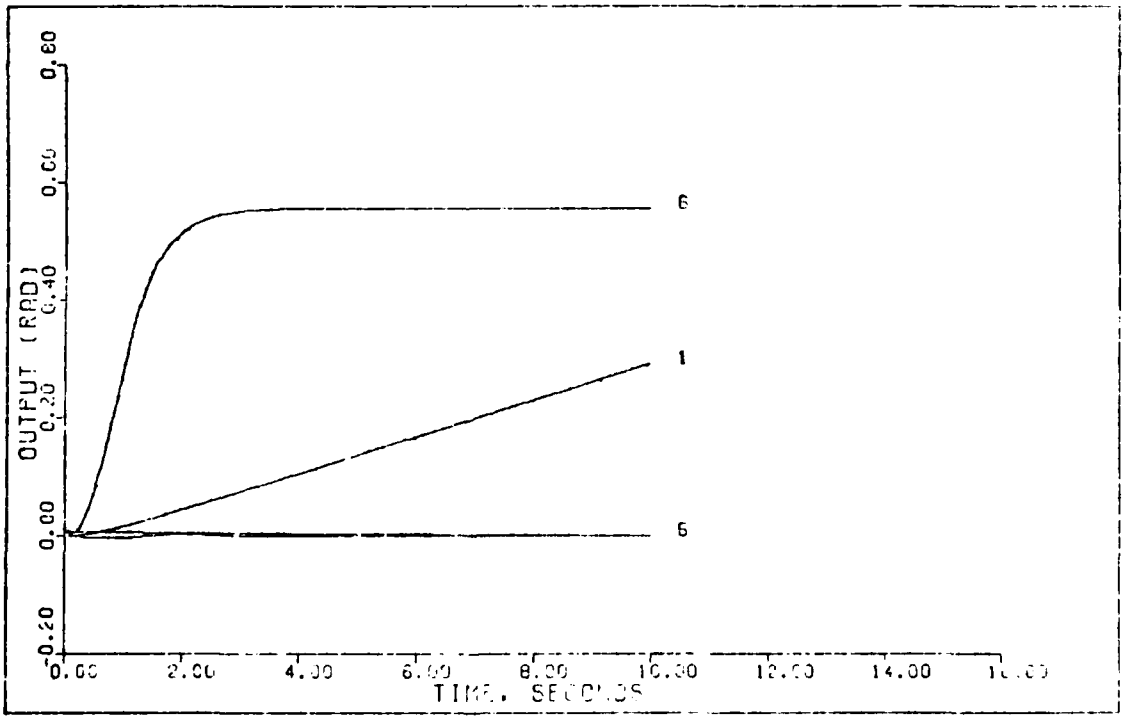
$$\dot{\psi}' \quad C_o\dot{\psi} = 0.001023 \text{ rad/sec}$$

$$\beta' \quad C_o\beta = 0 \text{ rad}$$




1=YAW ANGLE ($\psi$); 6=ROLL ANGLE ($\phi$)

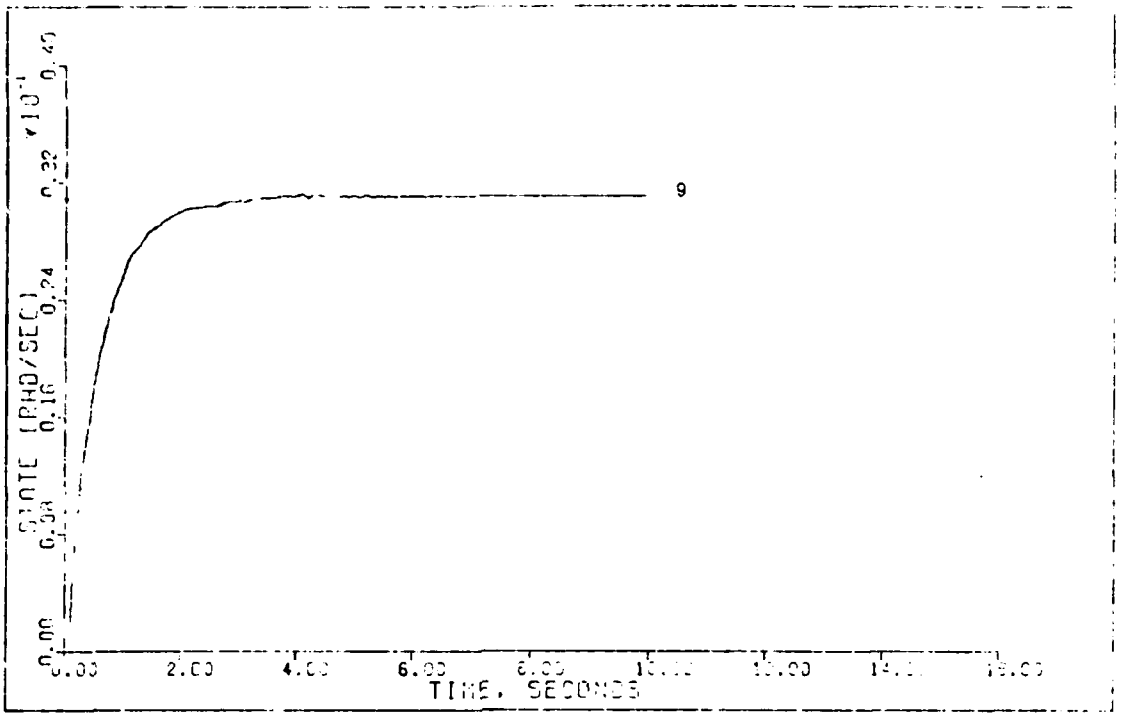
(a) $\psi$, $\phi$ Command Input




1=YAW ANGLE ($\psi$) 5=SIDESLIP ANGLE ($\beta$); 6=ROLL ANGLE ($\phi$)

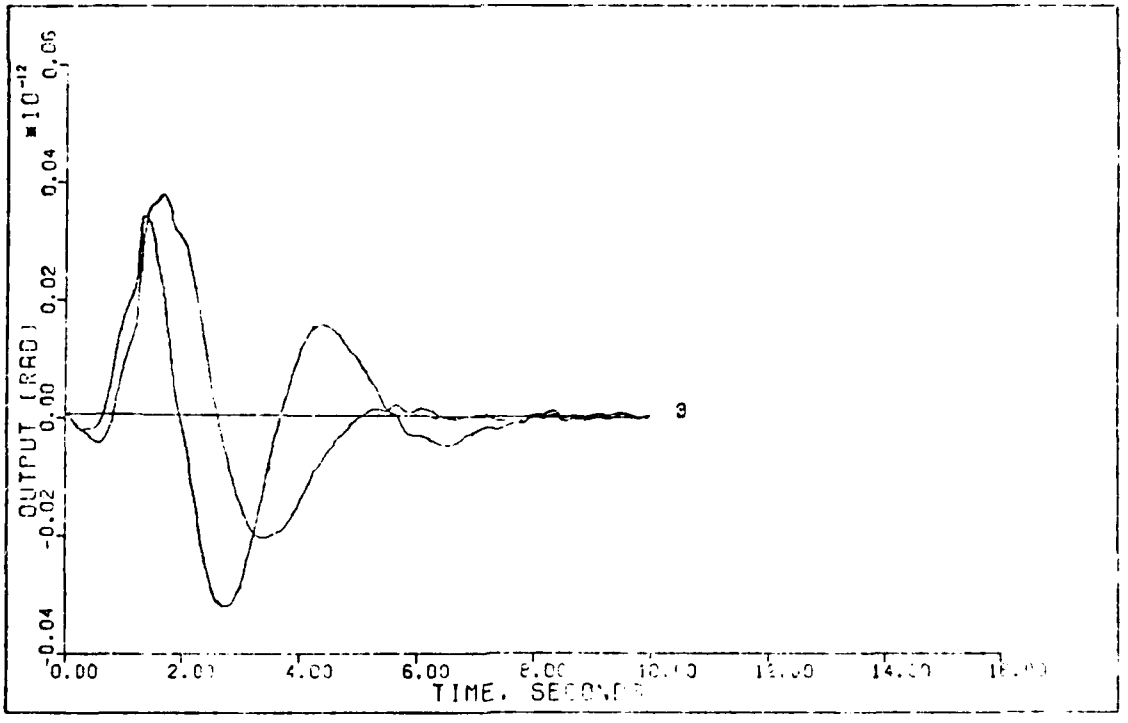
(b) $\psi$, $\beta$, $\phi$ Output Response

Figure 5-1. Configuration 1, 30° Coordinated Turn Commanded



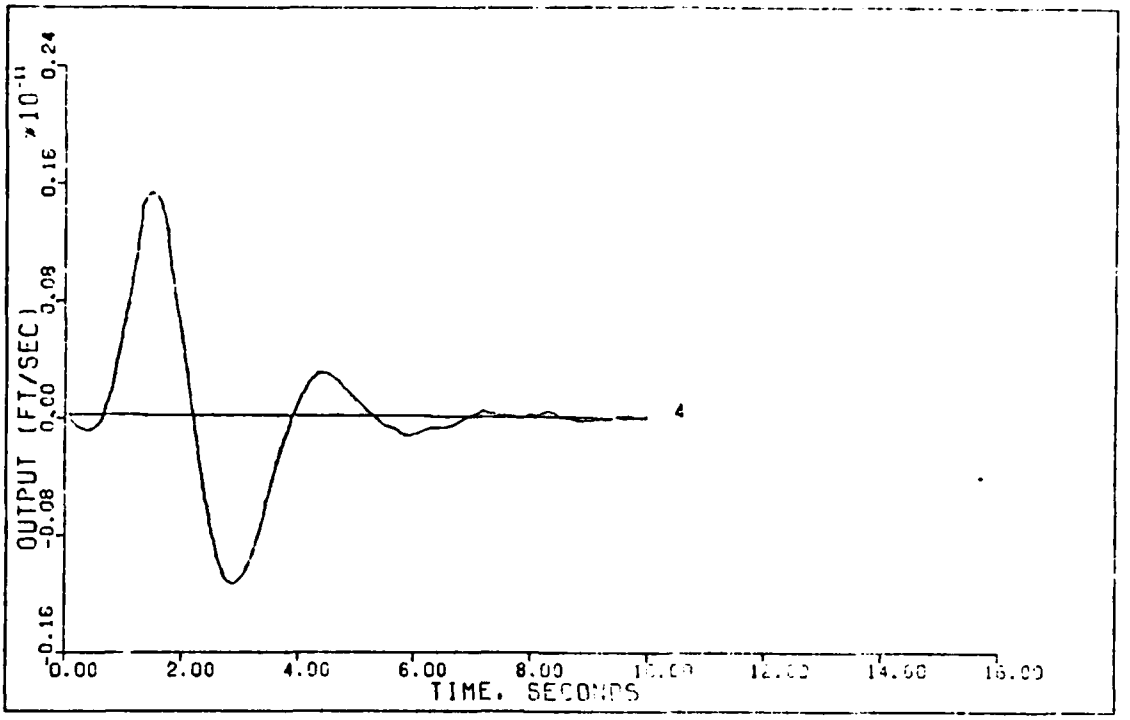

9=YAW RATE (R)

(c) r State Response



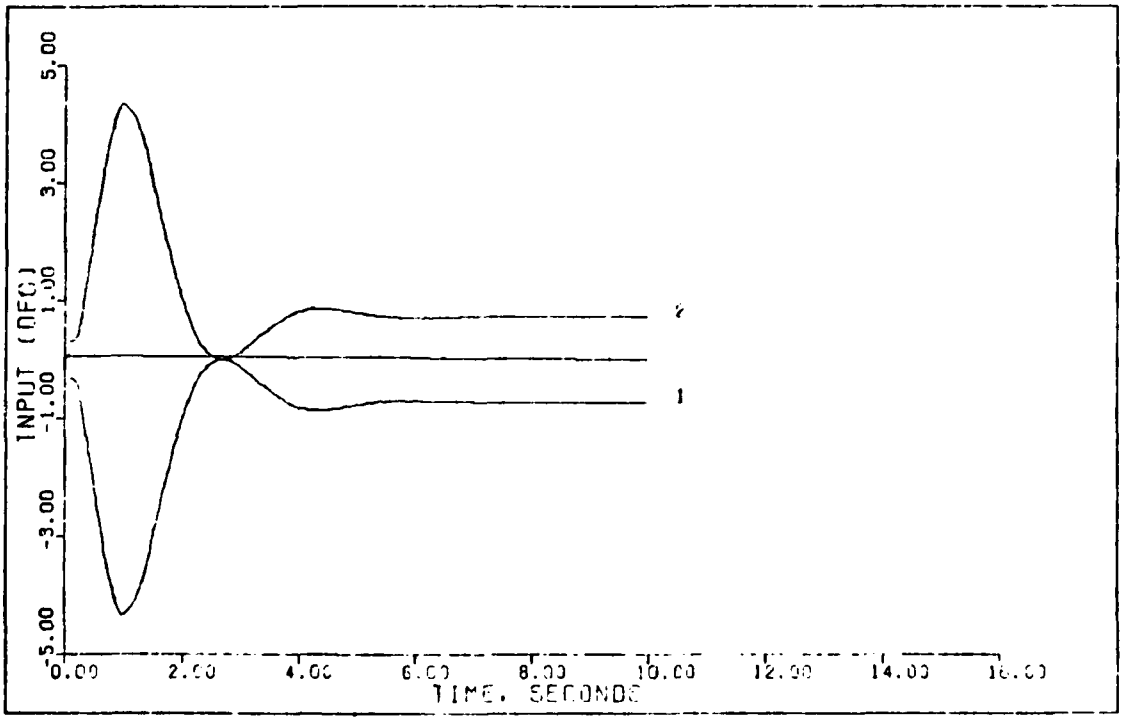

2=PITCH ANGLE (θ); 3=ANGLE OF ATTACK (α)

(d) θ, α Output Response



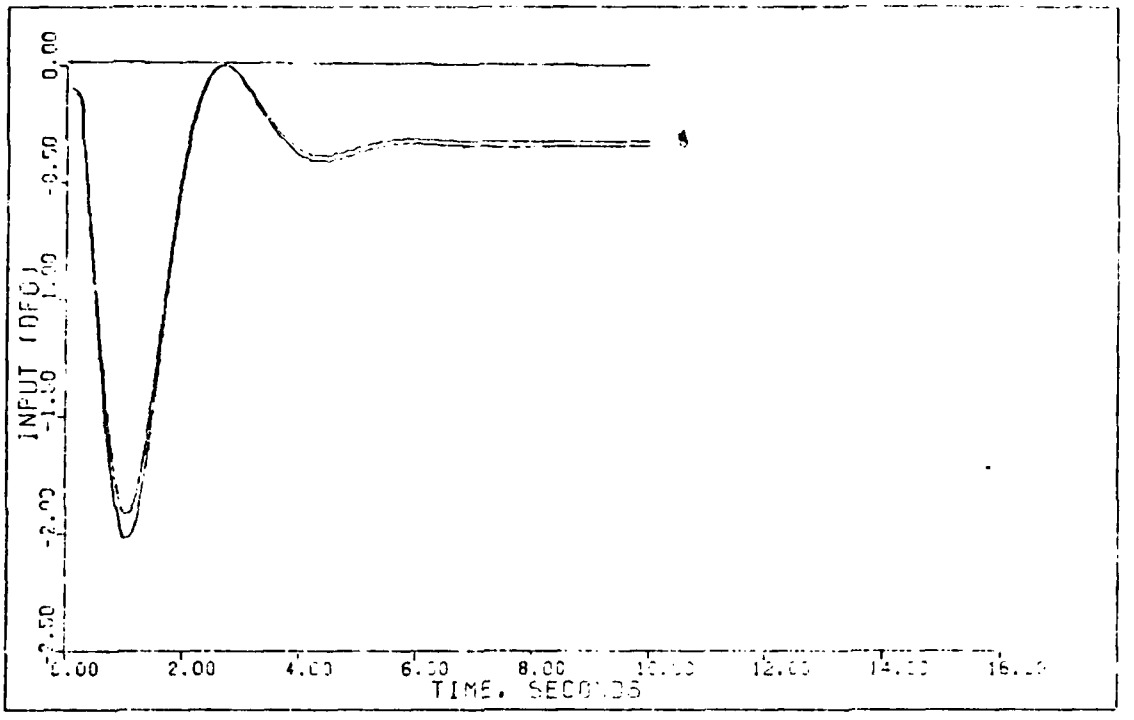

4=VELOCITY (U)

(e) n Output Response



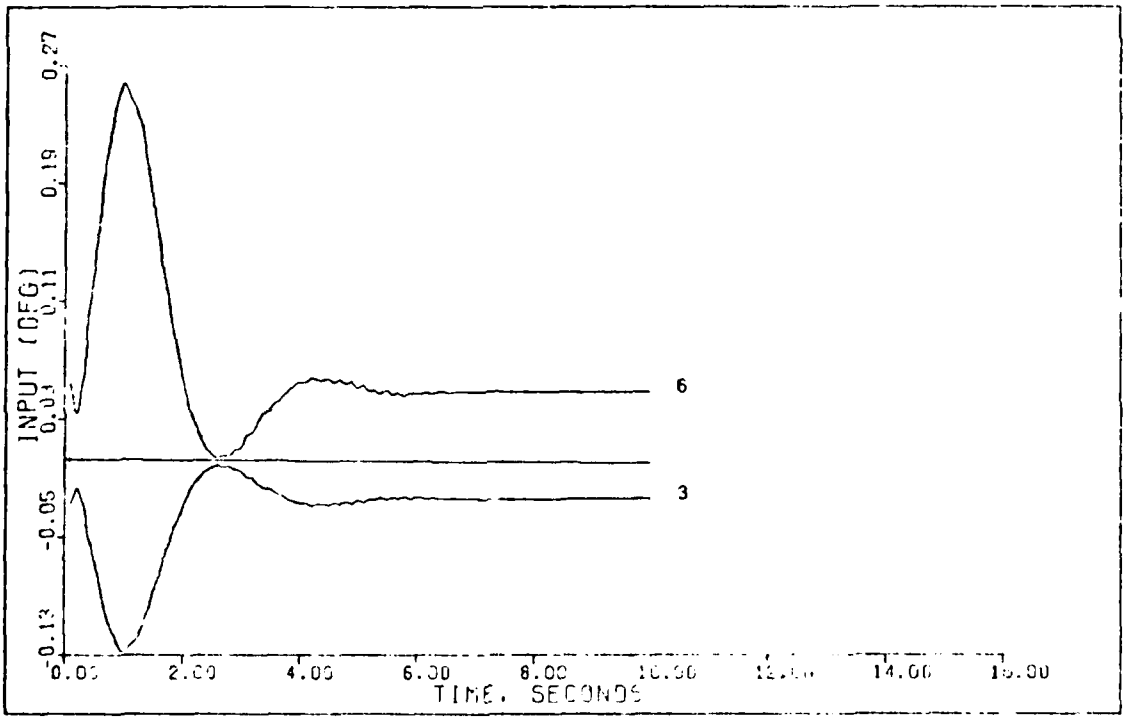

1=RIGHT TAIL ($\delta_{H_r}$); 2=LEFT TAIL ($\delta_{H_l}$)

(f) $\delta_{H_r}$, $\delta_{H_l}$ Control Input Response




4=RIGHT AILERON ($\delta_{a_r}$): 5=LEFT AILERON ($\delta_{a_l}$)

(g) $\delta_{a_r}$, $\delta_{a_l}$ Control Input Response




3=RUDDER ($\delta_r$): 6=SPOILER-FLAP ($\delta_{sf}$)

(h) $\delta_r$, $\delta_{s.f}$ Control Input Response

The command input vector for the coordinated turn maneuver is:

$$\underline{v} = \begin{bmatrix} 10,0.01023 \\ 0,0 \\ 0,0 \\ 0,0 \\ 0,0 \\ 1,0.0183 \end{bmatrix}$$

Blakelock (Ref 20) states that to achieve coordination for a given bank angle, there is one constant value of yaw rate, r, and is computed as:

$$r = \frac{g}{V_T} \sin \phi = 0.0254 \text{ rad/sec} \qquad (5\text{-}13)$$

Figure 5-1(c) shows the response of the state r for the maneuver. Note that the final value of r=0.0312 rad/sec is approximately 23% greater than that needed in Eq (5-13). This can be attributed to the fact that the aircraft is no longer in straight and level flight.

Figures 5-1(b), (d), and (e) illustrate the responses of the output variables. Figure 5-1(b) shows $\phi$ reaching its final value of $\phi$=0.524 rad=30° in approximately 2.5 sec with no overshoot, $\psi$ reaching its final value of $\psi$=0.01023 rad with a slope $\dot{\psi}$=0.001023 rad/sec, and $\beta$=0. Figure 5-1(d) shows the response of $\theta$ and $\alpha$. Note that the magnitude of these responses is on the order of $10^{-14}$ rad, thus $\theta=\alpha=0$. Similarly, Figure 5-1(e) shows the response u=0.

Figures 5-1(f), (g), and (h) illustrate the control surface deflections. Figure 5-1(f) shows the left and right horizontal tail moving in opposite directions, as expected, with a peak value of ±5° and a final value of ±1.6°. Figure 5-1(g) shows the left and right ailerons, by sign convention, moving in opposite directions with a peak value of -2.4° for $\delta_{a_r}$ and -2.3° for $\delta_{a_l}$ and a final value of -0.80° for $\delta_{a_r}$ and -0.75° for $\delta_{a_l}$. Figure 5-1(h) shows the responses of the rudder and the spoiler-flap. The peak value of rudder is -0.15° with a final value of -0.05°. The peak value of the spoiler-flap is 0.30° with a final value of 0.10°.

The results of the 30° coordinated turn for Configuration 1 are summarized in Table 5-1.

Control Surface Failures. The controller of Configuration 1 is used to examine the system response to control surface failures. Figure 5-2 is the command vector, $\underline{v}$, where $\theta$ and $\alpha$ are in radians and the scaling factor $c_o$ is the same as in Eq (5-12). Using Eq (5-12), the scaled commands for the 10° pitch-up maneuver are:

$$\theta' = c_o\theta = 0.0061 \text{ rad}$$

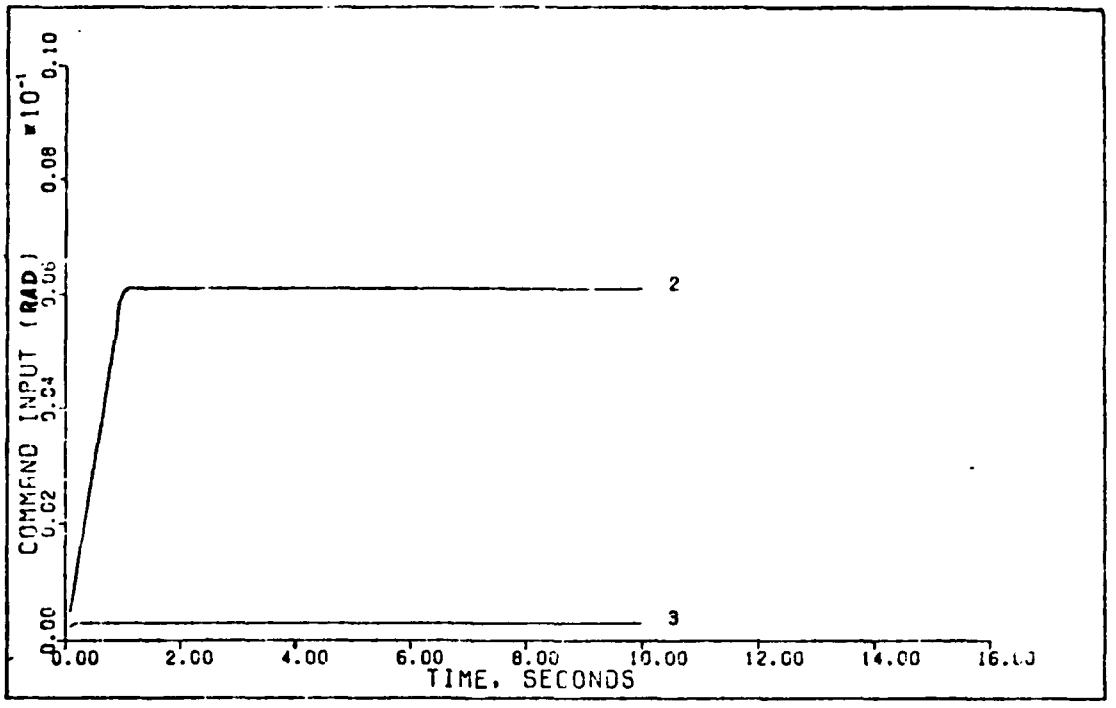
$$\alpha' = c_o\alpha = 0.0003 \text{ rad}$$

Table 5-1

Configuration 1 Results

| INPUT/ OUTPUT | $T_p$ (sec) | $T_s$ (sec) | $M_p$ | FINAL VALUE |
|---|---|---|---|---|
| $\psi$ * | 10 | - | 0.01023 | 0.01023 |
| $\theta$ | - | - | 0 | 0 |
| $\alpha$ | - | - | 0 | 0 |
| u ** | - | - | 0 | 0 |
| $\beta$ | - | - | 0 | 0 |
| $\phi$ | 3.6 | 3.0 | 0.524 | 0.524 |
| $\delta_{H_r}$ *** | 1 | 5.8 | -4.4 | -0.7 |
| $\delta_{H_l}$ | 1 | 5.8 | 4.4 | 0.7 |
| $\delta_r$ | 1 | 6.1 | -0.13 | -0.024 |
| $\delta_{a_r}$ | 1 | 5.8 | -1.9 | -0.3 |
| $\delta_{a_l}$ | 1 | 5.8 | -2.0 | -0.35 |
| $\delta_{sf}$ | 1 | 6.1 | 0.19 | 0.05 |

* - rad
** - ft/sec
*** - deg




2=PITCH ANGLE ($\theta$); 3=ANGLE OF ATTACK ($\alpha$)

Figure 5-2. Command Input for 10° Pitch-Up

Thus, the command input vector is:

$$\underline{v} = \begin{bmatrix} 0,0 \\ 1,0.0061 \\ 0.1,0.0003 \\ 0,0 \\ 0,0 \\ 0,0 \end{bmatrix}$$

Figures 5-3, 5-4, and 5-5 illustrate the system responses with failed rudder, ailerons, and spoiler-flap respectively. Figures B-7 through B-10 illustrate system response for system without failures. In each case, the controller performance is unsatisfactory in commanding $\theta$ and $\alpha$ to the desired steady-state values. Therefore, a separate controller is designed for the system with a failed control surface.

Configuration 2. This flight regime is identical to that of Configuration 1 with the exception that control limits are placed on the rudder. The maximum and minimum allowable deflections for the rudder are set at 0°. This effectively yields an inoperative control surface.

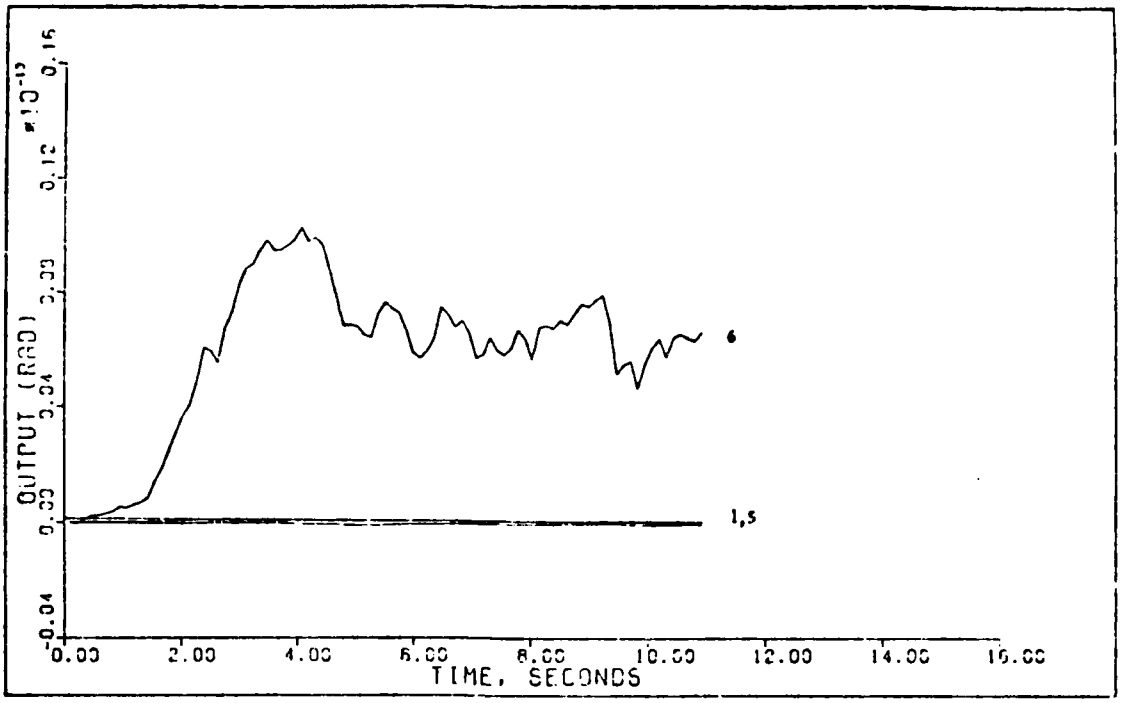
The design procedure yields a controller characterized by the parameter values:

$$T = 0.05 \text{ sec } (f = 20 \text{ hz}) \tag{5-14}$$

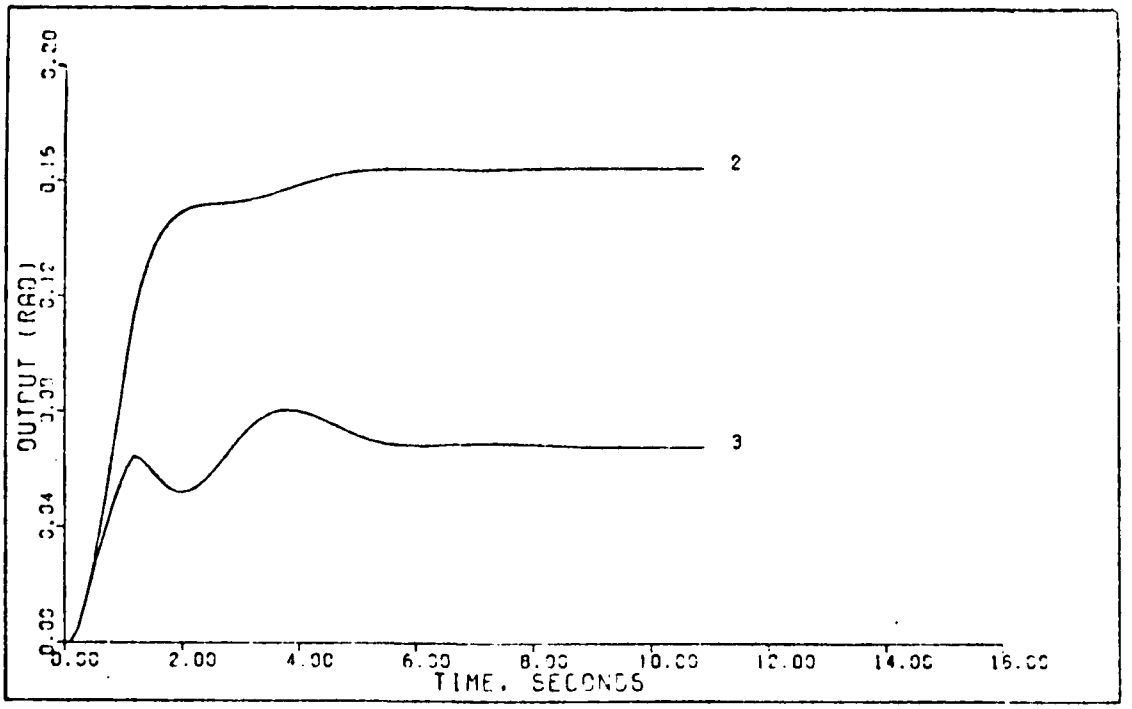
$$\alpha = 0.5 \tag{5-15}$$

$$\varepsilon = 1.0 \tag{5-16}$$

$$\underline{\Sigma} = \text{diag}\{0.08, 0.8, 3.75, 0.1, 0.1, 0.75\} \tag{5-17}$$

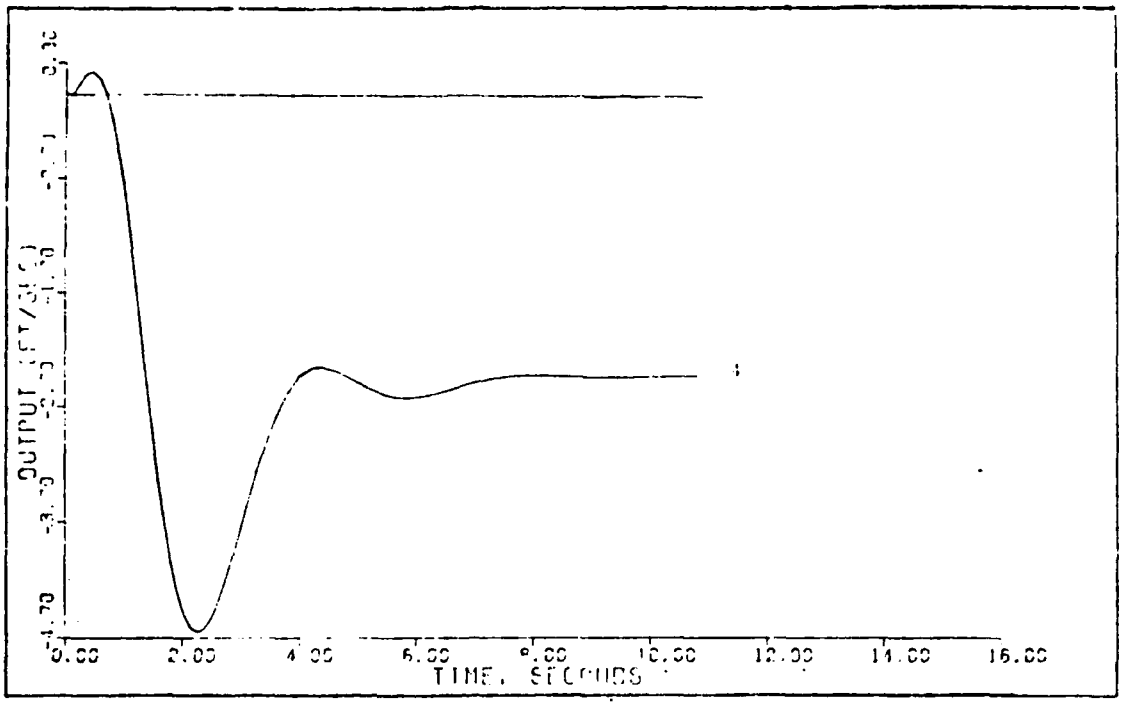



1=YAW ANGLE ($\psi$); 5=SIDESLIP ANGLE ($\beta$); 6=ROLL ANGLE ($\phi$)
(a) $\psi$, $\beta$, $\phi$ Output Response



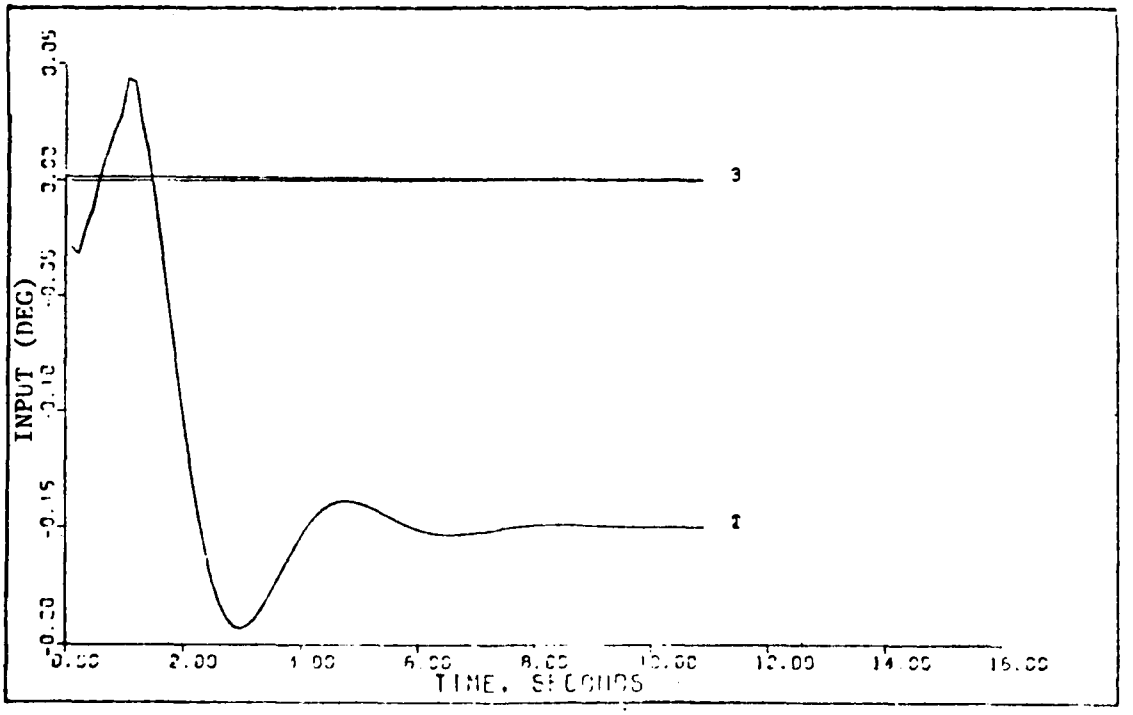

2=PITCH ANGLE ($\theta$); 3=ANGLE OF ATTACK ($\alpha$)
(b) $\theta$, $\alpha$ Output Response

Figure 5-3. Configuration 2, 10° Pitch-Up Commanded



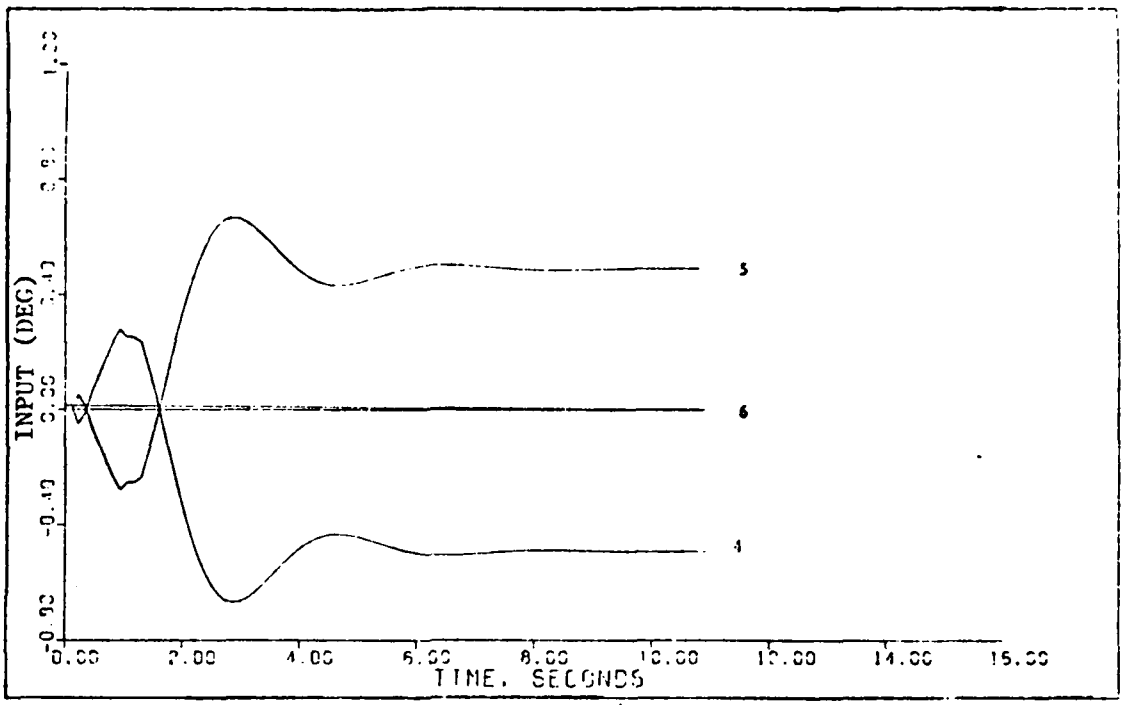

1-VELOCITY (U)

(c) u Output Response



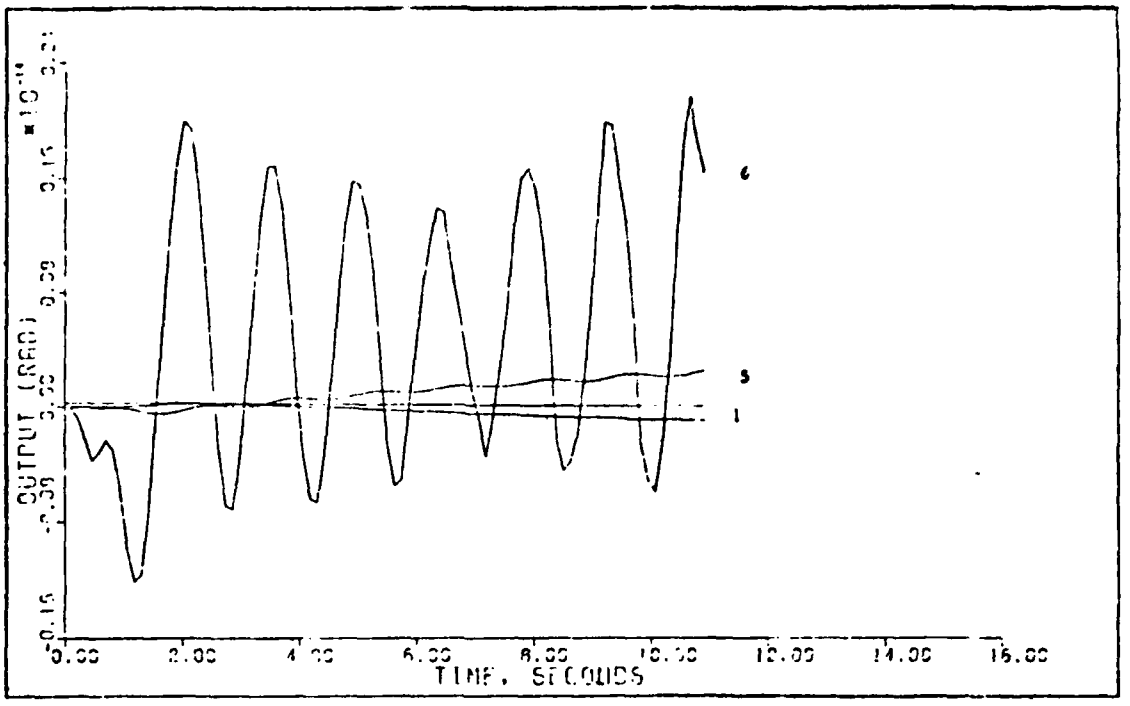

1-RIGHT TAIL ($\delta_{H_r}$); 2-LEFT TAIL ($\delta_{H_l}$); 3-RUDDER ($\delta_r$)

(d) $\delta_{H_r}$, $\delta_{H_l}$, $\delta_r$ Control Input Response



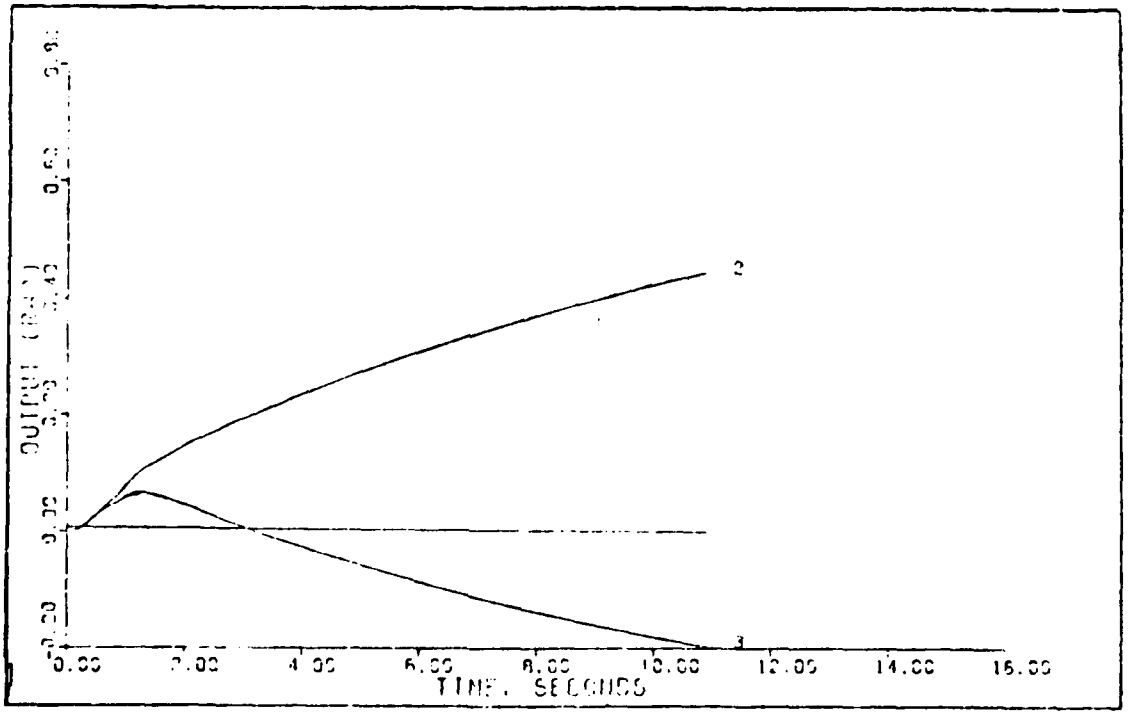

4=RIGHT AILERON ($\delta_{a_r}$);5=LEFT AILERON ($\delta_{a_l}$);6=SPOILER-FLAP ($\delta_{sf}$)

(e) $\delta_{a_r}$, $\delta_{a_l}$, $\delta_{sf}$ Control Input Response




1-YAW ANGLE ($\psi$): 5-SIDESLIP ANGLE ($\beta$): 6-ROLL ANGLE ($\phi$)

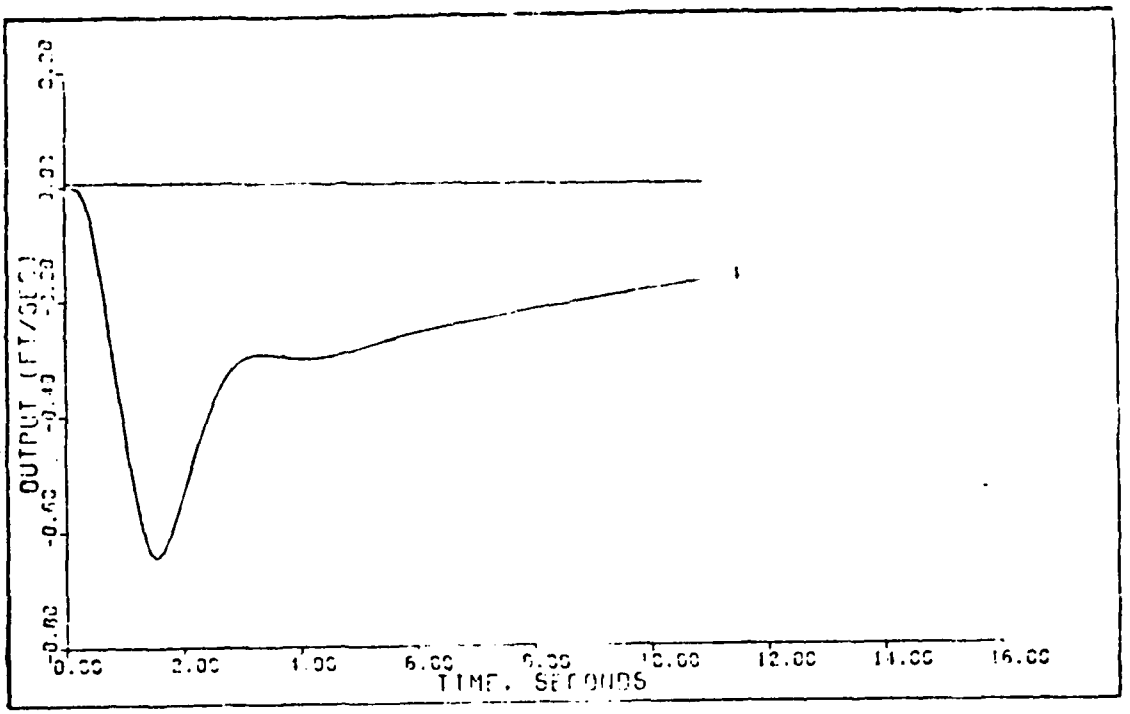
(a) $\psi$, $\beta$, $\phi$ Output Response




2-PITCH ANGLE ($\theta$): 3-ANGLE OF ATTACK ($\alpha$)

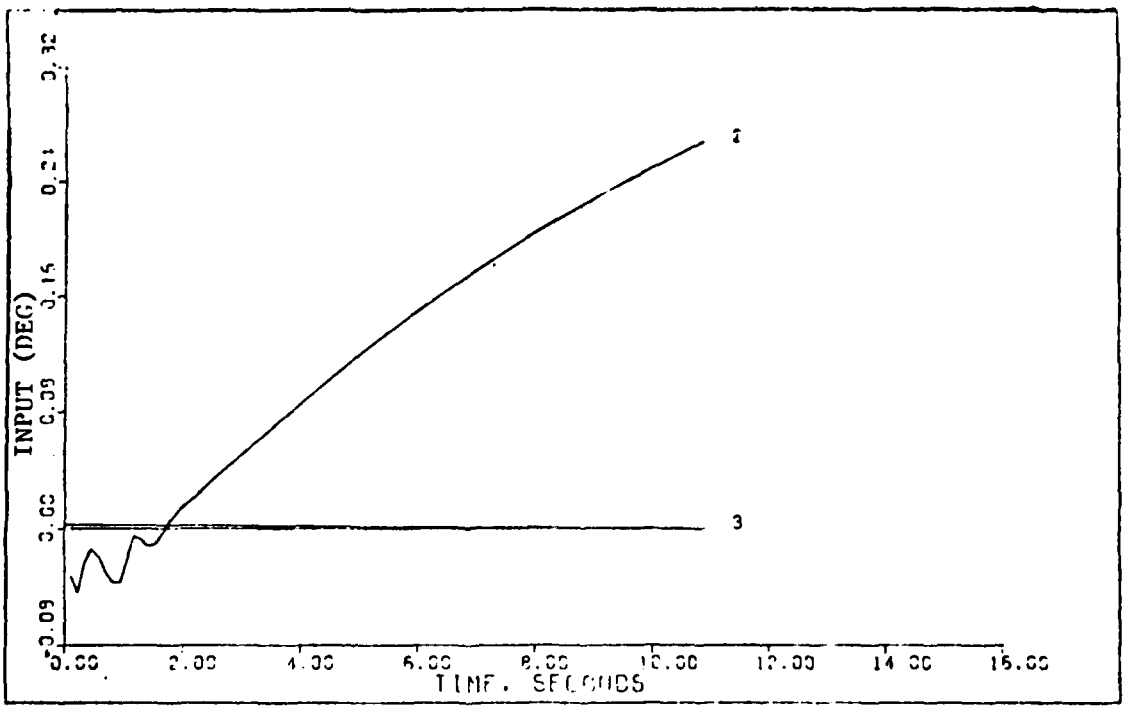
(b) $\theta$, $\alpha$ Output Response

Figure 5-4. Configuration 3, 10° Pitch-Up Commanded



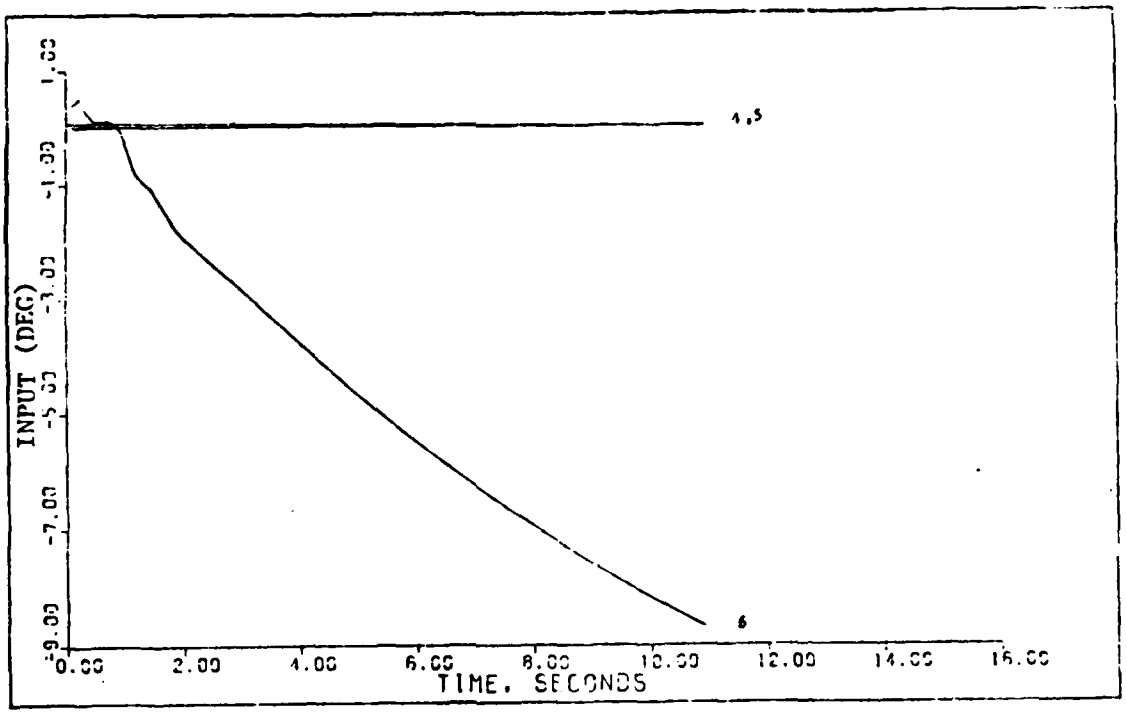

4=VELOCITY (U)

(c) u Output Response



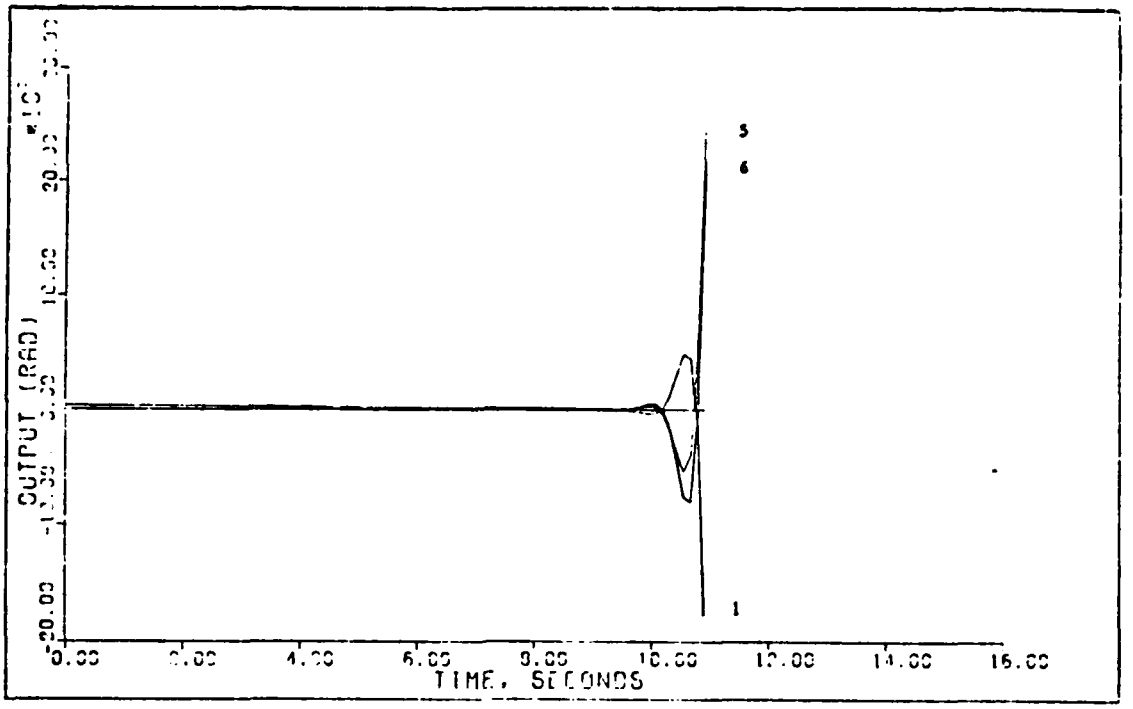

1=RIGHT TAIL ($\delta_{H_r}$): 2=LEFT TAIL ($\delta_{H_l}$): 3=RUDDER ($\delta_r$)

(d) $\delta_{H_r}$, $\delta_{H_l}$, $\delta_r$ Control Input Response



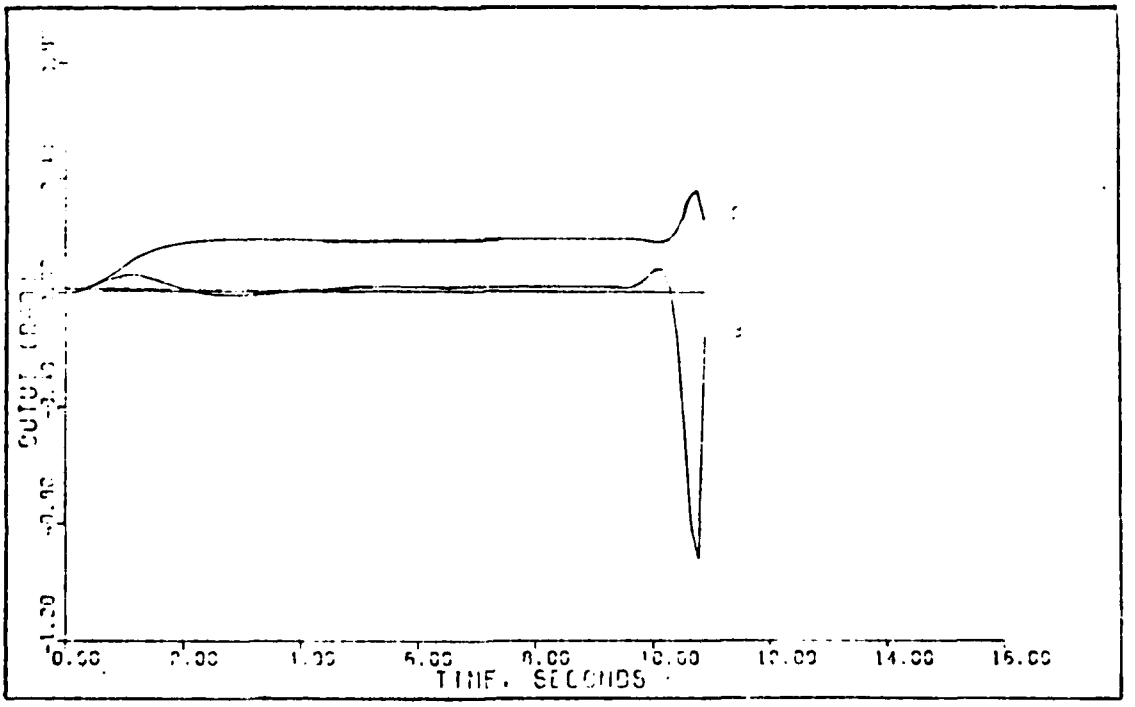

4=RIGHT AILERON ($\delta_{a_r}$);5=LEFT AILERON ($\delta_{a_l}$);6=SPOILER-FLAP ($\delta_{sf}$)

(e) $\delta_{a_r}$, $\delta_{a_l}$, $\delta_{sf}$ Control Input Response




1=YAW ANGLE ($\psi$); 5=SIDESLIP ANGLE ($\beta$); 6=ROLL ANGLE ($\phi$)

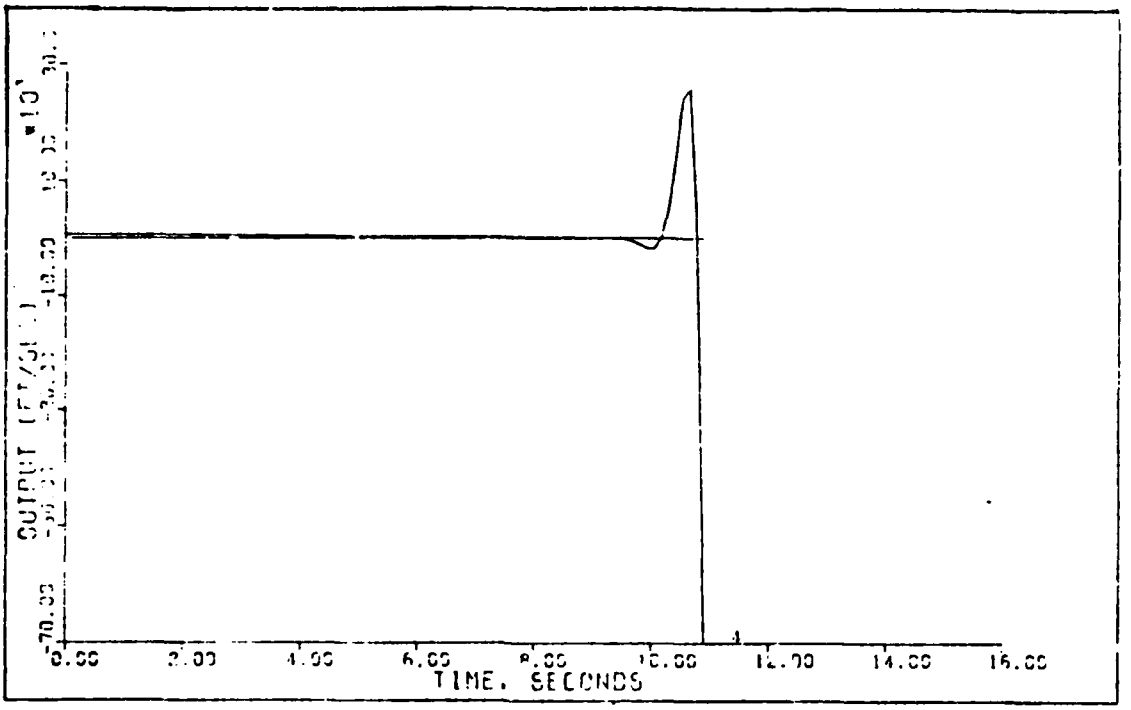
(a) $\psi$, $\beta$, $\phi$ Output Response




2-PITCH ANGLE ($\theta$); 3-ANGLE OF ATTACK ($\alpha$)

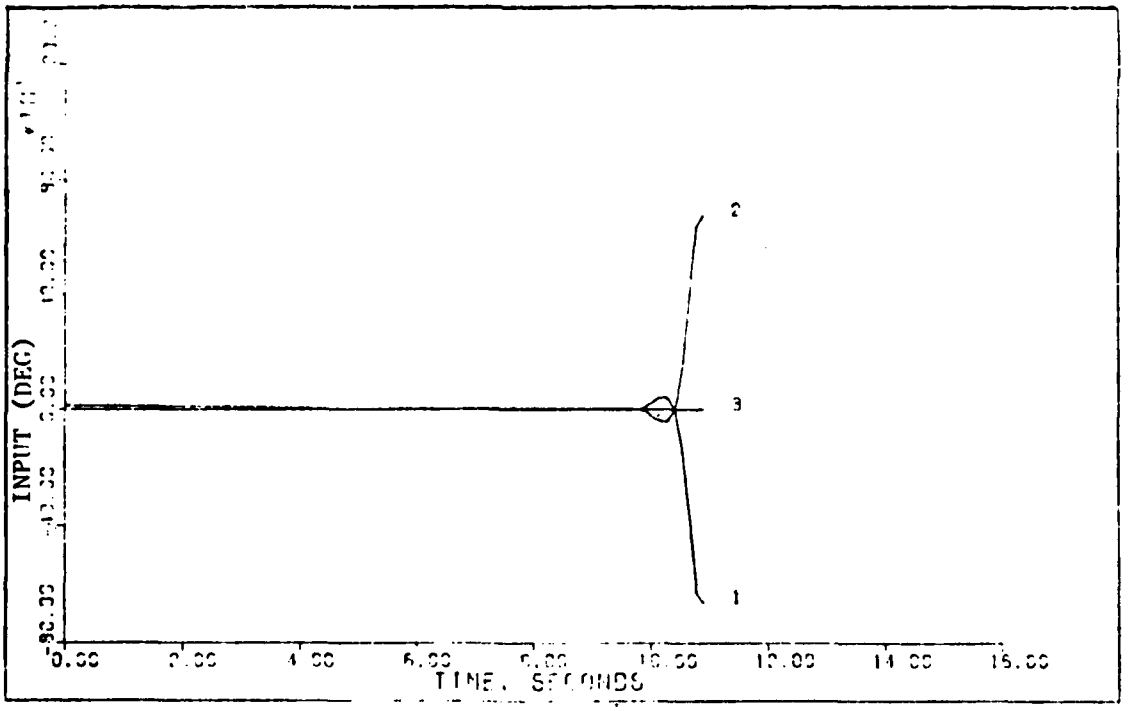
(b) $\theta$, $\alpha$ Output Response

Figure 5-5. Configuration 4, 10° Pitch-Up Commanded



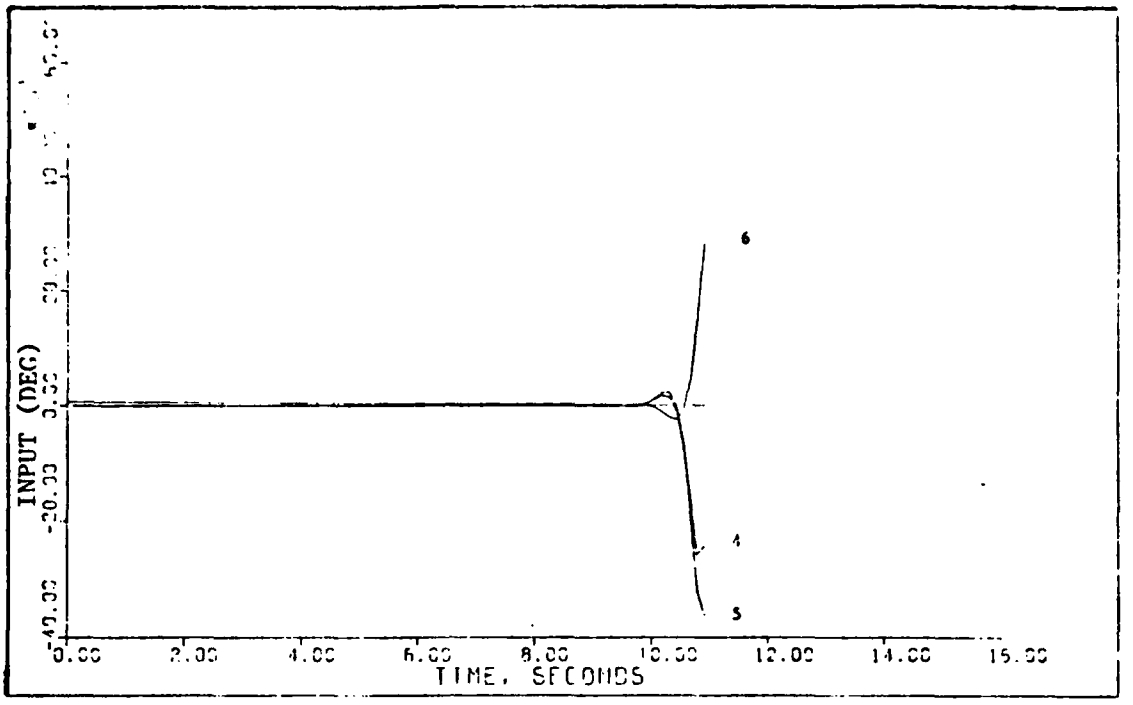

4-VELOCITY (U)

(c) u Output Response




1-RIGHT TAIL ($\delta_{H_r}$); 2-LEFT TAIL ($\delta_{H_l}$); 3-RUDDER ($\delta_r$)

(d) $\delta_{H_r}$, $\delta_{H_l}$, $\delta_r$ Control Input Response




4-RIGHT AILERON ($\delta_{a_r}$):5-LEFT AILERON ($\delta_{a_l}$):6=SPOILER-FLAP ($\delta_{sf}$)

(e) $\delta_{a_r}$, $\delta_{a_l}$, $\delta_{sf}$ Control Input Response

These parameter values yield the irregular plant control matrices, $\underline{K}_o$ and $K_1$, as:

$$\underline{K}_o = \begin{bmatrix} -.1[illegible]4E+01 & -.7090E+00 & -.2582E+01 & -.3813E-03 & -.1226E+02 & -.1483E+01 \\ .1[illegible]7E+01 & -.7090E+00 & -.2582E+01 & -.3813E-03 & .1230E+02 & .1488E+01 \\ -.[illegible]E+00 & .4595E-14 & 0. & -.3829E-17 & -.3554E+00 & -.3674E-01 \\ -.[illegible]E+00 & .3028E+01 & -.8554E+01 & -.2730E-02 & -.5537E+01 & -.1280E+00 \\ .8[illegible]E+00 & -.3028E+01 & .8554E+01 & .2730E-02 & -.5628E+01 & -.1581E+00 \\ .4[illegible]E+00 & .8340E+01 & .[illegible]E+02 & -.1341E-01 & .7156E+00 & .7698E-01 \end{bmatrix}$$

(5-18)

$$K_1 = \begin{bmatrix} -.[illegible]E+01 & -.1418E+01 & -.[illegible]E+01 & -.7626E-03 & -.2452E+02 & -.2967E+01 \\ .5[illegible]E+01 & -.1418E+01 & -.5168E+01 & -.7626E-03 & .2460E+02 & .2975E+01 \\ -.4[illegible]E+00 & .9[illegible]E-14 & 0. & -.7659E-17 & -.7108E+00 & -.7348E-01 \\ -.1[illegible]E+01 & .6055E+01 & -.1[illegible]E+02 & -.5461E-02 & -.1[illegible]E+02 & -.2560E+00 \\ -.1[illegible]E+01 & -.6055E+01 & .1[illegible]E+02 & .5461E-02 & -.1[illegible]E+02 & -.3163E+00 \\ .8[illegible]E+00 & .1655E+02 & .[illegible]E+02 & -.2663E-01 & .1431E+01 & .1480E+00 \end{bmatrix}$$

(5-19)

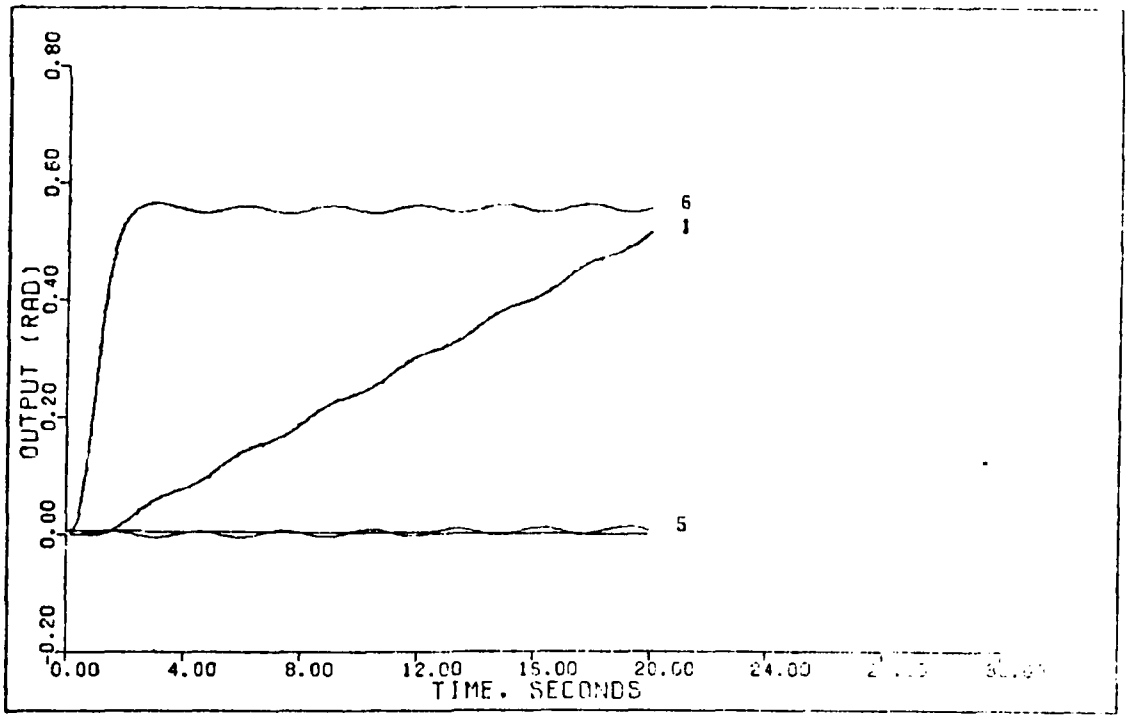
The measurement matrix for the irregular plant is:

$$\underline{M} = \begin{bmatrix} 0.05 & 0 & 0 \\ 0 & 0.02 & 0 \\ 0 & 0 & 0 \\ 0 & 0 & 0 \\ 0 & 0 & 0 \\ 0 & 0 & 0.02 \end{bmatrix} \qquad (5\text{-}20)$$

Figures 5-6(a), (b), and (c) illustrate the responses of the output variables. Figure 5-6(a) shows that the maneuver can still be performed without the rudder; however, some oscillation has crept into the response. The loss of the rudder has produced a more lightly damped system as evidenced in Figures 5-6(a) through (f). The oscillatory and divergent behavior of the ailerons and horizontal tail, shown

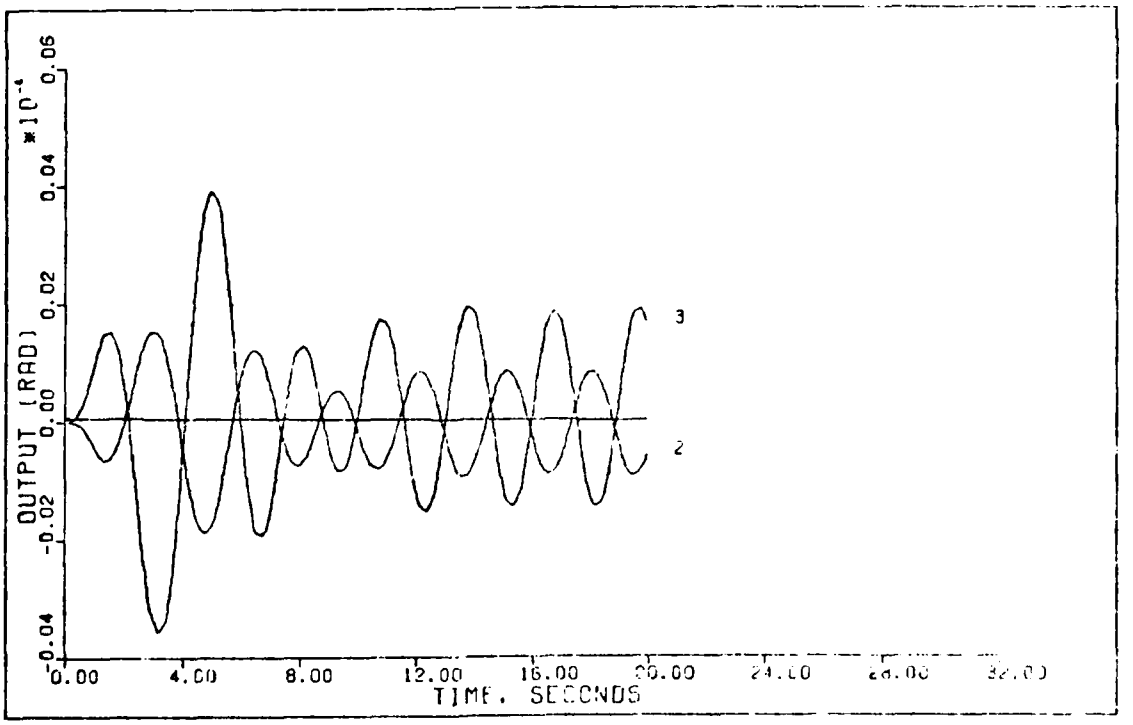


Reproduced from best available copy.




1=YAW ANGLE ($\psi$); 5=SIDESLIP ANGLE ($\beta$); 6=ROLL ANGLE ($\phi$)

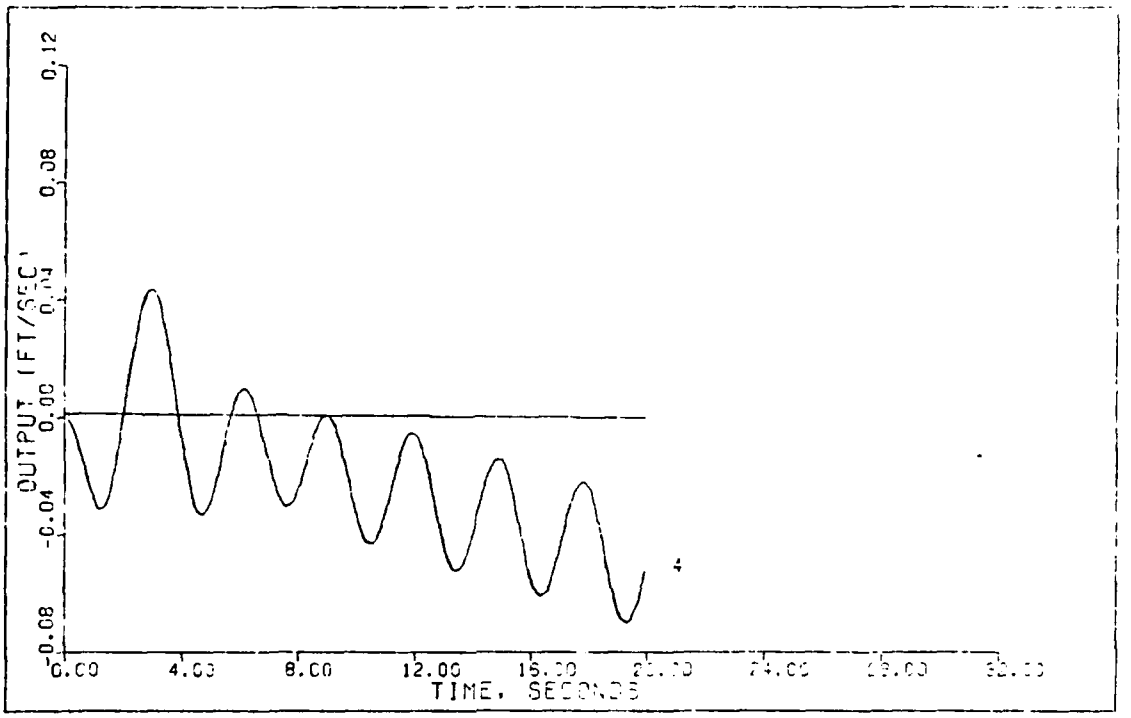
(a) $\psi$, $\beta$, $\phi$ Output Response




2=PITCH ANGLE ($\theta$); 3=ANGLE OF ATTACK ($\alpha$)

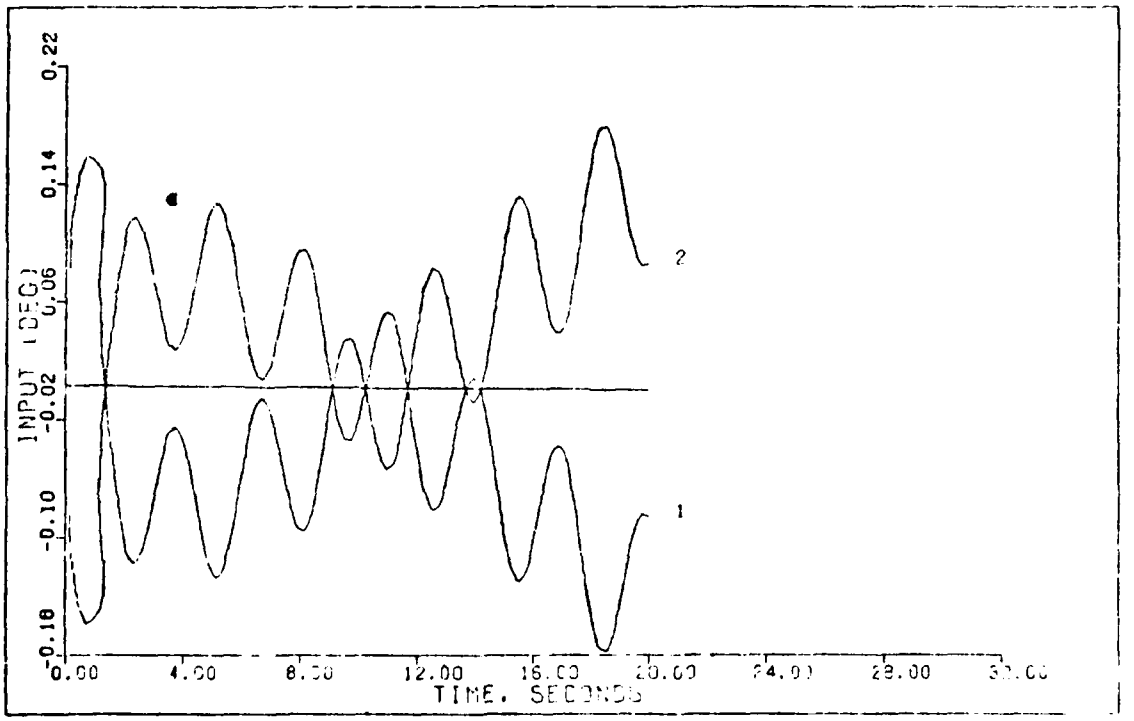
(b) $\theta$, $\alpha$ Output Response

Figure 5-6. Configuration 2, 30° Coordinated Turn Commanded



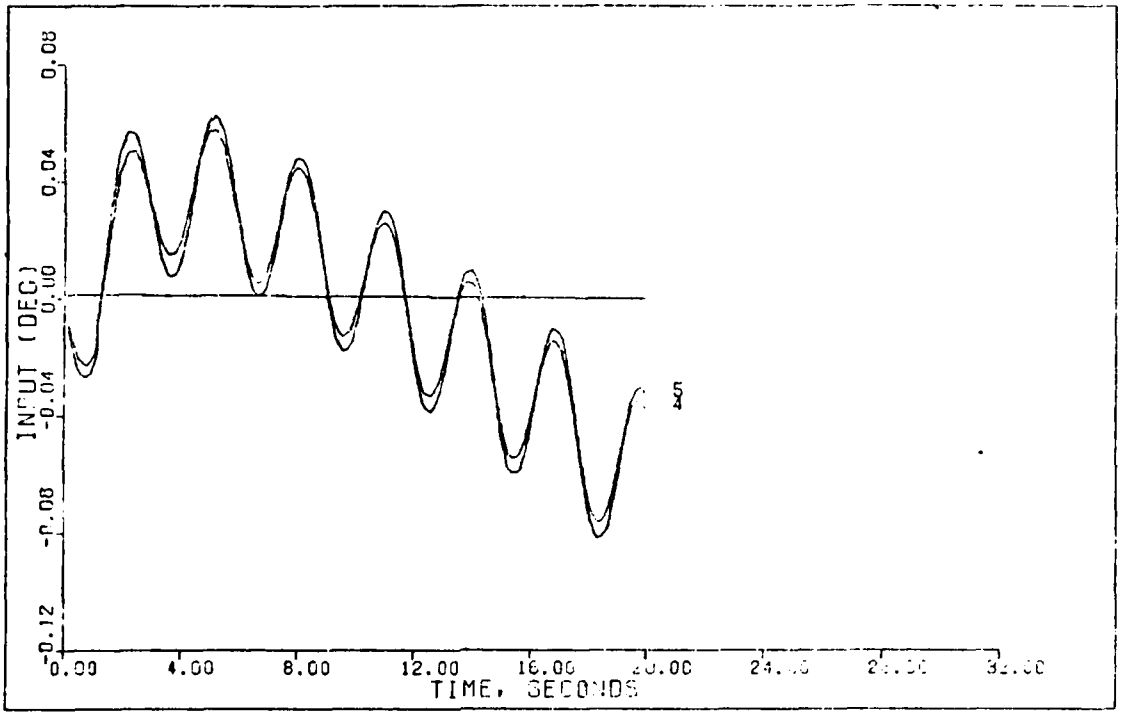

4=VELOCITY (U)

(c) u Output Response



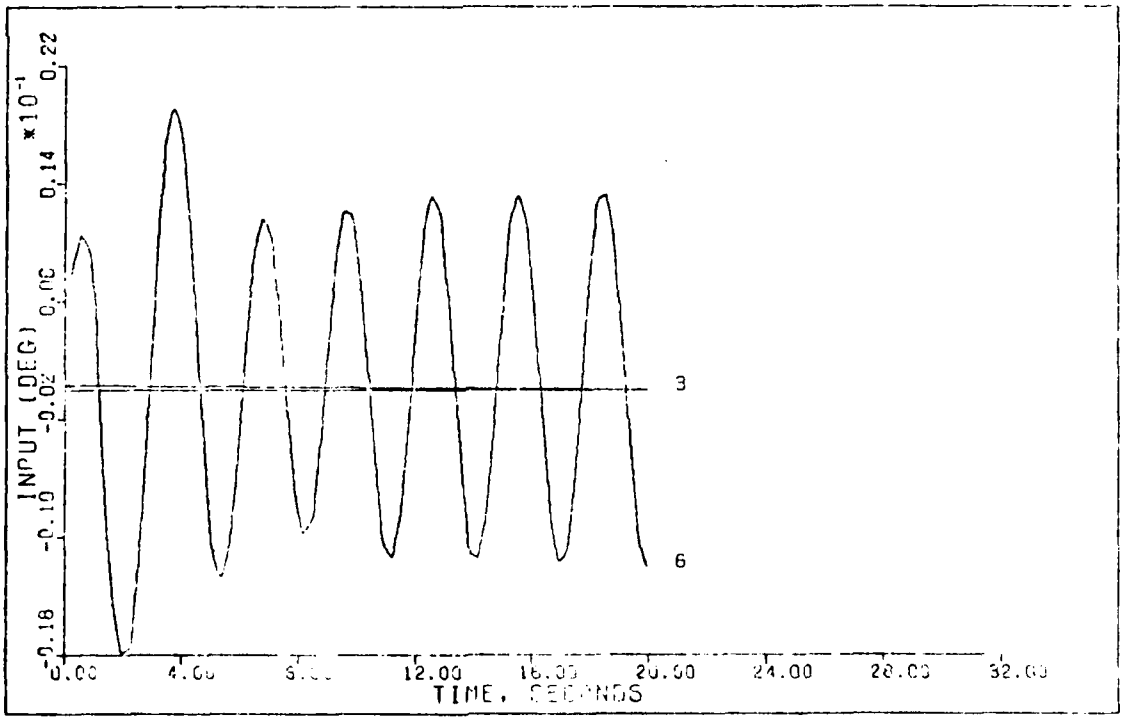

1=RIGHT TAIL ($\delta_{H_r}$): 2=LEFT TAIL ($\delta_{H_l}$)

(d) $\delta_{H_r}$, $\delta_{H_l}$ Control Input Response




4=RIGHT AILERON ($\delta_{a_r}$); 5=LEFT AILERON ($\delta_{a_l}$)

(e) $\delta_{a_r}$, $\delta_{a_l}$ Control Input Response




3=RUDDER ($\delta_r$); 6=SPOILER-FLAP ($\delta_{sf}$)

(f) $\delta_r$, $\delta_{sf}$ Control Input Response

in Figures 5-6(d) and (e), illustrate how the differential surfaces attempt to "fill in" for the absence of the rudder. The oscillatory and divergent behavior of the spoiler-flap, Figure 5-6(f), illustrates the controller's attempt to maintain $\theta = \alpha = 0$ without the aid of the ailerons and horizontal tail.

The results of the maneuver for Configuration 2 are summarized in Table 5-2.

Configuration 3. This flight regime is identical to Configuration 1 with the exception that control limits are placed on the ailerons. Initially, only one aileron is failed; however, the remaining aileron continues to operate as if both ailerons are present. This produces unsatisfactory results in both the longitudinal and lateral-directional modes. If further modelling of the dynamics of the aileron is developed to account for this phenomena, the problem can be avoided. As a result, it is assumed that an aileron failure implies both left and right ailerons become inoperative. The control limitations placed on the ailerons are the same as those placed on the rudder.

The design procedure yields a controller characterized by the parameter values:

$$T = 0.05 \text{ sec } (f = 20 \text{ hz}) \tag{5-21}$$

$$\varkappa = 1.0 \tag{5-22}$$

$$\varepsilon = 1.0 \tag{5-23}$$

Table 5-2

Configuration 2 Results

| INPUT/ OUTPUT | $T_p$ (sec) | $T_s$ (sec) | $M_p$ | FINAL VALUE |
|---|---|---|---|---|
| $\psi$ * | 10 | - | 0.50 | 0.50 |
| $\theta$ | - | - | 0 | 0 |
| $\alpha$ | - | - | 0 | 0 |
| u ** | - | - | $\infty$ | $\infty$ |
| $\beta$ | 1.5 | - | 0.01 | 0.01 |
| $\phi$ | 2.8 | 2.0 | 0.5 | 0.524 |
| $\delta_{H_r}$ *** | - | - | $\infty$ | $\infty$ |
| $\delta_{H_l}$ | - | - | $\infty$ | $\infty$ |
| $\delta_r$ | - | - | 0 | 0 |
| $\delta_{a_r}$ | - | - | $\infty$ | $\infty$ |
| $\delta_{a_l}$ | - | - | $\infty$ | $\infty$ |
| $\delta_{sf}$ | - | - | $\infty$ | $\infty$ |

* - rad
** - ft/sec
*** - deg

$$\underline{\Sigma} = \text{diag}\{0.05, 1, 0.01, 0.1, 0.1, 0.5\} \qquad (5\text{-}24)$$

These parameter values yield the irregular plant control matrices, $\underline{K}_o$ and $\underline{K}_1$, as:

$\underline{K}_o = K_1 =$

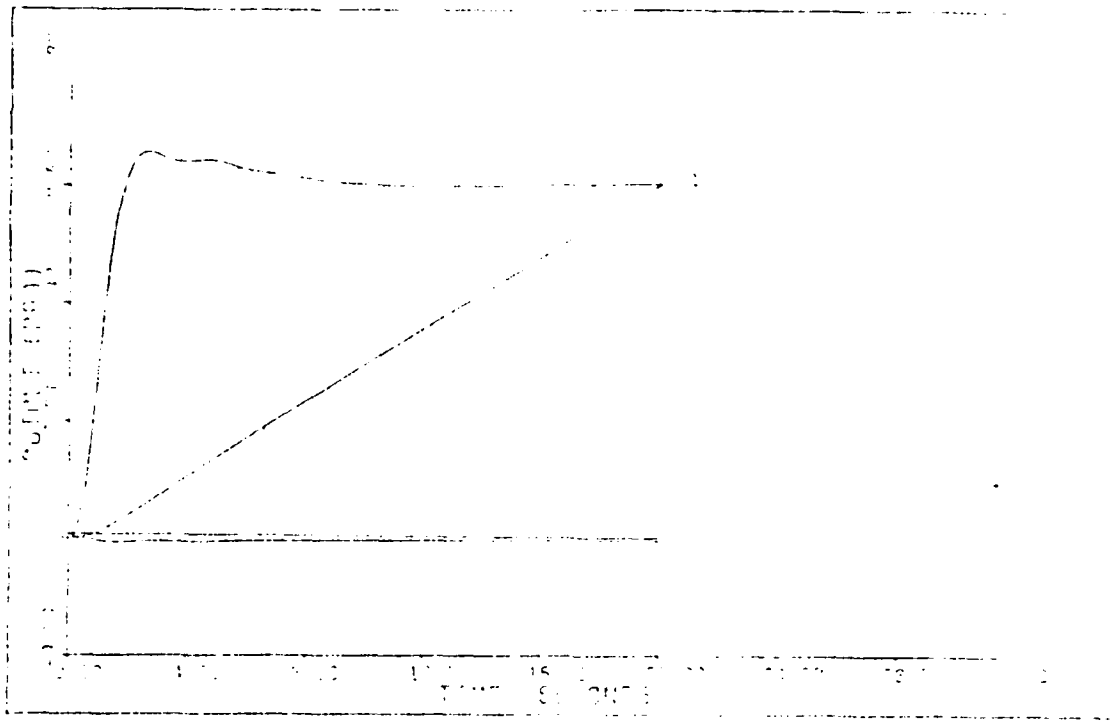
$$\begin{bmatrix}
-.5942E+01 & -.3545E+01 & -.1377E-01 & -.7e2eE-03 & -.245eE+02 & -.1[illegible]E+01 \\
.5e1eE+01 & -.3545E+01 & -.1377E-01 & -.762eE-03 & .2460E+02 & .1[illegible]E+01 \\
-.6414E+00 & .2298E-13 & 0. & -.7659E-17 & -.7109E+00 & -.4[illegible]E-01 \\
-.2[illegible]E+01 & .1514E+02 & -.456eE-01 & -.5[illegible]E-02 & -.11e7E+01 & -.1[illegible]E+01 \\
-.27e1E+01 & -.1514E+02 & .4562E-01 & .5461E-02 & -.11e6E+01 & -.2[illegible]E+01 \\
.1292E+01 & .4170E+02 & .1620E+00 & -.2683E-01 & .1431E+01 & .9[illegible]E-01
\end{bmatrix}$$

(5-25)

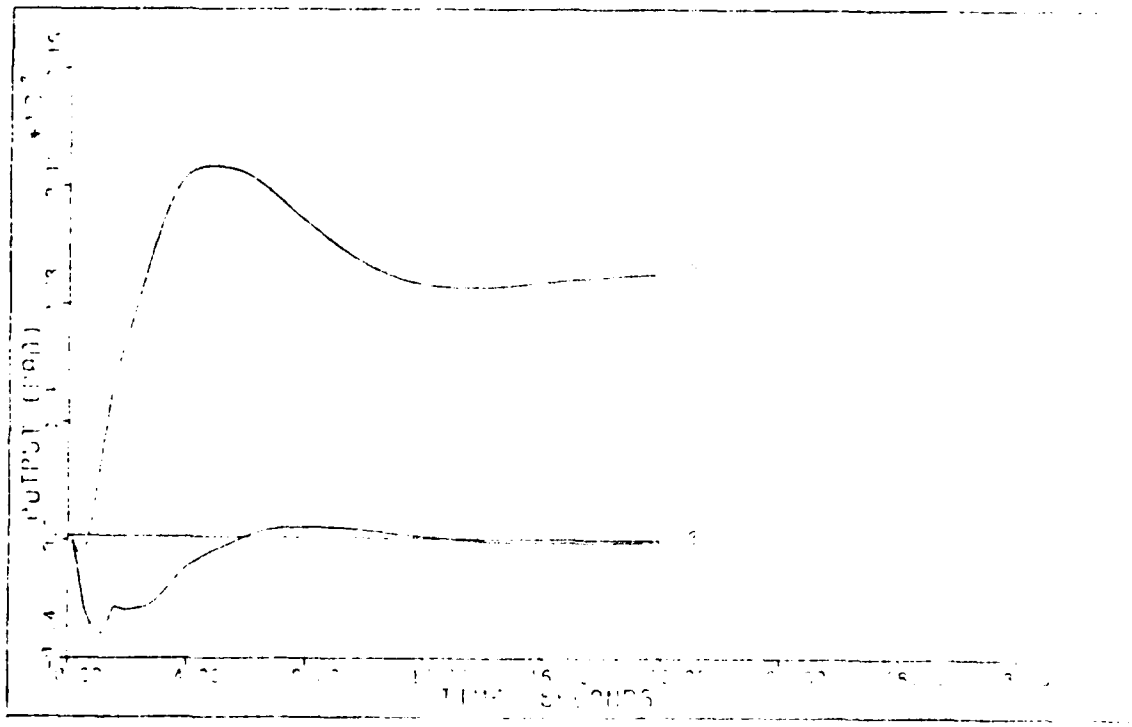
The measurement matrix for the irregular plant is:

$$\underline{M} = \begin{bmatrix}
0.02 & 0 & 0 \\
0 & 0.01 & 0 \\
0 & 0 & 0 \\
0 & 0 & 0 \\
0 & 0 & 0 \\
0 & 0 & 0.02
\end{bmatrix} \qquad (5\text{-}26)$$

Figures 5-7(a), (b), and (c) illustrate the responses of the output variables. Figure 5-7(a) shows that the coordinated turn maneuver can still be performed without the ailerons; however, the performance of the system is degraded somewhat. The final value of $\phi$=34.4°=0.60 rad indicates that without the ailerons, the controller is unable to stop the aircraft from rolling as quickly. Figures 5-7(b) shows the importance of the ailerons in controlling the longitudinal variables, that is, without the ailerons the controller



(a) $\psi$, $\beta$, $\phi$ Output Response

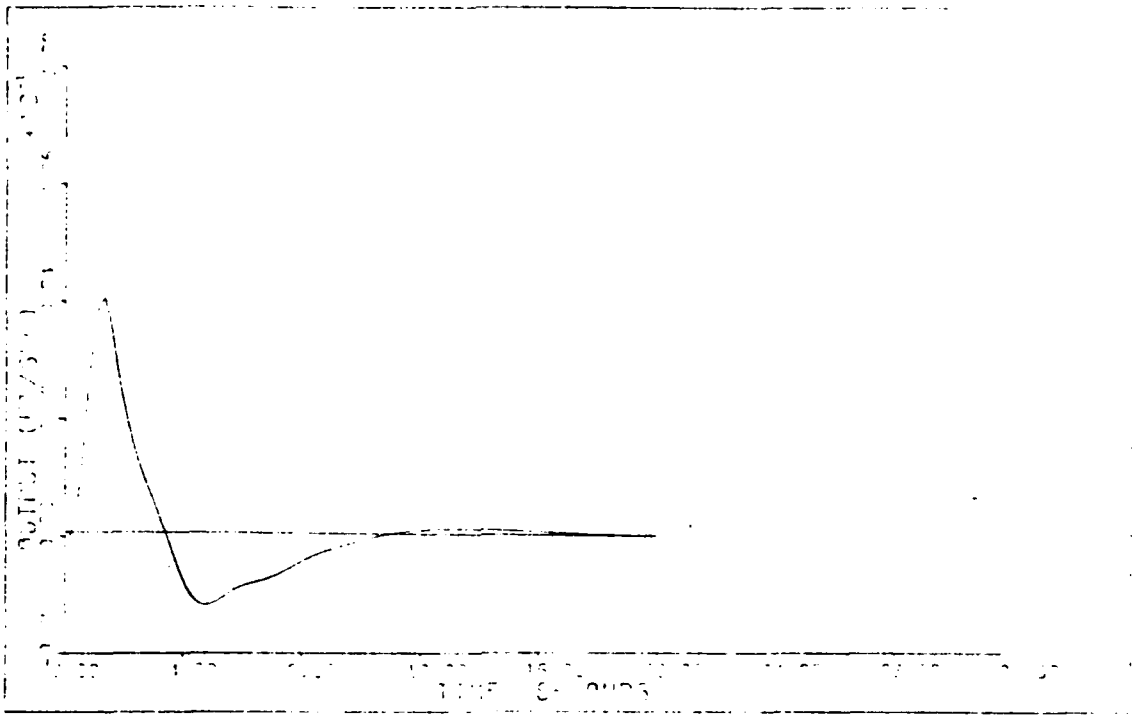


(b) $\theta$, $\alpha$ Output Response

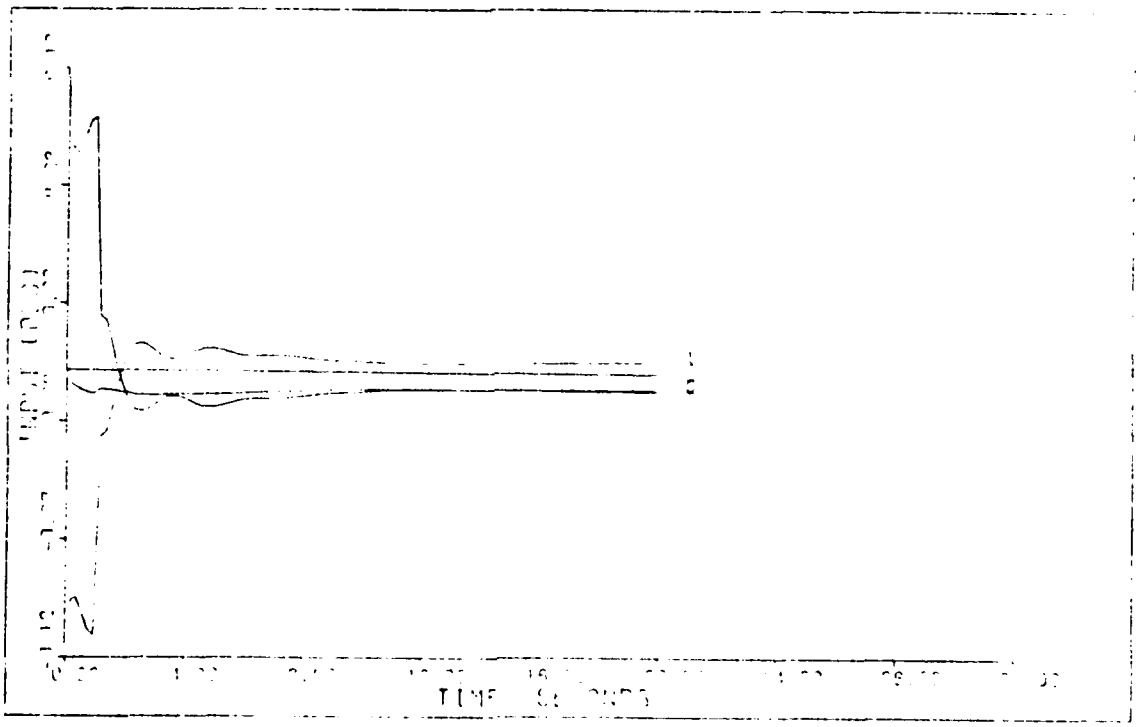
Figure 5-7. Configuration 3, 30° Coordinated Turn Commanded



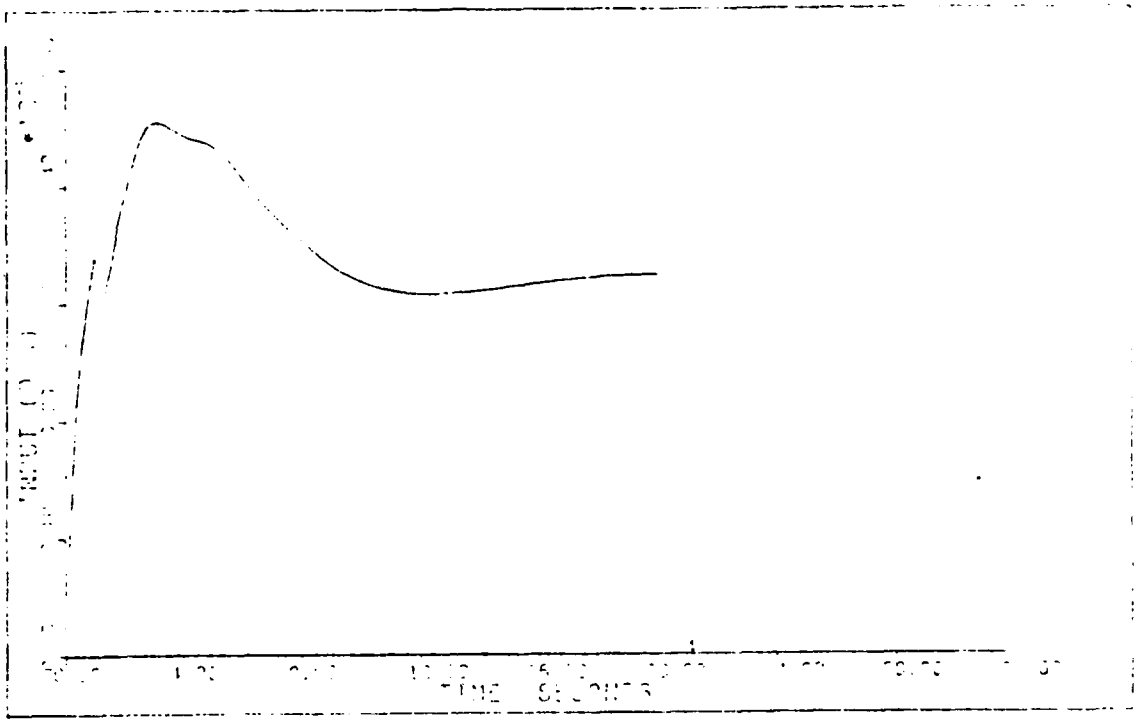
Copy available to DTIC does not permit fully legible reproduction



(c) u Output Response



(d) $\delta_{H_r}$, $\delta_{H_l}$, $\delta_r$ Control Input Response



(e) $\delta_{a_r}$, $\delta_{a_l}$, $\delta_{sf}$ Control Input Response

Copy available to DTIC does not

is unable to command $\alpha=0$ . Figures 5-7(d) and (e) illustrate the control surface deflections.

The results of the coordinated turn maneuver for Configuration 3 are summarized in Table 5-3.

Configuration 4. This flight regime is identical to Configuration 1 with the exception that control limits are placed on the spoiler-flap. The control limitations placed on the spoiler-flap are the same as those placed on the rudder.

The design procedure yields a controller characterized by the parameter values:

$$T = 0.02 \text{ sec } (f \approx 50 \text{ hz}) \tag{5-27}$$

$$\alpha = 0.5 \tag{5-28}$$

$$\varepsilon = 1.0 \tag{5-29}$$

$$\Sigma = \text{diag}\{1.25, 0.8, 4.0, 0.1, 2.5, 0.75\} \tag{5-30}$$

These parameter values yield the irregular plant control matrices, $\underline{K}_0$ and $\underline{K}_1$, as:

$$\underline{K}_0 = \begin{bmatrix} -.6923E-02 & -.1773E+01 & -.2754E+01 & -.3813E-03 & -.3065E+03 & -.1403E+01 \\ .7020E+02 & -.1773E+01 & -.2754E+01 & -.3813E-03 & .3073E+03 & .1433E+01 \\ -.8013E+01 & .1149E-13 & 0. & -.3829E-17 & -.8885E+01 & -.3674E-01 \\ -.2794E+02 & .7569E+01 & -.9124E+01 & -.2730E-02 & -.1364E+03 & -.1261E+02 \\ -.3451E-12 & -.7569E+01 & .9124E+01 & .2730E-02 & -.1457E+03 & -.1531E+02 \\ .1614E+02 & .2095E+02 & .3240E+02 & -.1341E-01 & .1764E+03 & .3178E+02 \end{bmatrix} \tag{5-31}$$

Table 5-3

Configuration 3 Results

| INPUT/ OUTPUT | $T_p$ (sec) | $T_s$ (sec) | $M_p$ | FINAL VALUE |
|---|---|---|---|---|
| $\psi$ * | 20 | - | 0.60 | 0.60 |
| $\theta$ | 1 | 11 | -0.00032 | 0 |
| $\alpha$ | 4.4 | 19 | 0.00128 | 0.00084 |
| u ** | 1.75 | 10 | 0.004 | 0 |
| $\beta$ | - | - | 0 | 0 |
| $\phi$ | 3.8 | 8.0 | 0.712 | 0.60 |
| $\delta_{H_r}$ *** | 0.8 | 10.4 | -0.115 | 0.012 |
| $\delta_{H_l}$ | 0.8 | 10.4 | 0.115 | -0.012 |
| $\delta_r$ | 5.2 | 8.8 | -0.015 | -0.01 |
| $\delta_{a_r}$ | - | - | 0 | 0 |
| $\delta_{a_l}$ | - | - | 0 | 0 |
| $\delta_{sf}$ | 5.2 | 11.2 | 0.068 | 0.056 |

* - rad
** - ft/sec
*** - deg

$$\underline{K}_1 = \begin{bmatrix} -.1386E+03 & -.3515E+01 & -.5509E+01 & -.7626E-03 & -.6151E+03 & -.2907E+01 \\ .1404E+03 & -.3545E+01 & -.5509E+01 & -.7626E-03 & .6151E+03 & .2907E+01 \\ -.1604E+02 & .2298E-13 & 0. & -.7659E-17 & -.1777E+02 & -.7348E-01 \\ -.5589E+02 & .1514E+02 & -.1825E+02 & -.5461E-02 & -.2768E+03 & -.1260E+00 \\ -.6902E+02 & -.1514E+02 & .1825E+02 & .5461E-02 & -.2911E+03 & -.1363E+00 \\ .3229E+02 & .4170E+02 & .6480E+02 & -.2693E-01 & .3578E+02 & .1460E+00 \end{bmatrix}$$

(5-32)

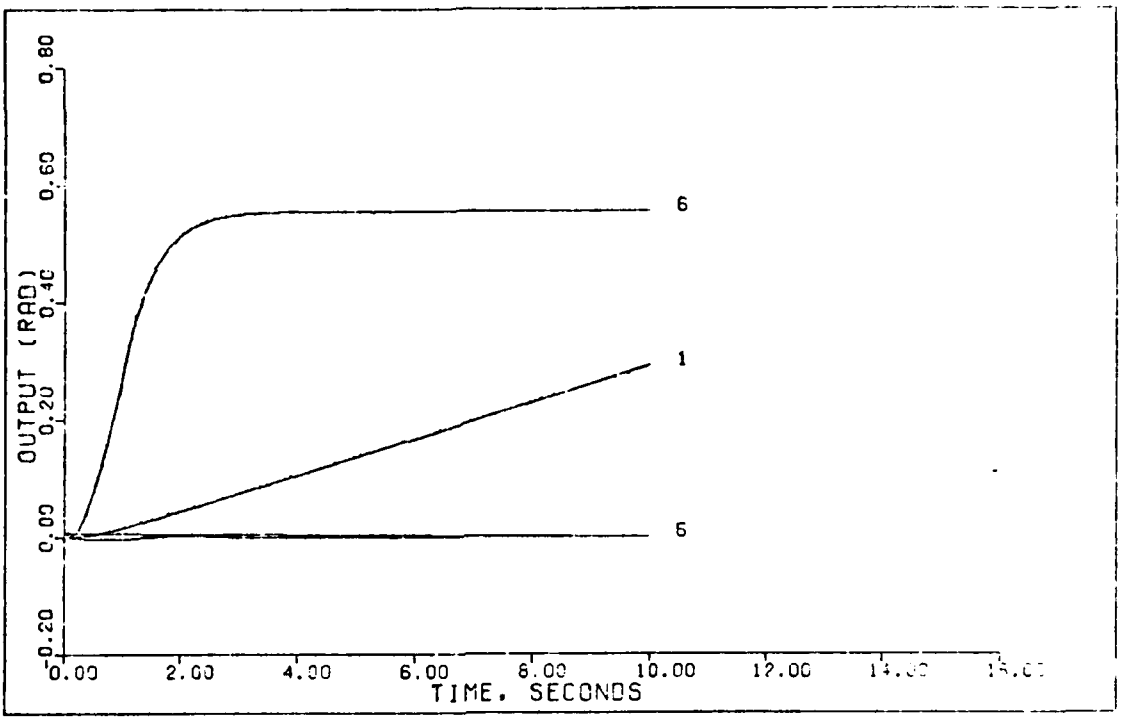
The measurement matrix for the irregular plant is:

$$\underline{M} = \begin{bmatrix} 0.02 & 0 & 0 \\ 0 & 0.008 & 0 \\ 0 & 0 & 0 \\ 0 & 0 & 0 \\ 0 & 0 & 0 \\ 0 & 0 & 0.02 \end{bmatrix} \qquad (5\text{-}33)$$

Figures 5-8(a), (b), and (c) illustrate the responses of the output variables. The responses for $\psi$, $\phi$, $\beta$, $\delta_{H_1}$, $\delta_r$, $\delta_{a_r}$, and $\delta_{a_l}$, (Figures 5-8(a), (d), and (e)), are identical to those of Figure 5-1 for Configuration 1. The importance of the spoiler-flap is seen in Figures 5-8(b) and (c) where the controller is unable to drive $\theta$, $\alpha$, and u to zero. Although these variables do not assume their commanded values, they do exhibit stable responses with final values of $\theta$=0.00085 rad, $\alpha$=-0.0019 rad, and u=0.30 ft/sec.

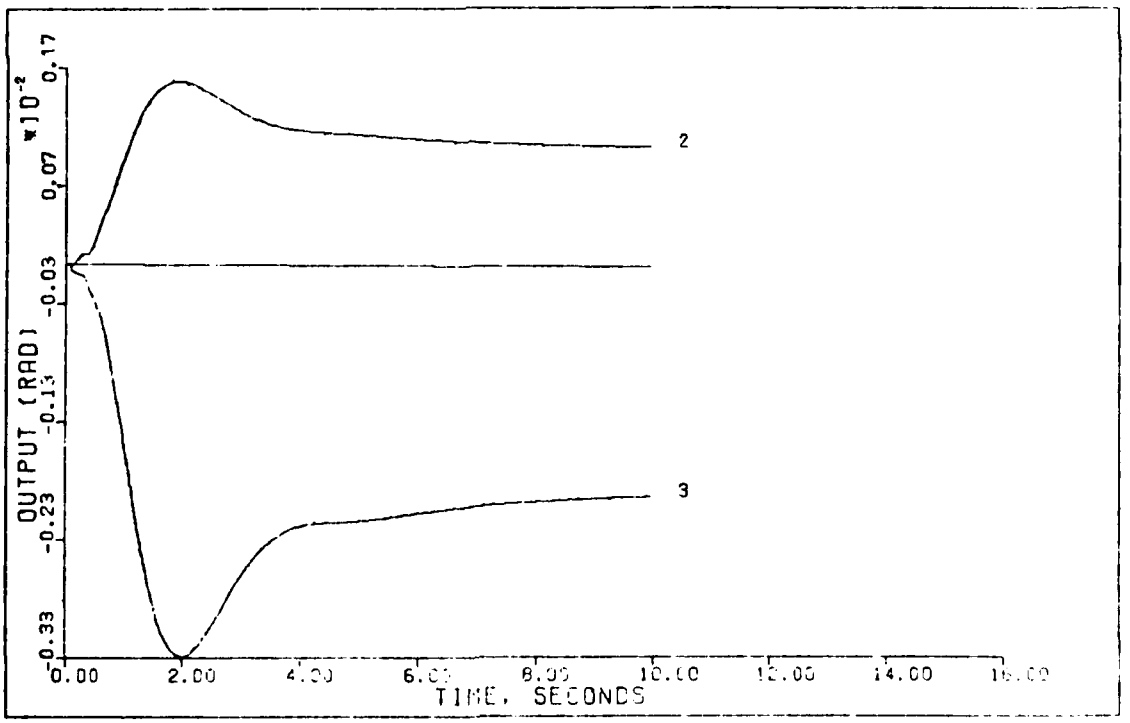
The results of the coordinated turn maneuver for Configuration 4 are summarized in Table 5-4.

Configuration 5. The system model used for this regime is that outlined in Eqs (A-12), (A-18), and (A-22).




1=YAW ANGLE ($\psi$) 5=SIDESLIP ANGLE ($\beta$); 6=ROLL ANGLE ($\phi$)

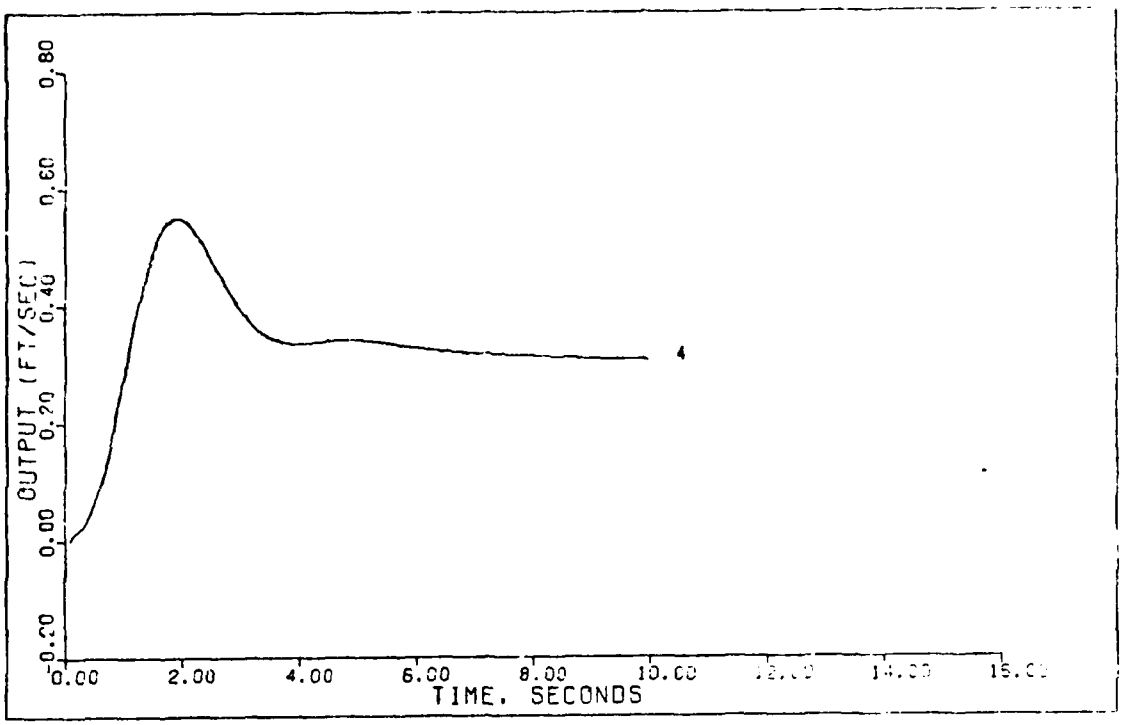
(a) $\psi$, $\beta$, $\phi$ Output Response




2=PITCH ANGLE ($\theta$); 3=ANGLE OF ATTACK ($\alpha$)

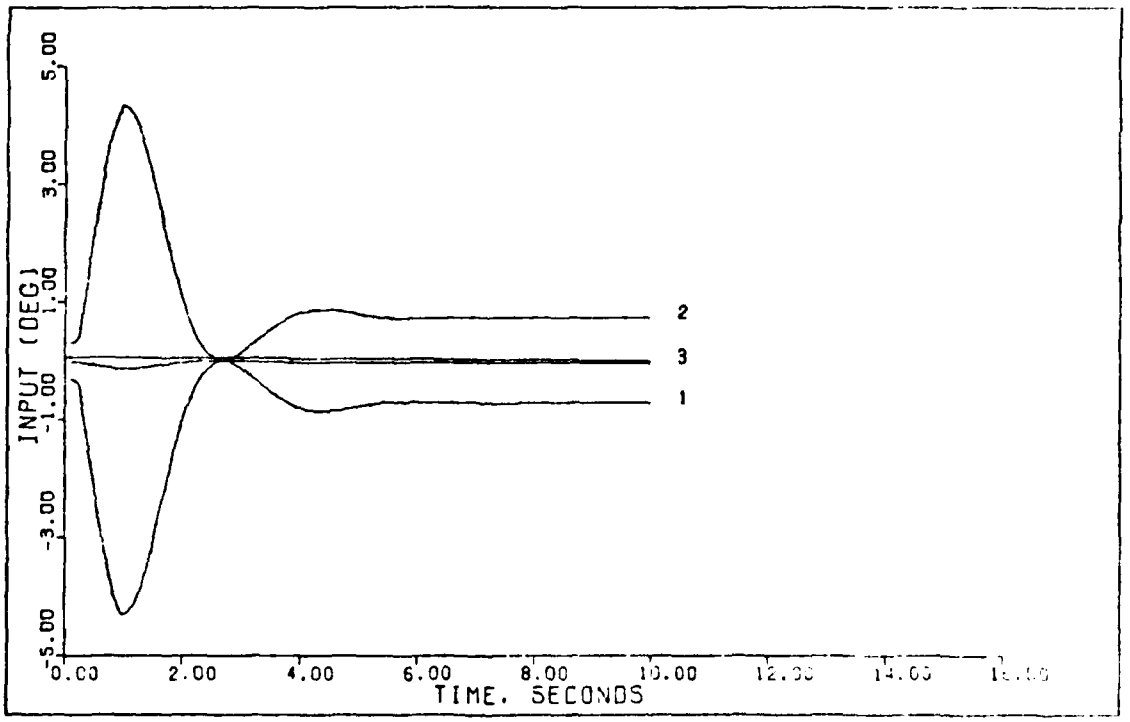
(b) $\theta$, $\alpha$ Output Response

Figure 5-8. Configuration 4, 30° Coordinated Turn Commanded



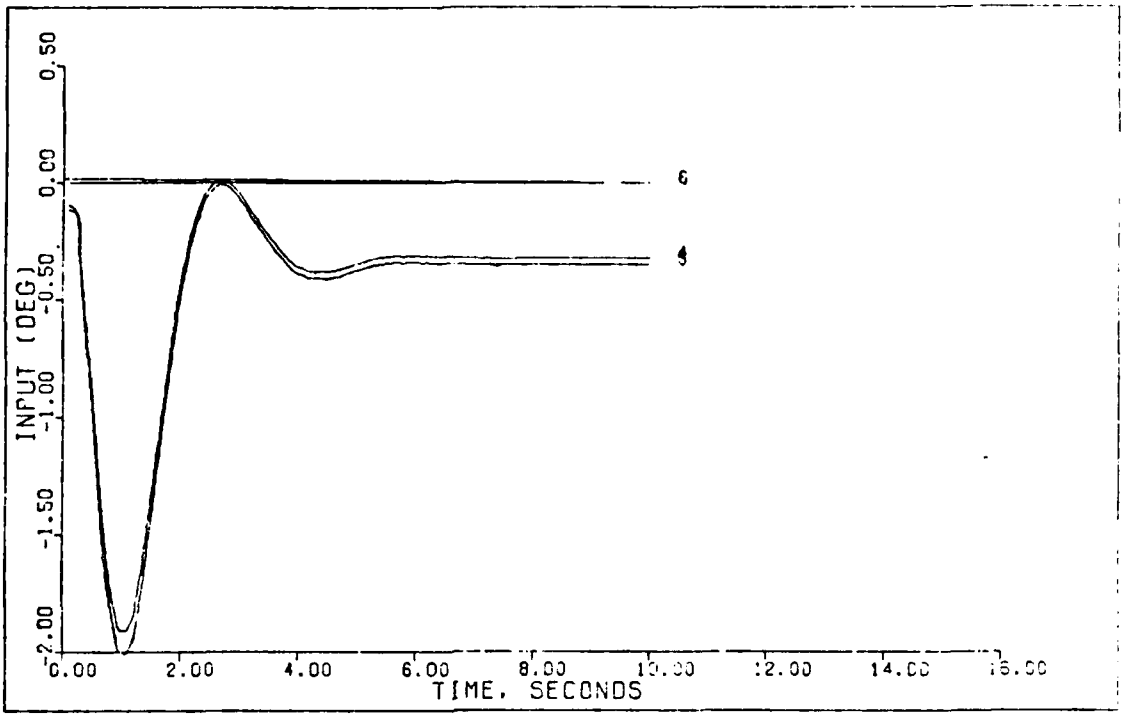

4=VELOCITY (U)

(c) u Output Response




1=RIGHT TAIL ($\delta_{H_r}$); 2=LEFT TAIL ($\delta_{H_l}$); 3=RUDDER ($\delta_r$)

(d) $\delta_{H_r}$, $\delta_{H_l}$, $\delta_r$ Control Input Response




4=RIGHT AILERON ($\delta_{a_r}$);5=LEFT AILERON ($\delta_{a_l}$);6=SPOILER-FLAP ($\delta_{sf}$)

(e) $\delta_{a_r}$, $\delta_{a_l}$, $\delta_{sf}$ Control Input Response

Table 5-4

Configuration 4 Results

| INPUT/ OUTPUT | $T_p$ (sec) | $T_s$ (sec) | $M_p$ | FINAL VALUE |
|---|---|---|---|---|
| $\psi$ * | 10 | - | 0.293 | 0.293 |
| $\theta$ | 2 | 8 | 0.00155 | 0.00085 |
| $\alpha$ | 2 | 15 | -0.0033 | -0.0019 |
| u ** | 2 | 12 | 0.54 | 0.30 |
| $\beta$ | - | - | 0 | 0 |
| $\phi$ | 3.6 | 3.0 | 0.524 | 0.524 |
| $\delta_{H_r}$ *** | 1 | 5 | -4.2 | -0.6 |
| $\delta_{H_l}$ | 1 | 5 | 4.2 | 0.6 |
| $\delta_r$ | 1 | 3.1 | -0.2 | -0.05 |
| $\delta_{a_r}$ | 1 | 5.4 | -1.9 | -0.35 |
| $\delta_{a_l}$ | 1 | 5.4 | -2.0 | -0.4 |
| $\delta_{sf}$ | - | - | 0 | 0 |

* - rad
** - ft/sec
*** - deg

The design includes the same actuator and sensor dynamics used in Configuration 1 through 4.

The design procedure yields a controller characterized by the parameter values:

$$T = 0.02 \text{ sec } (f = 50 \text{ hz}) \tag{5-34}$$

$$\alpha = 1.0 \tag{5-35}$$

$$\epsilon = 1.0 \tag{5-36}$$

$$\underline{\Sigma} = \text{diag}\{1.0, 0.75, 1.5, 0.1, 1.5, 0.5\} \tag{5-37}$$

These parameter values yield the irregular plant control matrices, $\underline{K}_o$ and $\underline{K}_1$, as:

$$\underline{K}_o = \underline{K}_1 =$$

$$\begin{bmatrix}
.5668E+02 & -.5477E+01 & -.1807E+01 & .2038E-03 & .4500E+02 & -.1461E+01 \\
-.5668E+02 & -.5477E+01 & -.1807E+01 & .2038E-03 & -.4500E+02 & .1461E+01 \\
.4717E+01 & -.4814E-14 & 0. & .3851E-17 & .1723E+02 & .1764E+00 \\
.2512E+02 & -.6767E+01 & -.9815E+01 & .2105E-02 & .1785E+02 & .9395E+00 \\
.2512E+02 & .6767E+01 & .9815E+01 & -.2105E-02 & .1785E+02 & .9395E+00 \\
-.2720E-11 & .7142E+02 & .2356E+02 & -.1180E-01 & -.2126E-11 & .4518E-13
\end{bmatrix} \tag{5-38}$$

The measurement matrix for the irregular plant is:

$$\underline{M} = \begin{bmatrix}
0.02 & 0 & 0 \\
0 & 0.02 & 0 \\
0 & 0 & 0 \\
0 & 0 & 0 \\
0 & 0 & 0 \\
0 & 0 & 0.02
\end{bmatrix} \tag{5-39}$$

Figure 5-9 illustrates the system response for a 30° coordinated turn. Figure 5-9(a) is the command vector, $\underline{v}$, where $\phi$ and $\psi$ are in radians, and the scaling factor $c_o$ is the same as in Eq (5-12). Using Eqs (5-2) and (5-12), the scaled commands are:

$$\phi' = c_o\phi = 0.0183 \text{ rad}$$

$$\dot{\psi}' = c_o\dot{\psi} = 0.00194 \text{ rad/sec}$$

$$\beta' = c_o\beta = 0 \text{ rad}$$

Thus, the command input vector for the coordinated turn maneuver is:

$$\underline{v} = \begin{bmatrix} 10,0.0194 \\ 0,0 \\ 0,0 \\ 0,0 \\ 0,0 \\ 1,0.0183 \end{bmatrix}$$

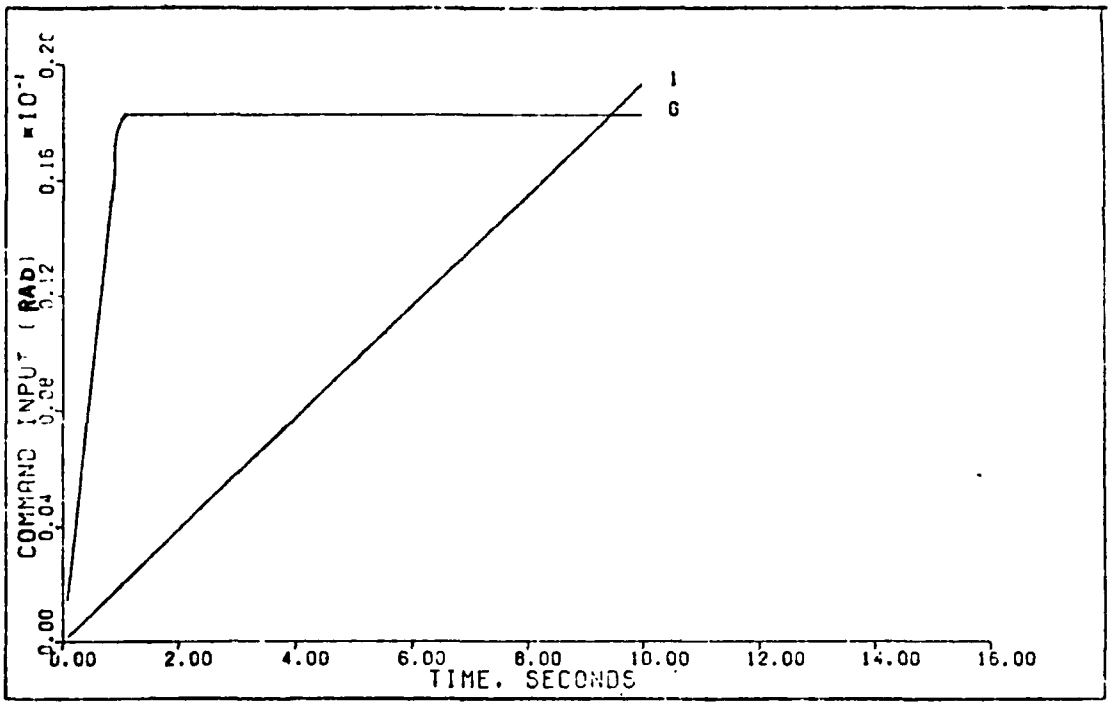
From Eq (5-13), the desired yaw rate, r, is:

$$r = 0.048 \text{ rad/sec}$$

Figure 5-9(c) shows the response of the state r for the maneuver.

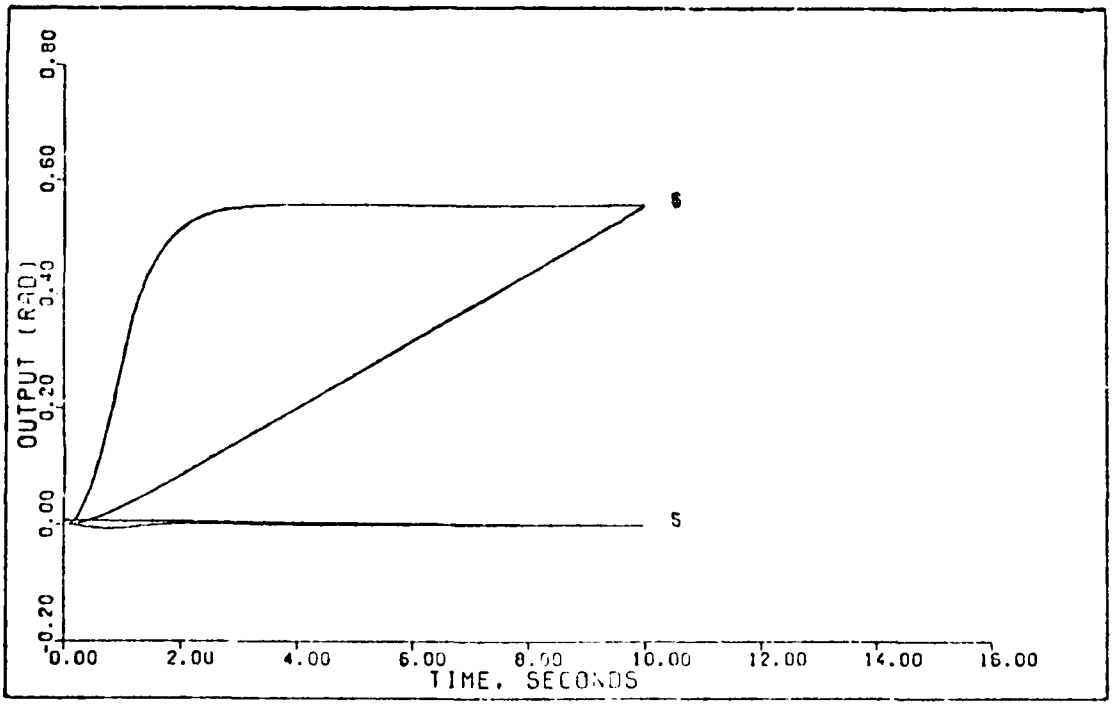
Figures 5-9(b), (d), and (e) illustrate the responses of the output variables. Figures 5-9(f) and (g) illustrate the control surface deflections for the system. The results of the coordinated turn maneuver for Configuration 5 are summarized in Table 5-5.

Configuration 6. The system model used for this regime is that outlined in Eqs (A-16), (A-20), and (A-22).




1=YAW ANGLE ($\psi$); 6=ROLL ANGLE ($\phi$)

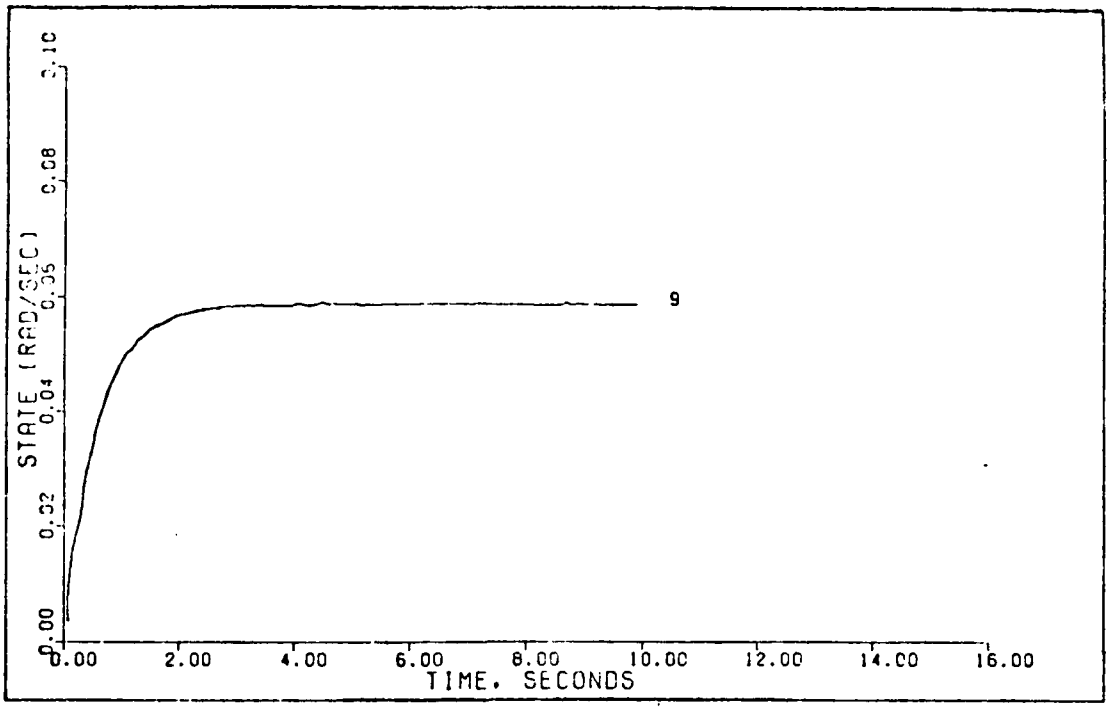
(a) $\psi$, $\phi$ Command Input




1=YAW ANGLE ($\psi$) 5=SIDESLIP ANGLE ($\beta$); 6=ROLL ANGLE ($\phi$)

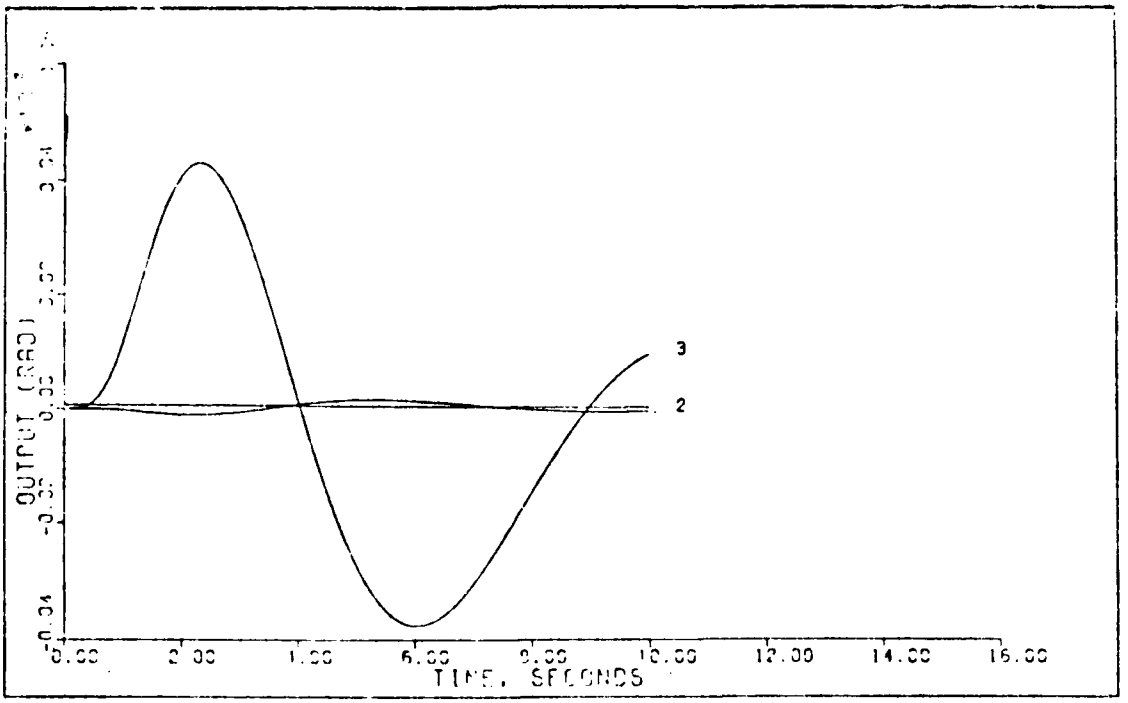
(b) $\psi$, $\beta$, $\phi$ Output Response

Figure 5-9. Configuration 5, 30° Coordinated Turn Commanded



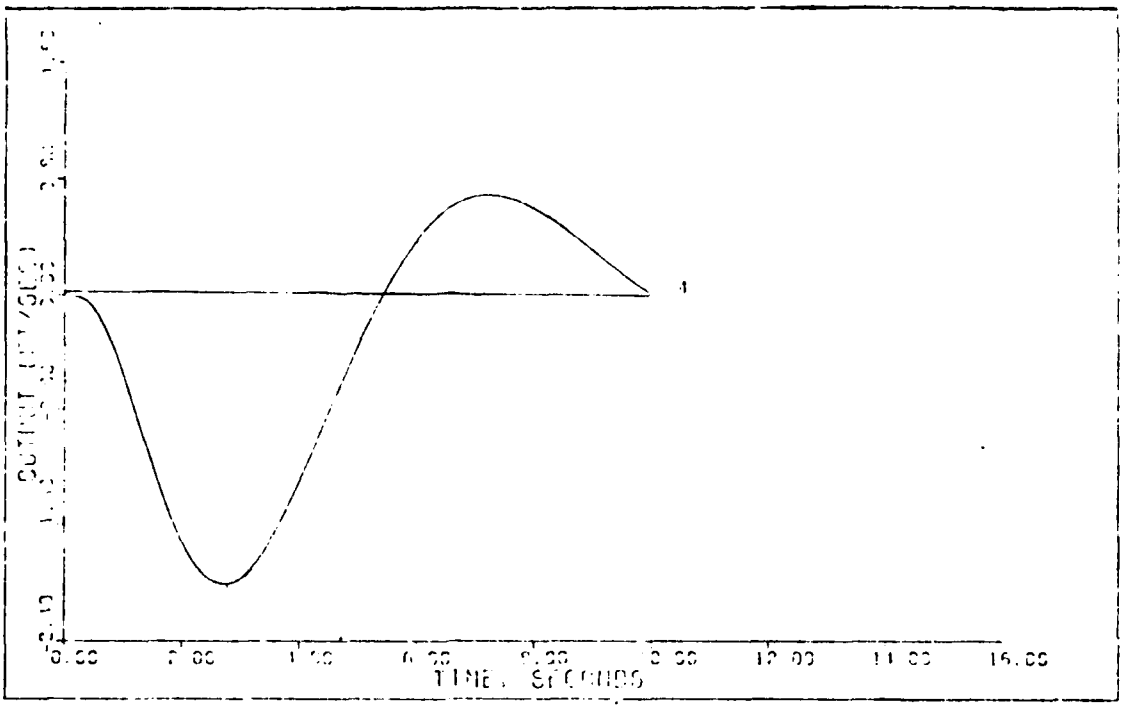

9=YAW RATE (R)

(c) r State Response



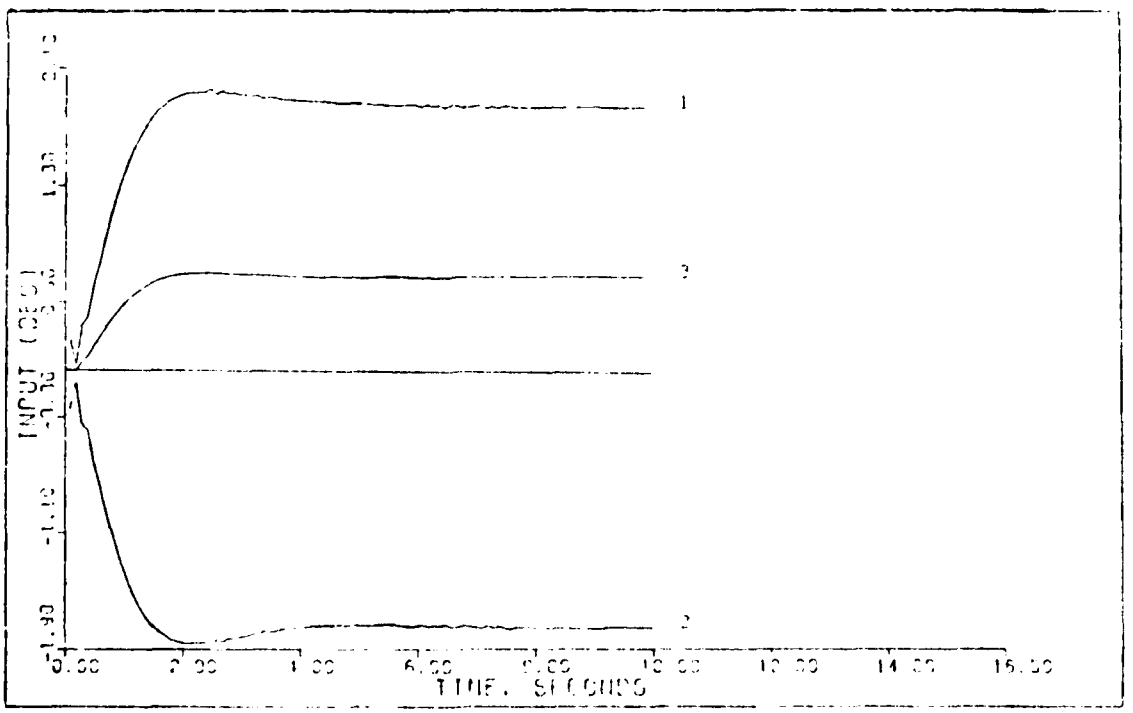

2-PITCH ANGLE ($\theta$); 3=ANGLE OF ATTACK ($\alpha$)

(d) $\theta$, $\alpha$ Output Response



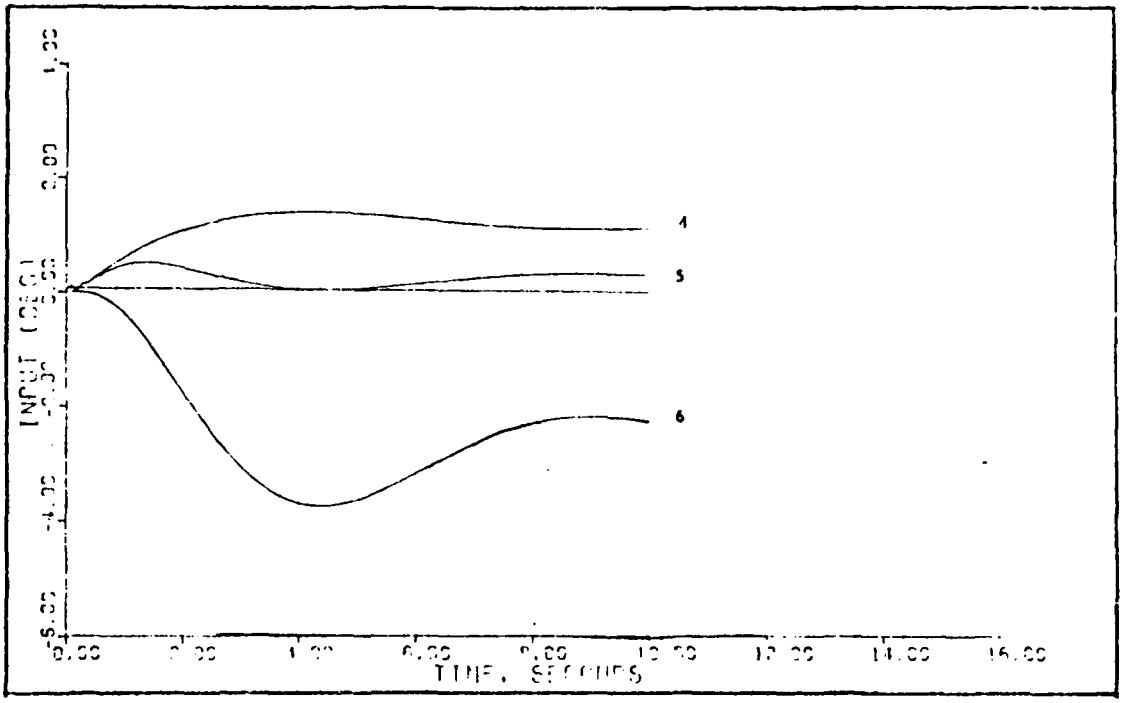

4-VELOCITY (U)

(e) u Output Response




1=RIGHT TAIL ($\delta_{H_r}$); 2=LEFT TAIL ($\delta_{H_l}$); 3=RUDDER ($\delta_r$)

(f) $\delta_{H_r}$, $\delta_{H_l}$, $\delta_r$ Control Input Response




4-RIGHT AILERON ($\delta_{a_r}$):5-LEFT AILERON ($\delta_{a_l}$):6-SPOILER-FLAP ($\delta_{sf}$)

(g) $\delta_{a_r}$, $\delta_{a_l}$, $\delta_{sf}$ Control Input Response

Table 5-5

Configuration 5 Results

| INPUT/ OUTPUT | $T_p$ (sec) | $T_s$ (sec) | $M_p$ | FINAL VALUE |
|---|---|---|---|---|
| $\psi$ * | 10 | - | 0.555 | 0.555 |
| $\theta$ | - | - | 0 | 0 |
| $\alpha$ | 2.2 | 25 | 0.043E-2 | 0 |
| u ** | 2.6 | 13 | -2.2 | 0 |
| $\beta$ | - | - | 0 | 0 |
| $\phi$ | 3.6 | 3.0 | 0.524 | 0.524 |
| $\delta_{H_r}$ *** | 2 | 4.8 | 1.94 | 1.86 |
| $\delta_{H_l}$ | 2 | 4.8 | -1.86 | -1.74 |
| $\delta_r$ | 2.1 | 3.4 | 0.66 | 0.60 |
| $\delta_{a_r}$ | 1.4 | 7 | 0.4 | 0.3 |
| $\delta_{a_l}$ | 4.2 | 7 | 1.4 | 1.1 |
| $\delta_{sf}$ | 4.3 | 10 | -3.8 | -2.4 |

* - rad
** - ft/sec
*** - deg

The design includes the same actuator and sensor dynamics used in Configurations 1 through 4.

The design procedure yields a controller characterized by the parameter values:

$$T = 0.02 \text{ sec } (f = 50 \text{ hz}) \tag{5-40}$$

$$\alpha = 1.0 \tag{5-41}$$

$$\varepsilon = 1.0 \tag{5-42}$$

$$\underline{\Sigma} = \text{diag}\{1.0, 0.75, 2.0, 0.1, 1.35, 0.75\} \tag{5-43}$$

These parameter values yield the irregular plant control matrices, $\underline{K}_o$ and $\underline{K}_1$, as:

$\underline{K}_o = \underline{K}_1 =$

$$\begin{bmatrix} .3521E+02 & -.1233E+01 & -.3819E+01 & .7509E-03 & .1638E+03 & .4207E+00 \\ -.3521E+02 & -.1233E+01 & -.3819E+01 & .7509E-03 & -.1638E+03 & -.4207E+00 \\ .4525E+01 & .8727E-16 & .3813E-13 & .9308E-17 & .4853E+02 & .2539E+00 \\ .1517E+02 & .9791E-01 & -.1452E+02 & .1842E-02 & .6560E+02 & .8509E+00 \\ .1517E+02 & -.9791E-01 & .1452E+02 & -.1842E-02 & .6560E+02 & .8509E+00 \\ -.2232E-11 & .1618E+02 & .5012E+02 & -.2862E-01 & -.1035E-10 & -.3166E-13 \end{bmatrix}$$

(5-44)

The measurement matrix for the irregular plant is:

$$\underline{M} = \begin{bmatrix} 0.02 & 0 & 0 \\ 0 & 0.02 & 0 \\ 0 & 0 & 0 \\ 0 & 0 & 0 \\ 0 & 0 & 0 \\ 0 & 0 & 0.02 \end{bmatrix} \tag{5-45}$$

Figure 5-10 illustrates the system response for a 30° coordinated turn. Figure 5-10(a) is the command vector, $\underline{v}$, where $\phi$ and $\psi$ are in radians and the scaling factor $c_o$ is the same as in Eq (5-12). Using Eqs (5-2) and (5-12), the scaled commands are:

$$\phi' = c_o\phi = 0.0183 \text{ rad}$$

$$\dot{\psi}' = c_o\dot{\psi} = 0.00068 \text{ rad/sec}$$

$$\beta' = c_o\beta = 0 \text{ rad}$$

Thus, the command input vector is:

$$\underline{v} = \begin{bmatrix} 10,0.0068 \\ 0,0 \\ 0,0 \\ 0,0 \\ 0,0 \\ 1,0.0183 \end{bmatrix}$$

From Eq (5-13), the desired yaw rate, r, is:

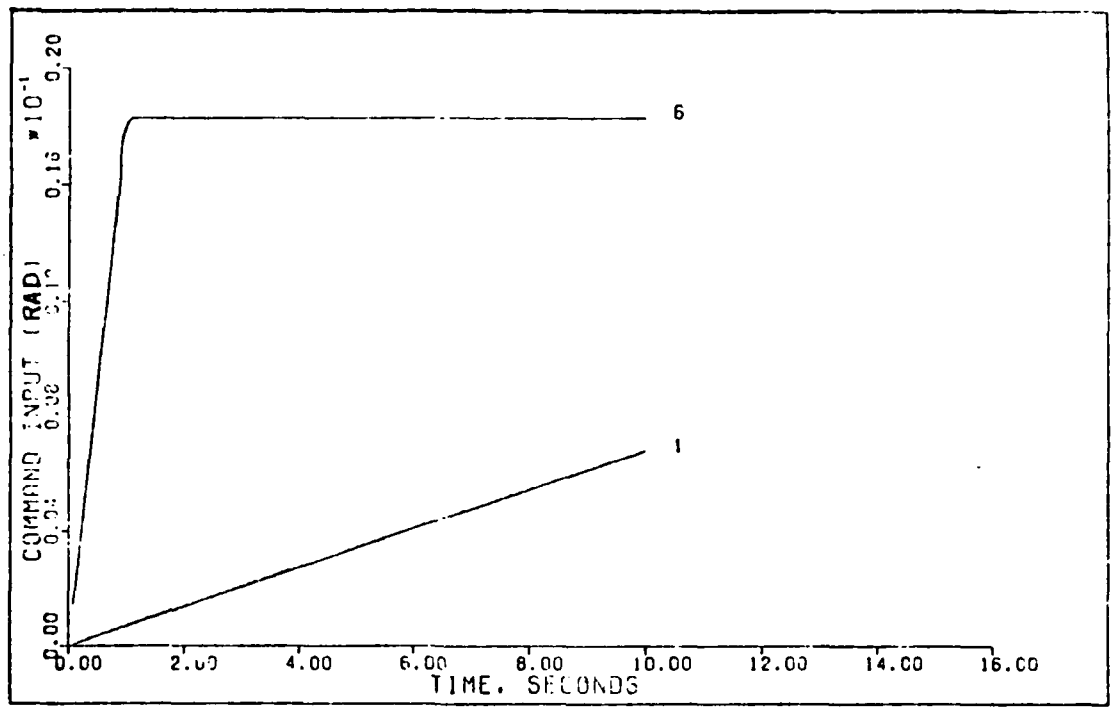
$$r = 0.0169 \text{ rad/sec}$$

Figure 5-10(c) shows the response of the state r for the maneuver.

Figures 5-10(b), (d), and (e) illustrate the responses of the output variables. Figures 5-10(f) and (g) illustrate the control surface deflections for the system. The results of the coordinated turn maneuver for Configuration 6 are summarized in Table 5-6.

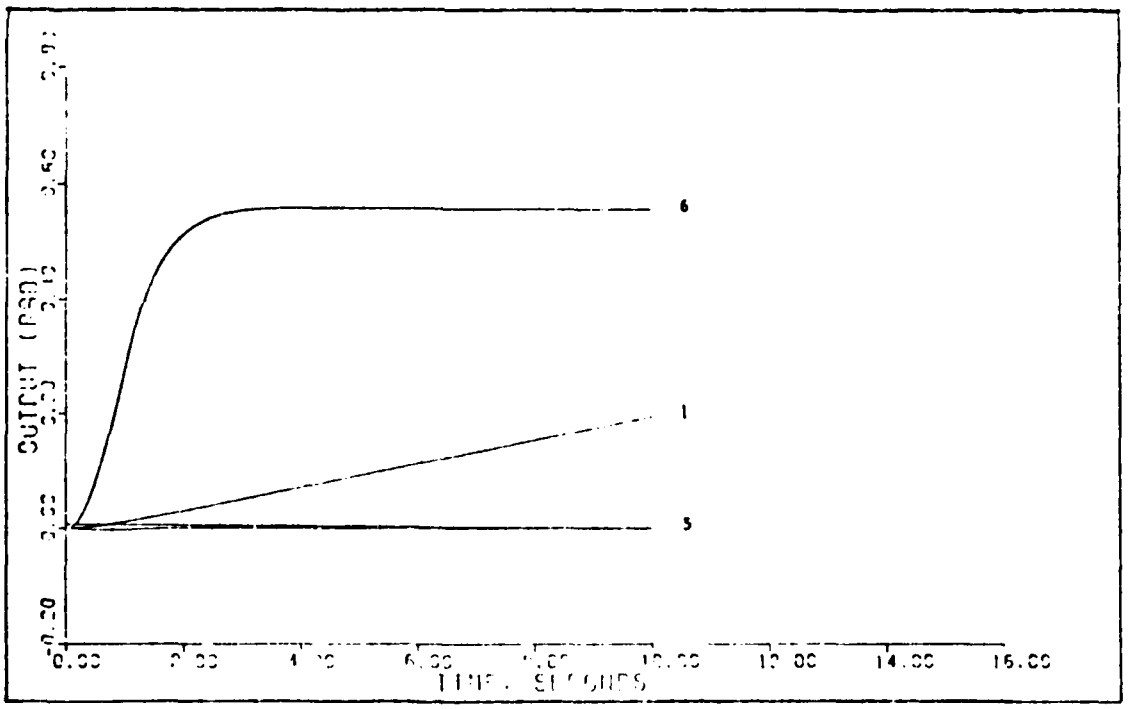
Robustness

The bulk of the design effort in this thesis is concentrated on obtaining controllers for the A-7D aircraft,




1=YAW ANGLE ($\psi$); 6=ROLL ANGLE ($\phi$)

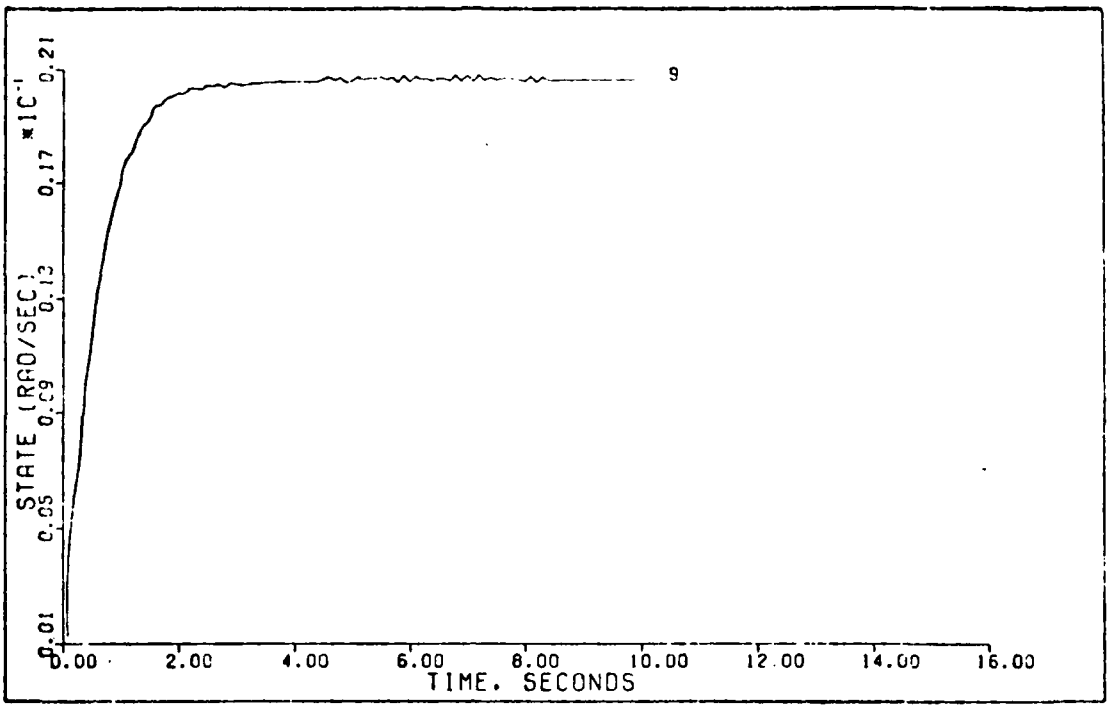
(a) $\psi$, $\phi$ Command Input




1=YAW ANGLE ($\psi$); 5-SIDESLIP ANGLE ($\beta$); 6-ROLL ANGLE ($\phi$)

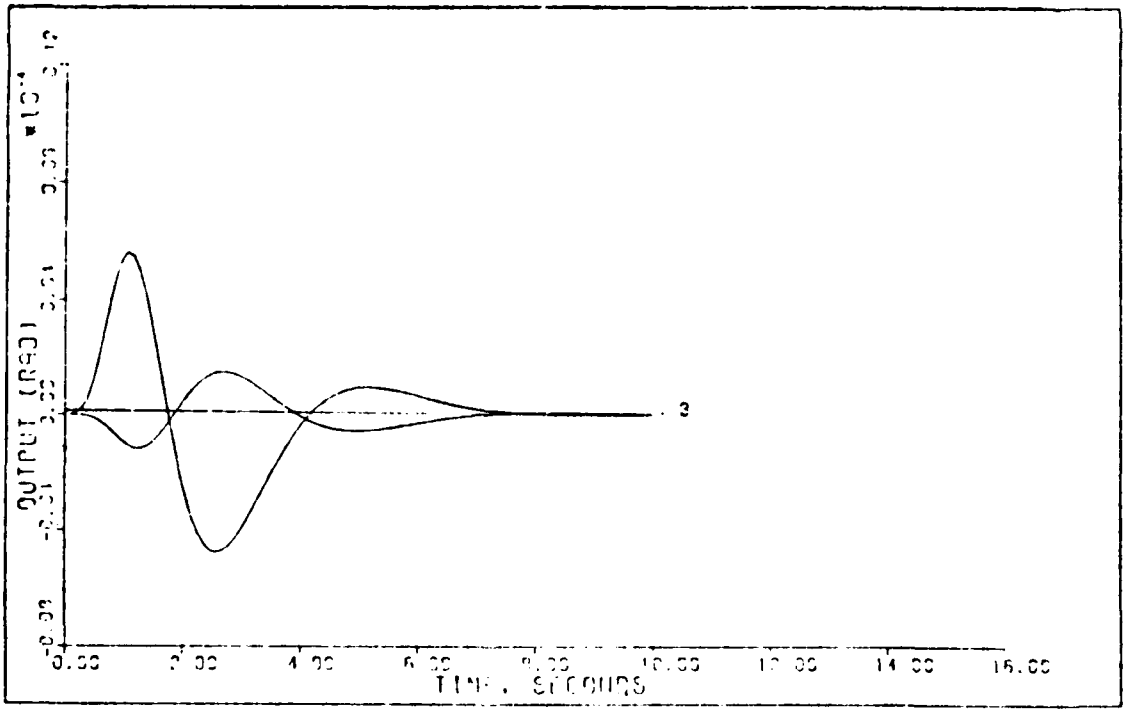
(b) $\psi$, $\beta$, $\phi$ Output Response

Figure 5-10. Configuration 6, 30° Coordinated Turn Commanded



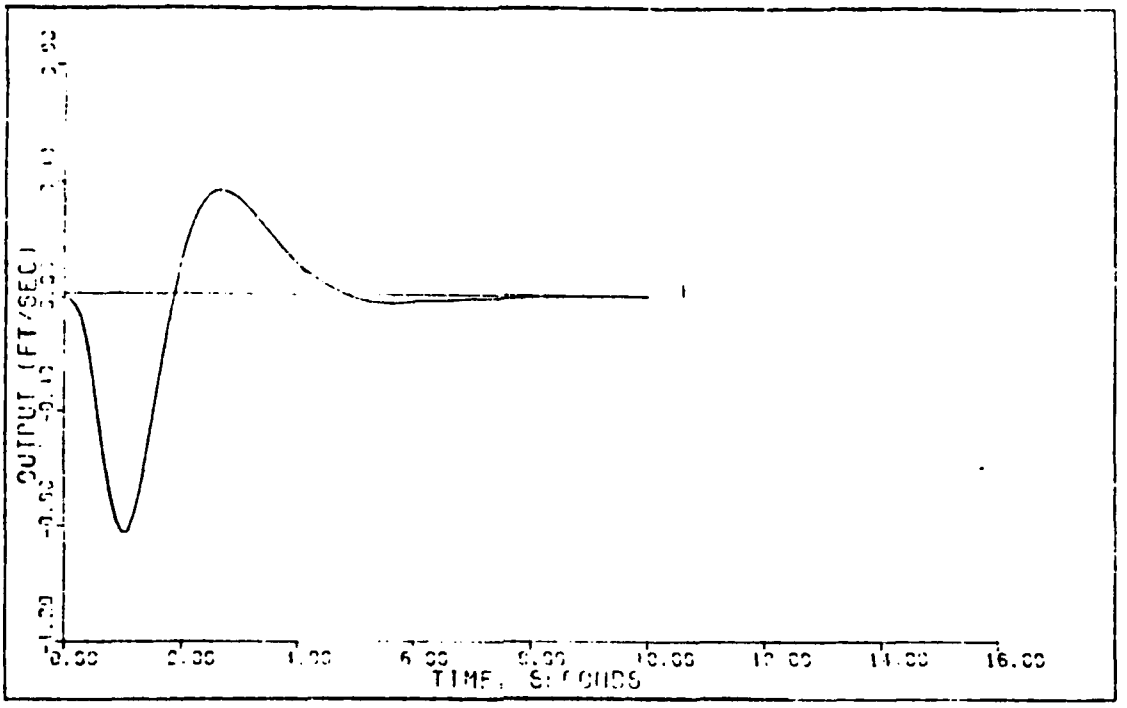

9=YAW RATE (R)

(c) r State Response



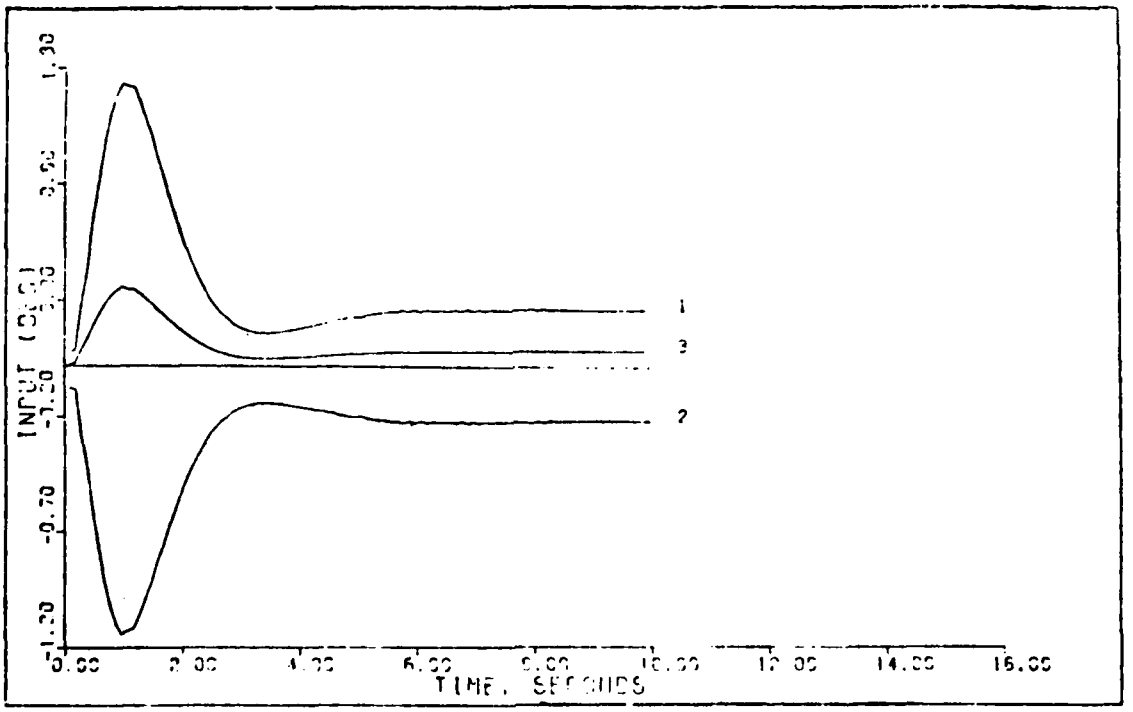

2-PITCH ANGLE (θ); 3 ANGLE OF ATTACK (α)

(d) θ, α Output Response



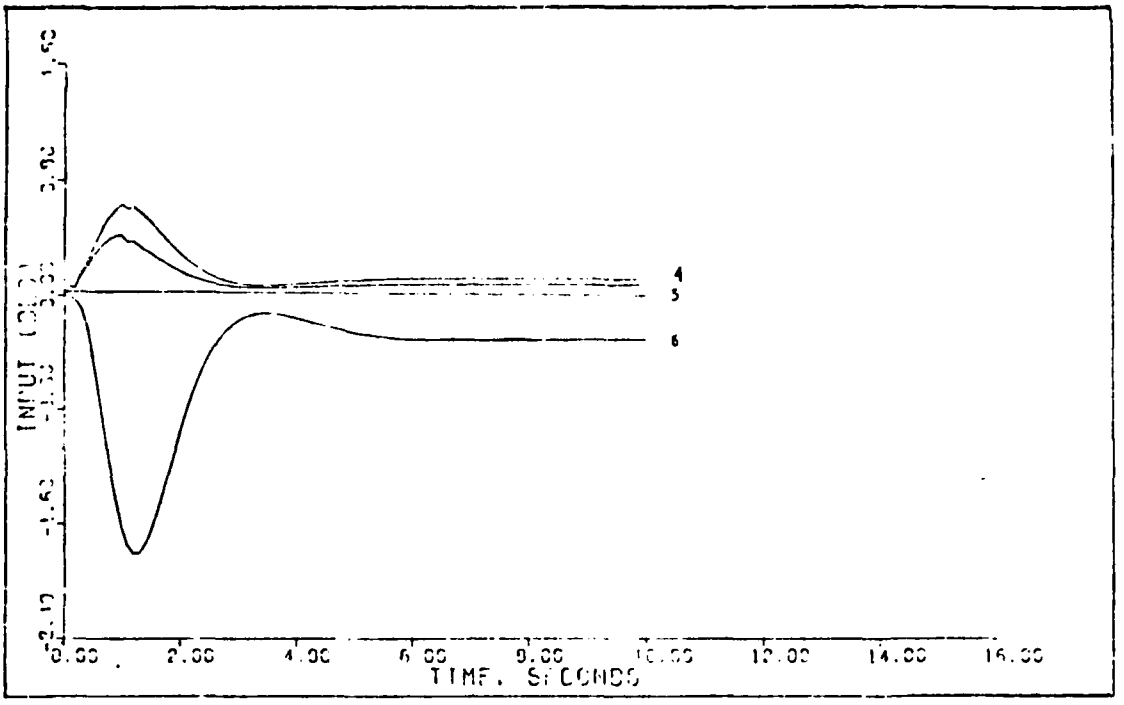

4-VELOCITY (U)

(e) u Output Response




1-RIGHT TAIL ($\delta_{H_r}$): 2-LEFT TAIL ($\delta_{H_l}$): 3-RUDDER ($\delta_r$)

(f) $\delta_{H_r}$, $\delta_{H_l}$, $\delta_r$ Control Input Response




4=RIGHT AILERON ($\delta_{a_r}$):5=LEFT AILERON ($\delta_{a_l}$):6=SPOILER-FLAP ($\delta_{sf}$)

(g) $\delta_{a_r}$, $\delta_{a_l}$, $\delta_{sf}$ Control Input Response

Table 5-6

Configuration 6 Results

| INPUT/ OUTPUT | $T_p$ (sec) | $T_s$ (sec) | $M_p$ | FINAL VALUE |
|---|---|---|---|---|
| $\psi$ * | 10 | - | 0.195 | 0.195 |
| $\theta$ | - | - | 0 | 0 |
| $\alpha$ | - | - | 0 | 0 |
| u ** | 1 | 7 | -0.84 | 0 |
| $\beta$ | - | - | 0 | 0 |
| $\phi$ | 3.6 | 3.0 | 0.524 | 0.524 |
| $\delta_{H_r}$ *** | 1 | 5.6 | 1.25 | 0.25 |
| $\delta_{H_l}$ | 1 | 5.6 | -1.15 | -0.25 |
| $\delta_r$ | 1 | 5.6 | 0.35 | 0.05 |
| $\delta_{a_r}$ | 1 | 5.6 | 0.64 | 0.12 |
| $\delta_{a_l}$ | 1 | 5.6 | 0.40 | 0.08 |
| $\delta_{sf}$ | 1.2 | 5.6 | -1.75 | -0.32 |

* - rad
** - ft/sec
*** - deg

with a variety of failed control surfaces, for the M=0.60 at 15,000 ft flight condition. The robustness of the design, that is, the ability of the controller to provide adequate tracking performance at flight conditions other than the one at which it is designed, is examined briefly.

The controllers designed at each flight condition, with all surfaces operative, are tested at each of the other two flight conditions. Each of the four maneuvers is performed using each controller. In all cases, the responses are unstable and highly oscillatory and are therefore not included in this thesis. Thus, none of the controllers are a "robust system."

The results of Bauschlicher and Masi (Ref 22; 23), however, show controllers which are robust over a wide range of flight conditions. An examination of their controller designs provides a possible clue to this apparent contradiction.

The robust designs of Bauschlicher and Masi are characterized by measurement matrix elements ranging from 0.25 to 1, that is, by transmission zeros located over the range -1 to -4 in the s-plane. The controllers developed in this thesis have measurement matrix elements ranging from 0.008 to 0.05, or transmission zeros located over the range -20 to -125 in the s-plane. It is beyond the scope of this thesis to determine whether or not there is a correlation between controller robustness and the location of transmission

zeros in the s-plane; however, this appears to be the only major difference in design parameters among the three thesis, and may perhaps have some significance.

Summary

This chapter presents the design procedure used to develop multivariable digital control laws for the A-7D DIGITAC II aircraft. The actual procedure is outlined and the control laws for six different configurations are presented. The chapter also addresses some of the problems encountered in modelling the aircraft as well as the maneuvers that are selected to develop the controllers. The chapter concludes with a brief discussion of the tests performed for controller robustness and presents a possible reason for the lack of robustness exhibited by the controllers.

The next chapter presents a suggested transition strategy from normal control laws to reconfigured control laws.

# VI Proposed Reconfiguration Strategy

## Introduction

This chapter presents one possible strategy for transitioning from the normal control laws for an aircraft with all surfaces operative, to a set of reconfigured control laws for an aircraft with a failed surface. The discussion begins with a definition of reconfiguration and why it is important. A transition strategy is then proposed, addressing the topics of failure detection and isolation, and implementation.

## Reconfiguration

Reconfiguration is a technique which shows promise in restoring aircraft stability and a degraded level of controllability in the event a primary control surface becomes inoperative. This technique implies that the control laws governing aircraft motion compensate for the failed surface by using the remaining surfaces to maintain control. In the past, pilots were sometimes able to do this manually, particularly if the aircraft was very stable aerodynamically.

The aircraft of today, however, are not necessarily stable and the use of closed-loop flight control systems leaves the pilot without direct control of the primary surfaces. The control laws of Chapter V provide the

independent control of each surface necessary to implement reconfiguration which deals with the new, highly coupled aerodynamics.

Transition Strategy

The development of reconfigurable digital control laws, such as those developed in this thesis, must include a method of failure identification and implementation of the revised control law. The key to reconfiguration is being able to determine when these laws should be used and how to switch to them from the normal control laws. Requiring the pilot to determine when and which surface has failed is an additional task that he may have little time for and may not be able to perform. Thus, a failure detection and isolation scheme must be developed.

The proposed failure detection and isolation system uses a set of redundant sensors, activated by stick movements, to determine if the hydraulic actuators are still operative. Should an actuator fail to move a control surface, the sensors notify a control surface monitor. The monitor validates the fail signal (voting between redundant monitors) and determines which control surface is inoperative.

The control surface monitor is the heart of the reconfigurable flight control system. When notified of a failure, the monitor informs a redundant set of flight control computers of the problem and provides the necessary

information concerning which set of new control laws should be used to calculate the appropriate surface deflections. The off-line flight control computer is programmed with the new control laws and then signals the on-line system that it is ready to assume control of the aircraft. Thus, the pilot is again able to fly a stable aircraft with some degree of control capability. The reconfigurable flight control system must be subject to some redundancy management scheme in order to prevent spurious data, noise, or sensor failure from precipitating an unneeded change from normal to reconfigured control laws.

Summary

This chapter presents one possible method for transitioning from normal control laws to a set of reconfigured control laws for an aircraft with a failed surface. The strategy requires the system to detect and isolate a surface failure and then transfer control to an off-line flight control computer which has been programmed with the new control laws.

The final chapter presents the conclusions drawn from this thesis effort and recommendations for further study.

# VII Conclusions and Recommendations

## Conclusions

The efforts of this thesis demonstrate that a multivariable digital tracker control law can be developed for the A-7D DIGITAC II aircraft for a number of different flight conditions. The performance of each controller is excellent for the flight condition at which it is designed. However, when a controller is used at a flight condition other than that at which it is designed, the system responses are unstable and highly oscillatory. Thus, none of the controllers provide a "robust system."

This thesis also demonstrates that reconfigured control laws can be developed for the A-7D DIGITAC II aircraft with a failed primary control surface. These reconfigured control laws perform conventional maneuvers satisfactorily. Depending on which control surface has failed, CCV maneuvers are also performed satisfactorily.

One of the most important things to come out of this thesis is that the design of multivariable control laws is a straightforward process. Once the engineer gains an understanding of the theory, and some experience applying the design procedure outlined in Chapter V, the development of control laws for a linear system is relatively simple.

The additional modifications to MULTI expand the usefulness of the program as a design tool. The transfer

function option provides the designer with the open-loop poles and zeros of the system and information about the stability of the basic plant. The modifications to the simulation program provide for a more accurate system representation when the plant contains actuators and/or sensors.

Recommendations

Based on the conclusions above, the following recommendations for further study are proposed:

1. The development of a more accurate model for the A-7D aircraft. Controllers developed for inaccurate models are of little use.

2. Expand the transfer function option to compute the closed-loop poles and zeros of the system. This will permit the calculation of the figures of merit which can also be added to MULTI.

3. An investigation of the relationship between the values of the measurement matrix elements (which directly determines the location of the transmission zeros) and the robustness of controllers.

4. An investigation of the effects of integration time delays on system performance and stability and the use of compensators to improve performance.

5. An examination of the use of compensation of plants with explicit actuator dynamics and the modifications to MULTI to account for such compensation (Ref 28).

## Bibliography


1. Porter, B. Design of High Performance Tracking Systems. USAME/DC/120/81. Air Force Flight Dynamics Laboratory, Wright-Patterson AFB OH. October 1981.

2. _____. Design of Set Point Tracking and Disturbance Rejection Controllers for Unknown Multivariable Plants. Progress Report for period 15 November 1980 to 31 December 1980. USAME/DC/101/81. Air Force Flight Dynamics Laboratory, Wright-Patterson AFB OH. January 1981.

3. _____, and A. Bradshaw. "High Gain Error-Actuated Controllers for a Class of Linear Multivariable Plants," Proceedings of the 18th IEEE Conference on Decision and Control, 322-325. Fort Lauderdale FL (December 1979).

4. _____. "Design of Error-Actuated Controllers for Unknown Multivariable Plants," Electronics Letters, 17(3): 106-107 (February 5, 1981).

5. _____, and A. Bradshaw. "Design of Linear Multivariable Discrete-Time Tracking Systems Incorporating Fast-Sampling Error-Actuated Controllers," International Journal of Systems Science, 11(7): 817-826 (July 1980)

6. _____. "Asymptotic Properties of Linear Multivariable Discrete-Time Tracking Systems Incorporating Fast-Sampling Error-Actuated Controllers," International Journal of Systems Science, 11(11): 1279-1293 (November 1980).

7. _____. "Design of Linear Multivariable Continuous-Time High-Gain Output Feedback Regulators," International Journal of Systems Science, 10(2): 113-121 (February 1979).

8. _____. "Design of Linear Multivariable Continuous-Time Tracking Systems Incorporating High-Gain Error-Actuated Controllers," International Journal of Systems Science, 10(4): 461-469 (April 1979).

9. _____. "Asymptotic Properties of Linear Multivariable Continuous-Time Tracking Systems Incorporating High-Gain Error-Actuated Controllers," International Journal of Systems Science, 10(12): 1433-1444 (December 1979).

10. Porter, B. "Singular Perturbation Methods in the Design of Stabilizing Feedback Controllers for Multivariable Linear Systems," International Journal of Control, 20(4): 689-692 (April 1974).

11. _____. "Singular Perturbation Methods in the Design of Observers and Stabilizing Feedback Controllers for Multivariable Linear Systems," Electronics Letters, 10 (23): 494-495 (November 14, 1974).

12. _____, and A. T. Shenton. "Singular Perturbation Methods of Asymptotic Eigenvalue Assignment in Multivariable Linear Systems," International Journal of Systems Science, 6(1): 33-37 (January 1975).

13. _____. "Singular Perturbation Analysis of the Transfer Function Matrices of a Class of Multivariable Linear Systems," International Journal of Control, 21(4): 655-660 (April 1975).

14. Porter, B. "Singular Perturbation Methods in the Synthesis of Feedback - Control Laws for Eigenvalue Assignment in Multivariable Linear Systems," International Journal of Systems Science, 7(5): 597-601 (May 1976).

15. _____. "Design of High-Gain Feedback Controllers for Linear Multivariable Systems," Electronics Letters, 14(8): 256-258 (April 13, 1978).

16. _____, and J. J. D'Azzo. "Transmission Zeros of Linear Multivariable Continuous-Time Systems," Electronics Letters, 13(24): 753-755 (November 24, 1977).

17. Porter, B. "Computation of the Zeros of Linear Multivariable Systems," International Journal of Systems Science, 10(12): 1427-1432 (December 1979).

18. Paschall, Randall N. Design of a Multivariable Control Law for the A-7D DIGITAC II Aircraft. MS thesis. Air Force Institute of Technology, Wright-Patterson AFB OH; December 1981. (AFIT/GE/EE/81D-47)

19. Porter, Douglas S. Design and Analysis of a Multivariable Digital Controller for the A-7D DIGITAC II Aircraft and the Development of an Interactive Computer Design Program. MS thesis. Air Force Institute of Technology, Wright-Patterson AFB OH; December 1981. (AFIT/GE/EE/81D-48)

20. Blakelock, John H. Automatic Control of Aircraft and Missiles. New York: John Wiley and Sons, Inc., 1965.

21. Ridgely, D. B., S. Banda, and J. J. D'Azzo. "Decoupling of High-Gain Multivariable Tracking Systems." Paper No. 83-0280 scheduled for presentation to the AIAA 21st Aerospace Sciences Meeting at Reno, Nevada, in January, 1983. Wright-Patterson AFB OH. June 1982.

22. Bauschlicher, Jon M. "Design of a Complete Multivariable Digital Flight Control System." Unpublished MS thesis. School of Engineering, Air Force Institute of Technology, Wright-Patterson AFB OH, December 1982.

23. Masi, Michael A. "Digital Multivariable Tracker Control Laws for the C-141 Aircraft." Unpublished MS thesis. School of Engineering, Air Force Institute of Technology, Wright-Patterson AFB OH, December 1982.

24. Barfield, A. Finley. "Multivariable Control Law Development for the AFTI/F-16." Unpublished MS thesis. School of Engineering, Air Force Institute of Technology, Wright-Patterson AFB OH, December 1982.

25. Potts, D. W. Direct Digital Design Method for Reconfigurable Multivariable Control Laws for the A-7D DIGITAC II Aircraft. MS thesis. Air Force Institute of Technology, Wright-Patterson AFB OH; December 1980. (AFIT/GE/EE/80D-36)

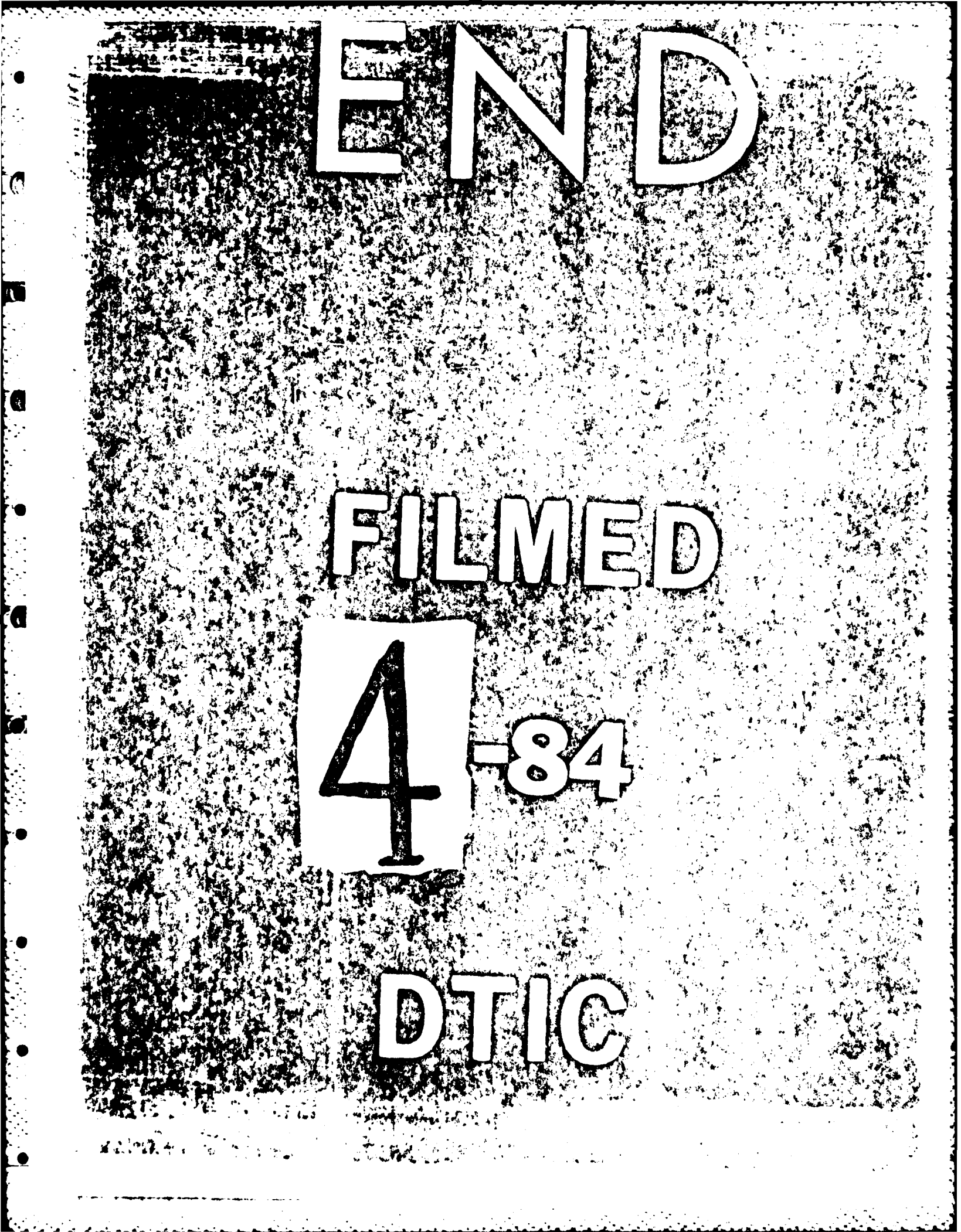
26. Bender, M., and A. Wolf. Flight Test Evaluation of a Digital Flight Control System for the A-7D Aircraft Simulation Test Plan. Contract F33601-73-C-3098. Wright-Patterson AFB OH: Aeronautical Systems Division, 15 February 1974.

27. LTV Vought Aeronautics Division. A-7 Aerodynamic Data Report. Report Number 2-53310/5R-1981, 21 May 1965.

28. Porter, B. "High-Gain Error-Actuated Controllers for Linear Multivariable Plants with Explicit Actuator Dynamics," Proceedings of the 2nd IFAC Symposium on Computer Aided Design of Multivariable Technological Systems. 61-65. West Lafayette IN, September 15-17, 1982.



*USGPO: 1984-759-062-686


END
FILMED
4-84
DTIC